



Australian Government
Geoscience Australia



Government of South Australia
Department for Manufacturing,
Innovation, Trade, Resources and Energy

The Frome airborne electromagnetic survey, South Australia:

Implications for energy, minerals and regional geology

Edited by I. C. Roach

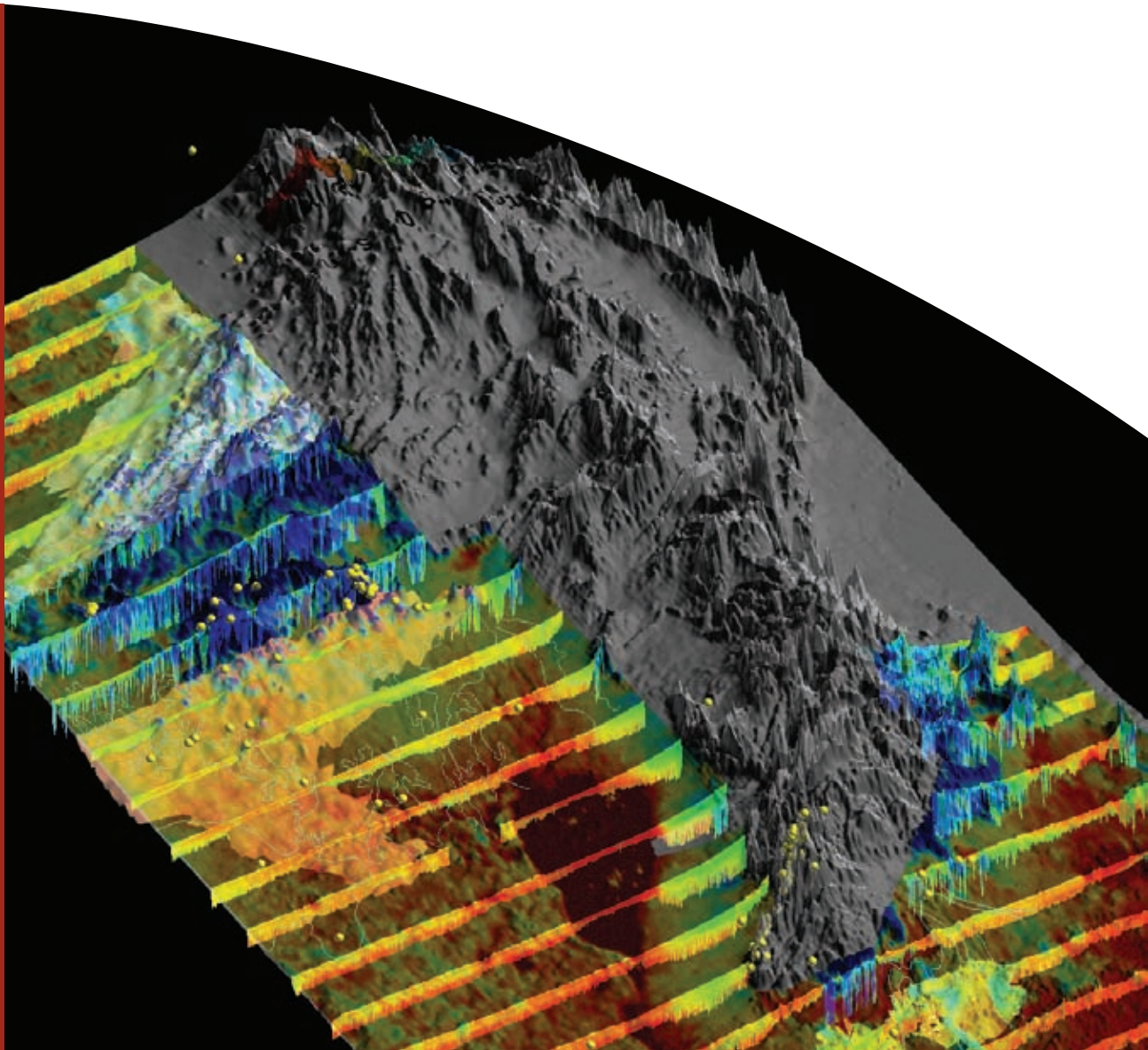
With contributions from: R. C. Brodie, M. T. Costelloe, A. J. Cross, T. Dhu, A. J. Fabris, S. B. Hore, E. A. Jagodzinski, S. Jaireth, L. F. Katona, J. L. Keeling, P. D. Magarey, A. B. Marsland-Smith, B. H. Michaelsen, I. C. Roach, C. E. Wade and T. Wilson

Record

2012/40

**GeoCat #
73713**

**DMITRE
Report Book
2012/00003**



The Frome airborne electromagnetic survey, South Australia: implications for energy, minerals and regional geology

GEOSCIENCE AUSTRALIA
RECORD 2012/40

GEOLOGICAL SURVEY OF SOUTH AUSTRALIA
REPORT BOOK 2012/00003

Edited by

I. C. Roach¹

With contributions from:

R. C. Brodie¹, M. T. Costelloe¹, A. J. Cross², T. Dhu³, A. J. Fabris³, S. B. Hore³, E. A. Jagodzinski³, S. Jaireth², L. F. Katona³, J. L. Keeling³, P. D. Magarey⁴, A. B. Marsland-Smith⁵, B. H. Michaelsen³, I. C. Roach¹, C. E. Wade³ and T. Wilson³.



Australian Government
Geoscience Australia



Government of South Australia
Department for Manufacturing,
Innovation, Trade, Resources and Energy

-
1. Continental Geophysics, Minerals and Natural Hazards Division, Geoscience Australia, GPO Box 387, Canberra ACT 2601 Australia.
 2. Resources, Advice and Promotions, Minerals and Natural Hazards Division, Geoscience Australia, GPO Box 387, Canberra ACT 2601 Australia.
 3. Geological Survey of South Australia, South Australia Department for Manufacturing, Innovation, Trade, Resources and Energy, GPO Box 1264, Adelaide SA 5001, Australia.
 4. South Australia Department for Water, Level 11, 25 Grenfell St, Adelaide, SA 5000, Australia
 5. Heathgate Resources Pty Ltd, Level 4, 25 Grenfell St, Adelaide, SA 5000, Australia

Department of Resources, Energy and Tourism

Minister for Resources and Energy: The Hon. Martin Ferguson, AM MP

Secretary: Mr Drew Clarke

Geoscience Australia

Chief Executive Officer: Dr Chris Pigram

South Australia Department for Manufacturing, Innovation, Trade, Resources and Energy

Minister for Mineral Resources and Energy: The Hon. Tom Koutsantonis, MP

DMITRE, Resources and Energy Group

Deputy Chief Executive: Dr Paul Heithersay



© Commonwealth of Australia (Geoscience Australia) 2012

With the exception of the Commonwealth Coat of Arms and where otherwise noted, all material in this publication is provided under a Creative Commons Attribution 3.0 Australia Licence (<http://www.creativecommons.org/licenses/by/3.0/au/>)

Geoscience Australia has tried to make the information in this product as accurate as possible. However, it does not guarantee that the information is totally accurate or complete. Therefore, you should not solely rely on this information when making a commercial decision.

ISSN 1448-2117

ISBN 978-1-922103-26-0 print

ISBN 978-1-922103-25-3 web

GeoCat # 73713

Bibliographic reference: Roach, I. C. ed. 2012. The Frome airborne electromagnetic survey, South Australia: implications for energy, minerals and regional geology. Geoscience Australia Record 2012/40 – DMITRE Report Book 2012/00003, 296 pp.

Contents

Executive Summary	1
1 Introduction (I. C. Roach and M. T. Costelloe)	3
1.1 Survey rationale	3
1.2 Survey location	3
1.3 Survey Geo-economic framework	5
1.3.1 Uranium mineral deposits	5
1.3.2 Metal deposits	8
1.3.3 Non-metal, industrial mineral and energy commodity deposits	9
1.3.4 Groundwater systems	9
1.3.5 Geothermal energy	9
1.4 Area Assessment	10
1.4.1 Targets: geo-electrical forward modelling for system selection	10
1.4.2 Terrain affecting aircraft operations (drape)	11
1.4.3 Aircraft access	13
1.4.4 Native title, no-fly zones and state government land access issues	13
1.4.5 Climate	15
1.4.6 Communication strategy	16
1.5 Survey infill partners and cost	17
1.6 Final survey design	18
1.7 References	21
2 Previous investigations (I. C. Roach, M. T. Costelloe and S. Jaireth)	23
2.1 Introduction	23
2.2 Geological mapping	23
2.2.1 Surface geology mapping	23
2.2.2 Solid geology mapping	23
2.3 Regolith-landform and soil mapping	26
2.4 Specialist geological publications	31
2.4.1 Geology and geodynamics	31
2.4.2 Regolith geology and geomorphology	32
2.4.3 Geochronology	33
2.4.4 Mineral resources and mineral systems	33
2.5 Drilling	35
2.6 Mineral exploration lease status before and after the survey	36
2.7 Geophysical mapping and remote sensing	38
2.7.1 Airborne geophysics	38
2.7.2 Seismic and magnetotellurics	41
2.7.3 Remote Sensing	41
2.8 3D models	43
2.9 Groundwater	43
2.10 References	44
3 Geology, physiography, landscape evolution and mineral systems (I. C. Roach, S. Jaireth, C. E. Wade, A. J. Cross, S. B. Hore and E. A. Jagodzinski)	53
3.1 Introduction	53
3.2 Regional geology	53
3.2.1 Paleo-Mesoproterozoic Curnamona Province	53
3.2.2 Neoproterozoic	58
3.2.3 Paleozoic	61
3.2.4 Mesozoic	61

The Frome airborne electromagnetic survey, South Australia: implications for energy, minerals and regional geology

3.2.5 Cenozoic	65
3.2.6 Quaternary	73
3.2.7 Granites and other felsic rocks	73
3.3 Physiography.....	79
3.4 Regolith geology.....	82
3.4.1 <i>In situ</i> regolith.....	84
3.4.2 Transported regolith.....	86
3.4.3 Indurated regolith	93
3.4.4 Vegetation.....	94
3.5 Landscape evolution	97
3.5.1 Proterozoic-Paleozoic	97
3.5.2 Mesozoic-Cenozoic	100
3.5.3 Evolution of the modern landscape	102
3.6 Mineral systems	105
3.6.1 Features of sandstone-hosted uranium systems in the Callabonna Sub-basin	108
3.6.2 Geological setting	108
3.6.3 Energy Drivers of the system	110
3.6.4 Source of uranium	112
3.6.5 Fluid pathways.....	114
3.6.6 Chemical and/or physical traps/gradients	115
3.6.7 Age of uranium systems	116
3.6.8 Preservation of uranium systems	116
3.7 References.....	117
4 AEM Geophysics (M. T. Costelloe and I. C. Roach)	125
4.1 Introduction.....	125
4.2 Released data	125
4.3 The TEMPEST™ AEM system.....	126
4.4 Background to the GA layered earth inversion.....	128
4.5 The GA layered earth inversion	129
4.5.1 Algorithm outline	129
4.5.2 Sample-by-sample (SBS) inversion.....	129
4.5.3 Conductivity model parameterization.....	130
4.5.4 Line-by-line (LBL) inversion	131
4.5.5 Reference Model.....	133
4.5.6 Data Misfit.....	133
4.5.7 Depth of Investigation	133
4.6 Geo-electrical models	134
4.7 GA-LEI products.....	135
4.7.1 Sections.....	135
4.7.2 Georeferenced JPEGs	135
4.7.3 GOCAD™ Triangulated Surfaces.....	137
4.7.4 Geoscience Australia layered earth inversion multiplots.....	137
4.7.5 Grids	137
4.7.6 Gridding Parameters	138
4.7.7 AEM Go-Map.....	139
4.7.8 Depth Slices.....	141
4.7.9 Elevation Slices	141
4.8 Discrete Conductors.....	144
4.9 Borehole conductivity validation	145
4.10 Statistical Comparison	147
4.11 Quality assurance and quality control	147
4.12 References.....	152

5 Interpretations of AEM Data	155
5.1 Introduction (I. C. Roach and M. T. Costelloe)	155
5.2 Mapping regional geology (I. C. Roach and M. T. Costelloe).....	157
5.2.1 Introduction	157
5.2.2 Mapping surface conductivity	159
5.2.3 Regional soil mapping with AEM	160
5.2.4 Peeling away cover	162
5.2.5 The DOI – decreasing exploration risk.....	163
5.2.6 PhiD – understanding misfits.....	165
5.2.7 Regional mapping of sedimentary facies.....	167
5.2.8 Mapping regional structure.....	169
5.2.9 Mapping regional geological surfaces	170
5.2.10 References	171
5.3 Mapping palaeovalley systems: Southern Callabonna Sub-basin (A. J. Fabris and I. C. Roach)	173
5.3.1 Introduction	173
5.3.2 Geological history and regional geology.....	173
5.3.3 Local geology: southwestern Callabonna Sub-basin	174
5.3.4 Local geology: southeastern Callabonna Sub-basin	175
5.3.5 Methods	178
5.3.6 Results	178
5.3.7 Discussion.....	189
5.3.8 Conclusion.....	191
5.3.9 References	192
5.4 Mapping palaeovalley systems: MacDonnell Creek and northern Flinders Ranges area (I. C. Roach and S. Jaireth).....	193
5.4.1 Introduction	193
5.4.2 Geology and geomorphology	193
5.4.3 AEM investigations	194
5.4.4 Methods	195
5.4.5 Interpretations from the Frome AEM Survey.....	197
5.4.6 Conclusions	203
5.4.7 References	204
5.5 Mapping basin architecture and salinity: A TEMPEST™ AEM interpretation of the Poontana Trough, northwestern Lake Frome region (B. H. Michaelsen, A. B. Marsland-Smith, P. D. Magarey, A. J. Fabris, I. C. Roach, T. Dhu, L. F. Katona and J. L. Keeling).....	205
5.5.1 Introduction	205
5.5.2 Basin-wide aquifer salinity model	210
5.5.3 Results and discussion	214
5.5.4 Conclusions	228
5.5.5 References	230
5.6 Mapping Structures: Interpretation of the Frome AEM Survey for the Leigh Creek-Marree region, South Australia (T. Wilson and I. C. Roach).....	231
5.6.1 Introduction	231
5.6.2 Outline of regional geology	232
5.6.3 Methods	233
5.6.4 Results	234
5.6.5 Discussion.....	241
5.6.6 Conclusion.....	242
5.6.7 References	242
5.7 Mapping structure-related mineral deposits: Gold deposits in the Nackara Arc and Copper-Molybdenum prospects associated with the Anabama Granite (S. Jaireth)	243

5.7.1 Introduction	243
5.7.2 AEM signatures of orogenic lode gold and porphyry copper-molybdenum deposits...	246
5.7.3. Conclusions	249
5.7.4 References	250
5.8 Mapping geological surfaces: Benagerie Ridge resistive basement and basin stratigraphy (I. C. Roach).....	251
5.8.1 Introduction	251
5.8.2 Creating the model.....	253
5.8.3 Results and discussion	253
5.8.4 Conclusions	258
5.8.5 References	258
6 Summary and conclusions (I. C. Roach and S. Jaireth)	259
6.1 Meeting the aims of the survey	259
6.1.1 Mapping Palaeovalley systems.....	259
6.1.2 Mapping basin architecture.....	259
6.1.3 Mapping sedimentary facies	260
6.1.4 Mapping geological structures.....	260
6.1.5 Mapping geological surfaces	260
6.1.6 Mapping groundwater resources.....	261
6.1.7 Data collection and inversion products.....	261
6.2 Implications for uranium systems	262
6.3 Implications for orogenic lode gold and porphyry copper-gold systems	263
6.4 References.....	264
7 Acknowledgements.....	269
Appendix 1: Additional climate data	271
Appendix 2: Summary of inversion products for the 400 m GA-LEI.....	275
Appendix 3: GA-LEI of TEMPEST Data (R. C. Brodie).....	278
A3.1 Introduction.....	278
A3.2 Formulation.....	278
A3.2.1 Coordinate System.....	278
A3.2.2 System Geometry.....	278
A3.2.3 Layered Earth.....	280
A3.2.4 Data.....	280
A3.2.5 Model Parameterisation	281
A3.2.6 Forward Model Derivatives	281
A3.2.7 Reference Model.....	282
A3.3 Objective Function	282
A3.3.1 Data Misfit.....	283
A3.3.2 Conductivity Reference Model Misfit	284
A3.3.3 System Geometry Reference Model Misfit	284
A3.3.4 Vertical Roughness of Conductivity	285
A3.4 Minimisation Scheme.....	285
A3.4.1 Linearisation	285
A3.4.2 Choice of the value of λ	286
A3.4.3 Convergence Criterion.....	287
A3.5 References	287
Appendix 4: GA-LEI output ASCII header information	288
A4.1 Sample-by-Sample Inversion Conductivity Header.....	288
A4.2 Line-by-Line Inversion Conductivity Header	291
Appendix 5: Technical specifications of map projections	295

Figures

Figure 1.1: Location map of the Frome AEM Survey area.....	4
Figure 1.2: Mineral occurrences in the Frome AEM Survey area.....	6
Figure 1.3: Uranium occurrences in the Lake Frome area.....	7
Figure 1.4: Geo-electrical Model 1.2. Eyre Formation palaeovalleys in Curnamona Province.....	11
Figure 1.5: Drape analysis of the Frome AEM Survey region.....	12
Figure 1.6: Native title determinations and applications in the Frome AEM Survey area.....	14
Figure 1.6: Legend for Figure 1.6.....	15
Figure 1.7: Cartoon of flight line planning including overfly areas.....	19
Figure 1.8: Final flight line spacings and infill areas for the Frome AEM Survey.....	20
Figure 2.1: 1:250 000 and 1:100 000 scale geological maps, Frome AEM Survey area.....	25
Figure 2.2: Solid geology maps of the Frome area.....	26
Figure 2.3: Time slices of geological provinces within the Frome AEM Survey area.....	27
Figure 2.4: Regolith-landform mapping within or intersecting the Frome AEM Survey area.....	30
Figure 2.5: Publicly-available drill hole data within and adjacent to the Frome AEM Survey area.....	35
Figure 2.6: Frequency versus depth histogram of all publicly-available drill holes.....	36
Figure 2.7: Exploration tenement status 2010-2012 over the Frome AEM Survey area.....	37
Figure 2.8: Regional geophysical datasets available for the Frome AEM Survey area.....	39
Figure 2.9: Publicly-available AEM survey boundaries for the Frome AEM Survey area.....	40
Figure 2.10: Location of seismic lines and associated magnetotelluric data.....	42
Figure 3.1: Geological domains of the Curnamona Province.....	54
Figure 3.2: Conceptual model of the Broken Hill rift.....	54
Figure 3.3: Depth to basement image of the Curnamona Province.....	55
Figure 3.4: Subdivisions of the Willyama Supergroup.....	56
Figure 3.5: First vertical derivative magnetic image of the Benagerie Ridge area.....	57
Figure 3.6: Location of the Frome AEM Survey compared to Neoproterozoic rocks.....	59
Figure 3.7: Stratigraphic column of Neoproterozoic rocks.....	60
Figure 3.8: Paleozoic solid geology of the Frome AEM Survey area.....	62
Figure 3.9: Mesozoic solid geology of the Frome AEM Survey area.....	63
Figure 3.10: Geology and stratigraphy of the Leigh Creek coalfield.....	64
Figure 3.11: Generalised stratigraphy of the Cretaceous portion of the Eromanga Basin.....	65
Figure 3.12: Cenozoic stratigraphy of the Lake Frome area and Murray-Darling Basin.....	66
Figure 3.13: Simplified surface geology of the Frome AEM Survey area.....	67
Figure 3.14: Cross-section of the Yarramba Palaeovalley at the Honeymoon uranium mine.....	68
Figure 3.15: Sketch of the Eyre Formation type section near Innamincka.....	69
Figure 3.16: Sketch of the stratigraphy of the Namba Formation outcrop.....	70
Figure 3.17: Stratigraphic logs of the Namba and Eyre formations at Oban.....	71
Figure 3.18: Interpreted palaeovalleys of the southern Callabonna Sub-basin.....	72
Figure 3.19: Distribution of the Ninnerie Supersuite granites.....	74
Figure 3.20: Physiographic regions of the Frome AEM Survey area.....	80
Figure 3.21: MRVBF index image of the Frome AEM Survey area.....	81
Figure 3.22: Regolith materials map of a portion of the Frome AEM Survey area.....	83
Figure 3.23: Examples of <i>in situ</i> regolith in the Frome AEM Survey area.....	84
Figure 3.24: Examples of <i>in situ</i> regolith in the Frome AEM Survey area.....	85
Figure 3.25: Examples of transported regolith in the Frome AEM Survey area.....	86
Figure 3.26: Ternary radiometric image of the Manunda Creek alluvial fan.....	87
Figure 3.27: Large alluvial fans systems of the northern Flinders Ranges.....	88
Figure 3.28: Palaeovalley outlines and modern drainage systems of the northern Olary Spur.....	89
Figure 3.29: Examples of colluvial regolith materials in the Frome AEM Survey area.....	90

Figure 3.30: Contour banded colluvial sheetwash lobes near Mingary, SA.	91
Figure 3.31: Aeolian sediments in or near the Frome AEM Survey area.	92
Figure 3.32: Examples of palaeolacustrine sediments in the Frome AEM Survey area.	92
Figure 3.33: Bioregions of the Frome AEM Survey area.	95
Figure 3.34: Examples of vegetation communities within the Frome AEM Survey area.	96
Figure 3.35: Landscape evolution model for the Mount Painter Inlier.	98
Figure 3.36: Deformation history of the Curnamona Province.	99
Figure 3.37: Drainage rearrangement and fault scarps.	103
Figure 3.38: Regolith-landform and geological components in the northern Flinders Ranges-Mount Painter Inlier-Mount Babbage Inlier area.	103
Figure 3.39: Regolith-landform and geological components in the Olary Spur-Barrier Ranges-southern Frome Embayment region.	104
Figure 3.40: Regolith-landform and geological components in the Nackara Arc- Murray-Darling Basin region.	104
Figure 3.41: Uranium occurrences in the Frome AEM Survey area.	105
Figure 3.42: Faults, basement structures and uranium deposit locations in the Beverley area. ...	111
Figure 3.43: Uranium source rocks and deposits in the northeastern Flinders Ranges- northwestern Lake Frome area.	112
Figure 3.44: Uranium source rocks and deposits in the Curnamona Province-southern Callabonna Sub-basin area.	114
Figure 4.1: Diagram of the 1D vertically smooth layered earth model used in the GA-LEI.	130
Figure 4.2: Spatial extent of the LBL inversion.	132
Figure 4.3: An example of a geo-electrical model (1.2) from the Frome AEM Survey area.	134
Figure 4.4: Georeferenced JPEG for a portion of line 1001002 (SBS GA-LEI).	136
Figure 4.5: Colour conductivity scale bars for georeferenced JPEGs.	136
Figure 4.6: An example of SBS GA-LEI GOCAD™ triangulated surfaces.	137
Figure 4.7: A SBS GA-LEI multiplot for a section of line 1001002.	139
Figure 4.8: The AEM Go-Map (DOI grid)	140
Figure 4.9: Depth slices showing 0-5 m, 30-40 m, 80-100 m and 150-200 m.	142
Figure 4.10: SBS GA-LEI elevation slices.	143
Figure 4.11: FAS multiplot for line 2005301.	144
Figure 4.12: Location of conductivity-logged boreholes and flight lines.	146
Figure 4.13: Scatter plots showing fiducial point comparisons for boreholes within 500 m and 1000 m of flight lines.	148
Figure 5.1.1: Frome AEM Survey case study areas.	155
Figure 5.2.1: 0-200 m conductance image of the Frome AEM Survey.	158
Figure 5.2.2: 0-200 m conductance image and 0-5 m conductivity depth slice image.	159
Figure 5.2.3: Soil Atlas of Australia polygons on the 0-5 m conductivity depth slice.	160
Figure 5.2.4: Sand dunes and playas in the northeast of the Frome AEM Survey area.	161
Figure 5.2.5: 200 m inversion product conductivity depth slices.	162
Figure 5.2.6: The DOI grid for the Frome AEM Survey.	163
Figure 5.2.7: Regional surface geology, 0-100 m conductance and detailed GA-LEI conductivity sections near the MacDonnell Creek uranium prospect.	165
Figure 5.2.8: SBS GA-LEI conductivity section and corresponding PhiD graph.	166
Figure 5.2.9: PhiD grid for the Frome AEM Survey.	167
Figure 5.2.10: Comparison of LBL GA-LEI and SBS GA-LEI with different colour stretches.	168
Figure 5.2.11: Validation of SBS GA-LEI conductivity sections with drill hole stratigraphy. ...	169
Figure 5.2.12: Ternary radiometric and conductance image, Murray-Darling Basin.	170
Figure 5.2.13: Resistive basement GOCAD™ model, northwestern Murray-Darling Basin.	171

Figure 5.2.14: Inversion conductivity profile and corresponding drill hole stratigraphic profile and drill hole stratigraphy, Murray-Darling Basin.	172
Figure 5.3.1: Location of the southern Callabonna Sub-basin and associated uranium deposits and prospects.	174
Figure 5.3.2: Idealised cross-section and AEM response, Billeroo Palaeovalley.	176
Figure 5.3.3: Schematic cross-section and AEM response of the Yarramba Palaeovalley.	177
Figure 5.3.4: Airborne electromagnetic images of the southern Callabonna Sub-basin.	179
Figure 5.3.5: 100-150 m conductivity depth slice, Billeroo and Curnamona palaeovalleys.	180
Figure 5.3.6: New interpretation of palaeovalley margins and thalwegs in the Curnamona-Billeroo-Lake Namba palaeovalley area.	181
Figure 5.3.7: 80-100 m depth slice of the Yarramba Palaeovalley.	182
Figure 5.3.8: LBL GA-LEI conductivity section highlighting the thickening of the Willawortina Formation towards the Flinders Ranges.	184
Figure 5.3.9: 100-150 m conductivity depth slice over the Honeymoon deposit.	185
Figure 5.3.10: GA-LEI conductivity sections and 100-150m conductivity depth slice, Honeymoon deposit.	186
Figure 5.3.11: SBS GA-LEI multiplot for flight line 2003501 illustrating the effects of incorrect AEM system geometry.	187
Figure 5.3.12: 100-150 m conductivity depth slice and linear colour stretched SBS GA-LEI conductivity sections, Goulds Dam deposit.	188
Figure 5.3.13: A drainage feature in the 20-30 m conductivity depth slice, Lake Frome.	189
Figure 5.4.1: Location of Cauldron’s Marree uranium project.	193
Figure 5.4.2: Local geology of the Blanchewater Palaeochannel-MacDonnell Creek area.	194
Figure 5.4.3: Redox conditions of the Eyre Formation in the Blanchewater Palaeochannel.	195
Figure 5.4.4: Location of Cauldron’s RepTEM™ survey.	196
Figure 5.4.5: Location of Frome AEM survey flight lines, Blanchewater Palaeovalley.	197
Figure 5.4.6: SBS GA-LEI conductivity sections, geology and Blanchewater Palaeovalley map.	198
Figure 5.4.7: Drill hole geology overlain on logarithmic (upper) and linear (lower) colour stretched SBS GA-LEI conductivity sections.	199
Figure 5.4.8: GOCAD™ model of the northern Flinders Ranges area with surface geology.	200
Figure 5.4.9: GOCAD™ model of the northern Flinders Ranges area with RepTEM™ data.	201
Figure 5.4.10: GOCAD™ model of the northern Flinders Ranges area with Proterozoic and Mesozoic surfaces.	202
Figure 5.5.1: Map of the Poontana Trough study area.	206
Figure 5.5.2: Landsat MSS mosaic of the Poontana Trough study area.	207
Figure 5.5.3: Surface geology of the Paralana Embayment.	208
Figure 5.5.4: Stratigraphic column of the northern Flinders Ranges and Poontana Trough.	209
Figure 5.5.5: Photographs of outcrop in the Dead Tree Section.	209
Figure 5.5.6: Localities described in the text.	210
Figure 5.5.7: The Paralana Embayment showing localities and uranium deposit outlines.	211
Figure 5.5.8: Regional salinity of bore-hole waters.	212
Figure 5.5.9: Examples of anthropogenic AEM anomalies, Moomba to Adelaide gas pipeline.	214
Figure 5.5.10: 0-200 m conductance image of the Poontana Trough area.	216
Figure 5.5.11: Conductivity depth slices showing selected groundwater salinity features.	217
Figure 5.5.12: LBL GA-LEI conductivity sections, drill holes and unconformity interpretations near the Wooltana 1 stratigraphic drill hole.	219
Figure 5.5.13: Central Poontana Trough in LBL GA-LEI conductivity sections and 60-80 m depth slice.	221

Figure 5.5.14: Heathgate gravity and magnetic images, central Poontana Trough.....	222
Figure 5.5.15: Interpreted structural features in the Beverley area.....	223
Figure 5.5.16: Interpreted unconformities within the greater Paralana-Beverley area.....	224
Figure 5.5.17: Namba Formation unconformity interpretation, Beverley area.....	226
Figure 5.5.18: Salinity (TDS ppm) of compliance water-monitoring bores on the periphery of Beverley uranium deposit.....	228
Figure 5.5.19: Stratigraphic, groundwater and anthropogenic features, northern Poontana Trough.....	229
Figure 5.6.1: Location of the Leigh Creek-Marree case study area.....	231
Figure 5.6.2: 5-10 m conductivity depth slice highlighting basement geology and cover.....	235
Figure 5.6.3: Conductivity anomalies in Neoproterozoic rocks.....	236
Figure 5.6.4: Conductivity structure associated with the Witchelina Diapir.....	238
Figure 5.6.5: Conductivity structures associated with magnesite deposits in the Skillogalee Dolomite.....	239
Figure 5.6.6: Conductivity structures associated with the Tapley Hill Formation and Leigh Creek coal mine.....	240
Figure 5.6.7: Conductivity anomalies associated with the Leigh Creek Coal Measures in the 5-10 m conductivity depth slice.....	241
Figure 5.7.1: Location map of gold and copper-molybdenum deposits associated with the Anabama Granite in the Nackara Arc region.....	244
Figure 5.7.2: 1VD TMI image showing the undercover extension of the Anabama Granite.....	248
Figure 5.7.3: 1VD TMI image and SBS GA-LEI conductivity sections, Anabama Granite.....	249
Figure 5.8.1: Benagerie Ridge depth to basement model.....	251
Figure 5.8.2: Geological domains of the Curnamona Province.....	252
Figure 5.8.3: Surface geology, GOCAD™ model.....	254
Figure 5.8.4: EM Flow™ CDI sections, GOCAD™ model.....	255
Figure 5.8.5: EM Flow™ CDI sections and resistive basement surface, GOCAD™ model.....	255
Figure 5.8.6: Comparison of the resistive basement surface and the Benagerie Ridge surface.....	256
Figure 5.8.7: Close-up view of the resistive basement surface and the Benagerie Ridge surface highlighting basin stratigraphy.....	257
Figure 6.1: Prospectivity analysis of the Frome AEM Survey area.....	265
Figure A1.1: Average number of thunder days for Australia.....	271
Figure A1.2: Average annual total lightning flashes for Australia.....	271
Figure A1.3: Rainfall and temperature averages for settlements within or near the survey area.....	272
Figure A1.4: Wind roses for 9 am wind directions and wind speeds.....	273
Figure A1.5: Wind roses for 3 pm wind directions and wind speeds.....	274
Figure A3.1: Schematic representation of the framework for GA-LEI inversion of TEMPEST™ AEM data.....	279

Tables

Table 1.1: Breccia complex deposit uranium resources in the Frome AEM Survey area.....	5
Table 1.2: Sandstone-hosted uranium resources in the Frome AEM Survey area	8
Table 1.3: Intrusive (magmatic-related) uranium resources in the Frome AEM Survey area.	8
Table 1.4: Metal resources in the Frome AEM Survey area.....	8
Table 2.1: 1:250 000 scale geological mapping available within the Frome AEM Survey area. .	24
Table 2.2: Regolith-landform mapping within or near the Frome AEM Survey area.....	28
Table 2.2 (continued): Regolith-landform mapping within or near the Frome AEM Survey area.	29
Table 2.3: Minerals systems references in and around the Frome AEM Survey area.	34
Table 2.4: Mineral resources references in and around the Frome AEM Survey area.....	34
Table 2.5: Geoscience Australia’s Uranium Systems Project publications.	34
Table 2.6: Impacts of the Frome AEM Survey on mineral exploration.....	36
Table 2.7: A compilation of early groundwater investigations in the Frome AEM Survey area. .	43
Table 3.1: Ages, uranium and thorium content of uranium-bearing granites and felsic rocks within the Curnamona Province, including the Ninnerie Supersuite.	75
Table 3.2: Important mineral systems within the Frome AEM Survey area.....	106
Table 3.3: Sandstone-hosted uranium deposits and prospects (Frome Embayment region).....	108
Table 4.1: Summary of TEMPEST™ AEM system specifications.	127
Table 4.2: The GA-LEI model layer thicknesses and depths from surface.....	131
Table 4.3: Conductivities used in the forward modelling.	134
Table 4.4: JPEG world file contents for line 1001002.....	135
Table 4.5: Panel descriptions for GA-LEI multiplots.	138
Table 4.6: Coordinates and depths of the 5 non-confidential boreholes logged at the Oban uranium deposit for the Frome AEM Survey.....	145
Table 4.7: Quality assurance and quality control steps.....	149
Table 4.8: X-component additive noise (standard deviation of high altitude data) for the Frome AEM Survey.	150
Table 4.9: Z-component additive noise (standard deviation of high altitude data) for the Frome AEM Survey.	151
Table 4.10: Panel descriptions for contractor supplied multiplots.....	151
Table 5.5.1: New terminology used in the Beverley-Poontana Trough area	213
Table 5.7.1: Significant orogenic lode gold and porphyry copper, molybdenum prospects.....	245
Table 6.1: Critical features of sandstone-hosted uranium systems in the Lake Frome region and the mineral potential of selected areas.....	267

The Frome airborne electromagnetic survey, South Australia: implications for energy, minerals and regional geology

Executive summary

The Frome Airborne Electromagnetic (AEM) Survey was designed to deliver reliable pre-competitive AEM data and scientific analysis to aid research into the potential of energy and mineral resources in the Lake Frome region of South Australia. The Survey was the third regional AEM survey conducted within the Onshore Energy Security Program (OESP) at Geoscience Australia (GA), following the Paterson and Pine Creek AEM surveys. The Survey was flown by Fugro Airborne Surveys (FAS) for GA between 22 May and 2 November 2010, using the TEMPEST™ time-domain electromagnetic (TEM) system. Survey lines were flown east-west at a nominal 100 m above ground level, and spaced 2.5 km or 5 km apart. A total of 32 317 line km of new data were collected over an area of 95 450 km², approximately one tenth of the area of South Australia.

The survey area extends from the South Australia-New South Wales border at Cameron Corner across to the Marree and Leigh Creek areas, skirts the highland of the northern Flinders Ranges, and includes the entire Lake Frome area, the Olary Spur between the towns of Yunta and Cockburn and the northwestern Murray-Darling Basin.

The Lake Frome region contains a large number of sandstone-hosted uranium deposits with known resources of ~60,000 tonnes of U₃O₈, constituting ~45% of uranium resources of this type in Australia. The Survey was conducted with the aims of reducing exploration risk, stimulating exploration investment and enhancing prospectivity within the region primarily for uranium, but also for other commodities including copper, gold, silver, lead, zinc, iron ore, coal and groundwater. The Frome AEM Survey was designed to be a regional mapping program for imaging surface and subsurface geological features that may be associated with sandstone-hosted uranium systems.

Interpretations of the Survey data have significant implications for the uranium prospectivity of the Survey area and surrounding region, as well as for the prospectivity of other commodities and knowledge of the geology under cover. The data have been shown to map:

- Basin architecture in the Lake Eyre Basin, Eromanga Basin and Murray-Darling Basin, all important for uranium and groundwater resource exploration;
- Uranium-bearing palaeovalley systems in the southern Lake Eyre Basin, northwestern Murray-Darling Basin and flanking the northern Flinders Ranges, to improve targeting of exploration efforts;
- Sedimentary facies changes in the Namba Formation and Eyre Formation of the Lake Eyre Basin, enhancing uranium systems understanding;
- Basement-cover relationships, for improved depth to target information, including:
 - ‘Basement’ surfaces of the Benagerie Ridge in the Lake Frome area underlying the Lake Eyre and Eromanga basins;
 - ‘Basement’ surfaces of the Flinders Ranges and possible Kanmantoo Group rocks underlying the Murray-Darling Basin;
 - Curnamona Province and Adelaidean rocks underlying the Lake Eyre Basin and Eromanga Basin, flanking the northern Flinders Ranges; and,
 - ‘Cover’ thickness of overlying Mesozoic and Cenozoic sediment of the Eromanga Basin, Lake Eyre Basin and Murray-Darling Basin.
- Faults involved in the preservation of uranium deposits or faults associated with gold-bearing fluids in the Nackara Arc;
- Structures in the Neoproterozoic rocks associated with copper-gold and magnesite deposits in the Leigh Creek area, as well as coal-bearing basins; and,
- Fresh and saline groundwater for exploitation by mineral explorers and graziers.

The Frome AEM Survey has provided new, low noise, repeatable, calibrated AEM data that are suitable for interpretation, enhancement and modelling. The consistent data quality ensures the usefulness and longevity of the data. The geophysical inversion of the Survey data produces subsurface electrical conductivity predictions using a layered earth inversion algorithm developed

The Frome airborne electromagnetic survey, South Australia: implications for energy, minerals and regional geology

by Geoscience Australia (the GA-LEI). The Frome AEM Survey data, inversion data and interpretation products have been released to the public domain to help facilitate further exploration by companies in the area.

Interpretations of the Frome AEM Survey data provide a regional overview of the under-cover geology of the entire survey area, as well as providing detailed along-line information to give users a greater understanding of previous detailed investigations within small areas. The data have mapped features of fertile sandstone-uranium systems and have highlighted many new areas of prospectivity for uranium and other commodities.

1 Introduction

I. C. Roach and M. T. Costelloe

1.1 SURVEY RATIONALE

The Frome Airborne Electromagnetic (AEM) Survey was designed to deliver reliable pre-competitive AEM data and scientific analysis to aid research into the energy resource potential of the Frome region of South Australia (Figure 1.1). The Survey was the third regional survey conducted within the Onshore Energy Security Program (OESP) at Geoscience Australia (GA), following the Paterson (Roach, 2010) and Pine Creek AEM surveys (Craig, 2011). The Survey was flown by Fugro Airborne Surveys (FAS) for GA, as a combined TEMPEST™ time-domain electromagnetic (TEM) and magnetic survey between 22 May and 2 November 2010, on east-west flight lines at ~100 m above ground level, totalling 32 317 line km of data collection over a survey area of 95 450 km².

The Survey was conducted with the aims of reducing exploration risk, stimulating exploration investment and enhancing prospectivity within the region primarily for uranium, but also for other commodities including copper, gold, silver, lead, zinc, iron ore, coal and potable groundwater. The Frome AEM Survey was primarily designed to be a regional mapping program for mapping surface and subsurface geological features that may be associated with sandstone-hosted uranium systems. The data are also capable of being interpreted for landscape evolution studies within the flanks of the tectonically active Curnamona Province and Flinders Ranges of South Australia.

1.2 SURVEY LOCATION

The Frome AEM Survey area lies in the eastern part of South Australia against the South Australia-New South Wales border (Figure 1.1). The Survey stretches in the south from near Redcliff and skirts the Danggali Conservation Park in the Murray-Darling Basin, extends north to cover almost the entire Lake Frome area and halts at Cameron Corner, where the South Australia, New South Wales and Queensland borders meet. The western margin of the Survey area extends nearly to Lake Eyre South, includes Marree and Leigh Creek and skirts the northern Flinders Ranges, but does not extend over the Flinders Ranges because of the risks the rugged terrain poses to low-flying fixed-wing aircraft.

The Survey area excludes the Vulkathunha-Gammon Ranges National Park and the Danggali Conservation Park, but includes portions of the Strzelecki Regional Reserve.

The Survey area covers much of the CALLABONNA, CHOWILLA, COPLEY, CURNAMONA, FROME, MARREE, OLARY and PARACHILNA 1:250 000 map sheets (Figure 1.1). The Survey area includes settlements at Marree, Lyndhurst, Leigh Creek, Copley, Yunta, Olary, Manna Hill and Cockburn, as well as numerous pastoral and mining settlements.

The Survey area is traversed in the south by the Barrier Highway, the major all-weather road between Broken Hill and Gawler, and the trans-Australian railway, linking Sydney to Perth. All-weather access is also afforded to the northwest by the road linking Hawker to Lyndhurst, however the road is unsealed north of Lyndhurst. The remainder of the Survey area may be accessed by dry weather-only major gravel roads including the Oodnadatta, Birdsville and Strzelecki tracks, the Yunta to Balcanoona road and numerous graded roads or tracks linking pastoral stations and other small settlements.

The Frome airborne electromagnetic survey, South Australia: implications for energy, minerals and regional geology

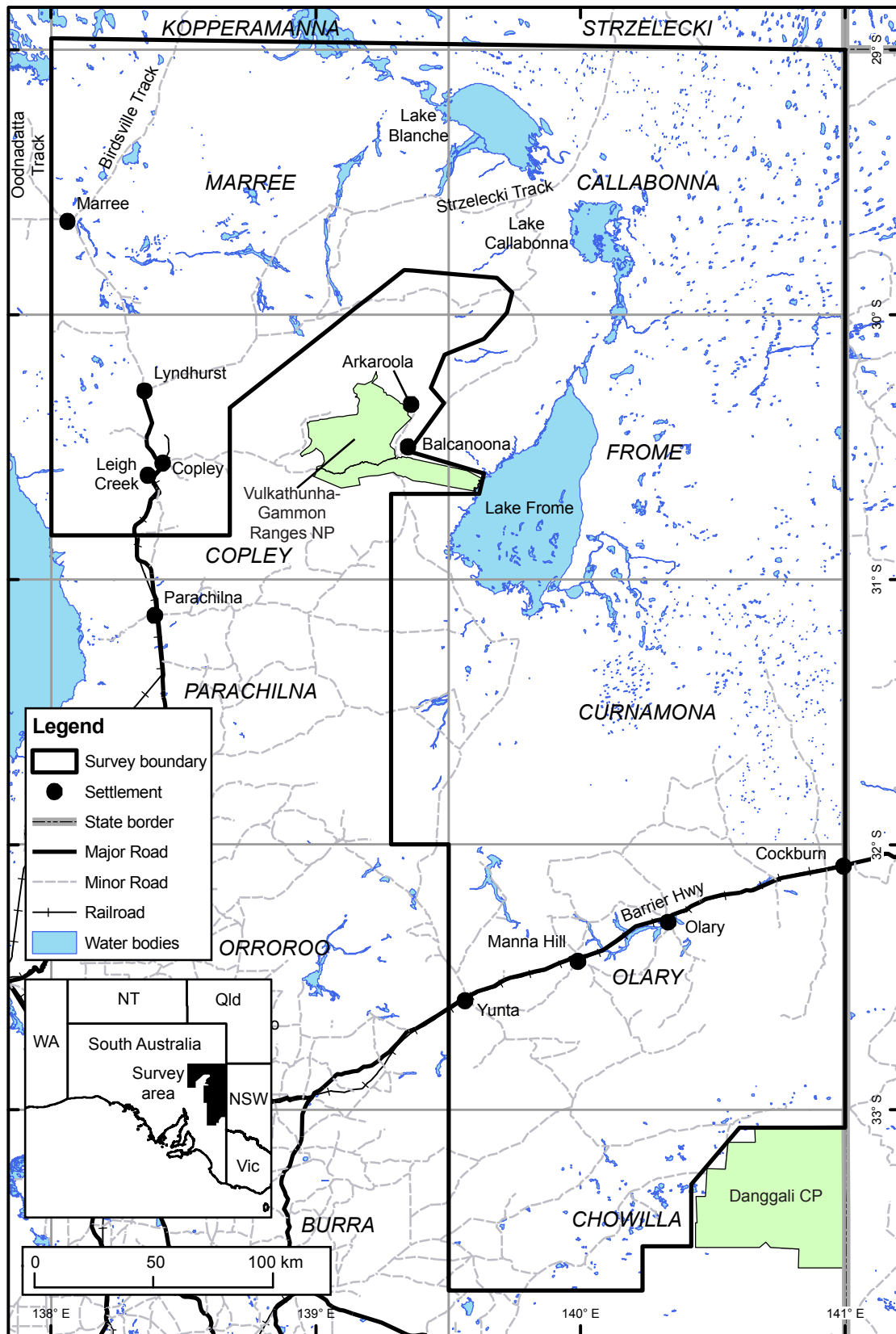


Figure 1.1: Location map of the Frome AEM Survey area.

1.3 SURVEY GEO-ECONOMIC FRAMEWORK

The Survey area is richly endowed with minerals, industrial minerals and energy commodities (Figure 1.2). There are a number of working mines including Beverley (uranium), Honeymoon (uranium), White Dam (gold), Mt Fitton (talc) and Leigh Creek (coal). There are also numerous deposits, prospects and historical workings within the Survey area, including Goulds Dam (uranium), Oban (uranium), East Kalkaroo (uranium), Mount Victoria (uranium), Crocker Well (uranium), MacDonnell Creek (uranium), Junction Dam (uranium), Radium Hill (uranium), Beltana (zinc), North Moolooloo (zinc), North Portia (copper-gold-molybdenum), Kalkaroo (copper-gold), Mountain of Light (copper), Anabama (copper), Yunta (iron), Mutooroo (copper, iron), Razorback (iron), Lake Frome (lithium), Myrtle Springs (magnesite), Paralana (geothermal), Goulds Dam (geothermal) and numerous industrial mineral deposits.

1.3.1 Uranium mineral deposits

There are a number of well-known uranium mineral systems in the Frome region (Figure 1.3) and the entire area is highly prospective for individual deposit styles, or a range of deposit styles, as listed below. This précis is condensed from descriptions of uranium resources in South Australia by McKay and Miezitis (2001), Skirrow (2009) and Wilson and Fairclough (2009). Deposit styles are arranged in order of their approximate Australian economic significance after McKay and Miezitis (2001).

1.3.1.1 Breccia complex deposits

Numerous small uranium deposits occur in the Mount Painter field in the northern Flinders Ranges. While this field does not lie within the Frome AEM Survey area, the type is important for its association with the Paleoproterozoic-Mesoproterozoic Curnamona Province, which underlies much of the Lake Frome area, and most particularly with the Mount Painter Inlier in the northern Flinders Ranges. The Mount Painter Group includes deposits at Mount Painter, Mount Gee, Radium Ridge, Armchair-Streitberg, Hodgkinson, Gunsight, Paralana Hot Springs, Valley and Shaft Prospects, Mount Shanahan, Monazite Hill, the British Empire mine and the Shamrock copper mine. Joint Ore Reserves Committee (JORC) reported amounts of contained uranium are listed in Table 1.1, for a potential total of > 35 558 t U₃O₈. These deposits may have acted as sources for other styles of deposits within the Frome region.

Table 1.1: Breccia complex deposit uranium resources in the Frome AEM Survey area.

NAME	APPROXIMATE JORC-REPORTED RESOURCE (t U ₃ O ₈)
Mt Gee	2722 (McKay and Miezitis, 2001) to 31 300 (Marathon, 2010)
Radium Ridge	2177 (McKay and Miezitis, 2001)
Armchair-Streitberg	1814 (McKay and Miezitis, 2001)
Hodgkinson	567 (McKay and Miezitis, 2001)

1.3.1.2 Sandstone-hosted deposits

Sandstone-hosted uranium deposits are a common feature within the Frome AEM Survey area, with a number of well-known deposits occurring in Callabonna Sub-basin sediments of the Lake Eyre Basin around the margins of the Lake Frome area in tabular and roll-front styles associated with palaeochannels and palaeovalleys. Perhaps the best known are the Beverley uranium deposit, in the northwest of the Lake Frome area, and the Honeymoon deposit, in the south of the Lake Frome area. Similar deposits may occur within the western Murray-Darling Basin and within the Lake Eyre Basin and Eromanga Basin east of Lake Frome and Lake Callabonna; there is much exploration activity in these areas. New discoveries are also being made to the north of the Flinders Ranges, including at MacDonnell Creek (Cauldron Energy Ltd, 2011).

The Frome airborne electromagnetic survey, South Australia: implications for energy, minerals and regional geology

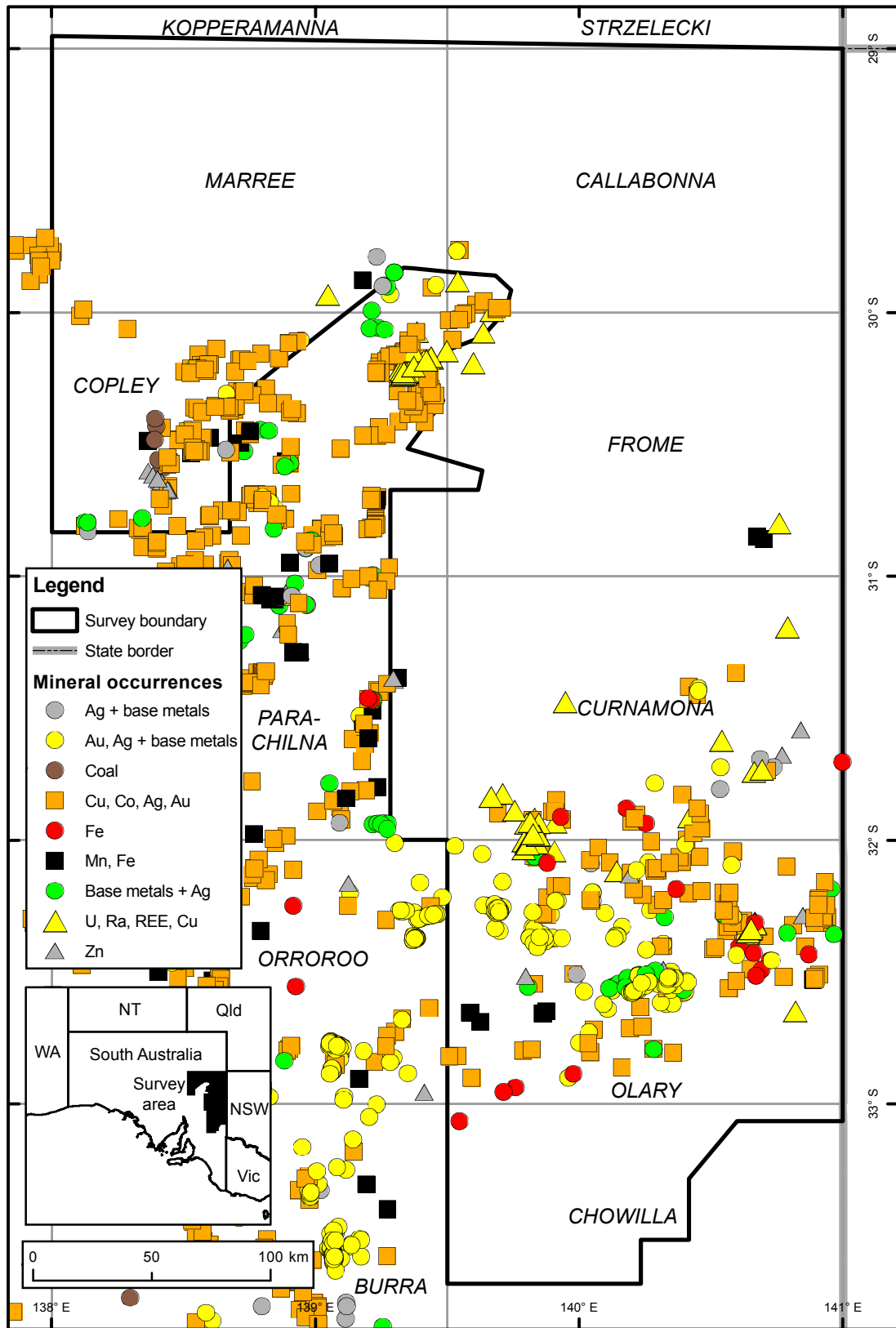


Figure 1.2: Mineral occurrences in the Frome AEM Survey area. Data from SARIG, downloaded February 2010.

The Frome airborne electromagnetic survey, South Australia: implications for energy, minerals and regional geology

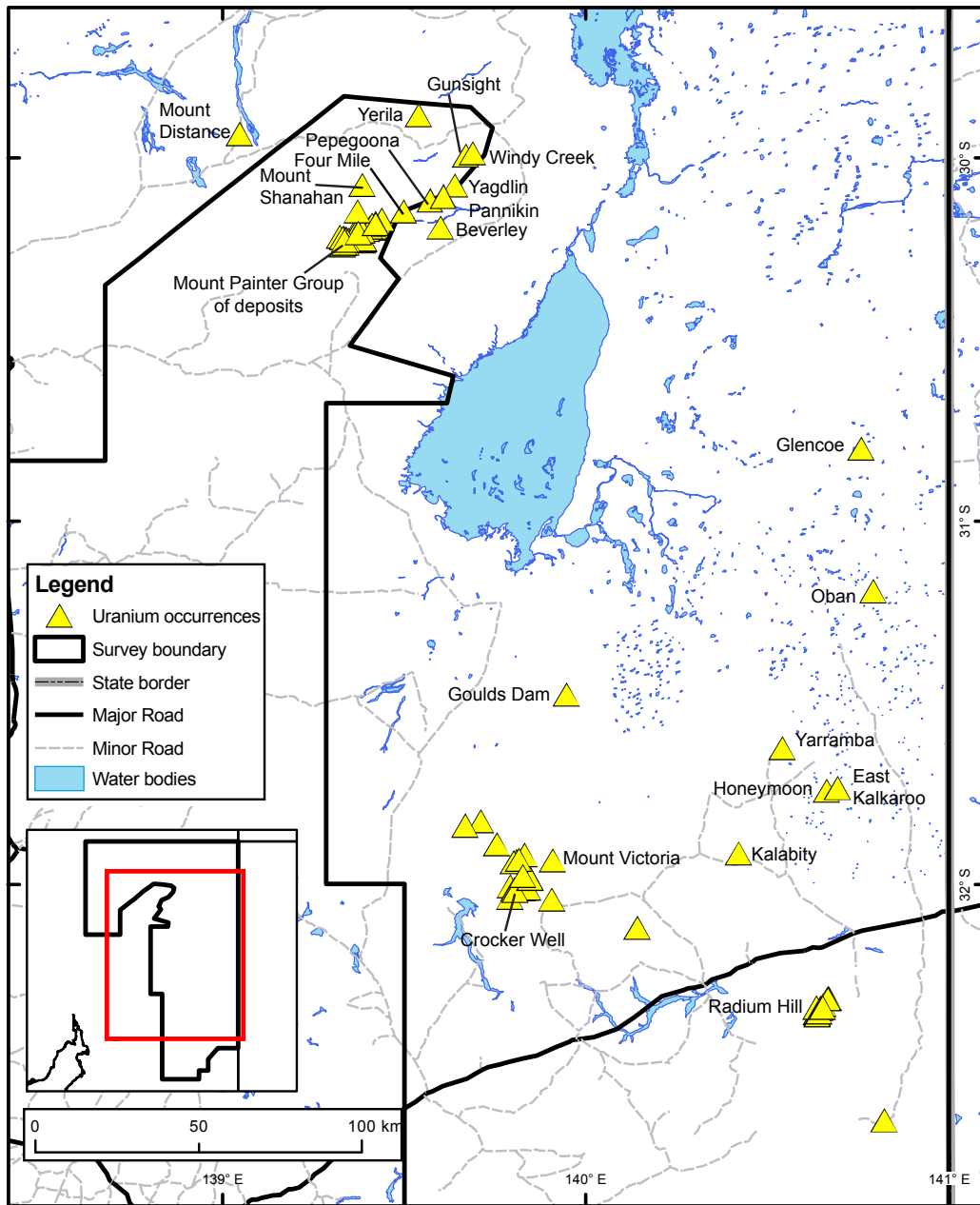


Figure 1.3: Uranium occurrences in the Lake Frome area. Data from SARIG, downloaded February 2010.

The Beverley area contains the greatest known resource of the Callabonna Sub-basin, with JORC-reported resources shown in [Table 1.2](#). The total potential sandstone uranium endowment within the Callabonna Sub-basin is > 60 310 t U₃O₈. Exploration for sandstone-hosted uranium deposits in the Murray-Darling Basin continues, with efforts focussed around Olary Creek, which drains Radium Hill, and Cronje Dam.

Table 1.2: Sandstone-hosted uranium resources in the Frome AEM Survey area.

NAME	APPROXIMATE JORC-REPORTED RESOURCE (t U ₃ O ₈)
Beverley	16 300 (OZMIN, 2009)
Four Mile West	19 000 (Alliance Resources Ltd, 2010)
Four Mile East	13 000 (Alliance Resources Ltd, 2010)
Billeroo	3600 (Southern Cross Resources, 2004)
Honeymoon	2900 (Wilson and Fairclough, 2009)
Goulds Dam	2500 (Southern Cross Resources, 2004)
Oban	2100 (Curnamona Energy Ltd, 2010)
East Kalkaroo	910 (Wilson and Fairclough, 2009)

1.3.1.3 Intrusive (magmatic-related) deposits

In the Frome area intrusive uranium deposits are associated with the Paleoproterozoic-Mesoproterozoic Curnamona Province, which hosts the Olary uranium field (McKay and Mieztis, 2001) in Mesoproterozoic granitoids of the Willyama Inlier. Known deposits are listed in Table 1.3. Radium Hill was mined between 1954 and 1961 and 852 t of U₃O₈ was sold (Parkin, 1965). A number of other, smaller, deposits and prospects are also known in around the three sites for a total of > 6552 t U₃O₈.

Table 1.3: Intrusive (magmatic-related) uranium resources in the Frome AEM Survey area.

NAME	APPROXIMATE JORC-REPORTED RESOURCE (t U ₃ O ₈)
Crocker Well	5290 (PepinNini Minerals Ltd, 2010)
Radium Hill	852* (Parkin, 1965)
Mount Victoria	410 (PepinNini Minerals Ltd, 2010)

* Amount sold during mine life, present resource unknown.

1.3.2 Metal deposits

The Proterozoic and Paleozoic rocks forming the basement of the Frome AEM Survey area are extensively mineralised and host numerous metal deposits and prospects including copper, gold, copper-gold, lead-zinc-silver, iron, magnesium, manganese, nickel, cobalt and molybdenum, some of which are listed in Table 1.4. The largest mineral deposit within the Curnamona Province is the world class Broken Hill lead-zinc-silver deposit in New South Wales.

Table 1.4: Metal resources in the Frome AEM Survey area.

NAME	APPROXIMATE JORC-REPORTED RESOURCE
White Dam	325 000 oz gold (Exco Resources Ltd, 2010)
Kalkaroo	320 000 t copper, < 1 000 000 oz gold (Havilah Resources NL, 2010)
Portia	67 000 oz gold (Havilah Resources NL, 2010)
North Portia	101 000 t copper, 234 000 oz gold, 5.680 Mkg molybdenum (Havilah Resources NL, 2010)
Mutooroo	6000 t copper (mined historically), 191 707 t copper, 17 542 t cobalt, 92 665 oz gold, 2.5 Mt sulfur (Havilah Resources NL, 2010)
Razorback Ridge	437 Mt @ 26% iron (Royal Resources Ltd, 2011)
Maldorky	147 Gt @ 30.1% iron (Havilah Resources NL, 2011)
Beltana	101 385 t zinc (Perilya Limited, 2011a)
North Moolooloo	73 530 t zinc (Perilya Limited, 2011b)
Leigh Creek area magnesite	Copley - 6000 t extracted; Myrtle Springs - 30 000 t extracted, 18.3 Mt resource; Termination Hill - 4 Mt resource; Witchelina - 23.7 Mt resource

There are also numerous small historical gold and copper workings within the Neoproterozoic sediments from which thousands of ounces of gold and tonnes of copper have been won historically. In the northern Flinders Ranges there are numerous copper, zinc, gold and silver prospects including the Flinders Zinc project, near Beltana.

There are numerous prospects around Cambrian granites related to the Kanmantoo Group, flanking and overlain by the Murray-Darling Basin in the southern Frome AEM Survey area, which are highly prospective for gold and copper. Prospects on the flanks of the Olary Range and further southeast in the overlying Murray-Darling Basin, including Anabama, are seeking to locate gold and copper mineralisation around historic workings in Neoproterozoic rocks and Delamerian intrusives within and under cover.

Finally, the Murray-Darling Basin and portions of the Callabonna Sub-basin of the Lake Eyre Basin are highly prospective for heavy mineral sand (HMS) deposits. Exploration for HMS deposits is presently occurring within the Murray-Darling Basin.

1.3.3 Non-metal, industrial mineral and energy commodity deposits

The Frome AEM Survey area includes Triassic coal measures at Leigh Creek as well as numerous sites where industrial minerals (barite, clay, aggregate, sand, gravel) have been or are being extracted. The Leigh Creek Coalfield sits within a series of Triassic-Early Jurassic intramontane basins, principally the Telford Basin, and is estimated to contain > 530 Mt (Springbett *et al.*, 1995) of low quality lignite and sub-bituminous coal (Kwitko, 1995) that is railed to Port Augusta to power the Playford and Northern power stations.

1.3.4 Groundwater systems

The Frome AEM Survey area contains three important groundwater basins including the Murray-Darling Basin, the Great Australian Basin (including numerous sub-basins) and the overlying Lake Eyre Basin. Bedrocks of the Flinders Ranges, the Olary Spur and the Barrier Ranges also contain fractured rock aquifers established in the Paleo-Mesoproterozoic rocks of the Curnamona Province, the Neoproterozoic Adelaidean succession and the overlying Cambrian succession of the Arrowie Basin.

Potable water is available in artesian and sub-artesian bores on the flanks of the Flinders Ranges and Olary Range, with salinity increasing towards Lake Frome and Lake Callabonna (Ker, 1965). Aquifers within the Lake Frome area occur within the Cenozoic and Mesozoic succession of the Lake Eyre Basin and the Eromanga Basin respectively. In the Murray-Darling Basin, a number of good aquifers are recognised within the Cenozoic succession, however, overall salinities appear to be higher than within the Lake Frome area (Ker, 1965; Shepherd, 1978).

Groundwater resources are essential for the exploitation of mineral resources and for agricultural purposes within the Frome AEM Survey area. Potable surface water is rare or non-existent and mining and pastoral communities rely almost entirely on bore water for their requirements.

1.3.5 Geothermal energy

The Lake Frome area-Murray-Darling Basin-Eromanga Basin region has potential for geothermal energy stored within hot dry rock (HDR) or heat producing granite (HPG) sources buried beneath Proterozoic, Paleozoic, Mesozoic and Cenozoic cover. Two active geothermal exploration fields currently exist within the Survey area and there are many more exploration tenements. The Petrathem Ltd Paralana field lies about 25 km east of the Beverley uranium mine and is targeting HPG of the Curnamona Province buried beneath up to 5 km of Neoproterozoic, Paleozoic (Cambrian), Mesozoic and Cenozoic sediments. Temperatures of up to 200°C occur “at drillable depths” and the site contain an estimated 230 000 ± 40 000 petajoules (PJ) of heat energy, which is expected to deliver 260 megawatts (MW) of base load electricity into the national grid in the long term (Petrathem Ltd, 2011).

Geothermal Resources Ltd identified an HPG source beneath Arrowie Basin (Paleozoic) and Callabonna Sub-basin (Cenozoic) sediments about 100 km northwest of Olary. The source is estimated to contain 84 000 PJ (Geothermal Resources Ltd, 2010).

These systems are too deeply buried to be imaged using AEM methods, however, are included for completeness.

1.4 AREA ASSESSMENT

The following section describes the assessments included in the survey planning in addition to the economic considerations detailed in the previous section ([Section 1.3](#)). Geological details of the Survey area are considered in [Chapter 3](#) of this Record.

1.4.1 Targets: geo-electrical forward modelling for system selection

Geoscience Australia's intention to conduct the Frome AEM Survey was advertised to airborne geophysical contractors registered on the GA Deed of Standing Offer on 24 March 2010. Three contractors offered expressions of interest using 4 AEM systems. Before the Survey could proceed, the different AEM systems needed to be assessed by forward modelling to test each system's theoretical expected performance in the Frome area. This was achieved by creating a series of synthetic geo-electrical models which approximated known target conditions in the Frome region. These models were transferred to GA-proprietary software to test for the probability of detection with a false alarm rate of 1%. When all scenarios were deemed of equal relevance, and when other survey factors were taken into account (such as survey logistics, availability, safety and cost), the TEMPEST™ system was assessed as most likely to be effective in the Frome AEM Survey area.

Geo-electrical models were developed using prior knowledge of the conductivity ranges of materials in the targeted geological units within the Survey area, gleaned from a literature review.

An example geo-electrical model (Model 1.2) is depicted in [Figure 1.4](#). Model 1.2 is based on conditions around the Honeymoon uranium deposit, which is hosted in Paleogene Eyre Formation sediments in the Yarramba Palaeovalley below the Neogene Namba Formation. A simplified geological cross-section is given in Model 1.2. The target palaeovalleys are incised directly into the Curnamona Province basement and the palaeovalleys are thought to be between 100 and 3000 m wide, extending laterally for tens of kilometres.

The Paleogene Eyre Formation consists of pyritic, carbonaceous sand with beds of lignite and clay (montmorillonite, kaolinite and illite). The Curnamona Craton basement is composed of Paleo-Mesoproterozoic metasedimentary and metavolcanic rocks and intrusives of the Willyama Supergroup.

More information on the use of forward modelling, a description of the FAS TEMPEST™ TEM system, the GA layered earth inversion (GA-LEI) method and GA-LEI data products is given in Roach (2010), Craig (2011) and Hutchinson *et al.* (2011).

Model 1.2: Tertiary Eyre Formation palaeovalleys in Paleo-Mesoproterozoic Curnamona Craton

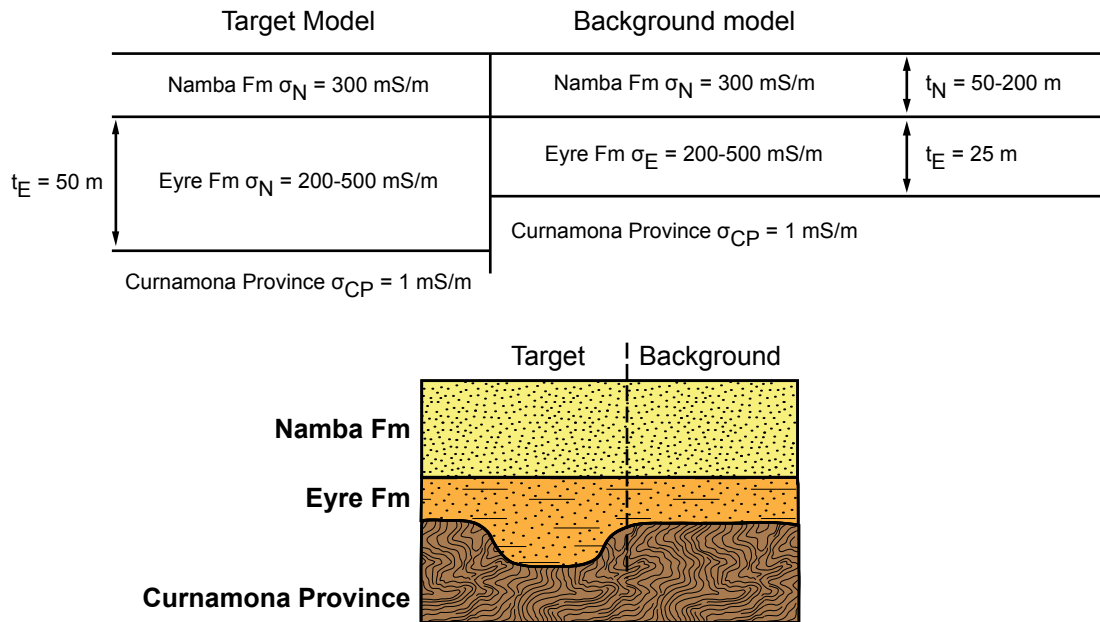


Figure 1.4: Geo-electrical Model 1.2. Eyre Formation palaeovalleys in Curnamona Province.

1.4.2 Terrain affecting aircraft operations (drape)

A ‘drape’ analysis is performed over a proposed survey area prior to a call for tenders. The analysis is necessary to ensure that the proposed survey can be performed by a nominated aircraft type within its own operating safety specifications, or whether the proposed flight plan or aircraft type needs to be altered. The aircraft type and operating specifications are set out in a Deed of Standing Offer between GA and survey contracting companies. The drape analysis is a necessary part of flight planning that ensures that it is legally possible to fly a survey with a nominated aircraft type within the federal government legislation governing aircraft operations.

The drape analysis is performed by entering a digital elevation model, in this case the Shuttle Radar Topographic Mission (SRTM) 90 m ground pixel resolution digital elevation model (DEM), into GA-proprietary software. The DEM is analysed, together with the specified aircraft average rate of climb, to highlight areas where the flight lines would cross terrain that would cause the aircraft to exceed its safe operating specifications. For instance, the FAS CASA 212-200 aircraft VH-TEM has an average rate of climb of only 100 m/km, whereas the FAS Short Skyvan VH-WGT has slightly better climb performance, when both are fitted with the TEMPEST™ TEM system. Figure 1.5 illustrates the results of the drape analysis for the FAS CASA aircraft, indicating that the bulk of the Survey area could be flown safely at the contracted nominal flying height of 100 m above ground. The Survey was, however, flown using the FAS Short Skyvan, therefore the drape analysis is seen as being conservative because of the aircraft’s better climb performance. In areas where the drape analysis indicated that the aircraft would exceed its average rate of climb specifications, permission was given to allow the aircraft to fly at slightly higher nominal altitude to provide adequate ground clearance.

The Frome airborne electromagnetic survey, South Australia: implications for energy, minerals and regional geology

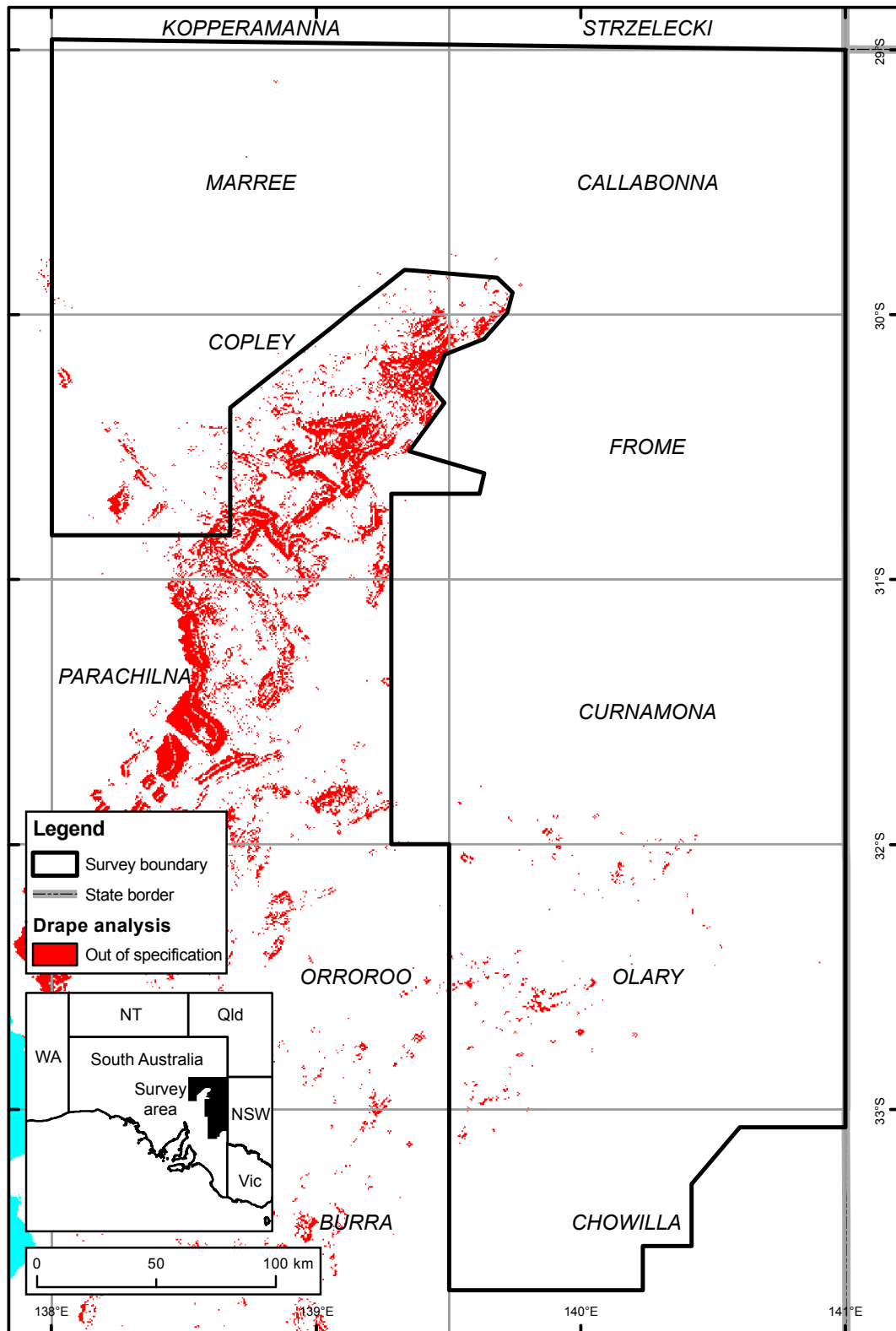


Figure 1.5: Drape analysis of the Frome AEM Survey region using the SRTM 90 m DEM, 100 m flying height and 100 m/km average climb rate. Figure shows areas where contract specifications were altered to allow safe ground clearance (red) and 1:250 000 map sheet names.

1.4.3 Aircraft access

The Frome AEM Survey area has reasonable aircraft access, particularly in the southern part. The survey aircraft flew out of Broken Hill, Jamestown, Leigh Creek and Marree, all of which offer all-weather access, refuelling and limited engineering facilities. Major aircraft maintenance was conducted at Parafield Airport in Adelaide.

Airstrips in case of emergency are also located at Arkaroola, Balcanoona (all-weather), Beverley uranium mine, Cockburn, Honeymoon uranium mine, Lyndhurst, Manna Hill, Olary, Parachilna, Smithville, Tibooburra, Yunta and most cattle stations.

1.4.4 Native title, no-fly zones and state government land access issues

A large proportion of the Frome AEM Survey area is under either a Native Title Determination or a Native Title Application (Figure 1.6). Advice from the Department of Manufacturing, Innovation, Trade, Resources and Energy South Australia (DMITRE) in the survey planning stage indicated that native title holders within the Survey area allowed aerial survey operations over their holdings or applications without the need for special consultation. Additionally, the survey aircraft was to be operated from registered public airfields in and around the Survey area. Therefore the Survey proceeded without further special consultation with native title holders or applicants.

A self-imposed no-fly zone was established within the confines of gazetted national parks, because of environmental and cultural sensitivities. In the Frome area this included only the Vulkathunha – Gammon Ranges National Park. The contractor avoided flying over the Park where practical, and data collected within the Park boundaries at the start or end of flight lines were cropped and deleted (see Section 1.6). Conservation Parks and Regional Reserves were included in the Survey, however the Dangdali Conservation Park in the Murray-Darling Basin was excluded for reasons of economy; the exclusion was due to the educated opinion that conductivity conditions within the Park would not allow reasonable signal penetration and therefore would not be good value for money. Flight line kilometres saved by this exclusion were programmed in other parts of the Survey area.

Self-imposed no-fly zones were also established around a number of pastoral settlements and mine sites. Pastoralists within the Survey area were contacted in the planning stage (see Section 1.4.6) and several asked that the aircraft not overfly their buildings. These requests were passed to FAS and were programmed into the flight plan. Mine sites were also avoided where practical, especially at the Honeymoon and Beverley uranium mines, where tall constructions could have possibly snagged the towed receiver bird and alternating current electricity supplies could affect the data quality.

On 28 March 2012 the NSW state government repealed the ban on uranium exploration in that state, however, the Frome AEM Survey was planned and flown while the ban was in place. A small amount of overfly into New South Wales was necessary as flight lines started or ended at the South Australia-New South Wales state border (see Section 1.6), and the aircraft was based in Broken Hill for a period. Any data collected within New South Wales at the start or end of a line was cropped to the state border and deleted by FAS before it was passed to GA to satisfy the New South Wales government's ban on uranium exploration and mining within that state at that time.

The survey aircraft was operated from commercial public airfields at all times; no other land access issues were reported.

The Frome airborne electromagnetic survey, South Australia: implications for energy, minerals and regional geology

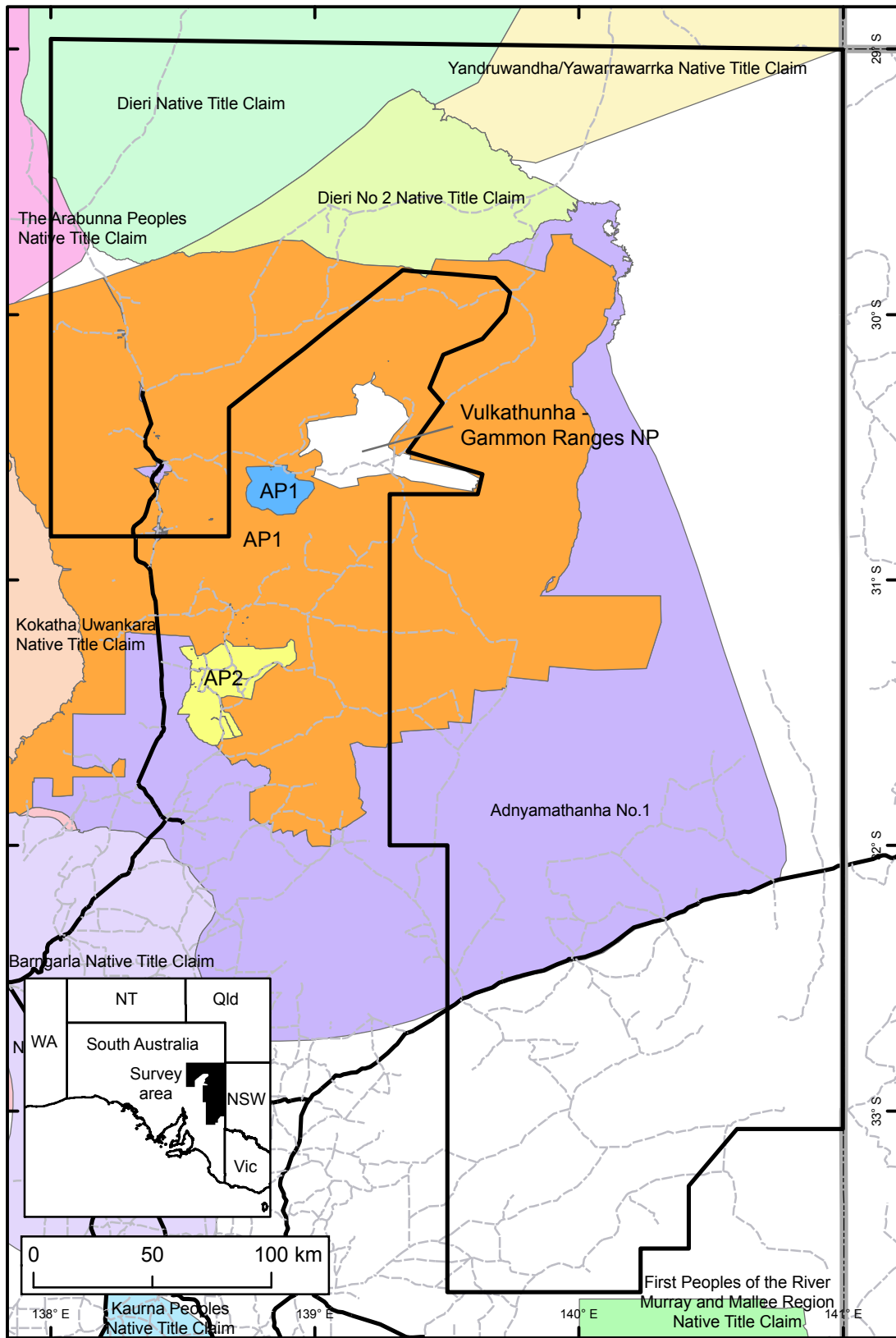


Figure 1.6: Native title determinations and applications in the Frome AEM Survey area, March 2011. See legend on next page.

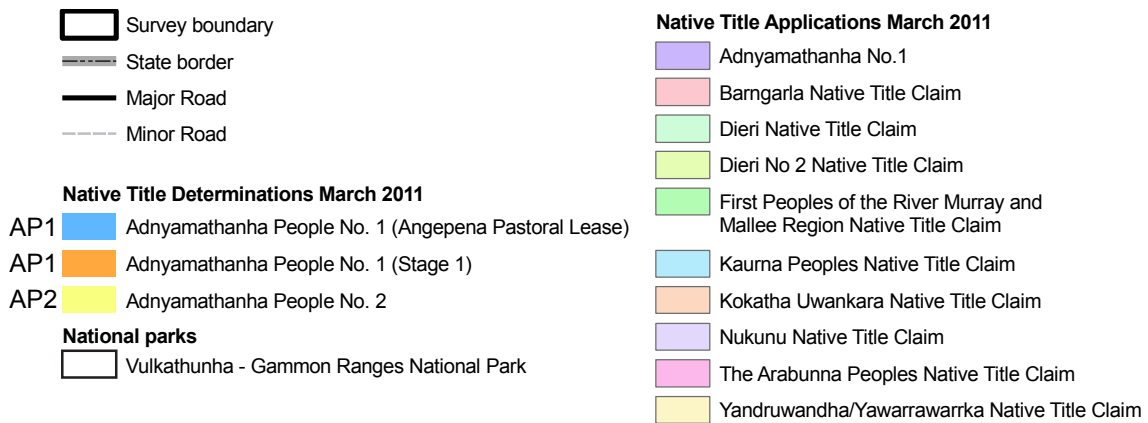


Figure 1.6 continued: Legend for Figure 1.6.

1.4.5 Climate

The Frome AEM Survey area sits largely within the Desert climate classification, but extends into the Grassland classification, of the modified Koeppen climate classification used by the Australian Bureau of Meteorology. The area is regarded as having low overall rainfall, but what rain the area receives is normally winter-dominated.

Knowledge of climatic conditions is important when planning any flight operations, but particularly so when planning for airborne geophysical operations because the aircraft fly much closer to the ground than during normal flight operations. For the Frome AEM Survey, the aircraft was contracted to fly at 100 m above ground, and the towed bird to fly at 60 m above ground, except in those areas where the drupe analysis (see Section 1.4.2) showed that this exceeded the safe climb performance characteristics of the aircraft and the aircraft was flown at slightly higher altitude.

A number of climate factors affect aircraft operations and the quality of recorded AEM data:

- Air temperature affects the maximum takeoff weight (MTOW) and aircraft flight endurance. See Appendix 1 of Roach (2010) for further information;
- High wind speed and air turbulence affect aircraft operations by lifting dust into the atmosphere causing reduced visibility and increased turbine and propeller wear. High winds affect low-altitude aircraft operations because of severe turbulence, up-drafts on the windward side and down-drafts on the leeward side of high-relief terrain. Severe air turbulence also affects the quality of recorded data by causing ‘coil knocks’, where the AEM receiver coils knock into the inside of the towed bird, adding noise to the data (Lawrence and Stenning, 2008). See Appendix 1 of Roach (2010) for more detail.
- The location and frequency of thunderstorms and lightning flashes affect AEM data. Lightning flashes cause noise ‘sferics’ in AEM data and can affect data collection from up to 1000 km away. The Frome AEM Survey area experiences one of the lowest lightning flash densities in Australia, with less than 5 flashes measured per square kilometre (< 5/km²) (BOM, 2011). See Figures A1.1 and A1.2 in Appendix 1 of this record for more detail.

In mid-2010 a major La Niña weather pattern was established in eastern Australia and the Survey area received above-average rainfall, commencing during the aerial survey, resulting in many lost flying days due to high wind, low cloud and widespread rain. Prevailing winds in the region are largely northerly to westerly but ‘southerly busters’ ahead of cold fronts are not uncommon. More information on local climate is included in Appendix 1 of this record.

1.4.6 Communication strategy

Geoscience Australia was aware of the potential impacts of aerial operations over pastoral land and built-up areas in the Frome region and the amount of interest that operations might generate with stakeholders within local, state and federal government agencies, exploration companies, title holders and the public. Working with FAS and the infill partners, GA developed a communication strategy to inform stakeholders of the survey activities within or near the Survey area, including:

- Letters and flyers to the relevant national park administrators;
- Letters and flyers to relevant indigenous communities;
- Letters and flyers to all landholders in the area;
- Letters, flyers and emails to all tenement holders in the area;
- Letters, posters and/or personal visits to as many local police stations, truck stops, public houses, hotels, motels and caravan parks as possible, within and outside the Survey area; and,
- Public notices in local newspapers.

Communication also included presentations to the academic community, state and federal government agencies and the minerals industry, including:

- Oral presentation at Australian Society of Exploration Geophysicists conference, Adelaide, February 2009;
- Shortcourse on uranium deposits, UWA Centre for Exploration Targeting, Perth, November 2009;
- Oral presentation at Australian Society of Exploration Geophysicists conference, Sydney, August 2010;
- Poster presentation at the Australian Regolith Geoscientist's Association conference at Arkaroola, SA, February 2010;
- Oral presentation at the Geological Survey of Western Australia in 2010;
- Oral presentation at the Australasian Institute of Mining and Metallurgy International Uranium Conference, Adelaide, June 2010;
- Oral presentations at Association of Mining and Exploration Companies congress, Perth, June 2010;
- Oral presentation at the Australian Earth Sciences Convention, Canberra, July 2010;
- Oral presentation at the Australian Uranium Conference, Fremantle July 2010;
- Oral presentation at the South Australian Resource and Energy Investment Conference, Adelaide, August 2010;
- Oral Presentation at the Society of Exploration Geophysicists conference, Denver USA, September 2010;
- Oral presentation at the Mining 2010 conference, Brisbane, October 2010;
- Oral presentation at the South Australian Explorer's Conference, November 2010;
- Oral presentation at the Centre of Excellence in Ore Deposits Shortcourse on Uranium Deposits, University of Tasmania, Hobart, November 2010;
- Oral presentation at GA in November 2010;
- Oral presentation at PIRSA in November 2010;
- Data workshop to stakeholders at Geoscience Australia, February 2011;
- Oral and poster presentation at the Prospectors and Developers Association of Canada (PDAC) convention, Toronto, Canada, March 2011;
- Oral presentation at the Annual Geoscience Exploration Seminar (AGES), Alice Springs, March 2011;
- Oral presentation at the South Australian Resource and Energy Investment Conference (SAREIC), Adelaide, May 2011;
- Oral presentation at the Association of Mining and Exploration Companies (AMEC) conference, Perth, June 2011;
- Oral presentation at GA, November 2011;

The Frome airborne electromagnetic survey, South Australia: implications for energy, minerals and regional geology

- 1-day data interpretation workshop at the University of Adelaide, November 2011;
- Oral presentation at South Australian Mineral Exploration Conference, December 2011;
- Poster presentation at the Australian Society of Exploration Geophysicists Conference, Brisbane, February 2012;
- Extended abstract at the Australian Regolith Geoscientists Association conference, Mildura, February 2012;
- Oral presentation at SAREIC 2012, 2 May 2012;
- Oral presentations at the AusIMM International Uranium Conference, Adelaide, June 2012; and,
- Oral presentation at the International Geological Congress, Brisbane, 2012.

1.5 SURVEY INFILL PARTNERS AND COST

Geoscience Australia invited state government agencies and mineral exploration companies to participate in the Frome AEM Survey in the interests of stimulating further exploration in the region. The intention to fly the Survey was advertised in GA's Minerals Alert and by email to individual agencies and companies. The invitation asked for feedback on the geographical extent and line spacing of the proposed Survey and invited agencies or companies to become survey partners by purchasing infill within the targeted area.

A number of companies responded to the offer and asked for further details or modifications to the flight plan, including:

- Callabonna Uranium Ltd;
- Cameco Australia Pty Ltd;
- Curnamona Energy Ltd;
- ERO Mining Ltd (formerly Eromanga Uranium Ltd);
- EURO Exploration Services Pty Ltd;
- Gold Fields Australasia;
- Marathon Resources Ltd;
- Mega Hindmarsh Pty Ltd;
- Government of South Australia Department for Manufacturing, Innovation, Trade, Resources and Energy (DMITRE), formerly the Department of Primary Industries and Resources South Australia (PIRSA), which changed name in October 2011;
- Sinosteel-PepinNini Pty Ltd; and,
- Toro Energy Ltd.

A number of agencies or companies responded by offering in-kind support to the Survey, including:

- Adelaide Resources Ltd provided access to drill holes, geophysical and geophysical logs;
- Alinta Energy Ltd (Leigh Creek Coal Mine) provided access to drill holes, geophysical and geophysical logs;
- Areva Australia Pty Ltd provided geophysical data;
- Curnamona Uranium Ltd provided access to drill holes, geophysical and geophysical logs and accommodation;
- Gold Fields Australasia provided drill hole logs;
- Heathgate Resources provided access to drill holes, geophysical and geophysical logs and accommodation;
- Scimitar Resources Ltd (now Cauldron Energy Ltd) provided geophysical data; and,
- Uranium One Australia Pty Ltd provided access to drill holes, geophysical and geophysical logs and accommodation.

After further negotiations, and a 12-month spending moratorium due to the 2009-10 global financial crisis, only two respondents finally took up the offer of purchasing infill within the Survey:

- Government of South Australia Department for Manufacturing, Innovation, Trade, Resources and Energy (contributed A\$278 000); and,
- Callabonna Uranium Ltd consortium including Cauldron Energy Ltd (contributed A\$84 500).

Infill purchases contributed a total of A\$362 500 to the survey budget and GA, through funding provided by the OESP, provided A\$2 307 500 for a total survey cost of A\$2 670 000.

1.6 FINAL SURVEY DESIGN

The final survey design (Figure 1.7) of 32 317 line km and 95 450 km² was fixed after careful consideration by the Geological Reference and Geophysical Reference groups at GA and after consultation with infill partners. A wide range of cultural, geological, geophysical, remote sensing and topographic data were compiled covering the Frome AEM Survey area, including:

- Cultural data including mines, roads, tracks, pipe lines and power lines;
- Cadastral data including place names, native title determinations and claims;
- Topographic data from the TOPO 250k series;
- Hydrological data including water courses and lakes;
- Tenement boundaries from the PIRSA SARIG database;
- Mineral occurrences from the PIRSA SARIG database;
- Mineral exploration drill hole locations from the PIRSA SARIG database;
- Petroleum well locations from the PIRSA SARIG database;
- Geoscience Australia 1:1 000 000 Surface Geology of South Australia (Raymond, 2010);
- Geoscience Australia Radiometric Map of Australia (Minty *et al.*, 2009);
- Magnetic Anomaly of the Australian Region Map;
- Gravity Anomaly of the Australian Region Map;
- Reduced-to-pole (RTP) total magnetics;
- RTP 1st vertical derivative magnetics;
- Shuttle Radar Topography Mission (SRTM) 3 second (90 m) DEM;
- Shuttle Radar Topography Mission (SRTM) 1 second (30 m) smoothed DEM;
- Landsat Thematic Mapper mosaic;
- Advanced Spaceborne Thermal Emission and Reflection radiometer (ASTER) mosaic; and,
- Existing ground electromagnetic and AEM surveys.

Survey boundaries were determined by integrating the above data with the forward modelling parameters, industry feedback and political considerations, given that uranium exploration and/or mining was illegal in New South Wales at that time. Flight line spacing and areal extent were determined by assessing the extents of known geological units and structures and predicted uranium potential. Knowledge gained during the Paterson AEM Survey (Roach, 2010) and the Pine Creek AEM Survey (Craig, 2011) was also used to determine flight line spacing. The planning process used magnetics, gravity, radiometrics and geology associated with palaeovalley-hosted uranium mineralisation to identify subsurface geological features. The process indicated that mappable palaeovalley features should be > 5 km in lineal extent. This criterion helped define the final flight line spacings in the Survey area.

The final survey design also included four objectives against which the success of the Survey could be measured. The Survey should be able to:

1. Map facies associated with uranium mineralisation;
2. Map structures associated with uranium or other mineralisation;
3. Map palaeovalley architecture; and,
4. Map geological surfaces.

The Frome airborne electromagnetic survey, South Australia: implications for energy, minerals and regional geology

The final survey design included the following generalisations which influenced the line spacing and survey boundaries:

- High uranium prospectivity and low risk areas:
 - Lake Frome area including Beverley, Goulds Dam, Honeymoon, Oban, Mount Victoria, Crocker Well and Radium Hill uranium deposits – 2.5 km flight line spacing.
- Lower uranium prospectivity and higher risk areas:
 - Northern Flinders Ranges – 2.5 km flight line spacing;
 - Murray-Darling Basin – 2.5 km flight line spacing; and,
 - Northwestern Flinders Ranges, Marree – 5 km flight line spacing.

Other geological targets included:

- Benagerie Ridge – improved understanding of depth of cover, 2.5 km flight line spacing;
- Olary Range – improved understanding of structural relationships and under-cover extent of chemically-reactive rocks in Neoproterozoic sediments, 2.5 km flight line spacing;
- Murray-Darling Basin – improved understanding of Cenozoic stratigraphy and depth to Adelaidean-Kanmantoo Group basement, 2.5 km flight line spacing;
- Lake Frome area – improved understanding of Cenozoic and Mesozoic stratigraphy, 2.5 km flight line spacing;
- Northern Flinders Ranges – improved understanding of potential uranium systems and neotectonics in the southern Eromanga Basin and Lake Eyre Basin;
- Strzelecki and Simpson deserts – improved understanding of Cenozoic and Mesozoic stratigraphy, 5 km flight line spacing; and,
- Northwestern Flinders Ranges – assessment of AEM method in exploring for Leigh Creek-style coal deposits and Beltana-type zinc silicate mineralisation, 5 km flight line spacing.

A small amount of overfly was necessary at the start and end of each flight line in order to line the aircraft up properly with the contracted flight lines. In the case of the Frome AEM Survey the contractor required a 1 km overfly at the start and end of each line (Figure 1.7) to reduce geophysical data processing artefacts and to ensure correct AEM system geometry. Overfly data were cropped to the survey boundaries and deleted after final processing. In the Frome AEM Survey area, the regional flight line spacing was 5 km for the whole Survey, with most of the Survey conducted at 2.5 km line spacing; no other flight line spacings were used (Figure 1.8). These flight line spacings were chosen in order to provide a truly regional overview of the geology of the Survey area.

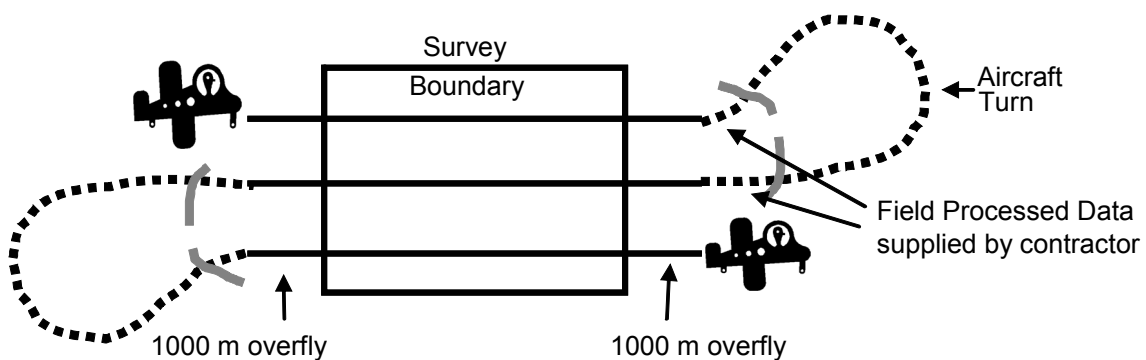


Figure 1.7: Cartoon of flight line planning including overfly areas.

The Frome airborne electromagnetic survey, South Australia: implications for energy, minerals and regional geology

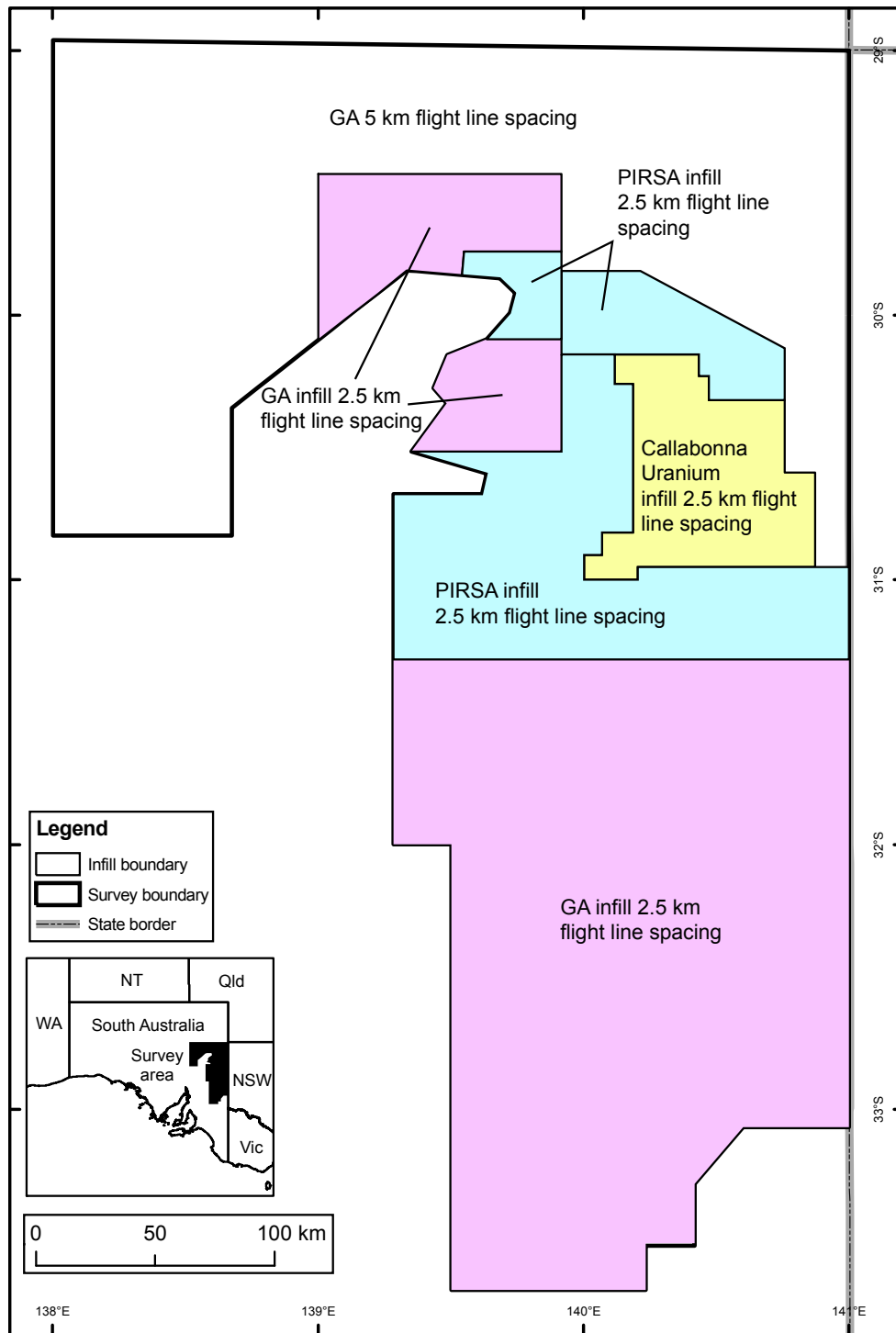


Figure 1.8: Final flight line spacings and infill areas for the Frome AEM Survey.

1.7 REFERENCES

- Alliance Resources Ltd, 2010. Alliance Resources Limited Annual Report 2010. 60 pp. Online: <http://www.allianceresources.com.au/>.
- BOM, 2011. Bureau of Meteorology. Online: <http://www.bom.gov.au>.
- Cauldron Energy Ltd, 2011. ASX Announcement: Quarterly Report for period ended 30 September 2011. Leederville WA, 19 pp. Online: http://www.cauldronenergy.com.au/_content/documents/548.pdf.
- Craig, M. A. (editor) 2011. Geological and energy implications of the Pine Creek region airborne electromagnetic (AEM) survey, Northern Territory, Australia. Geoscience Australia, Canberra. **Geoscience Australia Record 2011/18**.
- Curnamona Energy Ltd, 2010. Curnamona Energy Annual Report 2010. 47 pp. Online: http://www.curnamona-energy.com.au/pdf/CUY_Annual_Report_2010.pdf.
- Exco Resources Ltd, 2010. Exco Resources Ltd Annual Report 2010. 86 pp. Online: <http://www.excoresources.com.au/DownloadAsset.ashx?aid=fe6d7207-cdde-4010-82d3-6d39be95a340>.
- Geothermal Resources Ltd, 2010. Annual Report. Online: http://www.geothermal-resources.com.au/pdf/GHT_Annual_Report_2010.pdf.
- Havilah Resources NL, 2010. Havilah Resources NL Annual Report 2010. 63 pp. Online: http://www.havilah-resources.com.au/pdf/HAV_Annual_Report_2010.pdf.
- Hutchinson, D. K., Roach, I. C. and Costelloe, M., 2011. Logistics report for borehole conductivity logging in the Frome AEM survey area, South Australia, 2010. Geoscience Australia, Canberra, 20 pp. Online: https://www.ga.gov.au/products/servlet/controller?event=GEOCAT_DETAILS&catno=71566.
- Ker, D. S., 1965. Hydrology of the Frome Embayment in South Australia. Geological Survey of South Australia, Adelaide, **Report of Investigations No. 27**, 98 pp.
- Kwitko, G., 1995. Triassic intramontaine basins. In: Drexel, J. F. and Preiss, W. V. (editors), South Australia Geological Survey, The Geology of South Australia Volume 2 The Phanerozoic. **Bulletin 54**, 98-101 p.
- Lawrence, M. and Stenning, L., 2008. Paterson North Airborne Electromagnetic (AEM) Mapping Survey - Acquisition and Processing Report for Geoscience Australia. Fugro Airborne Surveys. **Unpublished report**, 108 pp.
- Marathon, 2010. Marathon Resources Ltd Annual Report 2010. 52 pp. Online: http://www.marathonresources.com.au/pdf/100929_Annual_Report_2010.pdf.
- McKay, A. D. and Miezitis, Y., 2001. Australia's uranium resources, geology and development of deposits. Mineral Resource Report, AGSO - Geoscience Australia, Canberra. **Mineral Resource Report 1, 1**, 200 pp.
- Minty, B. R. S., Franklin, R., Milligan, P. R., Richardson, L. M. and Wilford, J., 2009. The Radiometric Map of Australia. In: 20th International Geophysical Conference and Exhibition, Adelaide. Australian Society of Exploration Geophysicists.
- OZMIN, 2009. Geoscience Australia OZMIN database: uranium resources extracted February 2009.
- Parkin, L. W., 1965. Radium Hill uranium mine. In: McAndrew, J. (editor), Geology of Australian Ore Deposits. Australasian Institute of Mining and Metallurgy. 312-313 p.
- PepinNini Minerals Ltd, 2010. PepinNini Minerals Limited Annual Report 2010. Online: http://www.pepinnini.com.au/uploaded/docs/4cbf86dd34213_10382_Pepinnini_AR0910_3.pdf.
- Perilya Limited, 2011a. Flinders. Online: <http://www.perilya.com.au/our-business/development/flinders>.
- Perilya Limited, 2011b. Investor Presentation - Half Year Results September 2011. Online: http://www.perilya.com.au/articles/investor-presentation---half-year-results-september-2011/110901_-_Investor_Presentation_Half_Year_Results_Sept_2011.pdf.
- Petratherm Ltd, 2011. Paralana. Online: http://www.petratherm.com.au/_webapp_117685/Paralana.

The Frome airborne electromagnetic survey, South Australia: implications for energy, minerals and regional geology

- Raymond, O. L., 2010. Surface geology of Australia, 1:1,000,000 scale, 2010 edition. Geoscience Australia, Canberra. Online:
https://www.ga.gov.au/products/servlet/controller?event=GEOCAT_DETAILS&catno=70311.
- Roach, I. C. (editor) 2010. Geological and energy implications of the Paterson Province airborne electromagnetic (AEM) survey, Western Australia. Geoscience Australia, Canberra. **Geoscience Australia Record 2010/12**, 318 pp.
- Royal Resources Ltd, 2011. Royal Resources Ltd. Annual Report. Online:
[http://www.royalresources.com.au/documents/01822RR%20Annual%20Report%202011%20WEB\(1\).pdf](http://www.royalresources.com.au/documents/01822RR%20Annual%20Report%202011%20WEB(1).pdf).
- Shepherd, R. G., 1978. Underground water resources of South Australia. Geological Survey of South Australia, Adelaide, **Bulletin 48**, 67 pp.
- Skirrow, R. G. (editor) 2009. Uranium ore-forming systems of the Lake Frome Region, South Australia: Regional spatial controls and exploration criteria. Geoscience Australia, Canberra. **Record 2009/40**, 151 pp.
- Southern Cross Resources, 2004. Southern Cross Resources Annual Report 2004.
- Springbett, G. M., Kremor, A. G. and Brennan, S. H., 1995. Leigh Creek Coalfield. In: Ward, C. R., Harrington, H. J., Mallett, C. W. and Beeston, J. W. (editors), Geology of Australian coal basins. Geological Society of Australia Coal Geology Group. **Special Publication 1**, 513-524 p.
- Wilson, T. and Fairclough, M., 2009. Uranium and Uranium Mineral Systems in South Australia. South Australia, Department of Primary Industries and Resources, Adelaide. **Report Book 2009/14**, 182 pp.

2 Previous investigations

I.C. Roach, M.T. Costelloe and S. Jaireth

2.1 INTRODUCTION

This chapter collates geological and geophysical data available within the Frome AEM Survey area to provide context for the data collected in the Frome AEM Survey. This compilation describes publicly-available data within the survey area from state and federal government geological information sources including the Geoscience Portal (<http://www.geoscience.gov.au/>) at Geoscience Australia (GA), the South Australian Resources Information Geoserver (SARIG; <http://www.pir.sa.gov.au/minerals/sarig>), the Geophysical Archive Data Delivery System (GADDS; <https://www.ga.gov.au/gadds>) at GA and the Petroleum Data Repository at GA. This includes data gathered by state and federal government agencies and industry that is now in the public domain.

2.2 GEOLOGICAL MAPPING

2.2.1 Surface geology mapping

The Frome AEM Survey area is covered by geological mapping at various scales including a state 1:7 000 000 and 1:2 000 000 map and individual 1:250 000 and 1:100 000 maps. Only the 1:250 000 maps have explanatory notes; the digital-only 1:100 000 maps are regarded as the fundamental dataset from which all other scales of maps are drawn (Cowley, 2009).

The entire area is also mapped at 1:1 million scale in the GA Surface Geology of Australia map (Raymond, 2010), which joins seamlessly with the adjoining states of Queensland, New South Wales and Victoria. This map was compiled from 1:250 000 scale mapping in each state and was updated with revised mapping during the compilation process.

Figure 2.1 illustrates the 1:250 000 and 1:100 000 maps included within or intersecting the Frome AEM Survey area and Table 2.1 includes references to the available 1:250 000 map explanatory notes. All state maps are available for free download as GIS layers from the SARIG system and scanned versions of the original prints are also available from the Geoscience Portal. The GA 1:1 000 000 Surface Geology of Australia map is available for free download from GA's MapConnect service (<http://www.ga.gov.au/mapconnect/>).

2.2.2 Solid geology mapping

A range of solid geology maps for the state of South Australia are available for the Frome AEM Survey area, arranged into time slices, including (Cowley, 2009):

- Archean to Early Mesoproterozoic (Figure 2.2);
- Middle Mesoproterozoic;
- Late Mesoproterozoic; and,
- Neoproterozoic to Ordovician (Figure 2.2).

Geological province maps are also available for the state of South Australia (Figure 2.3), and arranged into time slices, including (Cowley, 2009):

- Archean to Mesoproterozoic;
- Middle to Late Mesoproterozoic;
- Neoproterozoic;
- Cambrian to Late Carboniferous;
- Late Carboniferous to Triassic;
- Jurassic to Cretaceous; and,
- Cenozoic.

The Frome airborne electromagnetic survey, South Australia: implications for energy, minerals and regional geology

Table 2.1: 1:250 000 scale geological mapping and explanatory notes available within the Frome AEM Survey area.

MAP NAME	AUTHOR(S), REFERENCE
CALLABONNA	Sheard, M.J. and Callen, R.A. 2000. CALLABONNA map sheet. South Australia Geological Survey. Geological Atlas 1:250 000 series, sheet SH 54-8. Sheard M.J. 2009. Explanatory notes for CALLABONNA 1:250 000 Geological Map, sheet SH 54-6. Division of Minerals and Energy Resources, Primary Industries and Resources South Australia, Report Book 2009/1. 204 pp.
CHOWILLA	Rogers P.A. 1977. CHOWILLA Sheet SI 54-6, First Edition. Rogers, P.A. 1978. 1:250 000 Geological Series – Explanatory Notes, CHOWILLA South Australia, Sheet SI/54-6 International Index. Department of Mines and Energy, State of South Australia, Geological Survey of South Australia. 25 pp.
COPLEY	Coats, R.P., 1973. COPLEY South Australia, Explanatory Notes 1:250 000 Geological Series—Sheet SH/54-9. Department of Mines, Geological Survey of South Australia. 38 pp. Coats, R.P., Callen, R.A. and Williams, A.F. 1973. COPLEY Sheet SH 54-9, First Edition.
CURNAMONA	Callen, R.A., 1986. CURNAMONA Sheet SH 54-14, First Edition. Callen, R.A., 1990. 1:250 000 Series—Explanatory Notes, CURNAMONA, South Australia, Sheet SH/54-14 International index. Department of Mines and Energy South Australia, Geological Survey of South Australia. 56 pp.
FROME	Callen, R. A. and Coats, R. P., 1975. Frome Sheet SH 54-10. 1:250 000 Geological Series, Geological Survey of South Australia, Department of Mines, Adelaide. First Edition. Callen, R. A., 1981. FROME, South Australia, Explanatory Notes, 1:250 000 Geological Series—Sheet SH/54-10. Geological Survey of South Australia, Adelaide. 42 pp.
MARREE	Forbes, B. G., Coats, R. P., Webb, B. P. and Horwitz, R. C., 1965. Marree Sheet H 54-5. 1:250 000 Geological Series, Geological Survey of South Australia, Department of Mines, Adelaide. First Edition.
OLARY	Forbes, B. G., 1989. OLARY Sheet SI 54-2. 1:250 000 Geological Series, Geological Survey of South Australia, Department of Mines and Energy, Adelaide. First Edition. Forbes, B. G., 1991. 1:250 000 Geological Series—Explanatory Notes, OLARY, South Australia, Sheet SI 54-2 International Index. Geological Survey of South Australia, Department of Mines, Adelaide. 47 pp.
PARACHILNA	Reid, P. and Preiss, W. V., 1999. PARACHILNA Sheet SH 54-13. 1:250 000 Geological Series, Geological Survey of South Australia, Department of Primary Industries and Resources SA, Adelaide. Second Edition. Preiss, W. V., 1999. 1:250 000 Geological Series—Explanatory Notes, PARACHILNA, South Australia, Sheet SH54-13 International Index, Second Edition. Primary Industries and Resources SA, Geological Survey of South Australia, Adelaide. 52 pp.

The Frome airborne electromagnetic survey, South Australia: implications for energy, minerals and regional geology

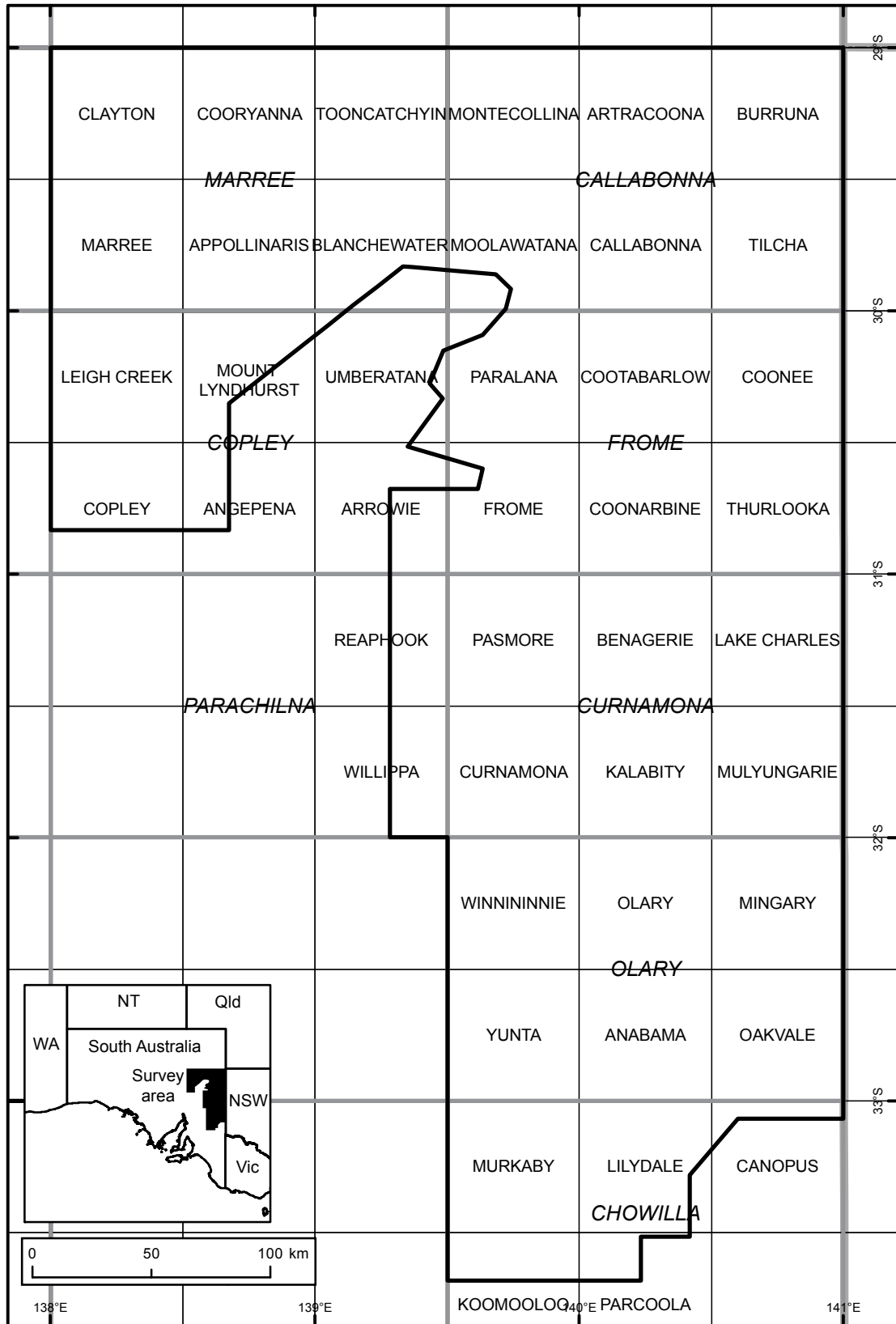


Figure 2.1: 1:250 000 (*italics*) and 1:100 000 scale geological maps within or intersecting the Frome AEM Survey area.

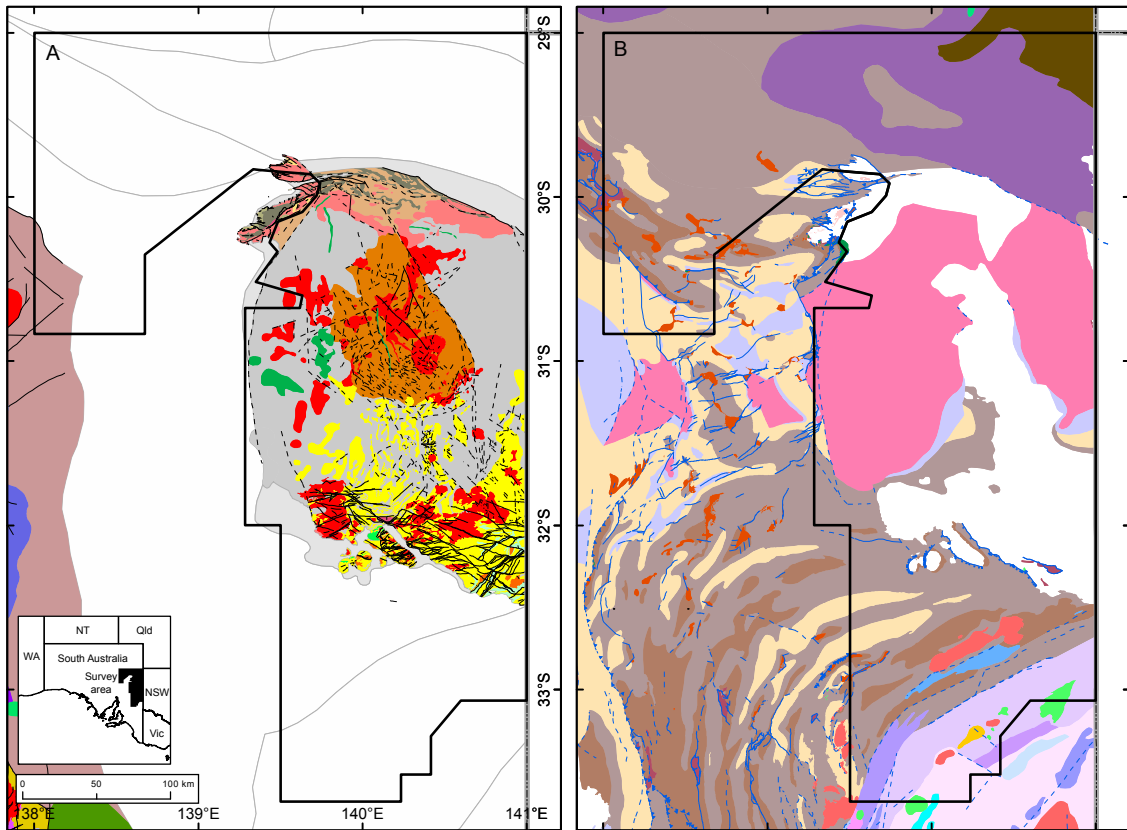


Figure 2.2: Solid geology maps of the Frome area, illustrating: A: Archean to Paleoproterozoic solid geology; and, B: Neoproterozoic to Ordovician solid geology (right), from SARIG. The Middle and Late Mesoproterozoic time slices are not strongly represented in the Frome AEM Survey area (see [Figure 2.3](#)). These images are discussed in more detail in [Chapters 4 and 5](#).

2.3 REGOLITH-LANDFORM AND SOIL MAPPING

The Frome AEM Survey area includes or intersects a number of regolith-landform maps at various scales, which are described in [Table 2.2](#) and [Figure 2.4](#). A significant number of the maps relevant to the Frome AEM Survey area were constructed as part of research projects conducted by the Cooperative Research Centre for Landscape Environments and Mineral Exploration (CRC LEME).

The Palaeodrainage and coastal barriers of South Australia 1:2 000 000 map (Hou *et al.*, 2007) and the new South Australia 1:1 000 000 regolith map (Krapf, in prep) are particularly useful references covering the whole of the Frome AEM Survey area.

The regolith-landform maps constructed as part of CRC LEME research activities within the Frome AEM Survey area are all available for individual free download from the CRC LEME website at <http://crcleme.org.au/> and from Geoscience Australia.

Small scale (large area) soil and landscape mapping is available for the Frome AEM Survey area via the Australian Soil Resource Information System (ASRIS) website (<http://www.asris.csiro.au/>), based on the 1:2 000 000 scale Atlas of Australian Soils (Northcote, 1979; Northcote *et al.*, 1960-1968).

The Frome airborne electromagnetic survey, South Australia: implications for energy, minerals and regional geology

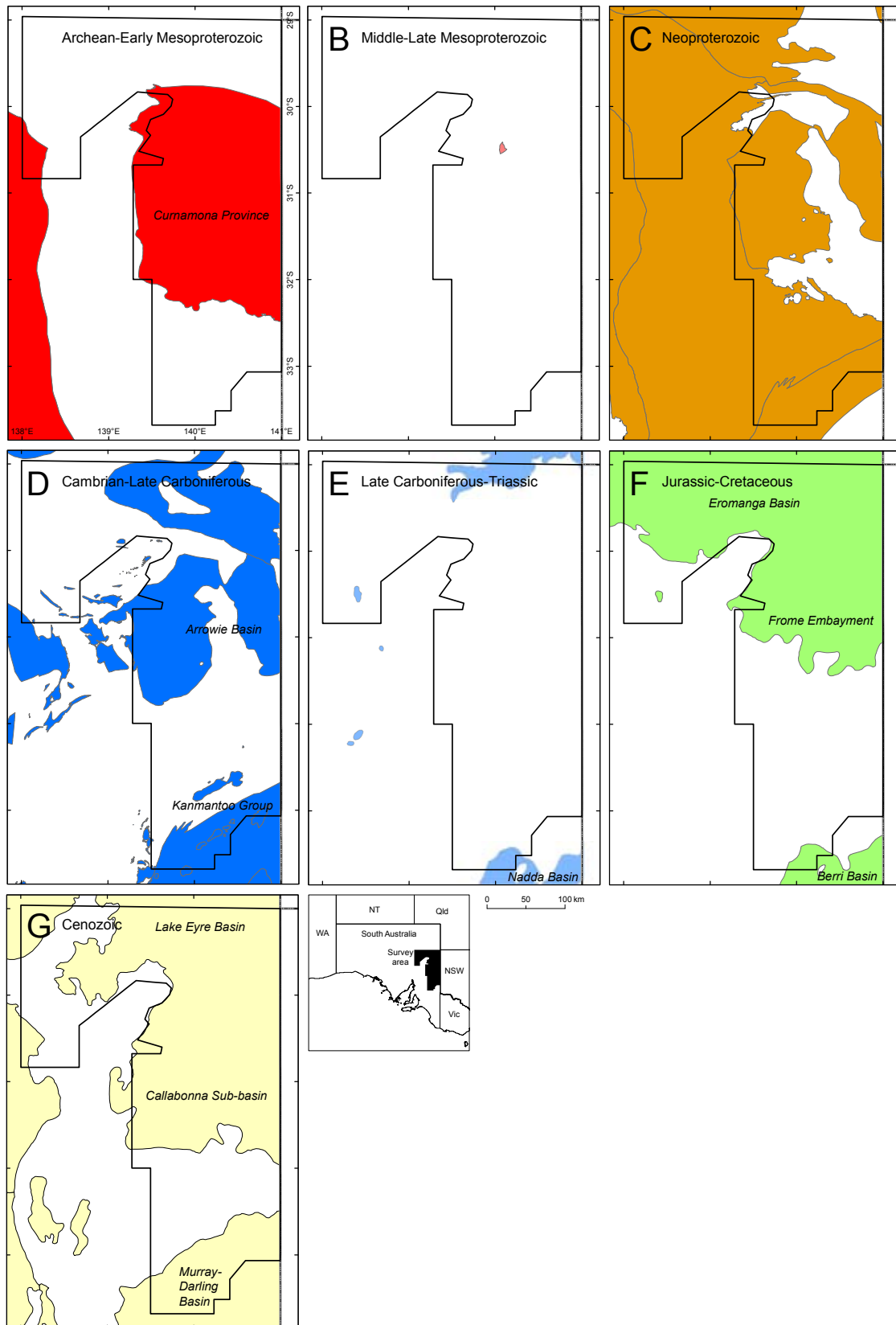


Figure 2.3: Time slices of geological provinces within the Frome AEM Survey area, from SARIG.

Table 2.2: Regolith-landform mapping within or near the Frome AEM Survey area.

MAP NAME	SCALE	AUTHOR(S), REFERENCE
Anabama	1:100 000	Skwarnecki, M. S., Shu, L. and Lintern, M. J., 2001. Geochemical dispersion in the Olary district, South Australia: investigations at
Blue Rose	1:12 000	Faugh-a-balagh Prospect, Olary Silver Mine, Wadnaminga Goldfield and Blue Rose Prospect. CRC LEME, Perth. Open File Report 113, 78 pp. Online: http://crcleme.org.au .
Faugh-a-balagh	1:5000	
Faugh-a-balagh	1:12 000	
Olary	1:100 000	
Wadnaminga	1:5000	
Bimbowrie Station, SA	1:150 000	Brown, A. D., 2006. Regolith landforms of Bimbowrie Station. MESA Journal 41(April 2006), 30-33. Online: http://crcleme.org.au/Pubs/MAPS/BimbowrieRegolithMap.pdf .
Broken Hill, NSW	1:500 000	Gibson, D. L., 1999. Explanatory notes for the Broken Hill and Curnamona Province 1:500 000 regolith landform maps. CRC LEME, Perth. Open File Report 77, 59 pp. Online: http://crcleme.org.au/Pubs/MAPS/broken_hill_500k.pdf and http://crcleme.org.au/Pubs/MAPS/curnamona_500k.pdf .
Curnamona, SA	1:500 000	
Four Mile	1:20 000	Dubieniecki, C. D. and Hill, S. M., 2007. Constraints on the Four Mile uranium mineralisation, resulting from neo-tectonic activity in the northern Flinders Ranges, SA. In: Cooper, B. J. and Keeling, J. L. (ed), 5th Sprigg Symposium, Adelaide, Geological Society of Australia, 15-18 pp.
Kalabity	1:100 000	Lawie, D. C., 2001. Exploration geochemistry and regolith geology over the northern part of the Olary Domain, South Australia. University of New England, Armidale NSW. PhD thesis. Online: http://crcleme.org.au/Pubs/MAPS/kalabity_region_100k.pdf .
Kalkaroo	1:25 000	Dawson, M. W., 2000. The geology of the Kalkaroo area. University of New England, Armidale, NSW. BSc Honours thesis. Online: http://crcleme.org.au/Pubs/MAPS/kalkaroo_25k.jpg .
Luxemburg	1:2500	Brown, A. D., Kernich, A. and Hill, S. M., 2002. Luxemburg Regolith-Landform map. In: Kernich, A., 2002. Weathering, erosion and element mobilisation in a catchment at the Luxemburg Copper/Gold site, Olary Domain, South Australia. University of Adelaide. BSc Honours thesis. Online: http://crcleme.org.au/Pubs/MAPS/luxemburg_2-5k.pdf .
Mingary	1:100 000	Crooks, A. and Hill, P., 2008. Mingary 7033. Department of Primary Industries and Resources SA, Adelaide. Online: http://www.pir.sa.gov.au/__data/assets/pdf_file/0016/132550/MINGARY_REGOLITH.pdf .
Mt Babbage Inlet	1:25 000	Davey, J. E., 2010. Mesozoic palaeolandscape reconstruction, southern Eromanga Basin margins. University of Adelaide. PhD thesis. Online: http://crcleme.org.au/Pubs/MAPS/mt_babbage_inlet_25k.pdf .
Parabarana, SA	1:25 000	Davey, J. E., McAvaney, D. J. and Hill, S. M., 2010. Parabarana, northern Flinders Ranges, Australia. In: Davey, J. E., 2010. Mesozoic palaeolandscape reconstruction, southern Eromanga Basin margins. University of Adelaide. PhD thesis. Online: http://crcleme.org.au/Pubs/MAPS/parabarana_25k.pdf .

Table 2.2 (continued): Regolith-landform mapping within or near the Frome AEM Survey area.

MAP NAME	SCALE	AUTHOR(S), REFERENCE
South Australian palaeochannel map	1:2 000 000	Hou, B., Zang, W., Fabris, A., Keeling, J., Stoian, L. and Fairclough, M., 2007. Palaeodrainage and coastal barriers of South Australia 1:2 000 000. CRC LEME, Geological Survey Branch, Primary Industries and Resources South Australia, Adelaide. Online: http://www.pir.sa.gov.au/__data/assets/pdf_file/0005/41486/palaeochannels_sa_map.pdf .
West Mt Neill palaeodrainage	1:25 000	Wilson (2007)
White Dam	1:2000 1:4000	Brown, A. D. and Hill, S. M., 2003. White Dam - detailed regolith-landform mapping as a tool for refining the interpretation of surface geochemical results. MESA Journal 31(October 2003), 6-8. Brown, A. D. and Hill, S. M., 2005. White Dam Au-Cu prospect, Curnamona Province, South Australia. In: Butt, C. R. M., Cornelius, M., Scott, K. M. and Robertson, I. D. M. (ed), Regolith Expression of Australian Ore Systems. CRC LEME, Perth. Online: http://crcleme.org.au/Pubs/MAPS/white_dam_2k.pdf . Brown, A. D. and Hill, S. M., 2004. Regolith-landform maps are an essential tool for interpreting regolith geochemistry: the White Dam, SA, experience. In: Roach, I. C. (ed), Regolith 2004, Canberra, CRC LEME, 37-41 pp. Online: http://crcleme.org.au/Pubs/MAPS/white_dam_4k.png and http://crcleme.org.au/Pubs/Monographs/regolith2004/Brown&Hill.pdf .
White Dam	1:30 000	Lau, I., 2004. Regolith-landform and mineralogical mapping of the White Dam Prospect, eastern Olary Domain, South Australia, using integrated remote sensing and spectral techniques. University of Adelaide. PhD thesis. Lau, I., 2004. White Dam South Australia. CRC LEME, Adelaide. Online: http://crcleme.org.au/Pubs/MAPS/white_dam_30k.pdf . Lau, I., Heinson, G. S. and Hill, S. M., 2004. Explanatory notes for the 1:30,000 regolith-landform map of White Dam, Olary Domain, South Australia. In: Roach, I. C. (ed), Regolith 2004, Canberra, CRC LEME, 188-193 pp.

Regolith- and regolith-landform mapping also considers the geochemistry of the land surface and a number of the publications listed in Table 2.2 contain surface geochemical sample analyses. A far broader survey of surface geochemistry on a catchment-by-catchment basis, the Geochemical Atlas of Australia, part of GA's National Geochemical Survey of Australia Project, was released in 2011. Data are available as a series of maps describing the distribution of individual elements across Australia, as well as a written record (Caritat, 2011) and an ASCII file of individual site analyses through the GA website (<http://www.ga.gov.au/energy/projects/national-geochemical-survey/atlas.html>).

The Frome airborne electromagnetic survey, South Australia: implications for energy, minerals and regional geology

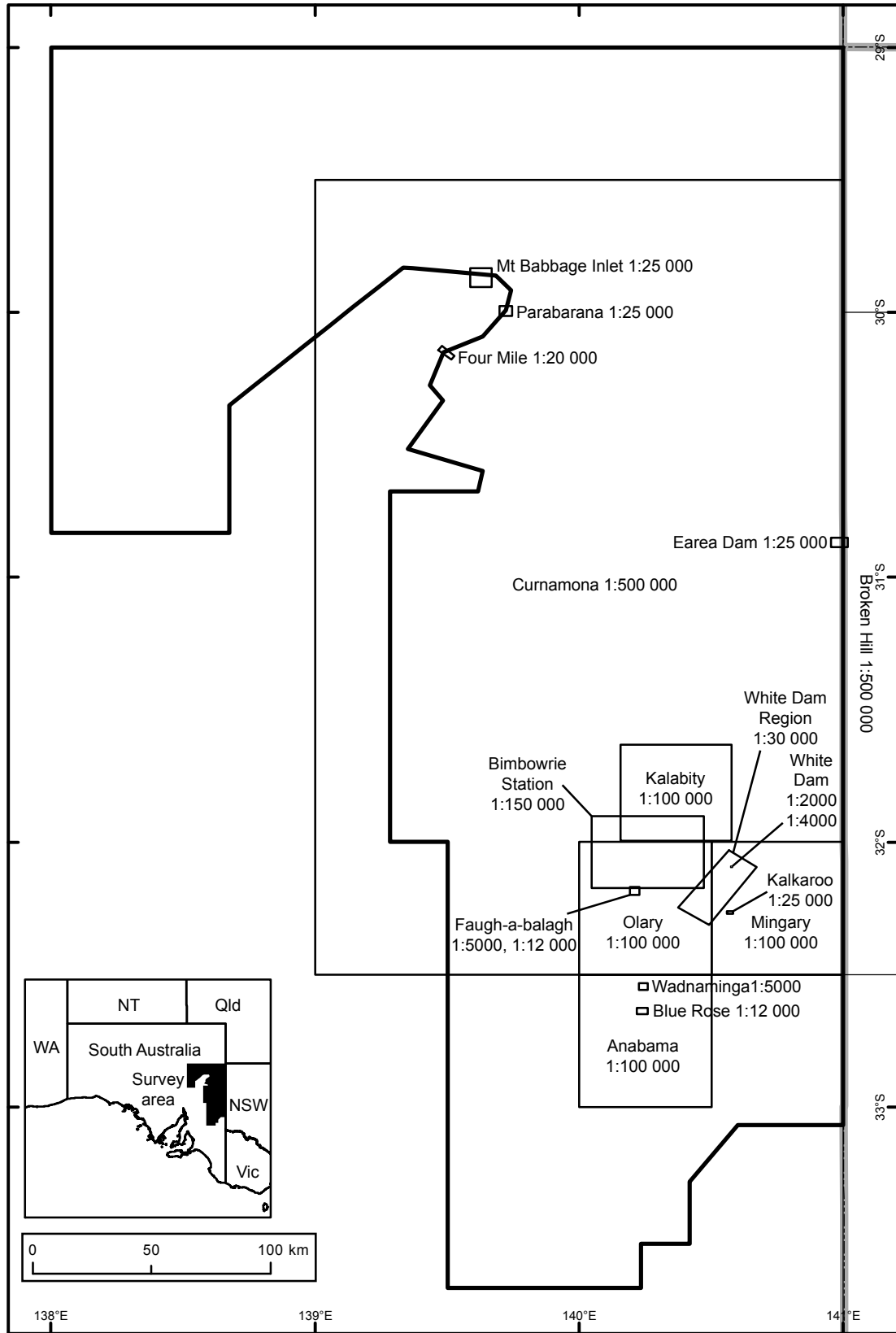


Figure 2.4: Regolith-landform mapping within or intersecting the Frome AEM Survey area.

2.4 SPECIALIST GEOLOGICAL PUBLICATIONS

A large number of specialist publications have been produced regarding the geology, geodynamics, geochronology and economic geology of features within the Frome AEM Survey area. These include studies into the detailed geology of particular geological regions, the geochronology of rocks, sediments or mineral deposits and mineral deposit styles.

Interpretations for the Frome AEM Survey rely primarily on 1:250 000 and 1:100 000 mapping described in [Section 2.2](#), however detailed knowledge of the mineral systems and bedrock geology and stratigraphy of the Lake Eyre Basin-Callabonna Sub-basin), the Eromanga Basin and the Murray-Darling Basin and their groundwater flow systems have also been consulted.

The following is a non-exhaustive summary of major publications that synthesise the geology, geodynamics, geochronology and economic geology of the Frome AEM Survey area.

2.4.1 Geology and geodynamics

Unlike other areas surveyed in the Onshore Energy Security Program AEM acquisition program within Australia (i.e., the Paterson area; Roach, 2010), the tectono-stratigraphic framework of South Australia is relatively well understood, and mature models of the surface geology, structural geology and stratigraphy of the Curnamona Province, Adelaide Geosyncline, Delamerian Orogen, Eromanga Basin, Lake Frome area and Murray-Darling Basin already exist.

As well as the 1:250 000 scale geological map explanatory notes ([Table 2.1](#)), there are a number of useful syntheses describing the geology of the entire Survey area, for instance “The geology of South Australia” volumes (Drexel and Preiss, 1995; Drexel *et al.*, 1993). Other syntheses concentrate on large parts of the Survey area, including the “Geodynamic Synthesis of the Gawler Craton and Curnamona Province” (Kositcin, 2010), the “Geology of the Adelaide Geosyncline” (Preiss, 1987), the detailed “Geology of the Olary Domain of the Curnamona Province” (Conor, 2004), the tectonic evolution of the Willyama Supergroup (Conor and Preiss, 2008) and the 3D shape of sedimentary basins covering the Curnamona Province (Fabris *et al.*, 2010). There are numerous reports, abstract volumes and journal articles regarding specific syntheses of the geology and geodynamics of the area including deep crustal seismic studies (Carr *et al.*, 2010; Korsch and Kositcin, 2010), structural geology (Marshak and Flöttmann, 1996) and geodynamics of the Curnamona Province as part of the larger Proterozoic of Australia (Fraser *et al.*, 2007). Coats and Blissett (1971) published an influential volume on the geology of the Mount Painter Province, including the western plains of Lake Frome in the Lake Frome area. Fricke (2008), Fricke and Hore (2010), Cowley *et al.* (2011) and Wade (2011) developed a new synthesis of granite occurrences in the Curnamona Province, collating granite geochemistry and geochronology across the region, and placed all of the Proterozoic granites into the “Ninnerie Supersuite”. Some granites of the Supersuite are highly uranium-enriched and act as sources for sandstone-hosted uranium deposits within the Callabonna Sub-basin and Murray-Darling Basin.

Syntheses of sedimentary basin cover over the Curnamona Province are detailed by Cowley (2006) and Hou *et al.* (2006). Mapped palaeovalleys are detailed in the Palaeovalley Map of South Australia (Hou *et al.*, 2007), including the current knowledge of those in the Lake Frome area. Knowledge of the stratigraphy of the Mesozoic sequences of the Eromanga Basin comes primarily from the petroleum literature (discussed in [Section 2.4.5](#)), but also from the likes of Ludbrook (1966) and numerous minerals industry reports, particularly those describing sedimentary uranium exploration. There are a number of publications describing the regional stratigraphy and sedimentology of the Lake Eyre Basin-Callabonna Sub-basin including Jack (1925; 1930), Ludbrook and Johns (1963), Wopfner *et al.* (1974) and Callen and Tedford (1976), as well as the synthesis of Drexel and Preiss (1995).

The stratigraphy and sedimentology of the Murray-Darling Basin have been described by Jack (1930), Barnes (1951), O’Driscoll (1960), Firman (1973), Ludbrook (1961), Bonnett and Lindsay

(1973), Shepherd (1978), Sprigg (1979), Brown and Stephenson (1991) and Fabris (2002; 2003a; b). Most recently, Cowley and Barnett (2007) redefined the stratigraphy of the Murray Group to bring nomenclature into line with that used in New South Wales and Victoria.

2.4.2 Regolith geology and geomorphology

The regolith geology and geomorphology of the Frome region has been described in geological and hydrological publications since the early 20th century as reports, journals articles, abstracts and maps. These commenced with the early geological investigation of South Australia and culminated in a series of focussed research projects examining specific aspects of the regolith geology and landscape evolution of the area, many of which are ongoing.

A great deal of interest has been shown in the geomorphological development of the region and there is still intense debate regarding the possible uses of indurated and weathered regolith to interpret large-scale weathering and tectonic events that may have occurred within the region. The arguments for and against the wide-scale correlation of indurated outcrops as tectonic and climatic marker horizons are outside the scope of this record, but further reading can be gleaned from the chief proponents of various theories including Alley (1977), Callen (1982), Milnes and Twidale (1983) and, more recently, Davey (2009), but also others included in the reference lists of those authors.

Early publications describing the Quaternary-Cenozoic and Mesozoic geology of the region (see [Section 2.4.1](#)) were also describing regolith and landscape features. A number of studies describe the geomorphological and/or environmental evolution of the Lake Frome area including the geomorphological history of the Lake Eyre Basin, e.g. Jack (1925; 1930), Ludbrook and Johns (1963), Ludbrook (1966), Wopfner and Twidale (1971), Wopfner *et al.* (1974), Callen and Tedford (1976) and Callen (1977), as well as the synthesis of Drexel and Preiss (1995). The Murray-Darling Basin has similarly been the focus of much interest in terms of its geomorphological and environmental evolution, almost too numerous to mention, including Jack (1930), Ludbrook (1961), Brown and Stephenson (1991), and summarised neatly by Fabris (2002) and Cowley and Barnett (2007).

A number of journal articles are devoted to determining the age of sand dunes within the Strzelecki, Simpson and Tirari deserts including Bowler (1976), Wopfner and Twidale (1988), Wasson *et al.* (1988), Gardner *et al.* (1987), Lomax *et al.* (2003), Fitzsimmons (2005) and Fitzsimmons *et al.* (2007), with the consensus being that dunes are multi-generational and maximum dune activity occurring during glacial maxima. Bowler *et al.* (2006) also described sand dune formation in the Mallee region of the Murray-Darling Basin. Quaternary alluvial sedimentation styles around the modern range fronts are also discussed in a number of publications including Wasson (1979), Wasson and Galloway (1986) and Bowler *et al.* (2006).

A large number of publications produced as contributions to the CRC LEME describe the regolith geology and geomorphology in and around the Frome AEM Survey area. The most recent, “A guide for mineral exploration through the regolith in the Curnamona Province, South Australia” (Fabris *et al.*, 2008) provides a précis of the regolith geology of the entire Curnamona Province. This includes much of the Frome AEM Survey area, and landscape evolution models for the northern Flinders Ranges and southern Lake Frome area for exploration for a range of commodities including sandstone-hosted, breccia complex and intrusive uranium deposits.

A number of publications describe and regolith-landform and landscape evolution aspects of field sites or small regions within or immediately adjacent to the Frome AEM Survey area, including a series of journals articles, reports, extended abstracts and regolith-landform or regolith maps (listed in [Table 2.2](#) and shown in [Figure 2.4](#)). Sheard (2008) and Fabris (2008) produced field trip guides for the northern and southern Curnamona Province, respectively, including sites around Broken Hill in New South Wales. A number of publications describe landscape evolution models within and adjacent to the Frome AEM Survey area including far western New South Wales (Hill, 2004a), the

Teilta area (Hill, 2004b), the northern Barrier Ranges (Gibson, 2004), the southern Barrier Ranges and northern Murray-Darling Basin (Hill *et al.*, 2004) and the Blue Rose district (Skwarnecki and Lintern, 2005). A number of PhD theses discuss aspects of the Mesozoic and Cenozoic regolith geology, landscape evolution and metallogeny of the region including Hill (2000), Lawie (2001), Lau (2004a), Fitzsimmons (2007), Wulser (2009) and Davey (2009). There are also numerous conference papers describing aspects of the regolith geology and landscape evolution the area included in Roach (2002; 2003; 2004; 2005) and Fitzpatrick and Shand (2006), as well as numerous Sprigg Symposia volumes (available online through the Geological Society of Australia – <http://www.gsa.org.au>).

2.4.3 Geochronology

Numerous publications describe the results and interpretations of geochronological data from within the Frome AEM Survey area. The sheer volume of data collected prohibits an exhaustive synthesis within this record, which is outside the scope of this document. However, a number of studies have focussed on sampling and analysing bedrock and sediment samples from the Flinders Ranges and Lake Frome area. These analyses have then been used to develop landscape evolution models for the uplift of the Flinders Ranges and for sediment provenance within the Lake Eyre Basin-Callabonna Sub-basin and Eromanga Basin. Neumann and Fraser (2007) synthesised the available geochronology for Proterozoic rocks on a province basis, concentrating on the Gawler Craton, Mount Isa Inlier and the Curnamona Province, to develop time-space plots. Cross *et al.* (2010) analysed detrital zircons from sediments in the Lake Eyre Basin-Callabonna Sub-basin and the Eromanga Basin, concentrating on drill core and surface exposures in the Beverley area, to determine the detrital zircon age populations present within specific stratigraphic units. This work has major implications for the geological evolution of the Flinders Ranges and onlapping basins in the Frome AEM Survey area. Wulser (2009) and Wulser *et al.* (2011) analysed uranium minerals in the Beverley uranium deposit in an attempt to date the age of mineralisation of this important deposit. Fraser and Neumann (2010) supplied new ages for granites in the Mount Painter Inlier.

Other workers have used different age determinations techniques including cosmogenic isotopic systems and fission track analysis in an attempt to explain the landscape evolution of the Flinders Ranges. Quigley *et al.* (2007) used ^{10}Be cosmogenic isotopes to determine a denudation history of Yudnamutana Creek gorge. Foster *et al.* (1994) and Mitchell *et al.* (2002) used fission track analysis of *in situ* bedrock samples from the northern Flinders Ranges, including the Mount Painter area, to determine a denudation history of the Ranges and a sedimentation history of the Lake Eyre Basin-Callabonna Sub-basin. Wulser (2009) synthesised the geochronology of the northern Flinders Ranges.

2.4.4 Mineral resources and mineral systems

A large number of publications are devoted to recording and interpreting the mineral deposits and mineral systems of the Curnamona Province and the overlying sedimentary basins. A synthesis of the major mineral systems is included in Table 3.2. A range of minor mineral deposits occur within the area, but a collation of these is beyond the scope of this record.

A number of useful syntheses describe the mineral systems and mineral resources of the Curnamona Province, Nackara Arc, Kanmantoo Trough, Eromanga Basin, Lake Eyre Basin-Callabonna Sub-Basin and Murray-Darling Basin. These are listed in Tables 2.3 and 2.4. While no means exhaustive, these syntheses cover the gamut of the major mineral systems and mineral resources of the Frome AEM Survey area.

Geoscience Australia's Uranium Systems Project produced a range of geoscience datasets including maps and 3D models regarding uranium mineral systems in the Lake Frome area. These are described in Table 2.5.

Table 2.3: Minerals systems references in and around the Frome AEM Survey area.

MINERAL SYSTEM	REGION	REFERENCE
U	East-central South Australia Lake Frome region South Australia Australia	Huston and van der Wielen (2011) Skirrow (2009) Wilson and Fairclough (2009) Bastrakov <i>et al.</i> (2010), Schofield (2009; 2010), Skirrow (2011), Skirrow <i>et al.</i> (2009)
Zn-Pb-Ag	Eromanga Basin Australia	van der Wielen <i>et al.</i> (2009) Page <i>et al.</i> (2005), Huston <i>et al.</i> (2006)
General	Northern Flinders Ranges	Cowley <i>et al.</i> (2009)

Table 2.4: Mineral resources references in and around the Frome AEM Survey area.

MINERAL RESOURCES	REGION	REFERENCE
U	South Australia Australia	Dickinson <i>et al.</i> (1954) McKay and Miezitis (2001)
Au	Nackara Arc	Morris and Horn (1990)
Fe	Nackara Arc	Whitten (1970)
Base metals	Northern Flinders Ranges	Johns (1972)
Heavy mineral sands	Murray-Darling Basin	Brown (1985), (Stewart, 1999), Whitehouse <i>et al.</i> (1999), Roy <i>et al.</i> (2000)
General	Australia and Papua New Guinea Australia South Australia Mount Painter Province Kanmantoo Trough	Hughes (1990) Geoscience Australia (2010) Cooper and McGeough (2006) Coats and Blissett (1971) Burt (2006)

Table 2.5: Geoscience Australia's Uranium Systems Project publications covering the Frome AEM Survey area.

TITLE	REFERENCE
Australia's uranium resources, geology and development of deposits	McKay and Miezitis (2001)
Uranium mineral systems: processes, exploration criteria and a new deposit framework	Skirrow <i>et al.</i> (2009)
Uranium content of igneous rocks of Australia 1:5 000 000 maps - Explanatory notes and discussion	Schofield (2009)
Uranium ore-forming systems of the Lake Frome Region, South Australia: Regional spatial controls and exploration criteria	Skirrow (2009)
Solubility of uranium in hydrothermal fluids at 25° to 300°C: implications for the formation of uranium deposits	Bastrakov <i>et al.</i> (2010)
Potential for magmatic-related uranium mineral systems in Australia	Schofield (2010)
SHRIMP U-Pb detrital zircon results, Lake Frome region, South Australia	Cross <i>et al.</i> (2010)
Uranium mineralisation events in Australia	Skirrow (2011)
Uranium systems processes in the Crocker Well Suite, South Australia	Schofield (2012)

2.5 DRILLING

Accurately located drill hole data are essential for interpreting AEM data. South Australia has a very sophisticated world wide web-based drill hole data delivery system within the SARIG database (<http://www.pir.sa.gov.au/minerals/sarig>), where drill hole data are available for free download. These include all minerals drill holes, all petroleum drill holes and drill holes from those two collections featuring lithology, stratigraphy and Hylogger data that have been lodged with, or logged by, DMITRE. All drill holes available within the Frome AEM Survey area (minerals, petroleum and geothermal) are shown in Figure 2.5 and a histogram of their frequency versus total depth is shown in Figure 2.6.

Drill hole data shown in this summary have been used to help interpret individual AEM conductivity sections and have also been included in 3D GOCAD™ models of the region to aid in the interpretation of conductivity volumes and the 3D relationships of geological surfaces and structures.

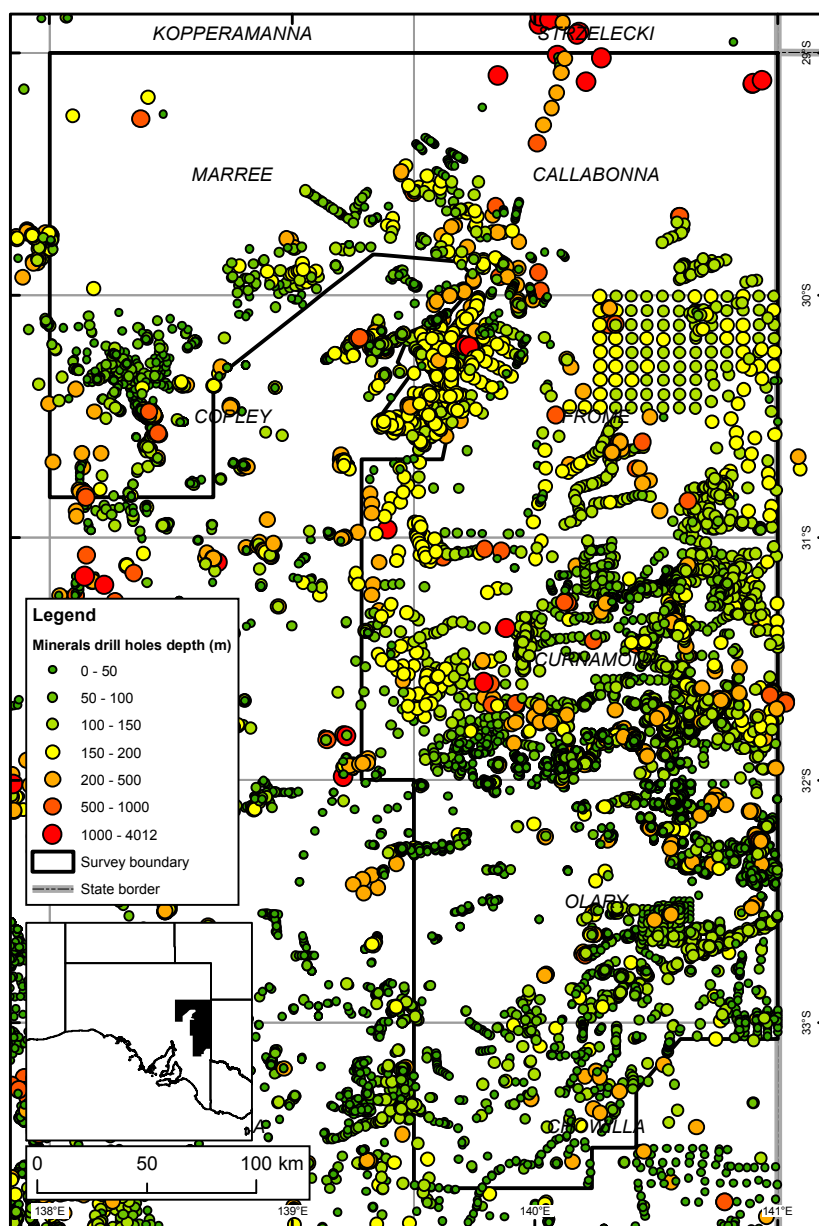


Figure 2.5: Distribution map of publicly-available drill hole data within and adjacent to the Frome AEM Survey area. Data downloaded from SARIG, January 2012.

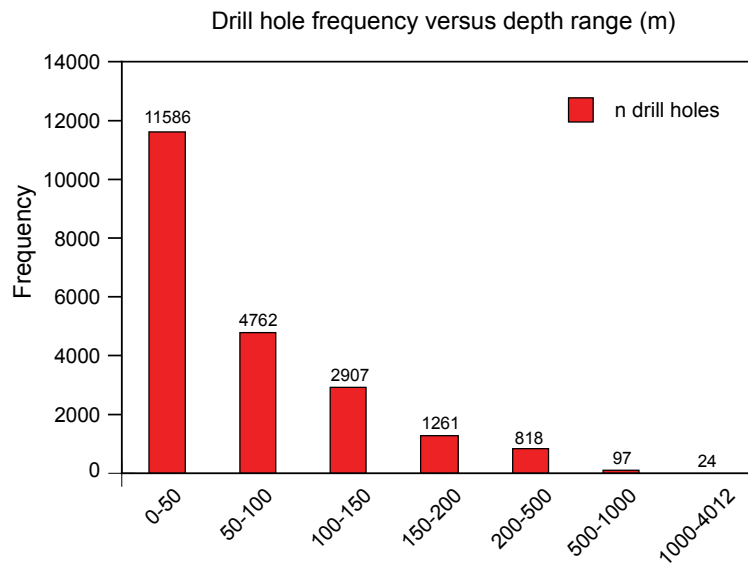


Figure 2.6: Frequency versus depth histogram of all publicly-available drill holes available within and adjacent to the Frome AEM Survey area. Data downloaded from SARIG, January 2012.

2.6 MINERAL EXPLORATION LEASE STATUS BEFORE AND AFTER THE SURVEY

The status of mineral exploration leases before and after the release of Frome AEM Survey data was monitored using data from SARIG. A map of pre- and post-data release mineral exploration lease holdings (Figure 2.7) shows a considerable increase (as of January 2012) since the Frome AEM Survey Phase-1 data were released on 2 November 2010. In September 2010, within the Frome AEM Survey area, mineral exploration lease holdings were approximately 65 414 km², but in January 2012 mineral exploration lease holdings were approximately 79 765 km² within the Frome AEM Survey area, with an additional 9 450 km² of mineral exploration lease applications pending, for a total of 89 215 km². This represents an approximately 36% increase in mineral exploration lease holdings or mineral exploration lease applications between September 2010 and January 2012.

A number of companies have mentioned using the Frome AEM Survey data in their Australian Stock Exchange (ASX) announcements and Quarterly and Annual reports. A compilation of these is listed in Table 2.6.

Table 2.6: Impacts of the Frome AEM Survey on mineral exploration.

COMPANY	COMMODITY	PURPOSE
Energia Minerals Ltd (2011)	U	Frome AEM data helps prioritise drilling program
Callabonna Uranium Ltd (2011)	U	Frome AEM Survey data used to map extensions to known palaeochannels in the Curnamona South area
Core Exploration Ltd (2011)	U	Frome AEM Survey data used to map palaeovalleys near Honeymoon uranium mine
(Renaissance Uranium Ltd, 2011a)	Cu-U	Exploration guided by Frome AEM Survey data, Marree West prospect
Renaissance Uranium Ltd (2011b)	Cu-U	Mapping electromagnetic conductors in a copper-uranium prospect near Farina

The Frome airborne electromagnetic survey, South Australia: implications for energy, minerals and regional geology

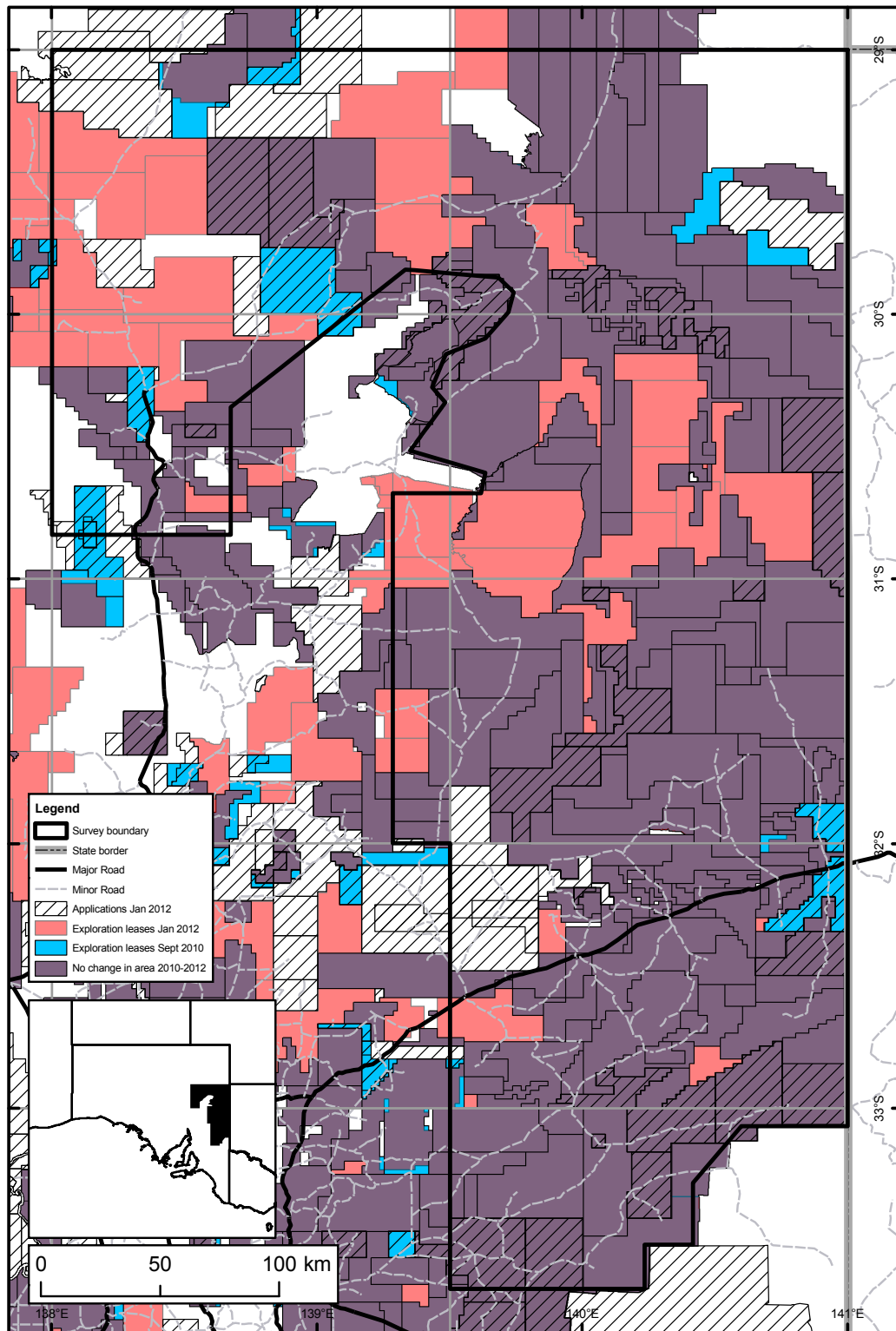


Figure 2.7: Exploration tenement status 2010-2012 over the Frome AEM Survey area. New leases are shown in orange, new applications are shown as oblique hachure. Data from SARIG.

2.7 GEOPHYSICAL MAPPING AND REMOTE SENSING

2.7.1 Airborne geophysics

A diversity of geophysical exploration techniques have been used within the Frome AEM Survey area. There are a range of publicly-available airborne geophysical datasets including detailed and regional magnetics, radiometrics, gravity, AEM and Digital Elevation Models (DEMs). These surveys have been commissioned by mineral exploration companies and state, federal or other government agencies. Publicly-available national airborne magnetic, airborne radiometric and gravity data are held within the Geophysical Archive Data Delivery System (GADDS) at GA and are available for free download through the Australian Geoscience Portal (<http://www.geoscience.gov.au/>). Publicly-available data held within DMITRE, including subsets of the national magnetic, radiometric and gravity data, but also elevation and seismic data, are available for free download through the South Australian Resources Information Geoserver (SARIG; <http://www.pir.sa.gov.au/minerals/sarig>).

Airborne surveys have been flown at a variety of line spacings using a variety of sampling rates, depending on the method and purpose. Company surveys have been flown with nominal line spacings of 100 m, for more detailed resolution, whereas regional state- and commonwealth-funded surveys have been flown with between 800 m and 3000 m line spacings (Percival, 2010a; b). High-resolution airborne surveys have been performed over most, if not all, of the mineral deposits and prospective areas within the Frome AEM Survey area, including the Beverley uranium mine (McConachy *et al.*, 2006).

Between March and December, 2007, GA contracted the Australia-wide airborne geophysical tie-line survey (AWAGS 2), which include parts of the Frome AEM Survey area (Johnson and McKay, 2007). This survey featured a single aircraft acquiring magnetics and radiometrics across the whole continent at 75 km line spacing with 300 km line spacing tie lines. The data were used to level magnetic and radiometric data sets across Australia to produce single, continent-wide magnetic and radiometric data sets. Data included in this report have been levelled according to the results of the AWAGS 2 survey.

Figure 2.8 illustrates the fundamental regional airborne magnetic, airborne radiometric and ground gravity geophysical data sets covering the Frome AEM Survey area. A number of other products are calculated from each data set, including First and Second Vertical Derivative (1VD, 2VD) gravity and magnetics (or variations thereon, including 0.5 and 1.5 VD magnetics) to highlight the rate of change of the potential fields, and various filters to highlight or subdue different wavelengths and directional trends. Radiometric data can also be displayed as single channel (potassium, thorium, uranium), total counts (dose rate), channel ratio (potassium/thorium, thorium/uranium, potassium/uranium) or variants thereon including uranium-squared/thorium (U^2/Th) and residual uranium, which can be used to highlight surface uranium concentrations for uranium prospecting (Mernagh *et al.*, 1998; Wilford *et al.*, 2009).

Other products generated from the regional airborne geophysical data sets include a depth to magnetic basement map (Meixner and Roy, 2010) which estimates the depth of non-magnetic cover to magnetic basement over the entire Gawler Craton and Curnamona Province.

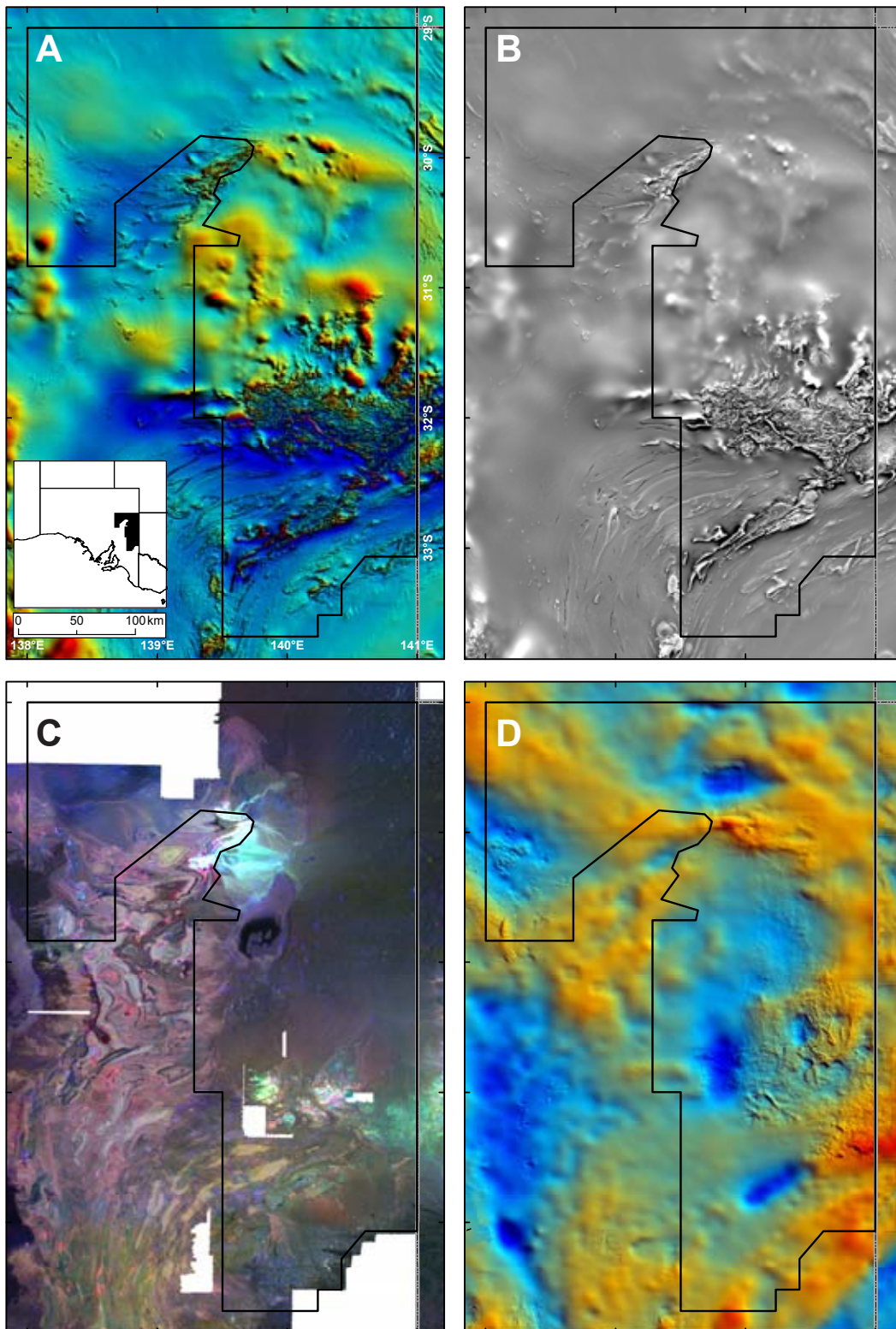


Figure 2.8: Regional geophysical datasets available for the Frome AEM Survey area. A: Sunshaded total magnetic intensity image; B: Sunshaded first vertical derivative of total magnetic intensity image; C: Ternary gamma-ray spectrometric image (KThU:RGB); D: Sunshaded Bouguer gravity anomaly (SA portion courtesy of DMITRE).

The Frome airborne electromagnetic survey, South Australia: implications for energy, minerals and regional geology

A number of AEM surveys have been undertaken within the Frome AEM Survey area, however most of the data are not in the public domain. [Figure 2.9](#) illustrates the results of a SARIG search which indicates that only two public-domain surveys are available: a 1991 BHP Minerals survey (magnetics, GES, TEM); and, a 1996 CRA Exploration survey (QUESTEM™, magnetics). A number of RESOLVE™ AEM surveys were flown along the River Murray further south of the Frome AEM Survey area and are described in reports published by CRC LEME.

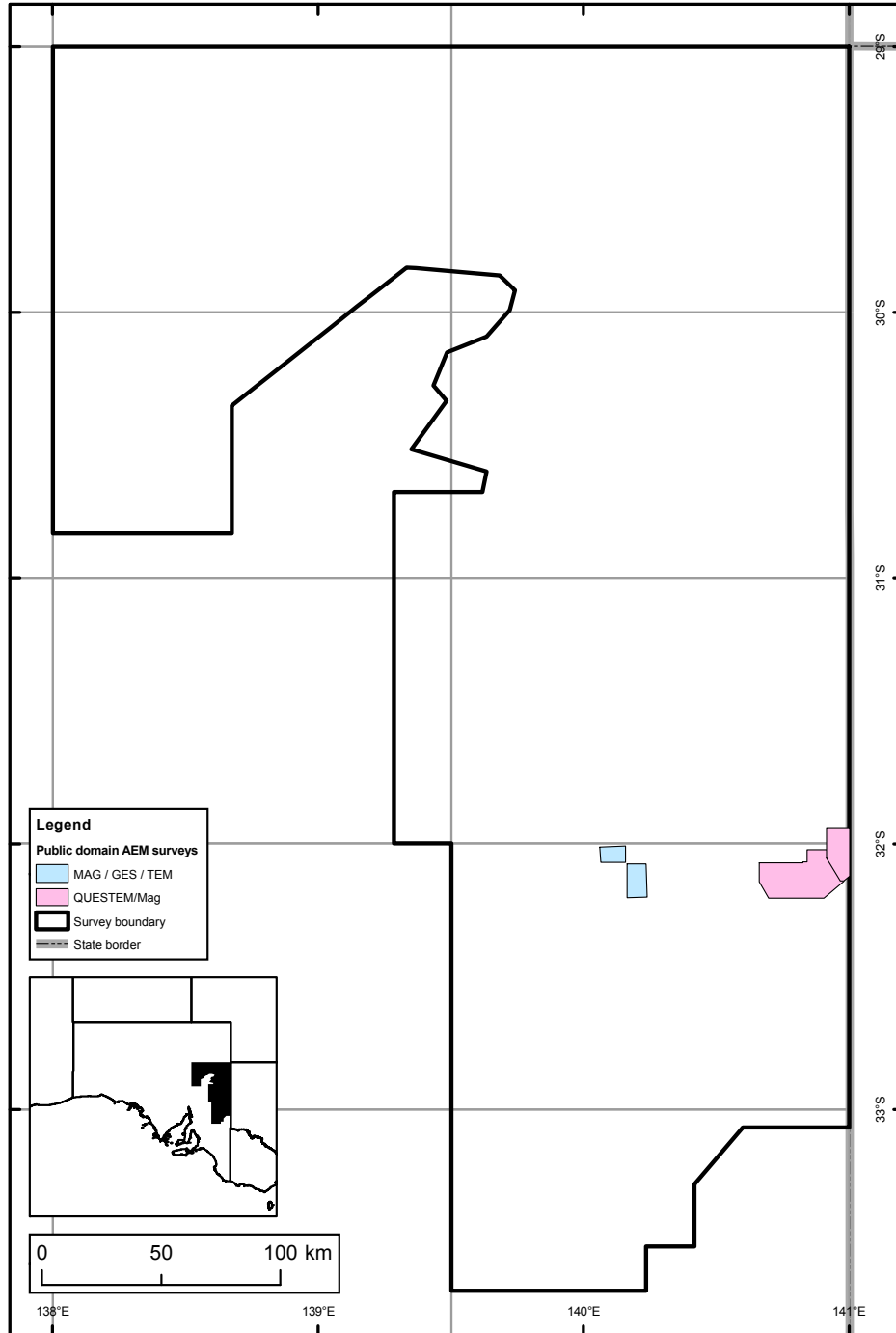


Figure 2.9: Publicly-available AEM survey boundaries for the Frome AEM Survey area.

2.7.2 Seismic and magnetotellurics

Between mid-2008 and early 2009, Geoscience Australia, in conjunction with PIRSA, acquired new deep seismic reflection data in the Frome AEM Survey area using vibroseis sources (Figure 2.10). The Curnamona Line, 262 kilometres in length, runs south to north across the Lake Frome area (08GA-C1) and the Curnamona-Gawler Link line, 144 kilometres in length, which links the Gawler and Curnamona Provinces across the Flinders Ranges (09GA-CG1). The survey transect (03GA-CU1) adjoins the deep crustal seismic transect (96AGS–BH1A), which was carried out across the Broken Hill region in NSW in 1996 using explosion sources.

These seismic lines were recorded to 20 seconds two-way-time and provide information on the crustal architecture of the southern Curnamona Province in both the highly prospective Paleo- and Mesoproterozoic rocks and the overlying Neoproterozoic and Cambrian succession in South Australia. A particular objective was the imaging of the deep crust and major structural features that may have influenced hydrothermal fluid flow, and hence mineralisation (Goleby *et al.*, 2006).

Magnetotelluric data were acquired for Geoscience Australia by contract along the north-south 08GA-C1-Curnamona seismic traverse, where 25 sites were spaced an average of 10 km apart, and five-component broadband data were recorded with a frequency bandwidth of 0.001 Hz to 250 Hz and dipole lengths of 100 m (Milligan and Lilley, 2010).

Numerous seismic reflection surveys were conducted over the decades since the 1960s in search of oil and gas within the Lake Frome area and Murray-Darling Basin, covering the Eromanga Basin and Arrowie Basin, but concentrating principally on the Cooper Basin in the north of the Frome AEM Survey area. These seismic surveys trace the history of the development of Cooper-Eromanga basins oil and gas reserves (Alexander and Sansome, 1996; O'Neill; O'Neill and Alexander, 2006).

Seismic refraction surveys of the area, such as the SKIPPY project (Kennett, 2003) focussed on the crust-mantle boundary and is more useful for interpreting magnetotelluric data.

There are also a wide range of commercial-in-confidence company data covering the area, including AEM, ground EM, magnetics, gravity and radiometrics, which can not be included in this compilation, but were available to GA for this interpretation.

2.7.3 Remote Sensing

The Frome AEM Survey area is covered by a range of remote sensing systems that provide geological, geomorphological and geobotanical information. From the point of view of the Frome AEM Survey, the most important of these is the Space Shuttle Radar Topographic Mission digital elevation model (SRTM DEM) data, which provides full coverage elevation data at 90 m (3 arc second) and 30 m (1 arc second) ground pixel resolution. A smoothed version, the SRTM DEM-S, has been modified to remove spikes, pits and the bulk of vegetation as well as many artefacts introduced during acquisition. The SRTM DEM-S is shown in Figure 3.19.

The SRTM DEM and its derivatives can be processed further to provide slope, aspect and surface drainage vector maps as well as having more advanced calculations such as the multi-resolution valley bottom flatness index (MRVBF) algorithm (Gallant and Dowling, 2003) applied, to highlight areas with low, moderate and high relief for landscape and surface hydrology studies (see Figure 3.20).

The 90 m (3 arc second) SRTM DEM is available for free download from the United States Geological Survey (USGS; <http://dds.cr.usgs.gov/srtm/>), however the 30 m (1 arc second) SRTM DEM is not available to public users. Other elevation data are available through GA at <http://www.ga.gov.au/topographic-mapping/digital-elevation-data.html>

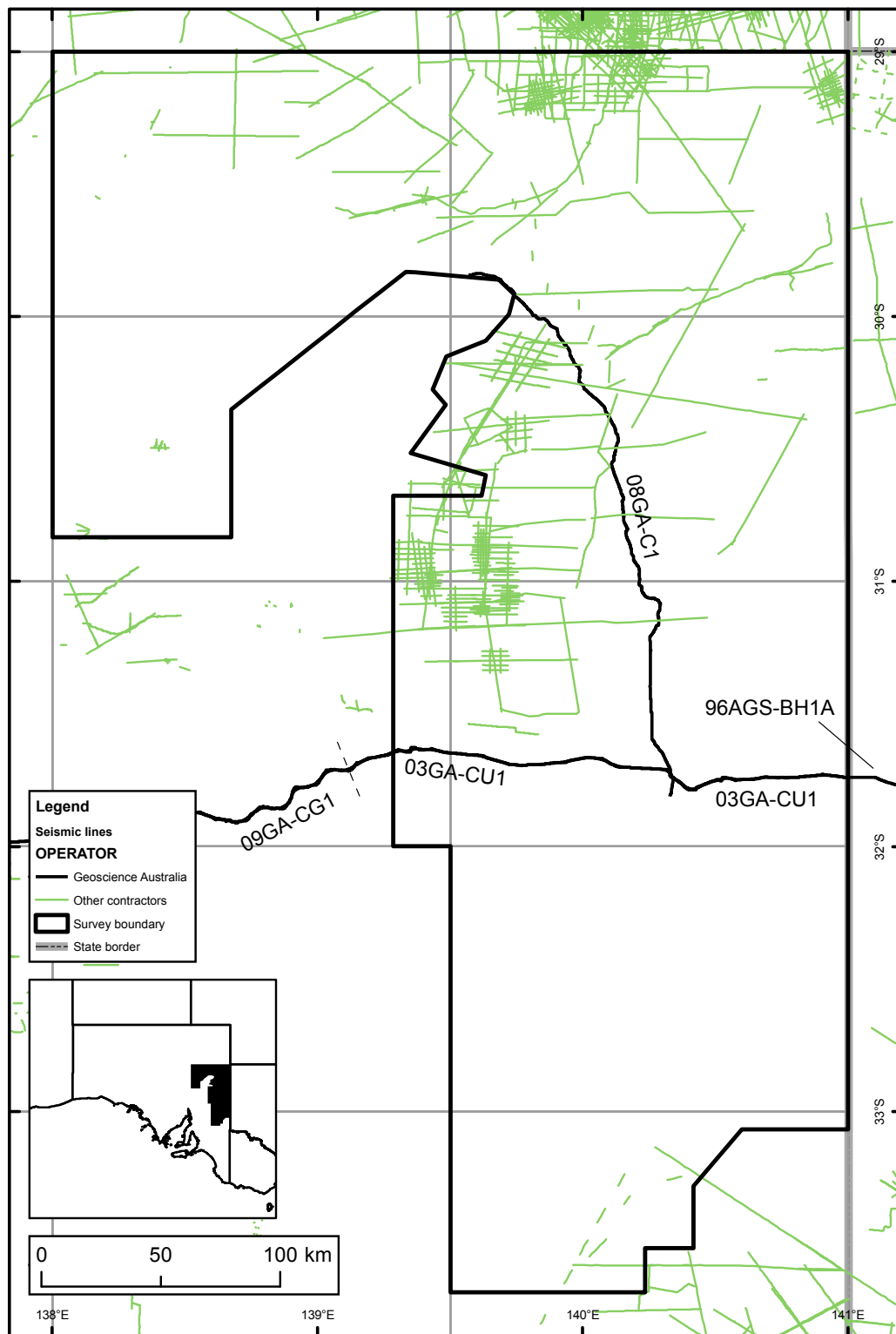


Figure 2.10: Location of seismic lines 08GA-C1 and 03GA-CU1 and associated magnetotelluric data together with undifferentiated industry seismic lines within the Frome AEM Survey area.

2.8 3D MODELS

A number of 3D models described various aspects of the Frome AEM Survey area. These have been derived from studies of seismic reflection data, other geophysical data and drill hole geology, including:

- Curnamona Province model (DMITRE, 2012a)
http://www.pir.sa.gov.au/__data/assets/pdf_file/0009/144549/Curnamona3D.pdf.
- Curnamona sedimentary basin 3D model (DMITRE, 2012b; Fabris *et al.*, 2010):
<ftp://central.pir.sa.gov.au/Minerals/CurnamonaSedimentaryBasin3DGocad.zip>.
<ftp://central.pir.sa.gov.au/Minerals/CurnamonaSedimentaryBasin3DPDF.zip>.
<ftp://central.pir.sa.gov.au/Minerals/CurnamonaSedimentaryBasin3DSourceData.zip>.
- Mount Painter 3D model, as part of the assessment of the mineral prospectivity of the northern Flinders Ranges (Cowley *et al.*, 2009; DMITRE, 2012c):
http://www.pir.sa.gov.au/__data/assets/pdf_file/0008/144548/MtPainter3D.pdf.
- State Model (SA 3D solid geology) (DMITRE, 2012d)
http://www.pir.sa.gov.au/__data/assets/pdf_file/0017/146024/State3DSolidG.pdf.
- Lake Frome area model (Skirrow, 2009):
https://www.ga.gov.au/products/servlet/controller?event=GEOCAT_DETAILS&catno=69697.

A range of products including maps and 3D models derived from seismic reflection studies, drilling and gravity data are also available for the Eromanga Basin and Cooper Basin from GA and DMITRE.

2.9 GROUNDWATER

There is a long history of groundwater investigations in and around the Frome AEM Survey area tied to the development of the South Australian inland regions for cattle grazing, cropping and mineral exploitation. A compilation of the earlier investigations is included in [Table 2.7](#).

Table 2.7: A compilation of early groundwater investigations in the Frome AEM Survey area.

AREA	REFERENCE
Lake Eyre Basin	Jack (1925), Kenny (1934), Ker (1965), Dennis and Lawson (1979)
Eromanga Basin – Great Artesian Basin	Jack (1925), Jack (1930), Kenny (1934), Ker (1965), Shepherd (1978), Dennis and Lawson (1979)
Murray-Darling Basin	Jack (1930), Kenny (1934), Barnes (1951), O’Driscoll (1960), Shepherd (1978), Ludbrook (1961)
Olary Spur	Ker (1965), Shepherd (1978)
Flinders Ranges	Jack (1930), Ker (1965), Shepherd (1978)
Barrier Ranges	Kenny (1934)

More recent research has resulted in a host of programs and publications by various state and federal government agencies, universities, private consultancies and mining companies. Comprehensive assessments of groundwater resources in the region include a review of the groundwater resources of the Lake Eyre Basin (ABARE AGSO and BRS, 1996), a consultants report on the hydrology of the Lake Eyre Basin (McMahon *et al.*, 2005), a technical report on the groundwater assessment of the Northern and Yorke natural resources management region (including parts of the Parachilna and Orroroo 1:250 000 maps sheets) (Alcoe and Berens, 2011), an assessment of the groundwater resources in the Broken Hill region including the Murray-Darling Basin and the Great Australian Basin (Lewis *et al.*, 2008) and numerous publications by the Murray-Darling Basin Authority (Murray-Darling Basin Commission), the New South Wales Department of Primary Industries, the National Water Commission, GA, and the Goyder Institute of South Australia.

There are a range of regional studies on the hydrogeochemistry of groundwater for mineral exploration including a number of studies based on the Curnamona Province and around Broken Hill examining water-rock interactions and the recognition of vectors towards mineralisation using isotopic systems and groundwater flow directions (Caritat and Kirste, 2004; 2005; Caritat *et al.*, 2005; Kirste *et al.*, 2003).

2.10 REFERENCES

- ABARE AGSO and BRS, 1996. Lake Eyre Basin: An Economic and Resource Profile of the South Australian Portion. Australian Bureau of Agricultural and Resource Economics, Canberra. **ABARE Research Report 96.1.**
- Alcoe, D. and Berens, V., 2011. Non-prescribed groundwater resources assessment - Northern and Yorke natural resources management region: Phase 1 - literature and data review. Science, Monitoring and Information Division, Department for Water, Government of South Australia, Adelaide, 92 pp. Online: https://www.waterconnect.sa.gov.au/BusinessUnits/InformationUnit/Technical%20Publications/DFW_TR_2011_17.pdf.
- Alexander, E. M. and Sansome, A., 1996. Lithostratigraphy and environments of deposition. In: Alexander, E. M. and Hibburt, J. E. (editors), Petroleum geology of South Australia Volume 2 - Eromanga Basin. SA Department of Mines and Energy, Adelaide. 49-86 p.
- Alley, N. F., 1977. Discussion: age and origin of laterite and silcrete duricrusts and their relationship to episodic tectonism in the mid-north of South Australia Reply. *Journal of the Geological Society of Australia* **24(7-8)**, 423-425.
- Barnes, T. A., 1951. Underground Water Survey of Portion of the Murray Basin (Counties Albert and Alfred). Geological Survey of South Australia, Department of Mines, Adelaide. **Bulletin No. 25**, 178 pp.
- Bastrakov, E. N., Jaireth, S. and Mernagh, T. P., 2010. Solubility of uranium in hydrothermal fluids at 25° to 300°C: implications for the formation of uranium deposits. Geoscience Australia, Canberra. **Record 2010/29**, 91 pp.
- Bonnett, J. E. and Lindsay, J. M., 1973. Tertiary stratigraphy of three deep bores in the Waikerie area of the Murray Basin. Geological Survey of South Australia, Adelaide. **Report of Investigations 38**.
- Bowler, J. M., 1976. Aridity in Australia: Age, origins and expression in aeolian landforms and sediments. *Earth-Science Reviews* **12(2-3)**, 279-310.
- Bowler, J. M., Kotsonis, A. and Lawrence, C. R., 2006. Environmental evolution of the Mallee region, western Murray Basin. *Proceedings of the Royal Society of Victoria* **118(2)**, 161-210.
- Brown, A. D., 2006. Regolith landforms of Bimbowrie Station. *MESA Journal* **41(April 2006)**, 30-33.
- Brown, A. D. and Hill, S. M., 2003. White Dam - detailed regolith-landform mapping as a tool for refining the interpretation of surface geochemical results. *MESA Journal* **31(October 2003)**, 6-8.
- Brown, A. D. and Hill, S. M., 2004. Regolith-landform maps are an essential tool for interpreting regolith geochemistry: the White Dam, SA, experience. In Roach, I. C. (editor): *Regolith 2004*, Canberra. CRC LEME, 37-41 pp. Online: <http://crcleme.org.au/Pubs/Monographs/regolith2004/Brown&Hill.pdf>.
- Brown, A. D. and Hill, S. M., 2005. White Dam Au-Cu prospect, Curnamona Province, South Australia. In: Butt, C. R. M., Cornelius, M., Scott, K. M. and Robertson, I. D. M. (editors), *Regolith Expression of Australian Ore Systems*. CRC LEME, Perth.
- Brown, A. D., Kernich, A. and Hill, S. M., 2002. Luxemburg Regolith-Landform map. CRC LEME, Perth. Online: http://crcleme.org.au/Pubs/MAPS/luxemburg_2-5k.pdf.
- Brown, C. M., 1985. Murray Basin, southeastern Australia: stratigraphy and resource potential - a synopsis. Bureau of Mineral Resources, Canberra. **Report 264**, 24 pp.
- Brown, C. M. and Stephenson, A. E., 1991. *Geology of the Murray Basin, Southeastern Australia*. Australian Govt. Pub. Service.

- Burt, A. C., 2006. Chapter 8 Kanmantoo Trough. In: Cooper, B. J. and McGeough, M. A. (editors), South Australia Mineral Explorers Guide. 2nd edition. South Australia Department of Primary Industries and Resources, Adelaide. **Mineral Exploration Data Package 11**, 38 p.
- Callabonna Uranium Ltd, 2011. Callabonna Uranium Limited Annual Report 2011. Online: http://www.callabonna.com.au/tasks/sites/cal/assets/File/AnnualReports/2011/CUU_AR2011_web.pdf.
- Callen, R. A., 1977. Late Cainozoic environments of part of northeastern South Australia. Journal of the Geological Society of Australia **24(3)**, 151-169.
- Callen, R. A., 1981. FROME, South Australia, Explanatory Notes, 1:250 000 Geological Series--Sheet SH/54-10. Geological Survey of South Australia, Adelaide, 42 pp.
- Callen, R. A., 1982. Late Tertiary 'grey billy' and the age and origin of surficial silicifications (silcrete) in South Australia. Journal of the Geological Society of Australia **30**, 393-410.
- Callen, R. A., 1986. CURNAMONA Sheet SH 54-14. 1:250 000 Geological Series, Geological Survey of South Australia, Department of Mines and Energy, Adelaide. First Edition.
- Callen, R. A., 1990. 1:250 000 Series—Explanatory Notes, CURNAMONA, South Australia, Sheet SH/54-14 International index. Department of Mines and Energy South Australia, Geological Survey of South Australia, Adelaide, 56 pp.
- Callen, R. A. and Coats, R. P., 1975. FROME Sheet SH 54-10. 1:250 000 Geological Series, Geological Survey of South Australia, Department of Mines, Adelaide. First Edition.
- Callen, R. A. and Tedford, R. H., 1976. New Late Cainozoic rock units and depositional environments, Lake Frome area, South Australia. Transactions of the Royal Society of South Australia **100(3)**, 125-167.
- Caritat, P. d., 2011. National Geochemical Survey of Australia: The Geochemical Atlas of Australia. Geoscience Australia, Canberra. **Record 2011/020**. Online: https://www.ga.gov.au/products/servlet/controller?event=GEOCAT_DETAILS&catno=71973.
- Caritat, P. d. and Kirste, D., 2004. Teilta regolith project: groundwater geochemistry. CRC LEME, Perth. **Open File Report 158**. Online: http://crlceme.org.au/Pubs/OPEN%20FILE%20REPORTS/OFR%20158/CRCLEME_OFR158.pdf.
- Caritat, P. d. and Kirste, D., 2005. Hydrogeochemistry applied to mineral exploration under cover in the Curnamona Province. In, MESA Journal. Adelaide. **37**, 13-17. p.
- Caritat, P. d., Kirste, D., Carr, G. and McCulloch, M., 2005. Groundwater in the Broken Hill region, Australia: recognising interaction with bedrock and mineralisation using S, Sr and Pb isotopes. Applied Geochemistry **20(4)**, 767-787.
- Carr, L. K., Korsch, R. J., Jones, L., Holzscuh, J., Costelloe, R. D., Godsmark, B. and Matthews, C., 2010. Architecture of the Arrowie Basin, South Australia, based on deep seismic reflection data. In: Australian Earth Science Convention, Canberra. Geological Society of Australia, **Abstracts No. 98**(300 pp. Online: <http://www.ga.gov.au/servlet/BigObjFileManager?bigobjid=GA18094>.
- Coats, R. P., 1973. COPLEY South Australia, Explanatory Notes 1:250 000 Geological Series—Sheet SH/54-9. Department of Mines, Geological Survey of South Australia, Adelaide, 38 pp.
- Coats, R. P. and Blissett, A. H., 1971. Regional and economic geology of the Mount Painter Province. Geological Survey of South Australia, Department of Mines, Adelaide. **Bulletin 43**, 417 pp.
- Coats, R. P., Callen, R. A. and Williams, A. F., 1973. COPLEY Sheet SH 54-9. 1:250 000 Geological Series, Geological Survey of South Australia, Department of Mines, Adelaide. First Edition.
- Conor, C. H. H., 2004. Geology of the Olary Domain, Curnamona Province, South Australia. South Australia. Department of Primary Industries and Resources, Adelaide, **Report Book 2004/8**, 86 pp.
- Conor, C. H. H. and Preiss, W. V., 2008. Understanding the 1720-1640 Ma Palaeoproterozoic Willyama Supergroup, Curnamona Province, Southeastern Australia: Implications for tectonics, basin evolution and ore genesis. Precambrian Research **166(1-4)**, 297-317.
- Cooper, B. J. and McGeough, M. A. (editors), 2006. South Australian Mineral Explorers Guide, 2nd Edition. South Australia Department of Primary Industries and Resources, Adelaide. **Mineral Exploration Data Package 11**.
- Core Exploration Ltd, 2011. Projects Overview. Online: <http://coreexploration.com.au/projects>.

- Cowley, W., 2009. State geological map datasets and products, updated data and new projects. Primary Industries and Resources SA, Adelaide. Online:
http://www.pir.sa.gov.au/_data/assets/pdf_file/0007/104200/Cowley_Wayne.pdf.
- Cowley, W. M., 2006. Solid geology of South Australia: peeling away the cover. *MESA Journal* **43(December 2006)**, 4-15.
- Cowley, W. M. and Barnett, S. R., 2007. Revision of Oligocene-Miocene Murray Group stratigraphy for geological and groundwater studies in South Australia. *MESA Journal* **47**, 17-20.
- Cowley, W. M., Hore, S. B., Preiss, W. V., Sheard, M. J. and Wade, C. E., 2011. A revised stratigraphic scheme for the Mount Painter and Mount Babbage inliers. In: Forbes, C. J. (editor): 2011 Sprigg Symposium: Unravelling the northern Flinders Ranges, University of Adelaide. Geological Society of Australia **Abstracts No. 100**, 11-17 pp.
- Cowley, W. M., Katona, L. F. and Gouthas, G., 2009. Assessment of mineral prospectivity of the northern Flinders Ranges using GIS analysis. Primary Industries and Resources South Australia, Adelaide, **Report Book 2009/19**, 102 pp.
- Crooks, A. and Hill, P., 2008. Mingary 7033. Department of Primary Industries and Resources SA, Adelaide. Online:
http://www.pir.sa.gov.au/_data/assets/pdf_file/0016/132550/MINGARY_REGOLITH.pdf.
- Cross, A., Jaireth, S., Hore, S. B., Michaelsen, B. and Schofield, A., 2010. SHRIMP U-Pb detrital zircon results, Lake Frome region, South Australia. Geoscience Australia, Canberra. **Record 2010/46**, 28 pp.
- Davey, J. E., 2009. Tectonostratigraphic Evolution of an Intracontinental Terrain: The Geological Evolution of the Frome Embayment, Eromanga Basin, South Australia. CRC LEME, School of Earth and Environmental Sciences, Geology and Geophysics and Australian School of Petroleum, University of Adelaide. PhD thesis, unpublished.
- Davey, J. E., McAvaney, D. J. and Hill, S. M., 2010. Parabarana, northern Flinders Ranges, Australia. In: Davey, J.E. Mesozoic palaeolandscape reconstruction, southern Eromanga Basin margins. University of Adelaide PhD thesis. Online:
http://crlceme.org.au/Pubs/MAPS/parabarana_25k.pdf.
- Dawson, M. W., 2000. The geology of the Kalkaroo area. School of Environmental and Rural Science, University of New England, Armidale, NSW. BSc Honours thesis, unpublished.
- Dennis, K. J. and Lawson, J., 1979. Callabonna 1:250 000 sheet water well survey. Geological Survey Engineering Division, Department of Mines and Energy South Australia, Adelaide. **Report Book No. 79/13**, 24 pp.
- Dickinson, S. B., Sprigg, R. C., King, D., Wade, M. L., Webb, B. P. and Whittle, A. W. G., 1954. Uranium deposits in South Australia. Geological Survey of South Australia, Department of Mines, Adelaide. **Bulletin No. 30**, 183 pp.
- DMITRE, 2012a. Curnamona Province. Online:
http://www.pir.sa.gov.au/minerals/geology/3d_geological_models/curnamona_province.
- DMITRE, 2012b. Curnamona Sedimentary Basin Model. Online:
http://www.pir.sa.gov.au/minerals/geology/3d_geological_models/curnamona_sedimentary_basin_model#model.
- DMITRE, 2012c. Mount Painter Model. Online:
http://www.pir.sa.gov.au/minerals/geology/3d_geological_models/mt_painter.
- DMITRE, 2012d. State Model. Online:
http://www.pir.sa.gov.au/minerals/geology/3d_geological_models/state.
- Drexel, J. F. and Preiss, W. V. (editors), 1995. The Geology of South Australia: Volume 2, The Phanerozoic. **Bulletin 54(2)**, 357 pp.
- Drexel, J. F., Preiss, W. V. and Parker, A. J. (editors), 1993. The Geology of South Australia: Volume 1, The Precambrian. **Bulletin 54(1)**, 249 pp.
- Dubieniecki, C. D. and Hill, S. M., 2007. Constraints on the Four Mile uranium mineralisation, resulting from neo-tectonic activity in the northern Flinders Ranges, SA. In Cooper, B. J. and Keeling, J. L. (editors): 5th Sprigg Symposium, Adelaide. Geological Society of Australia, **Abstracts Number 87**(15-18 pp).

- Energia Minerals Ltd, 2011. Quarterly Report September 2011. Online:
<http://www.energiaminerals.com/files/20111014-ANN-Quarterly%20Sept%202011.pdf>.
- Fabris, A. J., 2002. Northwestern Murray Basin - stratigraphy, sedimentology and geomorphology. *MESA Journal* **27**, 20-24.
- Fabris, A. J., 2003a. North-western Murray Basin geological synthesis, South Australia. South Australia, Department of Primary Industries and Resources. **Report Book 2003/13**, 81 pp.
- Fabris, A. J., 2003b. Northwestern Murray Basin - revised interpretation from recent drilling and aeromagnetism. *MESA Journal* **30**, 39-45.
- Fabris, A. J., 2008. Southern Curnamona Province, regolith tour guide. Primary Industries and Resources South Australia, Adelaide. **Report Book 2008/9**, 35 pp.
- Fabris, A. J., Gouthas, G. and Fairclough, M. C., 2010. The new 3D sedimentary basin model of the Curnamona Province: geological overview and exploration implications. *MESA Journal* **58(September 2010)**, 16-24.
- Fabris, A. J., Sheard, M. J., Keeling, J. L., Hill, S. M., McQueen, K. G., Connor, C. H. H. and Caritat, P. d., 2008. A guide for mineral exploration through the regolith in the Curnamona Province, South Australia. Cooperative Research Centre for Landscape Environments and Mineral Exploration, Perth, WA. 150 pp.
- Firman, J. B., 1973. Regional stratigraphy of surficial deposits in the Murray Basin and Gambier Embayment. Geological Survey of South Australia. **Report of Investigations 39**, 68 pp.
- Fitzpatrick, R. W. and Shand, P. (editors), 2006. Regolith 2006: Consolidation and Dispersion of Ideas. CRC LEME, Perth. 386 pp.
- Fitzsimmons, K. E., 2005. From little things big things grow: reconstructing past environments from Quaternary desert dune sediments and stratigraphy. In Roach, I. C. (editor): Regolith 2005: Ten Years of CRC LEME, Canberra, Adelaide. CRC LEME, 102-106 pp. Online:
<http://crlceme.org.au/Pubs/Monographs/regolith2005/Fitzsimmons.pdf>.
- Fitzsimmons, K. E., 2007. The Late Quaternary history of aridity in the Strzelecki and Tirari desert dunefields, South Australia. CRC LEME, Department of geology, Australian National University, Canberra. PhD thesis, unpublished.
- Fitzsimmons, K. E., Rhodes, E. J., Magee, J. W. and Barrows, T. T., 2007. The timing of linear dune activity in the Strzelecki and Tirari Deserts, Australia. *Quaternary Science Reviews* **26(19-21)**, 2598-2616.
- Forbes, B. G., 1989. OLARY Sheet SI 54-2. 1:250 000 Geological Series, Geological Survey of South Australia, Department of Mines and Energy, Adelaide. First Edition.
- Forbes, B. G., 1991. 1:250 000 Geological Series--Explanatory Notes, OLARY, South Australia, Sheet SI 54-2 International Index. Geological Survey of South Australia, Department of Mines, Adelaide, 47 pp.
- Forbes, B. G., Coats, R. P., Webb, B. P. and Horwitz, R. C., 1965. MARREE Sheet H 54-5. 1:250 000 Geological Series, Geological Survey of South Australia, Department of Mines, Adelaide. First Edition.
- Foster, D. A., Murphy, J. M. and Gleadow, A. J. W., 1994. Middle Tertiary hydrothermal activity and uplift of the northern Flinders Ranges, South Australia: insights from apatite fission track thermochronology. *Australian Journal of Earth Sciences* **41**, 11-17.
- Fraser, G. L., Huston, D. L., Gibson, G. M., Neumann, N. L., Maidment, D., Kositcin, N., Skirrow, R. G., Jaireth, S., Lyons, P., Carson, C., Cutten, H. and Lambeck, A., 2007. Geodynamic and metallogenic evolution of Proterozoic Australia from 1870-1550 Ma; a discussion. *Geoscience Australia, Canberra. Record 2007/16*, 76 pp.
- Fraser, G. L. and Neumann, N. L., 2010. New SHRIMP U-Pb zircon ages from the Gawler Craton and Curnamona Province, South Australia, 2008-2010. *Geoscience Australia, Canberra. Record 2010/16*, 265 pp.
- Fricke, C., 2008. Definitions of Mesoproterozoic igneous rocks of the Curnamona Province: The Ninnerie Supersuite. Primary Industries and Resources South Australia, Adelaide. **Report Book 2008/4**, 86 pp.

- Fricke, C. E. and Hore, S., 2010. Definition of the Mesoproterozoic Ninnerie Supersuite, Curnamona Province, South Australia. Department of Primary Industries and Resources South Australia, Adelaide. **Report Book 2010/20**, 55 pp.
- Gallant, J. C. and Dowling, T. I., 2003. A multiresolution index of valley bottom flatness for mapping depositional areas. *Water Resource Research* **39**(12), 1347-1359.
- Gardner, G. J., Mortlock, A. J., Price, D. M., Readhead, M. L. and Wasson, R. J., 1987. Thermoluminescence and radiocarbon dating of Australian desert dunes. *Australian Journal of Earth Sciences* **34**(3), 343-357.
- Geoscience Australia, 2010. Australia's identified mineral resources 2010. Geoscience Australia, Canberra, 114 pp.
- Gibson, D. L., 1999. Explanatory notes for the Broken Hill and Curnamona Province 1:500 000 regolith landform maps. CRC LEME, Perth. **Open File Report 77**, 59 pp.
- Gibson, D. L., 2004. North Barrier Ranges region. In: Anand, R. R. and de Broekert, P. (editors), *Regolith Landscape Evolution Across Australia*. CRC LEME, Perth. 96-100 p. Online: <http://crcleme.org.au/RegLandEvol/NthBarrierRanges.pdf>.
- Goleby, B. R., Korsch, R. J., Fomin, T., Connor, C. C. H., Preiss, W. V., Robertson, R. S. and Burt, A. C., 2006. The 2003-2004 Curnamona Province seismic survey: Workshop notes. Geoscience Australia, Canberra. **Record 2006/12**, 96 pp.
- Hill, S. M., 2000. The regolith and landscape evolution of the Broken Hill Block. CRC LEME, Department of Geology, Australian National University, Canberra. PhD thesis, unpublished.
- Hill, S. M., 2004a. Regolith and landscape evolution of far western New South Wales. In: Anand, R. R. and de Broekert, P. (editors), *Regolith Landscape Evolution Across Australia*. CRC LEME, Perth. Online: <http://www.crcleme.org.au/RegLandEvol/Far%20Western%20NSW.pdf>.
- Hill, S. M., 2004b. Teilita, western New South Wales. In: Anand, R. R. and de Broekert, P. (editors), *Regolith landscape evolution across Australia*. CRC LEME, Perth. 110-117 p. Online: <http://www.crcleme.org.au/RegLandEvol/Teilita%20Western%20NSW.pdf>.
- Hill, S. M., West, D. S., Shirliff, G., Senior, A. B., Maly, B. E. R., Jones, G. L., Holzapfel, M., Foster, K. A., Debenham, S. C., Dann, R. and Brachmanis, J., 2004. Southern Barrier Ranges – Northern Murray Basin. In: Anand, R. R. and de Broekert, P. (editors), *Regolith Landscape Evolution Across Australia*. CRC LEME, Perth. 104-109 p. Online: <http://www.crcleme.org.au/RegLandEvol/SthBarrierRanges.PDF>.
- Hou, B., Fabris, A. J. and Rogers, P. A., 2006. Chapter 13 Cainozoic basins and channels. In: Cooper, B. J. and McGeough, M. A. (editors), *South Australia Mineral Explorers Guide*. 2nd edition. South Australia Department of Primary Industries and Resources, Adelaide. **Mineral Exploration Data Package 11**, 5 p.
- Hou, B., Zang, W., Fabris, A., Keeling, J., Stoian, L. and Fairclough, M., 2007. Palaeodrainage and coastal barriers of South Australia 1:2 000 000. CRC LEME, Geological Survey Branch, Primary Industries and Resources South Australia, Adelaide. Online: http://www.pir.sa.gov.au/_data/assets/pdf_file/0005/41486/palaeochannels_sa_map.pdf.
- Hughes, F. E. (editor) 1990. *Geology of the mineral Deposits of Australia and New Guinea*. Australasian Institute of Mining and Metallurgy, Melbourne.
- Huston, D. L., Stevens, B., Southgate, P. N., Muhling, P. and Wyborn, L., 2006. Australian Zn-Pb-Ag Ore-Forming Systems: A Review and Analysis. *Economic Geology* **101**(6), 1117-1157.
- Huston, D. L. and van der Wielen, S. E. (editors), 2011. An assessment of the uranium and geothermal prospectivity of east-central South Australia. Geoscience Australia, Canberra. **Record 2011/34**, 229 pp.
- Jack, R. L., 1925. Some developments in shallow water areas in the north-east of South Australia. Geological Survey of South Australia, Department of Mines, Adelaide. **Bulletin No. 11**, 70 pp.
- Jack, R. L., 1930. Geological Structure and other Factors in Relation to Underground Water Supply in Portion of South Australia. Geological Survey of South Australia, Department of Mines, Adelaide. **Bulletin No. 14**, 53 pp.
- Johns, R. K., 1972. Base metal occurrences within Lower Cambrian sediments of the northern Flinders Ranges. Geological Survey of South Australia, Adelaide. **Report of Investigations 37**, 67 pp.

- Johnson, J. and McKay, W., 2007. Flight to find new energy resources. In, AUSGEO news. Geoscience Australia. **88 Dec 2007**, 3-5 p.
- Kennett, B. L. N., 2003. Seismic structure in the mantle beneath Australia. In: Hillis, R. R. and Muller, R. D. (editors), Evolution and dynamics of the Australian plate. Geological Society of Australia Special Publication 22 and Geological Society of America Special Publication 372. 7-23 p.
- Kenny, E. J., 1934. West Darling District: A Geological Reconnaissance with Special Reference to the Resources of Subsurface Water. New South Wales Department of Mines Geological Survey, Sydney. **Mineral Resources No. 36**, 194 pp.
- Ker, D. S., 1965. Hydrology of the Frome Embayment in South Australia. Geological Survey of South Australia, Adelaide, **Report of Investigations No. 27**, 98 pp.
- Kernich, A., 2002. Weathering, erosion and element mobilisation in a catchment at the Luxemberg Copper/Gold site, Olary Domain, South Australia. School of Earth and Environmental Sciences, University of Adelaide. BSc Honours thesis, unpublished.
- Kirste, D., Caritat, P. d. and Dann, R., 2003. The application of the stable isotopes of sulfur and oxygen in groundwater sulfate to mineral exploration in the Broken Hill region of Australia. Journal of Geochemical Exploration **78-79(May 2003)**, 81-84.
- Korsch, R. J. and Kositsin, N. (editors), 2010. South Australian Seismic and MT Workshop 2010. Geoscience Australia, Canberra. 124 pp.
- Kositsin, N. (editor) 2010. Geodynamic synthesis of the Gawler Craton and Curnamona Province. Geoscience Australia, Canberra **Record 2010/27**.
- Krapf, C., in prep. 1 000 000 scale regolith-landform map of South Australia. DMITRE.
- Lau, I., 2004a. Regolith-landform and mineralogical mapping of the White Dam Prospect, eastern Olary Domain, South Australia, using integrated remote sensing and spectral techniques. CRC LEME, School of Earth and Environmental Science, University of Adelaide. PhD thesis, unpublished.
- Lau, I., 2004b. White Dam South Australia. CRC LEME, Adelaide. Online: http://crleme.org.au/Pubs/MAPS/white_dam_30k.pdf.
- Lau, I., Heinson, G. S. and Hill, S. M., 2004. Explanatory notes for the 1:30,000 regolith-landform map of White Dam, Olary Domain, South Australia. In Roach, I. C. (editor): Regolith 2004, Canberra. CRC LEME, 188-193 pp.
- Lawie, D. C., 2001. Exploration geochemistry and regolith geology over the northern part of the Olary Domain, South Australia. School of Environmental and Rural Science, University of New England, Armidale NSW. PhD thesis, unpublished.
- Lewis, S. J., Roberts, J., Brodie, R. S., Gow, L., Kilgour, P., Ransley, T., Coram, J. E. and Sundaram, B., 2008. Assessment of groundwater resources in the Broken Hill region. Geoscience Australia, Canberra. **Professional Opinion 2008/05**. Online: <http://www.environment.gov.au/water/publications/environmental/groundwater/pubs/broken-hill.pdf>.
- Lomax, J., Hilgers, A., Wopfner, H., Grün, R., Twidale, C. R. and Radtke, U., 2003. The onset of dune formation in the Strzelecki Desert, South Australia. Quaternary Science Reviews **22(10-13)**, 1067-1076.
- Ludbrook, N. H., 1961. Stratigraphy of the Murray Basin in South Australia. Geological Survey of South Australia, Department of Mines, Adelaide. **Bulletin No. 36**, 117 pp.
- Ludbrook, N. H., 1966. Cretaceous Biostratigraphy of the Great Artesian Basin on South Australia. Geological Survey of South Australia, Department of Mines, Adelaide. **Bulletin No. 40**, 268 pp.
- Ludbrook, N. H. and Johns, R. K., 1963. Investigation of Lake Eyre. Part 1, The sediments of the Lake Eyre Basin, evaporites and brines, their constitution and age. Part 2, Subsurface stratigraphy. Geological Survey of South Australia, South Australia Department of Mines, Adelaide. **Report of Investigations 24**, 104 pp.
- Marshak, S. and Flöttmann, T., 1996. Structure and origin of the Fleurieu and Nackara Arcs in the Adelaide fold-thrust belt, South Australia: Salient and recess development in the Delamerian Orogen. Journal of Structural Geology **18(7)**, 891-908.
- McConachy, G., McInnes, D. and Paine, J., 2006. Airborne electromagnetic signature of the Beverley uranium deposit, South Australia. SEG Technical Program Expanded Abstracts **25(1)**, 790-794.

- McKay, A. D. and Mieзитis, Y., 2001. Australia's uranium resources, geology and development of deposits. Mineral Resource Report, AGSO - Geoscience Australia, Canberra. **Mineral Resource Report 1, 1**, 200 pp.
- McMahon, T. A., Murphy, R., Little, P., Costelloe, J. F., Peel, M. C., Chiew, F. H. S., Hayes, S., Nathan, R. and Kandel, D. D., 2005. Hydrology of the Lake Eyre Basin. Sinclair Knight Merz, Malvern, Vic., 131 pp. Online: <http://www.lebmf.gov.au/publications/pubs/hydrology.pdf>.
- Meixner, A. J. and Roy, I. G., 2010. Depth to magnetic basement map of the Gawler-Curnamona region, South Australia. First Edition. Online: http://intranet.ga.gov.au:88/nas/cds/open/maps/geophysical/70594/D2B_Gawler_Curnamona.pdf.
- Mernagh, T. P., Wyborn, L. A. I. and Jagodzinski, E. A., 1998. 'Unconformity-related' U +/- Au +/- platinum-group-element deposits. AGSO Journal of Australian Geology and Geophysics **17(4)**, 197-205.
- Milligan, P. R. and Lilley, F. E. M., 2010. Magnetotelluric results along the N-S Curnamona seismic traverse to the east of Lake Frome, South Australia. ASEG Extended Abstracts **2010(1)**, 1-4.
- Milnes, A. R. and Twidale, C. R., 1983. An overview of silicification in Cainozoic landscapes of arid central and southern Australia. Australian Journal of Soil Research **21**, 387-410.
- Mitchell, M. M., Kohn, B. P., O'Sullivan, P. B., Hartley, M. J. and Foster, D. A., 2002. Low-temperature thermochronology of the Mt Painter Province, South Australia. Australian Journal of Earth Sciences **49**, 551-563.
- Morris, B. J. and Horn, C. M., 1990. Review of gold mineralisation in the Nackara Arc. Mines and Energy Review, South Australia, 51-58 pp.
- Neumann, N. L. and Fraser, G. L. (editors), 2007. Geochronological synthesis and Time-Space plots for Proterozoic Australia. Geoscience Australia, Canberra. **2007/06**, 216 pp.
- Northcote, K. H., 1979. A Factual Key for the Recognition of Australian Soils. 4th Edition. Rellim Technical Publishers, Glenside, South Australia.
- Northcote, K. H., Beckmann, G. G., Bettenay, E., Churchward, H. M., Van Dijk, D. C., Dimmock, G. M., Hubble, G. D., Isbell, R. F., McArthur, W. M., Murtha, G. G., Nicolls, K. D., Paton, T. R., Thompson, C. H., Webb, A. A. and Wright, M. J., 1960-1968. Atlas of Australian Soils, Sheets 1 to 10. With explanatory data. CSIRO and Melbourne University Press, Melbourne. Online: http://www.asris.csiro.au/themes/Atlas.html#Atlas_Downloads.
- O'Driscoll, E. P. D., 1960. The Hydrology of the Murray Basin Province in South Australia. Geological Survey of South Australia, Department of Mines, Adelaide. **Bulletin No. 35**, 173 pp.
- O'Neill, B. J., History of petroleum exploration and development. In: Gravestock, D. I., Hibbert, J. E. and Drexel, J. F. (editors), Petroleum geology of South Australia volume 4: Cooper Basin. Primary Industries and Resources South Australia, Adelaide. 7-36 p.
- O'Neill, B. J. and Alexander, E. M., 2006. History of petroleum exploration and development. In: Cotton, T. B., Scardigno, M. F. and Hibbert, J. E. (editors), The petroleum geology of South Australia Volume 2: Eromanga Basin. Primary Industries and Resources SA.
- Page, R. W., Conor, C. H. H., Stevens, B. P. J., Gibson, G. M., Preiss, W. V. and Southgate, P. N., 2005. Correlation of Olary and Broken Hill Domains, Curnamona Province: Possible Relationship to Mount Isa and Other North Australian Pb-Zn-Ag-Bearing Successions. Economic Geology **100(4)**, 663-676.
- Percival, P., 2010a. Gamma-ray data acquisition by Geoscience Australia & States map. Online: http://www.ga.gov.au/image_cache/GA17484.pdf.
- Percival, P., 2010b. Index of airborne geophysical surveys. Geoscience Australia, Canberra. **Record 2010/013**. Online: https://www.ga.gov.au/products/servlet/controller?event=GEOCAT_DETAILS&catno=70295.
- Preiss, W. V., 1987. The Adelaide Geosyncline. Late Proterozoic Stratigraphy, Sedimentation, Palaeontology and Tectonics. Geological Survey of South Australia, Department of Mines and Energy, Adelaide. **Bulletin 53**, 441 pp.
- Preiss, W. V., 1999. 1:250 000 Geological Series--Explanatory Notes, PARACHILNA, South Australia, Sheet SH54-13 International Index, Second Edition. Primary Industries and Resources SA, Geological Survey of South Australia, Adelaide, 52 pp.

- Quigley, M., Sandiford, M., Fifield, K. and Alimanovic, A., 2007. Bedrock erosion and relief production in the northern Flinders Ranges. *Earth Surfaces Processes and Landforms* **32**, 929-944.
- Raymond, O. L., 2010. Surface geology of Australia, 1:1,000,000 scale, 2010 edition. Geoscience Australia, Canberra. Online: https://www.ga.gov.au/products/servlet/controller?event=GEOCAT_DETAILS&catno=70311.
- Reid, P. and Preiss, W. V., 1999. PARACHILNA Sheet SH 54-13. 1:250 000 Geological Series, Geological Survey of South Australia, Department of Primary Industries and Resources SA, Adelaide. Second Edition.
- Renaissance Uranium Ltd, 2011a. ASX Announcement: MArree and Gairdner exploration leases granted. Online: http://www.renaissanceuranium.com.au/_literature_45834/Marree_and_Gairdner_Exploration_Leases_Granted.
- Renaissance Uranium Ltd, 2011b. ASX Announcement: Prominent electromagnetic conductors identified over historic mine in copper-uranium Farina project. Online: http://www.renaissanceuranium.com.au/_literature_49631/Prominent_EM_Conductors_in_Farina_Project.
- Roach, I. C. (editor) 2002. Regolith and landscapes in Eastern Australia. CRC LEME, Canberra. 136 pp.
- Roach, I. C. (editor) 2003. Advances in Regolith. CRC LEME, Canberra. 446 pp.
- Roach, I. C. (editor) 2004. Regolith 2004. CRC LEME, Canberra. 420 pp.
- Roach, I. C. (editor) 2005. Regolith 2005 - Ten Years of CRC LEME. CRC LEME, Canberra. 345 pp.
- Roach, I. C. (editor) 2010. Geological and energy implications of the Paterson Province airborne electromagnetic (AEM) survey, Western Australia. Geoscience Australia, Canberra. **Geoscience Australia Record 2010/12**, 318 pp.
- Rogers, P. A., 1977. CHOWILLA Sheet SI 54-6. 1:250 000 Geological Series, Geological Survey of South Australia, Department of Mines, Adelaide. First Edition.
- Rogers, P. A., 1978. 1:250 000 Geological Series – Explanatory Notes, CHOWILLA South Australia, Sheet SI/54-6 International Index. Department of Mines and Energy, State of South Australia, Geological Survey of South Australia, Adelaide, 25 pp.
- Roy, P. S., Whitehouse, J., Cowell, P. J. and Oakes, G., 2000. Mineral Sands Occurrences in the Murray Basin, Southeastern Australia. *Economic Geology* **95(5)**, 1107-1128.
- Schofield, A., 2009. Uranium content of igneous rocks of Australia 1:5 000 000 maps - Explanatory notes and discussion. Geoscience Australia Record, Geoscience Australia, Canberra. **Record 2009/17**, 20 pp.
- Schofield, A., 2010. Potential for magmatic-related uranium mineral systems in Australia. Geoscience Australia, Canberra. **Record 2010/20**, 61 pp.
- Schofield, A., 2012. Uranium systems processes in the Crocker Well Suite, South Australia. Geoscience Australia, Canberra. **Record 2011/45**, 39 pp. Online: https://www.ga.gov.au/products/servlet/controller?event=GEOCAT_DETAILS&catno=72058.
- Sheard, M. J., 2008. Northern Curnamona Province, regolith exposures, tour guide. Primary Industries and Resources South Australia, Adelaide. **Report Book 2008/8**, 26 pp.
- Sheard, M. J., 2009. Explanatory notes for CALLABONNA 1:250 000 Geological Map, sheet SH 54-6. Division of Minerals and Energy Resources, Primary Industries and Resources South Australia, Adelaide, 204 pp.
- Sheard, M. J. and Callen, R. A., 2000. CALLABONNA Sheet SH 54-8. 1:250 000 Geological Series, South Australia Geological Survey, Adelaide. First Edition.
- Shepherd, R. G., 1978. Underground water resources of South Australia. Geological Survey of South Australia, Adelaide, **Bulletin 48**, 67 pp.
- Skirrow, R. G. (editor) 2009. Uranium ore-forming systems of the Lake Frome Region, South Australia: Regional spatial controls and exploration criteria. Geoscience Australia, Canberra. **Record 2009/40**, 151 pp.
- Skirrow, R. G. (editor) 2011. Uranium mineralisation events in Australia. Geoscience Australia, Canberra. **Record 2011/12**, 90 pp.

- Skirrow, R. G., Jaireth, S., Huston, D. L., Bastrakov, E. N., Schofield, A., van der Wielen, S. E. and Barnicoat, A. C., 2009. Uranium mineral systems: processes, exploration criteria and a new deposit framework. Geoscience Australia, Canberra. **Record 2009/20**, 44 pp.
- Skwarnecki, M. S. and Lintern, M. J., 2005. Blue Rose Au-Cu prospect, South Australia. In: Butt, C. R. M., Robertson, I. D. M., Scott, K. M. and Cornelius, M. (editors), Regolith expression of Australian ore systems. CRC LEME, Perth. 359-361 p.
- Skwarnecki, M. S., Shu, L. and Lintern, M. J., 2001. Geochemical dispersion in the Olary district, South Australia: investigations at Faugh-a-balagh Prospect, Olary Silver Mine, Wadnaminga Goldfield and Blue Rose Prospect. CRC LEME, Perth. **Open File Report 113**, 78 pp.
- Sprigg, R. C., 1979. Stranded and submerged sea-beach systems of southeast South Australia and the aeolian desert cycle. *Sedimentary Geology* **22**, 53-96.
- Stewart, R. (editor) 1999. Murray Basin Mineral Sands Conference. Extended Abstracts. Australian Institute of Geoscientists, Victoria Park WA. **Bulletin No. 26**, 259 pp.
- van der Wielen, S. E., Kirkby, A., Britt, A., Schofield, A., Bastrakov, E., Cross, A., Nicoll, M., Mernagh, T. and Barnicoat, A. C., 2009. Large-scale exploration targeting for uranium mineral systems within the Eromanga Basin. In: Society for Geology Applied to Mineral Deposits.
- Wade, C. E., 2011. Definition of the Mesoproterozoic Ninnerie Supersuite, Curnamona Province, South Australia. *MESA Journal* **62**, 25-42.
- Wasson, R. J., 1979. Sedimentation history of the Mundi Mundi alluvial fans, Western New South Wales. *Sedimentary Geology* **22(1-2)**, 21-51.
- Wasson, R. J., Fitchett, K., Mackey, B. and Hyde, R., 1988. Large-scale patterns of dune type, spacing and orientation in the Australian continental dunefield. *Australian Geographer* **19(1)**, 89-104.
- Wasson, R. J. and Galloway, R. W., 1986. Sediment Yield in the Barrier Range Before and After European Settlement. *The Rangeland Journal* **8(2)**, 79-90.
- Whitehouse, J., Roy, P. S. and Oakes, G. M., 1999. Mineral sand resource potential of the Murray Basin. In: Stewart, J. R. (editor), Geological Survey of New South Wales Department of Mineral Resources, **Geological Survey Report GS 1999/038**, 74 pp.
- Wilford, J., Worrall, L. and Minty, B., 2009. Radiometric Map of Australia provides new insights into uranium prospectivity. In, AusGeo News. Geoscience Australia. **No. 95**. Online: <http://www.ga.gov.au/ausgeonews/ausgeonews200909/radiometric.jsp>.
- Wilson, R. L., 2007. Palaeodrainage reconstruction at 'The Pimples', west of Mt Neill, northern Flinders Ranges: Implications for uranium mineralisation and exploration. CRC LEME, Department of Geology and Geophysics, University of Adelaide, Adelaide. BSc Honours thesis, unpublished.
- Wilson, T. and Fairclough, M., 2009. Uranium and Uranium Mineral Systems in South Australia. South Australia, Department of Primary Industries and Resources, Adelaide. **Report Book 2009/14**, 182 pp.
- Wopfner, H., Callen, R. and Harris, W. K., 1974. The Lower Tertiary Eyre Formation of the southwestern Great Artesian Basin. *Journal of the Geological Society of Australia* **21(1)**, 17-51.
- Wopfner, H. and Twidale, C. R., 1971. Geomorphological History of the Lake Eyre Basin. In: Jennings, J. N. and Mabbutt, J. A. (editors), Landform Studies from Australia and New Guinea. Australian National University Press, Canberra. 119-143 p.
- Wopfner, H. and Twidale, C. R., 1988. Formation age of desert dunes in the Lake Eyre depocentres in central Australia. *Geologische Rundschau* **77(3)**, 815-834.
- Wulser, P.-A., 2009. Uranium metallogeny in the North Flinders Ranges region of South Australia. Department of Geology and Geophysics, University of Adelaide, Adelaide. PhD thesis, unpublished.
- Wulser, P.-A., Brugger, J., Foden, J. and Pfeifer, H.-A., 2011. The sandstone-hosted Beverley uranium deposit, Lake Frome Basin, South Australia: mineralogy, geochemistry, and a time-constrained model for its genesis. *Economic Geology* **106**, 835-867.

3 Geology, physiography, landscape evolution and mineral systems

I. C. Roach, S. Jaireth, C. E. Wade, A. J. Cross, S. B. Hore and E. A. Jagodzinski

3.1 INTRODUCTION

I. C. Roach

The Simpson Desert, Strzelecki Desert, Frome Embayment, Flinders Ranges, Olary Spur, Barrier Ranges and Murray-Darling Basin host a wide variety of mineral deposits in a variety of landscape settings in rocks ranging from Paleoproterozoic to Cenozoic in age. A large number of authoritative texts already exist describing the physiography and geology of the region; South Australia is favoured by having a relatively recent record describing its geological history (Drexel and Preiss, 1995; Drexel *et al.*, 1993). There are also many specialist volumes describing aspects of the geology, economic geology and regolith geology of the region detailed in [Chapter 2](#) of this record. This chapter does not seek to duplicate those efforts, but instead to synthesise the information relevant to the Frome AEM Survey and its objectives, described in [Chapter 1](#).

This chapter reviews the geology, physiography and mineral systems of the Frome AEM Survey area in terms of their relevance to AEM survey operations and to uranium and other element (gold, copper, lead-zinc-silver, and iron) mineralisation. A new synthesis of time-space relations between mineralising events is presented, describing important mineralising events for uranium systems from the Proterozoic to Cenozoic including important breaks in sedimentation related to tectonic uplift, mineralisation and fluid flow.

3.2 REGIONAL GEOLOGY

3.2.1 Paleo-Mesoproterozoic Curnamona Province

The Paleoproterozoic to Mesoproterozoic rocks of the Curnamona Province are the oldest outcropping rocks of economic importance within the Frome AEM Survey area. The Curnamona Province was sub-divided into a series of domains by Conor and Preiss (2008), as shown in [Figure 3.1](#) and [Figure 3.2](#), and is interpreted to have been deposited in a rift setting (Conor and Preiss, 2008). The best known domain, the Broken Hill Domain, containing the ~1720-1640 Ma Willyama Supergroup (Conor and Preiss, 2008), occupies the southern portion of the Curnamona Province and hosts the giant Broken Hill zinc-lead-silver deposit, the world's largest deposit of this type (Huston *et al.*, 2006), as well as numerous other smaller deposits of copper, gold, lead-zinc-silver and uranium. Rocks within the Curnamona Province fall into two main age intervals: metasediments and metavolcanics of the Willyama Supergroup, and associated intrusives, which were all deformed and metamorphosed during the Late Paleoproterozoic-Early Mesoproterozoic Olarian Orogeny (~1620-1580 Ma); and, Early Mesoproterozoic volcanic and sedimentary rocks and granitoids (Kositcin, 2010; Robertson *et al.*, 2006). The basement to the Curnamona Province may be Archean or older Paleoproterozoic (Cutten *et al.*, 2006). Archean to Mesoproterozoic rocks of the Gawler Craton appear to form the basement to Lake Torrens in the west of the survey area (Conor and Preiss, 2008; Kositcin, 2010), but Archean rocks are not known to outcrop within the Survey area.

Following Conor and Preiss (2008), the Curnamona Province is divided into a series of domains ([Figure 3.1](#)) based on differences in age, sedimentary facies, metamorphism and magmatism. The total thickness of the Willyama Supergroup is unknown, but could be 5 km in the Olary Domain (Conor, 2004) and anywhere between 4.5 km and 13 km thick elsewhere (Willis *et al.*, 1983). The Olary Domain contains a thinner, less complex stratigraphy than the Broken Hill Domain, and

The Frome airborne electromagnetic survey, South Australia: implications for energy, minerals and regional geology

features outcrops of the basal Curnamona Group, the oldest part of the Willyama Supergroup (depicted as the Tommie Wattie Formation and the George Mine Formation in Figure 3.2) that are not seen in the Broken Hill Domain (Conor, 2004; Conor and Preiss, 2008). The Mulyungarie Domain lies largely under cover within the Frome Embayment and consists of Willyama Supergroup rocks (Kositcin, 2010). The Mulyungarie Domain contains a thick sulfidic succession (Conor and Preiss, 2008) and the stratigraphic model of Preiss (2011; Figure 3.2) indicates that the Mulyungarie Domain should contain the most comprehensive cross-section of Curnamona Province stratigraphy.

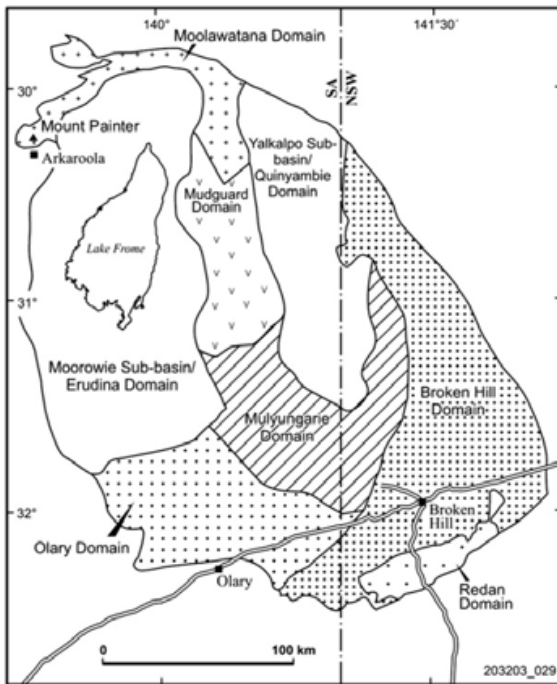


Figure 3.1: Geological domains of the Curnamona Province. From Conor and Preiss (2008). The Frome AEM Survey covers almost the entire portion of the South Australian side of the map, except Mount Painter-Arkaroola.

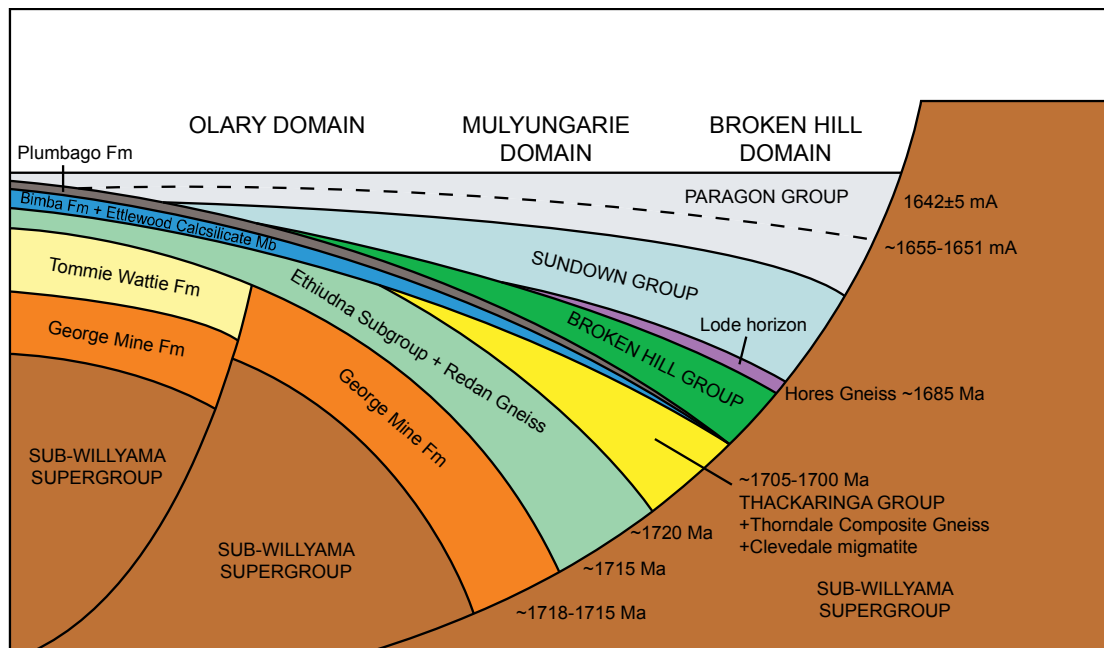


Figure 3.2: Conceptual model of the Broken Hill rift showing the stratigraphy of the Olary, Mulyungarie and Broken Hill domains. Modified after Preiss (2011).

The Frome airborne electromagnetic survey, South Australia: implications for energy, minerals and regional geology

The Moolawatana Domain consists of possible Paleoproterozoic and Early Mesoproterozoic rocks of the outcropping Mount Painter and Mount Babbage inliers and their extensions buried underneath sedimentary cover in the Lake Frome area to the east (Preiss, 2006). The Redan Domain contains rocks older than those in the Broken Hill Domain, including calc-silicate gneisses (Kositcin, 2010). The Mudguard Domain is regarded as containing a relatively undeformed sheet of ~1580 Ma Benagerie Volcanics overlying Willyama Supergroup rocks under relatively thin (50-200 m) cover on the Benagerie Ridge (Preiss, 2006), which is a raised portion of the Curnamona Province flanked to the east and west by younger rift-related sedimentary basins (Figure 3.3). The Erudina and Quinyambie domains consist of deeply buried Proterozoic basement rocks covered by Cambrian sediments of the Moorowie and Yalkalpo sub-basins of the Arrowie Basin (Kositcin, 2010).

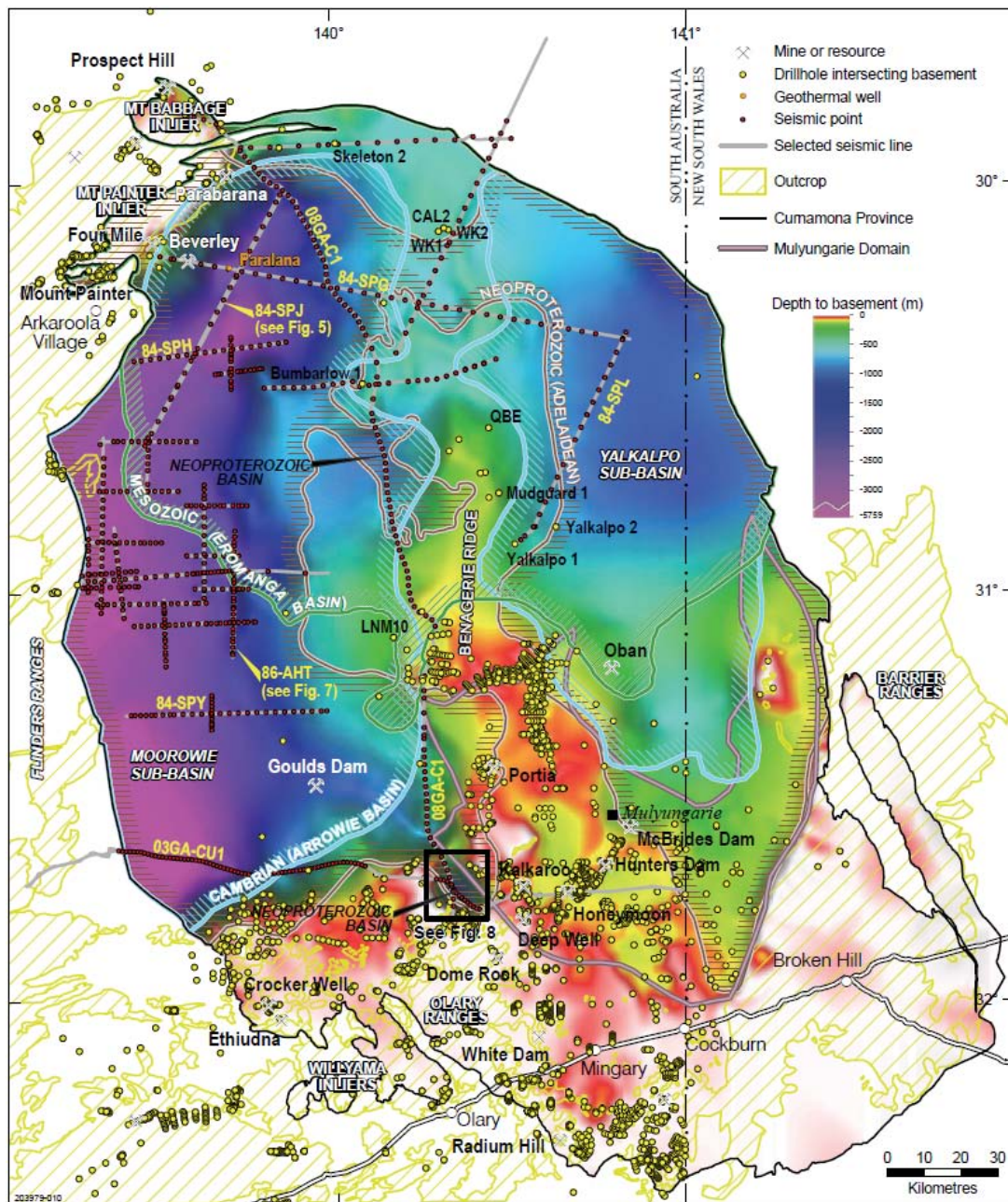


Figure 3.3: Depth to basement image of the Curnamona Province highlighting the location of the Benagerie Ridge and the estimated extents of sedimentary basin cover. From Fabris et al. (2010).

The Frome airborne electromagnetic survey, South Australia: implications for energy, minerals and regional geology

Models for the stratigraphic subdivision of the Willyama Supergroup continue to improve, synthesised most lately by Kositsin (2010; Figure 3.4).

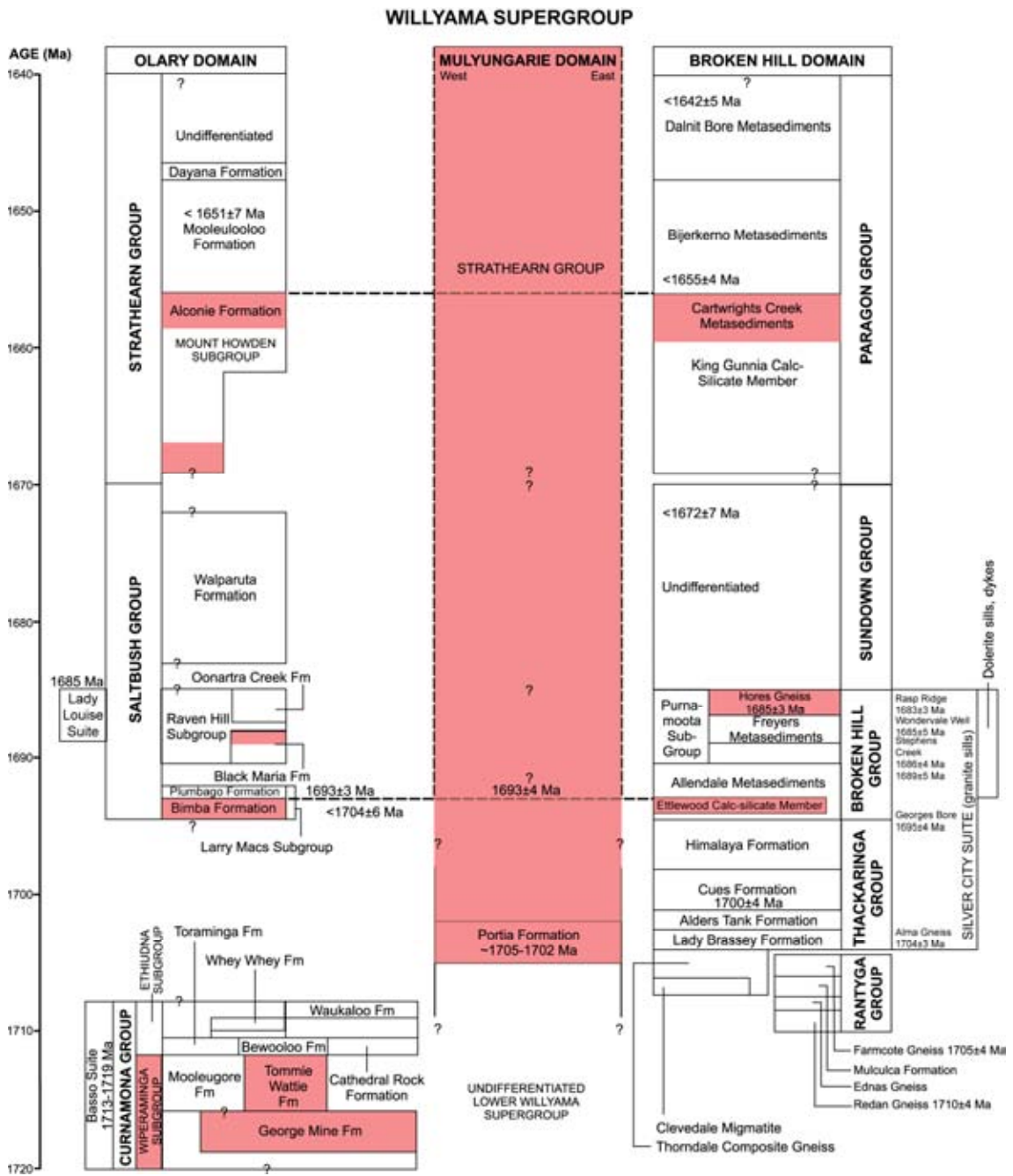


Figure 3.4: Subdivisions of the Willyama Supergroup in the Olary, Mulyungarie and Broken Hill domains with potential electrical conductors highlighted. Modified after Kositsin (2010).

A number of subdivisions within the Willyama Supergroup are potential electrical conductors (Figure 3.4). These include any units that contain large amounts of pyrite or other sulfides (excluding sphalerite, which is a resistor), carbon or graphite and salt water (Palacky, 1993). Potentially conductive rocks may include:

- The Bimba Formation (Bimba Sulphide Member; Conor, 2000; Conor and Preiss, 2008) near the base of the Saltbush Group in the Olary Domain and its lateral equivalent the

Ettlewood Calc-silicate Member near the base of the Broken Hill Group in the Broken Hill Domain;

- The rocks in the Mulyungarie Domain (Conor and Preiss, 2008);
- The main Broken Hill ore horizon within the Hores Gneiss of the Broken Hill Group, Broken Hill Domain (Conor and Preiss, 2008);
- Pyrite-bearing portions of the Wiperaminga Subgroup, Olary Domain (Conor, 2000);
- Graphitic portions of the Strathearn Group, Olary Domain (Conor, 2000);
- Graphitic portions of the basal Saltbush Group, Olary Domain (Conor, 2000);
- Pyritic basal Portia Formation, Olary Domain (Conor and Preiss, 2008);
- A graphite-bearing layer at the top of the Black Maria Formation, Olary Domain (Conor and Preiss, 2008); and,
- Graphitic portions of the Cartwrights Creek metasediments of the Broken Hill Domain and the Alconie Formation of the Olary Domain (Conor and Preiss, 2008).

Rocks containing magnetite tend to be resistive and are not visible within AEM images, but a first vertical derivative (1VD) magnetic image of the southern Frome Embayment area (Figure 3.5) is instructive for demonstrating the geological complexity within the Mulyungarie Domain, which should contain much electrically conductive material under relatively thin cover of the Callabonna Sub-basin (See Figure 2.3G for definition). Many of the units listed above are sub-aerially exposed (Broken Hill Domain, Olary Domain) or lie under relatively thin cover (Mulyungarie Domain) and can potentially be imaged by AEM. Salt water is present to greater or lesser extent throughout the survey area, but is concentrated in low-lying land within the Callabonna Sub-basin and Murray-Darling Basin, as will be demonstrated later.

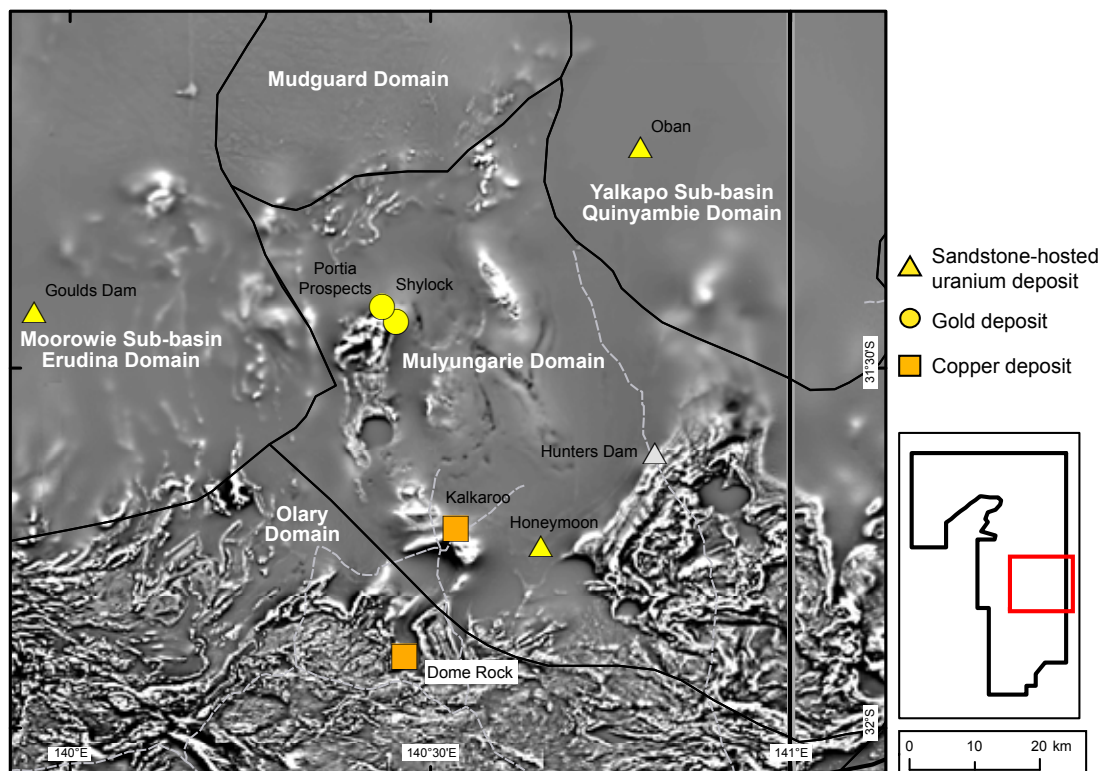


Figure 3.5: First vertical derivative magnetic image of the Benagerie Ridge area showing under-cover structures in the Mulyungarie and Mudguard domains.

3.2.2 Neoproterozoic

The Neoproterozoic sequence of the Adelaide Fold Belt (Nackara Arc) covers the Curnamona Province in part and forms the boundary between the Gawler Craton in the west and the Curnamona Province in the east. The Neoproterozoic sequence is fault-bounded against almost all other rocks within the Frome AEM Survey area, except in the Olary Spur where it lies unconformably over the Curnamona Province. The most comprehensive synthesis of the geology and evolution of the Neoproterozoic sequence comes from Preiss (1987), but a number of other publications provide overview and detail including Coats (1973), Coats *et al.* (1973), Rogers (1977; 1978), Forbes (1989; 1991), Drexel *et al.* (1993), Preiss (1999) and Riordan (2009).

The Neoproterozoic rocks within the Frome AEM Survey area are prospective principally for copper and gold, but also contain iron, magnesium, manganese, uranium and other metals in a large number of mineral deposits and prospects, some of which are considered in [Chapter 5](#) of this record.

The Frome AEM Survey area extends over Neoproterozoic rocks of the northern Flinders Ranges and Nackara Arc (Preiss, 1993; Preiss and Robertson, 2006) ([Figure 3.6](#)) including rocks of the Wilpena Group, Umberatana Group, Burra Group and Callanna Group, representing the entire stratigraphy of the South Australian Neoproterozoic succession. The Neoproterozoic rocks are believed to have been deposited in intracratonic rifts and basins (Preiss, 1993) under variable water depth regimes (Goleby *et al.*, 2006).

The Neoproterozoic succession has undergone low grade regional metamorphism resulting in hard quartzite beds that dominate the Flinders Ranges as characteristic strike ridges (see [Section 3.4](#) - physiography). Lithology is dominated by quartzite, siltstone, limestone and dolomite with prominent tillite of Sturtian age prominent in some areas. A number of subdivisions within the Neoproterozoic succession are potential electrical conductors, shown in [Figure 3.7](#), including any rocks that contain large amounts of pyrite, carbon or graphite and salt water. Potentially conductive rocks may include:

- Portions of the Black Knob Marble associated with copper sulfide deposits and secondary copper deposits;
- Portions of the Wywyana Formation associated with secondary copper minerals;
- Carbonaceous portions of the Boorloo Siltstone;
- Carbonaceous Portions of the Arkarba Hill Beds;
- The Kirwan Siltstone;
- Portions of the Niggly Gap Beds in the Blinman Diapir associated with copper mineralisation;
- Magnesite-bearing portions of the Skillogee Dolomite;
- Carbonaceous portions of the Saddleworth Formation;
- Carbonaceous portions of the Tapley Hill Formation;
- The Benda Siltstone;
- Pyritic and carbonaceous basal Tindelpina Shale Member; and,
- Magnesite-bearing portions of the Balcanoona Formation.

The Frome airborne electromagnetic survey, South Australia: implications for energy, minerals and regional geology

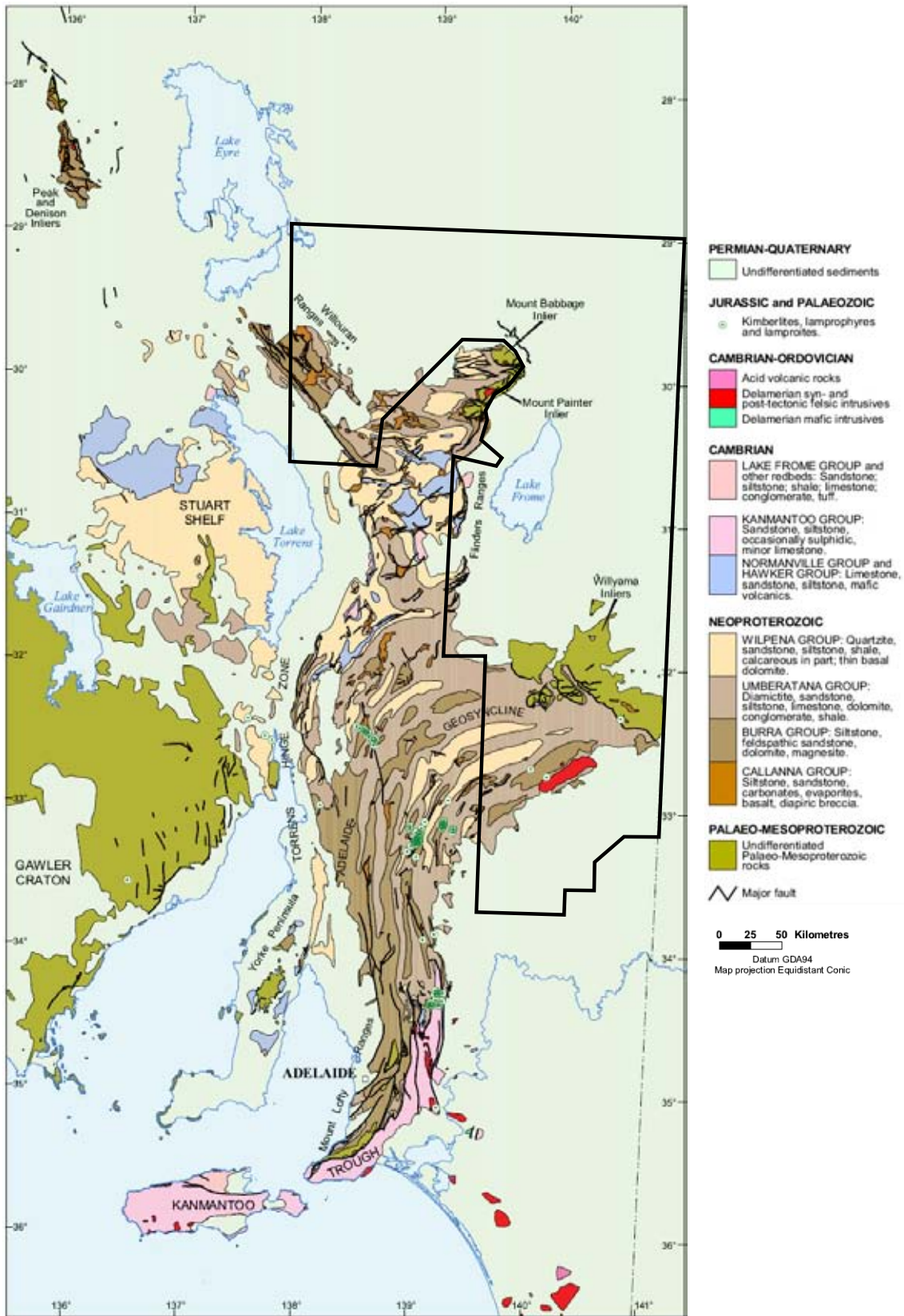


Figure 3.6: Approximate location of the Frome AEM Survey in comparison to major Neoproterozoic terrains of the Adelaide Geosyncline. Modified after Preiss and Robertson (2006).

The Frome airborne electromagnetic survey, South Australia: implications for energy, minerals and regional geology

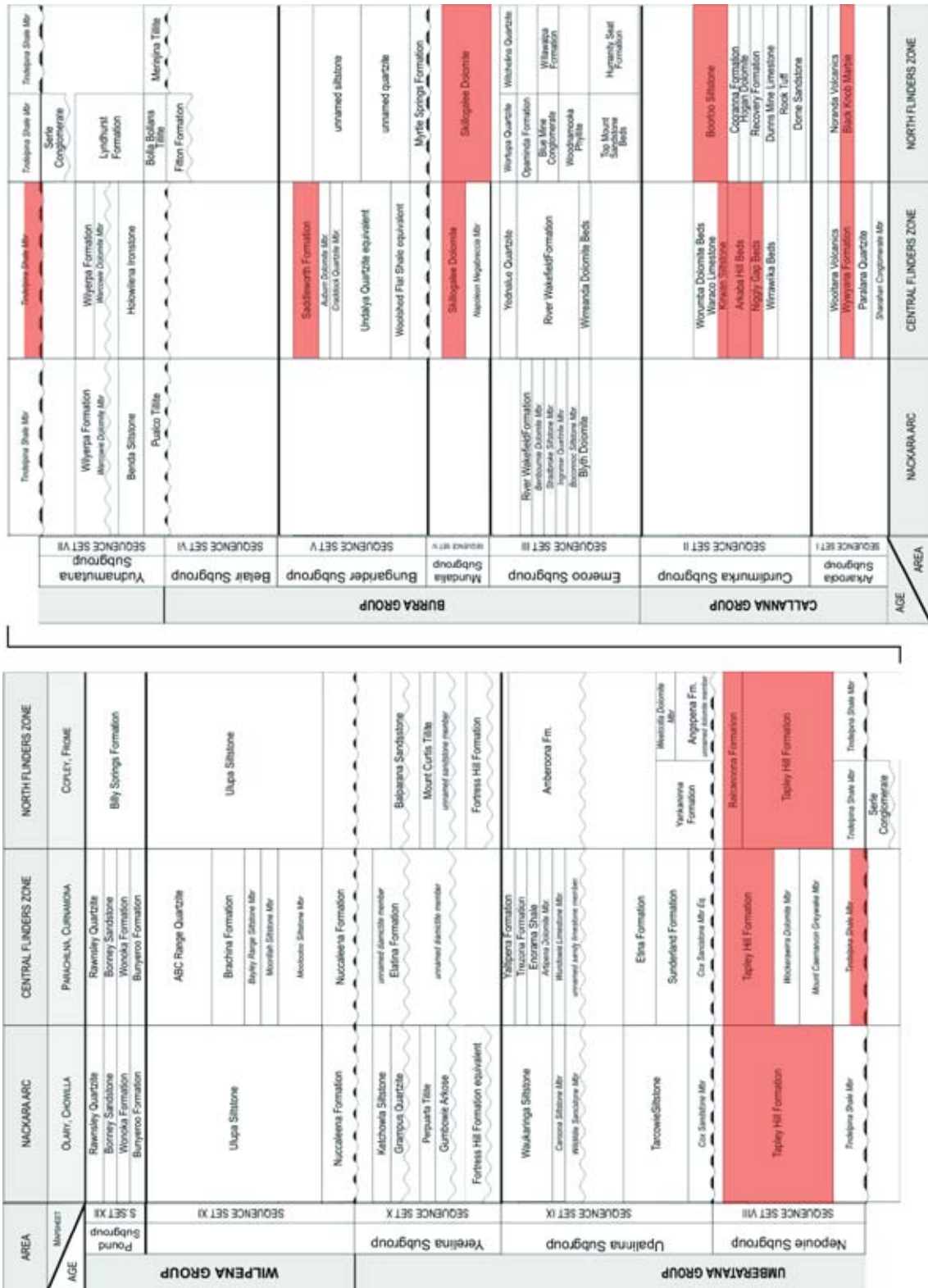


Figure 3.7: Stratigraphic column of Neoproterozoic rocks within the Frome AEM Survey area highlighting potential electrically conductive rocks. Modified after Riordan (2009).

3.2.3 Paleozoic

A range of intrusive and sedimentary Paleozoic rocks occur within the Frome AEM Survey area, although most of them do not outcrop. Paleozoic sedimentary rocks within the survey area include Cambrian rocks of the Arrowie Basin and Stuart Shelf. Successions up to 4 km thick occupy the Moorowie and Yalkapo sub-basins of the Arrowie Basin (Figure 3.8), which is a rift basin straddling the Benagerie Ridge (Figure 3.3). Cambrian sediments are marine in origin, believed to have been deposited in deep water environments in the central Arrowie Basin, but flanked to the west and east by shallower water on the Stuart Shelf and Curnamona Craton respectively (Gravestock and Cowley, 1995).

Cambro-Ordovician rocks of the Kanmantoo Trough outcrop to the southwest of the Frome AEM Survey area in the Mount Lofty Ranges, but do not outcrop within the survey area. There is a possibility that Kanmantoo Group rocks continue under cover of the Murray-Darling Basin, but drilling results reported by Farrand and Preiss (1995) indicate that the immediate basement to the Murray-Darling Basin is Neoproterozoic with Cambro-Ordovician intrusive rocks.

Sedimentation in the Adelaide Geosyncline (Arrowie and Kanmantoo basins) ceased during the Cambro-Ordovician Delamerian Orogeny, when syntectonic and post-orogenic granitoid intrusion occurred.

Paleozoic rocks associated with the Delamerian Orogeny occur in the south of the Frome AEM Survey area on the southeastern flanks of the Nackara Arc between it and the Murray-Darling Basin. The Anabama Granite is a zoned pluton, elongated along strike parallel to major faults defining the edge of the Nackara Arc and features prominently in magnetic and radiometric imagery. The Anabama Granite has a crystallisation age of 458 ± 62 Ma (Webb, 1976), also reported as 455 ± 7 (Farrand and Preiss, 1995), and is similar in age to the British Empire Granite of the Mount Painter Inlier with a garnet crystallisation age of 455 ± 8 Ma (Elburg *et al.*, 2003; McLaren *et al.*, 2002) or ~ 440 Ma (Wulser, 2009). Syntectonic granitoids are also present underneath the Murray-Darling Basin, although these have not been dated.

Arrowie Basin and possible Kanmantoo Trough sediments within the Frome AEM Survey area are mostly deeply buried under Mesozoic and Cenozoic cover, and are not generally visible in the AEM data.

3.2.4 Mesozoic

Mesozoic rocks of the Telford Basin, and associated basins, and the Eromanga Basin are exposed in the northern Frome AEM Survey area (Figure 3.9, Figure 3.13).

The Telford Basin (Figure 3.10) is the largest of five discrete coal-bearing basins known at Leigh Creek, which are interpreted to be Triassic-Jurassic terrestrial intramontaine basins containing > 500 Mt of coal collectively (Kwitko, 1995). Coal beds up to about 20 m thick are interbedded with mudstone, siltstone and sandstone in asymmetrical basins with dips of up to 80 degrees. While carbon is regarded as a good electrical conductor, it is anticipated that coal will not be a good electrical conductor because of the amount of sediment normally found within coal deposits, unless it is saturated with saline groundwater.

Sediments of the Eromanga Basin, part of the Great Australian Basin (Great Artesian Basin, GAB), are exposed at the surface around the northern Flinders Ranges and Strzelecki Desert areas by tectonic uplift of the underlying northern Flinders Ranges. Eromanga Basin sediments also occur under Cenozoic cover of the Callabonna Sub-basin within the Frome Embayment. In the Mount Babbage Inlier, Mesozoic sediments unconformably overlie Curnamona Province rocks (Davey, 2009; Twidale, 2007), where the marine Algebuckina Sandstone or the marginal marine Cadna-owie Formation caps Proterozoic granitoids and Neoproterozoic rocks. A basal conglomerate containing granitoid, volcanic and metamorphic lithic clasts occurs above the unconformity at the base of the Mesozoic sequence (Davey, 2009). Mesozoic sediments flanking the northern Flinders Ranges consist mainly of the Marree Subgroup (see Figure 3.11), comprising the Oodnadatta Formation, the

The Frome airborne electromagnetic survey, South Australia: implications for energy, minerals and regional geology

Coorikiana Sandstone and the Bulldog Shale, all marine sediments (Kreig and Rogers, 1995), and also the units mapped by Davey (2009).

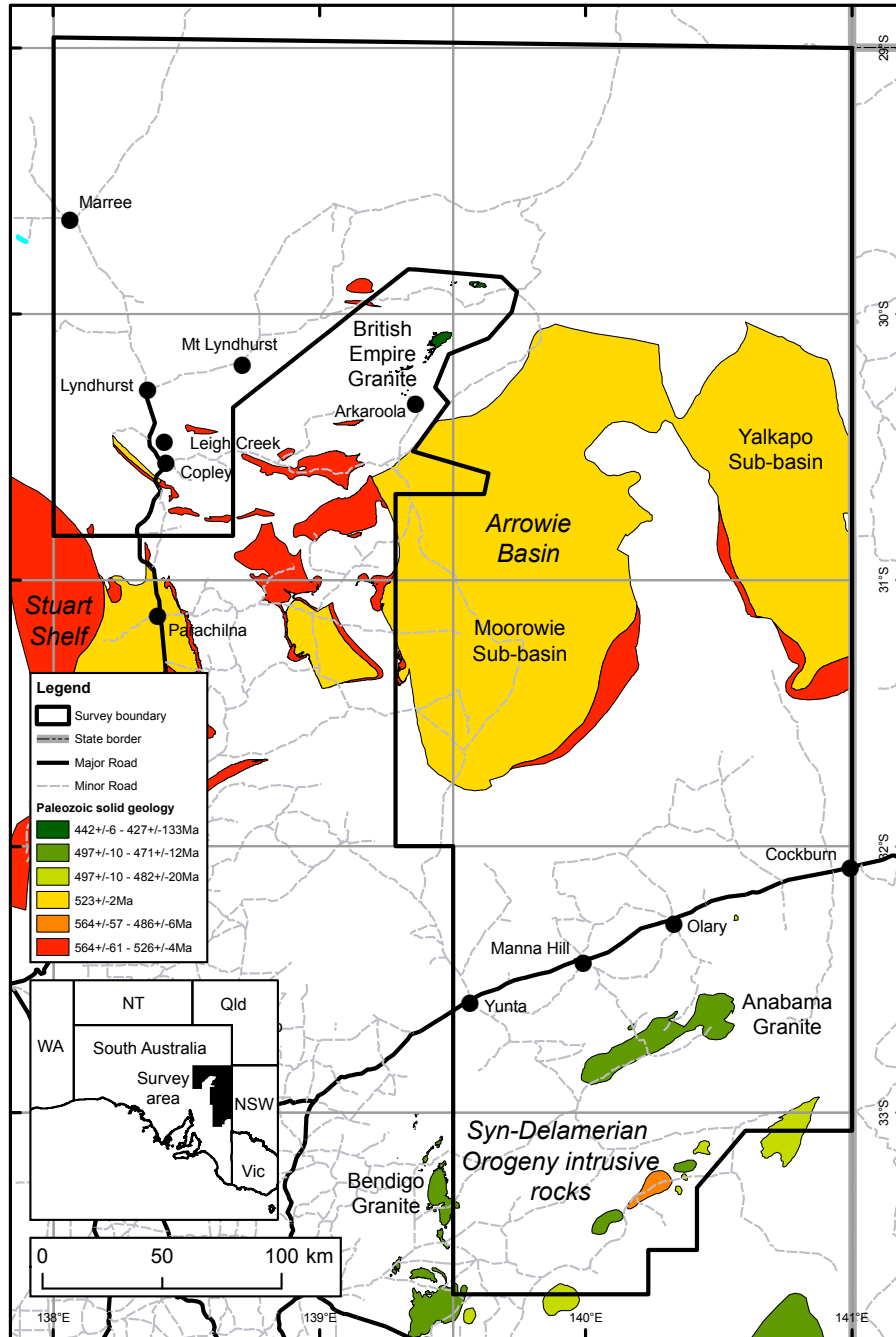


Figure 3.8: Paleozoic solid geology of the Frome AEM Survey area. Adapted from SARIG.

The Frome airborne electromagnetic survey, South Australia: implications for energy, minerals and regional geology

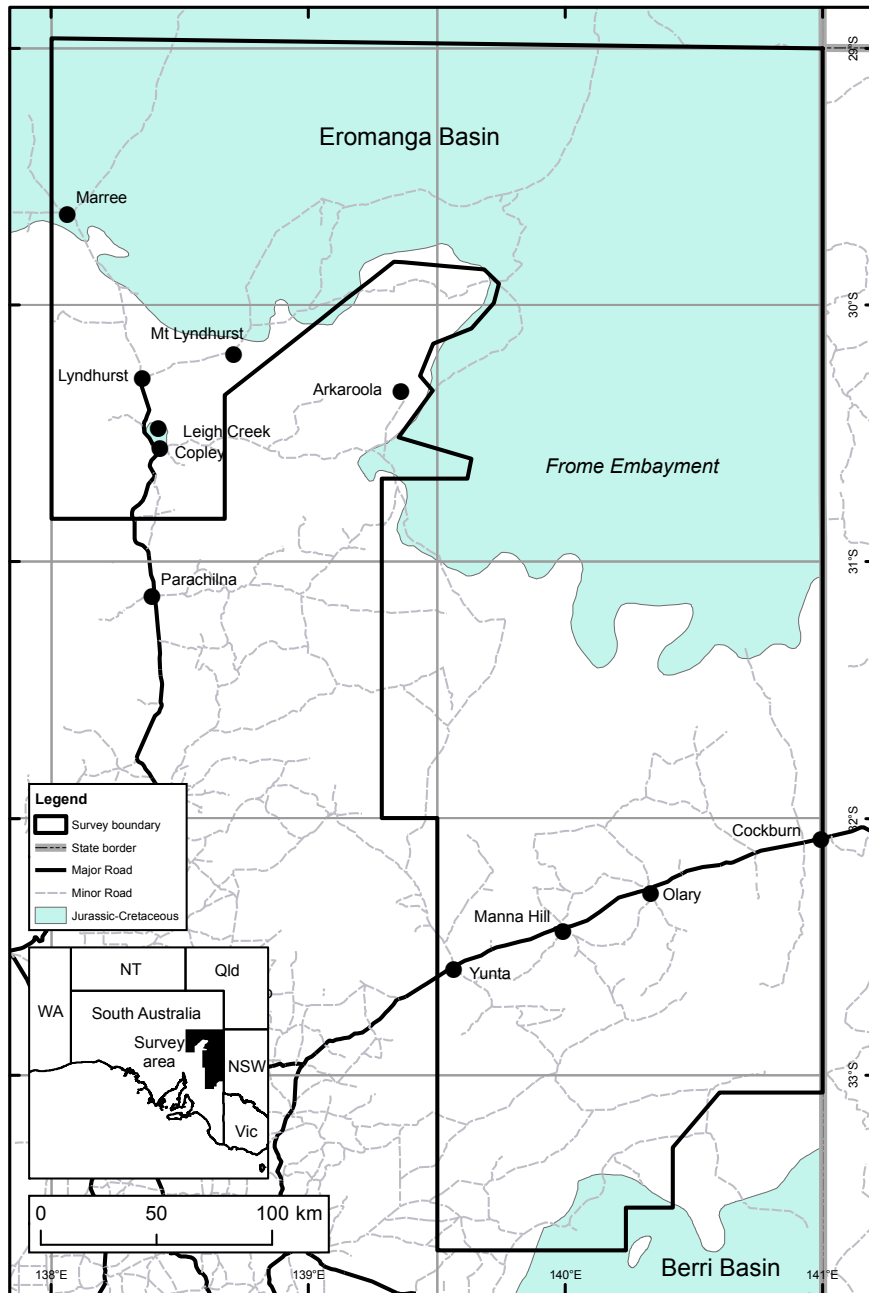


Figure 3.9: Mesozoic solid geology of the Frome AEM Survey area. From SARIG.

The Frome airborne electromagnetic survey, South Australia: implications for energy, minerals and regional geology

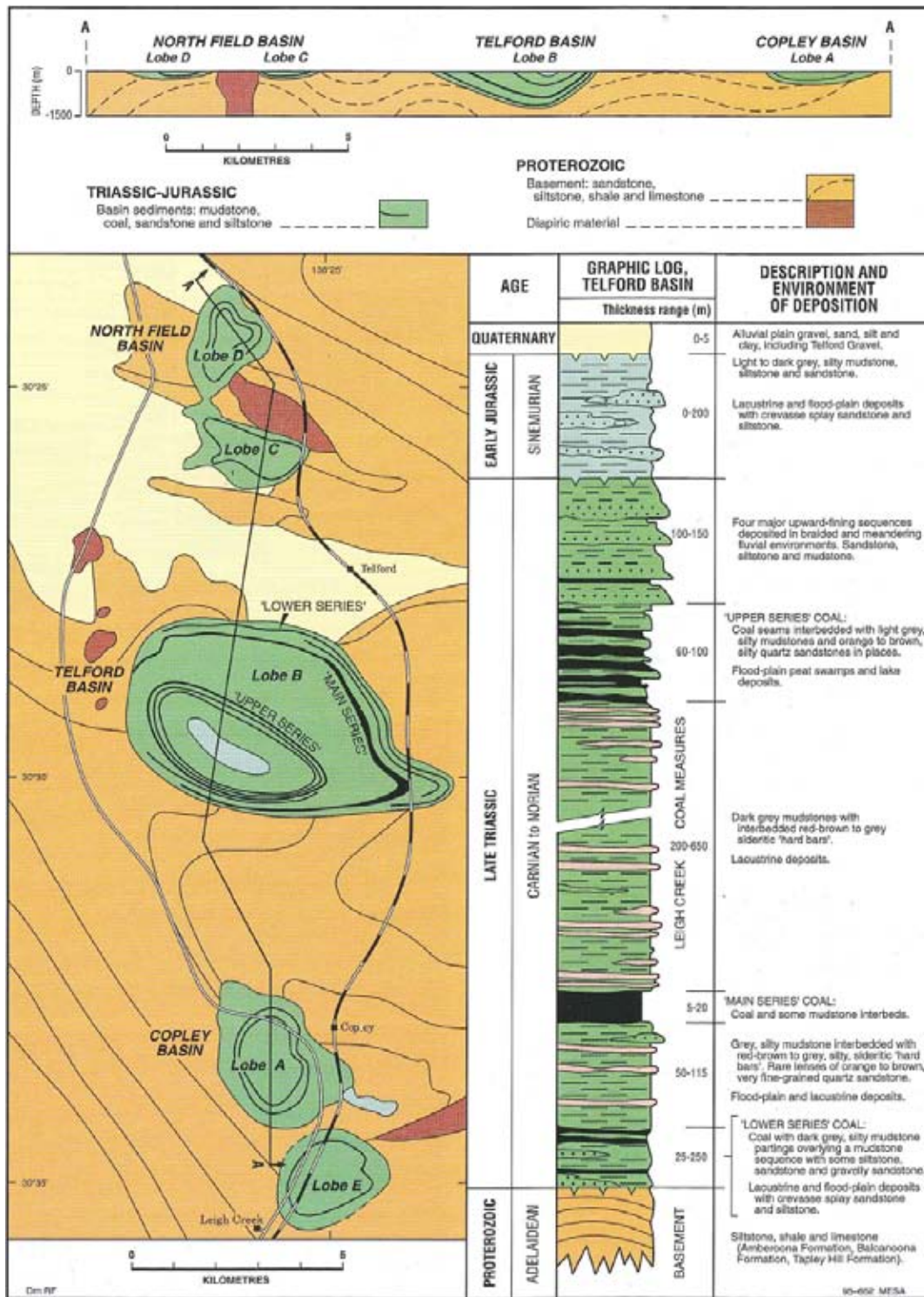


Figure 3.10: The geology and stratigraphy of the Leigh Creek coalfield. From Kwitko (1995).

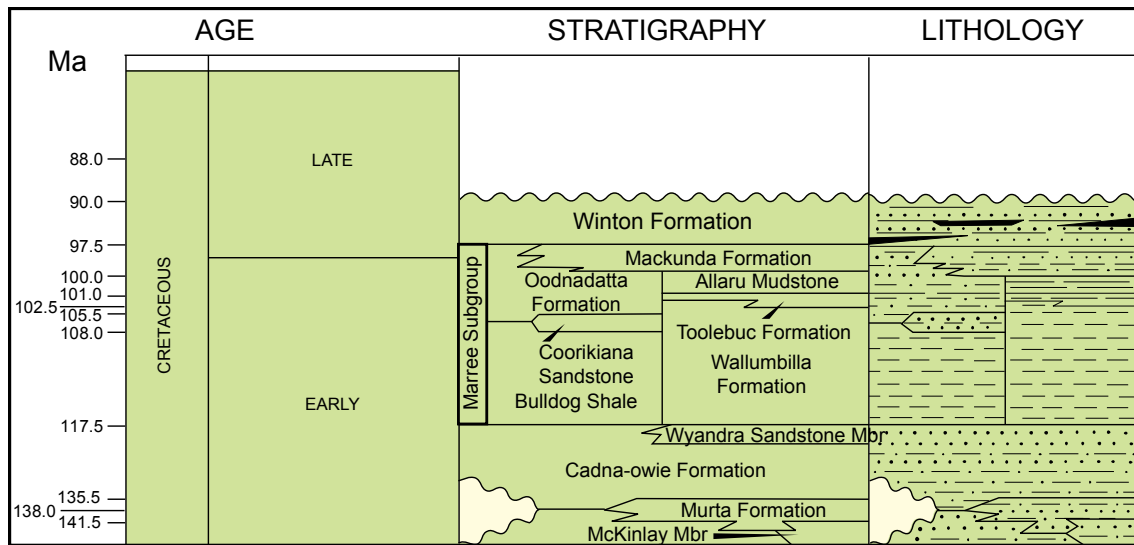


Figure 3.11: Generalised stratigraphy of the Cretaceous portion of the Eromanga Basin. The Marree Subgroup includes the Oodnadatta Formation, Coorikiana Sandstone and Bulldog Shale. Modified after Moussavi-Harami and Alexander (1998).

The Cadna-owie Formation is interpreted to contain glacial dropstones derived from Permian boulder clay (Kreig and Rogers, 1995), but may in places actually represent a Cretaceous diamictite (Alley, 1998; Hill and Hore, 2012; Hore and Hill, 2009). In the Strzelecki-Simpson deserts and the Marree and Blanchewater areas in the north of the Frome AEM Survey area the terrestrial Winton Formation, which consists of layered shale, siltstone, sandstone and minor coal layers overlying the Marree Subgroup, outcrops in creek cuttings and on some hilltops (Rogers, 1995b).

Mesozoic rocks of the Berri Basin (specifically the Canegrass Lobe) occur under the Murray-Darling Basin in the southern part of the Frome AEM Survey area (Figure 3.9, Figure 3.40). These rocks are hidden under thick terrestrial and marine cover of the Murray-Darling Basin, are not considered to be visible within the AEM data and are not included in this review. Likewise, older terrestrial sedimentary rocks of the Eromanga Basin are not considered within this review because they are too deeply buried to be visible in the AEM data.

Mesozoic rocks of the Eromanga Basin are anticipated to have variable electrical conductivity, dependent on mineral, carbon and salt water content. The Bulldog Shale is regarded as a poor resistor where fresh (Alexander and Hibbert, 1996), therefore a good conductor, and is noted in fresh exposures to contain abundant pyrite (Alexander and Sansome, 1996; Chivas *et al.*, 1991), carbon and plant fragments (Kreig and Rogers, 1995).

3.2.5 Cenozoic

Cenozoic sediments within the Frome AEM Survey area consist of terrestrial sediments within the Callabonna Sub-basin of the Lake Eyre Basin and terrestrial and marine sediments within the Murray-Darling Basin (Figures 3.12, 3.13, 3.34). Sedimentation in the Callabonna Sub-basin and the Murray-Darling Basin commenced in the Cenozoic at the end of a hiatus between the Cenomanian (Upper Cretaceous) and the Late Paleocene (Early Cenozoic) signifying the withdrawal of the Cretaceous inland sea, when weathering may have been dominant over erosion and deposition (Callen *et al.*, 1995a). Following this, renewed uplift, terrestrial erosion and sedimentation resulted in the deposition of the Eyre Formation (Eocene) in the Callabonna Sub-basin, with a hiatus and then deposition of the overlying Namba Formation (Miocene), which includes the Etadunna Formation within its base in the far north of the survey area. The hiatus between the deposition of the Eyre Formation and the deposition of the Namba Formation is indicated by a break in the sedimentary

The Frome airborne electromagnetic survey, South Australia: implications for energy, minerals and regional geology

record and silcrete formation on the top of the Eyre Formation in many places (Callen, 1982; Hill and Hore, 2012) (see [Section 3.3.3](#)).

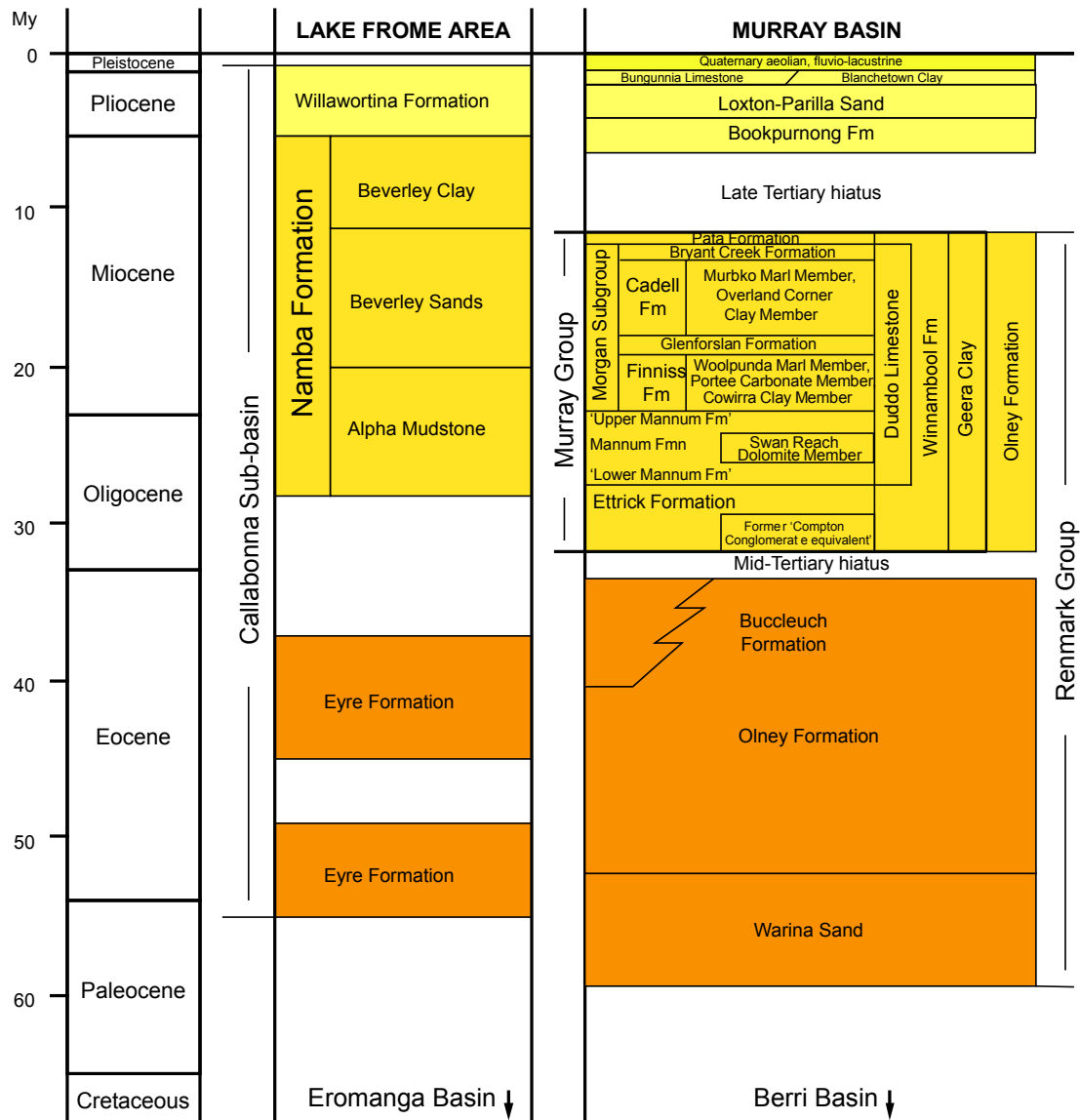


Figure 3.12: Cenozoic stratigraphy of the Lake Frome area and Murray-Darling Basin. Modified after Cowley and Barnett (2007), Skirrow (2009) and Whitehouse et al. (1999).

In the Murray-Darling Basin, age-equivalent terrestrial deposits of the Eyre and Namba formations occur in the Renmark Group (Figure 3.12), including the Warina Sand and the basal Olney Formation (Eocene), with more-or-less continuous sedimentation through to the top of the Olney Formation (Miocene) apart from a short hiatus in the mid-Tertiary. The age-equivalence of the sediments in the Callabonna Sub-basin and the Murray-Darling Basin has been previously noted by Jack (1930), Barnes (1951), O'Driscoll (1960), Ludbrook (1961), Wopfner *et al.* (1974) and Brown (1985).

The Frome airborne electromagnetic survey, South Australia: implications for energy, minerals and regional geology

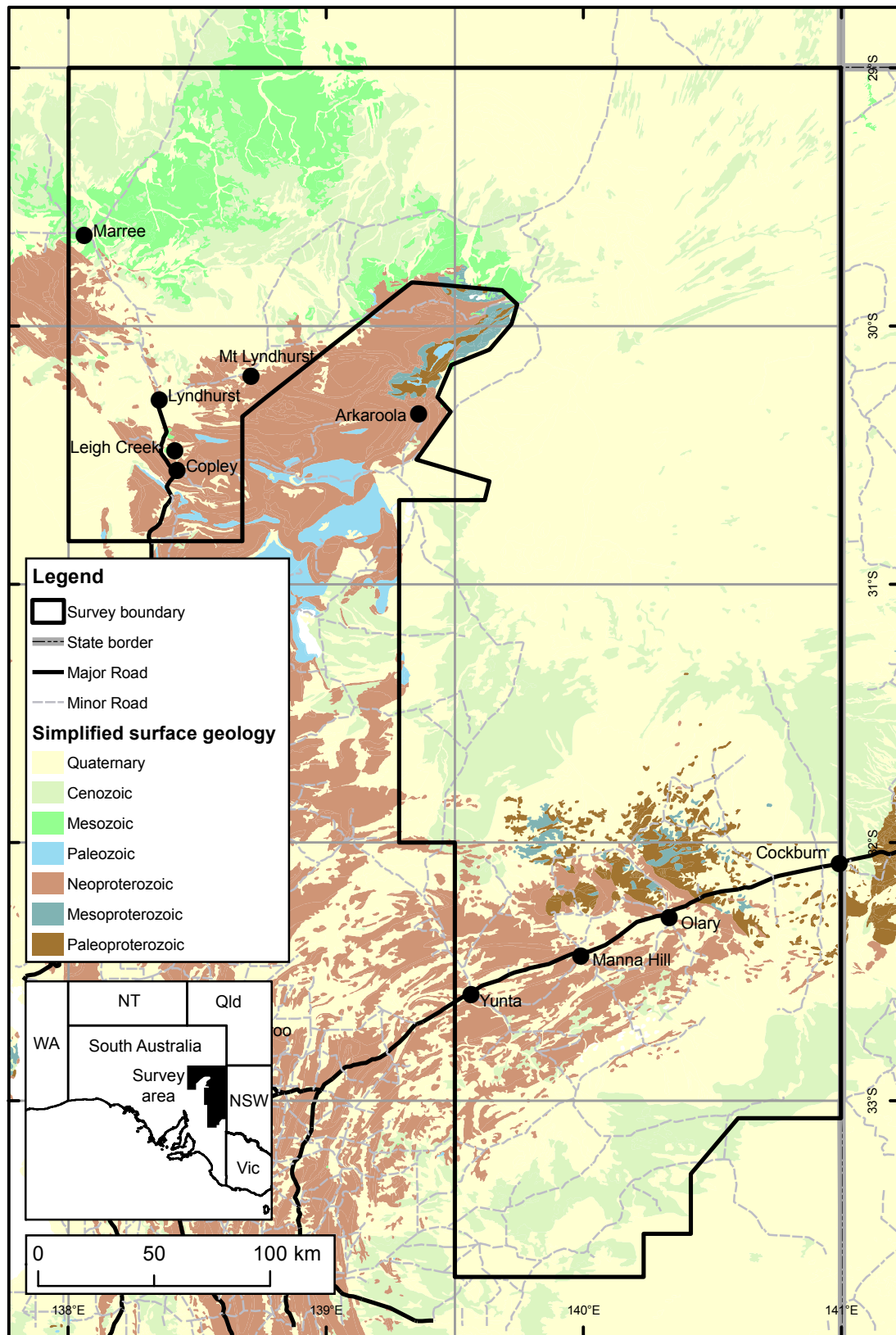


Figure 3.13: Simplified surface geology of the Frome AEM Survey area. Modified after the 1:1 million Surface Geology of Australia Map (Raymond and Retter, 2010).

The Murray-Darling Basin also includes marine sediments of the Buccleuch Formation and the Murray Group. The Buccleuch Formation was deposited during a minor marine transgression in the Late Eocene (Rogers *et al.*, 1995). The Murray Group was deposited during a major marine transgression-regression cycle spanning the Oligocene to Middle Miocene (Brown and Stephenson, 1991). The Loxton-Parilla Sand represents the final phase of marine deposition in the Murray-Darling Basin, where the regression left prominent a Pliocene barrier complex, younging towards the coast, which contain many large heavy mineral sand deposits (Roy *et al.*, 2000).

The Eyre Formation was deposited in a terrestrial setting in a series of meandering sandy streams, crevasse splays, alluvial fans, sand sheets and clayey overbank deposits close to the incipient Flinders-Barrier ranges and Olary Spur during a period of tectonic upheaval and erosional stripping following the Late Cretaceous-Early Paleocene hiatus. The Eyre Formation is predominantly sandy, consisting principally of mature, pyritic, carbonaceous sand. Grainsize varies from silt to gravel, with occasional patches of cobbles, all of which are subangular to subrounded (Callen *et al.*, 1995). Interbeds of clay-rich sediment (shale, siltstone and clayey sand) are present, as are areas of lignite and randomly-distributed woody fragments. The lower Eyre Formation is reported as containing up to 5 vol. % pyrite (Ellis, 1974), or as being “highly pyritic carbonaceous sand” (Brunt, 1975). Carbonaceous woody fragments and lignite beds occur frequently (Figure 3.14). The type section for the Eyre Formation, near Innamincka, contains abundant sandstone occasionally displaying cross-bedding, often with basal conglomerate or intra-bed channel-bottom conglomerate, and minor clayey lenses (Figure 3.15). In the type section the upper Eyre Formation is heavily indurated by silcrete, and this has been used to recognise the Eyre Formation regionally, however, silcrete does not occur at (or near) the top of the Eyre Formation everywhere. Pyrite and carbonaceous material are completely oxidised in outcrop, but are abundant in drill holes throughout the Eyre Formation.

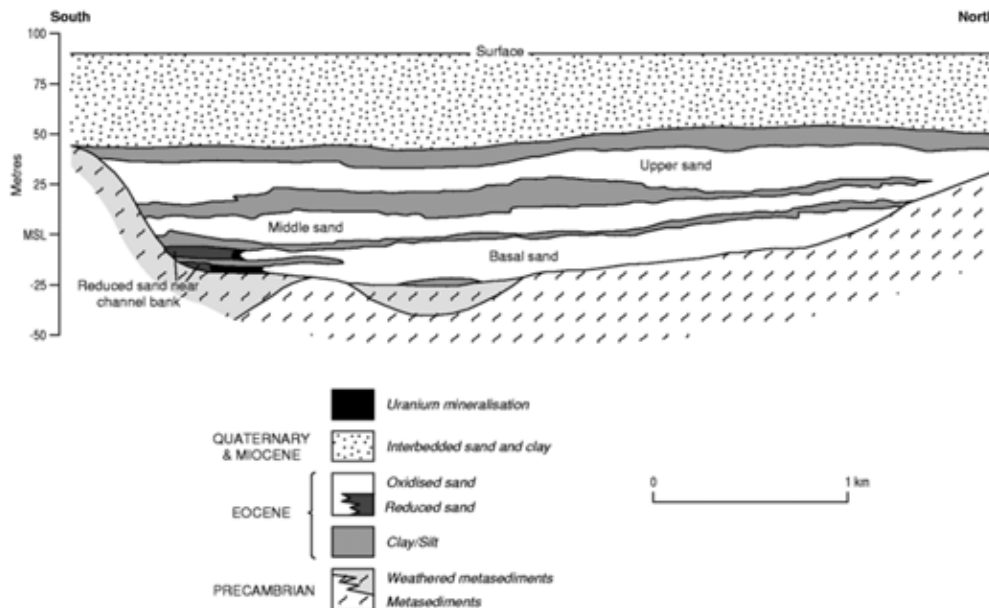


Figure 3.14: Cross-section of the Yarramba Palaeovalley at the Honeymoon uranium mine. From McKay and Mieztis (2001). Pyrite, lignite and woody fragments occur within the “Basal sand”. The Quaternary alluvial and aeolian succession and the Namba Formation have not been divided in this cross-section.

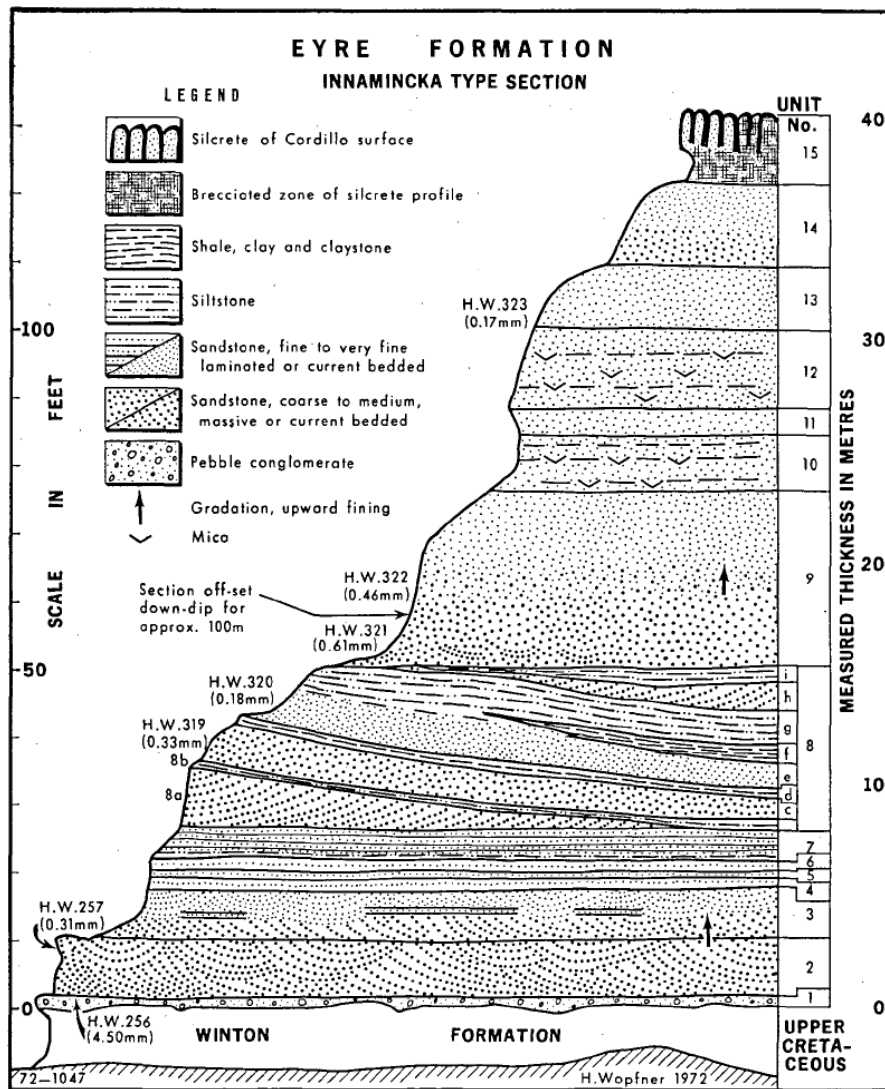


Figure 3.15: Sketch of the Eyre Formation type section near Innamincka. From Wopfner et al. (1974).

The Namba Formation disconformably overlies the Eyre Formation and was deposited in a terrestrial setting. It is far more clay- and carbonate-rich than the Eyre Formation, and has sandy interbeds (Callen, 1977; Callen et al., 1995a) (Figure 3.16). The Namba Formation is interpreted to have been deposited under a different, less energetic palaeoenvironment to the Eyre Formation, in which the lower-relief landscape was dominated by carbonate- and alkali-rich lakes fed by sand-dominated streams with wide clayey overbank deposits. A number of dolomite-rich interbeds may occur, and a layer of palygorskite clay-rich sediment occurs almost universally in the lower part of the Formation, witnessed in a number of stratigraphic drill holes in the Frome Embayment including Yalkapo 1 and Woltana 1 (Callen et al., 1995a). Callen (1977) informally divided the Namba Formation into an upper and lower sequence, dominated by illite-kaolinite clay and smectite-carbonate respectively.

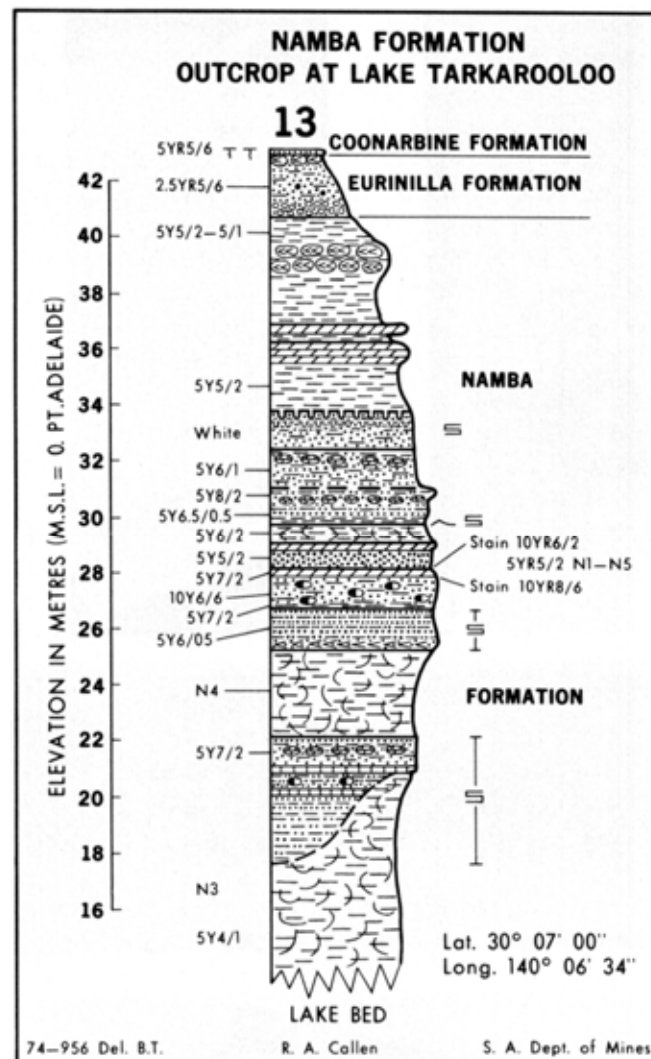


Figure 3.16: Sketch of the stratigraphy of the Namba Formation outcrop, with Munsell colours, at Lake Tarkarooloo. From Callen and Tedford (1976).

The internal facies of the Namba Formation vary widely, resulting in very different sand:clay ratios at the same elevation between closely-spaced drill holes. This is not surprising given the palaeoenvironmental conditions that the Namba Formation was deposited under. Lateral facies change is illustrated at the Oban uranium deposit in the southeastern Lake Frome area, where sandy interbeds representing shallow alluvial channels, and dolomitic clay layers representing lacustrine deposits, appear and disappear over the space of several hundred metres between successive drill holes (Figure 3.17).

The terrestrial sediments of the Renmark Group in the Murray-Darling Basin are interpreted to have been deposited under similar conditions to the Eyre and Namba formations in the Callabonna Sub-basin. The Paleocene-Eocene sediments in the Renmark Group were probably deposited in fluvial braided streams and associated flood plains with intercalated swamps forming peaty deposits (Brown, 1985) between periods where eustasy or tectonics caused absolute or relative sea level change.

The Frome airborne electromagnetic survey, South Australia: implications for energy, minerals and regional geology

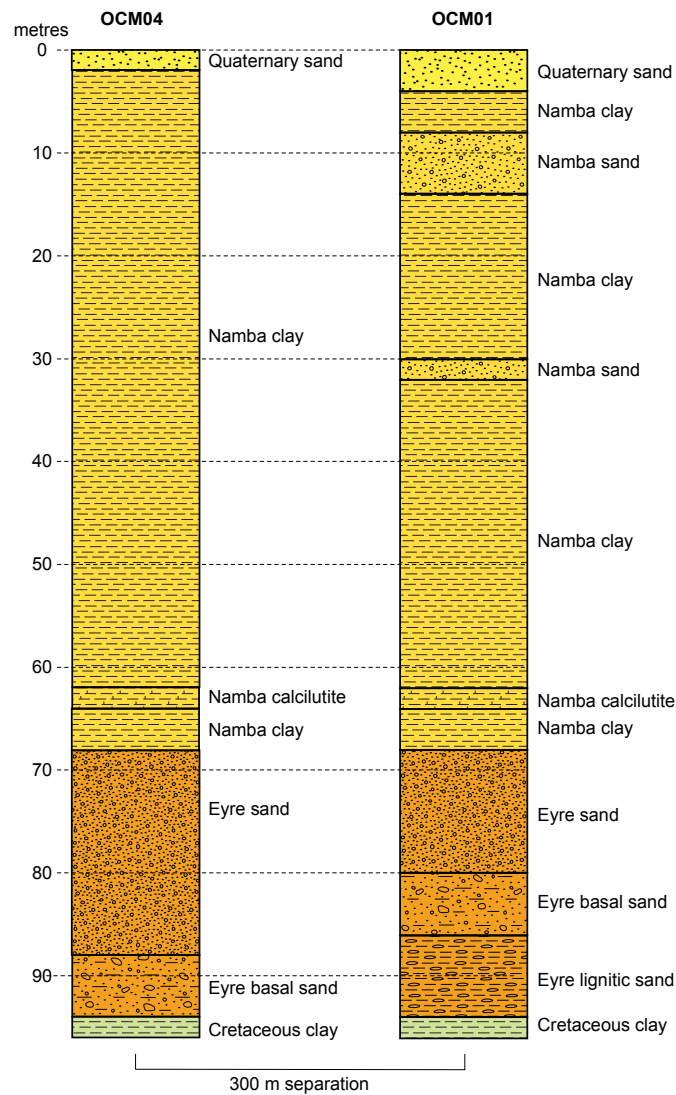


Figure 3.17: Stratigraphic logs illustrating lateral facies variation in the Namba and Eyre formations between close-spaced drill holes at the Oban uranium deposit, southeastern Lake Frome area. Modified from Curnamona Energy Ltd logging (Randell pers. comm. 2010).

The Eyre Formation is incised into the underlying basement rocks in a number of places within the southern Callabonna Sub-basin and the Lake Eyre Basin flanking the northern Flinders Ranges. In the Southern Callabonna Sub-basin, the Eyre Formation is incised into Paleo-Mesoproterozoic rocks of the Willyama Supergroup, Neoproterozoic rocks of the Adelaide Geosyncline, Cambrian rocks of the Arrowie Basin and Mesozoic sediments of the Eromanga Basin. A number of palaeovalleys systems are mapped in this area, some of which are associated with known uranium deposits and prospects including Goulds Dam, Honeymoon and Oban (Figure 3.18). Palaeovalley boundaries have been mapped using a variety of techniques including drill hole geology, ground EM and AEM and are drawn with varying degrees of confidence, because of the paucity of geological control in some areas, particularly in the western Callabonna Sub-basin.

The Willawortina Formation overlies the Eyre Formation and the Namba Formation flanking the northern Flinders Ranges. The Willawortina Formation consists of ~74 m of interbedded sandy mud and silty dolomite units in the Wooltana 1 drill hole, and ~95.5 m in the WC 2 drill hole at the Beverley uranium mine, that inter-finger with coarser-grained facies closer to the Flinders Ranges

The Frome airborne electromagnetic survey, South Australia: implications for energy, minerals and regional geology

where debris flow deposits consisting of poorly sorted coarse angular lithic fragments, sand and clay are mixed with finer-grained stream bed facies in alluvial-colluvial fan deposits radiating from the Flinders Ranges (Callen *et al.*, 1995b). The Willawortina Formation is regarded as having formed in response to the last pulse of tectonic uplift of the northern Flinders Ranges, perhaps over the last 4 million years (Quigley *et al.*, 2007). The Willawortina Formation is not known to host uranium mineralisation, but may be anomalous for uranium due to uranium-bearing groundwaters and uranium-bearing fragments of granitoids from the Mount Painter and Mount Babbage inliers.

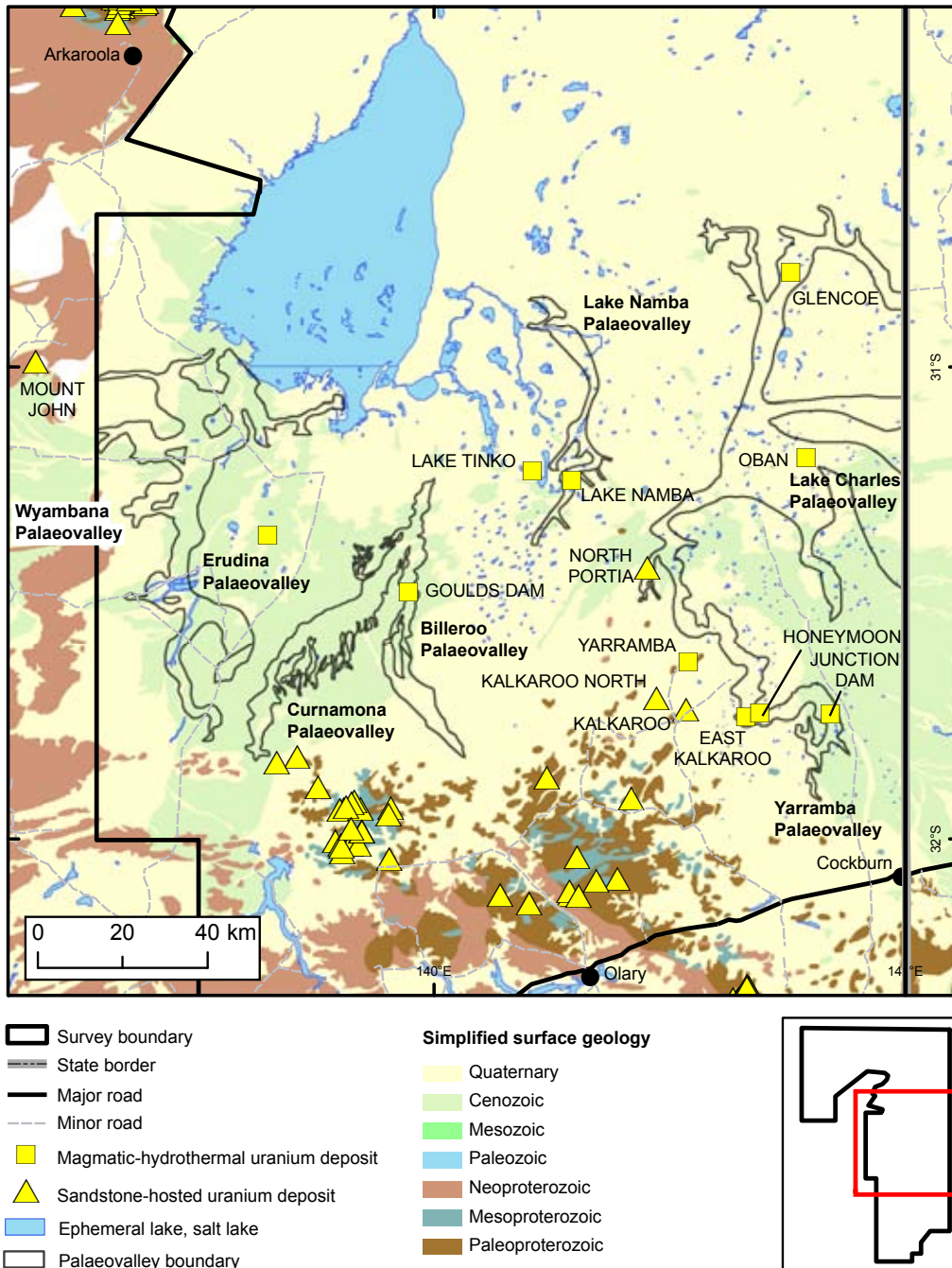


Figure 3.18: Interpreted palaeovalleys of the southern Callabonna Sub-basin, from the first release of the SA Palaeovalley Map (Hou *et al.*, 2007), overlain on simplified 1:1 million Surface Geology of Australia Map (Raymond and Retter, 2010).

3.2.6 Quaternary

Quaternary cover occurs throughout the Frome AEM Survey area and includes aeolian, fluvial and colluvial deposits. These are described in more detail as part of the regolith geology in [Section 3.4.2](#).

3.2.7 Granites and other felsic rocks

S. Jaireth and C. E. Wade

Many granites and other felsic rocks in the Curnamona Province are enriched in uranium. In some, uranium is present in an easily leachable form. These granites are potential sources of uranium for sandstone-hosted uranium deposits in the Lake Frome region. This section summarises important features of granites and other felsic rocks which could be important for uranium systems discussed in more detail in the following sections.

Granites have been described in some detail by Sheard *et al.* (1992), Teale (1993), Neumann (2001), Elburg *et al.* (2008), Budd *et al.* (2001) and McLaren *et al.* (2006). Wade (2011) collated the available geochronological data for granites within the Curnamona Province ([Table 3.1](#)) and grouped some of them into the Ninnerie Supersuite ([Figure 3.19](#)). Granites in the Curnamona Province belong to three broad age groups:

1. Ninnerie Supersuite (~1600 Ma to 1570 Ma) mapped in the Olary Domain as well as in the Mount Painter and Mount Babbage inliers;
2. Granites with emplacement age of ~1560 Ma;
3. Granites of Cambrian-Ordovician age (including the ~450 Ma British Empire Granite, Paralana Granodiorite, Mudnawatana Tonalite and pegmatites and ~460 Ma Anabama Granite).

The Ninnerie Supersuite comprises felsic S-type granites to intermediate and alkaline I-type granites, and A-type felsic volcanics (Wade, 2011). The granites are enriched in rare earth elements and high-field-strength elements. In the Olary Domain some granites were emplaced during brittle deformation, however, the majority of the Supersuite is interpreted to postdate the main deformation stages of the Olarian Orogeny (~1620-1580 Ma). Kositcin (2010) associated the emplacement of these granites with a continental-scale thermal event which also formed the bi-modal Gawler Range Volcanics and Hiltaba Granite Suite in the Gawler Craton. In the Mount Painter and Mount Babbage inliers the granites underwent metamorphism at ~1555 Ma (Fraser and Neumann, 2010). High grade metamorphism produced the uranium-enriched Hot Springs Gneiss from granites emplaced at ~1580 Ma ([Table 3.1](#); Fraser and Neumann, 2010).

Felsic magmatism in the Mount Babbage Inlier occurred at ~1560 Ma when the uranium-enriched Yerilla Granite was emplaced. This event also includes the Prospect Hill, White Well, Terrapinna and Wattleowie granites and Petermorra Volcanics ([Table 3.1](#)). The Yerilla Granite has the greatest potential as a source of uranium. It is an I-type, highly fractionated granite enriched in high field strength elements which include rare earth elements, zirconium, niobium, thorium, yttrium and tungsten (Teale, 1993).

The Ordovician British Empire Granite is a pegmatoidal garnet-muscovite granite comprising of I- and S-type phases (Elburg *et al.*, 2003; McLaren *et al.*, 2006) located in the Mount Painter Inlier. These phases were intruded during the ~440 Ma Rodingan Movement of the Alice Springs Orogeny, which is coeval with the Benambran Orogeny in Eastern Australia. Diopside-titanite veins, pegmatites and uranium mineralisation in the Mount Painter Inlier were also emplaced at this time. Wülser (2009) associates metasomatic overprints on the Mount Neill Granite and Hot Springs Gneiss with this event. The importance of this event in generating an easily leachable source of uranium is discussed in the section on sandstone-hosted uranium mineral systems ([Section 3.5](#)).

The Anabama Granite, dated at 468 ± 62 Ma (Stevenson and Webb, 1976), intrudes rocks of the Neoproterozoic Umberatana Group. It consists of biotite granodiorite interlayered with

The Frome airborne electromagnetic survey, South Australia: implications for energy, minerals and regional geology

microgranodiorites and is crosscut by several quartz porphyry and dacite porphyry dykes. Locally the granite is completely altered to a greisen-like assemblage containing quartz and muscovite.

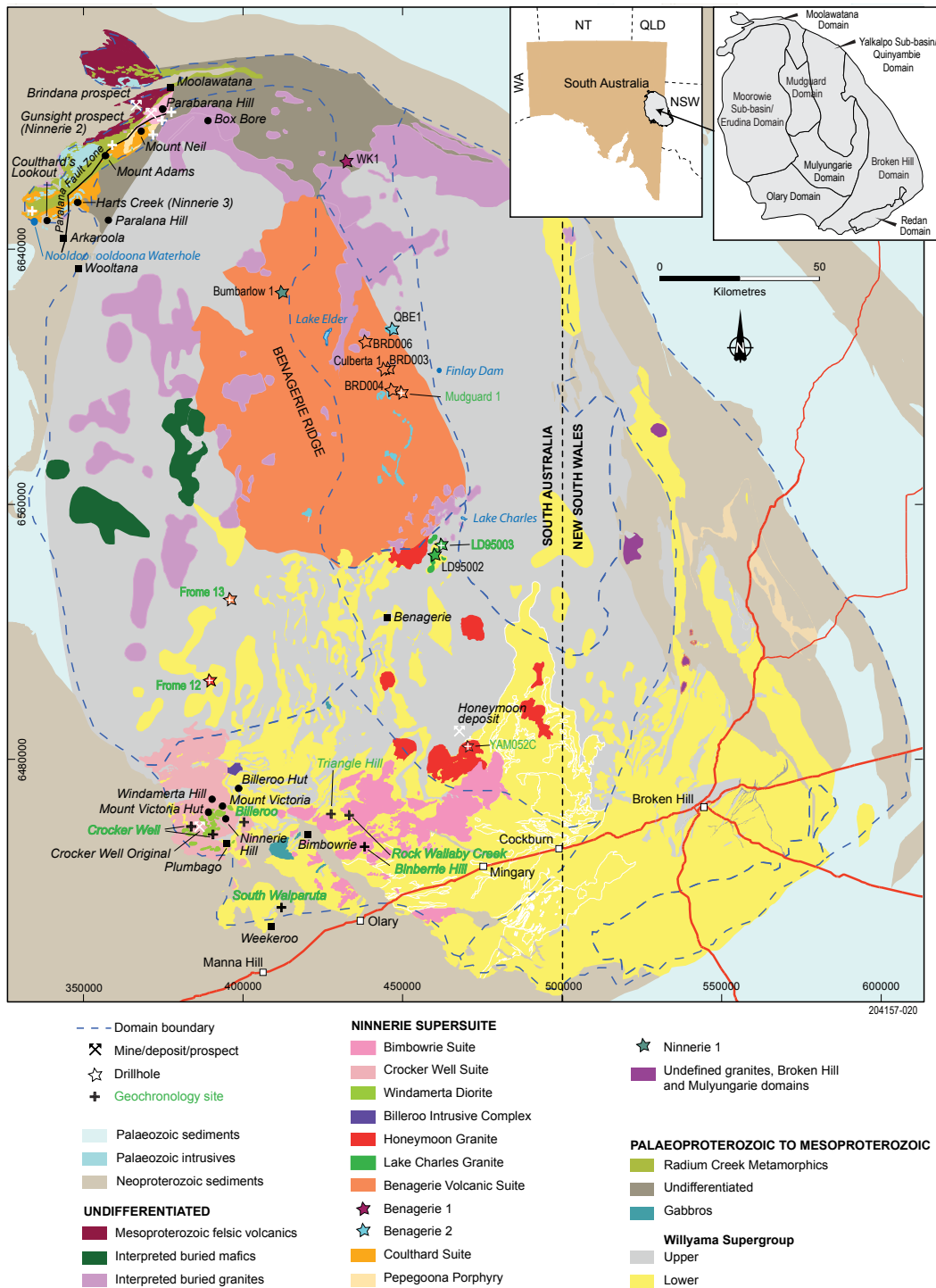


Figure 3.19: Distribution of the Ninnerie Supersuite granites within the Curnamona Province. Modified after Wade (2011).

The Frome airborne electromagnetic survey, South Australia: implications for energy, minerals and regional geology

Table 3.1: Ages, uranium and thorium content of uranium-bearing granites and felsic rocks within the Curnamona Province, including the Ninnerie Supersuite.

DOMAIN	PROVINCE	NAME	AGE Ma	± Ma	DESCRIPTION	COMMENTS	REFERENCE	U RANGE PPM	U AVG PPM	Th AVG PPM	Th/U AVG	MAIN U- BEARING MINERALS
Moolawatana	Mount Babbage	Terrapinna Granite	1560	3	Coarse-grained granite	Magmatic crystallisation age	Fraser and Neumann (2010)	2-28	8	49	7	Zircon, monazite, allanite
		Yerilla Granite	1558	4	Coarse-grained granite	Magmatic crystallisation age	Fraser and Neumann (2010)	4-270	107	355	4.1	Uraninite in pyrite, monazite, xenotime, allanite, zircon, apatite, titanite (Ti-silicate)
		Wattleowie Granite	1563	3	Biotite granite with biotite foliation	Magmatic crystallisation age	Fraser and Neumann (2010)	2-50	7	35	6.2	Zircon, monazite
		Petermorra Volcanics	1560	3	Deformed felsic extrusive, volcaniclastics, epiclastic sandstone	Magmatic crystallisation age	Teale and Flint (1993)	2-34	10	32	6.4	Zircon, monazite, allanite
		White Well Granite	1556	4	Biotite granite	Age assumed to be similar to the Yerilla Granite	Sheard <i>et al.</i> (1992)	4-16	9	45	7.1	Zircon, monazite
		Prospect Hill Granite	1556	4	Biotite granite	Age assumed to be similar to the Yerilla Granite	Sheard <i>et al.</i> (1992)	-	96	207	2.2	Monazite, allanite
		Mount Painter	Mount Neill Granite, Coulthard Suite	1585	3	Coarse-grained granite	Magmatic crystallisation age	Fraser and Neumann (2010)	3-380	30	90	5.4
		Box Bore Granite, Coulthard Suite	1583	2	Coarse-grained granite, gneissic fabric	Magmatic crystallisation age	Fraser and Neumann (2010)	5-79	41	130	4.2	Allanite, monazite, zircon

The Frome airborne electromagnetic survey, South Australia: implications for energy, minerals and regional geology

DOMAIN	PROVINCE	NAME	AGE Ma	± Ma	DESCRIPTION	COMMENTS	REFERENCE	U RANGE PPM	U AVG PPM	Th AVG PPM	Th/U AVG	MAIN U- BEARING MINERALS
Moolawatana	Mount Painter	Nooldoonooldoon a Trondhjemite, Coulthard Suite	1575	3	Na-altered Mount Neill Granite	Magmatic age of precursor Mount Neill Granite. Age of metasomatism ?1555 Ma	Elburg <i>et al.</i> (2008)		17	67	3.9	Zircon, monazite
		Hot Springs Gneiss	1582	6	Coarse-grained augen granitic gneiss with strong biotite foliation	Magmatic crystallisation age	Fraser and Neumann (2010)	7-427	98	330	3.4	Zircon, trace allanite
		Hodgkinson Granodiorite (4 Mile Creek)	1552	4	Medium-grained granodiorite	Magmatic crystallisation age	Neumann (2001)		5	12	2.4	Zircon
		Pepegoona Porphyry	1576	2	Rhyolitic and rhyodacitic metavolcanics	Magmatic crystallisation age	Teale and Flint (1993)	13-34	24	72	3.2	Zircon, titanite, ?xenotime
		British Empire Granite	455	8	Granite batholith with S-type intruded by I-type	Pb-Pb stepwise leaching of garnet	McLaren <i>et al.</i> (2002), Elburg <i>et al.</i> (2003)	2-32	11	9	1.2	Zircon, monazite, xenotime
		Radium Creek Metamorphics (Lower metasediments)	1600	8	Quartzofeldspathic gneiss with bands of heavy minerals	Maximum age of deposition	Fraser and Neumann (2010)	2-5	3	16	5.7	Zircon
		Radium Creek Metamorphics (Upper metasediments)	1591	6	Quartzofeldspathic gneiss with bands of heavy minerals	Maximum age of deposition	Fraser and Neumann (2010)	2-5	3	16	5.7	Zircon
		Golden Pole Granite	1560		Even textured brick red coloured granite	Maximum interpreted age of emplacement	Wall (1995)	1-10	4	36	18	Zircon, xenotime

The Frome airborne electromagnetic survey, South Australia: implications for energy, minerals and regional geology

DOMAIN	PROVINCE	NAME	AGE Ma	± Ma	DESCRIPTION	COMMENTS	REFERENCE	U RANGE PPM	U AVG PPM	Th AVG PPM	Th/U AVG	MAIN U- BEARING MINERALS
Moolawatana	Olary	Honeymoon Granite	1541	59	Quartz-plagioclase-alkali feldspar-muscovite-biotite granite	Concordia intercept age	Jagodzinski and Fricke (2010)	13.5-40	27.6	8.4	0.4	Monazite, zircon, apatite, allanite, titanite, U-oxides in pyrite
		Lake Charles Diorite	1585	195	Medium- to fine-grained hornblende-bearing diorites to granodiorites	Magmatic crystallisation age	Fanning (2009)	0.4-6	2.4	7	3.1	Zircon
Olary		Mindamereeka Trondhjemite, Crocker Well Suite	1580	21	White, coarse-grained and massive leucocratic phlogopite trondhjemites grading into alaskites, characterised by opalescent blue quartz	Magmatic crystallisation age	Ludwig and Cooper (1984)	0.9-110	13.9	72.8	13	Allanite, monazite, zircon, thorium brannerite
		Mount Victoria Granite, Crocker Well Suite	1579	2	Biotite-only to biotite-muscovite-bearing monzogranites	Magmatic crystallisation age	Ludwig and Cooper (1984)	0.5-19.1	7	60.3	11.6	Zircon, monazite
		Bimbowrie Suite	1581	3	Medium- to coarse-grained muscovite-biotite granite characterised by large K-feldspar phenocrysts	Magmatic crystallisation age	Page <i>et al.</i> (in prep)	0.1-35	8.5	38.1	6.3	Zircon
		Windamerta Diorite	1581	6	Biotite and hornblende diorites, granodiorites and tonalites	Magmatic crystallisation age	Fanning (pers. Comm..)	0.3-51	9.2	47.2	2.3	Zircon, allanite

The Frome airborne electromagnetic survey, South Australia: implications for energy, minerals and regional geology

DOMAIN	PROVINCE NAME	AGE Ma	± Ma	DESCRIPTION	COMMENTS	REFERENCE	U RANGE PPM	U AVG PPM	Th AVG PPM	Th/U AVG	MAIN U- BEARING MINERALS
Olary	Billeroo Intrusive Complex	1610 to 1550	-	Alkaline magmatic rocks including syenite bodies, layered feldspathic ijolite phases and alkali lamprophyre dykes	Constrained by tectonic fabrics formed during the third phase of the Olarian Orogeny and layer parallel fabrics within Willyama Supergroup clasts	Rutherford (2006)	0.3-7.2	2.3	9.6	4.7	No information
Mudguard	Finlay Dam Rhyolite, Benagerie Volcanic Suite	1587	6	Porphyritic rhyolitic volcanic rocks	Magmatic crystallisation age	Jagodzinski and Fricke (2010)	11-21	16.2	55.1	3.4	Zircon
	Lake Elder Rhyodacite, Benagerie Volcanic Suite	~ 1585	-	Porphyritic rhyodacitic volcanic rocks	-	Wade (2011)	8.5-18.5	11.8	35.8	3	Zircon
	Benagerie 1, Benagerie Volcanic Suite	-	-	Extensively altered porphyritic amygdaloidal trachytes occurring as a series of flows with scoriaceous tops	-	Wade (2011)	8-18	10.8	37.6	3.6	No information
	Ninnerie 1, Ninnerie Supersuite	1550 - 1590	-	Fine-grained basalt	Max depositional ages of overlying and underlying sediments respectively	Fraser and Neumann (2010)	4-10.5	6.5	14.7	2.3	No information

Hydrothermal activity associated with uranium mineralisation probably continued into the Middle Paleozoic as sinter deposits in Mount Painter and Mount Gee. The actual age of the Mount Painter-Mount Gee epithermal system is controversial; it has been suggested that it represents the waning stages of intrusion of the British Empire Granite (Elburg *et al.*, 2003), but more recent work suggests that the epithermal activity occurred to < 315 Ma (Brugger *et al.*, 2011a; b)

Paleozoic intrusions are probably not electrically conductive (Palacky, 1993), unless their weathered zones are saturated with salty water, and they are believed to be a major uranium source for sandstone-hosted uranium deposits within the Callabonna Sub-basin and Murray-Darling Basin. Paleozoic intrusive rocks are also associated with epithermal copper, gold and base metal mineralisation within themselves and the surrounding Neoproterozoic rocks. These mineral systems are described in more detail in [Section 3.6](#).

3.3 PHYSIOGRAPHY

I. C. Roach

The Frome AEM Survey area contains a variety of landforms that are generated by neotectonic, eustatic, alluvial or aeolian processes. The description here is generally limited to those that are visible in the AEM data or that affect the operation of the survey aircraft.

The survey area is dominated by the high- to moderate relief Flinders, Olary Spur and Barrier Ranges, part of the Nackara Arc (Marshak and Flöttmann, 1996) which are included, respectively, in the Flinders-Lofty Ranges, Olary Spur and Barrier Ranges physiographic regions of the Australian Collaborative Land Evaluation Program (ACLEP; Pain *et al.*, 2011) ([Figure 3.20](#)). Relief within the survey area is ca. 865 m, from highs on the flanks of the Flinders Ranges and Olary Spur (up to 859 m above sea level), to lows of 6 m below sea level on the Eyre-Frome Plains. The Flinders-Lofty Ranges and Olary Spur and Barrier Ranges are typified by bedrock-dominated rises (9-30 m relief), low hills (30-90 m relief), hills (90-300 m relief) and rare mountains (>300 m relief, except for the Barrier Ranges, where there are none). In the Flinders-Lofty Ranges (relief ca. 836 m within the survey area), these landscape features are often strike ridges, chiefly composed of slightly weathered, openly-folded Neoproterozoic rocks, mainly quartzite with interbedded shale/slate, conglomerate or tillite and dolomite. In the Olary Spur (relief ca. 591 m within the survey area) these features are a mixture of strike ridges composed of Neoproterozoic rocks (mainly quartzite) and slightly to moderately weathered, rounded rises to hills of Paleo-Mesoproterozoic metamorphic rocks of the Curnamona Province. In the Barrier Ranges (relief ca. 144 m within the survey area), the landscape consists almost entirely of rises to hills of rounded, slightly to moderately weathered metamorphic rocks of the Curnamona Province. Valleys everywhere are filled with Quaternary colluvium and alluvium, and where more deeply incised, may contain Cenozoic sediments (Namba Formation and possibly thin Eyre Formation) under Quaternary cover; these have dendritic to linear drainage patterns visible in the multiresolution valley bottom flatness (MRVBF; Gallant and Dowling, 2003) index image ([Figure 3.21](#)), depending on the nature of the substrate (Paleo-Mesoproterozoic or Neoproterozoic).

Low-lying areas within the survey area include land within the Strzelecki Plains, the Simpson Desert Plains, the Torrens-Gulf Plains, the Eyre-Frome Plains, the West-Turkey Plains and the Ivanhoe Plains ([Figure 3.20](#)). The Strzelecki Desert Plains (relief 132 m within the survey area) and the Simpson Desert Plains (relief 44 m within the survey area) are dominated by longitudinal Holocene sand dunes up to about 20 m high (Bowler, 1976; Fitzsimmons *et al.*, 2007; Wasson *et al.*, 1988), visible in [Figure 3.20](#), and thin sand sheets with numerous claypans and salt lakes within the dune swales. These plains feature disrupted linear and dendritic drainage patterns depending on the dune frequency, sand sheet height or nature of the substrate. The Simpson Desert Plains are constructed on weathered Mesozoic sediments and feature dendritic drainage patterns for the most part ([Figure](#)

3.21). The Torrens-Gulf Plains (220 m relief within the survey area) consist largely of gently sloping outwash fans from the western Flinders Ranges draining into Lake Torrens.

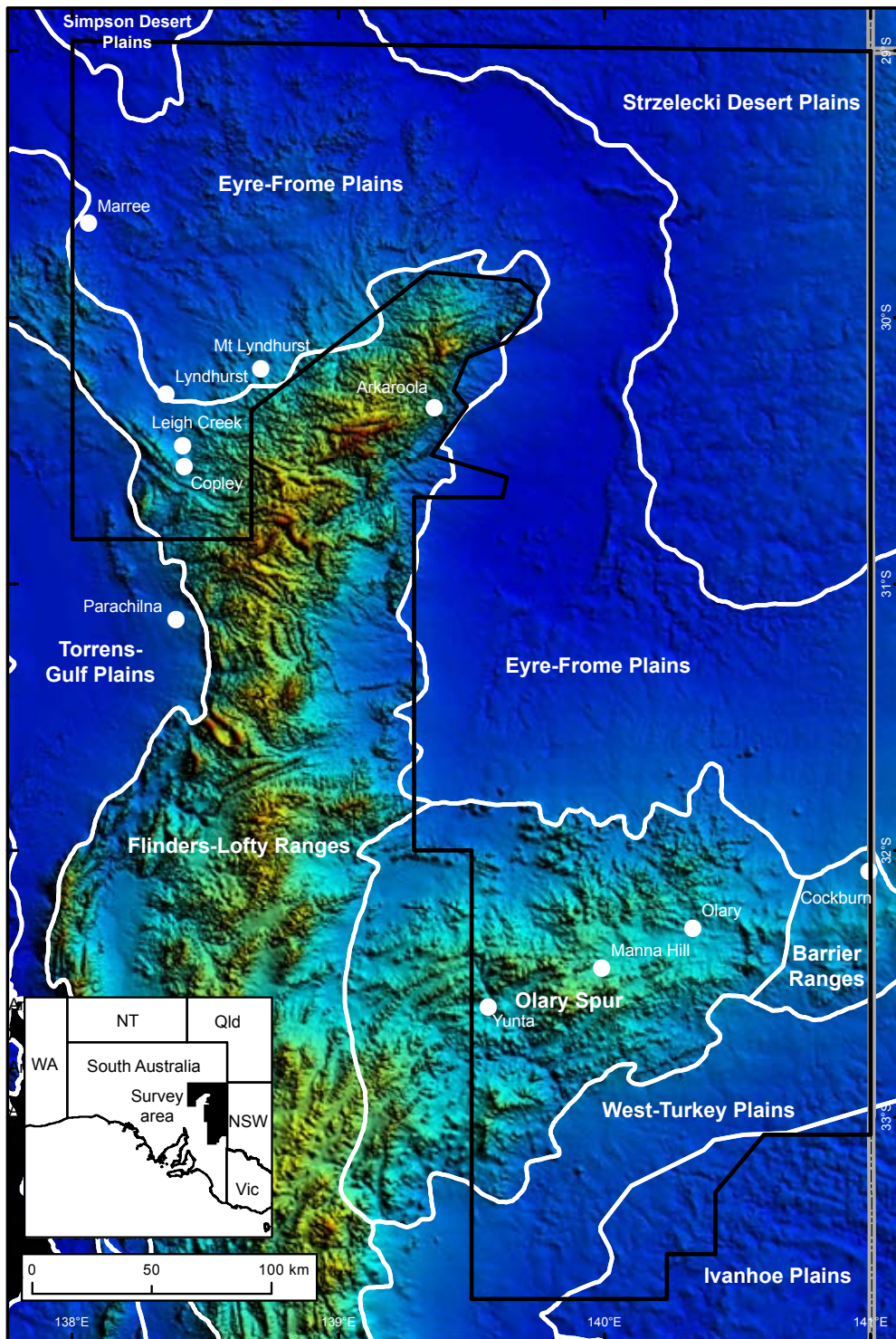


Figure 3.20: Physiographic regions of the Frome AEM Survey area. Physiographic regions are from the Australian Collaborative Land Evaluation Program (ACLEP; Pain et al., 2011) overlain on a sunshaded image of the SRTM DEM-S.

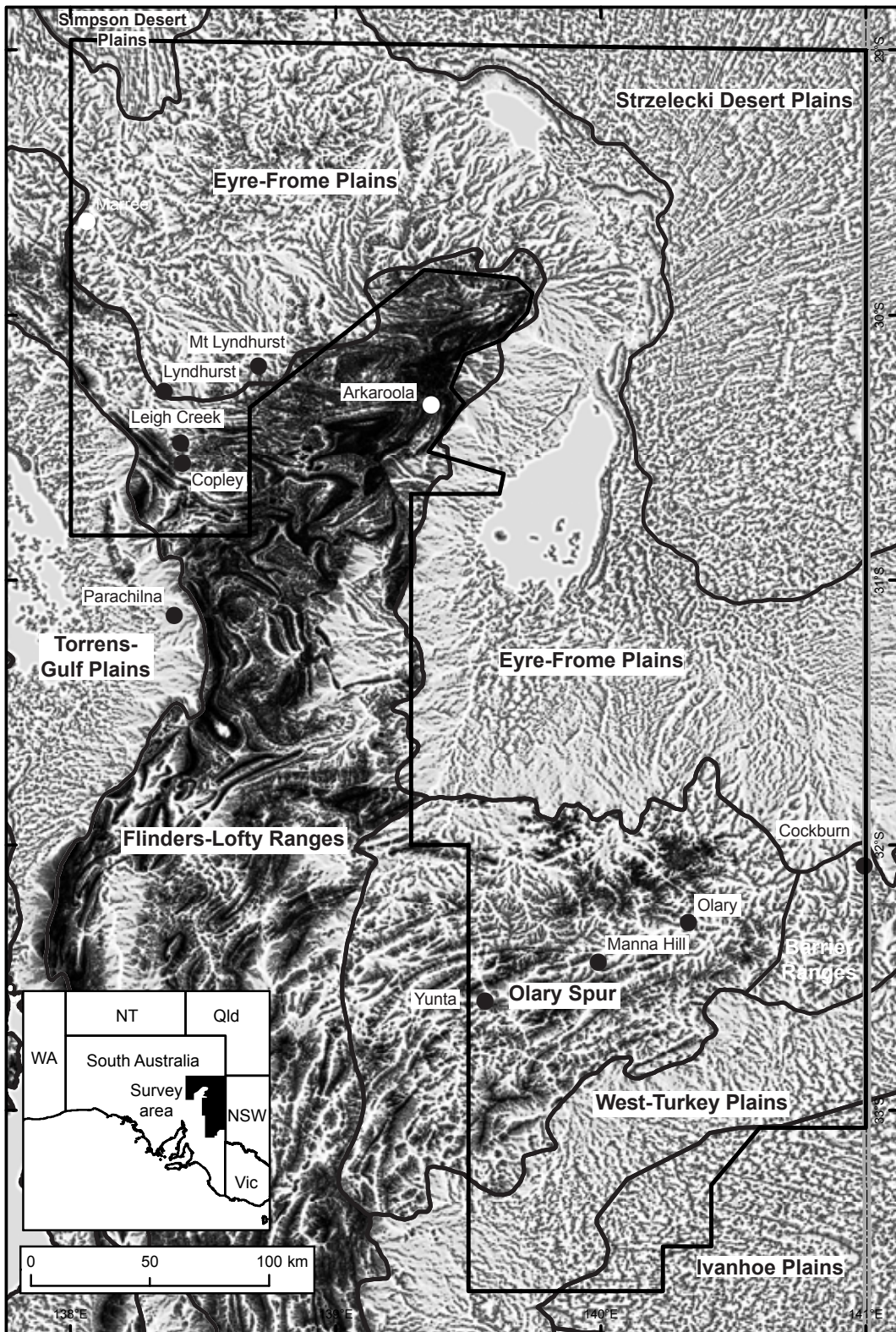


Figure 3.21: Multi resolution valley bottom flatness step 4 (MRVBF4; Gallant and Dowling, 2003) index image of the Frome AEM Survey area highlighting differences in drainage patterns between physiographic regions (Pain et al., 2011). The image is derived from the smoothed 1 second SRTM DEM.

The Eyre-Frome Plains (357 m relief within the survey area) include the lowest parts of the survey area (6 m below sea level) and are dominated by gently sloping outwash plains from the Flinders, Olary Spur and Barrier Ranges, into the Frome Embayment, together with source-bordering dunes and lunettes on the leesides of the larger drainage channels and lakes including lakes Frome, Callabonna and Blanche. To the north of the Flinders Ranges, the Eyre-Frome Plains feature well-developed dendritic drainage patterns on dissected plateaux (generally rises of 9-30 m relief) of Mesozoic sediments of the Eromanga Basin, little affected by sparse Holocene dunes and sand sheet cover.

The West-Turkey Plains (relief 219 m within the survey area) are gently sloping outwash plains from the Olary and Barrier Ranges into the Murray-Darling Basin, draining onto the Ivanhoe Plains (relief 56 m within the survey area), into which the modern day floodplain of the Murray River is incised. Long, low, Pliocene beach ridges in the Murray-Darling Basin (Brown, 1985; Brown and Stephenson, 1991; Roy *et al.*, 2000; Wallace *et al.*, 2005) are major landscape features in the Ivanhoe Plains and extend partially into the West-Turkey Plains, where they appear to be overlain or eroded by outwash fans from the Olary Spur. The beach ridges were deposited during the last sea level regression in the Murray-Darling Basin.

Aircraft operations were not hampered in the low-relief parts of the survey area, however flight planning had to be altered in the higher-relief parts including within the Flinders-Lofty Ranges and the Olary Spur. The Flinders-Lofty Ranges physiographic region was largely excised from the survey area because of the hazard that the high relief posed to low-flying, fixed-wing aircraft operations. More detail on the effects of terrain on the aircraft are included in [Section 1.4.2](#).

3.4 REGOLITH GEOLOGY

The regolith of the Frome AEM Survey area is highly complex and has been modified by the effects of neotectonic, eustatic, fluvial and aeolian processes, as well being deeply weathered in many places. A number of detailed maps and texts describe the regolith, regolith-landforms and landscape evolution of the Lake Frome area, Olary Spur, Barrier Ranges and northern Flinders Ranges, most particularly those developed from work conducted by the Cooperative Research Centre for Landscape Environments and Mineral Exploration (CRC LEME). This synthesis relies largely on the Curnamona 1:500 000 regolith-landforms map of Gibson (1999) ([Figure 3.22](#)), which provides a reasonable description of the regional regolith-landforms of the Frome Embayment, and the Curnamona Explorer's Guide (Fabris *et al.*, 2008).

The Frome airborne electromagnetic survey, South Australia: implications for energy, minerals and regional geology

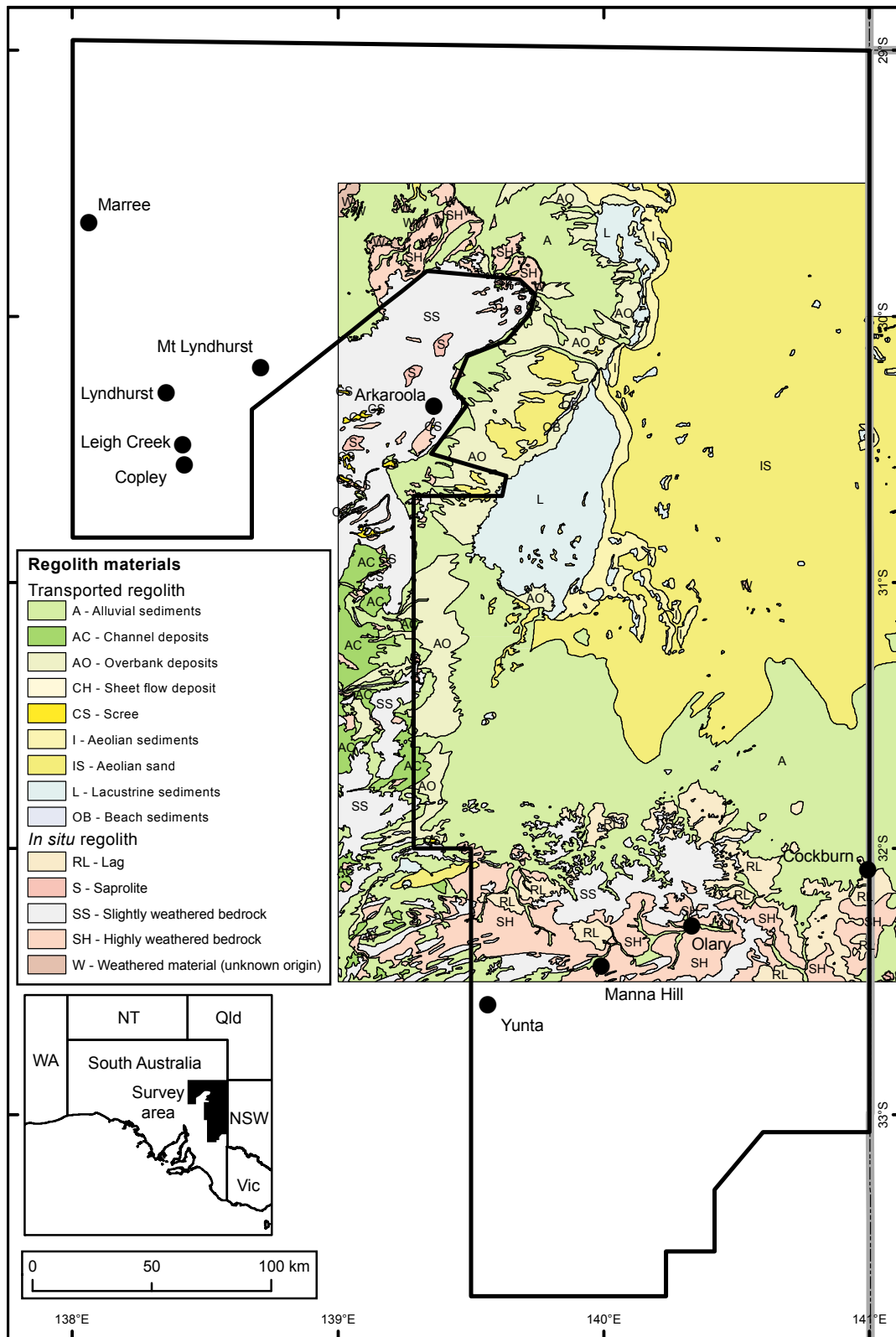


Figure 3.22: Regolith materials map of a portion of the Frome AEM Survey area, simplified from the Curnamona and Broken Hill 1:500 000 regolith-landforms maps of Gibson (1999).

3.4.1 *In situ* regolith

In situ regolith refers to weathered basement rocks, which may be apparently fresh, with < 5% of weatherable minerals altered, common in Neoproterozoic quartzite of the Nackara Arc, to highly weathered basement rocks, with > 50% of weatherable minerals altered to secondary minerals such as kaolinite, hematite and/or goethite, common in metasediments of the Paleoproterozoic Willyama Supergroup. Fresh rock, saprock (> 5 - < 20% of weatherable minerals are altered) and saprolite (> 20% of weatherable minerals are altered) occur throughout the Flinders and Barrier ranges and Olary Spur to a greater or lesser extent. Weathering criteria used here are after Eggleton (2001).

In the Paleo-Mesoproterozoic Willyama Supergroup of the Barrier Ranges and Olary Spur, bedrocks are largely highly weathered according to the classification of Gibson (1999), although local variation in weathering grade exists. Figure 3.23 illustrates some examples of moderately to highly weathered bedrocks of the Willyama Supergroup in the Mingary Pit beside the Barrier Highway, southwest of Cockburn SA. Here, the bedrocks have most of the feldspars and ferromagnesian minerals weathered to kaolinite and iron oxyhydroxides, respectively. The rock still maintains its original metamorphic texture but displays a typical weathering profile of (from the surface down): a quartzose and ferruginous colluvial gravel lag consisting of angular to subangular quartz fragments of local quartz veins, subrounded to rounded maghemite nodules and subangular to subrounded, ferruginised bedrock fragments (Figure 3.23A); a mottled zone consisting of kaolinite-rich saprolite with ferruginous mottles (Figure 3.23B, C); a bleached plasmic (clay-rich) zone (Figure 3.23B) and saprolite with obvious original metamorphic rock textures (Figure 3.23D).

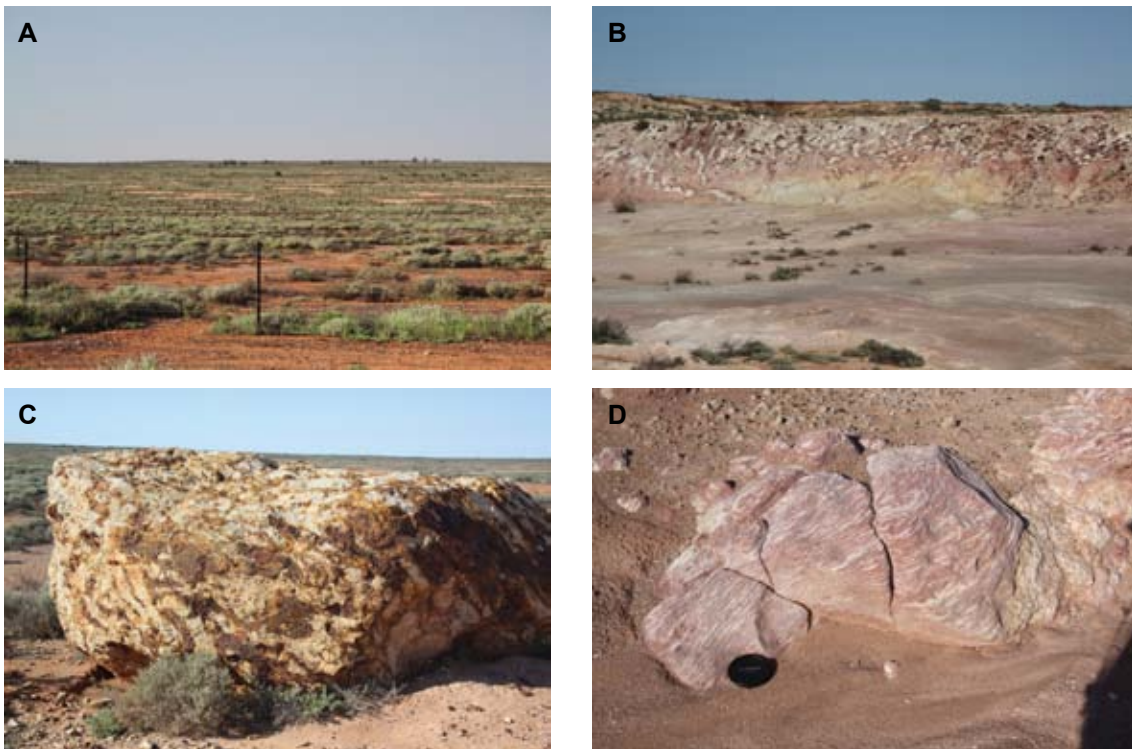


Figure 3.23: Examples of *in situ* regolith in the Frome AEM Survey area, Barrier Ranges physiographic region, Mingary Pit (GR 479180 mE 6446200 mN MGA54). A: Thin colluvial sheetwash cover with contour banding over weathered Willyama Supergroup bedrocks near the Mingary Pit; B: Mottled zone (upper) and plasmic zone (lower) on a weathering profile of Willyama Supergroup schists at Mingary Pit; C: Mottled saprolite boulder, Mingary Pit; D: Highly weathered schist, displaying original metamorphic rock texture.

The Frome airborne electromagnetic survey, South Australia: implications for energy, minerals and regional geology

A large portion of the Barrier Ranges physiographic region within the Frome AEM Survey area consists of rolling topography with little surface outcrop, much like the area around the Mingary Pit. Outcrops of Willyama Supergroup tend to have subdued relief and are highly ferruginised or coated in a silica-rich skin of ‘desert varnish’ or a manganese oxide-rich coating from the weathering of manganese-rich garnet, common in the Willyama Supergroup.

The Neoproterozoic rocks of the Flinders Ranges and Olary Spur are generally slightly to moderately weathered, according to Gibson’s (1999) classification. Where these rocks outcrop, the landscape is dominated by moderate to high relief strike ridges of slightly weathered quartzite (Figure 3.24A) or quartzose conglomerate (often Sturtian tillite). These are interbedded with dolomite, dolomitic shale or mudstone (Figure 3.24B). Where weathered, the rocks display dominantly ferruginous staining or mottling or development of calcrete-rich lithosols, depending on the original rock type. Much of the present day landscape within the Flinders Ranges and Olary Spur has been generated by tectonic and neotectonic activity within the Nackara Arc since the Late Cretaceous (Mitchell *et al.*, 2002) and into the Miocene (Foster *et al.*, 1994) or Late Quaternary (Quigley *et al.*, 2007), leading to the dramatic, jagged, high relief landscape visible today (Figure 3.24C, D). Away from active faults, landforms are more rounded and of low to moderate relief (Figure 3.24B). Landscape evolution is discussed in more detail in Section 3.6.

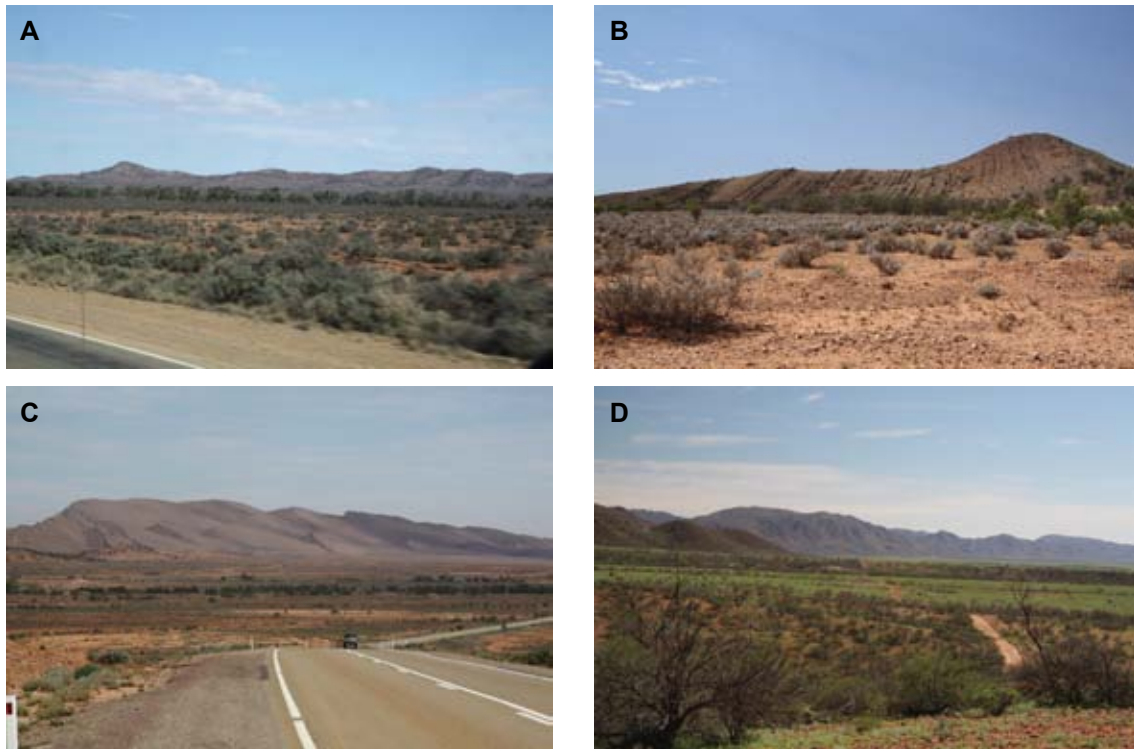


Figure 3.24: Examples of *in situ* regolith in the Frome AEM Survey area in the Olary Spur and Flinders Ranges physiographic regions. A: Slightly to moderately weathered quartzite strike ridges, Barrier Highway between Manna Hill and Yunta, SA; B: Slightly to moderately weathered, interbedded quartzite and dolomitic shale in a dissected strike ridge, north of Yunta SA; C: Cuestas and flatirons on slightly weathered, dipping quartzite beds, western flinders Ranges south of Leigh Creek, SA; D: Rugged terrain on slightly to moderately weathered bedrock, eastern Flinders Ranges, looking north from East Painter Creek towards Paralana Creek (approx GR 349000 mE 6653000 mN MGA54).

In the northern Flinders Ranges, Gibson (1999) mapped igneous and metamorphic rocks of the Mount Painter and Mount Babbage inliers as slightly weathered saprolith. These inliers consist largely of slightly weathered, but heavily incised, granites and metamorphic rocks of the Moolawatana Domain which have been intruded through by granites of Ordovician age, most notably the British Empire Granite. The Frome AEM Survey skirts the edges of the Flinders Ranges, excludes the outcropping Mount Painter Inlier, but includes a small portion of the outcropping Mount Babbage Inlier. Neotectonic fault activity has raised the Northern Flinders Ranges and it present has up to 836 m of relief within the survey area, but over 1000 m within the Flinders Ranges proper. Gibson (1999) mapped a series of highly weathered bedrock features to the north of the Flinders Ranges, composed of weathered Mesozoic sediment, as highly weathered saprolith or “weathered material (unknown origin)” (Figure 3.22). These have been subsequently mapped by Davey (2009) as colluvium and are included as transported regolith in the descriptions of Fabris *et al.* (2008). Gibson (1999) also mapped large areas of colluvium as “lag”; these units are both recognised as transported regolith and are described in Section 3.4.2 below.

3.4.2 Transported regolith

The transported regolith-landforms of the Frome AEM Survey area are dominated by alluvial, colluvial and aeolian regolith materials (Figure 3.22) lying principally within the Eyre-Frome Plains and Strzelecki Desert Plains physiographic regions (Figure 3.20, 3.21). Mesozoic and Cenozoic terrestrial and marine sediments of the Lake Eyre Basin-Callabonna Sub-basin and the Eromanga Basin have been extensively reworked by modern alluvial, colluvial and aeolian processes, as well as being extensively weathered and indurated in parts, and are here regarded as transported regolith.

Modern alluvial systems emanate from the uplands of the Flinders-Lofty Ranges, Olary Spur and Barrier Ranges physiographic regions, draining into the Lake Eyre Basin to the north, the Murray-Darling Basin to the south and to Lake Torrens in the west, as ephemeral streams. These systems carry a bedload of clay- to boulder-sized particles, depending on proximity to source and the relief of the channel bed (Figure 3.25A, B).

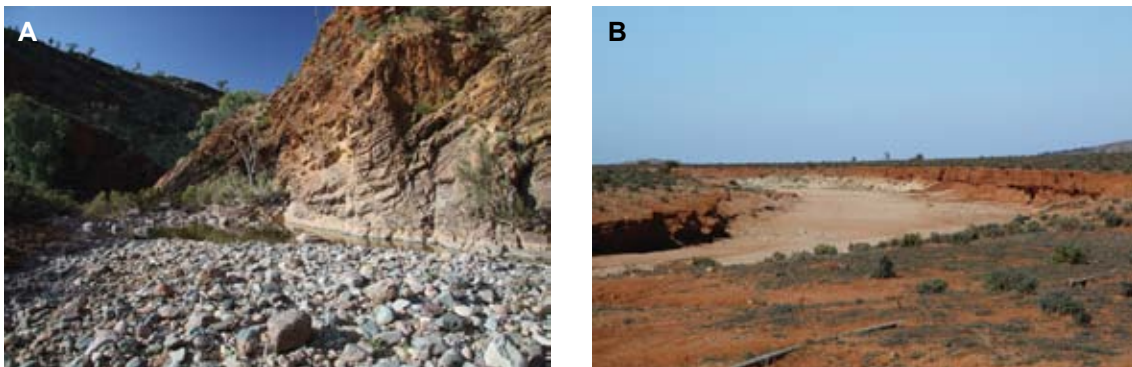


Figure 3.25: Examples of transported regolith in the Frome AEM Survey area. A: Stubbs Waterhole in Arkaroola Creek, Arkaroola Wilderness Sanctuary, showing source-proximal fine sand to boulder sized bedload of dominantly Neoproterozoic rocks; B: Gorge Creek (GR 420000 mE 6364500 mN MGA54), near Cronje Dam in the Murray-Darling Basin, showing source-distal clay to pebble size bedload and erosion of desert loam soils of the floodplain and a rock bar of heavily calccreted Neoproterozoic dolomite.

Particles are sourced from local bedrocks which may be Paleo-Mesoproterozoic Willyama Supergroup rocks, Neoproterozoic rocks of the Nackara Arc, Cambro-Ordovician rocks of the Kanmantoo Group, reworked Mesozoic-Cenozoic material from the Eromanga Basin, Lake Eyre Basin and Murray-Darling Basin, reworked aeolian sand from dune fields or clay to silt-sized aggregates of parna (wind-blown dust). These alluvial systems commonly feature levees and

The Frome airborne electromagnetic survey, South Australia: implications for energy, minerals and regional geology

floodplains of clay to granule sized particles, often with colluvially-rearranged gravel lag on the surface, source-bordering dunes on the larger systems, and have extensively developed alluvial fan systems, including Manunda Creek which drains into the Murray-Darling Basin (Figure 3.26).

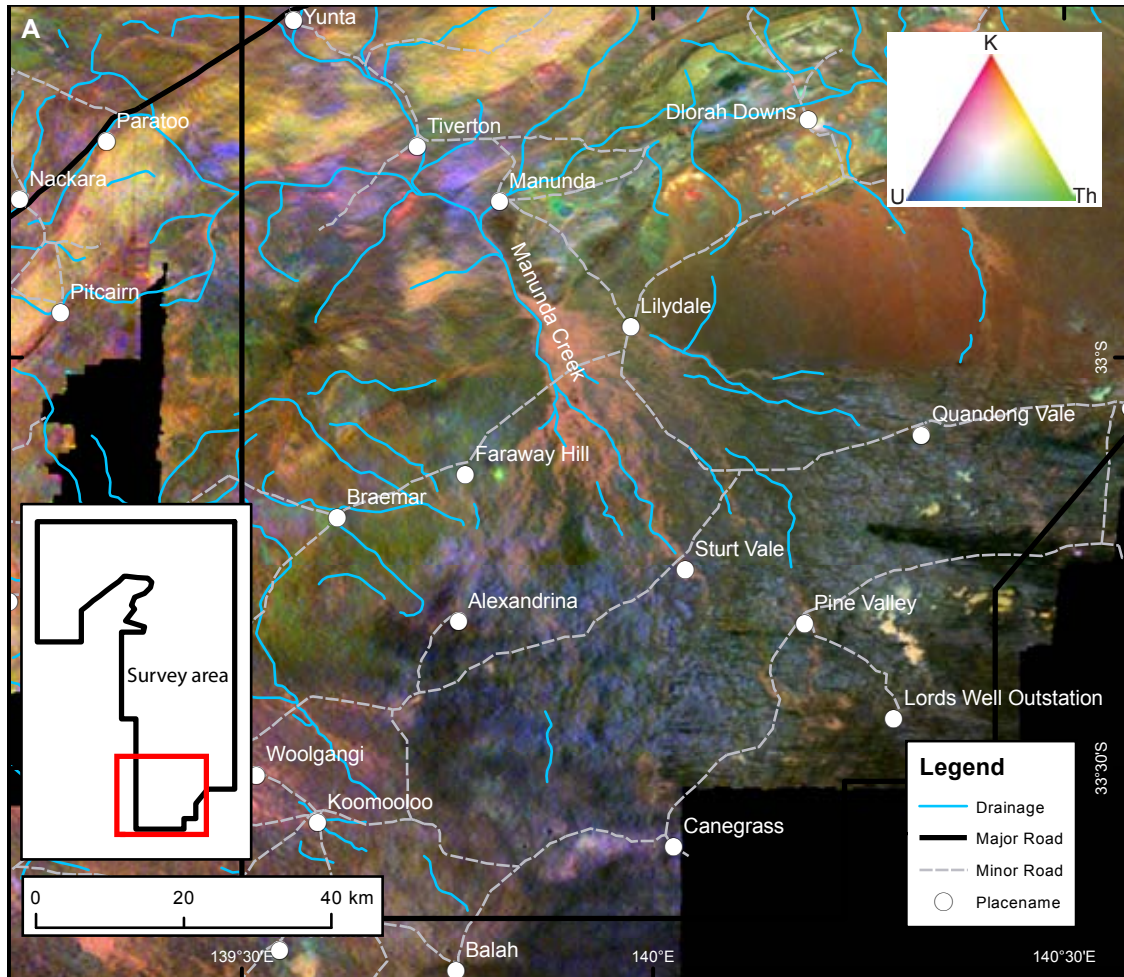


Figure 3.26: Ternary radiometric image of the Manunda Creek alluvial fan overlying the Murray-Darling Basin. The radiometric image has been created by merging different surveys of varying flight line spacing and has significant gaps where no radiometric information has been collected.

Most alluvial systems terminate in the dune fields of the Eyre-Frome Plains or the West-Turkey Plains, where surface water percolates underground, however, a few larger systems are persistent enough to terminate at the edges of the large salt lake systems including Lake Frome, Lake Callabonna and Lake Blanche, some as prograding deltas (Figure 3.27). Numerous small ephemeral streams are present within the dune swales of the Strzelecki Desert and Simpson Desert. These only flow after heavy rain and are typical of low relief, arid zone drainage systems, having floodplains with anastomosing gravelly channels, clayey and silty overbank deposits and numerous small ephemeral swamps or playas. Many of these systems are interrupted by sand dunes, however a number of the larger ones, e.g., Strzelecki, Coonee, Yandama and Tilcha creeks, have excavated courses through the dunes to reach Lake Frome.

Many of the modern alluvial systems have partially occupied the courses of, and are reworking sediments from, older Neogene and Paleogene palaeodrainage systems within the Lake Eyre Basin-Callabonna Sub-basin and may be hydraulically connected to these older systems. This is

The Frome airborne electromagnetic survey, South Australia: implications for energy, minerals and regional geology

particularly evident in modern and palaeodrainage systems draining north from the Olary Spur into the Callabonna Sub-basin including Pine Creek and Mingary Creek, which now partially occupy the headwater of the older Yarramba Palaeovalley, and Whey Whey Creek and Bimbowrie Creek which partially occupy the headwaters of the Billeroo Palaeovalley (Figure 3.28). Similarly, drainage eastwards from the Flinders Ranges (Wilpena, Balcoracana and Bendieuta creeks) now occupies the headwaters of the Wyambana Palaeovalley (Figure 3.28).

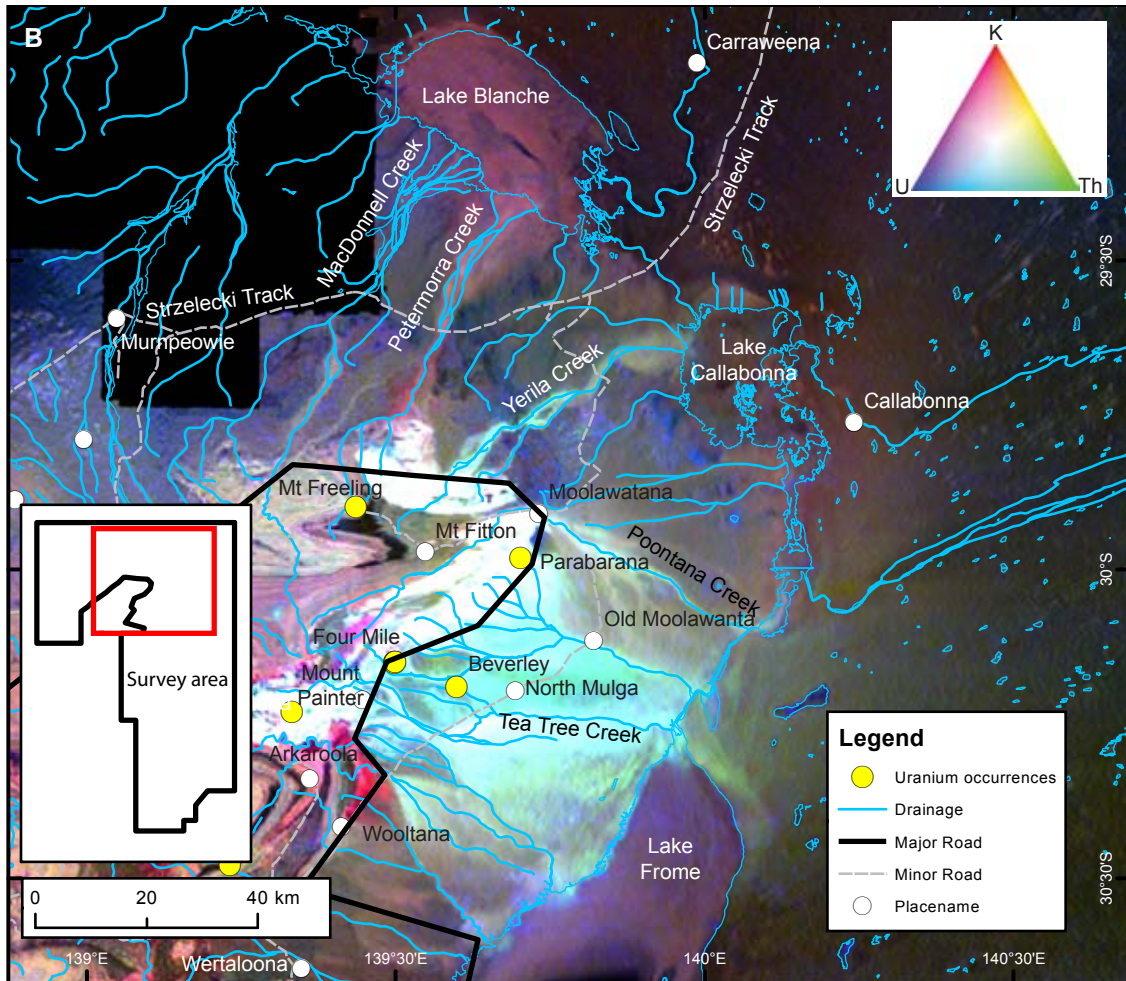


Figure 3.27: Large alluvial fans systems of the northern Flinders Ranges. The radiometric image has a significant gap where no data has been collected in the northwest.

Older sediments are exposed by neotectonic activity and along the flanks of the Flinders Ranges, particularly in the western Frome Embayment and the northern Flinders Ranges. Here, Cenozoic and Mesozoic sediments of the Lake Eyre Basin-Callabonna Sub-basin and Eromanga Basin are exposed in creek and river cuttings or as mesas of indurated remnants to the north of the Flinders Ranges.

Where sedimentary systems are not active, much of the older, indurated sediment and bedrock under shallow cover now have an extensive colluvial mantle, as do the flanks of higher relief landforms. Much of what Gibson (1999) mapped as alluvium is actually now being reworked by colluvial processes, and should be considered as colluvium modified by gilgai. In low relief areas, the colluvial mantle consists of sheetwash that may contain clasts of local bedrock, reworked Cenozoic and Mesozoic sediments, indurated materials such as silcrete and ferricrete and the ever-present parna consisting of red-brown fine sand and silt (Figure 3.29A). Commonly, this sheetwash displays

The Frome airborne electromagnetic survey, South Australia: implications for energy, minerals and regional geology

a contour banded pattern (Dunkerley and Brown, 1995; Wakelin-King, 1999) which is very noticeable at the Mingary Pit site (Figure 3.23A, 3.29A, 3.30), but is present within low-relief landforms across the entire region. Contour banding is typical of the rangelands within the semi-arid and arid zone and features vegetated bands, which act as sinks for surface water and nutrients, with stony interbands, which armour the land surface and prevent erosion. The vegetated bands commonly contain crabhole gilgai, which allow hydraulic connection from the surface to the subsurface. In areas where there is extensive contour banded colluvial sheetwash local relief is no more than about 50 m, and lag, derived from weathered quartz veins, recycled quartz particles from older deposits and broken down of ferruginous mottles, is distributed over the surface by shallow overland water flow during catastrophic rain events (usually thunder storms). In these areas, colluvial cover is generally quite thin, often no more than 1 m, but deepens towards drainage channels. The contour banding phenomenon is common over the low-relief land in the Frome AEM Survey area, but can also be seen in high relief areas as terracettes picked out by bands of *Spinifex* sp. (Figure 3.29D). Colluvial material is also present around the bases of high relief features in the Flinders Ranges and Olary Spur as colluvial footslopes consisting of colluvial fans (Figure 3.29C) or debris flows, and higher-relief scree slopes at the bases of cliffs.

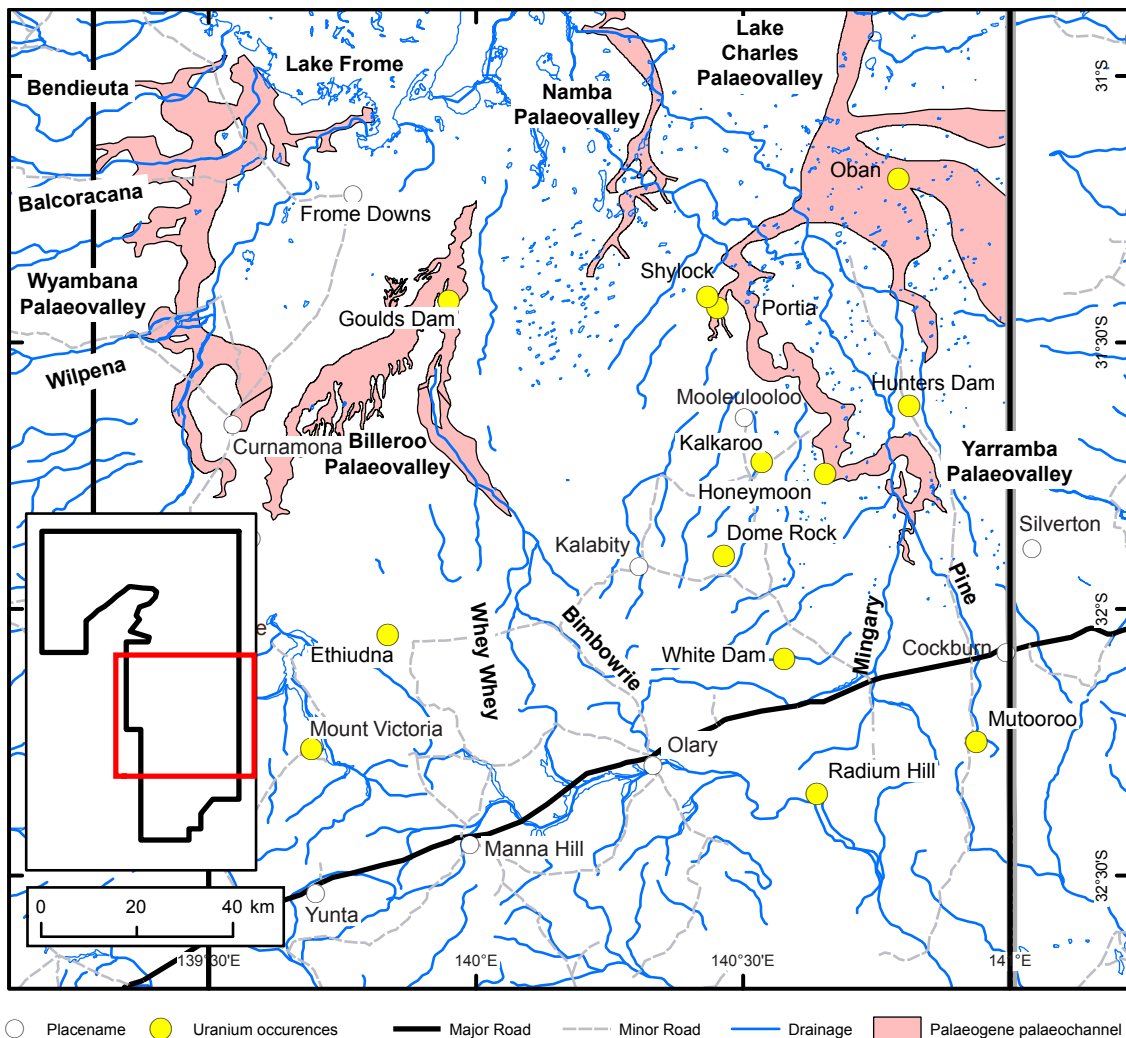


Figure 3.28: Palaeovalley outlines (from SARIG 2011) and modern drainage systems of the northern Olary Spur physiographic region. Many modern drainage systems occupy the headwaters of palaeodrainage systems.

Aeolian sediments are very common within the Frome AEM Survey area, especially within the Eyre-Frome Plains, Strzelecki Plains, Simpson Desert Plains, West-Turkey Plains, Ivanhoe Plains and Torrens-Gulf Plains physiographic regions, where erosion rates are low. Aeolian sediments most commonly occur as large seif (longitudinal) sand dunes (Figure 3.31A, B), with a small proportion of other types, in the Strzelecki and Simpson deserts, but sand plains extend into the southern Lake Frome area (Fabris *et al.*, 2008) (Figure 3.31B, C) and are labelled as “IS” in Gibson’s (1999) map (Figure 3.22). Extensive sand plains and low sand dunes also occur in the northeastern Murray-Darling Basin (Brown, 1985). Sand dunes within the Simpson and Strzelecki deserts are noted to have brilliant red or deep blood red colours (Figure 3.31A), but these colours are noted to alter with distance from sand sources; Wopfner and Twidale (1988) commented that dunes proximal to sediment sources tended to be brilliant white, but changed colour to more red hues as sand grains took on hematite coatings with distance, becoming deep red on the far lee sides of sediment sources (Figure 3.31A). Wopfner and Twidale (1988) also noted that sand dunes may change colour across drainage lines, being deep red at the entry point, but white or fawn at the exit point.



Figure 3.29: Examples of colluvial regolith materials in the Frome AEM Survey area. A: Contour banding on colluvial sheetwash at the Mingary Pit; B: Mixed lag including ferruginised bedrock fragments, vein quartz and maghemite nodules at Mingary; C: Colluvial footslopes, eastern Flinders Ranges near Arkaroola Creek, Arkaroola Wilderness Sanctuary; D: A high-angle, contour banded colluvial fan at Four Mile Creek, Arkaroola Wilderness Sanctuary.

Seif dunes within the Simpson Desert extend laterally for several hundred kilometres (Wopfner and Twidale, 1988), making them amongst the longest in the world. The dunes rest on a substrate of lacustrine sediments, gibber or indurated older sediment of the Lake Eyre Basin or Eromanga Basin, from which they partially draw their sediment supply; the rest is supplied by rivers flowing into the Lake Eyre Basin. Recent advances in dating sand dunes using optically stimulated luminescence (OSL) reveals the large seif dunes to be multi-generational, with dune cores in the Simpson and Tirari deserts noted by Fitzsimmons *et al.* (2007) to have episodes of activity at 73-66 ka, 35-32 ka, 22-18 ka and 14-10 ka. Hesse and Simpson (2006) noted dune cores of over 80 ka in age near

Birdsville. Nanson *et al.* (1992; 1995) noted dune cores in the Finke region of the Northern Territory were up to 100 ka in age. Gardner *et al.* (1987) used thermoluminescence dating to determine that some dune cores in the northern Strzelecki Desert near Moomba were as old as 243 ± 23 ka.

A number of drainage systems and lakes have extensive source-bordering dune systems on their lee sides, labelled as “T” in Gibson’s (1999) map (Figure 3.22), as do bedrock outcrops (Figure 3.31D). These dunes may be composed of quartz sand and silt blown from drainage channels and floodplains, or may be almost completely gypseous around salt lakes within the central Lake Frome area, particularly on the large lakes such as lakes Frome, Callabonna and Blanche, but also the smaller lakes such to the east of Lake Frome as lakes Namba, Tarkarooloo and Moko. These are noticeable on the DEM and MRVBF images (Figure 3.20, 3.21).

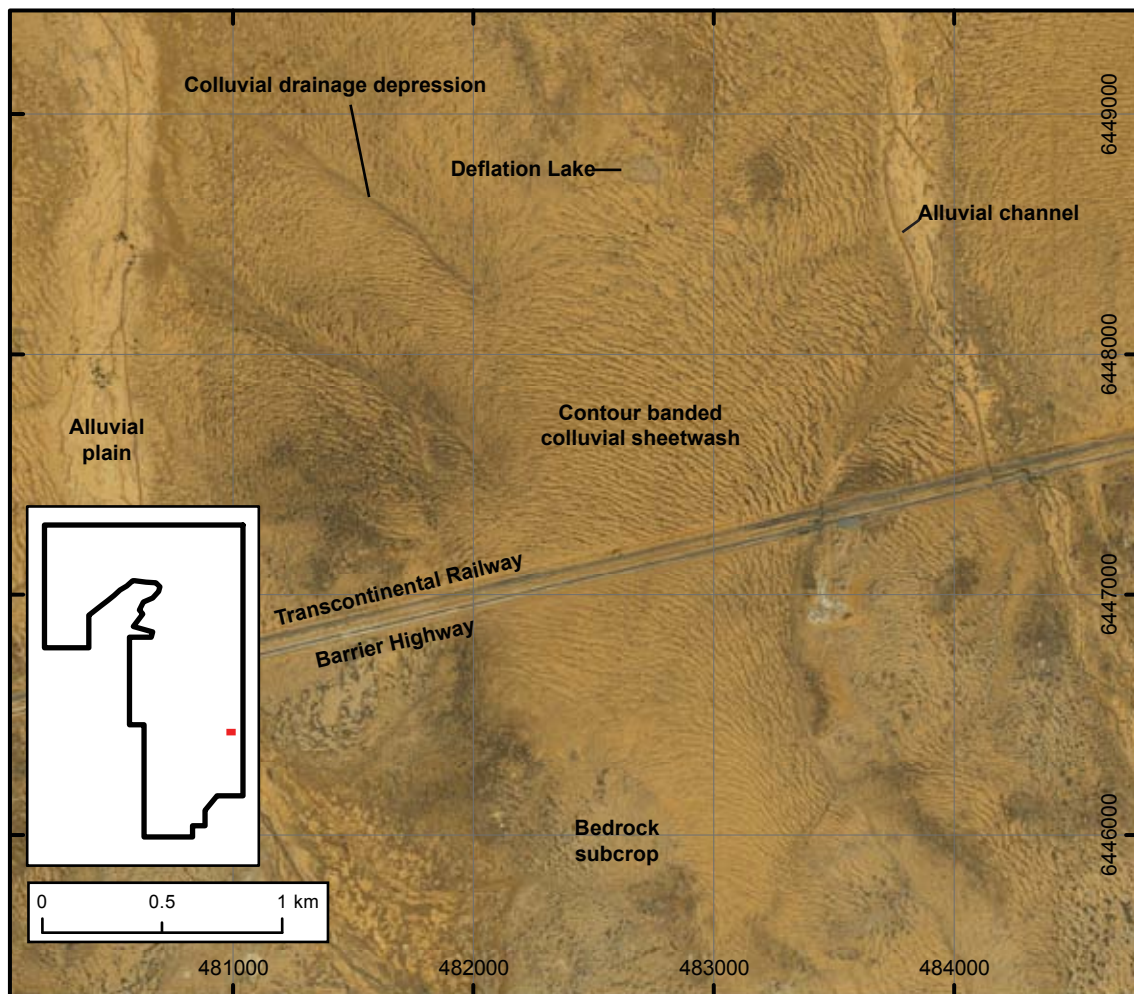


Figure 3.30: An example of contour banded colluvial sheetwash lobes crossed by the Barrier Highway and Transcontinental Railway near Mingary, SA. Background: SPOT image.

Lacustrine sediments are common within the Frome AEM Survey area in extant lakes or playas, but are also being increasingly noted within palaeolakes within the Cenozoic succession, most particularly within the Namba Formation (Figure 3.32A, B). Sediments in the extant lakes are dominantly clays, however, alluvial fans of silt, sand and gravel enter the larger lakes from a number of creeks draining the Flinders Ranges. Lakes contain a large proportion of chemically precipitated sediment, principally halite, but also of gypsum and other salts. Gypseous source-bordering dunes are recognised in a number of locations; many of these have been recrystallised to form gypcrete.

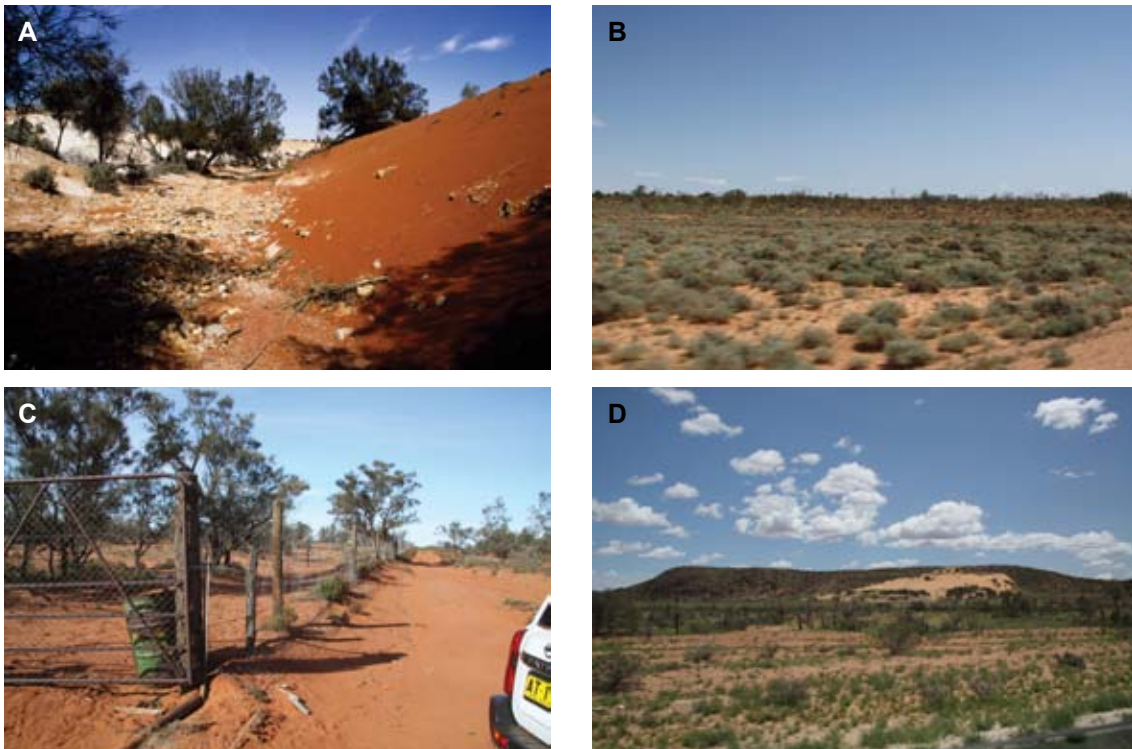


Figure 3.31: Aeolian sediments in or near the Frome AEM Survey area. *A:* Deep red hematitic quartz sand dunes on the edge of the Strzelecki Desert at Teilta, NSW, overlying gypcrete deposits and highly weathered saprolite of Paleo-Mesoproterozoic Willyama Supergroup rocks; *B:* Low (< 2 m relief) sand dunes on a sand plain near Wilpena Creek, Yunta to Balcanoona Road; *C:* Aeolian sand piled up at the base of the vermin proof fence, near Lake Namba. Note the addition of new fencing material to increase the fence's height; *D:* A sand blow on the lee side of Prism Hill, a Cambrian bedrock ridge, near Moro Creek, Yunta to Balcanoona Road.



Figure 3.32: Examples of palaeolacustrine sediments in the Frome AEM Survey area, Lady Buxton Creek, Arkaroola Wilderness Sanctuary, described by Hill and Hore (2012). *A:* View westward towards an outcrop of iron-indurated, mottled, clay-rich, dolomitic Namba Formation lacustrine sediments; *B:* A domal stromatolite from the dolomitic palaeolake deposits shown in Figure 3.12A, Namba Formation.

Older lacustrine sediments have been recognised within the Cenozoic succession, especially within the Namba Formation (Callen, 1977; Hill and Hore, 2012) and to a lesser extent the Eyre Formation (Wopfner *et al.*, 1974). Within the Namba Formation (Figure 3.32A, B), lacustrine sediments consist of carbonaceous clay deposits, dolomitic clay, palygorskite clay (a magnesium-rich clay) and dolomite with poorly-preserved domal stromatolites (Figure 3.32B), all accumulated in alkaline lakes within the Lake Eyre Basin (Callen, 1977). Within the Eyre Formation, lacustrine sediments consist of carbonaceous silty clays and interbedded lignite (Wopfner *et al.*, 1974) deposited within channels, floodplains and swamps of the Lake Eyre Basin.

3.4.3 Indurated regolith

Indurated regolith is present across much of the Frome AEM Survey area as materials that have been cemented by silica, iron oxyhydroxides, carbonate, sulfate, chloride or manganese oxyhydroxides. Silicified and ferruginised regolith commonly occurs as an induration of bedrock units of the Curnamona Province, the Adelaidean rocks and Mesozoic and Cenozoic sediments, particularly (but not solely) those that are enriched with silica or iron. Mesas, cuestas and buttes of silcrete- or ferricrete-indurated sediments are common in the Strzelecki and Simpson deserts in the northern part of the Frome AEM Survey area due to relief inversion of the indurated, weathering-resistant materials. Silcrete commonly occurs on or within the Cadna-owie Formation, the Parabarana Sandstone, the Marree Subgroup, the Eyre Formation and the Namba Formation. It has often been used as a diagnostic to locate the top of the Eyre Formation. Ferricrete occurs across a wide range of iron-bearing rocks or where iron-rich groundwaters come to the surface.

Regolith carbonate accumulations (or calcrete) are common within the Frome AEM Survey area and are concentrated over carbonate-bearing bedrocks including Neoproterozoic dolomitic rocks where there is a strong carbonate source. Concentration of calcrete within the regolith decreases in the north of the Frome AEM Survey area across the broad summer-winter rainfall divide that separates calcium-poor, summer-dominated monsoonal rainfall from the north from calcium-rich, winter-dominated rainfall from the Southern Ocean (Chen *et al.*, 2002; Dart *et al.*, 2007). Groundwater calcretes may form thick, massive accumulations in valley floors of around the flanks of salt lakes in conjunction with other precipitates including sulfates and halides (Chen *et al.*, 2002).

Gypseous regolith occurs in many of the low-lying landscape settings of the Frome AEM Survey, but also anywhere there is a sulfur source. Many of the playas in the region contain evaporitic gypsum and have gypseous lunettes on their lee sides, commonly recrystallised to form gypcrete. Gypsum is also common within soil profiles mixed with regolith carbonate accumulations. Gypsum commonly occurs over sulfur sources, including over sulfide deposits in the Broken Hill-Benagerie Ridge area, but also occurs on pyritic sediments of the Marree Subgroup (Fabris *et al.*, 2008), which may have abundant pyrite up to 10-15% of their volume. Gypsum may also occur where sulfate-bearing groundwaters are concentrated by evapotranspiration (Hill, 2000; Shirliff, 1998). Gypsum is commonly transported as aeolian dust, and may occur away from sulfur sources where parna collects (Chivas *et al.*, 1991).

Chloride-rich regolith, more particularly halite (or salcrete) commonly occurs in low-lying parts of the landscape within soil profiles, drainage channels and around saline playas and may crystallise in association with calcrete and gypsum. Manganese oxyhydroxides (or manganocrete) commonly occur as the weathering product of Paleo-Mesoproterozoic rocks of the Willyama Supergroup, most particularly those containing spessartine garnet. These commonly occur within gossans and weathering surfaces on the Willyama Supergroup, forming a black, sometimes iridescent coating.

Much of the lag material commonly seen on the surface within the Frome AEM Survey area is derived from indurated bedrock and sediments and may include ferricrete from eroded mottled zones or ferruginous caps and silcrete from Mesozoic and Cenozoic sediments, and less commonly manganocrete from weathered Willyama Supergroup bedrocks. These may be mixed with lag derived from the erosion of local bedrocks of the Curnamona Province, Adelaidean and Mesozoic of

Cenozoic basins. Depending on the distance to source, these may supply lithic fragments and grains, often angular to sub-rounded milky quartz from the abundant quartz veins within the Paleoproterozoic rocks of the Curnamona Craton, but also lithic fragments of quartzite, from overlying Neoproterozoic rocks. Mesozoic and Cenozoic rocks within the Frome AEM Survey area may supply recycled lithic fragments and quartz, commonly rounded to well rounded. Another common component of lag is maghemite, consisting of rounded grains, pisoliths and nodules that may be derived from local weathered bedrock, but may be chemically precipitated from iron-bearing groundwaters. More information regarding indurated regolith is included in Fabris *et al* (2008).

3.4.4 Vegetation

In the semi-arid and arid lands of Australia, particularly where vegetation has not been stripped by overgrazing or over-exploitation for agriculture or wood harvesting, much of the vegetation has a close geobotanical relationship with the regolith-landforms in which it occurs. This summary is taken from the Interim Biogeographic Regionalisation for Australia (IBRA), Version 6.1, of the National Land and Water Resources Audit (2001), the Australian Natural Resources Atlas (ANRA, 2011) and Fabris *et al.* (2008). Examples of commonly-occurring vegetation communities are shown in [Figure 3.34A-F](#)

Five main geobotanical associations exist within the Frome AEM Survey area ([Figure 3.34](#)):

1. Simpson Strzelecki Dunefields;
2. Stony Plains;
3. Flinders Lofty Block;
4. Broken Hill Complex; and,
5. Murray Darling Depression.

The Simpson Strzelecki Desert bioregion is dominated by hummock grasslands and open acacia woodlands with riparian woodlands along major drainage courses. Sand dune crests and the upper slopes of sand dunes are dominated by sandhill canegrass (*Zygochloa paradoxa*) and hard spinifex (*Triodia basedowii*). Dune swales are dominated by spinifex hummock grassland. The dune flanks have areas of sparse tall shrubland to low woodlands dominated by sandhill wattle (*Acacia ligulata*), mulga (*A. aneura*), whitewood (*Atalaya hemiglauca*) and needlewood (*Hakea spp.*). White cypress pine (*Callitris glaucophylla*) woodlands or individual trees extend across part of the Strzelecki Desert in the northeastern Frome Embayment. Riparian woodlands of coolibah (*Eucalyptus coolabah*), river cooba (*Acacia stenophylla*) and broughton willow (*Acacia salicina*) occur either side of major watercourses. Playa lakes support samphire and chenopod scrublands of old man saltbush (*Atriplex nummularia*), Queensland bluebush (*Chenopodium auricomum*), lignum (*Muehlenbeckia cunninghamii*) and canegrass (*Eragrostis australasica*).

The Stony Plains bioregion is dominated by ephemeral or short-lived species that germinate and set seed rapidly after rain. Tablelands covered in gilgai and gibber support chenopod shrublands containing saltbush (*Atriplex spp.*) and bluebush (*Maireana spp.*) vegetation. Gidgee (*Acacia cambagei*), coolibah (*Eucalyptus coolabah*) and river red gum (*E. camaldulensis*) form riparian woodlands along drainage lines. Mulga (*Acacia aneura* and *A. stowardii*) woodland or sandhill canegrass (*Zygochloa paradoxa*) are found on sand plains and sand dunes. Gibber plains support little vegetation regardless of the season.

The Flinders Lofty Block supports diverse vegetation which varies on climate, slope, aspect and geological substrate. Where rainfall is high, typically on the western side of the Flinders-Mount Lofty ranges, vegetation is dominated by eucalypt species including blue gum (*Eucalyptus leucoxylon*) in the far south, long leaf box (*E. goniocalyx*) and gum-barked coolibah (*E. intertexta*) in the north. The understorey consists of saltbush (*Atriplex spp.*), wattles (*Acacia spp.*) and spear wallaby grasses (*Danthonia spp.*). Where rainfall is less abundant, eucalyptus species are replaced by acacia species, dominantly mulga (*Acacia aneura*), and black oak (*Casuarina spp.*), native pine (*Callitris spp.*) and teatree (*Leptospermum spp.*), with the understorey consisting of scrub containing

The Frome airborne electromagnetic survey, South Australia: implications for energy, minerals and regional geology

acacias, cassias (*Senna spp.*) and hopbush (*Dodonaea spp.*). The driest stony hills often have groundsel (*Senecio spp.*), dead finish (*Acacia tetragonophylla*) and rock fuschia (*Eremophila freelingii*), or occasionally just spinifex (*Triodia spp.*). River red gums (*E. camaldulensis*) occur in riparian woodlands along larger creeks with prickly wattle (*Acacia victoriae*).

The Broken Hill Complex consists of downs country dominated by chenopod shrublands, principally various burrs with black blueblush (*Maireana pyramidata*) and pearl bluebush (*Maireana sedifolia*) where soils are calcareous, and saltbushes (*Atriplex spp.*). Drainage channels have riparian woodlands of river red gum (*E. camaldulensis*), *Casuarina spp.*, prickly wattle (*A. victoriae*), *Eremophila spp.*, *Dodonaea spp.* and ephemeral plants. Hilltops may have scattered mulga (*Acacia aneura*) and rosewood (*Alectryon oleifolius*) and hillslopes scattered belah (*Casuarina cristata*) and dead finish (*A. tetragonophylla*).

The Murray Darling Depression is dominated by mixed mallee species including the red mallee (*Eucalyptus oleosa*) and the ridge-fruited mallee (*E. incrassata*), on sandplains becoming dominated by the pointed fruit mallee (*E. socialis*) and yorrel (*E. gracilis*). Woodlands dominated by belah (*Casuarina pauper*) and rosewood (*Alectryon oleifolius*) also occur. Sandplain communities also include shrub lands and grass lands with the shrub layer dominated by black bluebush (*Maireana pyramidata*), pearl bluebush (*M. sedifolia*), nitre bush (*Nitraria billardiarei*) and saltbushes such as bladder saltbush (*Atriplex vesicaria*). The ground layer has a variety of native and introduced grasses and forbs. Riparian woodlands occur on the alluvial plains, riverbanks, swamps and billabongs. These include continuous stands of river red gum (*E. camaldulensis*) and black box (*Eucalyptus largiflorens*), sometimes as mixed stands but often as monocultural woodlands.

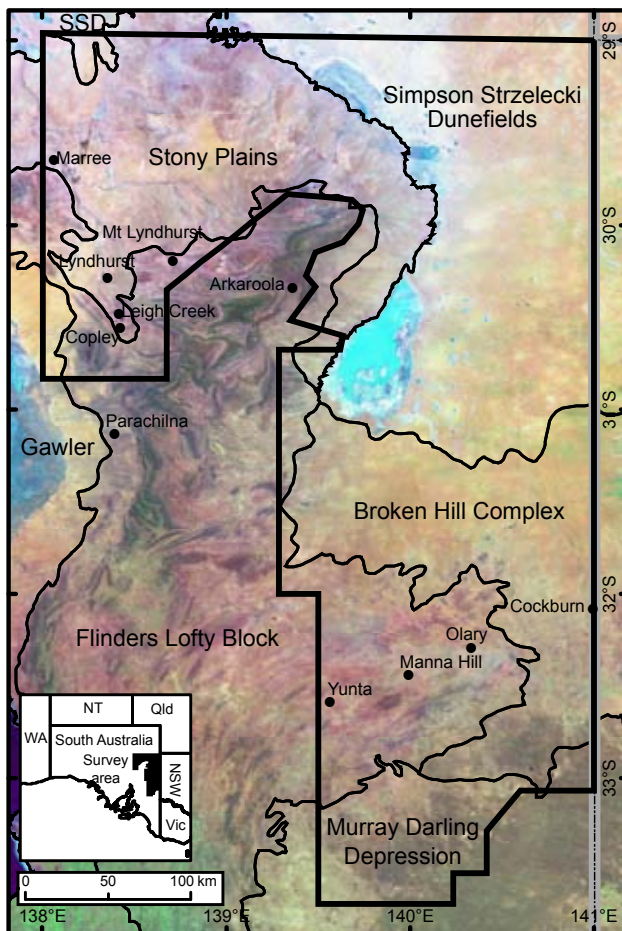


Figure 3.33: Bioregions of the Frome AEM Survey area. From the Interim Biogeographic Regionalisation of Australia (IBRA) version 6.1 database (ANRA, 2011). Background image: Landsat TM mosaic of Australia.

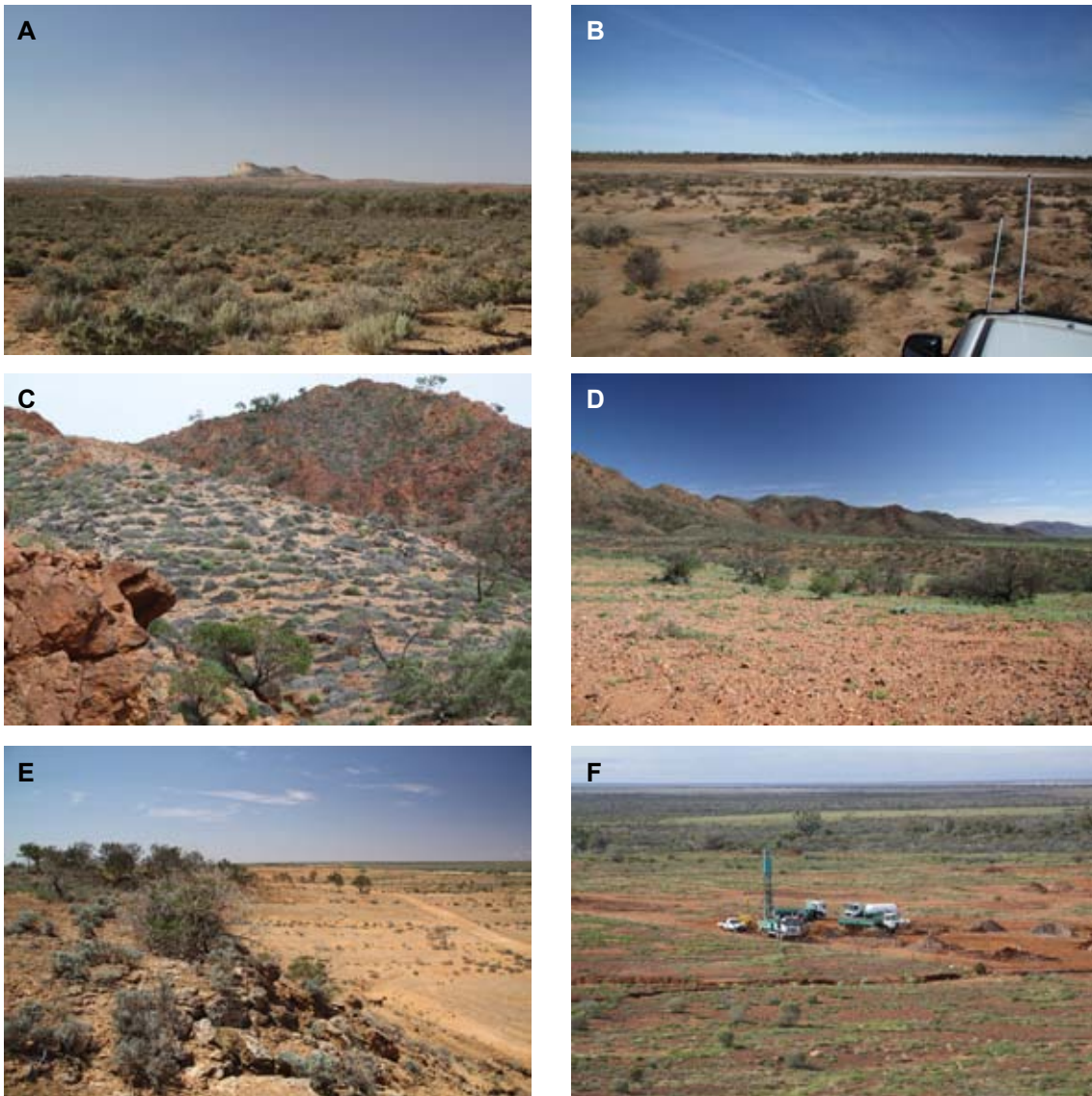


Figure 3.34: Examples of vegetation communities within the Frome AEM Survey area. **A:** mixed chenopod-burr shrubland and open belah-rosewood woodland looking south to Oratan Rock near Lilydale. **B:** Mixed halophytes and chenopods with an open belah woodland on the lunette near Lake Namba. **C:** Spinifex contour bands on a high-angle colluvial fan, with scattered *Eremophila* sp. on the footslopes and coolabahs on the upper slopes, Four Mile Creek, Arkaroola Wilderness Sanctuary. **D:** Chenopod-burr shrubland with scattered *Acacia* sp. and *Eremophila* sp. on footslopes, with open Belah woodland on the upper slopes, near Paralana Creek, eastern Flinders Ranges. **E:** Open belah woodland with an understory of *Eremophila* sp., chenopods and burrs, Wilpena Creek near Frome Downs. **F:** Mixed chenopod shrubland between ephemeral stream channels populated by mixed river red gum, coolabah, teatree, *Acacia* sp. and *Eremophila* sp., Four Mile Creek, Pepegoona area, Beverley uranium mine.

3.5 LANDSCAPE EVOLUTION

I. C. Roach, S. Jaireth, A. J. Cross, S. B. Hore and E. A. Jagodzinski

Here we consider the factors that have created the landscape within and around the Frome AEM Survey area, concentrating on the northern Flinders Ranges as they are today, and the evolving structure of the region as it relates to uranium mineralisation within the Lake Eyre Basin-Callabonna Sub-basin and the Murray-Darling Basin. Tectonics and neotectonics appears to have had a strong control over the locations of mineral deposits as we currently find them, so it is important to be able to reconstruct major episodes of tectonism, erosion and sedimentation within the Frome AEM Survey area.

The dominant landscape structure in the region, the Flinders Ranges, has a complex tectonic history that has been the source of great debate for many decades. Cyclical uplift and erosion of the Flinders Ranges, and the proto-Flinders Ranges, since the Delamerian Orogeny have created a complex sedimentological and thermal history that has most recently been synthesised by Davey (2009), Wülser (2009) and Cross *et al.* (2010). Figure 3.35 combines results of these studies into a single landscape evolution model using the thermal, isotopic, zircon provenance and sedimentological history of the Mount Painter Inlier and Northern Flinders Ranges-Beverley area. This model is used to explain the locations and timing of uranium deposits throughout the Lake Eyre Basin-Callabonna Sub-basin and Murray-Darling Basin. The Mesozoic-Cenozoic evolution of the region can be interpreted using zircon provenance, thermochronology and sedimentology (Figure 3.35A) and the post Delamerian-Orogeny evolution of the region can be interpreted using the thermochronology and isotopic dating data collation (Figure 3.35B). A useful précis based on geological and regolith-landform mapping is also given in Hill and Hore (2012).

Long-lived geological structures have shaped the morphology of the Flinders Ranges, Olary Spur, Barrier Ranges, Eyre-Frome Plains and the Murray-Darling Basin. These structures have controlled the juxtapositions of basement rocks of the Curnamona Province and Adelaide Geosyncline against sedimentary basins and have controlled the amount of sedimentary fill in the basins themselves. Some of these structures continue to be active to the present day. While it is neotectonics that have shaped the Flinders Ranges as we currently know them, the evidence points towards long-term uplift and erosion within the Flinders Ranges, proto-Flinders Ranges and wider Curnamona Province, controlled by long-lived structures, as being a major influence over the location and preservation of sandstone-hosted uranium deposits. It is the continued reactivation of older structures that shapes the current architecture of the region today.

3.5.1 Proterozoic-Paleozoic

The earliest faults interpreted to have affected the landscape evolution of the region are what SRK Consulting (SRK; Teasdale *et al.*, 2001) and FrOG Tech Pty Ltd (FrOG Tech; de Vries *et al.*, 2006; FrOG Tech, 2005) interpreted as Paleoproterozoic faults of the Calvert Extension (1730-1690 Ma) and the Leibig (1640-1690 Ma) and Warakurna (1090-1050 Ma) events, affecting the Archean and Paleo-Mesoproterozoic basement of the Curnamona Province including the Willyama Supergroup. After these, marine sedimentation in the Neoproterozoic was controlled by northeast-southwest opening of underlying northwest-southeast basement structures established during the Olarian Orogeny (Preiss, 1987; Teasdale *et al.*, 2001) and shaped the overall northwest-southeast axis of sediment deposition in the region (Figure 3.36).

The Frome airborne electromagnetic survey, South Australia: implications for energy, minerals and regional geology

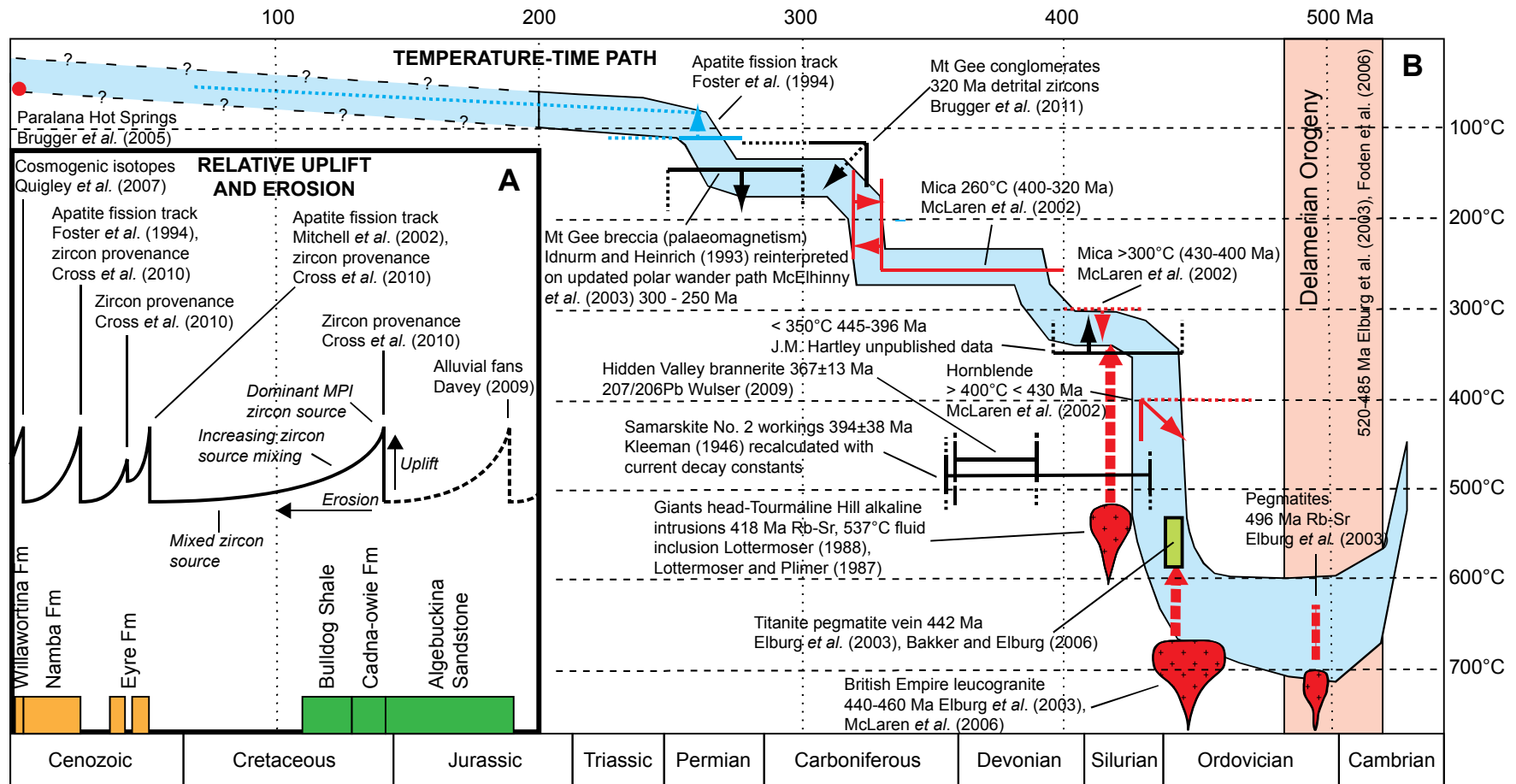


Figure 3.35: Landscape evolution model for the Mount Painter Inlier (MPI). **A:** Relative uplift and erosion events interpreted using cosmogenic isotopic dating, apatite fission track dating, zircon provenance studies and regolith-landform mapping. **B:** Thermochronology-isotopic dating-palaeomagnetic dating and thermal history path modified from Wülser (2009). Figure includes data from Bakker and Elburg (2006), Brugger et al. (2005), Brugger et al. (2011a), Cross et al. (2010), Davey (2009), Elburg et al. (2003), Foden et al. (2006), Foster et al. (1994), J. M. Hartley (pers. comm. to P.-A. Wülser, 2009), Idnurm and Heinrich (1984), Kleeman (1946), Lottermoser (1988), Lottermoser and Plimer (1987), McElhinny et al. (2003), McLaren et al. (2002), McLaren et al. (2006) and Wülser (2009).

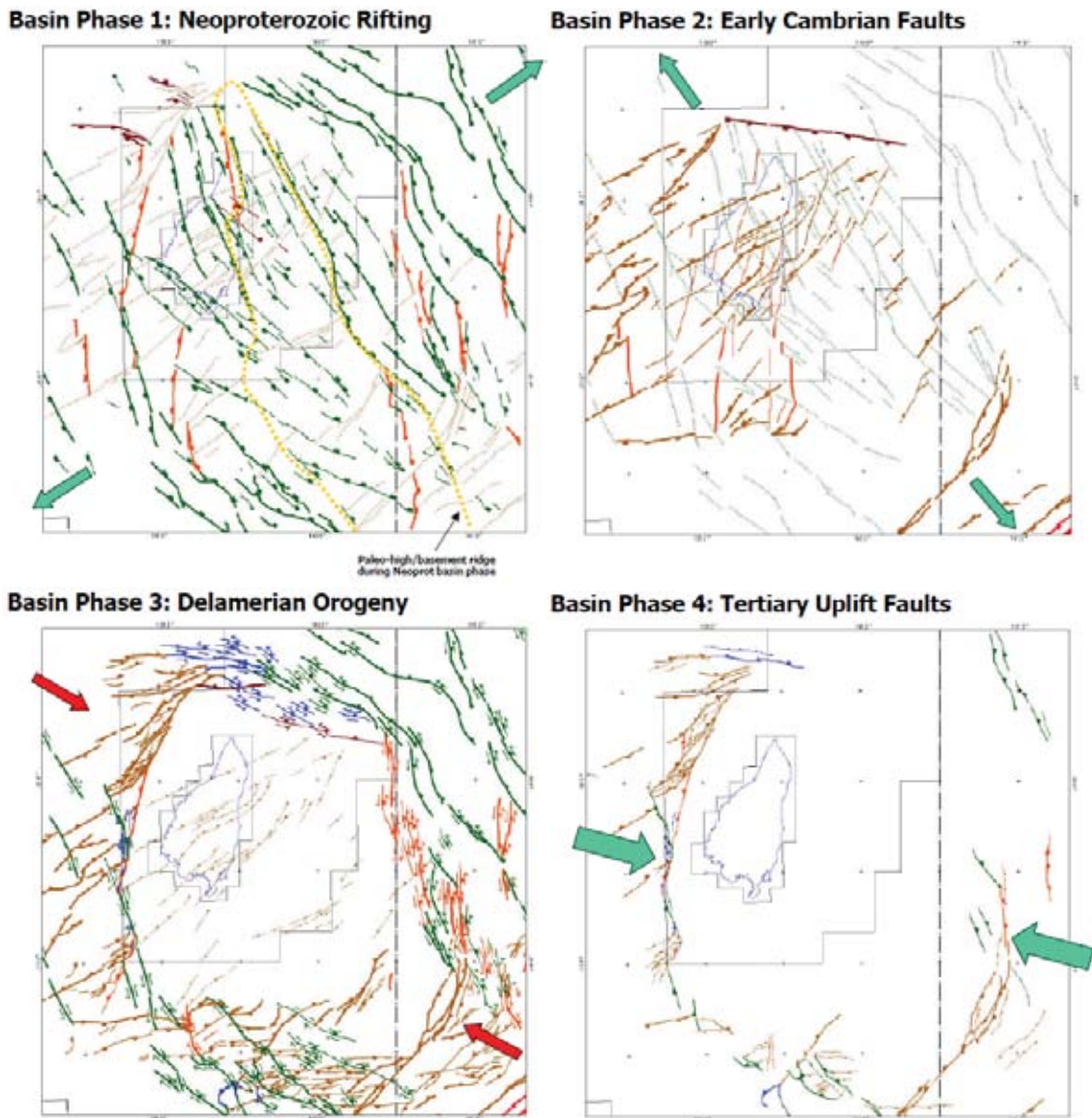


Figure 3.36: Deformation history of the Curnamona Province, modified from Teasdale et al. (2001).

In the Early Cambrian, a reversal of crustal stresses led to northwest-southeast rifting along dominantly northeast-southwest faults and the establishment of the Arrowie Basin, rifted into the underlying Neoproterozoic sedimentary pile and the Paleo-Mesoproterozoic Curnamona Province (Figure 3.7, 3.36). A number of large, crustal-scale faults were developed at this stage, or were reactivated from older fault systems, and controlled the shape and amount of sedimentary fill in the Arrowie Basin, which straddles the Benagerie Ridge (Figure 3.3). These include:

- The Paralana Fault, the Wooltana Range Front Fault (Vidnee Yarta Fault Zone), the Wooltana Fault, the Four Mile Fault and the Poontana Fault Zone in the Mount Painter Inlier area, controlling the western Arrowie Basin;
- The Mundi Mundi Fault and the Kantappa Fault controlling the eastern Arrowie Basin;
- The Redan Fault Zone, which bounds the eastern side of the Curnamona Province and wraps around the southern side of the Barrier Ranges and Olary Spur, forming the boundary between these and the Murray-Darling Basin; and,
- Un-named faults either side of the Benagerie Ridge.

Extensive Early-Middle Cambrian rifting deposited > 5.5 km of largely deep water marine sediment into the Moorowie Sub-basin on the western side of the Benagerie Ridge, and perhaps 2 km of more shallow marine sediment into the Yalkapo Sub-basin on the eastern side of the Benagerie Ridge, which has a thin shallow to shoaling marine cover over its central portion, and may have been sub-aerially exposed in some places. The Benagerie Ridge surface slopes upwards to the south to the Olary Spur and Barrier Ranges, where there is no evidence of Cambrian sedimentation.

Sedimentation in the Arrowie Basin ceased with the onset of the Delamerian Orogeny at ~500 Ma (Preiss, 1987). The Arrowie Basin was inverted by northwest-southeast compression during the Delamerian Orogeny, introducing normal faults and folds. Granitoid intrusion commenced in the Mount Painter Inlier during the Delamerian Orogeny as pegmatite veins (Elburg *et al.*, 2003) and continued with post-orogenic intrusions of the British Empire Granite at 440-460 Ma (Bakker and Elburg, 2006; Elburg *et al.*, 2003; McLaren *et al.*, 2006) and the Giants Head-Tourmaline Hill alkaline intrusions at 418 Ma (Lottermoser, 1988; Lottermoser and Plimer, 1987). These intrusions were concomitant with mountain building and elevation of the Mount Painter Inlier with a resultant cooling from ~700°C to ~300°C by the Early Silurian, according to Wülser (2009), and shaped the proto-Flinders Ranges. Cambro-Ordovician granitoid intrusion also occurred in the Nackara Arc south of the Olary Spur and Barrier Ranges during the Delamerian Orogeny (Preiss, 1995).

Further periods of uplift continued to elevate the proto-Flinders Ranges through to about 250 Ma (Foster *et al.*, 1994), but the Mount Painter Inlier was probably sub-aerially exposed by at least 330 Ma. Dykes of diamicite in the flanks of Mount Gee (Sprigg's Costean) have been shown to contain 320 Ma zircons and are interpreted to be Permian glacial till indicating that Mount Gee was sub-aerially exposed at this time (Brugger *et al.*, 2011a; b). The Mount Gee and Mount Painter breccias are interpreted to have been formed by near-surface boiling at about this time, adding further weight to the interpretation that the Mount Painter Inlier was elevated above water-level at this time (Brugger *et al.*, 2011a; b). Subsidence to the north of the Flinders Ranges during the Late Carboniferous resulted in the formation of the Cooper Basin, which has a thick Late Carboniferous and Permian terrestrial sedimentary succession. Subsidence to the south of the Olary Spur-Barrier Ranges resulted in the formation of the Nadda Basin (underneath the Canegrass Lobe of the Berri Basin; [Figure 3.9](#)), which also has a thick Permian terrestrial sedimentary succession. Subsidence in the Cooper Basin continued into the mid- to Late Triassic (Hill and Gravestock, 1995).

3.5.2 Mesozoic-Cenozoic

The temperature-time curve collated by Wülser (2009) does not contain any useful information from ~250 Ma to the present, apart from a near-present day temperature estimate of the Paralana Hot Springs by Brugger *et al.* (2005), but the sedimentary record of Mesozoic and Cenozoic sediments, zircon provenance data obtained from drill cores at Beverley and samples from around the northern Flinders Ranges, apatite fission track thermochronology and cosmogenic isotopic data can be used to fill in the remaining detail. Here, the Mesozoic-Cenozoic landscape evolution history of the Mount Painter Inlier and surroundings is reconstructed using these methods, described in [Figure 3.35A](#).

The post-Paleozoic landscape in the Mount Painter Inlier most likely consisted of sub-aerially exposed basement rocks with unknown but likely moderate relief and unknown thicknesses of Permian cover, which is now largely non-existent in the northern Flinders Ranges except for a small deposit near Blinman (Alley, 1995). Subsidence to the north of the Flinders Ranges during the Late Paleozoic and Early Mesozoic resulted in the formation of the Cooper Basin. Terrestrial sedimentation in the Cooper Basin continued into the Early Triassic (Kreig, 1995), but sedimentation continued in the nearby Simpson Basin into the Late Triassic (Gravestock, 1995).

Terrestrial sedimentation in the Eromanga Basin was triggered by northeast-southwest opening and renewed subsidence to the north of the northern Flinders Ranges in the Early Jurassic, followed by marine sedimentation from the Early Cretaceous. The Berri Basin to the south of the Olary Spur also subsided for a short period in the late Early Cretaceous, receiving marine sediments (Gravestock,

1995; Rogers, 1995a). Around the Mount Painter Inlier, and at Beverley in particular, the Eromanga Basin succession consists of the Algebuckina Sandstone overlain by Cadna-owie Formation and the Marree Subgroup, containing the Bulldog Shale (or their equivalents) wrapping around the northern Flinders Ranges and extending into the Frome Embayment, partially covering the Benagerie Ridge. These sediments represent the change from terrestrial (Algebuckina Sandstone) to transitional (Cadna-owie Formation) to marine (Marree Subgroup) sedimentation (Kreig and Rogers, 1995).

Regolith-landform mapping by Davey (2009) around the Mount Babbage Inlier–Parabarana area shows that a series of alluvial fans extended from the Mount Babbage Inlier, with palaeocurrent directions indicating dominantly northerly flow, in what is most likely the Algebuckina Sandstone, but possibly the Cadna-owie Formation; the state of the outcrop meant that it was difficult for Davey to determine specifically which of the two units was actually present. However, this mapping does indicate a highland to the south, supplying terrestrial sediments to the Eromanga Basin, and implies that there was significant relative or absolute uplift in the northern Flinders Ranges concomitant with subsidence in the Eromanga Basin. This is indicated in [Figure 3.35A](#) as an inferred uplift of the Mount Painter Inlier at the start of deposition of the Algebuckina Sandstone and the supply of sediment from erosion of the northern Flinders Ranges.

Detrital zircon uranium-lead (U-Pb) data obtained using the Sensitive High Resolution Ion Microprobe (SHRIMP) from Cross *et al.* (2010) are combined in [Figure 3.35A](#) with apatite fission track thermochronology results from Mitchell *et al.* (2002) and Foster *et al.* (1994) and cosmogenic isotopic dating by Quigley *et al.* (2007), which help to interpret the post-Jurassic uplift and erosion history of the Mount Painter Inlier and its influence on its surroundings. Zircons in a sample from the base of the Cadna-owie Formation at the Dead Tree Section at the base of the Paralana Fault scarp near Beverley (Hore and Hill, 2009) are strongly euhedral and consist almost entirely of a Mount Painter Inlier-age (~1.58 Ga) population, indicating strong uplift and erosion of the Mount Painter Inlier at this time, shedding terrestrial sediment, or perhaps even diamictite (Alley and Frakes, 2003; Hill and Hore, 2012), into the adjacent Cadna-owie Formation around the flanks of the Mount Painter Inlier. Further up-stratigraphy in the Cadna-owie Formation, a sample of Cretaceous diamictite from drill hole AKC130 at the Four Mile West uranium deposit yielded a mixed population of rounded zircons, with ages ranging from ~570 Ma to > 2700 Ma. This sample signifies the decreased dominance of Mount Painter Inlier-aged zircons and the admixture of zircons with different ages ranging from Neoproterozoic to Archean, implying a decrease in erosion from the Mount Painter Inlier by landscape lowering and the addition of sediment from around the region including the Gawler Range Volcanics and other Archean to Neoproterozoic bedrocks. Deposition in the Eromanga Basin continued through to the Late Cretaceous to the north of the northern Flinders Ranges in what are now the Strzelecki and Simpson deserts, but rocks of this age are missing from the stratigraphy in the vicinity of the Mount Painter Inlier.

A hiatus marks the boundary between the Eromanga Basin and the Lake Eyre Basin-Callabonna Sub-basin, which commenced deposition after yet another uplift of the Flinders Ranges that Teasdale *et al.* (2001) associated with the reactivation of major faults surrounding the Arrowie Basin.

Samples of the Eyre Formation taken from the Dead Tree Section again have large numbers of euhedral, Mount Painter Inlier-aged zircons, but with the addition of small numbers of ~900 Ma and ~485 Ma populations. This coincides with a period of cooling in apatite fission track thermochronology data (Foster *et al.*, 1994; Mitchell *et al.*, 2002). A brief hiatus in sedimentation in the Eyre Formation in the Callabonna Sub-basin (Callen *et al.*, 1995a) would have been followed by renewed minor uplift of the Mount Painter Inlier, as indicated in [Figure 3.35A](#). A sample of the lower Namba Formation from the Dead Tree Section is again dominated by Mount Painter Inlier-aged zircons, this time sub-rounded, but shows the addition of lesser amounts of ~1.68 Ga, ~1.73 Ga, ~1.77 Ga, ~1.87 Ga and ~2.4-2.6 Ga zircons. This appears to indicate moderate uplift and erosional stripping of the Mount Painter Inlier at this time. A sample of the Beverley Sands from the upper Namba Formation contains only small numbers of Mount Painter Inlier-aged zircons, and is

dominated young zircons between ~105 Ma and ~470 Ma, with small numbers of zircons at ~700 Ma, ~1.0-1.2 Ga, ~1.56 Ga (Mount Painter Inlier), ~2.3 Ga and ~2.7 Ga.

In the Murray-Darling Basin, sedimentation was largely contemporaneous with sedimentation in the Lake Eyre Basin and Callabonna Sub-basin (Figure 3.12), with the exception of a large marine incursion in the Oligo-Miocene (Murray Group; deposited more-or-less contemporaneously with the Namba Formation) and a small marine incursion in the Pliocene (Loxton-Parilla Sand; deposited more-or-less contemporaneously with the Willawortina Formation).

Finally, cosmogenic isotope dating by Quigley *et al.* (2007) led to their conclusion the last major uplift of the Mount Painter Inlier occurred at around 4 Ma, forming the northern Flinders Ranges as they are currently seen.

3.5.3 Evolution of the modern landscape

By the mid-Neogene (Pliocene), the landscape within the Frome AEM Survey area had settled into an approximation of what we see today, with the last large uplift of the Flinders Ranges occurring at ~4 Ma (Quigley *et al.*, 2007). The Willawortina Formation represents the outwash from this major uplift (Hill and Hore, 2012), consisting of poorly sorted, angular sand- to boulder-sized clasts, near the Flinders Ranges, to mixed silt and gravel closer to Lake Frome.

The discussions of Palaeozoic and Mesozoic-Cenozoic tectonics in the previous sections describe the gross architecture of the Lake Frome area and the structural features that formed the Proterozoic basement, Arrowie Basin, Eromanga Basin and Callabonna Sub-basin, but ignore more subtle features that are now becoming apparent in high resolution geophysical surveys including gravity, magnetics, seismic and AEM that are being performed in the Lake Frome area, particularly in the northwest around the Beverley uranium mine.

The Willawortina Formation covers much of the evidence for previous tectonics that has shaped the landscape (except, of course, for the Flinders Ranges), but in some areas neotectonic activity can be observed as surface-rupturing faults that offset the Willawortina Formation to produce small fault scarps and drainage re-arrangements that signal tectonic activity to the present day. Similarly, small scarps are visible in the Murray-Darling Basin offsetting the Pooraka Formation. Prominent fault scarps are visible in satellite digital elevation models (e.g. STRM DEM-S) in the Lake Frome area, associated with the Poontana Embayment near Beverley (Figure 3.37A), and in the Murray-Darling Basin, associated with the Redan Fault Zone (Figure 3.37B). The actual age of these scarps is not known, but given that they are visible as drainage re-arrangements and prominent scarps affecting the Willawortina Formation (Poontana Embayment) and Pooraka Formation (Murray-Darling Basin), they must be relatively young.

In the Pleistocene, the landscape has been modified by colluvial, alluvial and aeolian processes through a number of glacial cycles, resulting in the creation of the large seif (longitudinal) sand dunes in the Strzelecki and Simpson deserts and small longitudinal dunes overprinting the larger Plio-Pleistocene beach ridges of the Loxton-Parilla Sand in the Murray-Darling Basin (Bowler, 1976; Bowler *et al.*, 2006; Fitzsimmons *et al.*, 2007; Gardner *et al.*, 1987; Hesse and Simpson, 2006; Wopfner and Twidale, 1988). Modern alluvial and aeolian systems are currently reworking the sand dune materials into alluvial systems. The overall drying-out of the landscape over the Pleistocene-Holocene has resulted in the salinisation of the landscape and the creation of the extensive salt lake systems, occupying previous freshwater lake systems that we see today.

The relationships between basement rocks, cover materials, tectonics and landscape are depicted in a series of block diagrams describing the northern Curnamona Province (Figure 3.38; northern Flinders Ranges), the southern Curnamona Province (Figure 3.39; northern Olary Spur-Barrier Ranges-southern Lake Frome area) and Murray-Darling Basin (Figure 3.40; southeastern Nackara Arc-Murray-Darling Basin).

The Frome airborne electromagnetic survey, South Australia: implications for energy, minerals and regional geology

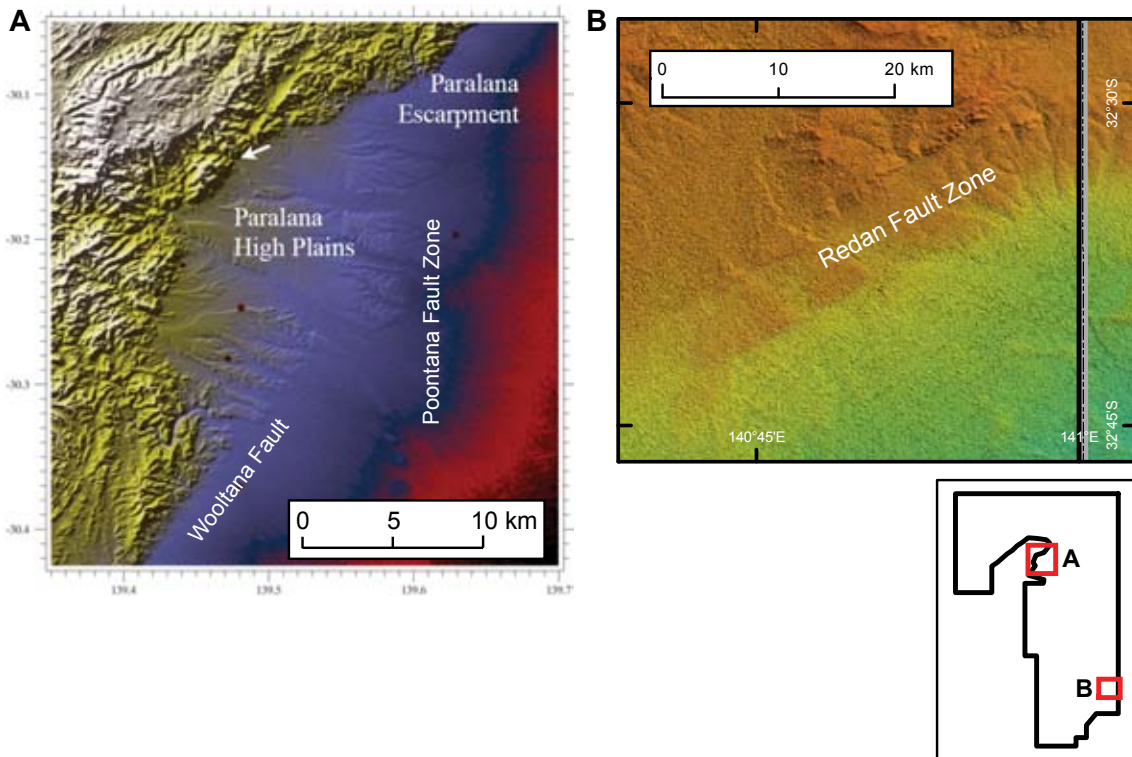


Figure 3.37: Drainage rearrangement and fault scarps. *A*: Paralana Embayment, also described as the Paralana High Plains by Sandiford (2008) (modified after Sandiford, 2008); and, *B*: Murray-Darling Basin highlighting fault scarps on the Redan Fault Zone, using the SRTM DEM-S.

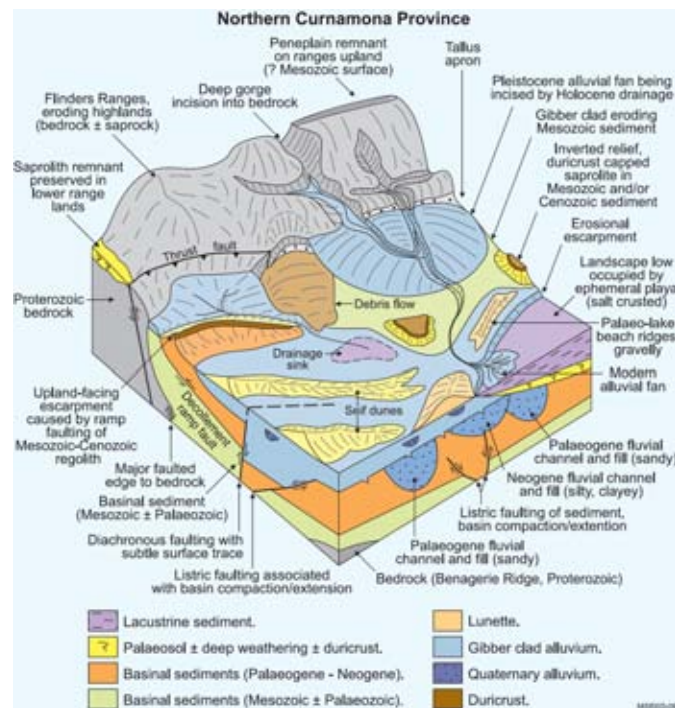


Figure 3.38: Block diagram summarising the regolith-landform and geological components in the northern Flinders Ranges-Mount Painter Inlier-Mount Babbage Inlier area. From Fabris et al. (2008).

The Frome airborne electromagnetic survey, South Australia: implications for energy, minerals and regional geology

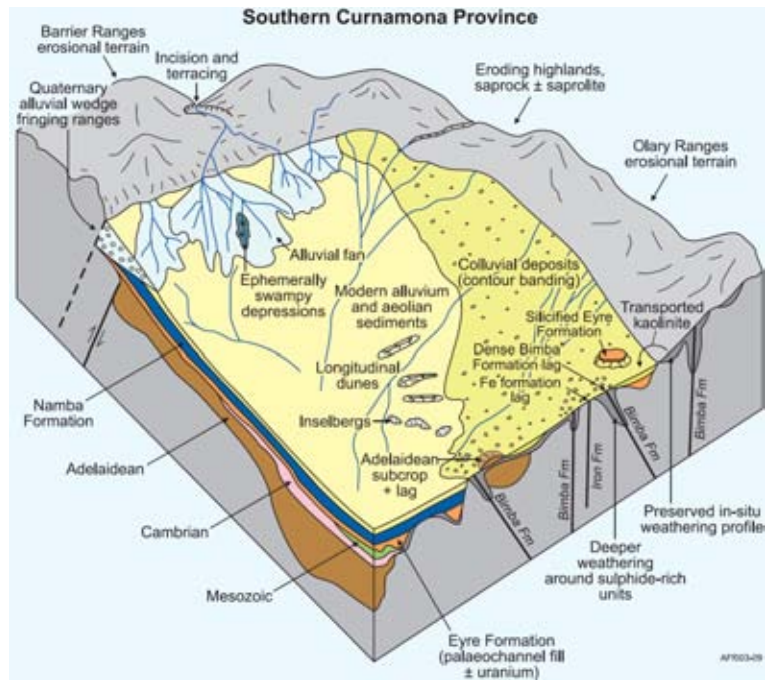


Figure 3.39: Block diagram summarising the regolith-landform and geological components in the Olary Spur-Barrier Ranges-southern Frome Embayment region. From Fabris et al. (2008).

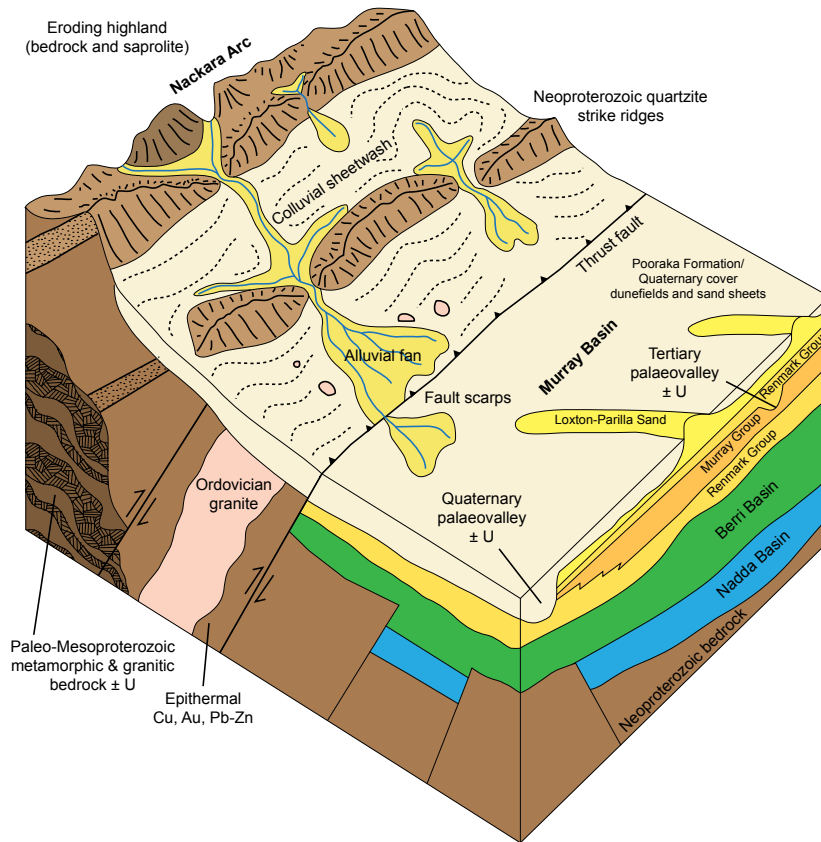


Figure 3.40: Block diagram summarising the regolith-landform and geological components in the Nackara Arc-Murray-Darling Basin region.

3.6 MINERAL SYSTEMS

S. Jaireth and I. C. Roach

The Lake Frome area and the adjoining Curnamona Province within the Survey area are host to several types of mineral systems (Table 3.2). Mineral deposits and prospects in the survey area have been described in detail in several publications (e.g. Coats and Blissett, 1971; Drexel and Major, 1990; Morris and Horn, 1990; Robertson *et al.*, 1998; Stevens *et al.*, 1990).

The Olary Domain also hosts several orthomagmatic and magmatic-hydrothermal (hard rock) uranium deposits and prospects spatially and genetically associated with alkaline rocks of the Crocker Well and Bimbowrie suites. More detailed descriptions of these can be found in McKay and Miezitis (2001), Ashley (1984) and Ludwig and Cooper (1984). As the focus on of the Frome AEM Survey is on sandstone-hosted uranium mineral systems in the Lake Frome region (Figure 3.41), this section summarises important features of these systems.

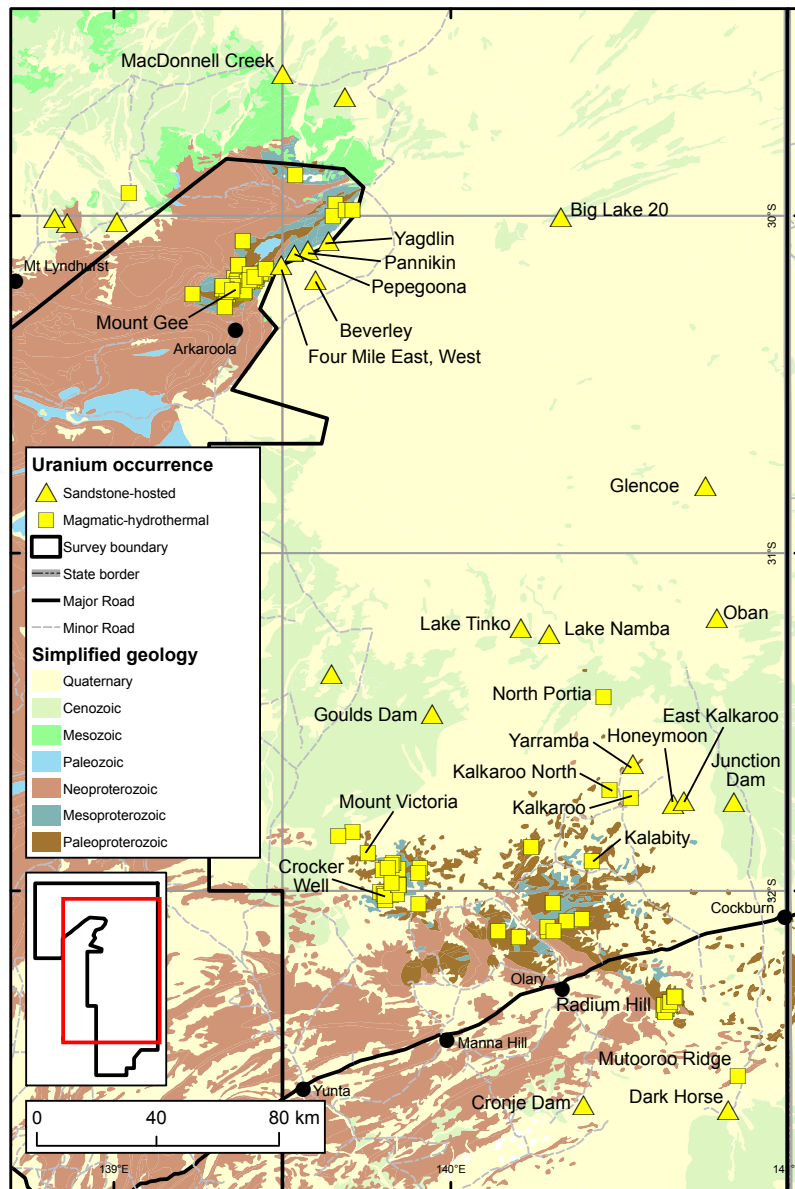


Figure 3.41: Uranium occurrences in the Frome AEM Survey area. Modified from SARIG and the 1:1 million Surface Geology Map of Australia (Raymond and Retter, 2010).

Table 3.2: Important mineral systems within the Frome AEM Survey area.

System	Main commodities	Age	Known example(s)	Host rock(s)	Reference(s)
Iron oxide uranium	U, REE (Cu, Au)	460 to 360 Ma	Mount Gee, Gunsight	Mesoproterozoic Mount Painter Inlier intruded and brecciated by post-Delamerian granitoids	Elburg <i>et al.</i> (2003), Wülser (2009); Skirrow (2011)
Sandstone-hosted uranium	U	~ 6 Ma (Beverley)	Four Mile East, Four Mile West, Beverley, Goulds Dam, Honeymoon, Oban	Mesozoic and Cenozoic sedimentary rocks including the Bulldog Shale, Cadna-owie Formation, Namba Formation and Eyre Formation	Wülser (2009)
Pegmatite uranium	U	1580 Ma	Radium Hill	I-type granitoids of the Olarian Orogeny intruding meta-sediments and metaigneous rocks of the Willyama Supergroup	Ludwig and Cooper (1984)
Orthomagmatic uranium (associated with alkaline rock)	U	1580 Ma	Crocker Well, Mount Victoria	I-type granitoids of the Olarian Orogeny intruding meta-sediments and metaigneous rocks of the Willyama Supergroup	Ludwig and Cooper (1984), Skirrow (2009)
Orogenic lode gold	Au	524 to 485 Ma	Teetulpa, Wadnaminga, Waukaringa	Principally Neoproterozoic Umberatana Group, but also Burra Group	Morris and Horn (1990)
Iron oxide copper gold	Cu, Au (U)	1630 to 1610 Ma	White Dam, Kalkaroo, Portia	Mulyungarie Domain, Curnamona Province	Williams and Skirrow (2000)

The Frome airborne electromagnetic survey, South Australia: implications for energy, minerals and regional geology

System	Main commodities	Age	Known example(s)	Host rock(s)	Reference(s)
Porphyry copper gold	Cu, Au (Mo)	468 Ma	Anabama	Cambro-Ordovician granitoids intruding Neoproterozoic sediments	Steveson and Webb (1976)
Sediment-hosted copper	Cu	Neoproterozoic (maximum)	Mountain of Light, Blinman, Lorna Doone, Lynda	Neoproterozoic	Cowley <i>et al.</i> (2009)
Sedimentary (Stratiform Iron)	Magnetite, hematite	Neoproterozoic (maximum)	Lilydale, Razorback, Mutooroo, Maldorky	Neoproterozoic Braemar Formation, Umberatana Group	Robertson <i>et al.</i> (1998)
Shear-hosted copper	Cu	1585 Ma (?)	Parabarana Mine		Cowley <i>et al.</i> (2009)
Copper skarn	Cu	Unknown	Yudnamutana Field		Cowley <i>et al.</i> (2009)
Stratiform and stratabound zinc, lead, silver	Zn, Pb, Ag (Cu)	Paleoproterozoic	Hunters Dam, Ram Dam Prospect	Mulyungarie Domain, Curnamona Province	Robertson <i>et al.</i> (1998)
Zinc silicate in hydrothermal karsts	Zn, Pb, As	435 Ma	Beltana	Lower Cambrian carbonate rocks, Arrowie Basin	Groves <i>et al.</i> (2003)
Chemical sedimentary (with supergene enrichment)	Mn	Neoproterozoic (maximum)	Martins Well Prospect, Eregunda, Boolcunda, Toothy Nob Mine		SARIG
Black coal	Coal	Triassic	Leigh Creek	Triassic Telford Basin and associated basins	Kwitko (1995)

3.6.1 Features of sandstone-hosted uranium systems in the Callabonna Sub-basin

In recent years sandstone-hosted uranium deposits in the Callabonna Sub-basin have become the focus of renewed studies. The deposits and prospects have been described in many individual and review papers such as Curtis *et al.* (1990), McKay and Miezitis (2001), Skirrow (2009) and Bastrakov *et al.* (2010). Important sandstone-hosted uranium deposits and prospects in the Lake Frome region are listed in the Table 3.3 and shown in Figure 3.34.

Table 3.3: Sandstone-hosted uranium deposits and prospects (Frome Embayment region).

DEPOSIT/ PROSPECT	PALAEOVALLEY	HOST SEQUENCE	AGE HOST SEQUENCE	RESOURCES (TONNES U ₃ O ₈)	RESOURCES (%)
Beverley	Beverley	Namba Formation	Late Oligocene to Miocene	16 310	27
MacDonnell Creek	Blanchewater	Eyre Formation	Paleocene to Eocene	Unknown	0
East Kalkaroo	Channel not identified	Eyre Formation	Paleocene to Eocene	889	1.5
Four Mile East	Channel not identified	Eyre Formation	Paleocene to Eocene	12 718	21
Four Mile West	Channel not identified	Bulldog Shale	Cretaceous	18 604	31
Goulds Dam	Billeroo	Eyre Formation	Paleocene to Eocene	6340	11
Honeymoon	Yarramba	Eyre Formation	Paleocene to Eocene	2882	5
Kalkaroo	Yarramba	Eyre Formation	Paleocene to Eocene	Unknown	0
Oban	Lake Charles	Eyre Formation	Paleocene to Eocene	2133	3.6
Pannikin	Channel not identified	Eyre Formation	Paleocene to Eocene	Unknown	0
Pepegoona	Channel not identified	Eyre Formation	Paleocene to Eocene	Unknown	0
Yagdlin	Channel not identified	Namba Formation	Late Oligocene to Miocene	Unknown	0
Yarramba	Yarramba	Eyre Formation	Paleocene to Eocene	Unknown	0

Sandstone-hosted uranium deposits have resulted from fertile uranium systems which operated in the Callabonna Sub-basin. Hence, the description focuses on important constituent features of the system. A mineral system (Bowler, 1986; Jaques *et al.*, 2002; Knox-Robinson and Wyborn, 1997) is generally defined by the following constituent elements: geological setting; sources of energy driving the system; sources of fluids, metals and ligands; pathways along which melt or fluid move; chemical and/or physical traps/gradients in proximity to pathways; outflow zones for discharge of residual fluids; and, preservation.

3.6.2 Geological setting

An important feature of the Lake Frome region is its embayment shape, in which the mineralized sedimentary basins are surrounded on three sides by Proterozoic rocks enriched in uranium (Figure

3.19). Similar shapes are observed in many mineralized areas such as the Chu-Sarysu and Syr Dariya basins in Kazakhstan (Jaireth *et al.*, 2008). This particular shape of the embayment has resulted from the prolonged geological history of the region.

In the south, the basins in the Lake Frome area are bounded by Paleoproterozoic metasediments of the Willyama Supergroup (southern Curnamona Province). The north-south trending Benagerie Ridge runs in the central part of the Lake Frome area and is entirely concealed by Phanerozoic sediments. In the west the Lake Frome area is flanked by the Proterozoic Mount Painter and Mount Babbage inliers (Northern Curnamona Province), part of the northern Flinders Ranges.

The Lake Frome area is filled with sediments of three major basins: the Arrowie Basin (Cambrian); the Eromanga Basin (Early Jurassic to Late Cretaceous); and, the Callabonna Sub-basin (part of the Lake Eyre Basin, Cenozoic). The gross architecture of the Lake Frome area is largely determined by the structures generated during a series of Neoproterozoic to Cenozoic basin-forming and orogenic events (Figure 3.36). These events created new structures and reactivated older structures (Teasdale *et al.*, 2001), including:

- Neoproterozoic intracratonic rifting (northeast-southwest extension) in the eastern Arrowie Basin, which led to the deposition of up to 4 km of sediments in a north-northwest-trending graben to the west of the Benagerie Ridge (Moorowie Sub-basin) and a half graben to the east of the Benagerie Ridge (Yalkapo Sub-basin);
- Early Cambrian northwest-southeast extension, which caused reactivation of old northeast-trending basement structures. Up to 3 km of sediments were deposited in northeast-trending graben and half graben. During this episode old Paleoproterozoic north-south structures were also reactivated;
- Northwest-southeast compression during the Delamerian Orogeny, which caused minor deformation in the eastern Arrowie Basin generating inversion of Cambrian normal faults. In the Adelaide Fold Belt, however, Early Cambrian sediments of the Arrowie Basin were folded and faulted;
- Deposition of Early Jurassic to mid-Cretaceous Eromanga Basin sediments, triggered by tectonic subsidence in the Arrowie Basin separated by the Benagerie Ridge; and,
- Deposition of fluvial and lacustrine sediments of the Cenozoic Callabonna Sub-basin, which host more than 90% of known sandstone-hosted uranium mineralisation in the Lake Frome region. Teasdale *et al.* (2001) associate this event with Cenozoic uplift caused by west-northwest—east-southeast compression during which major faults surrounding the Arrowie Basin were reactivated. The uplift generated minor foreland flexure in the area and up to 800 m of clastic sediments were deposited.

A number of major faults have been mapped in the Beverley area (Figures 3.42 and 5.5.14-5.5.17). Most of them are long-lived structures with a prolonged history of reactivation. These faults are considered to have played important roles in determining the present-day and palaeo-architecture of the Lake Frome area. Some of the important faults include the:

- Paralana Fault: a shallow west-dipping thrust fault which has been active since the Neoproterozoic (as a normal fault) which controlled deposition of Adelaidean sediments. The Paralana Hot Springs are controlled by this fault;
- Wooltana Range Front Fault (also known as the Vidnee Yarta Fault Zone near Beverley): a west-dipping thrust fault with splays mapped along the eastern scarp of the Flinders Ranges near Wooltana Station;
- Wooltana Fault: a steep west-dipping fault outlined on gravity data (Heathgate Resources, 2007);
- Four Mile Fault: northeast-southwest trending fault running west of the Four Mile East and Four Mile West deposits; and,
- Poontana Fault Zone: a west-dipping thrust fault with splays identified in drilling through variations in the thickness of the Cenozoic units on either side.

Movements along the Paralana Fault could have controlled paleorelief in the Lake Frome region, especially near the Beverley and Four Mile deposits. Drill hole and geophysical data suggest that a block defined by the Wooltana Fault in the west and the Poontana Fault Zone in the east forms an upthrust inlier (the Poontana Inlier) separating the Beverley deposit to its east and the Four Mile deposits to its west (Figure 3.42).

The Paralana Embayment to the west of the Poontana Inlier hosts the Paralana Trough, which contains several important uranium deposits and prospects (Heathgate Resources, 2008; McConachy, 2009). Movements along the Poontana Fault Zone could have also controlled the shape of the Miocene palaeovalley which hosts the Beverley deposit (Heathgate Resources, 2006).

3.6.3 Energy Drivers of the system

In a single-fluid model of sandstone-hosted uranium systems (Jaireth *et al.*, 2008) uranium is transported in oxidised shallow groundwater through sandstone aquifers. The flow of groundwater in this model is gravity driven and is controlled by hydrostatic head (created by relief) at the time when the uranium mineral system was established. The landscape evolution history outlined in Section 3.5 summarises important episodes of cooling/uplifting in the Lake Frome region. Of these, 2 episodes are considered critical for generating uranium systems are:

- Paleocene to Eocene (<65 Ma), caused either by the removal of ~1.5-2.0 km of rocks or by a decrease in geothermal gradient accompanied by minor erosion (Mitchell *et al.*, 2002). The uplifted Mount Painter Inlier could have not only provided material for the Eyre Formation sediments, but also created the needed hydrostatic head to generate fluid flow in Mesozoic aquifers (such as the Algebuckina Sandstone and the Cadna-owie Formation); and,
- Pliocene (~4 Ma), when the present day relief was formed from tectonic movement along major faults such as the Paralana Fault (Quigley *et al.*, 2007). This episode is broadly related to the formation of the Willawortina Formation which unconformably overlies the Namba Formation which hosts the Beverley uranium deposit. The tectonic uplift in the Pliocene thus created the needed hydrostatic head for fluids in the sandy aquifers of the Namba Formation.

A hiatus (~5 million years) in sedimentation is recorded between the Lower and Upper Eyre Formations in the southern Callabonna Sub-basin (Alley, 1998). A more prolonged hiatus (~15 million years) is also documented between the Upper Eyre Formation and the Namba Formation (Alley, 1998). Zircon provenance studies summarised in Section 3.5.2 show that sediments of both the Eyre Formation and the Namba Formation could have been partially derived from rocks in the Mount Painter Inlier, indicating that the provenance area (Mount Painter Inlier) was uplifted during the Middle Oligocene (~30 Ma). This indicates the presence of a possible hydrostatic head necessary to drive fluids in the aquifers of the Eyre Formation.

A two-fluid model (Jaireth *et al.*, 2008), considered to be important for some sandstone-hosted uranium systems, can not be ruled out for Lake Frome region. In this model uranium precipitation is caused by interaction with mobile reductants (hydrocarbons and/or H₂S). Mobile reductants can be derived either from hydrocarbon accumulations in the Eromanga and Arrowie basins or from thermal degradation of organic material in the sediments. Reactivation of faults in the Lake Frome region can trigger movement of reductants from underlying basins. Hot fluids along the Paralana Fault (such as the Paralana hot springs) can also cause reduction of uranium-bearing fluids in the aquifer. The principal driver of the hot springs is probably the thermal gradient created by the high heat flow zone in the Mount Painter Inlier. Apatite fission-track thermochronology studies near the Paralana Fault indicate that it created heating of > ~100°C in the area at ~20-25 Ma (Mitchell *et al.*, 2002). This heating is capable of generating mobile reductants from the degradation of organic material from shales in various sedimentary rocks in the three basins, especially in the Eromanga Basin and Callabonna Sub-basin.

The Frome airborne electromagnetic survey, South Australia: implications for energy, minerals and regional geology

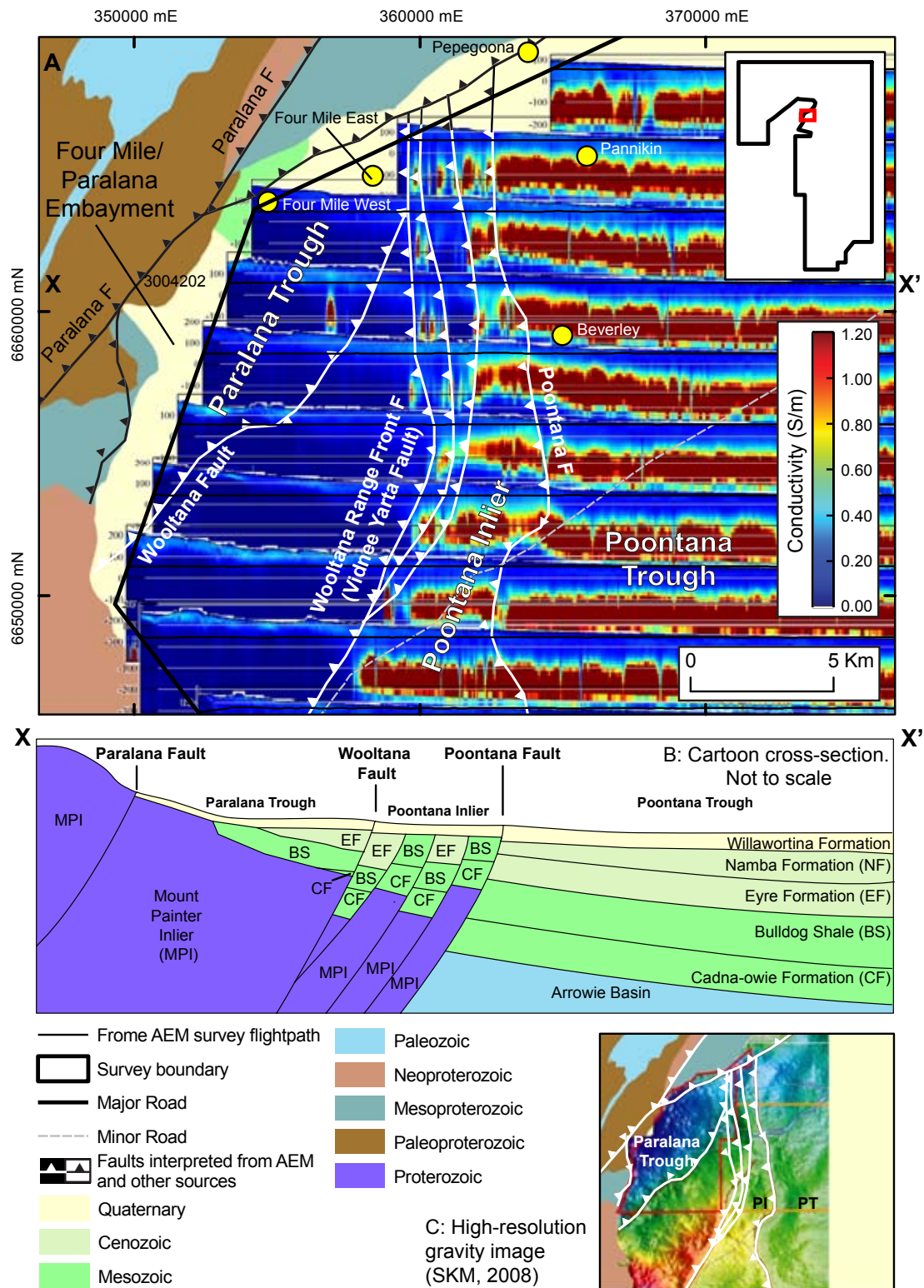


Figure 3.42: Faults, basement structures and uranium deposit locations in the Beverley area. Modified from SKM (2008). Faults in the Poontana Inlier are interpreted from linear colour-stretched SBS GA-LEI conductivity sections and conductivity depth slices and Heathgate Resources high-resolution gravity data.

3.6.4 Source of uranium

The Callabonna Sub-basin is surrounded on three sides by felsic rocks enriched in uranium (Table 3.1; Section 3.2.7). The average uranium concentration in the rocks varies between 4 ppm and 100 ppm, but some felsic rocks in the Mount Painter and Mount Babbage inliers contain up to 400 ppm uranium (Table 3.1, Figure 3.43). However, the total uranium in rocks only provides a rough guide to their potential as a source of uranium. A more important guide is the concentration of readily-leachable uranium in the rocks. Most leachable uranium-bearing minerals in rocks are uranium oxides (such as uraninite). In their absence uranium-bearing rock-forming and accessory minerals (e.g. allanite, monazite, xenotime, zircon, epidote and apatite) become important. Limited experimental leaching studies indicate that in minerals such as allanite, 80% of uranium is leachable (Larsen and Gottfried, 1961).

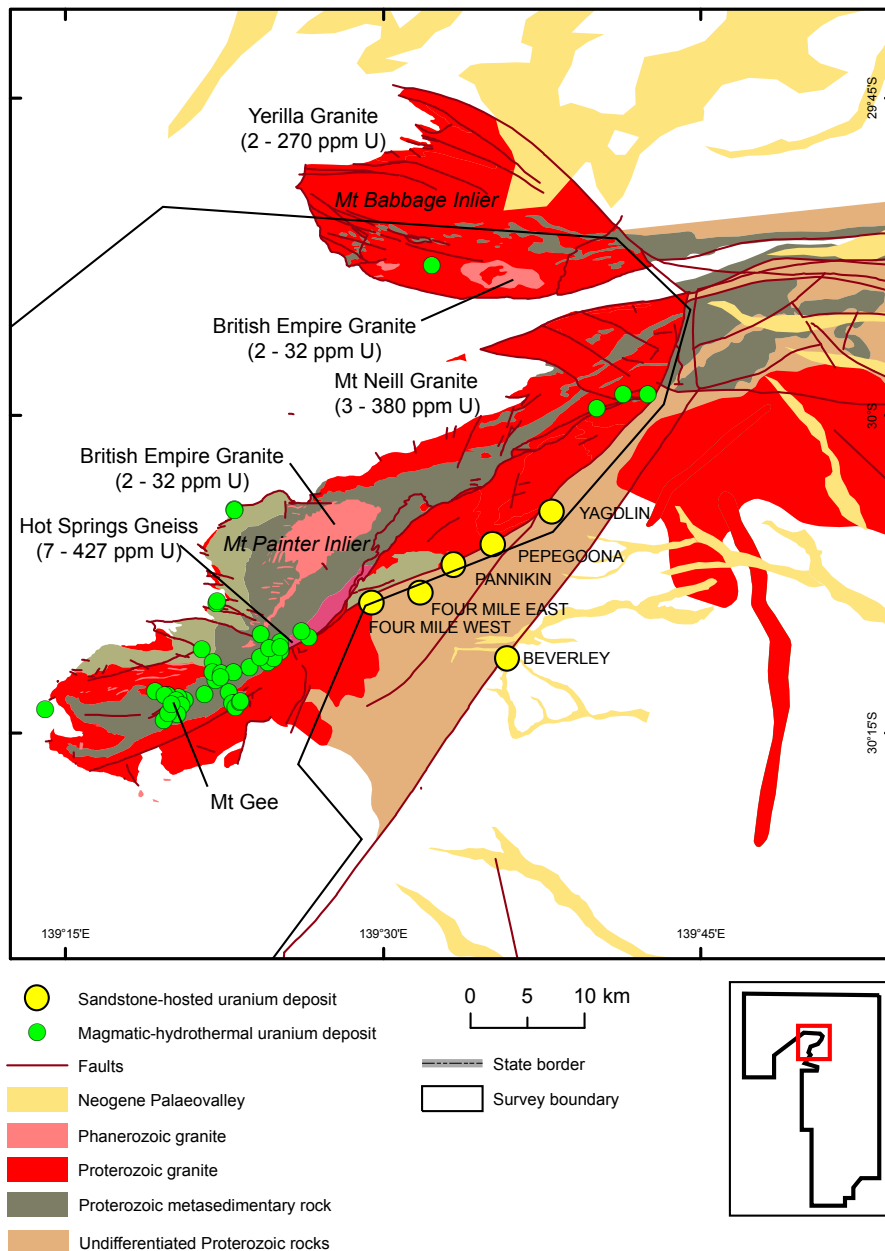


Figure 3.43: Uranium source rocks and deposits in the northeastern Flinders Ranges-northwestern Lake Frome area. Modified from SARIG.

The Yerilla Granite (4 to 270 ppm uranium) in the Mount Babbage Inlier, the Mount Neill Granite (3 to 380 ppm uranium) and the Hot Spring Gneiss (7 to 427 ppm) in the Mount Painter Inlier are possibly the best sources of leachable uranium (Table 3.1, Figure 3.43). The medium- to coarse-grained Yerilla Granite contains uraninite and other uranium-bearing accessory minerals including monazite, allanite, zircon, apatite and xenotime. It also shows extreme enrichment in REE, Nb, F, Th, Y and W (Teale, 1993). Wülser *et al.* (2009) document intensive metasomatic overprints (Proterozoic and Ordovician in age) and the gneissic varieties contain allanite-rich lenses. Uraninite and uranothorite inclusions are present in zircons. The uranium-enriched Hot Springs Gneiss also shows a similar metasomatic overprint (Wulser, 2009). A red metasomatic gneiss contains brannerite veins, allanite-rich zones and thorite mineralisation. Elburg *et al.* (2008) explain the presence of trondhjemite, gneiss and schist within the Mount Neill Granite as a result of metasomatic alteration. It is possible that some samples containing up to 300 ppm uranium represent metasomatic altered A-type Mount Neill Granite.

In addition to uranium-enriched felsic rocks, the Mount Painter Inlier also contains a variety of magmatic-hydrothermal and epithermal prospects and deposits of uranium such as Mount Gee, Mount Painter and Radium Ridge. Uraninite is the major ore mineral in these prospects. Other uranium-bearing minerals are brannerite, xenotime, allanite, apatite, titanite, ilmenite and zircon (Drexel and Major, 1990).

More than 80% of uranium resources in the Lake Frome region are located in close proximity to the Mount Painter and Mount Babbage inliers. A number of deposits (Four Mile East, Four Mile West, Pepegoona and Pannikin) are also within the Paralana Embayment (Paralana Trough), to the south-western end of which are located not only uranium-enriched felsic rocks (Hot Springs Gneiss, Mount Neill Granite), but also many uraninite-bearing deposits and prospects (Figure 3.43). The relatively high uranium endowment of this area could thus be associated with the presence of source rocks containing leachable uranium.

Uranium-enriched felsic rocks (average concentration of uranium varying between 2 ppm and 28 ppm) are also present in the southern Lake Frome region (Table 3.1, Figure 3.44). However, the maximum uranium maximum concentration is less than 110 ppm (Table 3.1). The most enriched of these is the Mindamereeka Trondhjemite (Crocker Well Suite) with up to 110 ppm uranium and the Honeymoon Granite with up to 40 ppm uranium. The trondhjemites have undergone intensive sodic metasomatism and grade into alaskites, which occur as dykes, veins and pegmatitic bodies (Wade, 2011). The Honeymoon Granite, which is considered to be spatially associated with the Honeymoon and East Kalkaroo uranium deposits, contains up to 40 ppm uranium. The Granite shows locally intensive potassic alteration (Fricke and Reid, 2009). Unaltered Honeymoon Granite, however, has an abundance of uranium-bearing minerals (uranium oxides in pyrite, monazite, allanite, zircon and apatite).

The felsic rocks in the Olary Domain are associated with a number of orthomagmatic and hydrothermal uranium deposits (Crocker Well, Mount Victoria and Radium Hill). The main uranium mineral at the Crocker Well deposit is thorian brannerite. Davidite is the main uranium mineral at the Mount Victoria and Radium Hill deposits. These deposits also contain monazite and xenotime and minor uranophane (McKay and Mieztis, 2001). Thus, although uranium-bearing minerals are present in felsic rocks and deposits in this part of the Lake Frome region, they are not as readily leachable as uraninite, which is far more abundant in the Mount Painter and Mount Babbage inliers.

In the Murray-Darling Basin, uranium mineralisation occurs in the Olary Palaeovalley (see Figures 5.2.12 and 6.1), filled with Tertiary sediments, at the Cronje Dam and Mutooroo Ridge prospects (Alley, 1995; U3O8 Limited, 2012), downstream of the Radium Hill mine. Sediments are Namba Formation age-equivalent sediments of the Renmark and Murray groups. No significant uranium mineralisation has been found on the southern side of the Olary Spur to date, most likely because of the orthomagmatic-hydrothermal source rocks and the lack of sufficient leachable uranium.

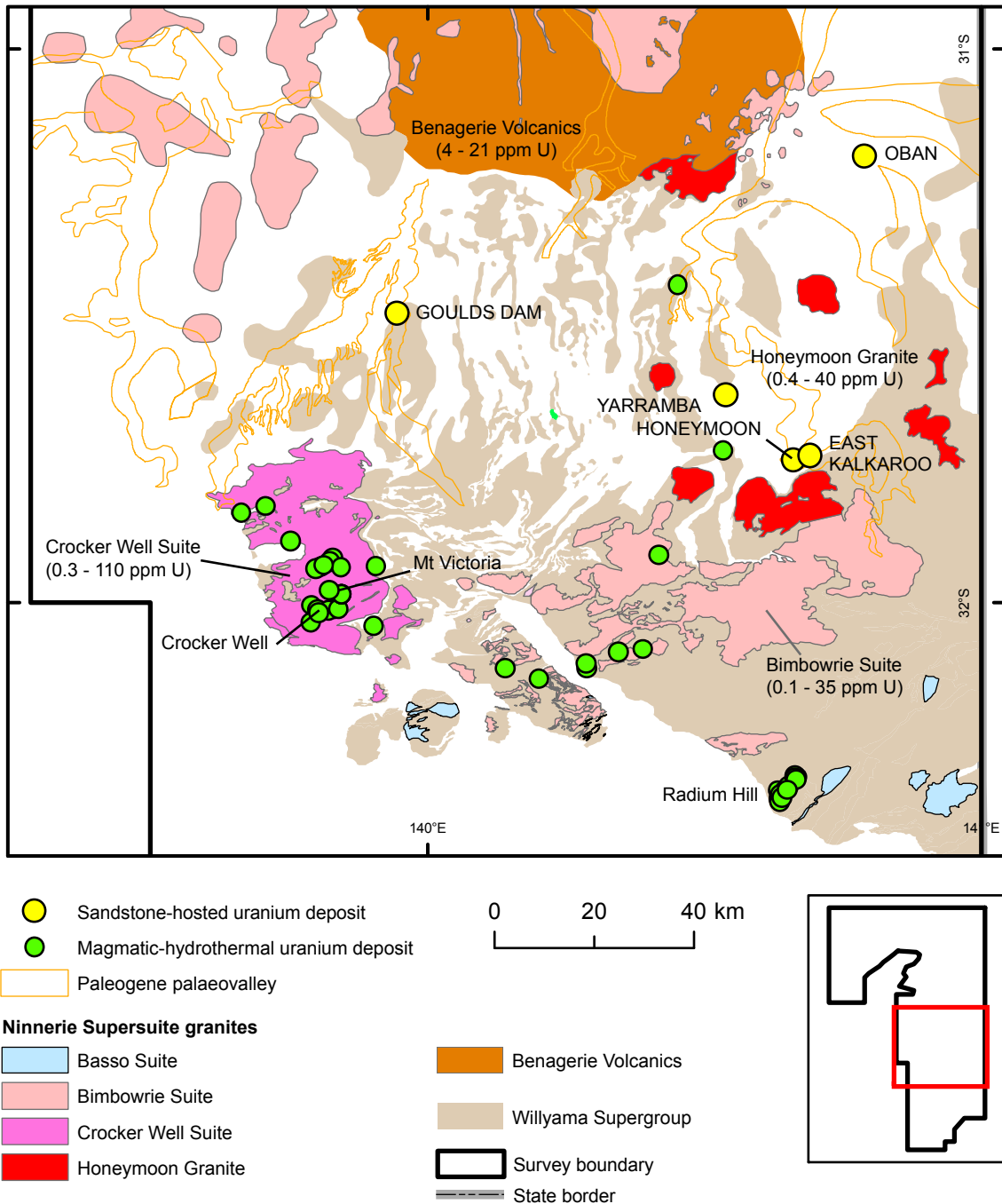


Figure 3.44: Uranium source rocks and deposits in the Curnamona Province—southern Callabonna Sub-basin area, modified from SARIG. Includes palaeovalley outlines from Hou et al. (2007).

3.6.5 Fluid pathways

Sandstone-hosted uranium deposits are formed by oxidised uranium-bearing fluids flowing in permeable sandstones sandwiched between relatively impermeable shaly sediments. Eyre Formation sands, which host more than 90% of known mineralisation, are highly permeable. The mature, fine- to coarse-grained, unconsolidated, carbonaceous, pyritic sands give a measured permeability of 5 m/day in the Four Mile East ore zone (Heathgate Resources, 2008). The overlying Namba Formation is characterised by an overall low permeability.

The lenticular Beverley Sands, which host the Beverley Deposit, are sandwiched between the Beverley Clay and the Alpha Mudstone. The Beverley Sands aquifer is made up of four units, of which the main mineralised sands have moderate hydraulic transmissivity, whereas the two underlying sandy units are more permeable (Heathgate Resources, 2006).

An important factor in the formation of sandstone-hosted uranium systems is the direction of fluid-flow at the time of mineralisation. In many mineralised basins it is known to be different from the present-day fluid-flow direction. In the southern part of the Lake Frome region mineralisation is located in the Eocene palaeovalley/channel systems which generally run northward from the uplifted parts of the Olary Domain (Alley, 1998). Some of these channels (e.g. Lake Charles, which hosts the Oban deposit) run southeast to northwest. Generally, the fluid-flow in the sands filling the channels is along the channels (e.g. northwards in the southern part of the Lake Frome region). Eyre Formation sediments in the northern part of the Lake Frome region were deposited predominantly in alluvial fans (Alley, 1998), although some palaeovalley/channel deposits may also be present to the north of the Mount Babbage Inlier. The top of the Eyre Formation in the Paralana Trough (Figure 3.42), which hosts significant uranium deposits, slopes southwest to northeast. Present-day hydrogeological measurements in wells show that the present-day groundwater flow is from southwest to northeast (SKM, 2008). It is therefore possible that in the Eocene, when uranium deposits were formed, the groundwater also flowed in the same direction, linking the waters with the source of leachable uranium (Figure 3.43).

The Beverley Palaeochannel represents a cyclic cut-and-fill (channel-in-channel) system and is filled with Beverley Sands (Namba Formation) incised into Alpha Mudstone. It runs generally from northwest to southeast. Its shape is controlled by movements along the Poontana Fault Zone, which was active during deposition of the Beverley sequence and also after the Willawortina Formation (Heathgate Resources, 2008). If the fluid-flow during the formation of the Beverley deposit was also from northwest to southeast, it would link the fluids with the sources of leachable uranium in the northern Mount Painter and Mount Babbage inliers, rather than bringing fluids across the hydrological barrier formed by the uplifted Poontana Inlier.

3.6.6 Chemical and/or physical traps/gradients

The presence of redox fronts in uranium deposits shows that uranium deposition was caused predominantly by reduction of oxidised uranium-bearing fluids flowing in sandy aquifers. In most cases reduction occurs from reaction with an *in situ* reductant (organic material in the aquifer and/or in the shaly sediments underlying it). The role of a mobile reductant (hydrocarbons, H₂S) in this process remains undocumented.

The Eyre Formation is known to be rich in organic material. In the Yarramba Palaeovalley, which hosts the Honeymoon deposit, it contains an average 0.3% organic material in the form of lignite, plant fragments and woody material (Bampton *et al.*, 2001; Skidmore, 2005). The sediments are also locally enriched in pyrite (averaging 7%), estimated on the basis of sulphur analysis by Bampton *et al.* (2001).

The Beverley Sands in the Namba Formation do not contain organic material but the Alpha Mudstone underlying the sands is enriched in carbonaceous matter. The ore zones contain 0.05% to 0.5% organic carbon in grey sands and up to 2% in selected samples (Heathgate Resources, 2006). The Alpha Mudstone has abundant plant fragments and large pieces of carbonised wood (Heathgate Resources, 2006).

Michaelsen and Fabris (2011) have recently identified six organic facies of which three are in the Eyre Formation and two are in the Namba Formation. Their “Namba Facies 1” is dominated by liptinite and contains abundant lamalginite and telaginite. The facies is developed at the base of the Namba Formation. Their “Namba Facies 2” is developed within mudstones and the humic material is considered to have undergone extensive transportation and oxidation. As the upper Namba

Formation lacks effective (hydrogen-rich detrital organic) reductants, mobile reductants (hydrocarbon gases) could have been involved in the formation of the Beverley uranium deposit (Michaelsen and Fabris, 2011).

In palaeovalleys, mineralisation is often located in the basal scours, bends, sites of confluences with tributaries, areas of channel-widening and bar-heads (Jaireth, 2010). At this stage the processes which influence accumulation of uranium mineralisation at these sites are not clear, but they may be related to the amount of organic material concentrated in the sediments. These sites may also exert control on the changes in the fluid-flux of groundwater in the channel sands.

3.6.7 Age of uranium systems

Wülser *et al.* (2011) dated coffinite grains at the Beverley deposit. The grains were inhomogeneous and porous and the Laser Ablation Inductively Coupled Plasma-Mass Spectrometry (LA ICP-MS) analysis showed the presence of high proportions of common lead, indicating that the grains were open to lead loss since their formation. Three intersects on the concordia plot of Wülser *et al.* (2011) gave sub-concordant to concordant apparent ages between 6.7 Ma and 0.4 Ma. Uranium-lead (U-Pb) dating by LA ICP-MS of carnotite disseminated in the Beverley Sands (upper mineralization zone) and also filling cracks within kaolinite and alunite in the Beverley Clay unit, gave concordant to sub-concordant ages between 5.5 Ma and 3.4 Ma (Wulser *et al.*, 2011).

Based on the disequilibrium $^{234}\text{U}/^{238}\text{U}$ ratio in groundwaters in the Pepegoona deposit, Murphy *et al.* (2011) suggest that uranium mineralization has probably been deposited or remobilized within 1 Ma.

The history of landscape evolution in the Lake Frome region (summarized and discussed in preceding sections) suggests at least three episodes (Figure 3.35) which could have generated flows of uranium-bearing fluids in sandy aquifers : at ~65 Ma (uranium systems in Mesozoic aquifers); at ~ 30 Ma (uranium systems in Eocene aquifers); and, ~6 Ma to 4 Ma (uranium systems in Miocene aquifers). It is possible that emplacement of younger systems not only remobilized uranium formed during preceding events, but also formed new zones of mineralization in older aquifers (i.e. the Miocene event could have formed new uranium deposits in Mesozoic and Eocene aquifers as well as redistributed mineralization formed during Mesozoic and Eocene events).

3.6.8 Preservation of uranium systems

High solubility of uranium in oxidised fluids raises the problem of preserving uranium mineralization formed in aquifers. Dispersion of U-series isotopes around known deposits shows that in many mineralized areas the mineralization is actively remobilized by groundwaters (e.g. Pepegoona deposit). The flow of groundwaters is controlled predominantly by hydrogeological gradient, which depends on the reactivation of faults. In the Lake Frome region, the present-day groundwater flow is controlled by relief generated during the uplift (< ~5 Ma) in the Mount Painter and Mount Babbage inliers. Penetration of groundwaters in Mesozoic and Cenozoic aquifers is remobilizing uranium from known deposits.

The reactivation of faults in the Lake Frome region has also led to selective erosion of aquifers. In the Poontana Inlier the Eyre Formation has been eroded, which means that mineralised zones, if formed, were destroyed resulting from movement on the Wooltana Fault in west and Poontana Fault Zone in the east.

3.7 REFERENCES

- Alexander, E. M. and Hibburt, J. E. (editors), 1996. Petroleum geology of South Australia Volume 2 - Eromanga Basin. SA Department of Mines and Energy, Adelaide.
- Alexander, E. M. and Sansome, A., 1996. Lithostratigraphy and environments of deposition. In: Alexander, E. M. and Hibburt, J. E. (editors), Petroleum geology of South Australia Volume 2 - Eromanga Basin. SA Department of Mines and Energy, Adelaide. 49-86 p.
- Alley, N. F., 1995. Late Palaeozoic. In: Drexel, J. F. and Preiss, W. V. (editors), The Geology of South Australia Volume 2: The Phanerozoic. Geological Survey of South Australia, Adelaide. **Bulletin 54**, 63-65 p.
- Alley, N. F., 1998. Cainozoic stratigraphy, palaeoenvironments and geological evolution of the Lake Eyre Basin. Palaeogeography, Palaeoclimatology, Palaeoecology **144**, 239-263.
- Alley, N. F. and Frakes, L. A., 2003. First known Cretaceous glaciation: Livingston Tillite Member of the Cadna-owie Formation, South Australia. Australian Journal of Earth Sciences **50(2)**, 139-144.
- ANRA, 2011. Australian Natural Resources Atlas. Online: <http://www.anra.gov.au/topics/vegetation/assessment/sa/index.html>.
- Ashley, P. M., 1984. Sodic granitoids and felsic gneisses associated with uranium-thorium mineralisation, Crockers Well, South Australia. Mineralium Deposita **19**, 7-18.
- Bakker, R. J. and Elburg, M. A., 2006. A magmatic-hydrothermal transition in Arkaroola (northern Flinders Ranges, South Australia): from diopside-titanite pegmatites to hematite-quartz growth. Contributions to Mineralogy and Petrology **152**, 541-569.
- Bampton, K. F., Haines, J. B. and Randell, M. H., 2001. Geology of the Honeymoon uranium project. The AusIMM Proceedings **306(2)**, 17-27.
- Barnes, T. A., 1951. Underground Water Survey of Portion of the Murray Basin (Counties Albert and Alfred). Geological Survey of South Australia, Department of Mines, Adelaide. **Bulletin No. 25**, 178 pp.
- Bastrakov, E. N., Jaireth, S. and Mernagh, T. P., 2010. Solubility of uranium in hydrothermal fluids at 25° to 300°C: implications for the formation of uranium deposits. Geoscience Australia, Canberra. **Record 2010/29**, 91 pp.
- Bowler, J. M., 1976. Aridity in Australia: Age, origins and expression in aeolian landforms and sediments. Earth-Science Reviews **12(2-3)**, 279-310.
- Bowler, J. M., 1986. Spatial variability and hydrologic evolution of Australian lake basins: analogue for Pleistocene hydrologic change and evaporite formation. Palaeogeography, Palaeoclimatology, Palaeoecology **54**, 21-41.
- Bowler, J. M., Kotsonis, A. and Lawrence, C. R., 2006. Environmental evolution of the Mallee region, western Murray Basin. Proceedings of the Royal Society of Victoria **118(2)**, 161-210.
- Brown, C. M., 1985. Murray Basin, southeastern Australia: stratigraphy and resource potential - a synopsis. Bureau of Mineral Resources, Canberra. **Report 264**, 24 pp.
- Brown, C. M. and Stephenson, A. E., 1991. Geology of the Murray Basin, Southeastern Australia. Australian Govt. Pub. Service.
- Brugger, J., Long, N., McPhail, D. C. and Plimer, I., 2005. An active amagmatic hydrothermal system: The Paralana hot springs, Northern Flinders Ranges, South Australia. Chemical Geology **222**, 35-64.
- Brugger, J., Wülser, P.-A. and Foden, J., 2011a. Genesis and preservation of a uranium-rich Palaeozoic epithermal system with a surface expression (northern Flinders Ranges, South Australia). Astrobiology **11**, 499-508.
- Brugger, J., Wülser, P.-A. and Foden, J., 2011b. Mt Gee and Mt Painter: Genesis and preservation of a U-rich Palaeozoic epithermal system with a surface expression. In: Forbes, C. J. (editor): 2011 Sprigg Symposium: Unravelling the northern Flinders and beyond, University of Adelaide. Geological Society of Australia **Abstracts No. 100**, 5-6 pp.
- Brunt, D. A., 1975. Mines Administration Pty Ltd Quarterley Report South Eagle farm-in portion of EL 132. South Australia Department of Mines. **ENV02511**.

- Budd, A. R., Wyborn, L. A. I. and Bastrakova, I. V., 2001. The metallogenic potential of Australian Proterozoic granites. Geoscience Australia, Canberra. **Record 2001/12**.
- Callen, R. A., 1977. Late Cainozoic environments of part of northeastern South Australia. *Journal of the Geological Society of Australia* **24(3)**, 151-169.
- Callen, R. A., 1982. Late Tertiary 'grey billy' and the age and origin of surficial silicifications (silcrete) in South Australia. *Journal of the Geological Society of Australia* **30**, 393-410.
- Callen, R. A., Alley, N. F. and Greenwood, D. R., 1995a. Lake Eyre Basin. In: Drexel, J. F. and Preiss, W. F. (editors), *The geology of South Australia. Volume 2: The Phanerozoic*. South Australia Geological Survey, Adelaide. **Bulletin 54**, 188-194 p.
- Callen, R. A., Sheard, M. J., Benbow, M. C. and Belperio, A. P., 1995b. Alluvial fans and piedmont slope deposits. In: Drexel, J. F. and Preiss, W. V. (editors), *The Geology of South Australia Volume 2: The Phanerozoic*. Geological Survey of South Australia, Adelaide. 241-243 p.
- Callen, R. A. and Tedford, R. H., 1976. New Late Cainozoic rock units and depositional environments, Lake Frome area, South Australia. *Transactions of the Royal Society of South Australia* **100(3)**, 125-167.
- Chen, X. Y., Lintern, M. J. and Roach, I. C., 2002. Calcrete: characteristics, distribution and use in mineral exploration. Cooperative Research Centre for Landscape Environments and Mineral Exploration. 160 pp.
- Chivas, A. R., Andrew, A. S., Lyons, W. B., Bird, M. I. and Donnelly, T. H., 1991. Isotopic constraints on the origin of salts in Australian playas. 1. Sulphur. *Palaeogeography, Palaeoclimatology, Palaeoecology* **84**, 309-322.
- Coats, R. P., 1973. COPLEY South Australia, Explanatory Notes 1:250 000 Geological Series—Sheet SH/54-9. Department of Mines, Geological Survey of South Australia, Adelaide, 38 pp.
- Coats, R. P. and Blissett, A. H., 1971. Regional and economic geology of the Mount Painter Province. Geological Survey of South Australia, Department of Mines, Adelaide. **Bulletin 43**, 417 pp.
- Coats, R. P., Callen, R. A. and Williams, A. F., 1973. COPLEY Sheet SH 54-9. 1:250 000 Geological Series, Geological Survey of South Australia, Department of Mines, Adelaide. First Edition.
- Conor, C. H. H., 2000. Definition of major sedimentary and igneous units of the Olary Domain, Curnamona Province. *MESA Journal* **19(October 2000)**, 51-56.
- Conor, C. H. H., 2004. Geology of the Olary Domain, Curnamona Province, South Australia. South Australia. Department of Primary Industries and Resources, Adelaide, **Report Book 2004/8**, 86 pp.
- Conor, C. H. H. and Preiss, W. V., 2008. Understanding the 1720-1640 Ma Palaeoproterozoic Willyama Supergroup, Curnamona Province, Southeastern Australia: Implications for tectonics, basin evolution and ore genesis. *Precambrian Research* **166(1-4)**, 297-317.
- Cowley, W. M. and Barnett, S. R., 2007. Revision of Oligocene-Miocene Murray Group stratigraphy for geological and groundwater studies in South Australia. *MESA Journal* **47**, 17-20.
- Cowley, W. M., Katona, L. F. and Gouthas, G., 2009. Assessment of mineral prospectivity of the northern Flinders Ranges using GIS analysis. Primary Industries and Resources South Australia, Adelaide, **Report Book 2009/19**, 102 pp.
- Cross, A., Jaireth, S., Hore, S. B., Michaelsen, B. and Schofield, A., 2010. SHRIMP U-Pb detrital zircon results, Lake Frome region, South Australia. Geoscience Australia, Canberra. **Record 2010/46**, 28 pp.
- Curtis, J. L., Brunt, D. A. and Binks, P. J., 1990. Tertiary palaeochannel uranium deposits of South Australia. In: Hughes, F. E. (editor), *Geology of the mineral deposits of Australia and Papua New Guinea*. Australasian Institute of Mining and Metallurgy, Melbourne. **Volume 2**, 1631-1636 p.
- Cutten, H. N. C., Korsch, R. J. and Kositsin, N., 2006. Tectonic synthesis of the Curnamona Province, southern Australia, using a time-space framework. In: Korsch, R. J. and Barnes, R. G. (editors), *Broken Hill Exploration Initiative, Abstracts*. Geoscience Australia. **Record 2006/21**, 36-45 p.

- Dart, R. C., Barovich, K. M., Chittleborough, D. J. and Hill, S. M., 2007. Calcium in regolith carbonates of central and southern Australia: Its source and implications for the global carbon cycle. *Palaeogeography, Palaeoclimatology, Palaeoecology* **249(3–4)**, 322-334.
- Davey, J. E., 2009. Tectonostratigraphic Evolution of an Intracontinental Terrain: The Geological Evolution of the Frome Embayment, Eromanga Basin, South Australia. CRC LEME, School of Earth and Environmental Sciences, Geology and Geophysics and Australian School of Petroleum, University of Adelaide. PhD thesis, unpublished.
- de Vries, S., Fry, N. and Pryer, L., 2006. OZ SEEBASE Proterozoic Basins Study, Report to Geoscience Australia. FrOG Tech Pty Ltd, Canberra.
- Drexel, J. F. and Major, R. B., 1990. Mount Painter uranium-rare earth deposit. In: Hughes, F. E. (editor), *Geology of the mineral deposits of Australia and Papua New Guinea*. Australasian Institute of Mining and Metallurgy, Melbourne. **Volume 2**, 993-998 p.
- Drexel, J. F. and Preiss, W. V. (editors), 1995. *The Geology of South Australia: Volume 2, The Phanerozoic*. **Bulletin 54(2)**, 357 pp.
- Drexel, J. F., Preiss, W. V. and Parker, A. J. (editors), 1993. *The Geology of South Australia: Volume 1, The Precambrian*. **Bulletin 54(1)**, 249 pp.
- Dunkerley, D. L. and Brown, K. J., 1995. Runoff and runoff areas in a patterned chenopod shrubland, arid western New South Wales, Australia: characteristics and origin. *Journal of Arid Environments* **30**, 41-55.
- Eggleton, R. A. (editor) 2001. *The Regolith Glossary*. CRC LEME, Perth. 144 pp.
- Elburg, M. A., Bons, P. D., Foden, J. and Brugger, J., 2003. A newly defined Late Ordovician magmatic-thermal event in the Mt Painter Province, northern Flinders Ranges, South Australia. *Australian Journal of Earth Sciences* **50(4)**, 611-631.
- Ellis, G. K., 1974. Pacminex Pty Ltd Quarterly report to 12 February 1975. South Australia Department of Mines. **ENV02362**.
- Fabris, A. J., 2008. Southern Curnamona Province, regolith tour guide. Primary Industries and Resources South Australia, Adelaide. **Report Book 2008/9**, 35 pp.
- Fabris, A. J., Gouthas, G. and Fairclough, M. C., 2010. The new 3D sedimentary basin model of the Curnamona Province: geological overview and exploration implications. *MESA Journal* **58(September 2010)**, 16-24.
- Fabris, A. J., Sheard, M. J., Keeling, J. L., Hill, S. M., McQueen, K. G., Connor, C. H. H. and Caritat, P. d., 2008. A guide for mineral exploration through the regolith in the Curnamona Province, South Australia. Cooperative Research Centre for Landscape Environments and Mineral Exploration, Perth, WA. 150 pp.
- Farrand, M. G. and Preiss, W. V., 1995. Delamerian igneous rocks. In: Drexel, J. F. and Preiss, W. V. (editors), *The Geology of South Australia Volume 2: The Phanerozoic*. Geological Survey of South Australia, Adelaide. 54-57 p.
- Fitzsimmons, K. E., Rhodes, E. J., Magee, J. W. and Barrows, T. T., 2007. The timing of linear dune activity in the Strzelecki and Tirari Deserts, Australia. *Quaternary Science Reviews* **26(19-21)**, 2598-2616.
- Foden, J., Elburg, M. A., Dougherty-Page, J. and Burt, A., 2006. The timing and duration of the Delamerian Orogeny: correlation with the Ross Orogen and implications for Gondwana assembly. *The Journal of Geology* **114**, 189-210.
- Forbes, B. G., 1989. OLARY Sheet SI 54-2. 1:250 000 Geological Series, Geological Survey of South Australia, Department of Mines and Energy, Adelaide. First Edition.
- Forbes, B. G., 1991. 1:250 000 Geological Series--Explanatory Notes, OLARY, South Australia, Sheet SI 54-2 International Index. Geological Survey of South Australia, Department of Mines, Adelaide, 47 pp.
- Foster, D. A., Murphy, J. M. and Gleadow, A. J. W., 1994. Middle Tertiary hydrothermal activity and uplift of the northern Flinders Ranges, South Australia: insights from apatite fission track thermochronology. *Australian Journal of Earth Sciences* **41**, 11-17.
- Fraser, G. L. and Neumann, N. L., 2010. New SHRIMP U-Pb zircon ages from the Gawler Craton and Curnamona Province, South Australia, 2008-2010. Geoscience Australia, Canberra. **Record 2010/16**, 265 pp.

- Fricke, C. and Reid, A., 2009. Alteration of uranium-rich granite and its relationship to uranium mineralisation in the Honeymoon area, South Australia. Department of Primary Industries and Resources South Australia, Adelaide, **Report Book 2009/4**, 19 pp.
- FrOG Tech, 2005. OZ SEEBASE Study 2005, Public Domain Report to Shell Development Australia. FrOG Tech Pty Ltd, Canberra.
- Gallant, J. C. and Dowling, T. I., 2003. A multiresolution index of valley bottom flatness for mapping depositional areas. *Water Resource Research* **39(12)**, 1347-1359.
- Gardner, G. J., Mortlock, A. J., Price, D. M., Readhead, M. L. and Wasson, R. J., 1987. Thermoluminescence and radiocarbon dating of Australian desert dunes. *Australian Journal of Earth Sciences* **34(3)**, 343-357.
- Gibson, D. L., 1999. Explanatory notes for the Broken Hill and Curnamona Province 1:500 000 regolith landform maps. CRC LEME, Perth. **Open File Report 77**, 59 pp.
- Goleby, B. R., Korsch, R. J., Fomin, T., Conor, C. C. H., Preiss, W. V., Robertson, R. S. and Burt, A. C., 2006. The 2003-2004 Curnamona Province seismic survey: Workshop notes. Geoscience Australia, Canberra. Record 2006/12.
- Gravestock, D. I., 1995. Simpson Basin. In: Drexel, J. F. and Preiss, W. V. (editors), *The Geology of South Australia Volume 2: The Phanerozoic*. Geological Survey of South Australia, Adelaide. **Bulletin 54**, 93-97 p.
- Gravestock, D. I. and Cowley, W. M., 1995. Arrowie Basin. In: Drexel, J. F. and Preiss, W. V. (editors), *The Geology of South Australia Volume 2, The Phanerozoic*. Geological Survey of South Australia, Adelaide. 20-31 p.
- Groves, I., Carman, C. E. and Dunlap, W. J., 2003. Geology of the Beltana Willemite Deposit, Flinders Ranges, South Australia. *Economic Geology* **98**, 797-818.
- Heathgate Resources, 2006. Mining Proposal for proposed extension of Beverley Mine. Heathgate Resources Pty Ltd, Adelaide.
- Heathgate Resources, 2008. Beverley Four Mile project public environment report and mining lease proposal. Heathgate Resources Pty Ltd, Adelaide.
- Hesse, P. P. and Simpson, R. L., 2006. Variable vegetation cover and episodic sand movement on longitudinal desert sand dunes. *Geomorphology* **81(3-4)**, 276-291.
- Hill, A. J. and Gravestock, D. I., 1995. Cooper Basin. In: Drexel, J. F. and Preiss, W. V. (editors), *The Geology of South Australia Volume2: The Phanerozoic*. Geological Survey of South Australia, Adelaide. **Bulletin 54**, 78-87 p.
- Hill, S. M., 2000. The regolith and landscape evolution of the Broken Hill Block. CRC LEME, Department of Geology, Australian National University, Canberra. PhD thesis, unpublished.
- Hill, S. M. and Hore, S. B., 2012. Key insights into range-front mineral system expression and evolution from regolith and long-term landscape history, NE Flinders Ranges. *MESA Journal* **63**, 20-31.
- Hore, S. B. and Hill, S. M., 2009. Palaeoredox fronts: setting and associated alteration exposed within a key section for understanding uranium mineralisation at the Four Mile West deposit. *MESA Journal* **December 2009**, 34-39.
- Hou, B., Zang, W., Fabris, A., Keeling, J., Stoian, L. and Fairclough, M., 2007. Palaeodrainage and coastal barriers of South Australia 1:2 000 000. CRC LEME, Geological Survey Branch, Primary Industries and Resources South Australia, Adelaide. Online: http://www.pir.sa.gov.au/_data/assets/pdf_file/0005/41486/palaeochannels_sa_map.pdf.
- Huston, D. L., Stevens, B., Southgate, P. N., Muhling, P. and Wyborn, L., 2006. Australian Zn-Pb-Ag Ore-Forming Systems: A Review and Analysis. *Economic Geology* **101(6)**, 1117-1157.
- Jack, R. L., 1930. Geological Structure and other Factors in Relation to Underground Water Supply in Portion of South Australia. Geological Survey of South Australia, Department of Mines, Adelaide. **Bulletin No. 14**, 53 pp.
- Jagodzinski, E. A. and Fricke, C. E., 2010. Compilation of new SHRIMP U-Pb geochronological data for the southern Curnamona Province, South Australia, 2010. Department of Primary Industries and Resources, Adelaide. **Report Book 2010/00014**, 56 pp.
- Jaireth, S., Clarke, J. and Cross, A., 2010. Exploring for sandstone-hosted uranium deposits in paleovalleys and paleochannels. *AUSGEONews* **97**, 21-25.

- Jaireth, S., McKay, A. and Lambert, I., 2008. Association of large sandstone uranium deposits with hydrocarbons. *AUSGEONews* **89**, 8-12.
- Jaques, A. L., Jaireth, S. and Walshe, J. L., 2002. Mineral systems of Australia; an overview of resources, settings and processes. *Australian Journal of Earth Sciences* **49(4)**, 623-660.
- Kleeman, A. W., 1946. An age determination of samarskite from Mount Painter, South Australia. *Transactions of the Royal Society of South Australia* **70**, 175-177.
- Knox-Robinson, C. M. and Wyborn, L. A. I., 1997. Towards a holistic exploration strategy: using geographic information systems as a tool to enhance exploration. *Australian Journal of Earth Sciences* **44**, 453-463.
- Kositcin, N. (editor) 2010. Geodynamic synthesis of the Gawler Craton and Curnamona Province. Geoscience Australia, Canberra **Record 2010/27**.
- Kreig, G. W., 1995. Chapter 9: Mesozoic. In: Drexel, J. F. and Preiss, W. V. (editors), *The Geology of South Australia Volume 2: The Phanerozoic*. Geological Survey of South Australia, Adelaide. **Bulletin 54**, 93 p.
- Kreig, G. W. and Rogers, P. A., 1995. Stratigraphy - marine succession. In: Drexel, J. F. and Preiss, W. V. (editors), *The Geology of South Australia Volume 2 - The Phanerozoic*. Geological Survey of South Australia, Adelaide. 112-123 p.
- Kwitko, G., 1995. Triassic intramontane basins. In: Drexel, J. F. and Preiss, W. V. (editors), *South Australia Geological Survey, The Geology of South Australia Volume 2 The Phanerozoic*. **Bulletin 54**, 98-101 p.
- Lottermoser, B. G., 1988. A carbonatitic diatreme from Umberatana, South Australia. *Journal of the Geological Society, London* **145**, 505-513.
- Lottermoser, B. G. and Plimer, I. R., 1987. Chemical variation in tourmalines, Umberatana, South Australia. *Neues Jahrbuch für Mineralogie Monatshefte* **1987**, 314-326.
- Ludbrook, N. H., 1961. Stratigraphy of the Murray Basin in South Australia. Geological Survey of South Australia, Department of Mines, Adelaide. **Bulletin No. 36**, 117 pp.
- Ludwig, K. R. and Cooper, J. A., 1984. Geochronology of Precambrian granites and associated U–Ti–Th mineralisation, northern Olary Province, South Australia. *Contributions to Mineralogy and Petrology* **86**, 298–308.
- Marshak, S. and Flöttmann, T., 1996. Structure and origin of the Fleurieu and Nackara Arcs in the Adelaide fold-thrust belt, South Australia: Salient and recess development in the Delamerian Orogen. *Journal of Structural Geology* **18(7)**, 891-908.
- McConachy, G., 2009. Pepegoona Depoist Northern Flinders Ranges, SA. In: SA Explorer's Conference, Adelaide.
- McElhinny, M. W., Powell, C. M. and Pisarevsky, S. A., 2003. Paleozoic terranes of eastern Australia and the drift history of Gondwana. *Tectonophysics* **362**, 41-65.
- McKay, A. D. and Miezitis, Y., 2001. Australia's uranium resources, geology and development of deposits. Mineral Resource Report, AGSO - Geoscience Australia, Canberra. **Mineral Resource Report 1, 1**, 200 pp.
- McLaren, S., Dunlap, W. J., Sandiford, M. and McDougall, I., 2002. Thermochronology of high heat-producing crust at Mount Painter, South Australia: implications for tectonic reactivation of continental interiors. *Tectonics* **21(4)**, 1020-1037.
- McLaren, S., Sandiford, M., Powell, R., Neumann, N. and Woodhead, J., 2006. Palaeozoic intraplate crustal anatexis in the Mount Painter Province, South Australia: timing, thermal budgets and the role of crustal heat production. *Journal of Petrology* **47(12)**, 2281-2302.
- Michaelsen, B. H. and Fabris, A. J., 2011. Organic facies of the Frome Embayment and Callabonna Sub-basin: what are the U reductants? In: Forbes, C. J. (editor), 2011 Sprigg Symposium: Unravelling the northern Flinders and beyond. Geological Society of Australia, Adelaide. **Abstracts No. 100**, 49-52 p.
- Mitchell, M. M., Kohn, B. P., O'Sullivan, P. B., Hartley, M. J. and Foster, D. A., 2002. Low-temperature thermochronology of the Mt Painter Province, South Australia. *Australian Journal of Earth Sciences* **49**, 551-563.
- Morris, B. J. and Horn, C. M., 1990. Review of gold mineralisation in the Nackara Arc. *Mines and Energy Review, South Australia*, 51-58 pp.

- Moussavi-Harami, R. and Alexander, E., 1998. Tertiary stratigraphy and tectonics, Eromanga Basin region. *MESA Journal* **8**(February 1998), 32-36.
- Murphy, M. J., Dosseto, A., Schaefer, B. F., Turner, S. P. and Pearson, N. J., 2011. Application of U-series isotopes in understanding sandstone-hosted uranium mineralisation in the Frome Embayment, South Australia. In: Forbes, C. J. (editor), 2011 Sprigg Symposium: Unravelling the northern Flinders and Beyond., Geological Society of Australia, Adelaide. **Abstracts No. 100**, 53-56 p.
- Nanson, G. C., Chen, X. Y. and Price, D. M., 1992. Lateral migration, thermoluminescence chronology and colour variation of longitudinal dunes near Birdsville in the Simpson Desert, central Australia. *Earth Surface Processes and Landforms* **17**(8), 807-819.
- Nanson, G. C., Chen, X. Y. and Price, D. M., 1995. Aeolian and fluvial evidence of changing climate and wind patterns during the past 100 ka in the western Simpson Desert, Australia. *Palaeogeography, Palaeoclimatology, Palaeoecology* **113**(1), 87-102.
- Neumann, N. L., 2001. Geochemical and isotopic characteristics of South Australian Proterozoic granites: implications for the origin and evolution of high heat-producing terrains. Department of Geology and Geophysics, University of Adelaide, Adelaide. PhD thesis, unpublished.
- O'Driscoll, E. P. D., 1960. The Hydrology of the Murray Basin Province in South Australia. Geological Survey of South Australia, Department of Mines, Adelaide. **Bulletin No. 35**, 173 pp.
- Page, R. W., Conor, C. C. H. and Jagodzinski, E. A., in prep. Compilation of SHRIMP U-Pb geochronology for the southern Curnamona Province, South Australia, 1998-2004. South Australia Department of Primary Industries and Resources, **Report Book**.
- Pain, C., Gregory, L., Wilson, P. and McKenzie, N., 2011. The Physiographic Regions of Australia: Explanatory notes. Australian Collaborative Land Evaluation Program and National Committee on Soil and Terrain, CSIRO Land & Water, Canberra. 30 pp.
- Palacky, G. J., 1993. Use of airborne electromagnetic methods for resource mapping. *Advances in Space Research* **13**(11), 5-14.
- Preiss, W., 2011. Synthesising existing and new mapping in the southern Curnamona Province. PowerPoint presentation. Geological Survey of South Australia, Adelaide. Online: http://www.pir.sa.gov.au/_data/assets/pdf_file/0004/154777/Wolfgang_Preiss.pdf.
- Preiss, W. V., 1987. The Adelaide Geosyncline. Late Proterozoic Stratigraphy, Sedimentation, Palaeontology and Tectonics. Geological Survey of South Australia, Department of Mines and Energy, Adelaide. **Bulletin 53**, 441 pp.
- Preiss, W. V., 1993. Chapter 6: Neoproterozoic. In: Drexel, J. F., Preiss, W. V. and Parker, A. J. (editors), *The Geology of South Australia Volume 1: The Precambrian*. Geological Survey of South Australia, Adelaide. **Bulletin 54**, 171-202 p.
- Preiss, W. V., 1995. Early and Middle Palaeozoic orogenesis: Delamerian Orogeny. In: Drexel, J. F. and Preiss, W. V. (editors), *The Geology of South Australia Volume 2: The Phanerozoic*. Geological Survey of South Australia, Adelaide. **Bulletin 54**, 45-54 p.
- Preiss, W. V., 1999. 1:250 000 Geological Series--Explanatory Notes, PARACHILNA, South Australia, Sheet SH54-13 International Index, Second Edition. Primary Industries and Resources SA, Geological Survey of South Australia, Adelaide, 52 pp.
- Preiss, W. V., 2006. Tectonic overview of the Curnamona Province. In: Korsch, R. J. and Barnes, R. G. (editors): *Broken Hill Exploration Initiative: Abstracts for the September 2006 Conference, Broken Hill*. *Geoscience Australia Record* **2006/21**, 145-153 pp.
- Preiss, W. V. and Robertson, R. S., 2006. Chapter 7: Adelaide Geosyncline and Stuart Shelf. In: Cooper, B. J. and McGeough, M. A. (editors), *South Australia Mineral Explorers Guide*. 2nd edition., Geological Survey of South Australia, Adelaide. Online: http://www.pir.sa.gov.au/_data/assets/pdf_file/0014/20552/adelaide_geosyncline_intro.pdf.
- Quigley, M., Sandiford, M., Fifield, K. and Alimanovic, A., 2007. Bedrock erosion and relief production in the northern Flinders Ranges. *Earth Surfaces Processes and Landforms* **32**, 929-944.

- Raymond, O. L. and Retter, A. J., 2010. Surface geology of Australia 1:1 000 000 scale. Geoscience Australia, Canberra. 2010. Online: <http://www.ga.gov.au/mapconnect/>.
- Riordan, S. J., 2009. Characterization of Adelaidean rocks as potential geothermal reservoirs. The Australian School of Petroleum, University of Adelaide, Adelaide. **Final Report for PIRSA Project TIG 4.3**, 35 pp.
- Robertson, R. S., Conor, C. C. H., Preiss, W. V., Crooks, A. F. and Sheard, M. J., 2006. Chapter 5 Curnamona Province. In: Cooper, B. J. and McGeough, M. A. (editors), South Australia Mineral Explorers Guide. 2nd edition. South Australia Department of Primary Industries and Resources, Adelaide. **Mineral Exploration Data Package 11**, 51 p.
- Robertson, R. S., Preiss, W. V., Crooks, A. F., Hill, P. W. and Sheard, M. J., 1998. Review of the Proterozoic geology and mineral potential of the Curnamona Province in South Australia. AGSO Journal of Australian Geology and Geophysics **17(3)**, 169-182.
- Rogers, P. A., 1977. CHOWILLA Sheet SI 54-6. 1:250 000 Geological Series, Geological Survey of South Australia, Department of Mines, Adelaide. First Edition.
- Rogers, P. A., 1978. 1:250 000 Geological Series – Explanatory Notes, CHOWILLA South Australia, Sheet SI/54-6 International Index. Department of Mines and Energy, State of South Australia, Geological Survey of South Australia, Adelaide, 25 pp.
- Rogers, P. A., 1995a. Berri Basin. In: Drexel, J. F. and Preiss, W. V. (editors), The Geology of South Australia Volume 2: The Phanerozoic. Geological Survey of South Australia, Adelaide. **Bulletin 54**, 127-130 p.
- Rogers, P. A., 1995b. Stratigraphy - upper non-marine succession. In: Drexel, J. F. and Preiss, W. V. (editors), The Geology of South Australia Volume 2 - The Phanerozoic. Geological Survey of South Australia, Adelaide. 123-124 p.
- Rogers, P. A., Lindsay, J. M., Alley, N. F., Barnett, S. R., Lablack, S. R. and Kwitko, G., 1995. Murray basin. In: Drexel, J. F. and Preiss, W. V. (editors), The Geology of South Australia Volume 2: The Phanerozoic. Geological Survey of South Australia, Adelaide. 157-162 p.
- Roy, P. S., Whitehouse, J., Cowell, P. J. and Oakes, G., 2000. Mineral Sands Occurrences in the Murray Basin, Southeastern Australia. Economic Geology **95(5)**, 1107-1128.
- Rutherford, L., 2006. Developing a tectonic framework for the southern Curnamona Cu-Au Province: Geochemical and radiogenic isotope applications. Department of Geology and Geophysics, University of Adelaide, Adelaide. PhD thesis, unpublished.
- Sandiford, M., 2008. Four Mile Creek report for URS. In, Revised draft report: Ground motion response spectra, Four Mile Project. Prepared for Quasar Resources Pty Ltd., URS, Pasadena, California.
- Sheard, M. J., Fanning, C. M. and Flint, R. B., 1992. Chronology and definition of Mesoproterozoic volcanics and granitoids of the Mount Babbage Inlier, northern Flinders Ranges. Quarterly Geological Notes, the Geological Survey of South Australia **123(July 1992)**, 18-32.
- Shirtliff, G., 1998. Massive gypsum, ferricretes and regolith landform mapping of western Balaclava, Broken Hill, NSW. CRC LEME, Department of Geology, Australian National University, Canberra. BSc (Hons) thesis, unpublished.
- Skidmore, C., 2005. Geology of the Honeymoon uranium deposit. In Taylor, G. F. (editor): 4th Sprigg Symposium: Uranium, exploration, deposits, mines and minewaste disposal, Adelaide. Geological Society of Australia, Sydney, N.S.W., Australia, **Abstracts No. 78**
- Skirrow, R. G. (editor) 2009. Uranium ore-forming systems of the Lake Frome Region, South Australia: Regional spatial controls and exploration criteria. Geoscience Australia, Canberra. **Record 2009/40**, 151 pp.
- Skirrow, R. G. (editor) 2011. Uranium mineralisation events in Australia. Geoscience Australia, Canberra. **Record 2011/12**, 90 pp.
- SKM, 2008. Environmental studies for the Four Mile Project. Sinclair Knight Merz, Adelaide, 44 pp.
- Stevens, B. P. J., Barnes, R. G. and Forbes, B. G., 1990. Willyama Block-regional geology and minor mineralisation. In: Hughes, F. E. (editor), Geology of the mineral deposits of Australia and Papua New Guinea. Australasian Institute of Mining and Metallurgy, Melbourne. **Volume 2**, 1065-1072 p.

- Stevenson, B. G. and Webb, A. W., 1976. The geochronology of the granitic rocks of southeastern South Australia: AMDEL Progress Report 14. South Australia Department of Mines and Energy, Adelaide. **Open File Envelope 2136**.
- Teale, G. S., 1993. Geology of the Mount Painter and Mount Babbage inliers. In: Drexel, J. F., Preiss, W. V. and Parker, A. J. (editors), The Geology of South Australia Volume 1: The Precambrian. Geological Survey of South Australia, Adelaide. **Bulletin 54**, 149-156 p.
- Teale, G. S. and Flint, R. B., 1993. Curnamona Craton and Mount Painter Province. In: Drexel, J. F., Preiss, W. V. and Parker, A. J. (editors), The Geology of South Australia Volume 1: The Precambrian. Geological Survey of South Australia, Adelaide. **Bulletin 54**, 147-155 p.
- Teasdale, J., Pryer, L., Etheridge, M., Romine, K., Stuart-Smith, P., Cowan, J., Loutit, T., Vizy, J. and Henley, P., 2001. Eastern Arroyie Basin SEEBASE Project. SRK Consulting, Canberra. **SRK Project Code: PI12**.
- Twidale, C. R., 2007. Ancient Australian Landscapes. Rosenberg Publishing Pty Ltd, Dural NSW.
- U3O8 Limited, 2012. Olary Creek. Online:
http://www.u3o8.com.au/aurora/assets/user_content/file/Website%20Project%20Information%20in%20PDF/Olary%20Creek.pdf.
- Wade, C. E., 2011. Definition of the Mesoproterozoic Ninnerie Supersuite, Curnamona Province, South Australia. *MESA Journal* **62**, 25-42.
- Wakelin-King, G. A., 1999. Banded mosaic ('tiger bush') and sheetflow plains: a regional mapping approach. *Australian Journal of Earth Sciences* **46(1)**, 53-60.
- Wall, N., 1995. Observations on the role of thermal regime on basement-cover deformation. Department of Geology and Geophysics, University of Adelaide, Adelaide. BSc Honours thesis, unpublished.
- Wallace, M. W., Dickinson, J. A., Moore, D. H. and Sandiford, M., 2005. Late Neogene strandlines of southern Victoria: a unique record of eustacy and tectonics in southeastern Australia. *Australian Journal of Earth Sciences* **52**, 279-297.
- Wasson, R. J., Fitchett, K., Mackey, B. and Hyde, R., 1988. Large-scale patterns of dune type, spacing and orientation in the Australian continental dunefield. *Australian Geographer* **19(1)**, 89-104.
- Webb, A. W., 1976. Geochronology of eastern basement rocks - AMDEL Progress Report 11. Department of Mines and Energy, Adelaide. **Open File Envelope 2136**.
- Whitehouse, J., Roy, P. S. and Oakes, G. M., 1999. Mineral sand resource potential of the Murray Basin. In: Stewart, J. R. (editor), Geological Survey of New South Wales Department of Mineral Resources, **Geological Survey Report GS 1999/038**, 74 pp.
- Williams, P. J. and Skirrow, R. G., 2000. Overview of iron oxide-copper-gold deposits in the Curnamona Province and Cloncurry district (Eastern Mount Isa Block). In: Porter, T. M. (editor), Hydrothermal Iron Oxide Copper-Gold and Related Deposits: A Global Perspective. PGC Publishing, Adelaide. **1**, 105-122 p.
- Willis, I. L., Brown, R. E., Stroud, W. J. and Stevens, B. P. J., 1983. The Early Proterozoic Willyama Supergroup: stratigraphic subdivision and interpretation of high to low-grade metamorphic rocks in the Broken Hill Block. *Journal of the Geological Society of Australia* **30**, 195-224.
- Wopfner, H., Callen, R. and Harris, W. K., 1974. The Lower Tertiary Eyre Formation of the southwestern Great Artesian Basin. *Journal of the Geological Society of Australia* **21(1)**, 17-51.
- Wopfner, H. and Twidale, C. R., 1988. Formation age of desert dunes in the Lake Eyre depocentres in central Australia. *Geologische Rundschau* **77(3)**, 815-834.
- Wulser, P.-A., 2009. Uranium metallogeny in the North Flinders Ranges region of South Australia. Department of Geology and Geophysics, University of Adelaide, Adelaide. PhD thesis, unpublished.
- Wulser, P.-A., Brugger, J., Foden, J. and Pfeifer, H.-A., 2011. The sandstone-hosted Beverley uranium deposit, Lake Frome Basin, South Australia: mineralogy, geochemistry, and a time-constrained model for its genesis. *Economic Geology* **106**, 835-867.

4 AEM Geophysics

M. T. Costelloe and I. C. Roach

4.1 INTRODUCTION

Airborne electromagnetic (AEM) surveys are used to map the electrical conductivity of the subsurface over extents too large to be covered on the ground. A time-domain AEM system aircraft carries a transmitter loop through which a time-varying current is passed inducing eddy (secondary) currents to flow in any electrically conductive subsurface material. The secondary eddy currents are detected via the voltage that is induced in the receiver coils towed by the same aircraft. The current flow in the subsurface is related to its conductivity. An inversion of the received signal allows estimates of the conductivity to be made. The depth to which the signals can be used to map conductivity depends on the system configuration and the subsurface conductivity (Lane *et al.*, 2004; Smith, 2001).

The Frome AEM Survey was flown by Fugro Airborne Surveys (FAS) using the TEMPEST™ fixed wing AEM system. The TEMPEST™ survey data were publicly released by Geoscience Australia (GA) in March 2011.

4.2 RELEASED DATA

Data were delivered into the public domain in two Phases. Phase-1 data are quality controlled, contractor-supplied data owned by GA and the Government of South Australia Department of Manufacturing, Innovation, Trade, Resources and Energy (DMITRE). Phase-2 data are quality controlled GA layered earth inversions (GA-LEI) derived from Phase-1 data, also owned by GA and DMITRE. Phase-1 and Phase-2 data flown for subscriber companies have also been released to the public domain as detailed below.

Phase-1 GA- and DMITRE-owned data were released as one block known as the Frome AEM Survey. Internal to the main survey block are sub-areas of infill flying; these subdivisions are shown on the locality map (Figure 1.8). Under the terms of the funding agreements with the company subscribers, a moratorium was placed on the release of infill data until April 2012. All Phase-1 and Phase-2 subscriber company infill data have now been released to the public domain.

The Frome AEM Survey Phase-1 data release contained:

- The Survey operations and processing report;
- Point-located electromagnetic response data without correction to a standard geometry;
- Point-located electromagnetic response data with correction to a standard geometry;
- Point-located conductivity depth image (CDI) data derived using EM Flow™ software;
- Gridded electromagnetic response and CDI data; and,
- Graphical multiplot profiles showing electromagnetic, CDI and ancillary data for each line.

The Frome AEM Survey Phase-1 data are available from the GA Sales Centre and are also available by free download from the GA website using the following link:

Frome AEM Survey – GA and DMITRE infill Phase-1 data and processing report https://www.ga.gov.au/products/servlet/controller?event=GEOCAT_DETAILS&catno=71624.

Phase-1 data included CDIs generated by FAS using the EM Flow™ (v3.30) software package. The EM Flow™ CDI program is an industry-standard method for deriving conductivity estimates from AEM surveys.

The Phase-2 Frome AEM Survey TEMPEST™ conductivity estimates have been produced using one of two GA-LEI algorithms developed at GA: a sample-by-sample inversion (SBS GA-LEI); or a line-by-line inversion (LBL GA-LEI). The Phase-2 data release contains both the SBS GA-LEI and LBL GA-LEI 1D inversion data for the GA and DMITRE owned data, including:

- Frome AEM Survey inversion report;
- Shape files: flight lines, survey boundary and national parks;
- Point-located SBS GA-LEI inversion data and inversion products, which include:
 - SBS GA-LEI georeferenced Joint Photographic Experts Group (JPEG) format image conductivity sections;
 - SBS GA-LEI multiplots;
 - ER Mapper™ grids of depth slices, elevation slices (10 and 50 m slices), 0-200 m conductance, 0-400 m conductance, AEM Depth Of Investigation (DOI) Go-Map for SBS inversion data;
 - JPEG images of depth slices, elevation slices (10 and 50 m), 0-200 m conductance, 0-400 m conductance, AEM DOI Go-Map for SBS GA-LEI data; and,
 - GOCAD™ triangulated surfaces of conductivity sections;
- Point-located LBL GA-LEI inversion data and inversion products, for selected lines, which include:
 - Point-located LBL GA-LEI inversion data (secondary) used to calculate the percent data influence (PDI) for the inversion;
 - LBL GA-LEI georeferenced JPEG sections;
 - LBL GA-LEI multiplots; and,
 - GOCAD™ triangulated surfaces of conductivity line sections.

The Frome AEM Survey Phase-2 data for the GA- and DMITRE-owned data, released in July 2011 and containing a 30 layer inversion data to 400 m, are available from the GA Sales Centre and also by free download from the GA website at the following link:

https://www.ga.gov.au/products/servlet/controller?event=GEOCAT_DETAILS&catno=72589.

The Frome AEM Survey Phase-2 data for the GA- and DMITRE-owned data, including the Callabonna Uranium Ltd-owned infill area, released in June 2012 in conjunction with this interpretation record and containing a 30 layer inversion to 200 m, are available from the GA Sales Centre and also by free download from the GA website at the following link:

https://www.ga.gov.au/products/servlet/controller?event=GEOCAT_DETAILS&catno=73838.

The Frome AEM Phase-1 and Phase-2 data, containing a 30 layer inversion to 400 m, for the Callabonna Uranium (C1) infill area, are available from the GA Sales Centre and are also available by free download from the GA website. Downloads are available through the following link:

https://www.ga.gov.au/products/servlet/controller?event=GEOCAT_DETAILS&catno=73839.

The GA-LEI inversion products created for the Frome AEM Survey are documented in the inversion report (Hutchinson *et al.*, 2011a), which is summarised in [Section 4.7](#) and [Appendix 2](#). The remainder of this chapter discusses the 400 m inversion products only. More detail on the 200 m inversion is available from the GA website using the link above.

4.3 THE TEMPEST™ AEM SYSTEM

The Frome AEM Survey was flown using the TEMPEST™ AEM System (Lane *et al.*, 2000), installed on a Short Skyvan aircraft, registration VH-WGT. A summary of the system configuration, acquisition and processing is detailed in Bergeron and Lawrence (2010). A summary of the specifications of the TEMPEST™ system is shown in [Table 4.1](#).

Table 4.1: Summary of TEMPEST™ AEM system specifications.

SYSTEM	TEMPEST™
Contractor	Fugro Airborne Surveys
Platform type	Fixed-wing towed-bird
Base frequency	25 Hz
Transmitter area	186 m ²
Transmitter turns	1
Waveform	Square
Duty cycle	50%
Transmitter pulse width	10 ms
Transmitter off time	10 ms
Peak current	300 A
Peak moment	55 880 Am ²
Average moment	27 900 Am ²
Sample rate	75 kHz on X and Z
Sample interval	13.333 μs
Samples per half cycle	1500
System bandwidth	25 Hz to 37.5 kHz
Tx Loop Flying height nominal	100 m (subject to safety considerations)
Tx Loop Flying height average	101.2 m
EM sensor	Towed bird with 3 component dB/dt coils
Tx-Rx horizontal separation (primary field)	-114.8 m (survey average)
Tx-Rx vertical separation (primary field)	-40.7 m (survey average)
Tx-Rx horizontal separation (GPS)	-115.1 m (survey average)
Tx-Rx vertical separation (GPS)	-43.2 m (survey average)
Tx-Rx horizontal separation standard	-115.0 m (geometry corrected standard)
Tx-Rx vertical separation standard	-40.0 m (geometry corrected standard)
Stacked data output interval	200 ms (~12 m)
Number of output windows	15
Window centre times	13 ms to 16.2 ms
Magnetometer	Stinger mounted caesium vapour
Magnetometer compensation	Fully digital
Magnetometer output interval	200 ms (~12 m)
Magnetometer resolution	0.001 nT
Typical noise level	0.5 nT
GPS cycle rate (incl. bird GPS)	0.2 second (5 Hz)

TEMPEST™ is a fixed-wing, time-domain electromagnetic system. It employs an approximate square-wave, 50% duty cycle current waveform with a base frequency of 25 Hz. The current is transmitted through a single turn transmitter (TX) loop draped around the nose, wings and tail of the aircraft. The Survey was flown with the TX loop at an average of 101.2 m above ground level. The receiver (RX) coils are housed in a ‘bird’ towed approximately 115 m behind and 40 m below the aircraft. The RX consists of three orthogonal coils that sense the rate of change of the magnetic field (dB/dt) flux threading each coil. The axes of the three coils are nominally aligned in the horizontal flight line direction (X-component), horizontal direction perpendicular to the flight line (Y-component), and vertical direction (Z-component). However, only the X and Z components are recorded and processed at full resolution and are available for interpretation.

The TX height and the orientations and relative separations of the TX and RX are also known as the system geometry. The system geometry continuously varies as the aircraft moves along a flight line. The TEMPEST™ instrumentation includes a GPS unit for the aircraft’s position, radar and laser altimeters to measure its height above ground level and gyroscopes to measure its roll, pitch and yaw angles (i.e. its orientation). The relative separations of the TX and RX and the orientation of the RX are not normally measured by the system because of the logistical difficulty in doing so.

Since the system geometry affects the measured response, it must be input into quantitative forward modelling of the system response, and hence estimation of subsurface conductivity from the recorded data. Therefore, in the data processing the unmeasured elements of the system geometry need to be estimated. For the TEMPEST™ system this involves separation of the measured total field response into its primary field (due to direct coupling between TX and RX) and secondary field (due to eddy currents induced in the ground) components. This requires an assumption to be made about the unknown subsurface conductivity, which typically is that the subsurface is resistive at depth. Once separated into primary and secondary components, the horizontal and vertical offsets between the TX and RX can be analytically determined from the primary field if it is assumed that the receiver bird is oriented with zero roll, pitch and yaw. It is these estimated and assumed values of system geometry that are taken to be the real values in standard algorithms for estimating subsurface conductivity from the measured data.

For the first time in production a GPS receiver was introduced in the RX bird as a new feature in the TEMPEST™ system for this survey. This allowed a more accurate measurement of the relative separations of the TX and RX. Previously this separation was estimated from measurements of the primary field. Both the GPS and primary field estimates of the TX-RX separations are included in the data. The orientation of the RX is not measured by the system because of the logistical difficulty in doing so.

4.4 BACKGROUND TO THE GA LAYERED EARTH INVERSION

Conversion of the non-linear electromagnetic response data into estimates of subsurface conductivity allows for much easier and more accurate integration with independent subsurface information and facilitates better interpretation. The conversion can use either approximate transformation methods or geophysical inversion, both of which produce model-dependent conductivity estimates.

The Phase-1 data release of the Frome AEM data include conductivity predictions produced by FAS from the industry standard EM Flow™ algorithm (Macnae *et al.*, 1998; Stolz and Macnae, 1998). EM Flow™ is a fast approximate transformation method based on the concept that the response of a quasi-layered earth can be approximately represented by a mirror image of the transmitter dipole that recedes below the surface and expands with delay-time. By determining the vertical depth distribution of the mirror image dipoles a quasi-layered estimate of the subsurface conductivity can be estimated.

Some complications arise, however, because not all components of the TEMPEST™ system geometry are measured, and they must be estimated by FAS during the standard data processing.

Since the EM Flow™ routine relies on these estimates, the accuracy of the resultant conductivity estimates is dependent on the accuracy of the geometry estimates. Accordingly, the estimates tend to be biased towards producing results that are consistent with the assumptions made in the FAS data processing, typically a resistive basement earth model. This bias can in turn create an overestimate of the conductivity near the surface, since the model must compensate for the lack of conductance at depth (Brodie and Fisher, 2008; Lane *et al.*, 2004a).

A further problem is caused by the assumption made in the system geometry estimation that the receiver is in its nominal position (i.e. with zero roll, pitch and yaw). If the receiver is in fact rotated from its nominal position, which is generally the case, it may be impossible to simultaneously fit both the X- and Z-component data using the same subsurface conductivity distribution because the data are inconsistent with the system geometry information provided to the routine. For this reason it is often necessary to calculate the EM Flow™ estimates using just the X- or the Z-component data. While this is possible, a different conductivity model will result from each component.

These issues led to the development of the GA-LEI algorithm (Lane *et al.*, 2004). In the GA-LEI inversion algorithm, the idea is to not rely on the primary field separation and hence geometry estimates made in the standard FAS data processing. Instead, the total field (primary plus secondary) data are inverted directly. The inversion solves not only for a layered earth conductivity model, but it simultaneously solves for the horizontal and vertical separations between the TX and RX and the pitch of the receiver coils. By solving for the system geometry during the final inversion the method allows the information from both the X- and Z-components to be simultaneously fitted using a single common conductivity model. It prevents the assumptions made during the standard data processing from being automatically imposed onto the inversion results. Furthermore, if prior information exists about the electrical structure of the Survey area, these can be included as specific constraints on the inversion results.

Previous work at GA, in which down hole conductivity log data were compared to conductivity estimates (Brodie and Fisher, 2008; Lane *et al.*, 2004a; Reid and Brodie, 2006), has shown that improvements on the standard FAS EM Flow™ conductivity estimates can be made using the GA-LEI algorithm.

4.5 THE GA LAYERED EARTH INVERSION

4.5.1 Algorithm outline

The data from the Frome AEM Survey have been inverted to create subsurface conductivity models, referred to as Phase-2 data, using the GA-LEI. In previous GA surveys, such as Paterson (Roach, 2010) and Pine Creek (Craig, 2011), the data were inverted solely using a SBS inversion algorithm, which inverts each sample independently of its neighbours. For the Frome AEM Survey, we have released conductivity models using both the SBS inversion and a laterally-constrained LBL inversion.

In some parts of the Survey, the LBL inversion failed to converge to a solution that fitted the data. This was primarily caused by highly deformed, non-flat-lying geology in some areas of the Survey, where the laterally-continuous model, required by the LBL inversion, was not suitable for fitting the data. For this reason, we have released the LBL inversion data and limited products in selected areas only (see [Figure 4.2](#)).

4.5.2 Sample-by-sample (SBS) inversion

The SBS GA-LEI is a 1D inversion in which each of the airborne samples, acquired at

approximately 12 m intervals along a flight line, are inverted independently of their neighbours. The inversion of each individual sample involves the estimation of a 1D layered earth conductivity structure, and three elements of the system geometry, that are consistent with the data. A 1D layered earth conductivity structure means that the earth is considered to be a series of horizontal layers stacked in layer-cake fashion (Figure 4.1). Each layer extends to infinity in the horizontal direction and the conductivity within each layer is constant. Once all samples are inverted they are compiled into a pseudo-3D model by ‘stitching’ the 1D model together. A detailed technical description of the GA-LEI is provided in Appendix 3.

Since the data are non-linear with respect to the model parameters, an iterative inversion technique is used. Starting from an initial estimate, the layer conductivities and system geometry parameters are iteratively updated until the forward response of the model replicates the measured data satisfactorily (i.e. to within the noise levels). The estimated conductivity model is constrained to be vertically smooth and to be as close as possible to a reference conductivity model. The aim of these smoothness and reference model constraints is to ensure that the model is as simple as possible, and complex structure is only permitted where necessary, see for example Constable *et al.* (1987).

4.5.3 Conductivity model parameterization

In the Frome AEM Survey the subsurface was parameterized with 30 layers whose thicknesses were chosen and remained fixed throughout the inversion (i.e. they were not solved for). The layer thicknesses gradually increase from 4 m in the top layer of the model up to approximately 60 m in the second deepest layer. The bottom layer was set to infinite thickness and thus represents a halfspace below all other layers. The parameters of each layer used in the GA-LEI are shown in Table 4.2.

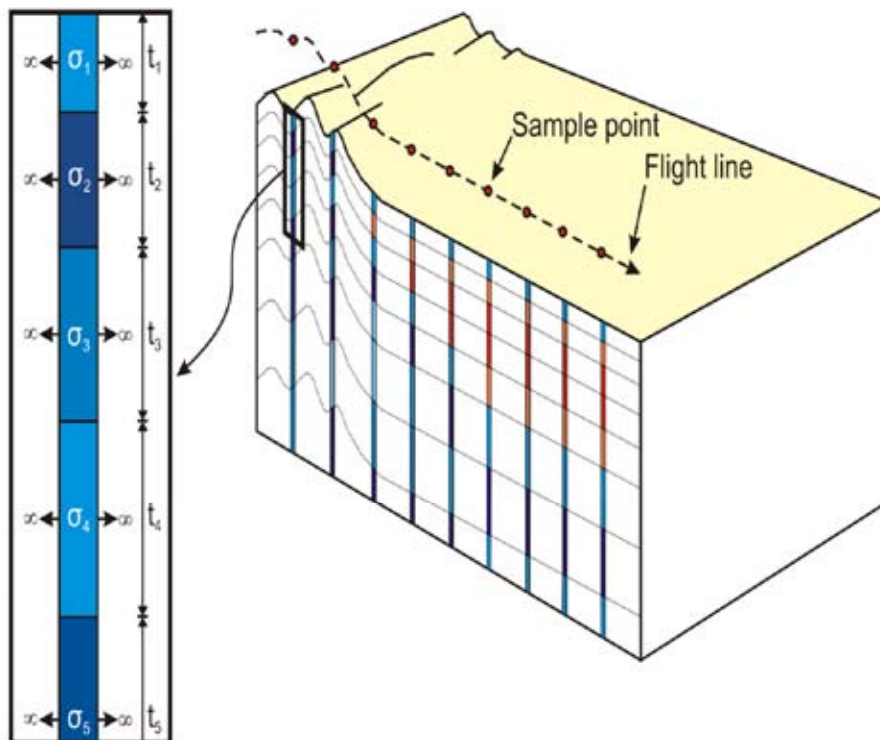


Figure 4.1: Schematic diagram of the 1D vertically smooth layered earth model used in the GA-LEI. The thickness of each layer (t_n) is fixed, but the conductivity (σ_n) is not fixed and can vary between layers. From Brodie and Fisher (2008).

Table 4.2: The GA-LEI model layer thicknesses and depths from surface. This layer structure is used for both the SBS and LBL inversions.

LAYER NUMBER	THICKNESS (m)	DEPTH TO BOTTOM (m)
1	4.00	4.00
2	4.40	8.40
3	4.84	13.24
4	5.32	18.56
5	5.86	24.42
6	6.44	30.86
7	7.09	37.95
8	7.79	45.74
9	8.57	54.31
10	9.43	63.74
11	10.37	74.11
12	11.41	85.52
13	12.55	98.07
14	13.81	111.88
15	15.19	127.07
16	16.71	143.78
17	18.38	162.16
18	20.22	182.38
19	22.24	204.62
20	24.46	229.08
21	26.91	255.99
22	29.60	285.59
23	32.56	318.15
24	35.82	353.97
25	39.40	393.37
26	43.34	436.71
27	47.67	484.38
28	52.44	536.82
29	57.68	594.50
30	∞	∞

The inversions were run using in-house software programs on the VAYU cluster computer at GA, or at the National Computational Infrastructure (NCI) resource at the Australian National University. The output ASCII header information from the inversions is in [Appendix 4](#), which contains details of the GA-LEI inversion of TEMPESTTM data.

4.5.4 Line-by-line (LBL) inversion

The LBL inversion algorithm is based on the same layered earth structure as the SBS inversion, with additional lateral constraints. The LBL inversion uses the same principle of fitting layered earth conductivity values to match the measured AEM data. Vertical smoothness and reference model constraints apply as above. However, a whole line of data is inverted at once using a cubic-spline parameterization of the conductivity of each layer and each system geometry parameter. This allows along-line smoothness and continuity constraints to be applied and for the solution at a particular sample to be influenced by its neighbours. A detailed description of the LBL inversion algorithm can be found in Brodie and Sambridge (2009) and Brodie (2010).

The horizontal smoothness of the model has the advantage of enhancing layered features of the geology, making such features more continuous and clearly defined. This smoothing also helps to

The Frome airborne electromagnetic survey, South Australia: implications for energy, minerals and regional geology

reduce the 1-dimensionality of the SBS inversion, and allows the model to give appropriate weighting to data trends in either a vertical or horizontal direction. By the same reasoning, horizontal smoothing can effectively smooth over discontinuous features in the data, such as discrete conductors. Discontinuous features may still be present in the data, but their magnitudes will be underestimated because of the numerical tendency to reduce the conductivity gradient between neighbouring data points.

In some areas of the Survey, especially in and around the Olary Spur, the LBL inversion algorithm was unable to converge to a solution that fitted the data. In these cases, the iterative process of finding a solution failed to improve the data misfit even from the initial homogeneous reference model. This was caused by 3D geology, especially where there were discrete or steeply-dipping conductors identified in the SBS inversion. It was also observed that the SBS inversion had discrete patches of high data misfit in these areas. Thus the laterally continuous requirement of the LBL inversion was not suitable in these areas. However, the LBL inversion fits the data well in areas characterised by layered sediments and thick regolith cover. [Figure 4.2](#) shows the portion of the Survey covered by the LBL inversion (the SBS inversion covers the whole Survey).

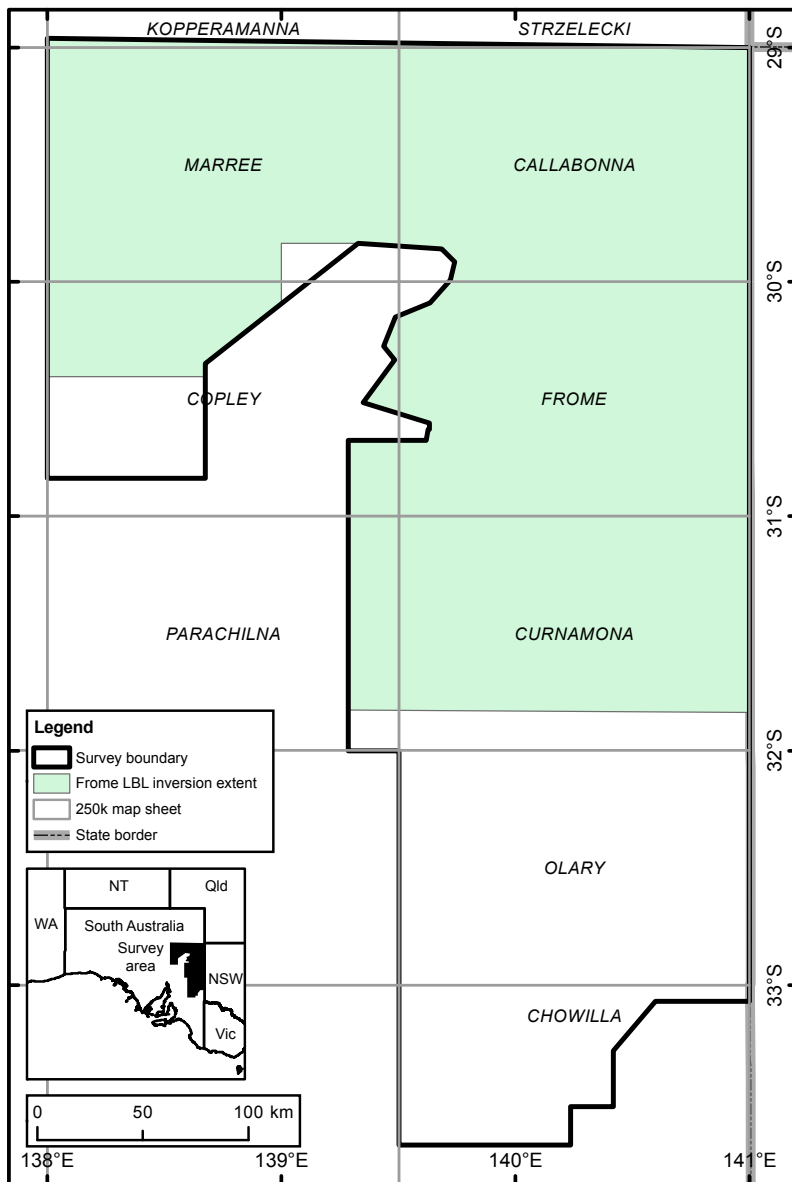


Figure 4.2: Spatial extent of LBL inversion data (blue) contained in the Phase 2 data release. The SBS inversion covers the entire survey area.

4.5.5 Reference Model

In principle, conductivity logs can be used to create a detailed reference model that varies across the Survey in order to constrain the inversion when the solution becomes non-unique. In the Frome AEM Survey, only 20 conductivity logs were available for use in the inversion. Since there were relatively few conductivity logs available over a large survey area, it was not feasible to constrain a detailed reference model from the conductivity logs. Therefore, the reference model used in this inversion is simply a half-space of homogeneous conductivity across the Survey area. We chose to use a conductivity reference value of 0.01 S/m, based on the average value of the resistive basement. The reference model was also used as the starting model for the iterative inversion.

For the TX to RX horizontal and vertical separation inversion model parameters we used the GPS-measured values delivered by FAS (i.e. different for each sample) as the starting and reference model values. We used zero for the starting and reference model value for the receiver coils' pitch parameter.

4.5.6 Data Misfit

The inversion would ideally converge until the data misfit (Φ_d) reaches a value of 1.0 as shown in Equation 1 below (Appendix 3). The data misfit Φ_d is a measure of the misfit, between the data (\mathbf{d}^{obs}) and the forward model of the model parameters ($\mathbf{f}(\mathbf{m})$), normalised by the expected error and the number of data, defined as:

$$\begin{aligned} \Phi_d &= \frac{1}{N_D} \sum_{k=1}^{N_D} \left(\frac{d_k^{obs} - f_k(\mathbf{m})}{d_k^{err}} \right)^2 \\ &= [\mathbf{d}^{obs} - \mathbf{f}(\mathbf{m})]^T \mathbf{W}_d [\mathbf{d}^{obs} - \mathbf{f}(\mathbf{m})] \end{aligned} \quad (1)$$

The data misfit is a measure of fit (agreement) between the forward response of the inversion model and the observed data. It is not a measure of confidence, certainty or uniqueness in the model parameters. In 1D geological environments (i.e. horizontal layering) it is usually possible to achieve a data misfit of 1.0 or close to 1.0. However, in geological environments with 2D (i.e. faulted horizontal layering) or 3D geology (i.e. folded, faulted layering), 1D inversions usually have a higher data misfit, reflecting the fact that a 1D model is insufficient to explain anomalies caused by the 2D or 3D geology.

The data misfit of the inversion is displayed on the GA-LEI multiplots as a number between 0 and 1000. When reviewing these multiplots, it is important to understand the data misfit is not a direct reflection of the quality of the AEM data, but reflects the ability of the inversion to fit the data to a geological model.

4.5.7 Depth Of Investigation

The Depth Of Investigation (DOI) is an important factor when interpreting the inversion results, as there are several factors that can limit the reliable depth of the conductivity results. The AEM signal penetration is highly variable and depends strongly on the ground conductivity. In highly conductive areas such as Lake Frome, a salt lake, the TEMPESTTM AEM signal penetration may be only a few tens of metres, whereas in resistive areas the signal penetration may be 400 m or more. It is important to ascertain whether the inversion result is influenced predominantly by AEM data or by assumptions inherent in the inversion. The DOI provides an important measure of how deep the inversion results are reliable.

For the SBS inversion, we calculate the DOI using a variation on the method of Christiansen and Auken (2010). For the LBL inversion, the DOI is based on the method of Oldenburg and Li (1999), which has been used in previous releases of the GA-LEI. This involves comparing the results of two separate inversions with different reference models, in order to determine a percent data influence

(PDI), indicating whether the results were data-driven or model-driven. While this method provides a useful DOI, a key limitation is that to separate ‘data-driven’ and ‘model-driven’ results, the DOI is set at the arbitrary threshold of 50% PDI. This does not account for the fact that the entire conductivity result is influenced by both the data and reference model (and indeed the inversion method). There is no distinct cut-off point between the data and model influences.

4.6 GEO-ELECTRICAL MODELS

Geo-electrical models were created utilising *a priori* knowledge of conductivity ranges for targeted geological units derived from literature reviews and personal communications. Table 4.3 is a summary of the conductivity ranges used for geological targets in the forward modelling exercise (Bakker and Elburg, 2006) and an example geo-electrical model is shown in Figure 4.3

Table 4.3: Conductivities used in the forward modelling.

Willawortina Formation	50 mS/m
Beverly Clay	630 mS/m
Beverly Sands	100 - 400 mS/m
Alpha Mudstone	600 mS/m
Namba Formation	300 mS/m
Eyre Formation	200 - 500 mS/m
Curnamona Craton	1 mS/m
Bulldog Shale	1000 mS/m

Model 1.2: Tertiary Eyre Formation palaeovalleys in Paleo-Mesoproterozoic Curnamona Craton

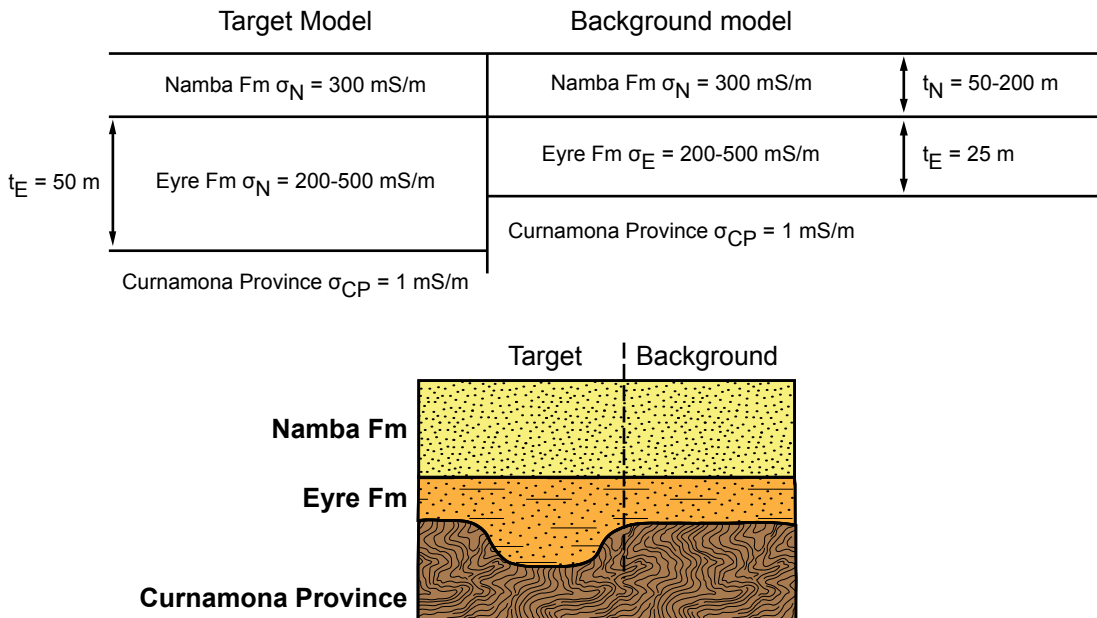


Figure 4.3: An example of a geo-electrical model (1.2) from the Frome AEM Survey area. Forward modelling of this scenario was used to predict if the presence of the palaeochannel, under 0 – 250 m of 200 - 500 mS/m cover sediments, could be detected within the AEM system noise levels.

Forward modelling results from the geo-electrical model in [Figure 4.3](#) indicated that, of the various AEM systems considered for the Frome AEM Survey, only two would be successful in detecting the target under up to 250 m of sediments (Namba and Eyre formations).

Similar forward modelling was undertaken on other geological targets in the Survey area to predict the likelihood of successfully detecting targets given different scenarios, for example, resolution of the near-surface and under varying degrees of cover. Modelling for the Frome AEM Survey predicted the TEMPEST™ system would best be able to detect target geology in these areas.

4.7 GA-LEI INVERSION PRODUCTS

4.7.1 Sections

The GA-LEI data are provided as sections in different formats including georeferenced JPEGs, GOCAD™ triangulated surfaces and multiplots with ancillary information. These line sections provide a detailed graphical representation of conductivity variations with depth and are suitable for viewing in Geographical Information System (GIS) applications. The multiplots are available as Portable Document Format (PDF) files and combine the conductivity data with data misfit, terrain clearance, system geometry and EM window data. The ancillary information can have a significant influence on the conductivity result and thus provides an important context for interpretation. Line sections for both SBS and LBL GA-LEI have been released into the public domain.

4.7.2 Georeferenced JPEGs

Conductivity sections are delivered as JPEG (.jpg) files, with an accompanying ‘world file’ (.jgw) which provides a spatial scale, position and orientation of the section. The x and y coordinates in the world file are provided as easting and northing values of the Map Grid of Australia Zone 54 (MGA Zone 54) using the Geodetic Datum of Australia 1994 (GDA94). See [Appendix 5](#) for the technical specifications of this map projection. The sections can be imported with their spatial coordinates recognised in GIS software. An example world file (.jgw) is shown in [Table 4.4](#).

The georeferenced JPEGs are configured to have a vertical exaggeration of 7.5 or 10.

Table 4.4: JPEG world file contents for line 1001002.

COLUMN	DATA
1 x scale (per pixel)	4.229174
2 rotation about y axis	0.001281
3 rotation about x axis	0.001281
4 y scale	-4.229174
5 x reference point	359133.712322
6 y reference point	6371643.528828

Georeferenced JPEGs have been included in the Phase-2 data release, with an example taken from line 1001002 shown in [Figure 4.4](#). The plot contains only a coloured conductivity section, either logarithmic or linear colour stretched, and a logarithmic or linear colour conductivity scale bar is provided as a separate file that applies to all of the georeferenced JPEGs in the dataset. This avoids superfluous colour bars when importing multiple line sections in a GIS. The colour conductivity scale bar images are shown in [Figure 4.5](#), and these are found in the same data directory as the georeferenced JPEGs in the data release. The logarithmic stretch colour scale has a range from 0.001 S/m to 3 S/m and the linear stretch colour scale has a range from 0 to 1.2 S/m.

The Frome airborne electromagnetic survey, South Australia: implications for energy, minerals and regional geology

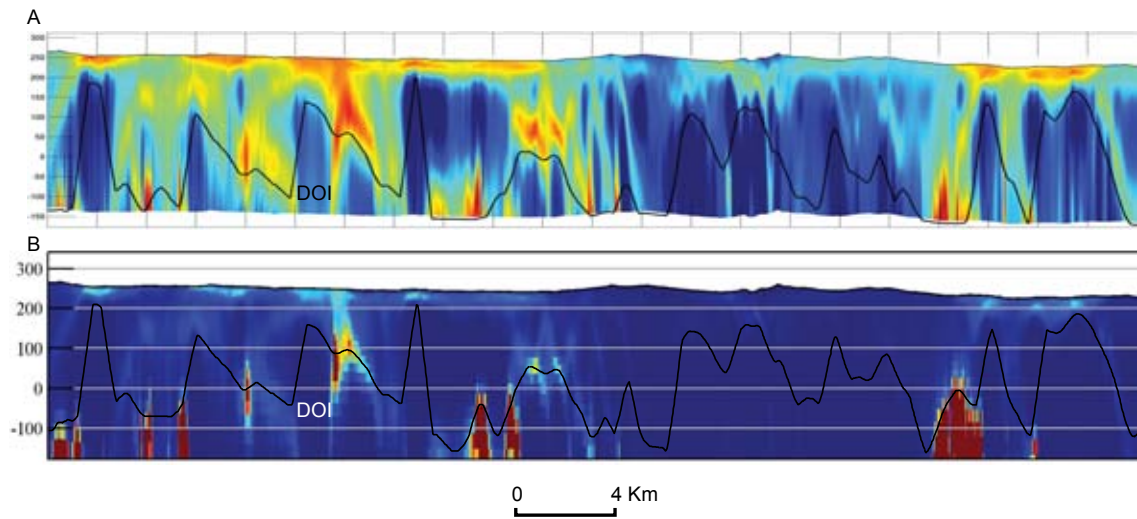


Figure 4.4: Georeferenced JPEG images for a portion of line 1001002 (SBS GA-LEI). Elevation above sea level is in metres and is labelled on the left hand side of each plot. The horizontal scale is provided in the accompanying .jgw world file. The black undulating line marks the DOI. **A:** logarithmic colour stretch; **B:** linear colour stretch.

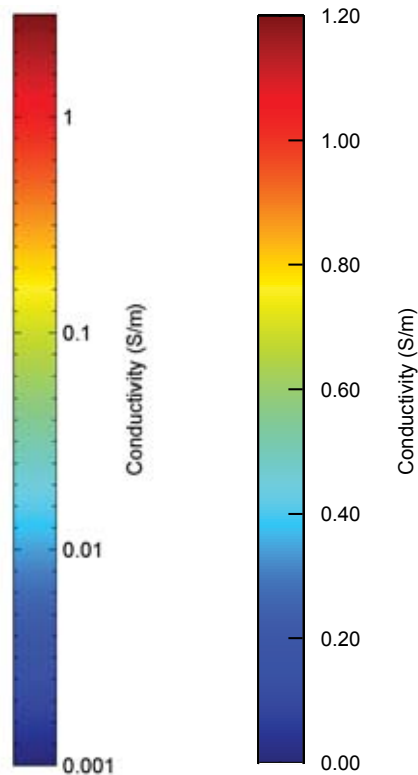


Figure 4.5: Colour conductivity scale bars for georeferenced JPEGs, with a logarithmic stretch ranging from 0.001 S/m to 3 S/m (left) and a linear stretch ranging from 0 to 1.2 S/m (right). One of the two colour bars is provided as a reference to all lines, depending on the colour stretch used.

4.7.3 GOCAD™ Triangulated Surfaces

Conductivity sections for both inversions are also provided as GOCAD™ triangulated surfaces (.ts), which allow for 3D viewing, flexible data display options and construction of 3D models. The triangulated surface files are coloured to the same conductivity range limits as the georeferenced JPEGs (described above), however the actual conductivity values are attached to each node in the triangulated surface, unlike the JPEG images which represent the conductivity values using a colour palette of 256 different colours. While the triangulated surfaces are configured to have a logarithmic stretch and the ‘classic’ GOCAD™ colour lookup table, users may choose a different colour stretch, or manipulate the display. In the triangulated surfaces, the conductivity data are sub sampled to every 2nd sample of the inversion data to conserve computer memory and enable faster viewing. This means the sample spacing is approximately 25 m rather than 12.5 m. This halves the memory requirement for each line, without losing any significant detail from the line section. An example of GOCAD triangulated surfaces is shown in Figure 4.6, with data values nulled below the DOI.

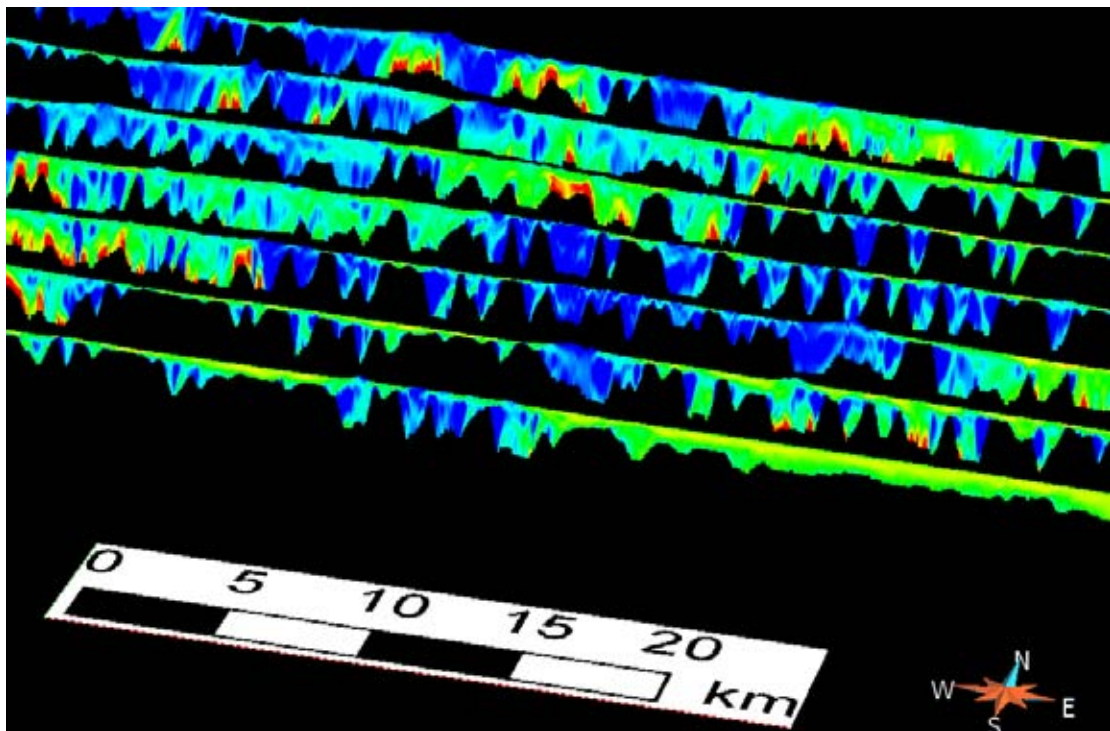


Figure 4.6: An example of SBS GA-LEI GOCAD™ triangulated surfaces.

4.7.4 Geoscience Australia layered earth inversion multiplots

The GA-LEI multiplots (example shown in Figure 4.7) for the Frome AEM Survey for both SBS and LBL GA-LEI contains a number of panels, described in Table 4.5.

4.7.5 Grids

The Phase-2 SBS GA-LEI data were released as a selection of 2D grids, presenting the inverted data across the Frome AEM Survey. These 2D grids have been created in three different categories:

1. As single inversion layers (the fundamental parameters from the 30 layer GA-LEI model);
2. As depth slices; and,
3. As elevation slices.

The LBL GA-LEI data were not released as grids.

Table 4.5: Panel descriptions for GA-LEI multiplots.

PhiD	Data misfit of the inversion. The optimal misfit is 1.0.
TX Height	Measured transmitter height in metres.
TX attitude	Measured transmitter pitch and roll in degrees.
Dx	Inline horizontal separation between the transmitter loop and the receiver coils in metres. Two traces show the processing estimate and output inversion model estimate.
Dz	Vertical separation between the transmitter loop and the receiver coils in metres. Two traces show the processing estimate and output inversion model estimate.
Rp	Receiver pitch in degrees. Two traces show the processing assumption (zero degrees) and output inversion model estimate.
X component	Non-geometry corrected X-component window data profiles scaled using the arcsinh function, in units of asinh(FT).
Z component	Non-geometry corrected Z-component window data profiles scaled using the arcsinh function, in units of asinh(FT).
Conductivity section	GA-LEI conductivity-depth section image with conductivity colour bar in S/m.

A conductivity depth slice is the average estimated conductivity over a given constant depth interval below the topographic surface. In contrast, an elevation slice is the average estimated conductivity over a given constant height interval above sea level. All of these grids present the data using the (base-10) logarithm of conductivity, since this is the value that enters into the inversion. We have found that geological structures are better defined in grids that use the logarithm of conductivity, than conductivity itself. Users who wish to grid the data without logarithms may obtain the data from the raw inversion output file in the Phase-2 data release.

4.7.6 Gridding Parameters

The Frome AEM Survey data were gridded using Intrepid™ software and are stored in binary files as ER Mapper™ single band IEEE4Byte Real data types. An ER Mapper™ header file (.ers) is associated with each grid file, which describes the data type and the coordinate systems used to spatially reference the grid. Gridded data are stored in a projected coordinate system only, in this case Universal Transverse Mercator (metric) coordinates of the MGA Zone 54 using the GDA94 datum.

The Frome AEM Survey has a regional line spacing of 5 km, with extensive areas of infill at 2.5 km line spacing. The gridding parameters were optimised for the 2.5 km spaced lines, with the grid cell size chosen to be 500 m (1/5th of the line spacing). The data were imported into an Intrepid™ database and transformed into the logarithm of conductivity prior to the gridding process. Each layer of conductivity was gridded using bicubic spline interpolation, with a first-pass Laplacian smoothing process. The extrapolation limit was set to 5 cells, allowing interpolation between the 5 km lines. This gridding method applies to the grids displayed below: the AEM Go-Map (Figure 4.8), depth slices (Figure 4.9) and elevation slices (Figure 4.10).

Once the data had been gridded in layers, they were combined into depth slices using a thickness-weighted average of the layer conductivities. In order to create elevation slices, the point-located inversion data were re-sampled into 10 m elevation intervals relative to sea level, creating another point-located dataset. This dataset was also gridded in logarithmic units (using the gridding method described above), and is available as 10 m elevation slice grids. The elevation grids were also combined into 50 m intervals, using the average conductivity values from 10 m elevation grids.

The Frome airborne electromagnetic survey, South Australia: implications for energy, minerals and regional geology

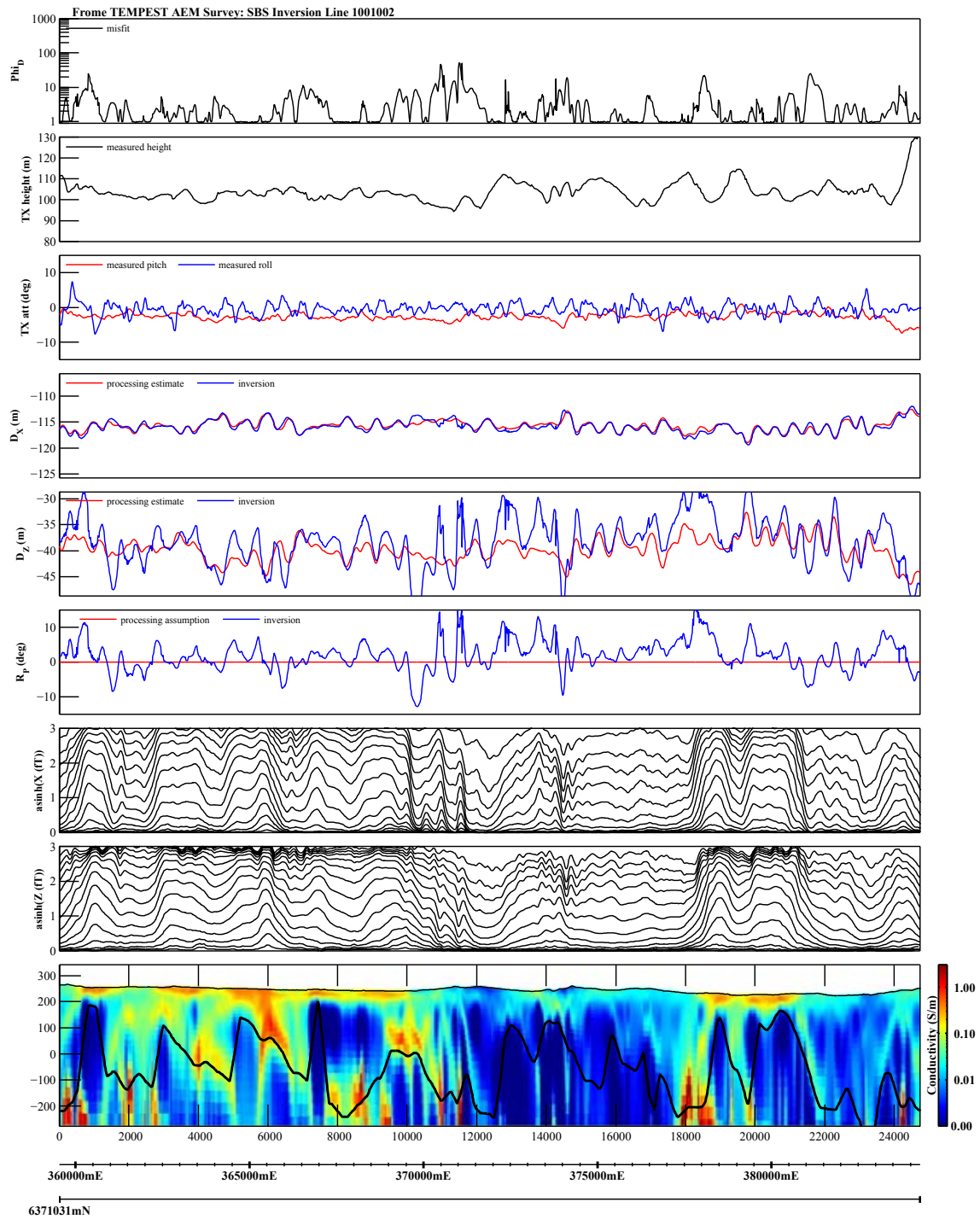


Figure 4.7: A SBS GA-LEI multiplot for a section of line 1001002.

4.7.7 AEM Go-Map

The DOI is presented as a 2D grid in Figure 4.8. Although the inversion layers extend to 595 m, the DOI was set to a maximum of 400 m depth, based on forward modelling estimates of the probability of detecting geological targets at depth. Given the system performance as specified by the contractor, it was found that the probability of detecting targets deeper than 400 was low. In the resistive areas of the Survey the DOI reaches this maximum depth.

The Frome airborne electromagnetic survey, South Australia: implications for energy, minerals and regional geology

The DOI shows a high degree of variability over the Survey, ranging from 30 m to 400 m. Red areas indicate very shallow areas of DOI, of the order of 40 m, while the yellow areas across much of the Survey indicate a DOI of about 100 to 200 m depth. In the northeast corner of the Survey, the DOI is deeper than 200 m in some parts. In the Olary Spur and the north-western edges of the Flinders Ranges, the DOI is as deep as 400 m, reflecting the predominantly resistive bedrock that outcrops in these areas. However, these resistive areas contain numerous discrete conductors that are reflected as shallower patches of the DOI.

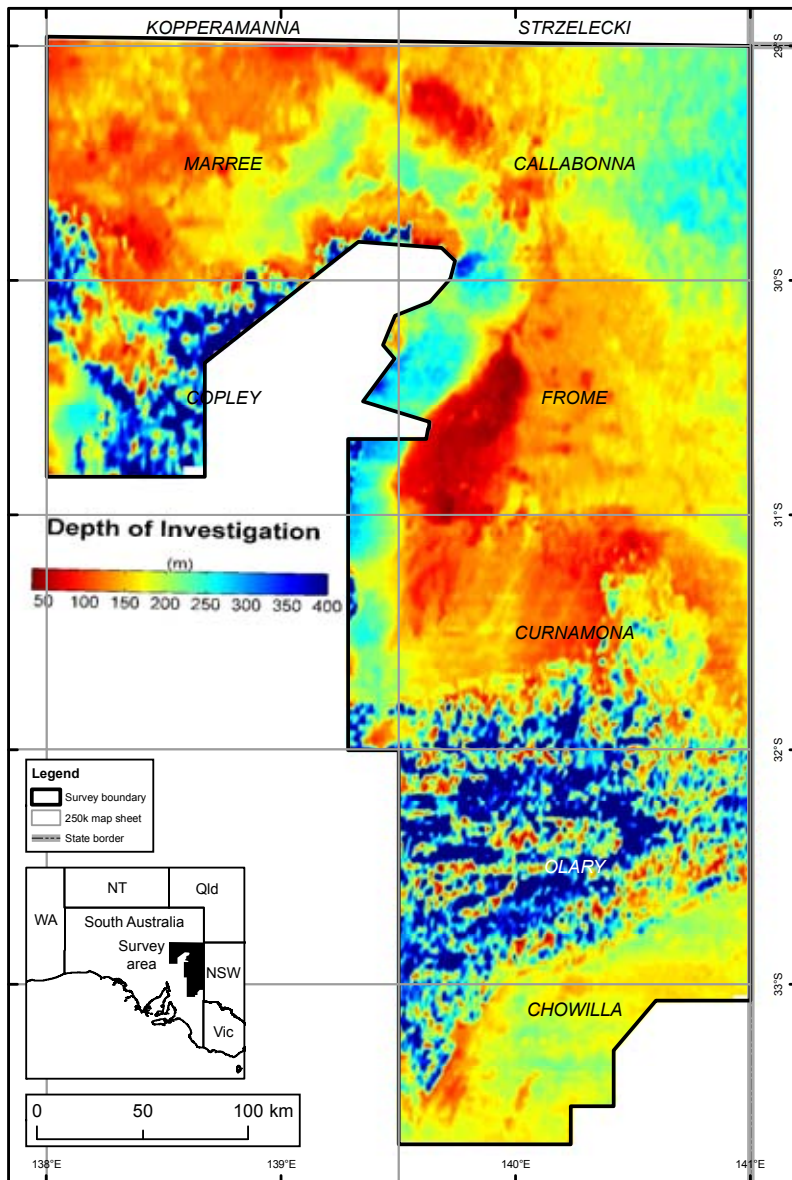


Figure 4.8: The AEM Go-Map (DOI grid) for the Frome AEM Survey created from the SBS GA-LEI.

The main gridded products of this AEM inversion are the depth slices and elevation slices. These grids present the inverted conductivity values in 2D spanning the entire Survey area. The DOI surface has been incorporated into these depth and elevation slice grids in order to mask out results that are below the DOI. The purpose of this masking is to focus attention on the data-driven results of the inversion and to ensure that spurious features from model-driven results are not misinterpreted as real geological structures or anomalies.

A key objective of this analysis was to determine where AEM surveys are likely to be effective as an aid to exploration in the Frome Embayment and Murray-Darling Basin. Airborne electromagnetic surveys carry an inherent risk, as the depth of penetration of the signal is highly variable. Furthermore, AEM surveys are relatively expensive compared to other geophysical techniques. The DOI grid presented here can reduce the risk for further AEM and ground EM surveys in the Survey area by showing where AEM and ground EM systems are likely to penetrate to a usable depth. The DOI grid can be interpreted as an AEM Go-Map. This DOI grid can reduce the risk of exploration using EM surveys, making EM surveying a more attractive tool for mineral exploration (Hutchinson *et al.*, 2010).

The DOI grid can also be used to estimate the effectiveness of AEM surveys in areas outside of the Frome AEM Survey area, where geological units have similar conductivities. An accurate downhole conductivity logging assessment and comparison of the conductivity signatures within a tenement to the Frome AEM Survey DOI can be used as an interpretative tool reducing risk when planning an AEM survey.

4.7.8 Depth Slices

A series of depth slices were created between 0 and 400 m, with the slices becoming progressively thicker with depth. The depth slices are set to 5 m thickness between 0 and 20 m depth, 10 m thickness between 20 and 40 m depth, 20 m thickness between 40 and 100 m depth, and 50 m thickness between 100 and 400 m depth. These increases in thickness reflect the greater sensitivity of the inversion at shallower depths.

A selection of four depth slices is illustrated in [Figure 4.9A-D](#), showing the A: 0-5 m; B: 30-40 m; C: 80-100 m; and, D: 150-200 m depth slice intervals. [Figure 4.9A](#) and [4.10B](#) shows a range of conductive and resistive areas and there is no DOI masking, since the depth slices are relatively shallow. However, [Figure 4.9C](#) shows some isolated areas of DOI masking, and [4.10D](#) shows substantial masking in broad conductive regions. This masking reflects the different penetration of the AEM signal in resistive (deep penetration) and conductive (shallow penetration) areas.

4.7.9 Elevation Slices

The elevation slices present the same inversion results, but the slices are referenced to the height above sea level rather than depth below surface. This gives the option of viewing data plotted along horizontal planes. The one drawback of using elevation slices over the entire survey is that there is a substantial altitude difference across some parts of the Frome AEM Survey. There is over 600 m of relief between the highest and lowest points of the Survey. Therefore, a given elevation slice may compare near-surface data from one corner of the Survey with much deeper data from other parts of the Survey.

Elevation slices were created from 200 m below sea level to 400 m above sea level at 10 m intervals. [Figure 4.10A-D](#) illustrates a selection of the elevation slices, showing A: 100-90 m below sea level (b.s.l.); B: 50-40 m b.s.l.; C: 0-10 m above sea level (a.s.l.); and, D: 50-60 m a.s.l. In both [Figures 4.10A](#) and [4.11B](#) there are substantial areas of masking under the DOI, since parts of these slices lie deep below the surface, and there is also a shallow DOI in some areas. In [Figure 4.10C](#) there is very little masking, however in [Figure 4.10D](#) there are substantial areas of null values due to the land surface being lower than the elevation slice itself. These null data values are especially prevalent around Lake Frome and in the north of the Survey, where the surface elevation is significantly lower than the 50-60 m elevation slice (in fact, Lake Frome is slightly below sea level).

The advantage of using elevation slices is that the undulations of topography are removed from the data. This may be useful when mapping palaeochannels, the Benagerie Ridge and other buried features, as these features may have profiles that do not follow the present day topography. In these cases, elevation above sea level may be a more relevant measure than depth below surface.

The Frome airborne electromagnetic survey, South Australia: implications for energy, minerals and regional geology

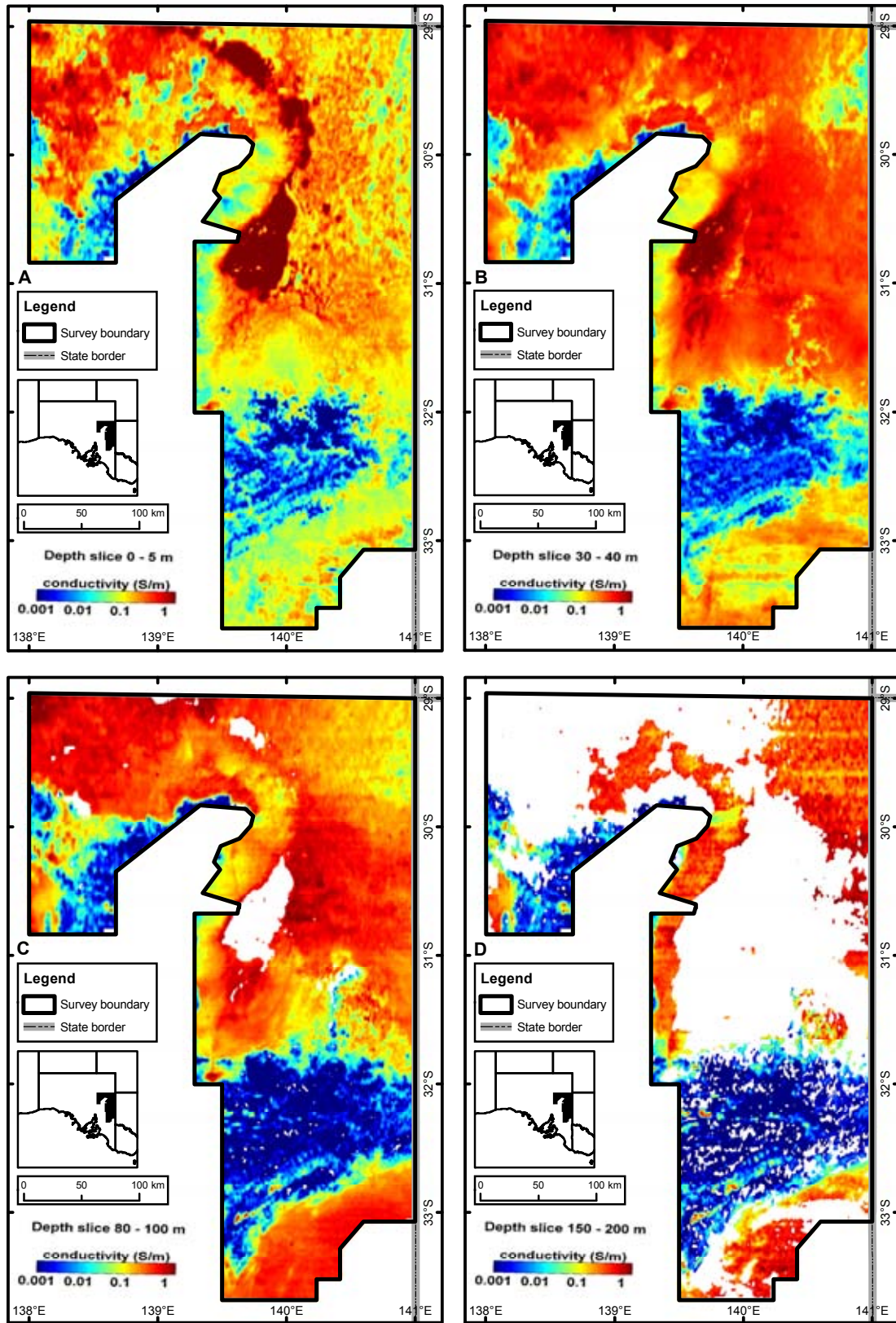


Figure 4.9: A selection of depth slices showing A: 0-5 m, B: 30-40 m, C: 80-100 m and D: 150-200 m. Data falling below the DOI have been masked out, and appear white.

The Frome airborne electromagnetic survey, South Australia: implications for energy, minerals and regional geology

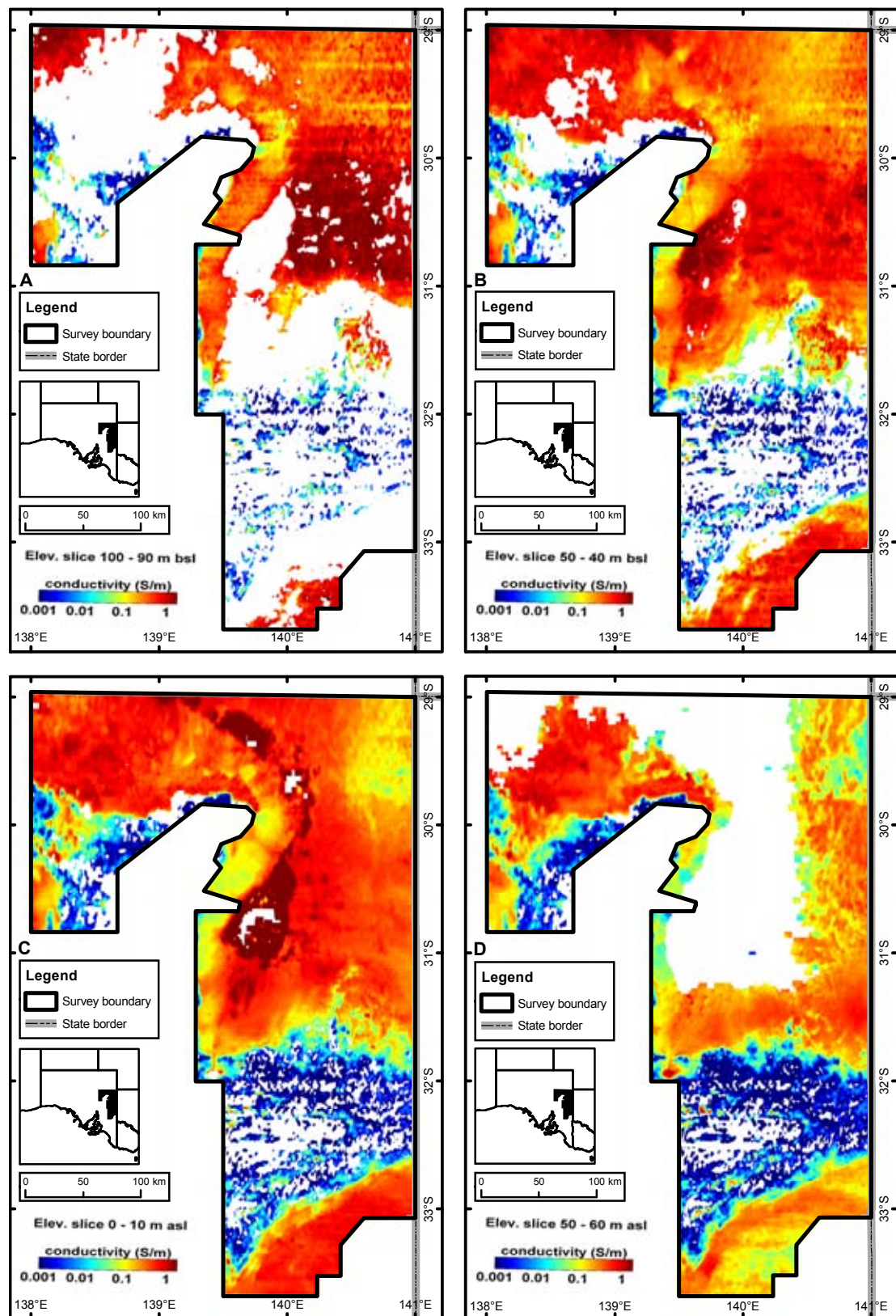


Figure 4.10: Selection of elevation slices, showing **A:** 100-90 m below sea level (b.s.l.); **B:** 50-40 m b.s.l.; **C:** 0-10 m above sea level (a.s.l.); and, **D:** 50-60 m a.s.l.

4.8 DISCRETE CONDUCTORS

The primary reason for conducting the Frome AEM Survey was to map regional geology, as well as palaeochannels, unconformities and faults that may host or affect uranium deposits. However, as a procedural step in the QA-QC process, the data were scanned for the presence of discrete conductors.

Multiplots delivered by FAS were used for interpreting the presence of discrete conductors using the process described by Lane and Worrall (2002). It is important to determine if the source of the discrete conductor effect is noise or variations in the subsurface conductivity distribution. The EM windowed amplitude responses can be affected by variations in system geometry, which affect the orientation of both the transmitter and receiver coils. The EM signal may also be affected by powerlines or ‘sferics’, which are noise spikes caused by lightning flashes within about 1500 km of the survey. Figure 4.11 shows an extract of a FAS multiplot for line 2005301, showing the X and Z component data along with system geometry, noise filters, and an EM FlowTM conductivity section. The plot shows a discrete conductor at fiducial 9430.

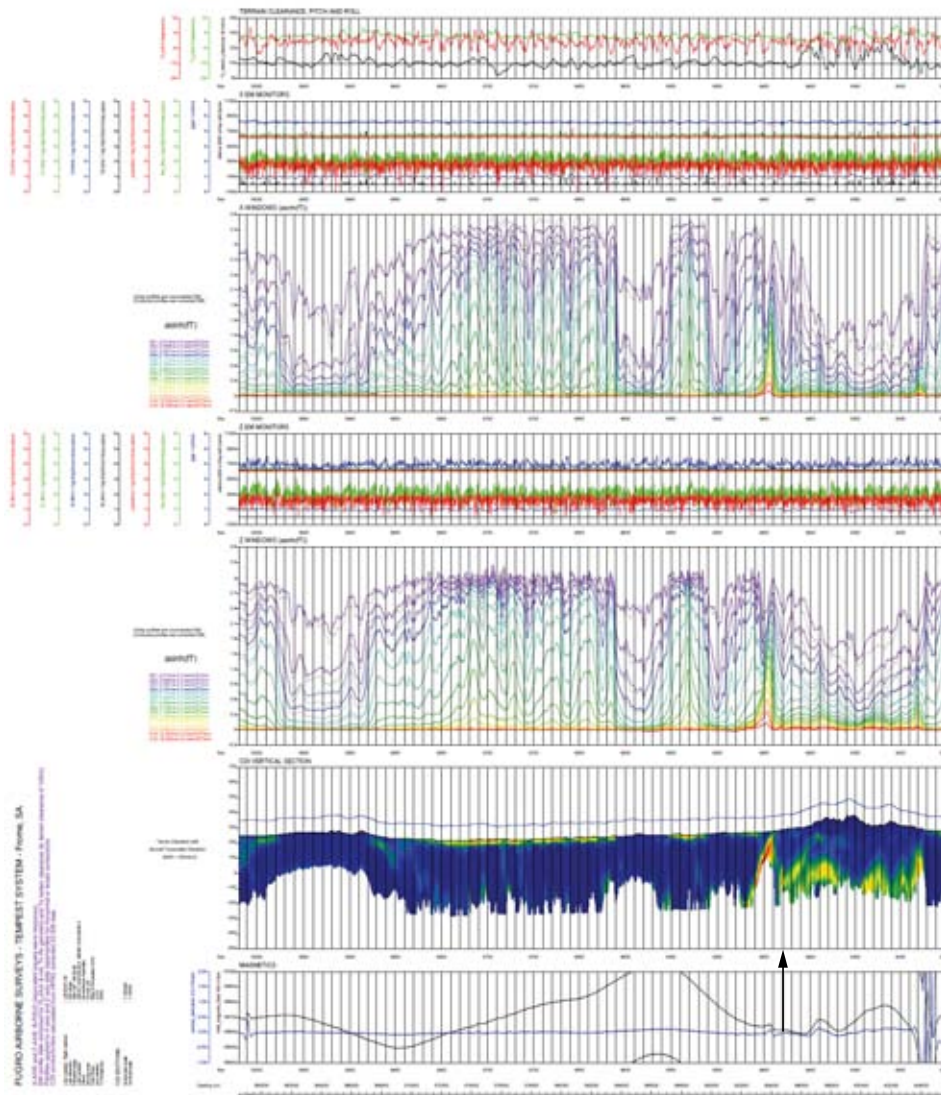


Figure 4.11: FAS multiplot for line 2005301, discrete conductor at fiducial 9430 (arrow).

4.9 BOREHOLE CONDUCTIVITY VALIDATION

Induction conductivity data were acquired in boreholes (referred to as conductivity logs) during July and August 2010 in support of the Frome AEM Survey. The data were acquired from a number of widespread boreholes across different geological formations. A total of 20 boreholes were logged. The logs were used to assist in generating reference models for geophysical inversions of the AEM data, as well as allowing the results of those inversions to be assessed against an independent dataset (Hutchinson *et al.*, 2011b).

Induction conductivity logging tools measure the electrical conductivity of the material surrounding the borehole and provide a detailed indication of changes in conductivity with depth. These tools permit measurements of the electrical conductivity of the ground outside uncased or PVC-cased boreholes, generally without being sensitive to the presence of more conductive borehole fluid within the hole. These tools are capable of making reliable scientific measurements, however, their method of use has not been standardised. The principle of operation of induction conductivity borehole logging tools (McNeill, 1986; McNeill *et al.*, 1990) and other conductivity logging information can be found in Hutchinson *et al.* (2011b).

In order to assess the performance of the inversion, we compare the results of the GA-LEI at selected points to the borehole conductivity logs collected in that part of the Survey area. There are limitations to this technique (Ley-Cooper and Davis, 2010; Reid and Vrbancich, 2004) related to the footprint of the conductivity log versus the AEM footprint.

The boreholes were selected based on accessibility, type of casing, depth of holes and location of the holes in relation to important geological units. The majority of the conductivity logs are commercial-in-confidence, however 5 of the logs are publicly available (Table 4.6). The approximate locations of all the boreholes are plotted over the Shuttle Radar Topographic Mission digital elevation model (SRTM DEM) in Figure 4.12.

Table 4.6: Coordinates (MGA Zone 54) and depths of the 5 non-confidential boreholes logged at the Oban uranium deposit for the Frome AEM Survey.

BOREHOLE	EASTING	NORTHING	COLLAR ELEVATION (m)	HOLE DEPTH (m)
OBM01	481050	6549516	70	96
OBM09	479368	6549076	66	84
OBM10	479764	6548141	68	96
OCM01	480233	6548814	67	96
OCM04	480232	6549114	69	96

The Frome airborne electromagnetic survey, South Australia: implications for energy, minerals and regional geology

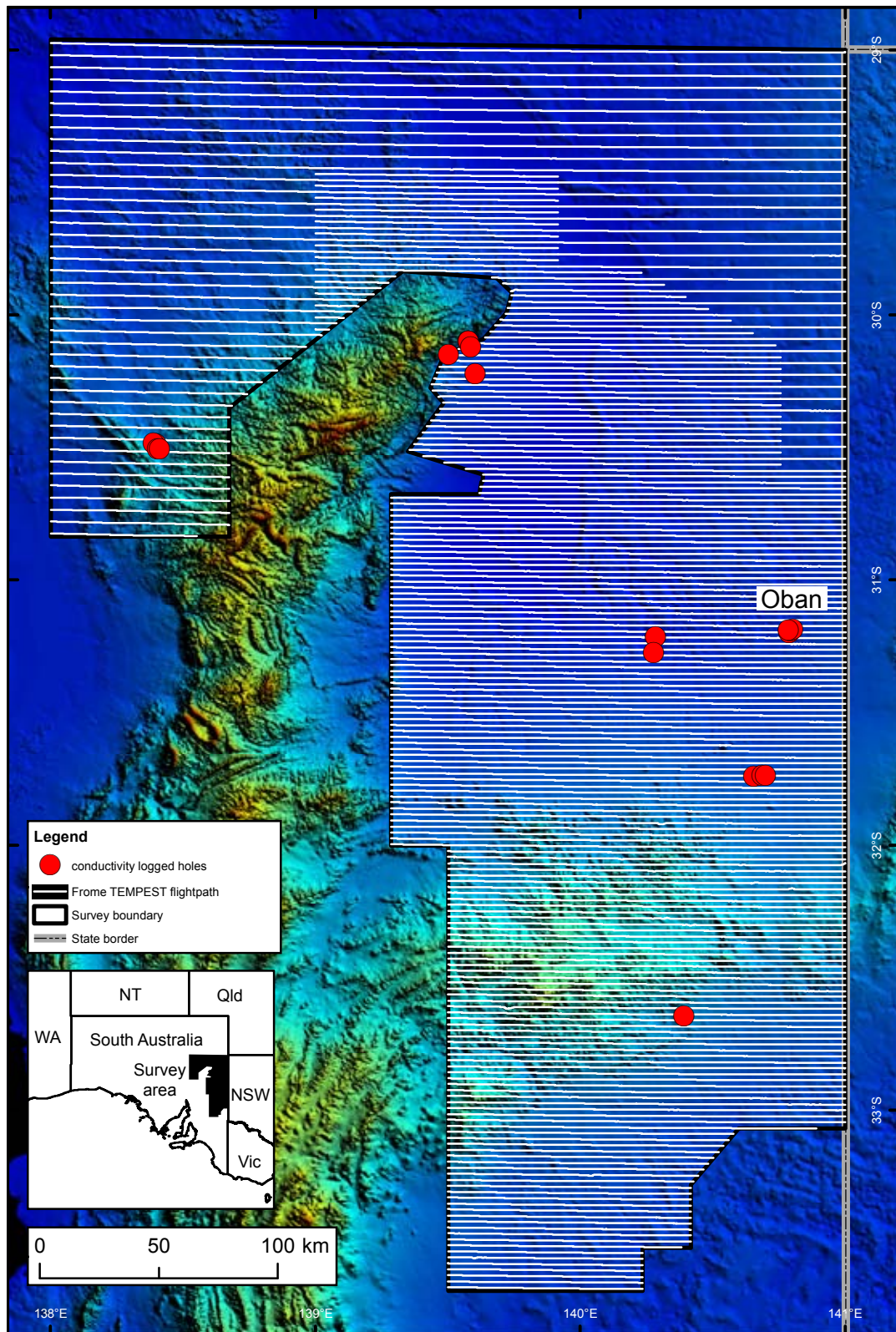


Figure 4.12: Location of conductivity-logged boreholes, flight lines and the survey boundary for the Frome AEM Survey, plotted over the 9-second (300 m ground pixel resolution) SRTM DEM.

4.10 STATISTICAL COMPARISON

Fiducial point comparisons for all of the 20 boreholes in the Survey were combined to produce a statistical correlation between the inversion conductivity estimates and the conductivity logs by Hutchinson *et al.* (2011a). This analysis re-sampled both the inversion results and the conductivity logs into 5 m depth intervals (to the maximum depth of the conductivity logs) using the average conductivity within each interval. Linear regressions in log-log space were performed between the re-sampled inversion and borehole data. This regression was applied to the SBS GA-LEI, the LBL GA-LEI and the FAS EM FlowTM data. The results of these regressions are shown in Figure 4.13. In parts (a), (c) and (e), the samples were limited to the boreholes within 500 m of the nearest flight line (the approximate radius of the AEM system footprint), whereas in (b), (d) and (f) the samples were extended to boreholes within 1000 m of the flight lines.

The scatter plots show that the SBS inversion conductivity estimates achieved the best fit to the borehole conductivity logs within the AEM footprint. The LBL inversion also achieved a better fit to the conductivity logs than the FAS EM FlowTM estimates. Even using boreholes up to 1000 m from the flight lines (well outside the AEM system footprint), the inversions produce conductivity estimates that show general agreement with the boreholes. This should be treated as an order-of-magnitude validation, showing that the inversion results agree with the broad-scale trends observed in the conductivity logs. Fine scale features in the conductivity logs cannot be reproduced by a smooth inversion such as the GA-LEI. However, these fine scale features do not significantly affect the regression across multiple boreholes.

It is worth noting that the EM FlowTM results use a look-up table, and are therefore limited to a discrete set of conductivity estimates. EM FlowTM also assumes a resistive basement and a resistive top layer, both of which produce conductivity estimates that are unrealistically low in some places. The results also rely on geometry assumptions inherent in the geometry-corrected AEM window data, whereas the GA-LEI varies the system geometry to achieve a better fit to the AEM data.

Further details of the conductivity logging conducted in the Frome AEM Survey can be found in the drill hole logging logistics report (Hutchinson *et al.*, 2011b), along with conductivity data from the 5 publicly available logs. Downloads are available through the following link:

https://www.ga.gov.au/products/servlet/controller?event=GEOCAT_DETAILS&catno=71566.

4.11 QUALITY ASSURANCE AND QUALITY CONTROL

Predicting earth conductivities from measured electromagnetic responses depends on window amplitudes, terrain clearance, aircraft attitude and estimates of changes in transmitter loop-to-receiver coil geometry. Before interpreting AEM data, it must be determined whether they are fit-for-purpose and contain sufficient information to justify being modelled and interpreted according to the survey objectives. To achieve this GA continually assessed the contractor's supplied data during survey flying and completed a data check list prior to inverting the data. The project geophysicist worked with the contractor to resolve any problems or discrepancies between delivered data and the contractual specifications.

The contractor performed numerous compensations and calibration flights in accordance with industry best practice and provided details of these procedures in the logistics report (Bergeron and Lawrence, 2010). The validation of electromagnetic calibration, navigation and flight path recovery, magnetic, diurnal, altimeter, RADAR, LASER, barometer, thermometer, video tracking and elevation data are conducted by the contractor and GA assessed the results prior to quality assurance and quality control (QA-QC) of the AEM data. The QA-QC checks on the Frome AEM Survey dataset, once flying was complete, are summarised in Table 4.7.

The Frome airborne electromagnetic survey, South Australia: implications for energy, minerals and regional geology

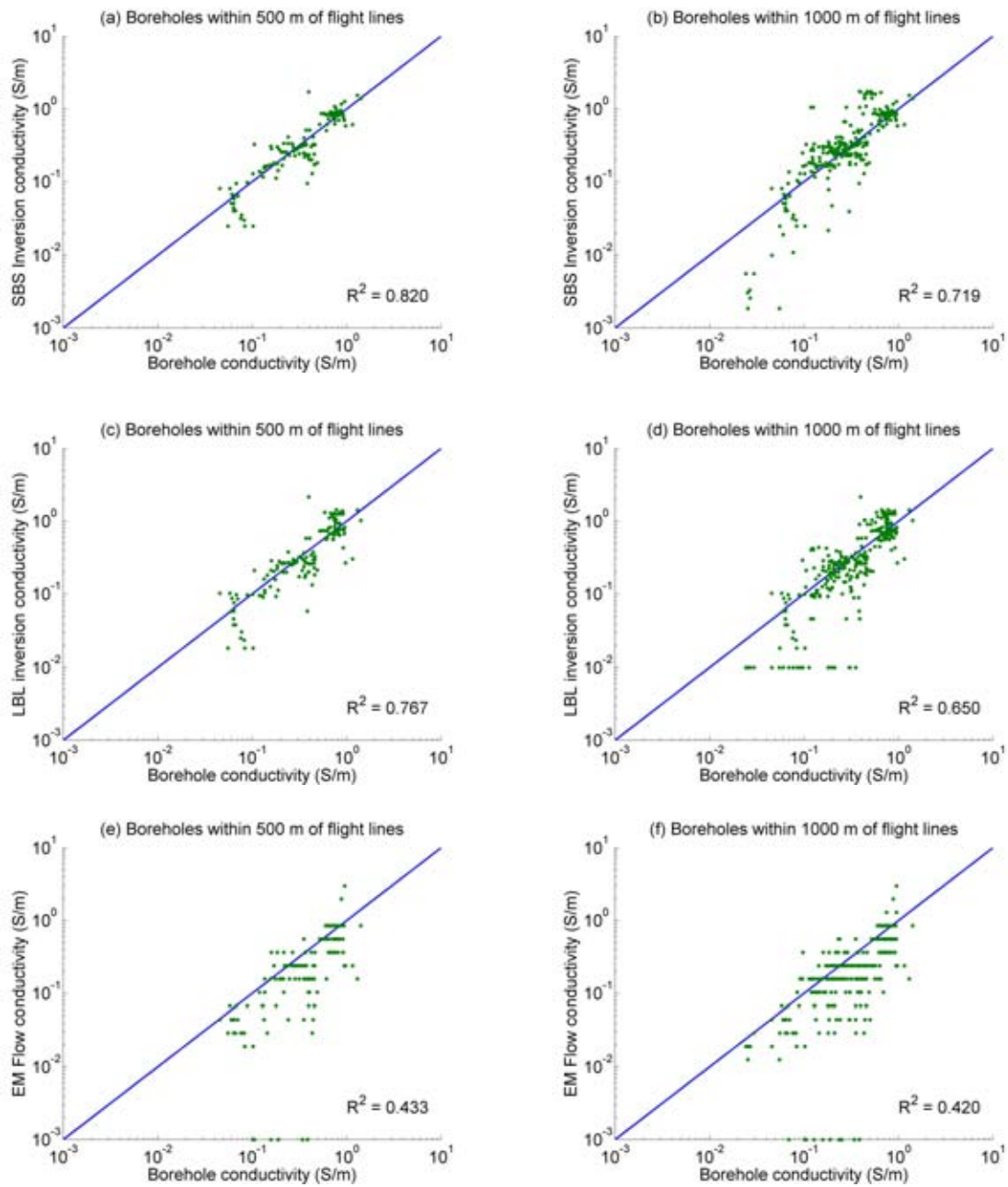


Figure 4.13: Scatter plots showing fiducial point comparisons for boreholes within 500 m of flight lines with corresponding values of (a) SBS GA-LEI, (c) LBL GA-LEI and (e) EM FlowTM conductivity; and for boreholes within 1000 m of flight lines for (b) SBS GA-LEI, (d) LBL GA-LEI and (f) EM FlowTM conductivity.

Table 4.7: Quality assurance and quality control steps.

STEP	DESCRIPTION
1	Check that all data have been delivered against contract specifications.
2	Check data have been supplied (format and detail) as per contract.
3	Noise analysis of high altitude data (X and Z component): <ul style="list-style-type: none"> • Calculate the additive noise, standard deviation and bias noise.
4	Repeat line analysis on repeat lines: <ul style="list-style-type: none"> • Calculate multiplicative noise estimates and assess system repeatability.
5	Create survey line database and assess statistics on all fields: <ul style="list-style-type: none"> • Note number of nulls, minimum, maximum, average.
6	Check flight path: <ul style="list-style-type: none"> • That all lines are flown, in the right direction, in the right location, that no flight line is more than 40 m off course over a continuous distance of 1500 m or more unless the deviation is required by civil aviation requirements.
7	Check flight path and terrain clearance: <ul style="list-style-type: none"> • The average transmitter terrain clearance for any flight line shall be within ± 5 m of the nominal transmitter terrain clearance.
8	Check altimeter corrections: <ul style="list-style-type: none"> • Compare LIDAR and RADAR altimeters.
9	Assess GPS height field: <ul style="list-style-type: none"> • Corrected altimeter–nvalue \approx SRTM DEM or gravity spot heights.
10	Grid elevation and magnetics: <ul style="list-style-type: none"> • Assess for nulls, level shifts and coherency.
11	Grid non-height-pitch-roll-geometry (HPRG) corrected and HPRG windows: <ul style="list-style-type: none"> • Assess for nulls, level shifts and coherency.
12	Grid all monitor channels: <ul style="list-style-type: none"> • Assess for nulls, level shifts.
13	Compute and tabulate minimum, maximum, mean and standard deviation of transmitter height (tx_height), transmitter-receiver x-separation distance (txrx_dx) and transmitter receiver z-separation distance (txrx_dz) for each line, each flight and whole survey and assess.
14	Assess EM Flow TM HPRG data: <ul style="list-style-type: none"> • Compare to drill hole data, known geology and geological targets.
15	Multiplot assessment: <ul style="list-style-type: none"> • For noise, interpretability and data consistency.
16	Check the logistics report and associated metadata.
17	Conductivity Logging: <ul style="list-style-type: none"> • Compare conductivity logs to geology.
18	GA layered earth inversion (GA-LEI) inversion: <ul style="list-style-type: none"> • Assess inversion parameters and compare to <i>a priori</i> information.

High altitude (zero-level) flights are used to characterise system noise in the absence of any ground effect. The high-altitude noise is considered as two components:

1. The mean of the processed data in each channel, that is, the window and component combination is calculated and termed the 'bias'; and,
1. The standard deviation of the processed data in each channel which is calculated and termed the 'additive noise'.

The high altitude noise analysis of the data revealed that noise was within acceptable levels. The additive noise is used as an input into the GA-LEI (see [Tables 4.8](#) and [4.9](#)).

Repeat line data is used to characterise the system noise at the specified survey altitude. The repeatability of the processed data is used to calculate the multiplicative noise for the survey (Green and Lane, 2003). For the Survey four repeat line locations were utilised due to the large areal extent of the Survey. An average multiplicative noise for the X component was calculated to be 1.86%, and Z component multiplicative noise was calculated to be 3.01%, both acceptable values. The multiplicative noise is an input parameter in the GA-LEI.

Flight path checks confirmed that no lines deviated more than 40 m off course over a continuous distance of 1500 m from the planned flight path.

The terrain clearance contract specification was that the average terrain clearance for any one flight should be within ± 5 m of the nominal aircraft terrain clearance (101.2 m). Several lines were outside this specification where the average transmitter height was greater than 105 m due to steep topographic gradients, and could not be flown at the nominal height for safety reasons. The contractor had ‘manually excluded’ such areas from the calculation of the average transmitter height.

Corrections to the RADAR and LIDAR were applied accurately by the contractor; it was found that the final contractor supplied elevation equalled the GA calculated elevation (GPS height - corrected LIDAR altimeter minus the nvalue) to within 0.2 m.

Table 4.8: X-component additive noise (standard deviation of high altitude data) for the Frome AEM Survey.

X WINDOW NUMBER	ADDITIVE NOISE (ft) SURVEY DATA	ADDITIVE NOISE (ft) CONTRACT SPECIFICATIONS
1	0.0119	0.0139
2	0.0117	0.0211
3	0.0093	0.0108
4	0.0061	0.0061
5	0.0057	0.0067
6	0.0054	0.0057
7	0.0051	0.0054
8	0.0048	0.0052
9	0.0046	0.0051
10	0.0044	0.0049
11	0.0043	0.0048
12	0.004	0.0044
13	0.0034	0.0038
14	0.0026	0.0029
15	0.0034	0.0035

Gridded data were used to check for data spikes, along-line data level shifts (drift) and system noise within flights. The EM Flow™ software CDI sections provided by the contractor for field data and repeat line analysis were also assessed for data coherency, relevance to known geology and noise.

Multiplot assessment was another important step in the quality control and interpretation of the Frome AEM data. The contractor-supplied multiplots (Figure 4.11) are a visual representation of relevant data in one frame at the highest possible resolution. They contain line data that has not been re-sampled and smoothed, unlike data in a gridded format. Discrete conductors are most effectively interpreted from line data presented in this multi-panel stacked profile format. Multiplots can also be used to assess artefacts that result from noise, system geometry and topography. For the Frome AEM Survey the multiplots delivered contain seven information panels, described in Table 4.10.

Table 4.9: Z-component additive noise (standard deviation of high altitude data) for the Frome AEM Survey.

Z WINDOW NUMBER	ADDITIVE NOISE (fT) SURVEY DATA	ADDITIVE NOISE (fT) CONTRACT SPECIFICATIONS
1	0.0094	0.0113
2	0.0084	0.016
3	0.0067	0.0081
4	0.0047	0.0048
5	0.0045	0.0053
6	0.0043	0.0045
7	0.0041	0.0043
8	0.0039	0.0041
9	0.0036	0.0038
10	0.0034	0.0037
11	0.0033	0.0036
12	0.003	0.0033
13	0.0024	0.0027
14	0.0017	0.002
15	0.0019	0.0021

Table 4.10: Panel descriptions for contractor supplied multiplots.

PANEL (FROM THE TOP) DESCRIPTION	
1.	Transmitter terrain clearance, pitch and roll of the transmitter.
2.	X EM monitors. X-component monitor values tracking sferics, coupling to the transmitter loop, low frequency signals induced by variations in the coupling of the receiver coils with the ambient magnetic field, powerline noise and coupling with VLF transmissions.
3.	X-component data. X-component window amplitude profiles compressed using an asinh function. HPRG and non-HPRG profiles are plotted.
4.	Z EM monitors. Z-component monitor values tracking sferics, coupling to the transmitter loop, low frequency signals induced by variations in the coupling of the receiver coils with the ambient magnetic field, powerline noise and coupling with VLF transmissions.
5.	Z-component data. Z-component window amplitude profiles compressed using an asinh function. HPRG and non-HPRG profiles are plotted.
6.	Conductivity Depth Image. EM Flow TM conductivity depth section Z-component.
7.	Magnetic data. Total magnetic intensity (TMI) and 1st vertical derivative.
8.	Location easting and northing information.

The multiplot panels are arranged to aid interpretation as well as being a quality control tool. The ability to assess if a response in the X and Z component is geological, or is just a variation in system geometry, topography or noise, is invaluable. Primary sources of EM noise include sferics, powerlines, VLF transmissions, electric fences and man-made metal objects on or just under the ground, such as sheds, mining structures or pipes. Weakly elevated conductivity artefacts, which apparently link near-surface flat-lying conductors to each other within the CDI section, are common artefacts. The artefacts are a result of 1D algorithm limitations in EM FlowTM and the GA-LEI, as well as the AEM system footprint (Sattell, 2004) and noise.

Metadata attached to the survey data are assessed for accuracy to facilitate data exchange and archiving between organisations with different hardware and software systems. Details such as text descriptions of the data and survey parameters, map datum and projection details, field names, units

of measurement, format, comments and missing data substitution values (nulls) are essential for the usefulness and longevity of the dataset. The metadata text describes the survey database which is in simple, multi-column ASCII files.

The accuracy, integrity and useability of AEM data are reliant on many factors including topography, system geometry, noise and location. Successful QA-QC of these factors allows the data to be deemed fit for original purpose as well as fit for future use. The QA-QC steps outlined above were used as a minimum standard to assess if AEM data were accurate and suitable to be inverted, manipulated and interpreted. It is important to consider improvements to the QA-QC process as requirements, technology and AEM systems change. It is also important to recognise that survey planning, forward modelling, inversion techniques, calibration tests, conductivity logging and DOI methods must be considered and completed to assure the successful completion of an AEM project.

4.12 REFERENCES

- Bakker, R. J. and Elburg, M. A., 2006. A magmatic-hydrothermal transition in Arkaroola (northern Flinders Ranges, South Australia): from diopside-titanite pegmatites to hematite-quartz growth. *Contributions to Mineralogy and Petrology* **152**, 541-569.
- Bergeron, M. C. and Lawrence, M., 2010. Frome Airborne Electromagnetic (AEM) Mapping Survey Acquisition and Processing Report for Geoscience Australia. Fugro Airborne Surveys, Perth. **Unpublished.**
- Brodie, R., 2010. Holistic Inversion of Airborne Electromagnetic Data. Research School of Earth Sciences, Australian National University, Canberra. PhD thesis, unpublished.
- Brodie, R. and Fisher, A., 2008. Inversion of TEMPEST AEM survey data, Honeysuckle Creek, Victoria. Geoscience Australia for the Bureau of Rural Sciences, Canberra. **Unpublished.**
- Brodie, R. and Sambridge, M., 2009. Holistic inversion of frequency-domain airborne electromagnetic data with minimal prior information. *Exploration Geophysics* **40**, 765-778.
- Christiansen, A. and Auken, E., 2010. A global measure for depth of investigation in EM and DC modelling. In, ASEG Conference 2010. Australian Society of Exploration Geophysicists, **Extended Abstracts.**
- Constable, S., Parker, R. and Constable, C., 1987. Occam's inversion; a practical algorithm for generating smooth models from electromagnetic sounding data. *Geophysics* **52**, 289-300.
- Craig, M. A. (editor) 2011. Geological and energy implications of the Pine Creek region airborne electromagnetic (AEM) survey, Northern Territory, Australia. Geoscience Australia, Canberra. **Geoscience Australia Record 2011/18.**
- Green, A. and Lane, R., 2003. Estimating Noise Levels in AEM Data. In, ASEG 16th Geophysical Conference and Exhibition, Adelaide. Australian Society of Exploration Geophysicists.
- Hutchinson, D. K., Brodie, R. C. and Costelloe, M. T., 2011a. Frome Embayment TEMPEST™ AEM Survey: Inversion Report. Geoscience Australia, Canberra. **GEOCAT #72589**, 57 pp.
- Hutchinson, D. K., Roach, I. C. and Costelloe, M., 2011b. Logistics report for borehole conductivity logging in the Frome AEM Survey area, South Australia, 2010. Geoscience Australia, Canberra, 20 pp. Online: https://www.ga.gov.au/products/servlet/controller?event=GEOCAT_DETAILS&catno=71566.
- Hutchinson, D. K., Roach, I. C. and Costelloe, M. T., 2010. Depth of investigation grid for regional airborne electromagnetic surveys. *Preview* **145**, 38-39.
- Lane, R., Brodie, R. and Fitzpatrick, A., 2004. A revised inversion model parameter formulation for fixed wing transmitter loop – towed bird receiver coil time-domain airborne electromagnetic data. In, ASEG 17th Geophysical Conference and Exhibition, Sydney.
- Lane, R., Brodie, R. and Fitzpatrick, A., 2004a. Constrained inversion of AEM data from the Lower Balonne area, Southern Queensland, Australia. Cooperative Research Centre for Landscape Environments and Mineral Exploration, Perth. **Open File Report 163**. Online: <http://croleme.org.au/Pubs/OPEN%20FILE%20REPORTS/OFR%20161-162-163-164-166-167/OFR163.pdf>.

- Lane, R., Green, A., Golding, C., Owers, M., Pik, P., Plunkett, C., Sattel, D. and Thorn, B., 2000. An example of 3D conductivity mapping using the TEMPEST airborne electromagnetic system. *Exploration Geophysics* **31(2)**, 162-172.
- Lane, R. and Worrall, L., 2002. Interpretation of Airborne Electromagnetic Data: Summary report on the Challenger Workshop. Geoscience Australia Gawler Craton Mineral Promotion Project Canberra. **Record 2002/2**.
- Ley-Cooper, U. and Davis, A., 2010. Can a borehole conductivity log discredit a whole AEM survey? ASEG Extended Abstracts 2010. In. Australian Society of Exploration Geophysicists **Extended Abstracts**.
- Macnae, J., King, A., Stolz, N., Osmakoff, A. and Blaha, A., 1998. Fast AEM processing and inversion. *Exploration Geophysics* **29**, 163-169.
- McNeill, J. D., 1986. Geonics EM39 borehole conductivity meter-theory of operation. Geonics Ltd, Mississauga, Ontario. **Technical Note 20(11)**. Online: <http://www.geonics.com/pdfs/technicalnotes/tn20.pdf>.
- McNeill, J. D., Bosnar, M. and Snelgrove, F. B., 1990. Resolution of an electromagnetic borehole conductivity logger for geotechnical and ground water applications. Geonics Limited, Mississauga, Ontario. **Technical Note TN-25**, 29 pp. Online: <http://www.geonics.com/pdfs/technicalnotes/tn25.pdf>.
- Oldenburg, D. W. and Li, Y., 1999. Estimating depth of investigation in DC resistivity and IP surveys. *Geophysics* **64**, 403-416.
- Reid, J. E. and Brodie, R. C., 2006. Preliminary inversions of Honeysuckle Creek airborne electromagnetic data: Comparison with borehole conductivity logs and previously derived conductivity models. Geoscience Australia for the Bureau of Rural Sciences. **Unpublished**.
- Reid, J. E. and Vrbancich, J., 2004. A comparison of the inductive-limit footprints of airborne electromagnetic configurations. *Geophysics* **69**, 1229-1239.
- Roach, I. C. (editor) 2010. Geological and energy implications of the Paterson Province airborne electromagnetic (AEM) survey, Western Australia. Geoscience Australia, Canberra. **Geoscience Australia Record 2010/12**, 318 pp.
- Sattel, D., 2004. The resolution of shallow horizontal structure with airborne EM. *Exploration Geophysics* **35**, 208-216.
- Smith, R. S., 2001. On removing the primary field from fixed wing time-domain airborne electromagnetic data: some consequences for quantitative modelling, estimating bird position and detecting perfect conductors. *Geophysical Prospecting* **49**, 405-416.
- Stolz, E. and Macnae, J., 1998. Evaluating EM waveforms by singular-value decomposition of exponential basis function. *Geophysics* **63**, 64-74.

The Frome airborne electromagnetic survey, South Australia: implications for energy, minerals and regional geology

5 Interpretations of AEM Data

M. T. Costelloe, T. Dhu, A. J. Fabris, S. Jaireth, L. F. Katona, J. L. Keeling, P. D. Margarey, A. B. Marsland-Smith, B. H. Michaelsen, I. C. Roach and T. Wilson

5.1 INTRODUCTION

I. C. Roach and M. T. Costelloe

This chapter discusses geological features that can be seen within the Frome AEM Survey data set. Some of the larger geological features within the region are discussed, and case studies are presented by different authors focusing on known mineral deposits or structures, highlighting the potential of the AEM dataset as a tool for regional geological investigations including mapping palaeovalley systems, basin architecture, sedimentary facies, structures that may control mineralisation, geological surfaces and water resources (Figure 5.1.1). These interpretations are only possible once the data set has been determined to be fit-for-purpose and has been inverted or otherwise processed, as discussed in Chapter 4 of this Record. Case studies presented here include:

- 5.2 Mapping regional geology;
- 5.3 Mapping palaeovalley systems: southern Callabonna Sub-basin;
- 5.4 Mapping palaeovalley systems: MacDonnell Creek and northern Flinders Ranges area;
- 5.5 Mapping basin architecture and salinity: a TEMPEST™ AEM interpretation of the Poontana Trough, northwestern Lake Frome region;
- 5.6 Mapping Structures: interpretation of the Frome AEM Survey for the Leigh Creek – Marree region;
- 5.7 Mapping structure-related mineral deposits: gold deposits in the Nackara Arc and Copper-Molybdenum prospects associated with the Anabama Granite; and,
- 5.8 Mapping geological surfaces: Benagerie Ridge resistive basement model.

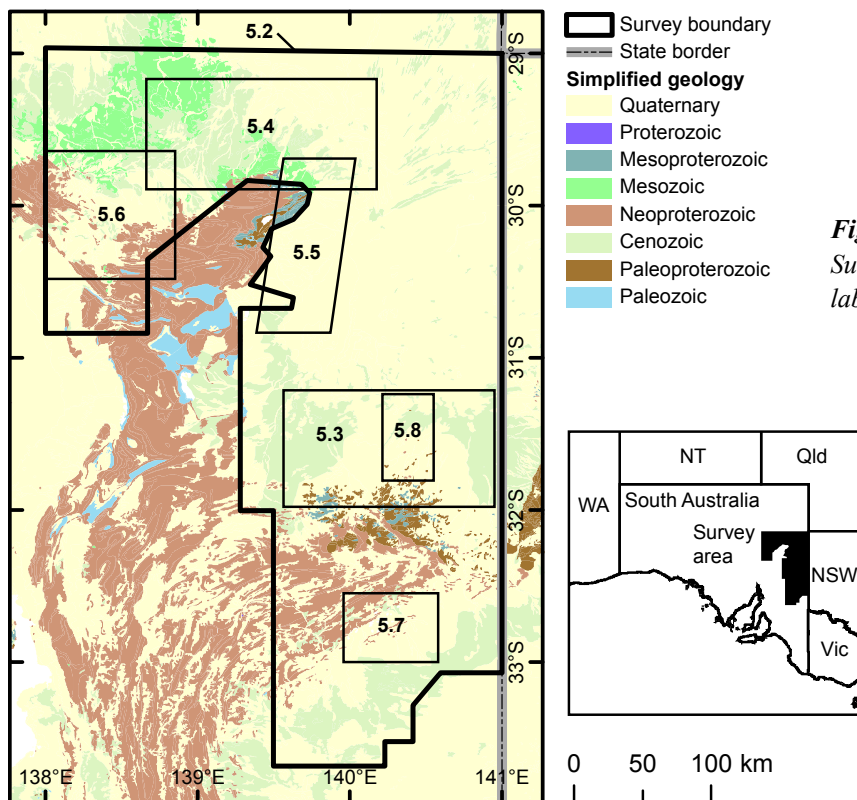


Figure 5.1.1: Frome AEM Survey case study locations, labelled by chapter section.

The Frome airborne electromagnetic survey, South Australia: implications for energy, minerals and regional geology

5.2 MAPPING REGIONAL GEOLOGY

I. C. Roach and M. T. Costelloe

5.2.1 Introduction

The Frome AEM Survey ([Figure 5.1.1](#)) maps geological environments and broad scale features such as the depth and electrical conductivity of cover over a large area, the extent and morphology of palaeovalley and basin systems and major geological structures. The survey was designed to use a wide line spacing to uncover new geological features and to possibly expand the area perceived to be prospective in the Lake Frome area. By mapping critical geological elements such as those being presented in this chapter, AEM has proven to be an important regional mapping tool.

The interpretation products demonstrate where AEM can be an effective tool, mapping to depth within the survey area, as well as informing about the relevance of using EM techniques in areas surrounding the survey with similar conductivity signatures.

The Frome AEM Survey, with 2.5 km and 5 km flight line spacing (see [Figure 1.8](#)), targets geological features with across-line extents greater than 15 km. The relatively broad line spacing was chosen as a compromise between providing regional coverage and local detail. Electrical conductivity data derived from the Sample-By-Sample Geoscience Australia Layered earth Inversion (SBS GA-LEI) were gridded with 500 m cells (1/5th of the minimum flight line spacing) and provide a regional overview of ground electrical conductivity, although along-line detail is available at far greater resolution in individual conductivity sections. Gridding allows a quick and instructive overview of millions of soundings from thousands of line kilometres of data and a wide variety of conductivity conditions within the Survey area.

A suite of interpretation products were created from the SBS GA-LEI as outlined in [Chapter 4](#). The gridded data, including 0-100 m and 0-200 m conductance, depth slices, elevation slices and the Depth Of Investigation (DOI), contain a host of information on the electrical conductivity of basement geology (Curnamona Province, Neoproterozoic rocks) as well as the overlying Paleozoic, Mesozoic and Cenozoic sedimentary basins. The conductance image ([Figure 5.2.1](#), [5.2.2A](#)) describes the summed electrical conductivity of the top 200 m of the earth's surface. The immediate impression of the regional conductance is that the ground is relatively conductive in the low-lying areas (Lake Torrens, the Marree area, the Strzelecki Desert, the Lake Frome area and the Murray-Darling Basin) and is variably resistive in the Flinders, Willouran and Barrier ranges and the Olary Spur. In terms of relative conductivity, this is a reasonable first impression because the low-lying ground consists of a number of sedimentary units that are known to be strongly or moderately conductive (e.g. the Marree Subgroup, the Bulldog Shale, the Eyre Formation, the Namba Formation and Murray Group sediments). The low-lying ground may also be saturated with saline water closer to the axes of the salt lakes within the survey area (Lake Blanche, Lake Callabonna and Lake Frome). However, on closer examination, it is possible to see geological detail within the conductance image, particularly within the Leigh Creek-Marree area and the southern Lake Frome area (southern Callabonna Sub-basin; see [Figure 2.3](#)), the Olary Spur and the northwestern Murray-Darling Basin.

The Frome airborne electromagnetic survey, South Australia: implications for energy, minerals and regional geology

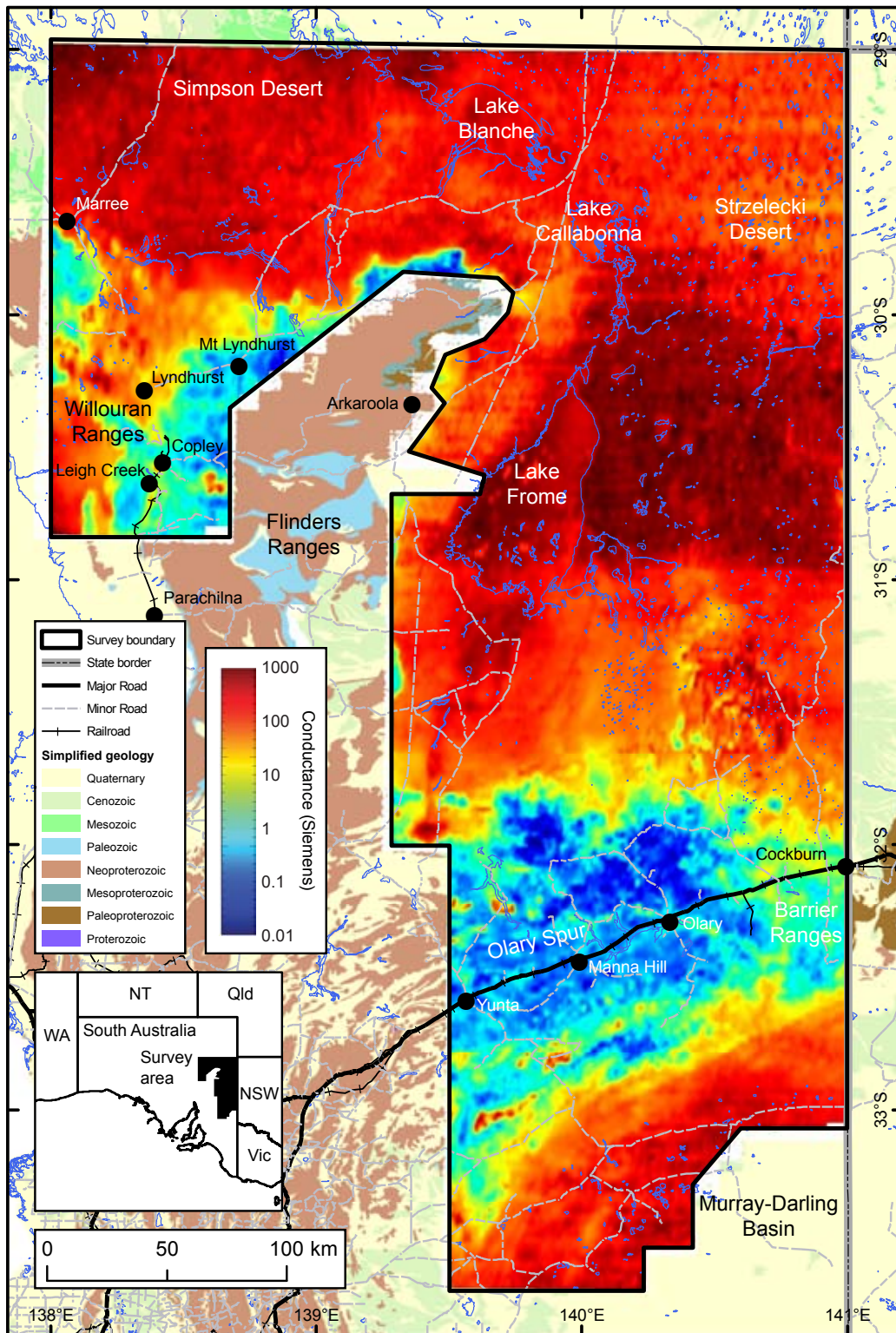


Figure 5.2.1: 0-200 m conductance image of the Frome AEM Survey indicating broad conductivity features relating to basement, basin geology and water bodies. Background: simplified 1:1 million Surface Geology of Australia Map (Raymond and Retter, 2010).

5.2.2 Mapping surface conductivity

Prominent surface high conductivity features are largely related to playas and salinas within the survey area. The large lakes (Blanche, Callabonna and Frome) each have high surface conductivity visible in the 0-5 m conductivity depth slice (Figure 5.2.2B). Numerous small playas or salinas are particularly visible on the eastern (leeside) of Lake Frome, as are saline drainage channels draining into the large playas or linking the playas in the central Lake Frome area. Drainage channels originating in the Olary Spur are observed to be quite resistive in their headwaters, gradually becoming more conductive as they enter the lowlands to the north and south, probably indicating that they contain relatively fresh water at their heads, but become progressively more saline downstream as water is lost due to evapotranspiration.

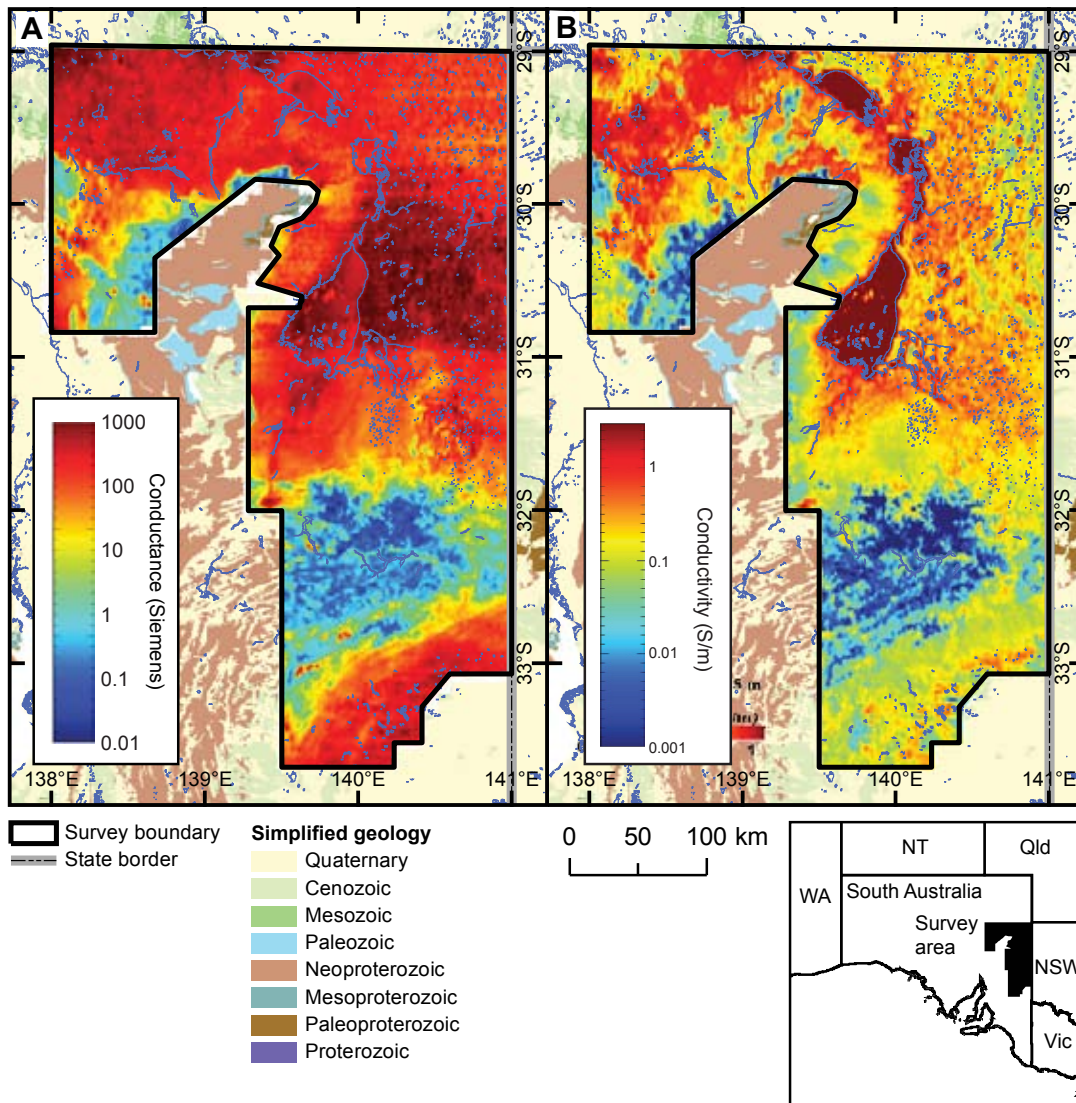


Figure 5.2.2: A: 0-200 m conductance image; and, B: 0-5 m conductivity depth slice image of the 400 m SBS GA-LEI product, with water bodies.

Not all conductive surface features are due to the presence of saline surface or groundwater; the northern Flinders Ranges is fringed by Mesozoic sediments of the Marree Subgroup, which includes the Bulldog Shale (see Figures 2.3 and 3.13). These are clearly visible in the conductance image (Figure 5.2.1, 5.2.2A) and the 0-5 m conductivity depth slice (Figure 5.2.2B). Much of the

- Unit Na4, between the Olary Spur and Barrier Ranges in the southeast of the Survey area, consists of undulating plains with low hillocks and remnants of dissected tablelands. The Soil Atlas of Australia notes that this area consists of crusty loamy soils with shallow calcareous loamy soils on plains, rock outcrops and shallow calcareous soils, and some sand dunes and drifts of brown sands close to valleys;
- Unit B60, on the eastern side of Lake Frome. The Soil Atlas of Australia notes that this unit consists of dune fields with variable inter-dune corridors and plains, some clay pans and ephemeral drainage (which were saturated by excessive rainfall during the Frome AEM Survey in 2010), dominated by on ~5 m average height sand dunes. This area has moderately to strong, mottled, conductivity patterns (Figure 5.2.4);

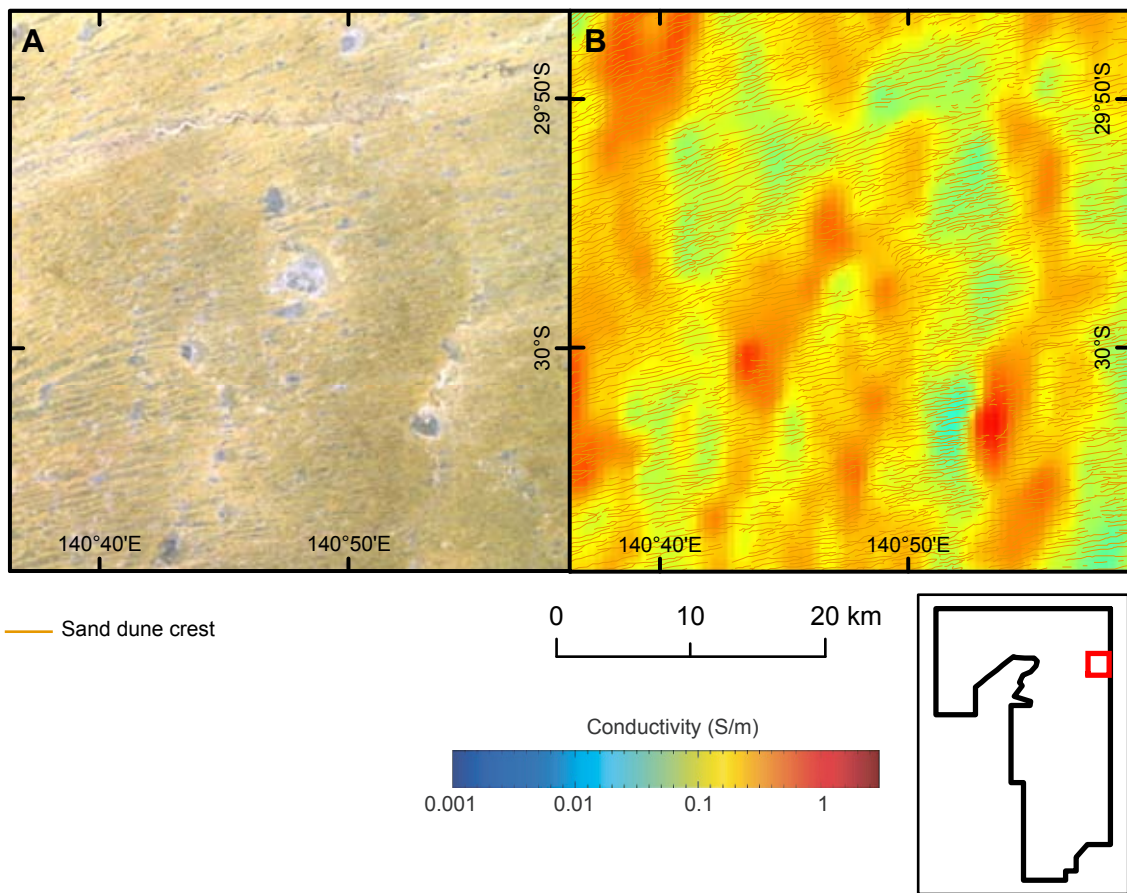


Figure 5.2.4: Sand dunes and playas in the northeast of the Frome AEM Survey area, described in the Soils Atlas of Australia as unit B60. **A:** Landsat MSS mosaic of the area showing playas, sand dune crests and ephemeral drainage channels. **B:** Sand dune crests overlain on the 0-5m conductivity depth slice. Conductivity anomalies are generally correlated with the lines of playas, here defining palaeodrainage lines.

- Unit CC118 is easily seen surrounding playas in the north of the Survey area. The Soil Atlas of Australia notes that this unit consist of plains with some low ridges, some tracts of low dunes and saline, normally dry lakes. Soils are very variable, but the dominant soils are swelling clays. This area was inundated during the survey, resulting in dissolution of salts and high conductivity. The outline of this unit matches well with the conductivity anomaly associated with the edges of Lake Callabonna. Flight lines were spaced at 5 km intervals in this area and the gridded data do well to match the boundaries of this unit;

- Unit DD2 in the southeast of the Survey area has a strong correlation to the Murray-Darling Basin region. The Soil Atlas of Australia notes that this unit consists of plains with isolated tracts of dunes, areas of exposed caliche (calcrete) and crusty loamy soils with claypans, saline soils, swamps, and intermittent lakes in the lower-lying portions; dunes of brown sands and brown calcareous earths. Small areas of alluvial soils and hard alkaline red soils occur on outwash adjacent to the Mount Lofty Ranges

There is great potential for the Soil Atlas of Australia to be updated using regional AEM data.

5.2.4 Peeling away cover

Conductive clays and saline groundwater yield conductivities of 1 to 3 S/m in the Frome AEM Survey data, and are easily mapped by their electrical conductivity. However, large areas of these near-surface sediments lack significant magnetic susceptibility contrasts (they are mostly poorly magnetised), and mapping the near-surface cover with magnetics is ineffective.

The gridded conductivity depth slice data, in conjunction with other *a priori* information, improve our understanding of cover structure in broad areas of the Frome AEM Survey, where mineral explorers are either seeking to explore within the cover (for uranium) or under cover (for gold, copper, lead, zinc and coal). Figures 5.2.5A and B highlight the difference between the 0-5 m and the 90-100 m depth slices from the 200 m SBS GA-LEI product.

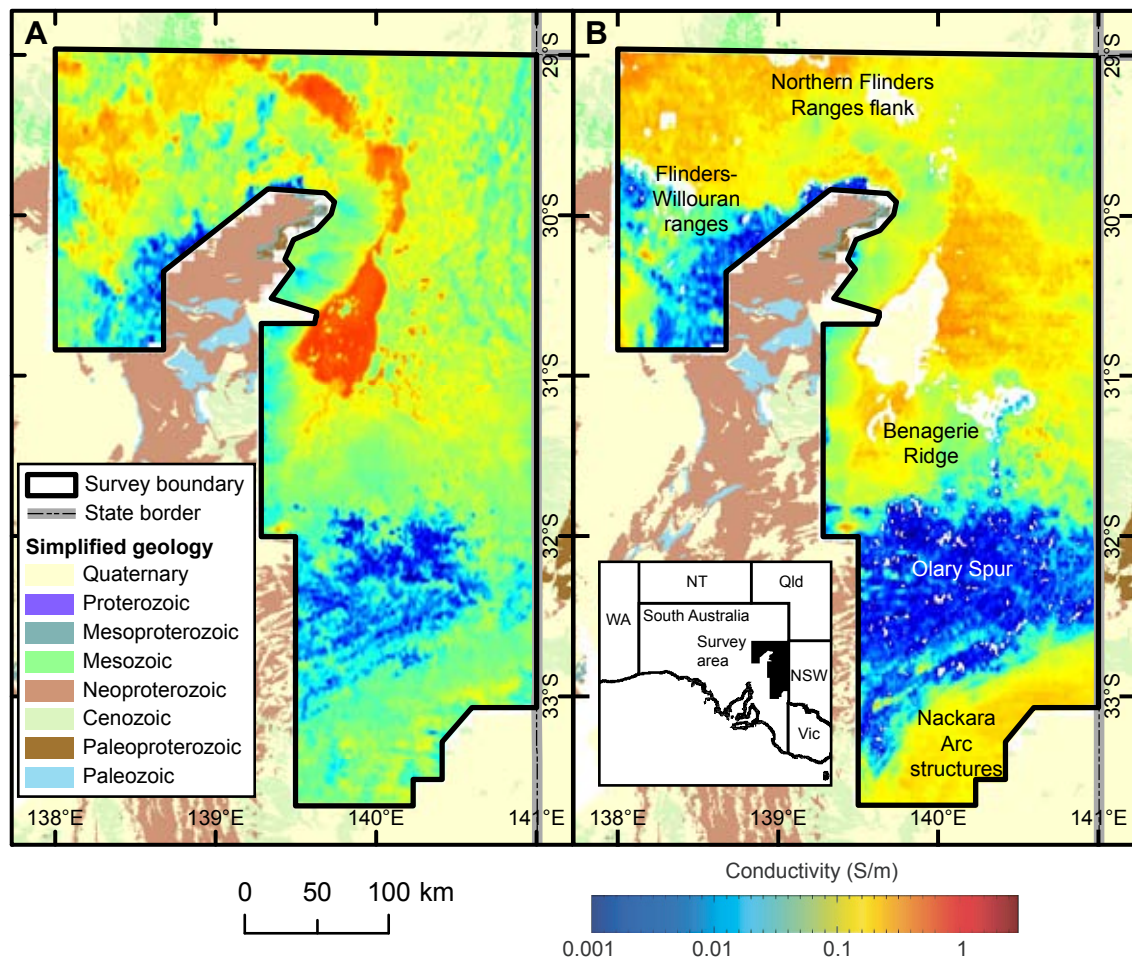


Figure 5.2.5: 200 m SBS GA-LEI product conductivity depth slices. A: 0-5 m. B: 90-100 m.

The differences between the two depth slices are dramatic in some areas. Where cover rests unconformably on resistive basement, the 90-100 m depth slices reveals new information about the thickness of cover and the nature of the resistive basement rocks underneath. A range of features are revealed including the extent of the resistive basement in the Benagerie Ridge, Neoproterozoic rocks under cover in the Flinders and Willouran ranges, the under-cover extent of resistive basement in the Olary Spur (at that depth) and regional-scale fault structures in the Nackara Arc under cover of the Murray-Darling Basin. The depth slices reveal much new information regarding the regional distribution of cover, but much more detailed information is available from individual conductivity sections for each flight line.

5.2.5 The DOI – decreasing exploration risk

The gridded DOI across the Frome AEM Survey area (Figure 5.2.6) is a useful tool for determining the depth of reliable signal penetration, which is a function of the bulk conductivity of the earth within the survey area. The DOI marks the threshold depth to which the inversion is more influenced by conductivity data rather than modelled assumptions.

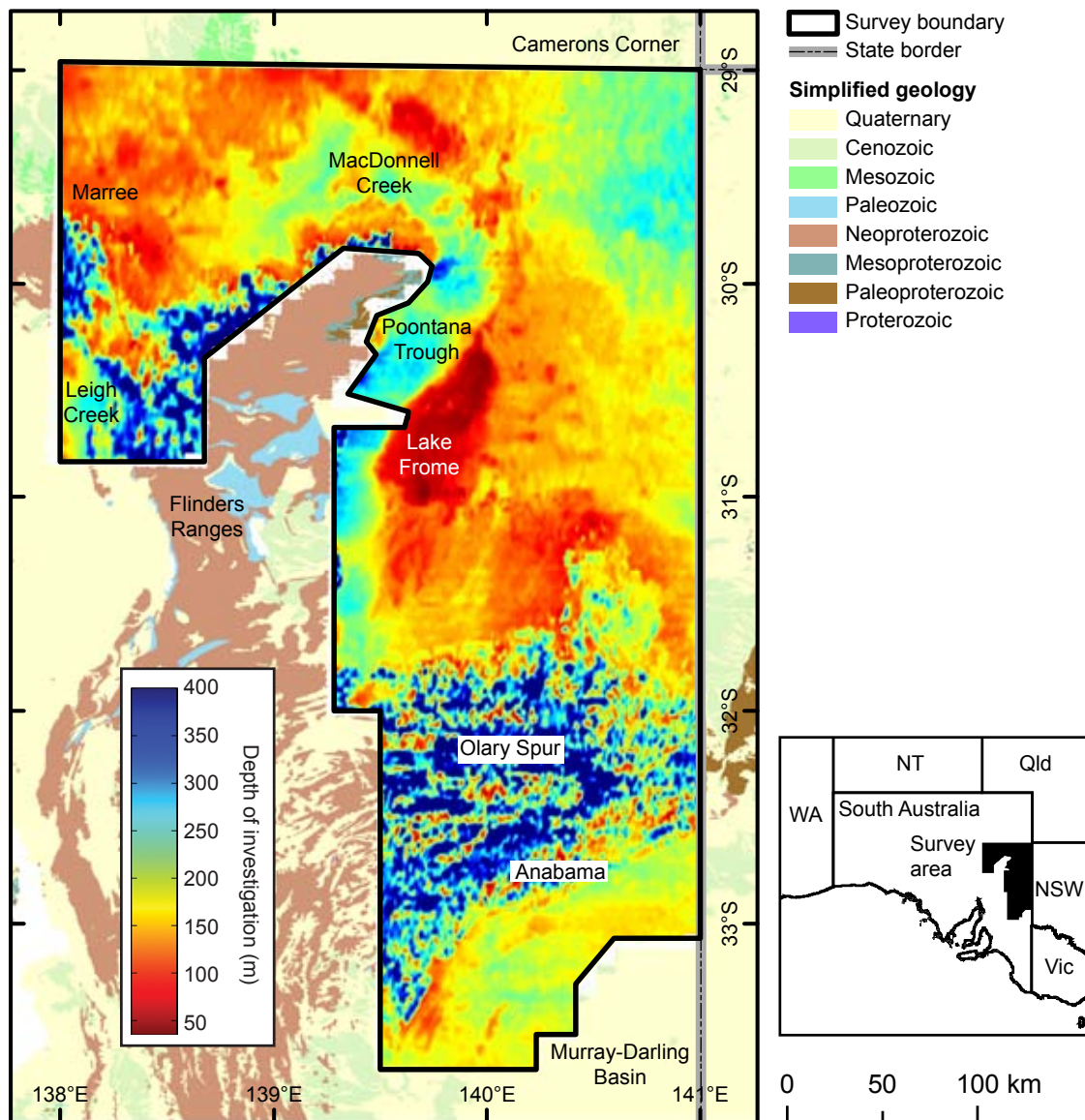


Figure 5.2.6: The DOI grid for the Frome AEM Survey.

The DOI grid is a useful tool for determining locations where further follow-up airborne or ground EM surveys are likely to be effective. It is directly relevant to industry because it allows explorers to decrease exploration risk by making informed decisions regarding the area and techniques used in follow up geophysical surveys. An explanation of the method used to calculate the DOI is included in [Section 4.7.7](#).

The DOI grid reveals variable reliable signal penetration in the upland areas of the Flinders Ranges and Olary Spur. This can be attributed to a number of factors including saline cover sediments and groundwaters collecting in alluvial systems between resistive hills, deep-seated conductors within the Neoproterozoic succession and artefacts caused by poor system geometry due to the survey aircraft flying over high relief in these areas. Conductors in Neoproterozoic rocks in the northwest of the survey area are discussed in greater detail in the case study describing the Leigh Creek-Marree area in [Section 5.6](#). Conductors in Neoproterozoic rocks in the Anabama area of the southwestern Nackara Arc are discussed in greater detail in [Section 5.7](#).

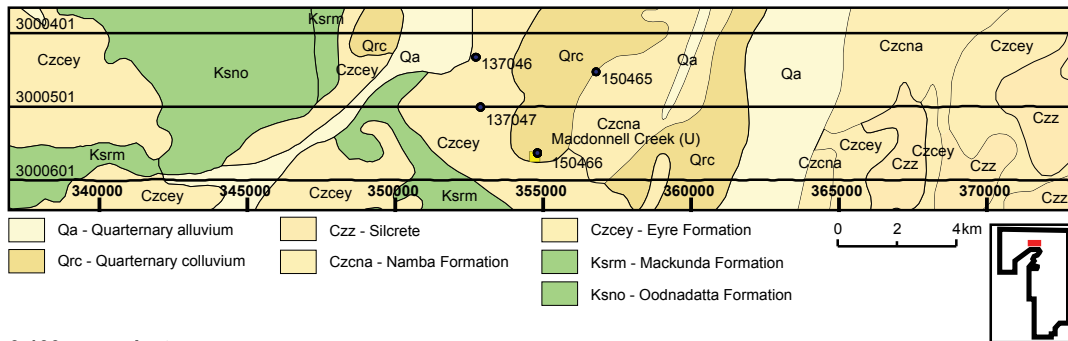
In areas with relatively flat topography, the DOI image appears smoother and reveals a great deal of information about the geology and groundwater conditions in the Lake Eyre Basin—Callabonna Sub-basin and Murray-Darling Basin. Signal penetration beneath the large salt lakes is calculated to be < 50 m, but can reach depths of 250-300 m in the flanks of the Flinders Ranges and in the northeast around Camerons Corner, signifying the potential for relatively fresh groundwater in these areas. Some of these groundwater features are discussed in more depth in the case study describing the basin architecture of the Poontana Trough (see [Section 5.5](#)). Signal penetration in the Murray–Darling Basin is overall less than in the Lake Eyre Basin—Callabonna Sub-Basin in the north of the survey area, but penetration of up to ~200 m is indicated in some areas within the DOI image. In the northern Flinders Ranges, signal penetration appears to be largely geologically-controlled, with low penetration around the flanks of the northern Flinders Ranges associated with outcropping Marree Subgroup sediments in the MacDonnell Creek area. The Marree Subgroup is either offset by faulting, or dips to the north due to uplift of the northern Flinders Ranges, resulting in increased signal penetration to ~200 m before the saline groundwaters associated with Lake Blanche and Lake Callabonna are encountered in the far north of the survey area. See [Section 3.5](#) for a discussion of the landscape evolution of this area and [Section 5.4](#) for more detail on structure and surface mapping in this area, and for a discussion of landscape evolution.

[Figure 5.2.7](#) highlights the variation in the DOI calculated in two different inversion products released for the Frome AEM Survey: the SBS GA-LEI; and, the Line-By-Line (LBL) GA-LEI (see [Chapter 4](#)). In this region of the Frome AEM Survey, the two different DOIs mimic each other in all but fine detail, and in this area lie near the top of the Bulldog Shale, a known strong conductor (~1000 mS/m) in the Marree Subgroup. The DOI for the LBL GA-LEI is not available as a gridded product because the LBL GA-LEI was only calculated for part of the Frome AEM Survey area.

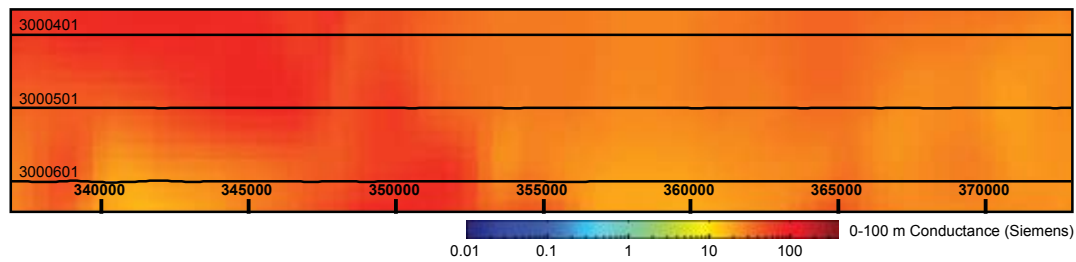
[Figure 5.2.8](#) depicts the variation in the DOI with changing bulk earth conductivity across a whole flight line (line 2000101A), which was flown over the eastern flanks of the Flinders Ranges and Lake Frome. The DOI varies with changing bulk earth conductivity, becoming shallower where surface conductivity is high, but is deeper where relatively fresh groundwater occurs on the flanks of the Flinders Ranges in the west of the image. This image also describes the saline plume around the edge of Lake Frome, which is also described in [Section 5.5](#).

Exploration risk in the area surrounding the Frome AEM Survey may be mitigated by extending the knowledge gained from the DOI calculated within the Survey area to areas outside the Survey area with similar basement geology, cover geology, groundwater salinity conditions and basement-cover relationships.

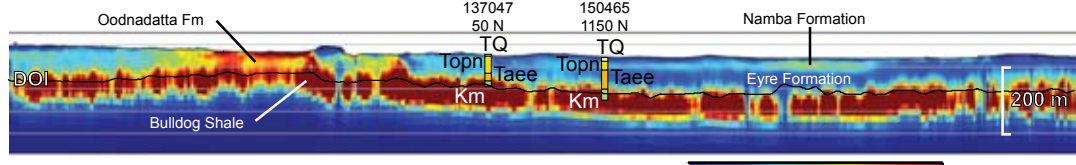
1:1 million scale Surface Geology of Australia map



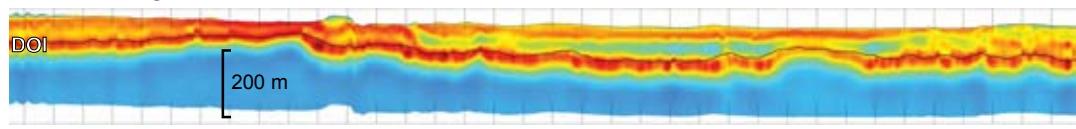
0-100 m conductance map



SBS GA-LEI linear colour stretch section line 3000501



LBL GA-LEI logarithmic colour stretch section line 3000501



Drill hole stratigraphy

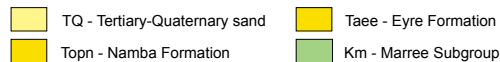


Figure 5.2.7: Regional surface geology, 0-100 m conductance and detailed GA-LEI conductivity sections (upper: SBS GA-LEI; lower: LBL GA-LEI) near the MacDonnell Creek uranium prospect, flanking the northern Flinders Ranges. This diagram highlights two different versions of the DOI, calculated for the SBS GA-LEI and the LBL GA-LEI, the variation in regional conductance compared to detailed conductivity sections, and a geological interpretation of detailed conductivity sections including two stratigraphic drill hole logs. Modified from Costelloe and Roach (2012).

5.2.6 PhiD – understanding misfits

The data misfit or PhiD is a data field provided in the SBS GA-LEI dataset and, when gridded, can be a useful reference tool. The PhiD quantifies the data misfit of an inversion; the target misfit being less than 1, assuring that the inversion has fitted the AEM data to the reference model. Where the inversion is successful the misfit is less than one and in areas where the inversion struggles to converge the data and the reference model, the misfit is greater than one. The PhiD (Figure 5.2.8.) shows that in the Lake Frome area the misfit is high, due to the super-saturation of the AEM signal in the highly conductive salt lake. However, in the Benagerie Ridge area the PhiD highlights areas where the inversion does not fit the data due to the complex 3D nature of the geology (folds and faults). In the Leigh Creek-Marree region the misfit reflects the complex structures in the area, further discussed in Section 5.6.

The gridded PhiD image (Figure 5.2.9) reveals much about the electrical conductivity conditions of the earth within the survey area, but also contains geological detail. A number of the larger Neoproterozoic sedimentary units within the Olary Spur have visibly coherent, similar PhiD numbers, which can be traced over many flight lines. Equally, high PhiD numbers occur clustered around large granitic bodies in the Nackara Arc (the Anabama Granite, for one; see Section 5.7) and the instance of high PhiD increases within rocks of the Curnamona Province corresponding to the Willyama Supergroup. In both these areas, the geology is dominated by complex folding and numerous vertical shear zones and faults, contributing to the high data misfit.

A linear PhiD anomaly can also be seen corresponding to the Moomba-to-Adelaide gas pipeline to the northeast of the northern Flinders Ranges. The pipeline is periodically energised with 50 Hz alternating current to prevent corrosion. The 50 Hz signal is a multiple of the 25 Hz base frequency of the TEMPEST™ AEM system and causes anthropogenic artefacts in the inversion data. See Chapter 4 for more information on quality assurance and quality control of AEM data and Section 5.5 for more information on the anthropogenic artefacts in this region.

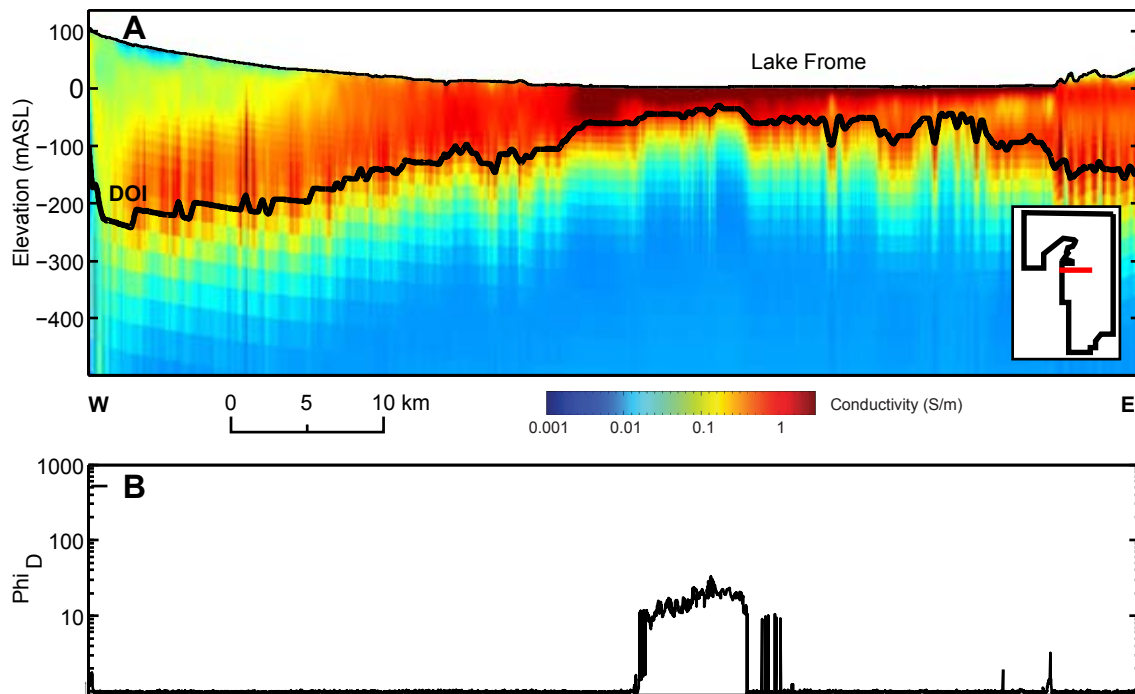


Figure 5.2.8: *A: SBS GA-LEI conductivity section; and, B: corresponding PhiD graph for flight line 2000101A. This diagram highlights the variation in the DOI in response to changing bulk earth conductivity, in this case from relatively resistive ground near the Flinders Ranges in the west to highly conductive, saline ground in the east at Lake Frome. The line is severely fore-shortened compared to actual GA-LEI data products. Note too the change in PhiD over the western side of Lake Frome due to excess surface conductivity.*

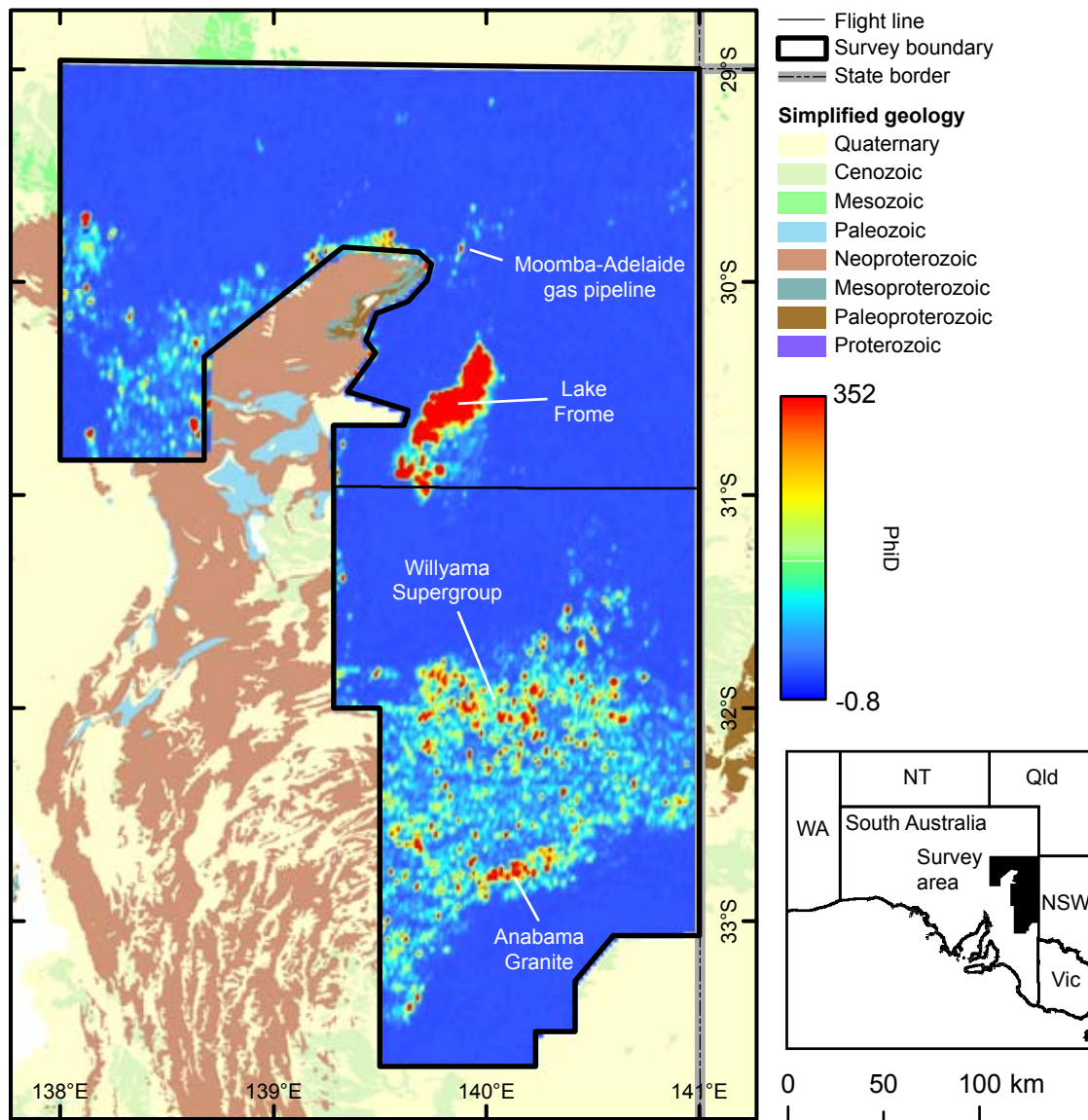


Figure 5.2.9: PhiD grid for the Frome AEM Survey.

5.2.7 Regional mapping of sedimentary facies

A regional AEM survey like the Frome AEM Survey allows users to make interpretations that are not normally possible within small, tenement-scale AEM surveys. The addition of geological data to maps and sections, and the use of the various different types of data products, including the different inversions (SBS GA-LEI and LBL GA-LEI) and colour stretches provided (logarithmic and linear) can highlight subtleties within the data that perhaps would not normally be apparent.

One of the stated aims of the Frome AEM Survey was to map basin architecture and sedimentary facies. The long flight lines easily allow basin features to be interpreted (see Sections 5.3, 5.4 and 5.5), but is it possible to map sedimentary facies, or facies changes within the data? Figure 5.2.10 illustrates drill hole stratigraphy drawn over the top of data products from the two different inversions produced for the Frome AEM Survey on a flight line from near the Honeymoon uranium mine in the southern Callabonna Sub-basin.

The Frome airborne electromagnetic survey, South Australia: implications for energy, minerals and regional geology

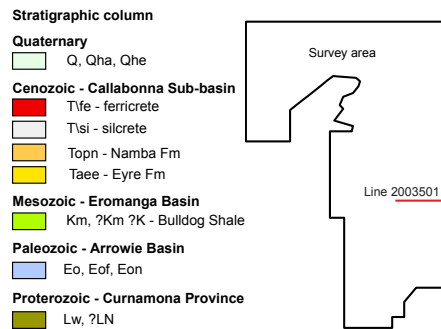
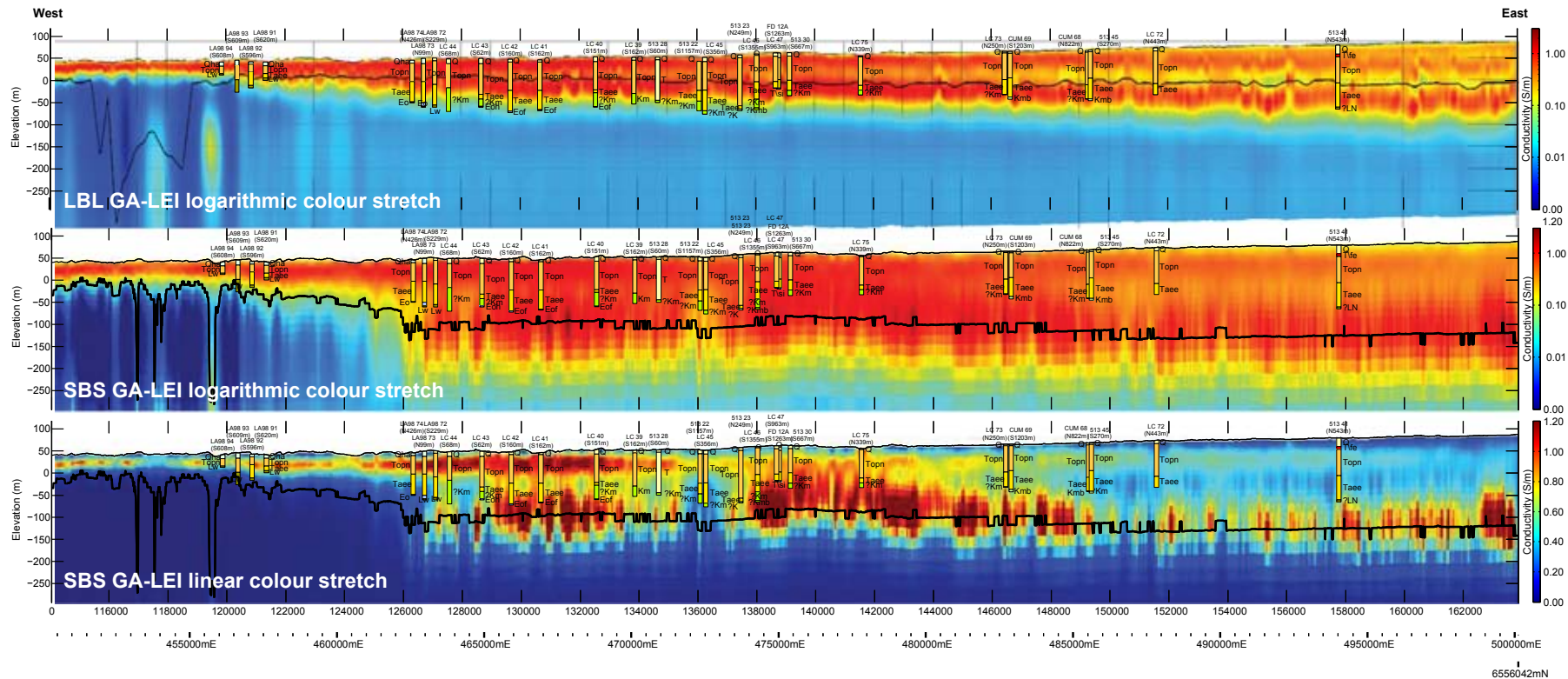


Figure 5.2.10: LBL GA-LEI (upper) and SBS GA-LEI (middle and lower) conductivity sections from flight line 2003501, near the Honeymoon uranium mine, southern Callabonna Sub-basin. The linear colour stretch SBS GA-LEI conductivity section at bottom enhances electrical conductivity variation in the Namba Formation related to horizontal facies changes better than the two upper conductivity sections. Modified after Roach (2012a). See Figure 5.2.11 for a close-up view of a portion of this flight line.

Figure 5.2.10 provides an overall picture of conductivity conditions along flight line 2003501. The different colour stretches, logarithmic and linear, enhance the data differently. The logarithmic colour stretch tends to show all moderate and strong conductors in “hot” colours (orange-red-brown) and is useful for separating conductive cover from resistive basement in this area. The linear colour stretch, however, separates the moderate conductors from the strong conductors, and in this area resolves resistive basement, the strong conductor of the Mesozoic Bulldog Shale and the moderate conductor associated with part of the Namba Formation. A close-up of this is shown in Figure 5.2.11.

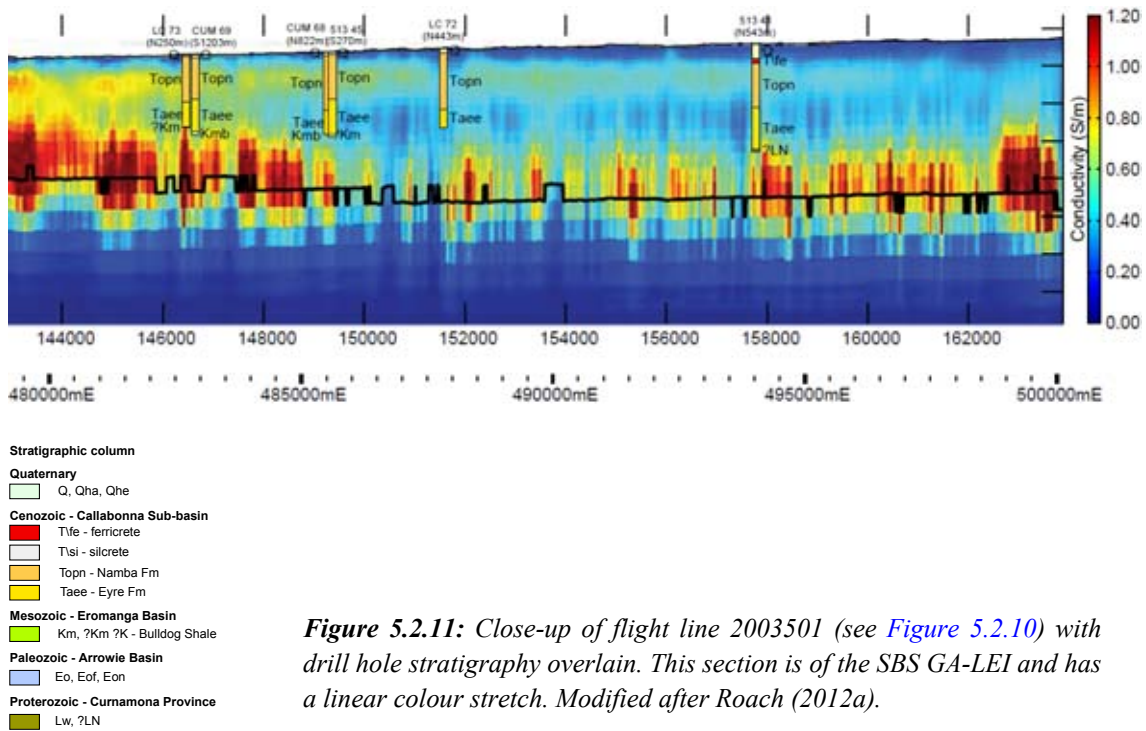


Figure 5.2.11: Close-up of flight line 2003501 (see Figure 5.2.10) with drill hole stratigraphy overlain. This section is of the SBS GA-LEI and has a linear colour stretch. Modified after Roach (2012a).

In this area the Namba Formation is known to be quite heterogeneous. Figure 3.17 demonstrates the lateral variation of facies within the Namba Formation at the Oban uranium deposit, ~60 km northeast of Honeymoon, where lateral variation between sand and clay occurs over several hundreds of metres. This is hardly surprising given that the depositional environment of the Namba Formation is interpreted to have been one of sandy meandering streams, clayey floodplains and alkaline lakes.

The variation in the conductivity of the Namba Formation illustrated in Figure 5.2.11 indicates lateral variation in the bulk conductivity of the unit, which is most likely caused by a change in the sand:clay ratio, altering porosity and permeability and therefore the bulk conductivity of this unit, which is known to be saturated with saline groundwater. Given adequate stratigraphic drill hole information, lateral conductivity variations correlated with facies variation can be mapped over large areas of the Frome AEM Survey area.

5.2.8 Mapping regional structure

The regional nature of the Frome AEM Survey has yielded excellent results in mapping large-scale structures that define the boundaries of major crustal elements within the Survey area. An example comes from the Murray-Darling Basin region in the south of the Survey area, where the relatively bland surface geology masks much of the neotectonic activity that occurs in what is actually a dynamic landscape. The most obvious landscape features in the area are large alluvial fans developed on creeks that drain the uplands of the Olary Spur; the Manunda Creek and Olary Creek fans are good examples (Figure 5.2.12A). The Cenozoic cover of the Murray-Darling Basin masks a

series of major thrust and strike-slip faults in the Anabama-Redan Fault Zone (Figure 5.2.12B), a major crustal suture that can be traced from the eastern Mount Lofty Ranges through the Survey area into New South Wales east of Broken Hill and north towards Tibooburra. In this area, conductivity depth slices and the conductance images highlight abrupt conductivity contrasts related to the fault systems, where conductive Murray Group marine sediments are juxtaposed against largely resistive Neoproterozoic rocks of the Nackara Arc and Delamerian granites including the Anabama Granite. A number of other conductivity features occur in the area, including conductive rocks of the Saddleworth Formation, a black, pyritic, carbonaceous shale unit similar to the Tapley Hill Formation, and a conductivity anomaly associated with the Olary Creek Palaeovalley, which is filled with conductive Murray Group sediments in electrical contrast to the surrounding Nackara Arc rocks. The data also map modern alluvial systems, which tend to be saturated with fresh to brackish groundwater and are relatively resistive in their upper reaches.

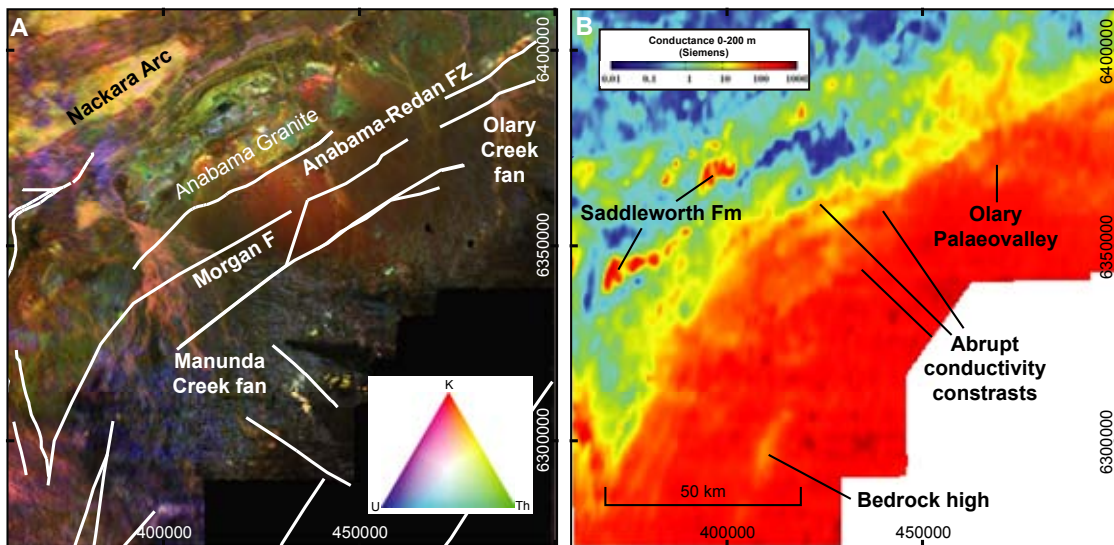


Figure 5.2.12: A comparison of surface features and under cover structure in the northwest Murray-Darling Basin and Nackara arc area. A: Ternary radiometric image. B: 0-200 conductance image. Mapped faults are from SARIG. Modified after Roach (2012b).

5.2.9 Mapping regional geological surfaces

The prominent electrical conductivity contrast between sediments of the overlying Murray-Darling Basin and the rocks of the underlying Neoproterozoic and Kanmantoo Group of the Nackara Arc (Figure 5.2.12) allows the construction of along-line profiles, which have been assembled into a 3D model of the resistive basement. Figure 5.2.13 illustrates a GOCAD™ model constructed using EM Flow™ conductivity depth interval (CDI) sections (which have no DOI) of the Frome AEM Survey. The EM Flow™ data were released as part of the Phase-1 data release.

The model shows the contact between the resistive basement and the overlying Murray-Darling Basin. The model was constructed by tracing the boundaries between the basement resistor and overlying conductive beds, which were then used to construct a surface in GOCAD™. These interpretations were validated using drill hole stratigraphic logs from SARIG, which were compared to SBS GA-LEI conductivity sections, and individual inversion conductivity profiles where possible (Figure 5.2.14). The CDI sections shown in the model highlight the contrast in conductivity between the Murray Group, which consists entirely of marine sediments, and the overlying Plio-Pleistocene succession which includes the Pooraka Formation, the Blanchetown Clay and the Parilla Sands, which are variably, but generally only relatively weakly conductive. The model also indicates the position of major faults associated with the Anabama-Redan Fault Zone as abrupt offsets in conductivity in individual CDI sections.

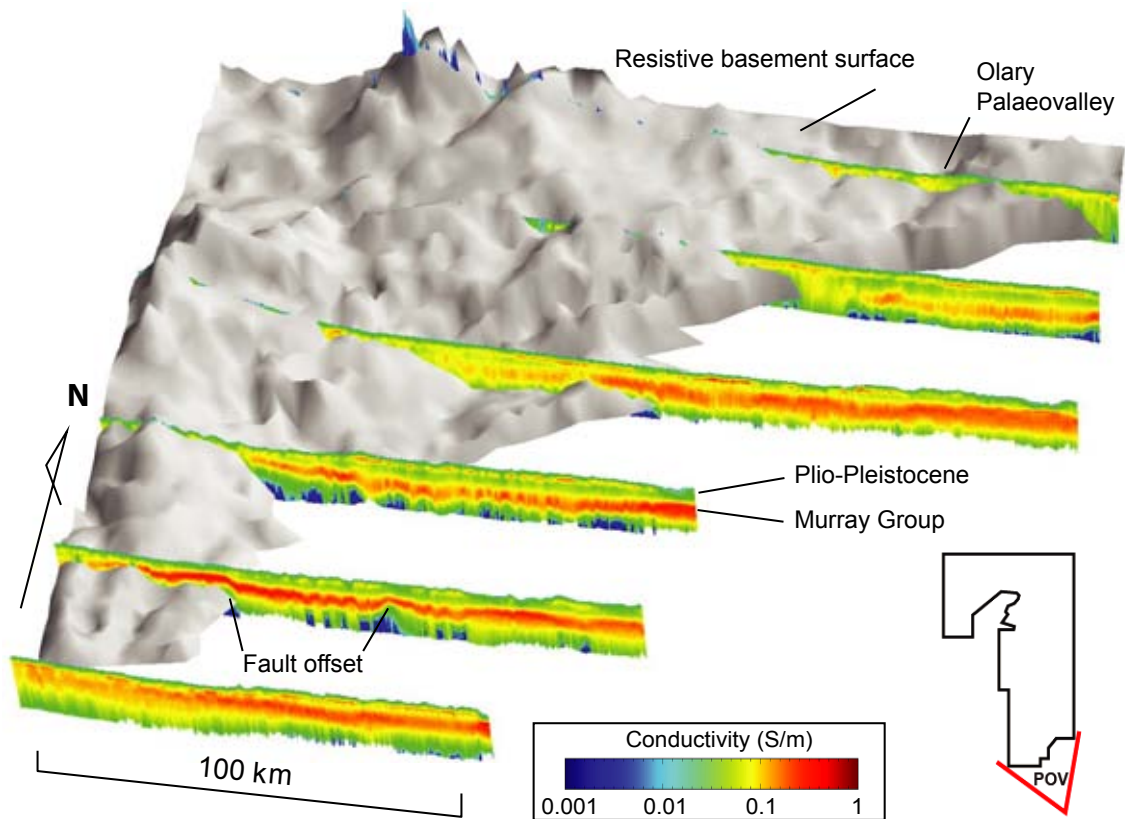


Figure 5.2.13: Resistive basement GOCAD™ model of the northwestern Murray-Darling Basin modified from Roach (2012b). The model is constructed from EM Flow™ CDI sections with the aid of stratigraphic drill hole data from SARIG.

5.2.10 References

- Costelloe, M. T. and Roach, I. C., 2012. The Frome AEM Survey, uncovering 10% of South Australia. Preview **158**.
- Northcote, K. H., Beckmann, G. G., Bettenay, E., Churchward, H. M., Van Dijk, D. C., Dimmock, G. M., Hubble, G. D., Isbell, R. F., McArthur, W. M., Murtha, G. G., Nicolls, K. D., Paton, T. R., Thompson, C. H., Webb, A. A. and Wright, M. J., 1960-1968. Atlas of Australian Soils, Sheets 1 to 10. With explanatory data. CSIRO and Melbourne University Press, Melbourne. Online: http://www.asris.csiro.au/themes/Atlas.html#Atlas_Downloads.
- Raymond, O. L. and Retter, A. J., 2010. Surface geology of Australia 1:1 000 000 scale. Geoscience Australia, Canberra. 2010. Online: <http://www.ga.gov.au/mapconnect/>.
- Roach, I. C., 2012a. The Frome airborne electromagnetic survey, South Australia. In: 22nd International Geophysical Conference and Exhibition, 26-29 February - Brisbane, Australia, Brisbane. Australia Society of Exploration Geophysicists, **ASEG Extended Abstracts 2012(1)**, 1-3 pp. Online: <http://www.publish.csiro.au/nid/267/paper/ASEG2012ab071.htm>.
- Roach, I. C., 2012b. Using airborne electromagnetic data for regional stratigraphic and landscape evolution studies, Murray Basin, South Australia. In: Australian Regolith and Clays Conference, Mildura, 7-10 February 2012, Mildura, Victoria. Australian Regolith Geologists Association/Australian Clay Minerals Society. Online: http://regolith.org.au/docs/ARGC-ACMS_2012/S1P_5_ARGA2_Roach.pdf.

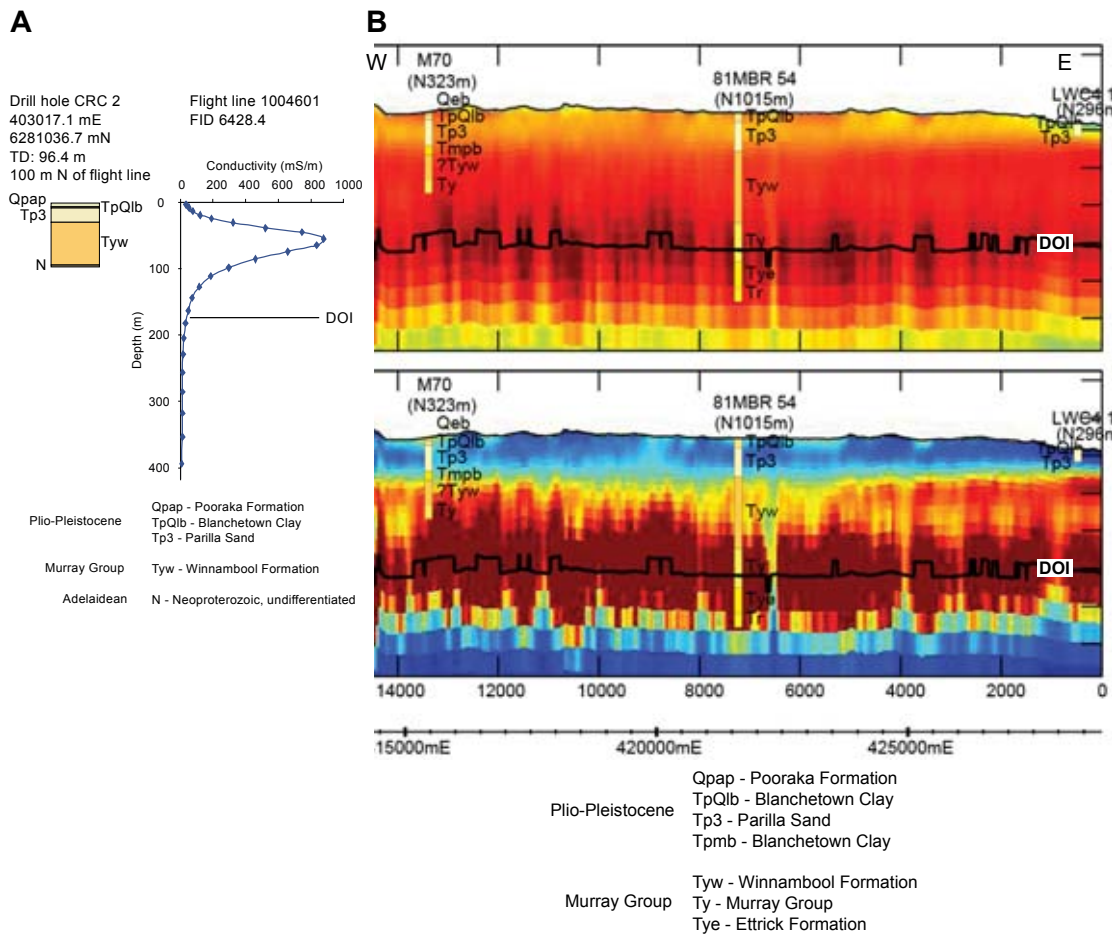


Figure 5.2.14: *A: An example inversion conductivity profile and corresponding drill hole stratigraphic profile showing resistive Blanchetown Clay and Parilla Formation over conductive Murray Group sediments and resistive Neoproterozoic basement. The conductivity profile is not directly measured, but is extracted from a data point in the SBS GA-LEI data set. See Section 4.9 for more information on independent validation of the inversions using calibrated bore hole conductivity logging. B: An example of drill hole stratigraphy plotted on logarithmic (top) and linear (bottom) colour-stretched SBS GA-LEI conductivity sections, flight line 1004501. Murray Group sediments are variably conductive, with the moderately conductive Winnambool Formation thickening to the east over highly conductive undifferentiated Murray Group and Ettrick Formation. The distance between the drill hole and the flight line is shown for each, e.g., N1015m, meaning the drill hole occurs 1015 metres north of the flight line. From Roach (2012b).*

5.3 MAPPING PALAEOVALLEY SYSTEMS: SOUTHERN CALLABONNA SUB-BASIN

A. J. Fabris and I. C. Roach

5.3.1 Introduction

The southern Callabonna Sub-basin, part of the Lake Eyre Basin, is host to several significant uranium mines or prospects, including the Honeymoon uranium mine and the Goulds Dam and Oban uranium prospects (Figure 5.3.1). These sandstone-hosted uranium occurrences demonstrate the process of uranium reduction and accumulation within Cenozoic sediments in this region. Uranium-rich granites and metasedimentary rocks of the Ninnerie Supersuite outcrop throughout the Olary Spur and Barrier Ranges and are known through drilling and potential field geophysics within the Benagerie Ridge (Fabris, 2004; Fricke, 2008; Hou *et al.*, 2007a). These provide a vast uranium source region, supplying uranium-rich fluids across the entire southern Callabonna Sub-basin. Fluids are diverted into palaeovalleys, including the Billeroo, Curnamona, Lake Namba, Lake Charles and Yarramba palaeovalleys, where uranium may be concentrated by interaction with a reductant within these palaeodrainage systems.

The Frome AEM Survey provides, for the first time, a regional dataset in which explorers can assess this region as a whole.

5.3.2 Geological history and regional geology

The Cenozoic Callabonna Sub-basin is the youngest of several basins overlying the Paleoproterozoic Curnamona Province. These include Neoproterozoic metasediments that extend from the Adelaide Geosyncline, Cambrian metasediments of the Arrowie Basin and Mesozoic sediments of the Eromanga Basin (see Chapter 3). The distribution of each of these basins within the southern Callabonna Sub-basin region is complex (Fabris *et al.*, 2004).

Prior to deposition within the Callabonna Sub-basin, a hiatus between the Late Cretaceous (Cenomanian) and Early Cenozoic (Late Paleocene; Callen *et al.*, 1995) marked a period of deep weathering (Figure 3.11, 3.12). By the Early Cenozoic, basement rocks of the Flinders Ranges, Olary Spur and Barrier Ranges were sufficiently weathered to provide significant volumes of kaolinitic sands in basins proximal to the uplands, and a mostly mature, quartz-dominated bedload elsewhere. These sediments were gradually stripped by erosion coincident with uplift along the Flinders-Olary-Barrier upland axis commencing in the Paleocene. Once this uplift was established, an extensive network of major river systems formed, draining in a predominantly northerly direction from the Olary Spur, west to northwest from the adjacent Barrier Ranges, and in a north to easterly direction from the incipient Flinders Ranges (Benbow *et al.*, 1995). The Murray-Darling Basin was also established to the south of this uplift, with river systems draining south and southeast from the Flinders-Olary-Barrier upland axis.

Sediment thickness within the Paleogene palaeodrainage features is commonly as much as 50 m. These dominantly fluvial sands make up the Eyre Formation (see Section 3.2.5) and have been the main target for uranium exploration in the southern Callabonna Sub-basin. Following a hiatus in deposition (see Figure 3.12), the Neogene Namba Formation was widely deposited in a number of different styles including lacustrine, overbank, channel and floodplain facies (Callen and Tedford, 1976; Hill and Hore, 2012). Channel sediments are common within the Namba Formation but are rarely more than a few metres thick in this region. Thus far, only limited assessment of their potential for sandstone-hosted uranium has been conducted, principally around the Beverley area in the northern Callabonna Sub-basin.

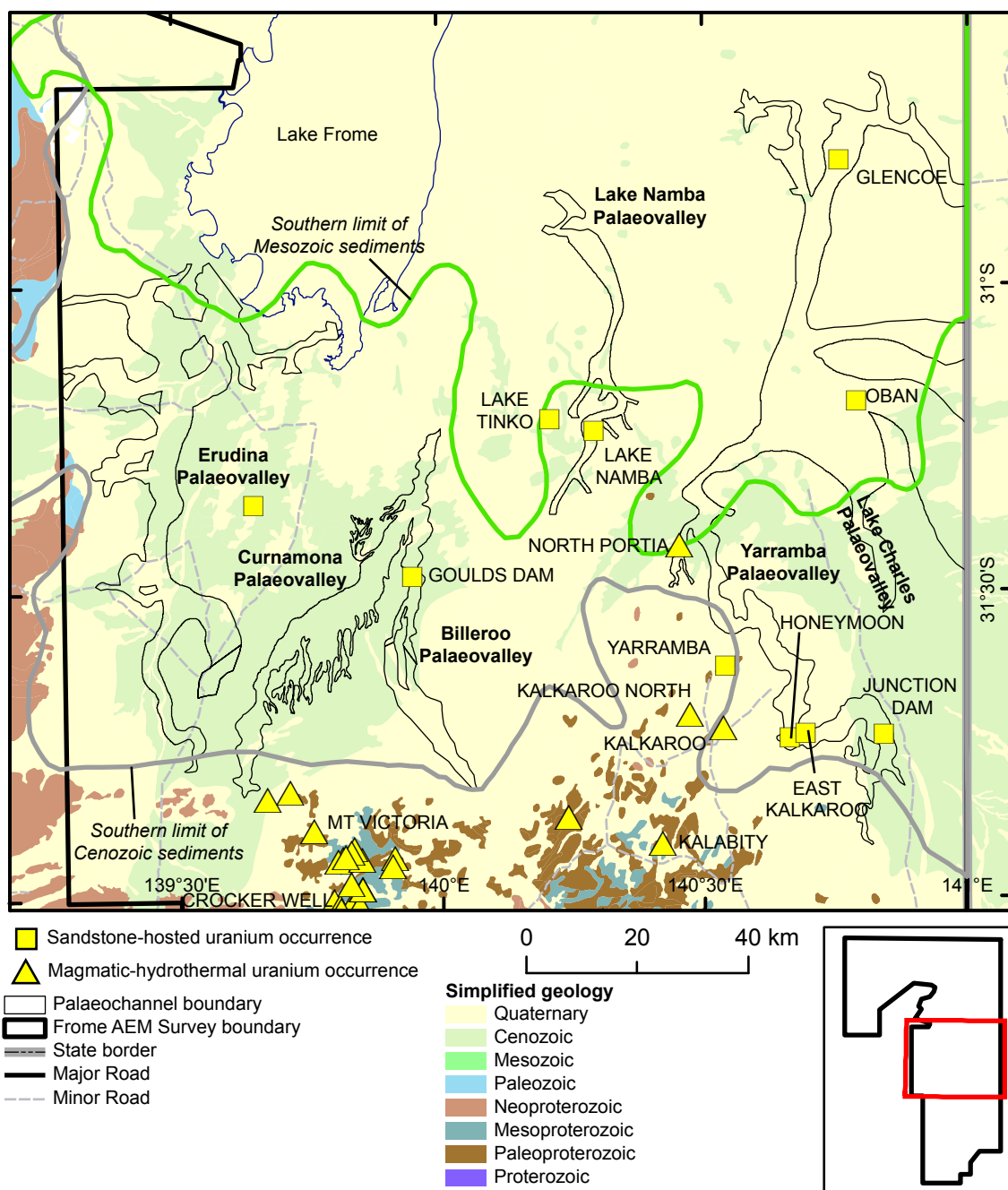


Figure 5.3.1: Location of the southern Callabonna Sub-basin and associated uranium deposits and prospects. Palaeovalley outlines are from version 1 of the South Australian Palaeovalley Map (Hou *et al.*, 2007b). Background: SRTM 9-second DEM.

5.3.3 Local geology: southwestern Callabonna Sub-basin

The stratigraphy of the Billeroo and adjacent Curnamona Palaeovalley system is best described at the Goulds Dam uranium deposit (Figure 5.3.1, Figure 5.3.2A) on the western side of the Benagerie Ridge (see Figure 3.3). Mineralisation at this location is within the lower Eyre Formation within a palaeovalley incised into Cambrian siltstones and sandstones of the Lake Frome Group, Arrowie Basin. The top of the Cambrian sequence is commonly between 110-150 m below the surface in the region (Fabris *et al.*, 2010). The Eyre Formation at Goulds Dam is typically 40 m thick and has informally been broken into three members, all of which contain fine to coarse-grained sands with

thin clay units. Only the lower member has significant organic matter and pyrite (Southern Cross Resources, 2000). This is overlain by 60-80 m of silty clays and thin sand lenses of the Namba Formation. Quaternary cover is typically 20 m thick and consists of sandy clays and aeolian sand spreads.

The base of the Eyre Formation along the western margin of the Callabonna Sub-basin is significantly deeper than it is around Goulds Dam and is covered by a greater thickness of Namba Formation and Willawortina Formation lying within the Poontana Trough (see [Section 5.5](#)). Drill logs commonly describe the Eyre Formation in this region as being dominated by clay to fine sand and lignite, which is not typical for a high-energy channel system as seen in other palaeovalleys in the southern Callabonna Sub-basin. This suggests that Paleogene deposition along this western margin was dominated by a floodplain environment with only minor channel development. The Namba Formation is typically > 80 m thick and the Quaternary sequence thickens dramatically towards the Flinders Ranges, where the Willawortina Formation may be greater than 50 m thick.

Conductance and conductivity images of the Billeroo Palaeovalley and Curnamona Palaeovalley ([Figure 5.3.2B](#)) show a variable depth of conductive cover, thickening at the palaeovalley axes, conforming to the Cenozoic sedimentary sequence. This overlies an undulating resistive basement surface, in this case Cambrian sediments of the Arrowie Basin. A relatively stronger conductance anomaly occurs in the Curnamona Palaeovalley (as compared to the Billeroo Palaeovalley) indicating that the valley may be more deeply incised into the underlying basement and has a slightly thicker Cenozoic sediment fill than the Billeroo Palaeovalley.

5.3.4 Local geology: southeastern Callabonna Sub-basin

Major palaeovalleys on the eastern side of the Benagerie Ridge include the Yarramba Palaeovalley (hosting the Honeymoon uranium deposit and the Junction Dam and East Kalkaroo uranium prospects), the Lake Charles Palaeovalley (hosting the Oban uranium prospect) and the Lake Namba palaeovalley ([Figure 5.3.1](#)). The bedrock that these channels incise is far more complex than that to the west of the Benagerie Ridge. The Yarramba palaeovalley incises Paleo-Mesoproterozoic Willyama Supergroup of the Mulyungarie Domain, the Lake Charles palaeovalley incises Mesozoic sediments, and the Lake Namba Palaeovalley incises a combination of Mesozoic, Cambrian, Neoproterozoic and Paleo-Mesoproterozoic Willyama Supergroup of the Mulyungarie Domain and Mudguard Domain (see [Figure 3.1, 3.5](#)). All of these bedrock types are commonly reduced and could act as potential uranium reductants. Cenozoic sedimentary cover is similar to that on the western side of the Benagerie Ridge. Uranium mineralisation has only been identified within the Eyre Formation, with the most significant example being the Honeymoon uranium deposit, although new results at the Junction Dam prospect, about 10 km east of the Honeymoon uranium mine, indicate an early resource of > 1500 t U₃O₈ (Marmota Energy Ltd, 2012). At Honeymoon, the uranium mineralisation is identified at the base of the Lower Eyre Formation ([Figure 5.3.3](#)).

Conductance and conductivity images of the Yarramba Palaeovalley ([Figure 5.3.3B](#)) show complex conductance within the region. Between Honeymoon, Oban and North Portia a roughly circular conductivity feature about 40 km in diameter occurs within the Willyama Supergroup of the Mulyungarie Domain. Other Proterozoic basement highs to the southwest are seen as resistive. The upper Yarramba Palaeovalley has a weak conductivity contrast with the surrounding rocks, and is best seen in the 80-100 m and 100-150 conductivity depth slices of the area.

The Frome airborne electromagnetic survey, South Australia: implications for energy, minerals and regional geology

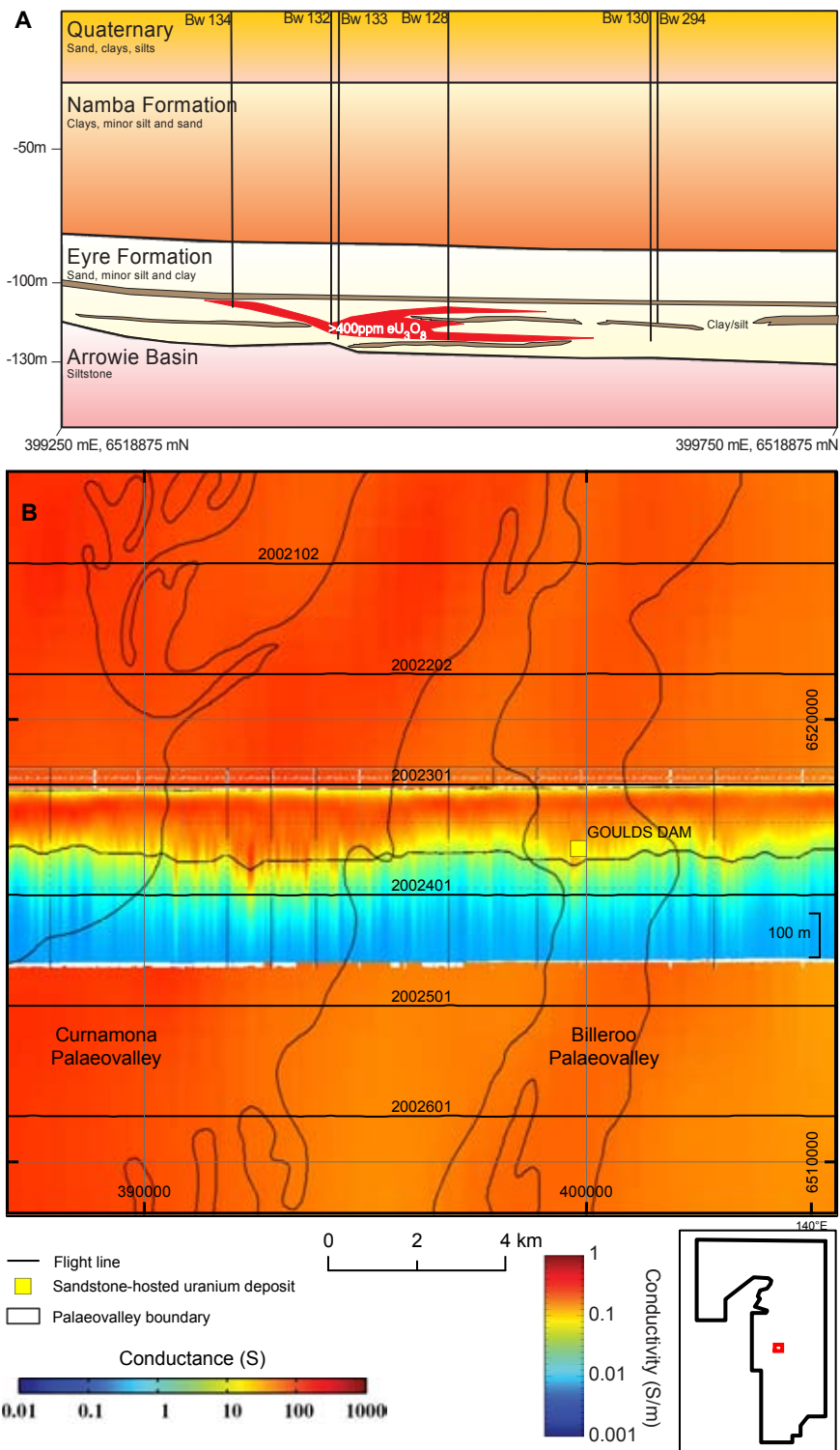


Figure 5.3.2: *A: Idealised cross-section of the Billeroo Palaeovalley showing the Goulds Dam uranium deposit. Actual location of the section is 1.5 km north of Goulds Dam along northing 6518875 mN. From Southern Cross Resources (2000). B: Airborne electromagnetic response through the Billeroo Palaeovalley near the Goulds Dam deposit, flight line 2002301. Background: 0-200 m conductance image; foreground: SBS GA-LEI conductivity section with a logarithmic colour stretch. Palaeovalley outlines are from Hou et al. (2007b).*

The Frome airborne electromagnetic survey, South Australia: implications for energy, minerals and regional geology

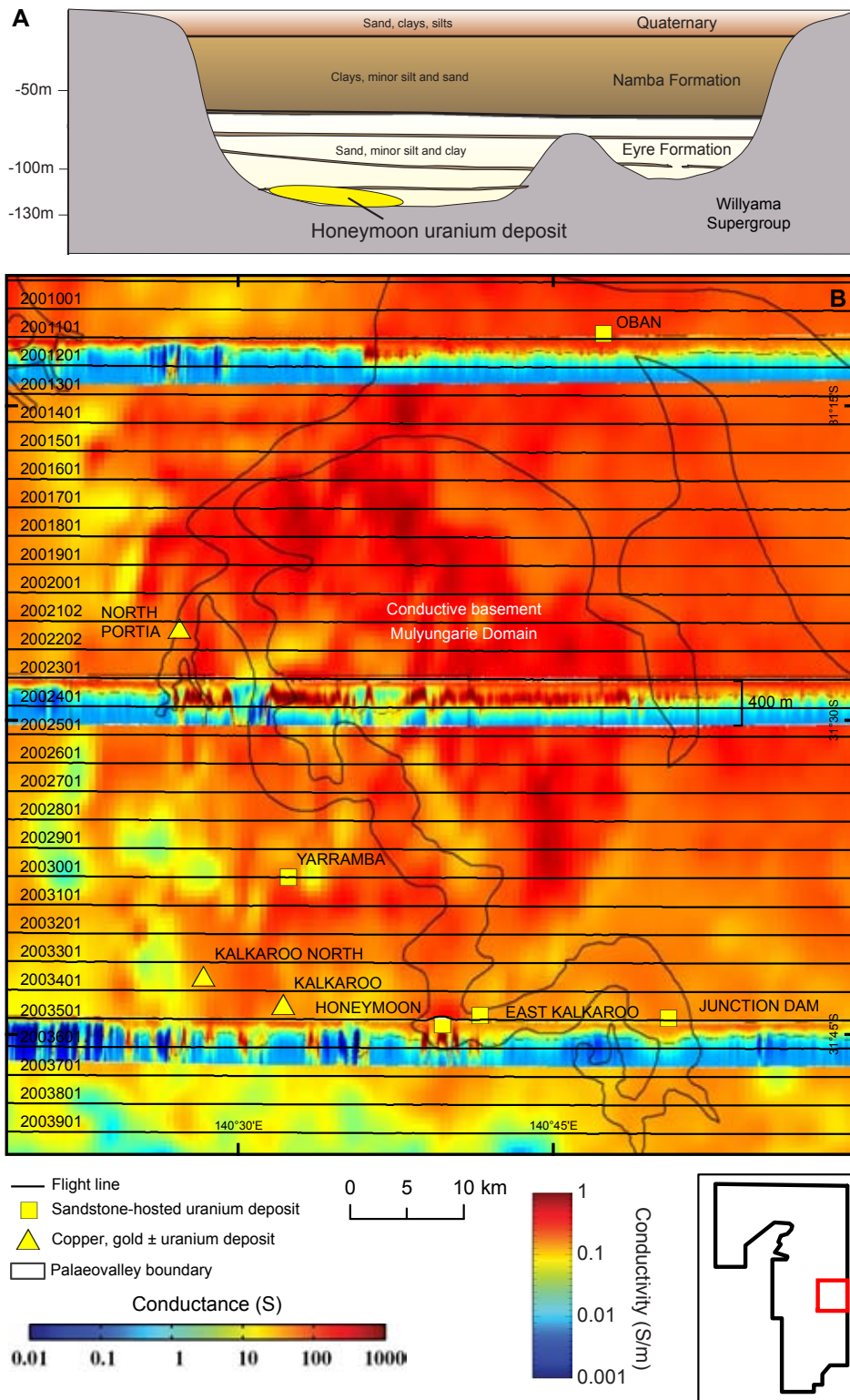


Figure 5.3.3: *A: Schematic cross-section through the Honeymoon deposit. The Willyama Supergroup forms the basement to the deposit and commonly occurs between 100 and 120 m below the surface. After Southern Cross Resources (2000). B: Airborne electromagnetic response of the Yarramba Palaeovalley. Background: 0-200 m conductance image; foreground: SBS GA-LEI conductivity sections with a logarithmic colour stretch. Palaeovalley outlines are from Hou et al. (2007b).*

Prior to the Frome AEM Survey, the boundaries of the Yarramba Palaeovalley had been constructed largely using drilling information. Undulations in the surface of the basement in drill hole stratigraphic data near Honeymoon-East Kalkaroo-Junction Dam reflect variation of relief and incision of the Yarramba Palaeovalley into the underlying Proterozoic basement. It is now possible to map these more comprehensively using the Frome AEM Survey data.

The Yarramba Palaeovalley is difficult to recognise over much of its length in the AEM images because of the conductive basement, apart from in its upper reaches in the south of [Figure 5.3.3B](#). The northern reaches of the Yarramba Palaeovalley where it merges with the Lake Charles Palaeovalley and the Beefsteak Palaeovalley are difficult to interpret solely using AEM because of the conductive basement, especially towards Oban where Mesozoic sediment of the relatively strongly electrically conductive Bulldog Shale underlies the Callabonna Sub-basin.

5.3.5 Methods

Interpretations of the Frome AEM Survey data are based on SBS GA-LEI depth slices, SBS GA-LEI conductivity sections, LBL GA-LEI conductivity sections, inversion multiplots, the depth to base of Cenozoic GOCAD™ surface generated from drill hole and seismic data (Fabris *et al.*, 2010), and several data layers from the DMITRE database (drill holes, palaeodrainage, modern drainage, water bodies, solid geology, surface geology and digital elevation model; available from SARIG). These data were used in ArcGIS™ and GOCAD™ projects, where the interpreted extents of the known palaeovalley systems, derived from detailed drill hole stratigraphy, were compared to the conductivity grids, sections and multiplots to observe any possible correlations, create empirical rules regarding these correlations and extrapolate these rules across the Frome AEM data set. These correlations were captured in ArcGIS™ maps and GOCAD™ models.

5.3.6 Results

An overview of the regional conductivity measured in the southern Callabonna Sub-basin can be gained using the 0-100 m and 0-200 m conductance images ([Figure 5.3.4A, B](#)). These show that basement rocks in the Olary Spur are generally resistive and that relatively shallowly-buried (<100 m thick cover) basement rocks of the Willyama Supergroup over the Benagerie Ridge are generally more resistive than surrounding covered areas, thereby effectively defining the extent of shallow basement. However, this relationship does not hold where basement rocks are conductive, such as the area of Willyama Supergroup in the Mulyungarie Domain between Honeymoon, Oban and North Portia where the basement is pelitic and contains graphitic rocks of the upper part of the Willyama Supergroup ([Figure 5.3.3](#)). These rocks are similarly shallowly-buried (<100 m thick cover), but form a prominent, highly conductive feature as visible in the 0-200 m conductance image ([Figures 5.3.3](#) and [5.3.4B](#)). A zone of high conductivity is also evident extending south of Lake Frome. This is discussed further in [Section 5.3.6.3](#).

The entire western margin of the southern Callabonna Sub-basin has relatively low conductivity, best seen in near-surface conductivity depth slices (e.g. [Figure 5.3.4C](#)). In detail, this zone can be subdivided into separate outwash fans of relatively fresh water, emanating from the Flinders Ranges, with much lower conductivity (lower salinity) than the sediments both further and deeper into the Sub-basin. The data therefore effectively maps freshwater influx into the Sub-basin and zones of mixing with more saline groundwater.

Some of the features relevant to palaeovalley mapping in the Frome AEM Survey dataset are described and discussed in the following sub-sections.

5.3.6.1 Palaeovalley systems

Palaeovalley systems within the southern Callabonna Sub-basin have previously been defined based on drilling, small industry AEM surveys and induced polarisation (IP) surveys. The depth to the top of the Eyre Formation (defined by the southern Callabonna Sub-basin model of Fabris *et al.*, 2010) varies between palaeovalleys:

The Frome airborne electromagnetic survey, South Australia: implications for energy, minerals and regional geology

- Typically from 130 m within the Erudina Palaeovalley;
- From 80 m within the Billeroo and Curnamona palaeovalleys;
- From 70 m within the Yarramba Palaeovalley;
- From 65 m in the Lake Charles Palaeovalley (Oban prospect); and,
- From 40 m within the Lake Namba Palaeovalley.

Where there are conductivity contrasts, the Eyre Formation can be located in conductivity depth slices as an anastomosing weak conductor over resistive basement, and in conductivity sections as conductivity anomalies at the base of Cenozoic cover, allowing us to reinterpret the courses of previously-mapped palaeovalleys, to add extensions to known palaeovalley systems and to map potential new palaeovalley systems using interpreted channel thalwegs (channel bottoms).

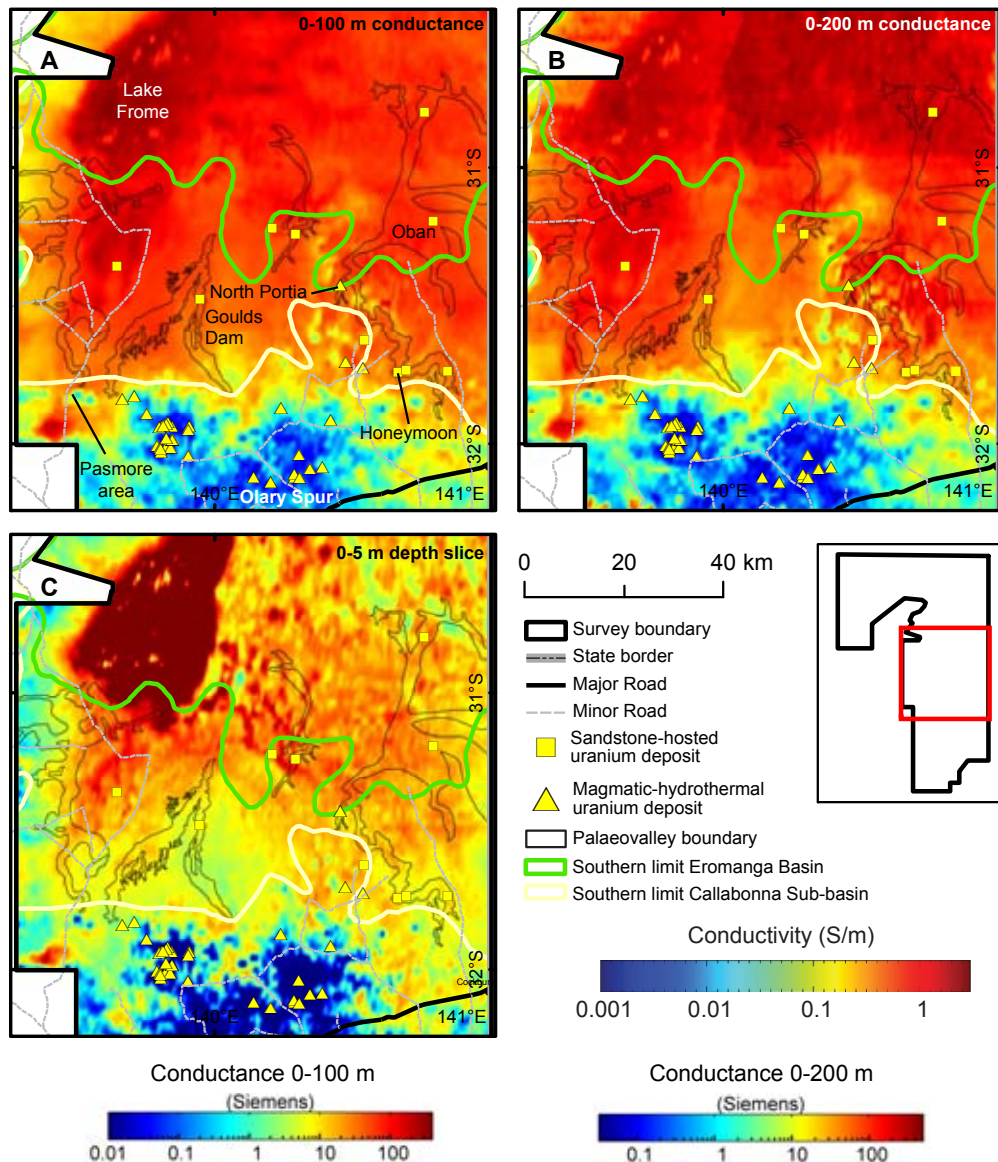


Figure 5.3.4: Airborne electromagnetic images of the southern Callabonna Sub-basin **A:** 0-100 m conductance image. **B:** 0-200 m conductance. **C:** 0-5 m conductivity depth slice image. The southern extents of the Eromanga Basin (green line) and Callabonna Sub-basin (cream line) are indicated. Palaeovalley outlines are from Hou et al. (2007b).

5.3.6.1.1 *Billeroo and Curnamona Palaeovalleys*

The Curnamona Palaeovalley and, perhaps more clearly the Billeroo Palaeovalley, have significant conductivity contrasts between the Eyre Formation and the underlying Cambrian and Neoproterozoic sedimentary basement that they incise. These palaeovalleys can most effectively be defined in the 0-200 m conductance image (Figure 5.3.2B, 5.3.4B) and the 100-150 m depth slice (Figure 5.3.5) as having locally high conductivity. They are also visible in the 80-100 m depth slice. An extension of a further 30 km to the north of the previously mapped extent of the Billeroo Palaeovalley is evident (Figure 5.3.5), and greater detail is available around the source region of the palaeovalley system in the Olary Spur (Figures 5.3.4-5.3.6).

Figure 5.3.6 illustrates the interpreted thalwegs and outlines of the known Eyre Formation in the Curnamona-Billeroo and Lake Namba palaeovalley systems, based on stratigraphic drill holes in the region. The conductivity anomalies associated with these palaeodrainage features also extend southwards towards the Olary Spur and are interpreted to involve the Namba Formation and perhaps the Quaternary sequence, which appears to have re-occupied the headwaters of the palaeodrainage systems as erosion occurs on the Olary Spur.

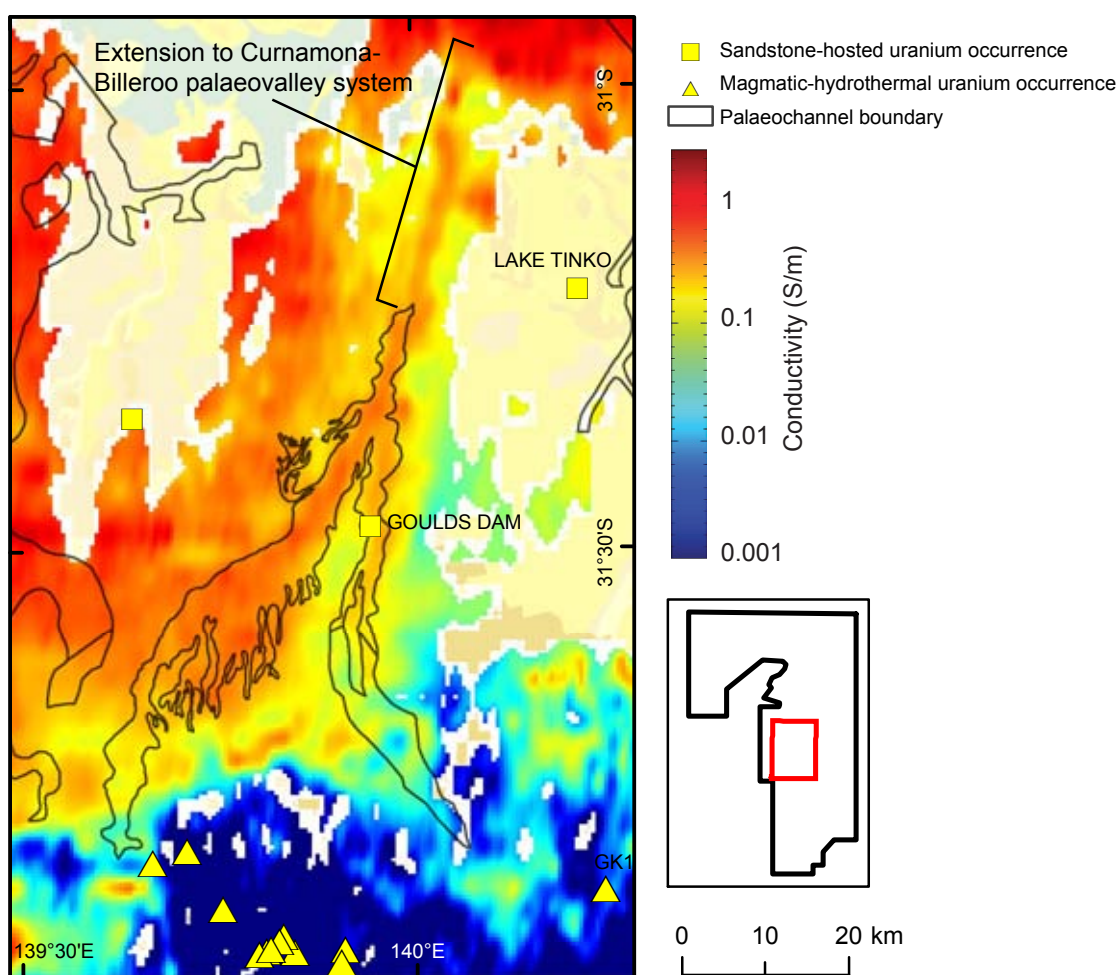


Figure 5.3.5: Conductivity depth slice for 100-150m depth can effectively be used to map the position of the Billeroo and Curnamona palaeovalleys. Palaeovalley outlines are from Hou et al. (2007b). The conductivity depth slice is transparent where the DOI occurs within the range of the depth slice (see section 4.5.7).

A new potential palaeodrainage feature is also outlined to the west of the Billeroo Palaeovalley (Figure 5.3.6). Due to very few drill holes in the region and the encroachment of a highly conductive zone (described in Section 5.3.6.3), that partly overlaps its western margin, it is not possible to confirm that this conductivity trend relates to Eocene palaeodrainage. However, the feature appears to lie at the same elevation as other conductivity features that are well correlated to known occurrences of the Eyre Formation in the known palaeovalley systems.

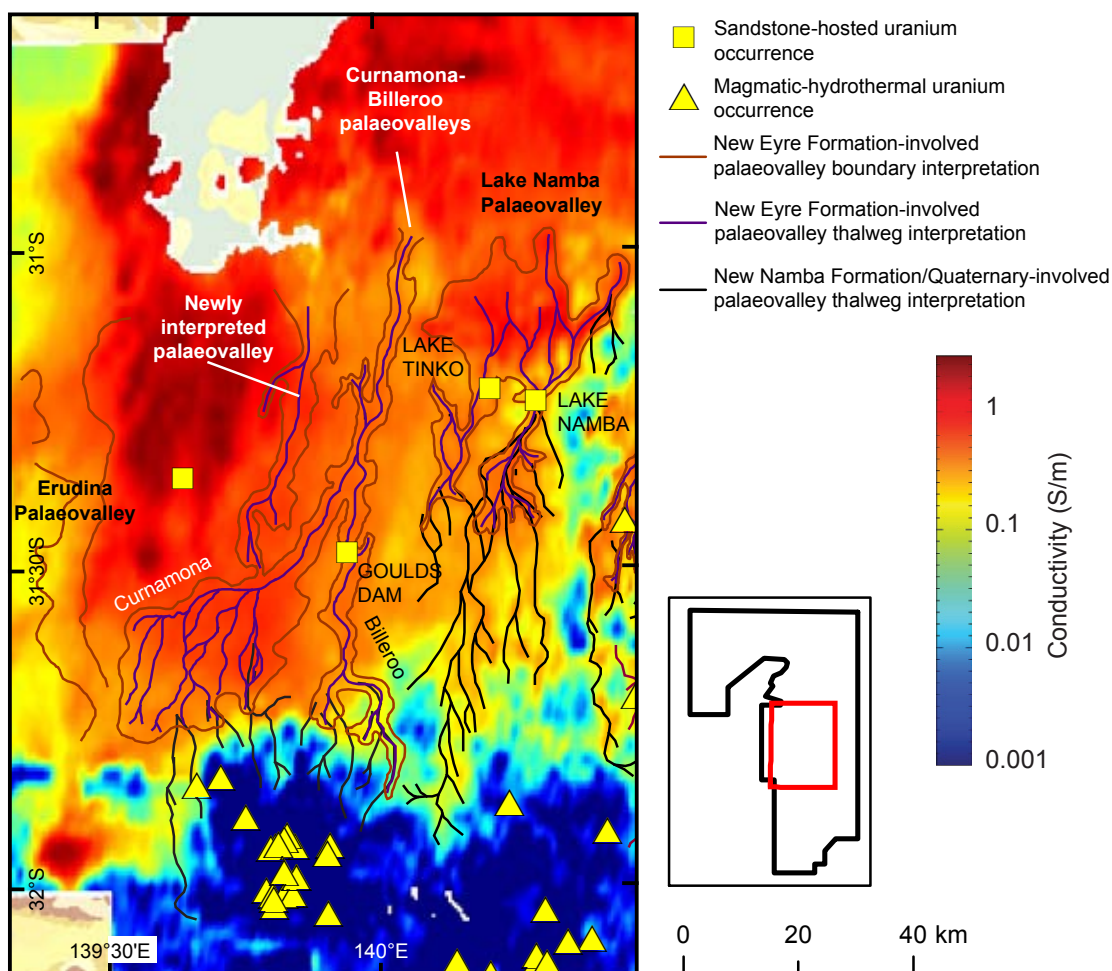


Figure 5.3.6: New interpretation of palaeovalley margins and thalwegs in the Curnamona-Billeroo-Lake Namba palaeovalley area with the 60-80 m conductivity depth slice as background. Palaeovalley boundaries depict the interpreted extent of the Eyre Formation from stratigraphic drilling information. The extent of the Namba Formation-involved palaeovalley thalwegs is interpreted from the Frome AEM Survey data.

5.3.6.1.2 Lake Namba Palaeovalley

The Lake Namba Palaeovalley is a drainage system developed on the Benagerie Ridge, which formed a basement high at the time of Eyre Formation deposition. It is the shallowest Eocene drainage system in the southern Callabonna Sub-basin. Basement geology to this drainage system varies considerably and includes Willyama Supergroup, Benagerie Volcanic Suite, Neoproterozoic and Cambrian metasediments and Cretaceous shales along its length. In spite of the varying 'basement' geology, palaeodrainage over the Benagerie Ridge can effectively be defined based on locally high conductivity anomalies using the 40-60 m, 60-80 m and 80-100 m depth slices and the 0-100 m and 0-200 m conductance images (Figure 5.3.4A, 5.3.4B, 5.3.6). Conductivity sections

outline the lowest-elevation parts of the channel system, although the system becomes more difficult to define and is eventually lost where the channels incise more highly conductive Cretaceous sediments of the Bulldog Shale.

A previously unrecognised drainage feature is evident about 10 km to the west of the upper Lake Namba Palaeovalley (Figure 5.3.6). This palaeodrainage feature merges with the Lake Namba Palaeovalley around Lake Tinko, where the combined system appears to flood out into an alluvial fan system.

5.3.6.1.3 Yarramba Palaeovalley

The Yarramba Palaeovalley was already reasonably well-defined by stratigraphic drilling and ground EM, but its extents can now be more accurately defined based on trends of locally high conductivity using conductivity depth slices from 80-100 m and 100-150 m and the 0-200 m conductance image (Figure 5.3.7). Extensions and corrections to the previously known channel boundaries are displayed in a new palaeovalley thalweg and boundary interpretation in Figure 5.3.7. Based on the Frome AEM Survey data, the upper reaches of the Yarramba Palaeovalley are interpreted to extend into New South Wales towards the Mundi Mundi Plain, which equates to an extension of approximately 20 km over its previously mapped length on the South Australian side of the border. Its course and extent in New South Wales is yet to be defined.

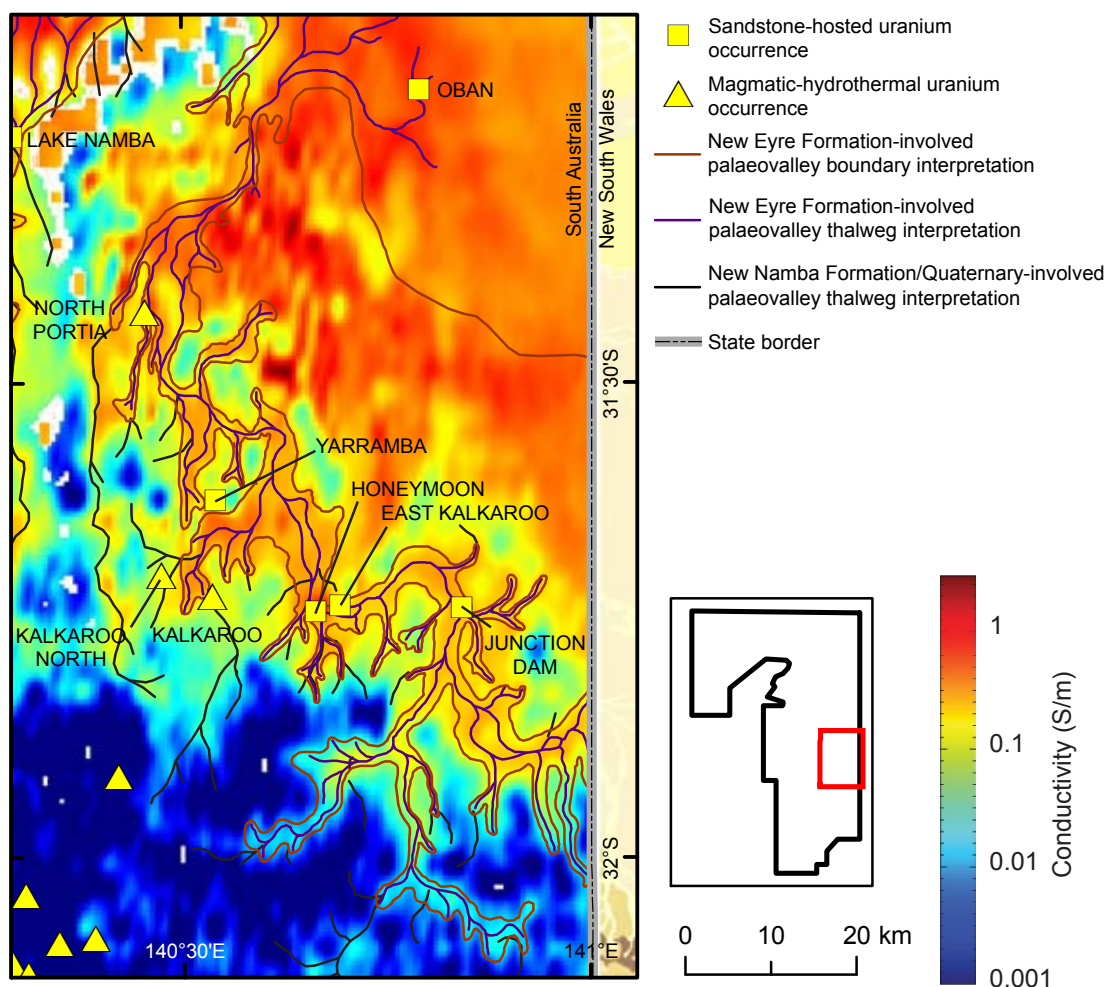


Figure 5.3.7: 80-100 m depth slice depicting the conductivity anomaly associated with the Yarramba Palaeovalley.

South of the North Portia deposit, the Yarramba Palaeovalley incises Willyama Supergroup metasediments which are less conductive than the Eyre Formation. Defining the palaeovalley becomes increasingly more difficult to the north of North Portia, where it incises the more highly conductive part of the Willyama Supergroup (Strathearn Group; see [Figure 3.4](#)). This is also true where the Yarramba Palaeovalley incises highly conductive Mesozoic Bulldog Shale in the Eromanga Basin along the northern reaches of the palaeovalley ([Figure 5.3.4A](#), [5.3.4B](#), [5.3.7](#)). Because of the lack of an adequate conductivity contrast between the Eyre Formation and the underlying Bulldog Shale, it has not been possible to define the previously interpreted Lake Carnanto and Yalkapo palaeovalleys, which were previously interpreted to feed into the Yarramba Palaeovalley, using the Frome AEM Survey data. Similarly, the previously mapped Lake Charles Palaeovalley, which is host to the Oban deposit, is difficult to differentiate in the Frome AEM data. Channel boundaries may be best defined using SBS GA-LEI conductivity sections. These outline shallower and narrower channels than interpreted within the Yarramba Palaeovalley. For simplicity, these palaeovalley systems have been included into a flood-out at the mouth of the Yarramba Palaeovalley near Oban, where the valley system may have emptied into a series of alluvial fans as a river delta.

Channel thalwegs, interpreted using conductivity sections combined with conductivity depth slices, map drainage into the main palaeovalley and highlight the presence of local sediment supply. Again, thalwegs mapped using conductivity are seen to join modern drainage systems and indicate that modern drainage is re-occupying palaeodrainage systems, and may be contributing saline water into the palaeodrainage systems.

5.3.6.1.4 Erudina Palaeovalley

The depth of investigation (DOI) along the western margin of the southern Callabonna Sub-basin is typically 150-200 m, up to 250 m in isolated areas (see [Figure 4.8](#)). While the Namba Formation-Eyre Formation boundary has been interpreted from drilling at between 130 to 150 m from the surface, the base of the Eyre Formation may be beyond the depth of investigation along much of the previously defined Palaeovalley. As a result, the Erudina Palaeovalley ([Figure 5.3.6](#)), previously interpreted from sparse drilling and geophysical data from small induced polarisation (IP) surveys, is not clearly defined within the Frome AEM Survey. It is likely that Eyre Formation deposition in this region is dominated by floodplain facies with only minor channel development, based on the limited stratigraphic drill hole information to hand. These smaller channel features are not defined by the Frome AEM dataset. The Erudina Palaeovalley, therefore, will remain poorly defined until such time as more detailed information becomes available.

Although unrelated to the mapping of the Erudina Palaeovalley, two prominent features in the LBL GA-LEI conductivity section data are seen in this region. These include a moderately conductive layer that dips gently to the west from the Benagerie Ridge high, and the top of a highly conductive zone at the base ([Figure 5.3.8](#)). Correlation from regional drilling suggests that the moderately conductive feature corresponds to the Willawortina Formation-Namba Formation contact or basal Namba Formation sands, and that the basal conductive layer is likely to represent the upper Eyre Formation. These features are indicative of sediment thickening that is typical along almost the entire length of the eastern Flinders Ranges from southwest of Lake Frome to Beverley (see [Section 5.4](#)). Relatively low conductivities in the Willawortina Formation and Namba Formation indicate that this area is likely to be charged with relatively fresh groundwater in comparison to water closer to Lake Frome.

The Willawortina Formation thickens towards the sediment source in the Flinders Ranges (west). The Namba Formation and the Eyre Formation dip gently to the west. Closer to the range front, the three units reverse their dip, and dip eastward, perhaps signifying drag folding on the eastern range front of the over-thrusting Flinders Ranges and the continued lowering of the Poontana Trough along the range front by neotectonic activity in the Flinders Ranges.

The Frome airborne electromagnetic survey, South Australia: implications for energy, minerals and regional geology

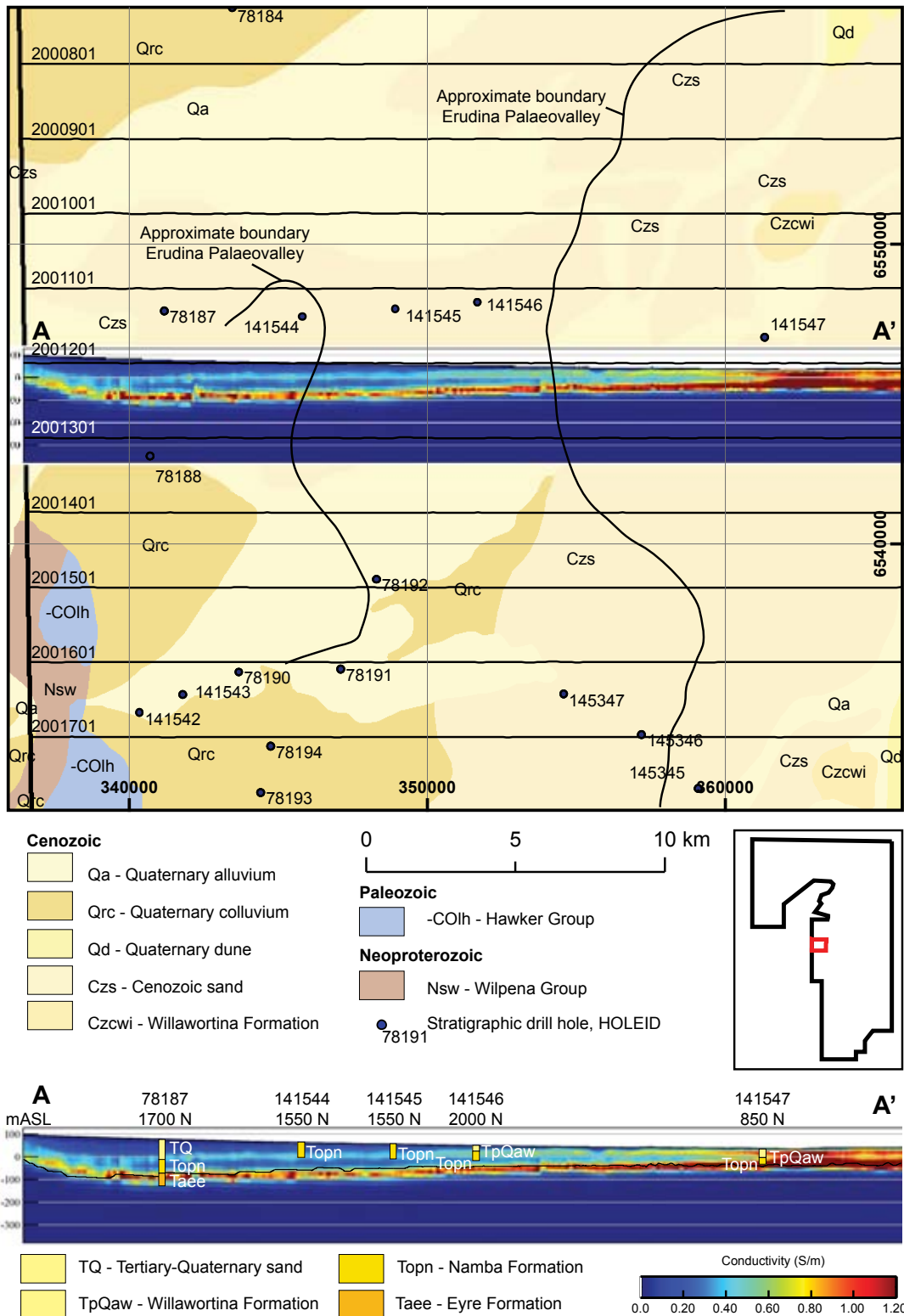


Figure 5.3.8: Linear colour-stretched LBL GA-LEI conductivity section (line 2001201) in the western Callabonna Sub-basin highlighting the thickening of the Willawortina Formation towards the Flinders Ranges in the west. Drill holes are labelled with their SARIG HOLEID number and distance from the flight line north (N) or south (S).

5.3.6.2 Detailed mapping of uranium deposits

Despite the regional nature of the Frome AEM Survey, and the relatively wide flight line spacing in the southern Callabonna Sub-basin area (2.5 km), it is possible to make detailed observations of palaeovalley morphology around uranium deposits over-flown by the Survey. Here we examine two of the larger deposits, Honeymoon and Goulds Dam.

5.3.6.2.1 The Honeymoon deposit

The Honeymoon deposit is located at a sharp bend in the Yarramba Palaeovalley. This is effectively imaged by the AEM data, particularly in the 100-150 m depth slice which includes the interval covered by the Eyre Formation in the base of the Palaeovalley. Despite the coarse pixel size of the gridded data (500 m cell size), several tributaries are also evident (Figure 5.3.9). This includes a tributary leading from the Honeymoon Granite (Fricke and Hore, 2010) that has previously been recognised in earlier, closer spaced industry TEMPEST™ AEM survey data (confidential reporting by Southern Cross Resources; Fricke and Reid, 2009). This may be responsible for supplying uranium-bearing groundwater from the weathering zone of the Honeymoon Granite to a suitable reductant in the Eyre Formation at Honeymoon.

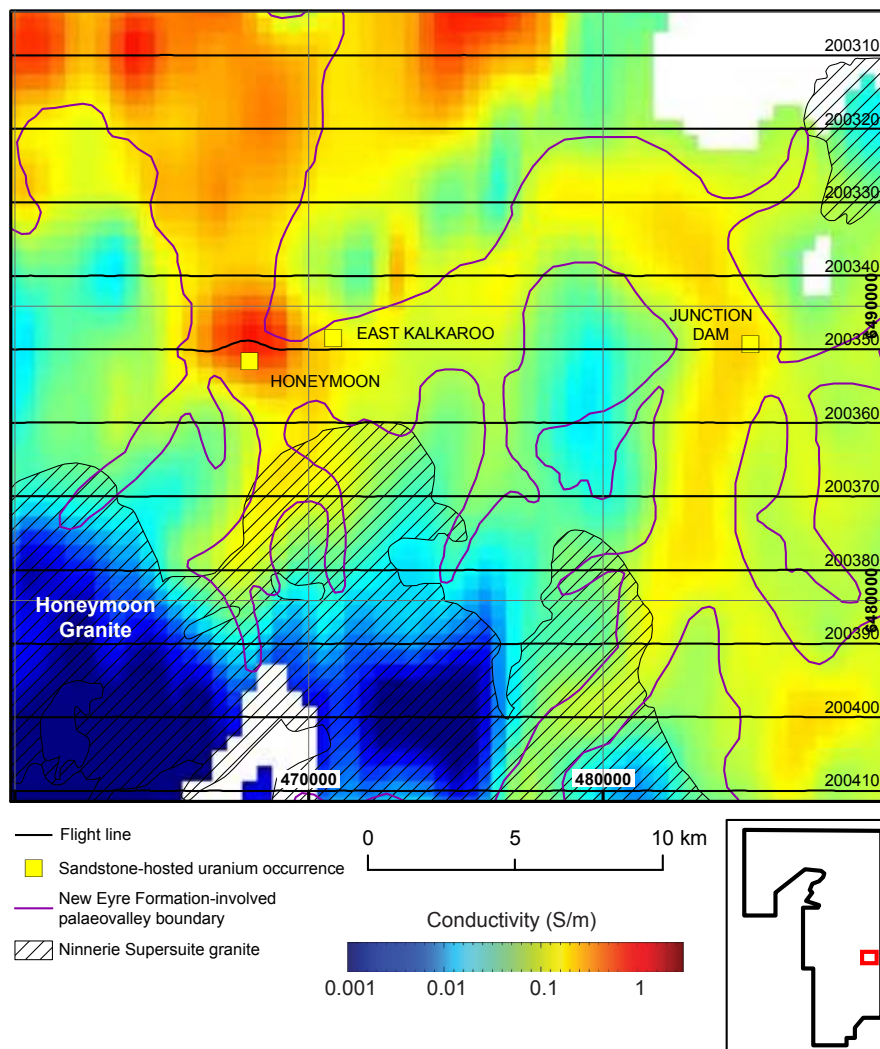


Figure 5.3.9: 100-150 m conductivity depth slice over the Honeymoon deposit. A tributary represented by a zone of high conductivity connects the Honeymoon Granite (resistive) with the Yarramba Palaeovalley and Honeymoon deposit. Granite boundary from SARIG.

The Honeymoon deposit appears to be located adjacent to a number of relatively highly conductive anomalies within the Yarramba Palaeovalley, as seen in Figure 5.3.10A. The conductivity section through the deposit (line 2003501) reveals several discrete, vertical, highly conductive areas in the SBS GA-LEI inversion data. Further checking of the data from the local area, in consultation with the multiplots of adjacent flight lines supplied with the data release, reveals these conductivity “anomalies” to be inversion artefacts caused by a change in the AEM system geometry as the aircraft turned to avoid the large tower at the Honeymoon processing plant (Figure 5.3.11). A comparison of the SBS GA-LEI data against the LBL GA-LEI data (Figure 5.3.10B) highlight the difference between the two inversions, and further illustrate the need to check the validity of “anomalies” within the data before drawing a geological conclusion. Palaeovalley thalweg interpretations detailed in earlier sections of this case study were checked using a similar process to ensure that they were not simply inversion artefacts.

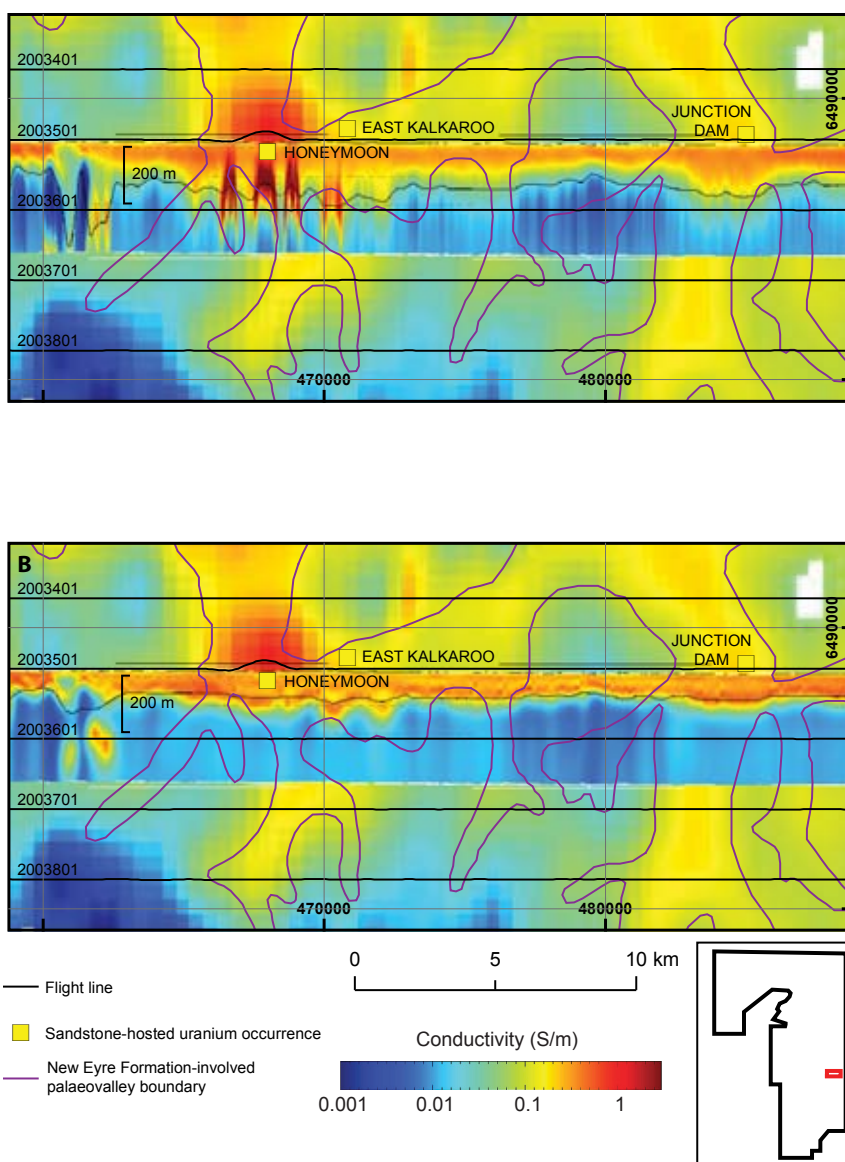


Figure 5.3.10: *A: SBS GA-LEI conductivity section for flight line 2003501 on the 100-150m conductivity depth slice, Honeymoon deposit. B: LBL GA-LEI conductivity section. Conductivity anomalies near the Honeymoon deposit in the SBS GA-LEI are not apparent in the LBL GA-LEI.*

The Namba Formation is imaged as a relatively weakly conductive layer throughout the Basin. In the Honeymoon region, significant variation in its thickness is evident (Figure 5.3.12). Facies variations in the Namba Formation are also noted within the data, especially in the linear colour stretched SBS-GA-LEI conductivity sections. In these the relative conductivity of the horizon correlated with the Namba Formation varies laterally, most likely caused by a change in the sand:clay ratio affecting porosity and permeability, signalled by a change in the bulk conductivity. The Namba Formation is noted to contain a variety of facies including sandy channels, clayey overbank deposits and alkaline lakes (Callen, 1977; Hill and Hore, 2012).

The Namba Formation is mapped as a shallow and laterally continuous moderate conductor in the SBS GA-LEI conductivity sections. Significant thinning occurs where Namba Formation laps onto basement highs around the Benagerie Ridge, especially evident near Honeymoon where the Proterozoic basement is resistive. Variations in the depth to the base of the Namba Formation are illustrated in Figures 5.3.10 and 5.3.11, where the moderate conductor of the Namba Formation overlies resistive basement of the Willyama Supergroup. It is not possible to separate the Namba Formation from the Eyre Formation in the logarithmic colour stretched SBS GA-LEI conductivity sections, but they may be differentiated in the linear colour stretched LBL GA-LEI conductivity sections, as illustrated in Figure 5.3.8.

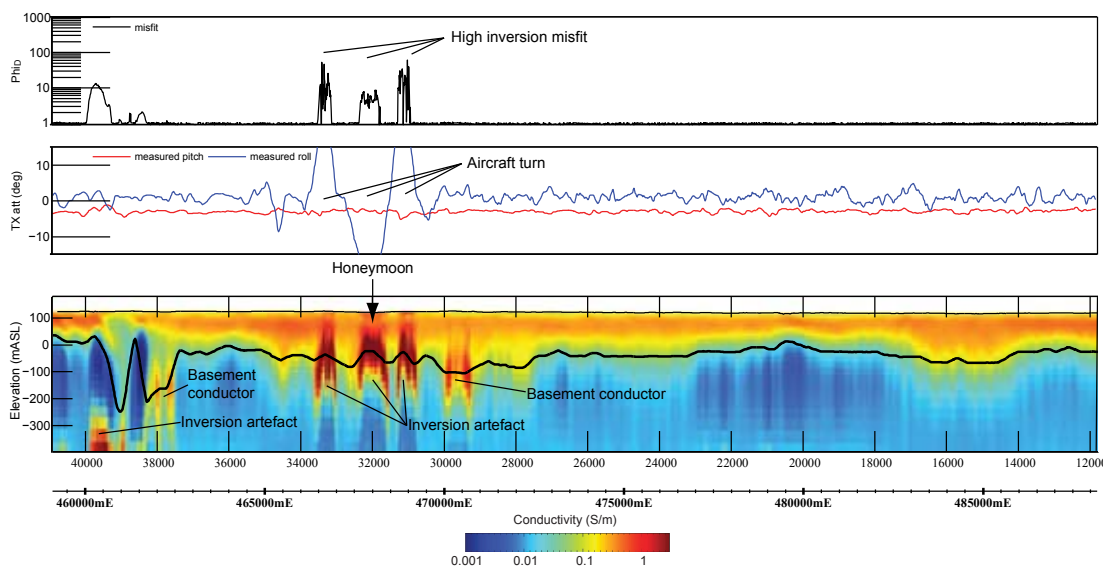


Figure 5.3.11: Subsection of the SBS GA-LEI multiplot for flight line 2003501 illustrating the effects of incorrect AEM system geometry (rapid changes in aircraft pitch and roll) on the SBS inversion. Rapid change in AEM system geometry results in high PhiD (inversion misfit) and creates artefacts in the inversion, seen in the conductivity section at bottom. The LBL inversion smooths over these artefacts (see Figure 5.3.10).

5.3.6.2.2 The Goulds Dam deposit

The Eyre Formation, which hosts uranium mineralisation at the Goulds Dam deposit, is relatively conductive compared to the basement rocks beneath the Billeroo Palaeovalley, in this case sediments of the Arrowie Basin. This contrast allows the boundaries of the Palaeovalley to be relatively easily defined. The overlying Namba Formation is represented by a flat lying, relatively moderately conductive layer that can be traced across many conductivity sections (Figure 5.3.12). The absolute conductivity difference between the Namba Formation and the Eyre Formation is difficult to determine in the logarithmic colour stretched SBS GA-LEI conductivity sections, however better differentiation is obtained using the linear colour stretched conductivity sections of either the SBS GA-LEI or the LBL GA-LEI (Figure 5.3.8, 5.3.12).

The orientation of the Billeroo Palaeovalley is controlled by the western edge of the Benagerie Ridge which is effectively mapped in the 80-100 m depth slice (not shown). Close observation of the 100-150 m depth slice shows that the deposit itself hugs the inside bend of a kink in the channel (Figure 5.3.12). A faint conductivity anomaly orientated NNE extending from the main channel is also evident. In line 2002301, this conductivity anomaly corresponds to a shallow channel feature.

Once the correlations between conductors and stratigraphy have been established in a local area (see Figure 5.3.8), the course of the Billeroo Palaeovalley becomes apparent in Figure 5.3.12 as concentrations of relatively strong conductors underneath a flat-lying, moderate conductor. The SBS inversion tends to smear conductivity anomalies vertically, but we are confident that the moderately strong conductors in the conductivity sections represent the basal Eyre Formation in the Billeroo Palaeovalley underneath the flat-lying Namba Formation that covers the area as a sheet.

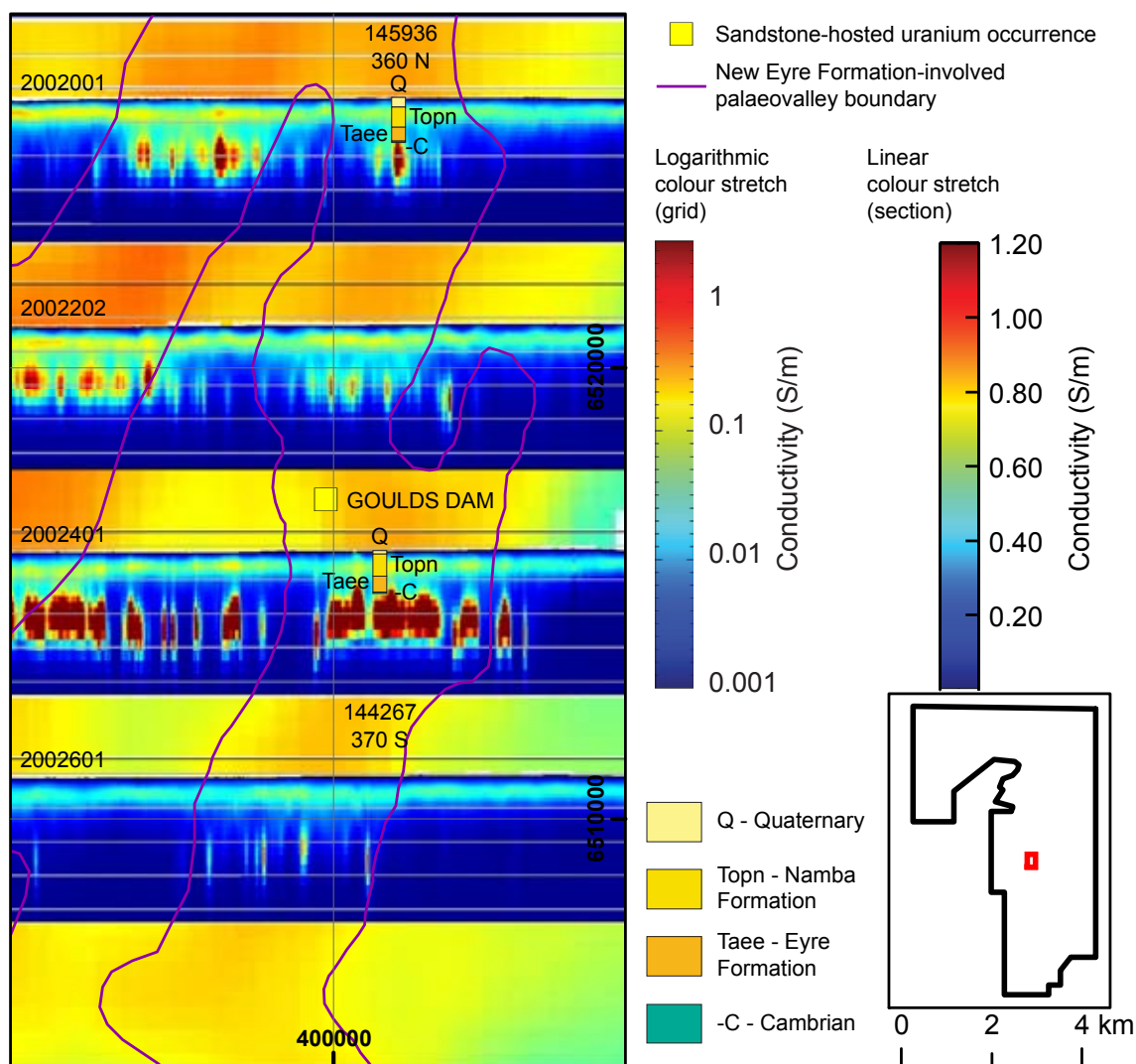


Figure 5.3.12: 100-150 m conductivity depth slice and linear colour stretched SBS GA-LEI conductivity sections, Goulds Dam deposit. The Goulds Dam deposit is situated at the inside bend of a kink in the channel and located close to the junction of a tributary with the Billeroo Palaeovalley. Selected drill holes show stratigraphy. Drill hole labels include the SARIG HOLEID number and distance from the flight line north (N) or south (S).

5.3.6.3 Drainage feature south of Lake Frome

A drainage feature that persists from the surface to about 80m depth is evident running south from the southern end of Lake Frome. The drainage system, as defined by very high relative conductivity, is sourced from the Erudina Station region and drains northwards, to Lake Frome. This zone of very high relative conductivity is evident from about 80 m to the surface, but is most clearly defined from the 20-30 m depth slice (Figure 5.3.13). Conductivity values are comparable with those in Lake Frome. This zone of high conductivity extends for up to 20 km in an east-west direction and is semicontinuous. This drainage feature shows a good correspondence with modern drainage and several small salt pans. This region encompasses the Pasmore River, which is known to have been a major river valley draining into Lake Frome in the mid-Pleistocene (Callen, 1990).

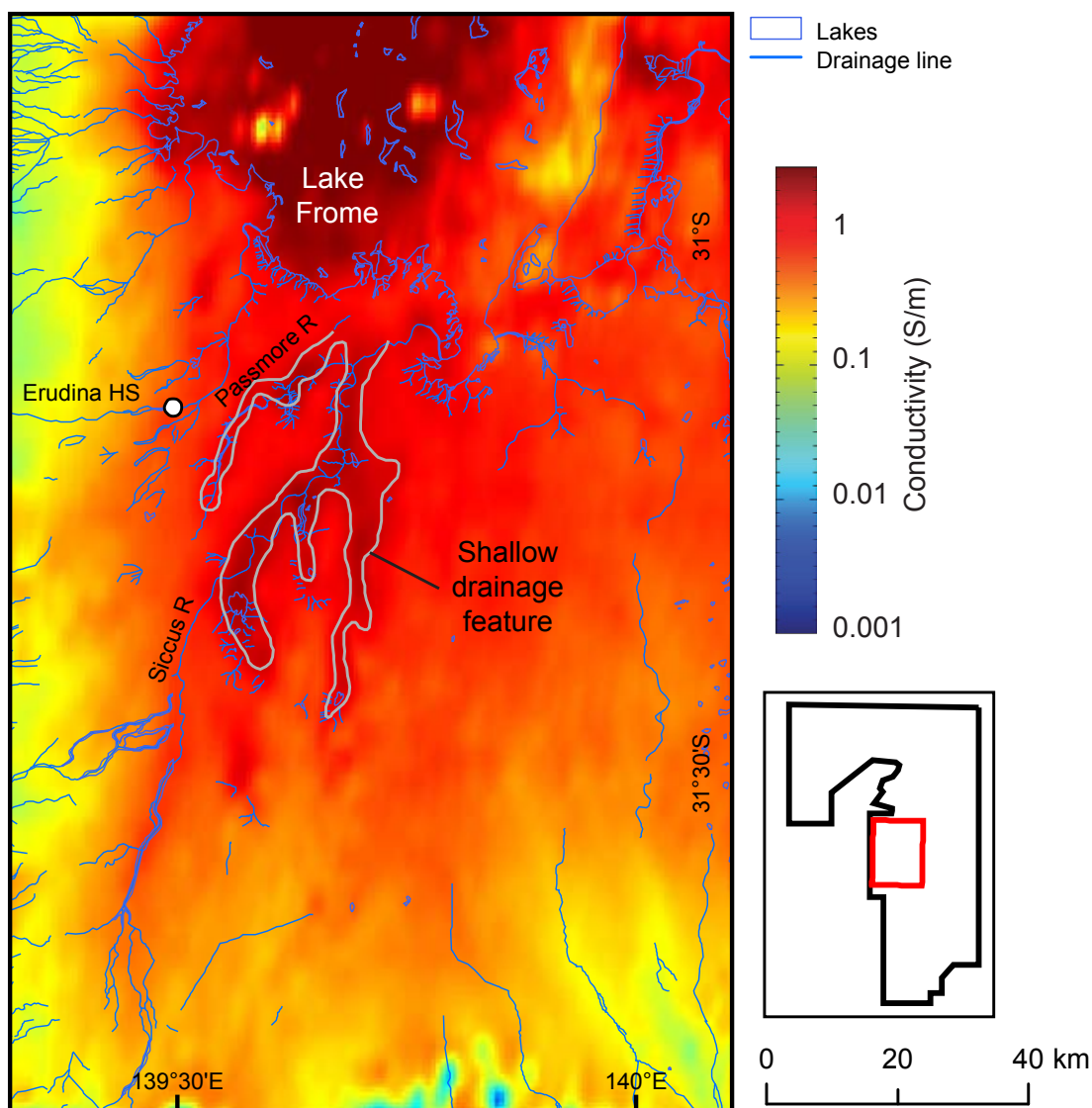


Figure 5.3.13: A zone of high conductivity defining a distinct drainage feature in the 20-30 m conductivity depth slice.

5.3.7 Discussion

Exploration for sedimentary uranium throughout the Callabonna Sub-basin has found that there are very few techniques other than AEM that can be used to image palaeovalley systems. This is largely

due to the shallow depth of the palaeovalleys, the dominance of clay within cover sequences affecting other geophysical techniques (e.g. IP, self potential), the lack of magnetic contrast of the palaeovalleys and their incision into underlying sedimentary basins rather than into highly contrasting basement rocks in all but the southeast of the region. For this reason, the Frome AEM Survey has valuable application to uranium exploration in the Curnamona region.

The majority of uranium exploration in the southern Callabonna Sub-basin has been for mineralisation hosted within large Eocene palaeovalley systems (Eyre Formation). The Frome AEM Survey data can be used to effectively map several of the known channel systems (Billeroo, Curnamona and Yarramba palaeovalleys) as well as enable mapping of extensions to these systems. In a few instances, known palaeodrainage could not be resolved; this highlights several important points to bear in mind when interpreting this dataset. Firstly, it is important to be aware of the DOI, which gives the local depth limitation on the inversion applied. While the existence of a major north-south draining palaeovalley, previously defined as the Erudina Palaeovalley is questionable (Figure 5.3.4, 5.3.6, 5.3.8), the base of the Eyre Formation along the western margin of the Callabonna Sub-basin has been identified by drilling to generally be greater than 180 m deep. This is close to the limits of the DOI for the technique in this area. Since drill hole logs do not support significant channel development as seen elsewhere in the Callabonna Sub-basin, there may be insufficient signal from material below any narrow and thin Eocene channel features to define their extent. Furthermore, the line spacing of the survey may be insufficient in this area. Secondly, geological interpretations are based on the premise that there will be a conductivity contrast between geological units. Within the Lake Charles Palaeovalley (Figure 5.3.1), Eocene channels incise Mesozoic sediments (Bulldog Shale) that are known regionally to be highly conductive. As a result, there is insufficient conductivity contrast to define channel boundaries, should they exist. It is therefore important to be aware of the geology of the Basin when interpreting possible palaeovalleys in the region.

The Billeroo Palaeovalley, hosting the Goulds Dam deposit, is clearly defined using the Frome AEM Survey data set. Exactly what controls the position of the Goulds Dam deposit is uncertain, however, some interesting observations can be made from close examination of the AEM data. The location of mineralisation is at the inside bend of a kink in the channel, similar to that noted at the Honeymoon deposit in the Yarramba Palaeovalley (Jaireth *et al.*, 2010). This represents a potential trap site for organic debris. The deposit is also very close to a previously unrecognised tributary into the channel. At the time of Eyre Formation deposition, this tributary would have drained Neoproterozoic metasediments on the Benagerie Ridge and may have influenced groundwater chemistry at the Goulds Dam deposit.

Airborne electromagnetics has previously been used in the definition of the Yarramba Palaeovalley and description of the geology around the Honeymoon deposit (Randell and Skidmore, 2003). Randell and Skidmore (2003) made the observation, in the vicinity of the Honeymoon deposit, that the Yarramba Palaeovalley follows a linear resistive body in a southwest direction before making a sharp turn to the northwest and then widening. Through correlation with other geophysical data sets, the resistive body that the channel follows can be correlated with a palaeo-ridge possibly of Strathearn Group (Willyama Supergroup), with the deposit occurring in the position where the channel has eroded its way through the rock bar. Further to this, the basement geology which the valley incises at this location includes the sulfidic Bimba Formation and graphitic Plumbago Formation. The Honeymoon deposit marks the position in which the basement stratigraphy goes from being oxidised to reduced and commonly graphitic. The AEM conductivity section through the deposit shows strong conductors within the basement. Some of these features have been shown to be artefacts that result from deviation in the flight path to avoid the towers at the Honeymoon site and resultant shift in the AEM system geometry. Conductors in adjacent lines, however, likely reflect real basement conductors and could relate to graphitic and/or sulfidic units. These may play a role in the reduction of uranium at Honeymoon. Of additional interest are numerous tributaries that can be mapped using the Frome AEM Survey depth slices. These provide avenues for uranium-bearing

fluid mixing and a local source of detritus and organic debris. Randell and Skidmore (2003) linked a tributary mapped using earlier AEM, close to the position of the deposit, to a uranium-bearing granite (The Honeymoon Granite, part of the Ninnerie Supersuite) and suggested that it was the likely uranium source for the deposit. This same correlation is evident in the Frome AEM Survey data. The Frome AEM Survey provides valuable regional context in the Honeymoon region and, together with other geophysical data, helps unravel the complex geology and build models to explain the mode of mineralisation. These key ingredients should be applied elsewhere in the region.

While Eocene palaeodrainage is readily mapped using the Frome AEM Survey data set in the southern Callabonna Sub-basin, Miocene palaeodrainage is not obvious. This is a function of the generally high salinity of the Namba Formation, and that channel sediments within the Namba Formation rarely exceed a few metres thickness in the southern Callabonna Sub-basin. It is therefore of particular interest that just south of Lake Frome, a conductivity anomaly that resembles a drainage feature, most obvious in the 20-30 m depth slice, is evident at the depth of the Namba Formation sediments (to 80 m deep).

There are a number of important observations that are relevant to the interpretation of this feature.

1. The conductivity anomaly occurs from the surface to include Quaternary sediments, and is not just within the Namba Formation;
2. In conductivity sections, the zone of very high conductivity is not confined to channel structures;
3. The conductivity anomaly is over 50 m thick, which is far beyond what is reasonable for sand thickness within the Namba Formation;
4. There is a very good correlation between the location of modern drainage, salt pans, and the conductivity anomaly; and,
5. Conductivity values exceed those of channel sediments in the Eyre Formation and are comparable to values within saline lakes such as Lake Frome.

The combination of these observations suggests that it is unlikely that this conductivity anomaly relates to Miocene drainage. Rather, it is likely that this drainage feature is associated with Quaternary to modern drainage. Callen (1990) described a mid-Pleistocene river system that drained into Lake Frome in this region (Pasmore River area). The drainage is sourced from the western Olary Spur. Modern drainage patterns suggest that very little runoff from the Olary Spur reaches Lake Frome. Instead, solutes concentrate in low lying areas such as within drainage features and local salt pans. The conductivity of the drainage features seen in depth slices is extremely high (approaching 1 S/m) and because of this, it is probable that the signal from the TEMPEST™ system has resonated within these shallow and highly conductive features, and this ‘ringing’ has produced a geophysical artefact at depth. As such, the interpretation of the AEM data below these shallow features is of questionable value.

5.3.8 Conclusion

Airborne electromagnetics has historically been a key exploration technique for sandstone-hosted uranium within the Callabonna Sub-basin. The Frome AEM Survey has provided continuous EM coverage over the Curnamona region and is available for public use. For the first time, this enables entire palaeovalley systems to be mapped at medium to coarse resolution. While uranium mineralisation does not have a distinctive conductance signature, channel sands which host a deposit often contain saline groundwater which makes them relatively conductive and they will often have a conductivity contrast with surrounding basement rocks. Airborne electromagnetic data can effectively be used to define the base of the Billeroo, Curnamona and Yarramba palaeovalleys in conductivity sections, and their extent using the 100-150 m depth slice. Several new palaeodrainage features have been defined as a result of the Frome AEM Survey and significant extensions and refinements to known palaeovalleys have been possible.

Both the Goulds Dam and Honeymoon deposits lie at bends in channels and are located close to tributaries. These features are only obvious in the Frome AEM Survey data set and provide potential ingredients for exploration in this region and assessment of the Frome AEM Survey data and industry AEM data elsewhere.

5.3.9 References

- Benbow, M. C., Alley, N. F., Callen, R. A. and Greenwood, D. R., 1995. Geological history and palaeoclimate. In: Drexel, J. F. and Preiss, W. V. (editors), *The Geology of South Australia. Volume 2: The Phanerozoic*. South Australia Geological Survey, Adelaide. **Bulletin 54**, 208-218 p.
- Callen, R. A., 1977. Late Cainozoic environments of part of northeastern South Australia. *Journal of the Geological Society of Australia* **24(3)**, 151-169.
- Callen, R. A., 1990. 1:250 000 Series—Explanatory Notes, CURNAMONA, South Australia, Sheet SH/54-14 International index. Department of Mines and Energy South Australia, Geological Survey of South Australia, Adelaide, 56 pp.
- Callen, R. A., Alley, N. F. and Greenwood, D. R., 1995. Lake Eyre Basin. In: Drexel, J. F. and Preiss, W. V. (editors), *The geology of South Australia. Volume 2: The Phanerozoic*. South Australia Geological Survey, Adelaide. **Bulletin 54**, 188-194 p.
- Callen, R. A. and Tedford, R. H., 1976. New Late Cainozoic rock units and depositional environments, Lake Frome area, South Australia. *Transactions of the Royal Society of South Australia* **100(3)**, 125-167.
- Fabris, A. J., 2004. Uranium prospects of the Southern Curnamona Province and cover sequences, South Australia. Department of Primary Industries and Resources, Adelaide. **Report Book 2004/22**.
- Fabris, A. J., Gouthas, G. and Fairclough, M. C., 2010. The new 3D sedimentary basin model of the Curnamona Province: geological overview and exploration implications. *MESA Journal* **58(September 2010)**, 16-24.
- Fricke, C., 2008. Definitions of Mesoproterozoic igneous rocks of the Curnamona Province: The Ninnerie Supersuite. Primary Industries and Resources South Australia, Adelaide. **Report Book 2008/4**, 86 pp.
- Fricke, C. and Reid, A., 2009. Alteration of uranium-rich granite and its relationship to uranium mineralisation in the Honeymoon area, South Australia. Department of Primary Industries and Resources South Australia, Adelaide, **Report Book 2009/4**, 19 pp.
- Fricke, C. E. and Hore, S., 2010. Definition of the Mesoproterozoic Ninnerie Supersuite, Curnamona Province, South Australia. Department of Primary Industries and Resources South Australia, Adelaide. **Report Book 2010/20**, 55 pp.
- Hill, S. M. and Hore, S. B., 2012. Key insights into range-front mineral system expression and evolution from regolith and long-term landscape history, NE Flinders Ranges. *MESA Journal* **63**, 20-31.
- Hou, B., Fabris, A. J., Keeling, J. L. and Fairclough, M. C., 2007a. Cainozoic palaeochannel-hosted uranium and current exploration methods, South Australia. *MESA Journal* **46**, 34-39.
- Hou, B., Zang, W., Fabris, A., Keeling, J., Stoian, L. and Fairclough, M., 2007b. Palaeodrainage and coastal barriers of South Australia 1:2 000 000. CRC LEME, Geological Survey Branch, Primary Industries and Resources South Australia, Adelaide. Online: http://www.pir.sa.gov.au/__data/assets/pdf_file/0005/41486/palaeochannels_sa_map.pdf.
- Jaireth, S., Clarke, J. and Cross, A., 2010. Exploring for sandstone-hosted uranium deposits in paleovalleys and paleochannels. *AusGeo News* **97**, 21-25.
- Marmota Energy Ltd, 2012. Marmota Energy ASX Release: Assay results show higher true grades >8,000 ppm U₃O₈ for Marmota's uranium project adjacent Honeymoon U mine. Online: http://www.marmotaenergy.com.au/site/investors/asx-announcements/doc_view/200-assay-results-received-for-junction-dam.html.
- Randell, M. H. and Skidmore, C. P., 2003. Tertiary uranium exploration - New developments in palaeochannel definition and deposit evaluation. In: Peljo, M. (editor), Broken Hill Exploration Initiative. Abstracts from the July 2003 Conference. Geoscience Australia. **Record 2003/13**.
- Southern Cross Resources, 2000. Honeymoon Uranium Project - draft environmental impact statement. Southern Cross Resources Australia Pty Ltd. **Unpublished**.

5.4 MAPPING PALAEOVALLEY SYSTEMS: MACDONNELL CREEK AND NORTHERN FLINDERS RANGES AREA

I. C. Roach and S. Jaireth

5.4.1 Introduction

Cauldron Energy Ltd's (Cauldron's) Marree Joint Venture uranium project is located in the Blanchewater area, straddling the Strzelecki Track on the flanks of the northern Flinders Ranges (Figure 5.4.1). Recent exploration by the company has identified a number of uranium targets in the area associated with Cauldron's 'Blanchewater Palaeochannel', including the promising MacDonnell Creek uranium target (Figure 5.4.2). No resource estimations are available, because work is still preliminary, but good intersections of uranium mineralisation have been obtained from a number of drill holes in the area (Cauldron Energy Ltd, 2011a; c). This case study describes the Blanchewater area as it appears within the Frome AEM survey dataset, and discusses the implications of the dataset for future uranium investigations within the wider northern Flinders Ranges flank region.

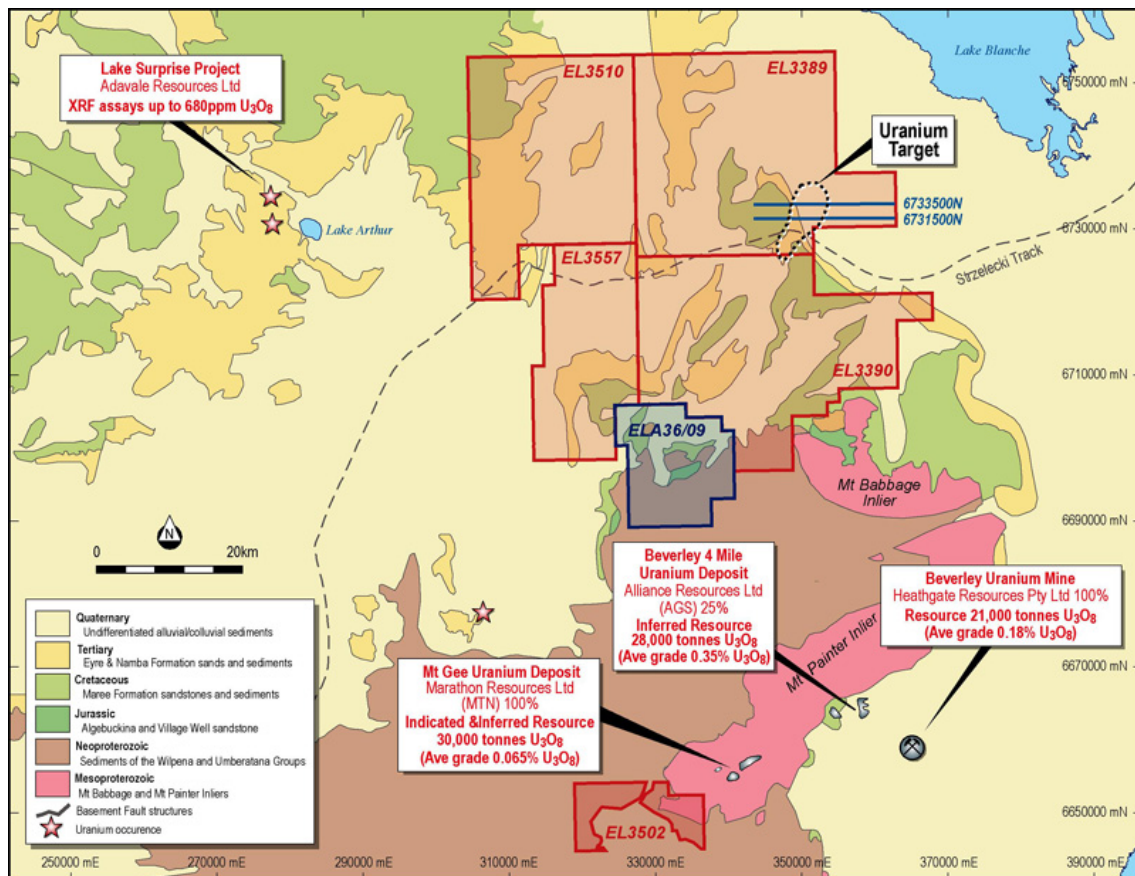


Figure 5.4.1: Location of Cauldron's Marree uranium project in relationship to other uranium deposits in the Lake Eyre Basin and northern Callabonna Sub-basin. From Cauldron Energy Ltd (2012).

5.4.2 Geology and geomorphology

The geology of the Blanchewater Palaeovalley site is complex; the site includes an up-thrown fault block of Mesozoic Marree Subgroup sediments which was incised and filled with Cenozoic Eyre Formation (Figure 5.4.2). Namba Formation sediments, should they have been deposited in this area, have now been stripped by post-tectonic erosion. On the down-thrown side, the Eyre Formation is covered by Namba Formation. A regional northward tilt from the northern Flinders Ranges further

complicates the geology, with Marree Subgroup exposed around the flanks of the Flinders Ranges gradually being covered by increasing thicknesses of Cenozoic sediment (Figure 5.4.1). Cauldron regards uranium mineralisation as being analogous to the Beverley-Four Mile uranium deposits, with mineralisation located in the Eyre Formation under a cap of Namba Formation (Cauldron Energy Ltd, 2011a). Drilling results indicate that Eyre Formation sediments on the southwest side of the fault are variably oxidised or reduced, but those on the northeastern side are entirely reduced, at the MacDonnell Creek uranium prospect (Figure 5.4.3).

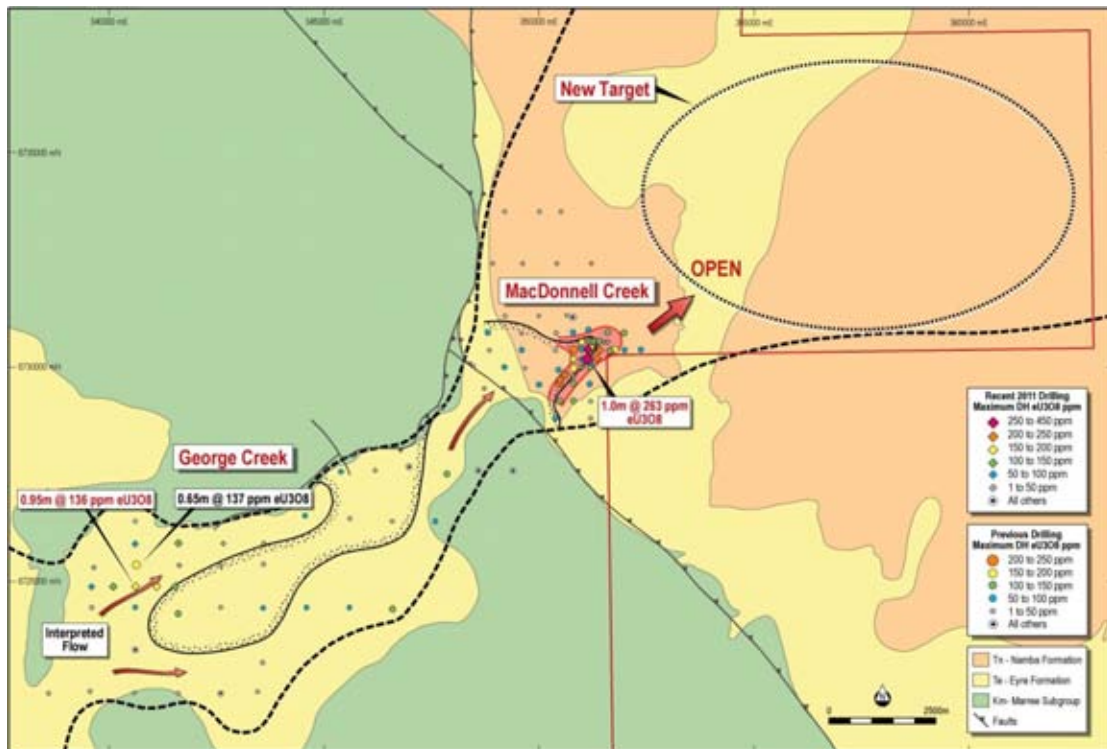


Figure 5.4.2: Local geology of the Blanchewater Palaeochannel-MacDonnell Creek area, Marree uranium project. This site is indicated as “Uranium Target” in Figure 5.1. From Cauldron Energy Ltd (2011b).

The site is in rolling country on the northern flanks of the northern Flinders Ranges. There is a low angle regional slope from the southwest to the northeast, with prominent ephemeral drainage channels draining from the northern Flinders Ranges into Lake Blanche further to the northeast. Incision along the channels exposes the Marree Subgroup and Eyre Formation in the MacDonnell Creek and George Creek systems. The Marree Subgroup and the Eyre Formation form prominent buttes and mesas, which have armoured, indurated top surfaces of groundwater silcrete and ferricrete.

Lithological and stratigraphic information of sub-surface geology comes from a series of publicly-available stratigraphic and mineral drill holes available through SARIG, as well as drill hole lithology and stratigraphy published in Cauldron’s company announcements.

5.4.3 AEM investigations

Cauldron obtained its own high-resolution AEM data using the RepTEM™ AEM system, which allowed the company to make interpretations of the morphology of the Blanchewater Palaeochannel due to conductivity differences between the Eyre Formation fill and the surrounding and underlying Marree Subgroup (Figure 5.4.4). These data have guided the exploration effort, by highlighting the location of Cenozoic sediments and major fault systems within the area that may have affected the location of uranium mineralisation.

The site is ideal for using AEM as part of an exploration strategy because, unlike in the southern Callabonna Sub-basin, it features relatively weakly to moderately conductive sediments of the Namba Formation (~300 mS/m) and the Eyre Formation (~200-500 mS/m) overlying a strong conductor in the Marree Subgroup (~1000 mS/m). This allows the interfaces between the Cenozoic and Mesozoic sedimentary units, and possibly intra-Cenozoic interfaces, to be mapped relatively easily, provided adequate drill hole control is available. Also, the site is in a relatively elevated position on the footslopes of the Flinders Ranges and groundwater, which is a major control on bulk conductivity, appears to be brackish rather than saline or hyper-saline, as it is further to the north in the creek systems and shorelines nearer Lake Blanche. This has a major effect on the ability of an AEM system to penetrate deeply enough, and resolve sufficient detail, to allow accurate mapping.

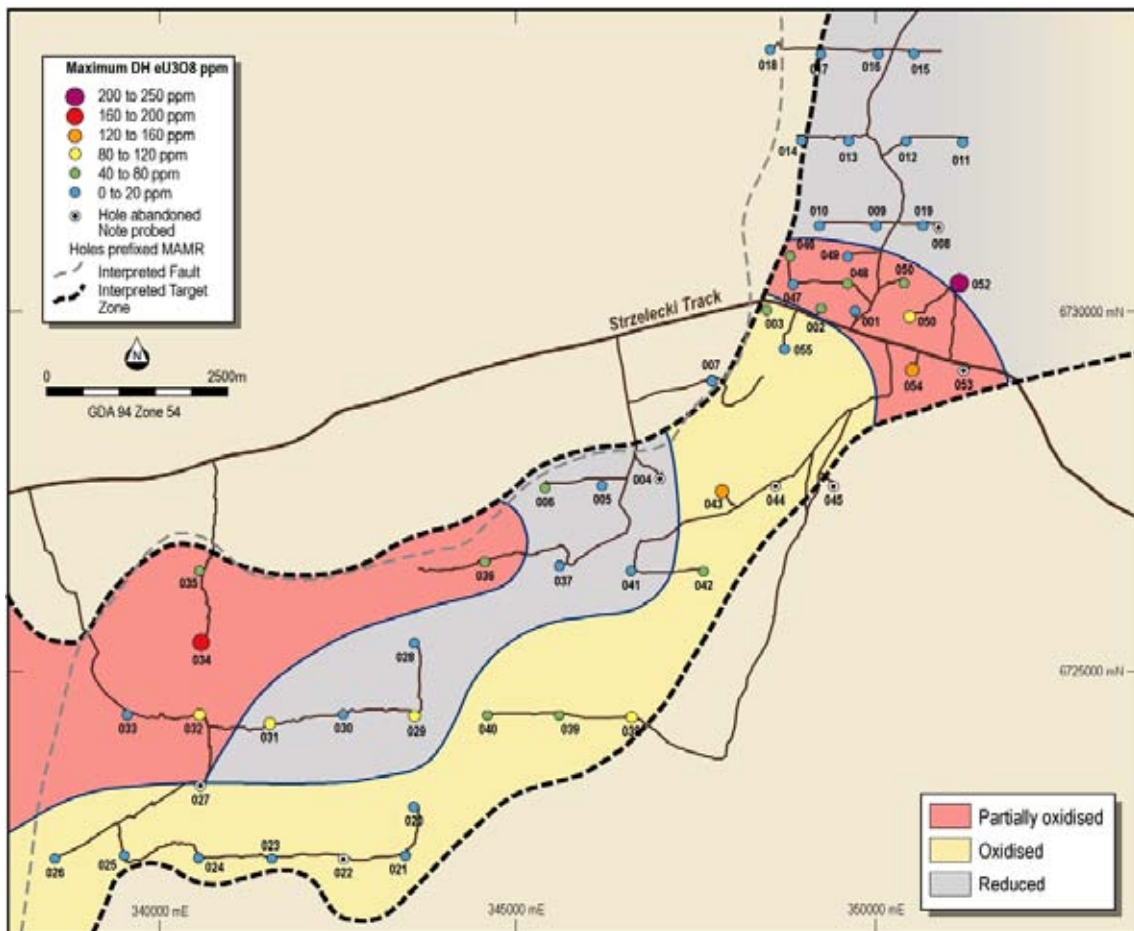


Figure 5.4.3: Redox conditions of Eyre Formation sediments in the Blanchewater Palaeochannel. From Cauldron Energy Ltd (2009).

5.4.4 Methods

Over the Marree uranium project area, the Frome AEM survey was flown mainly at 2.5 km line spacing, with 5 km line spacing data covering the far north towards Lake Blanche and the west towards Marree (Figure 5.4.5). The Frome AEM survey data were inverted using two separate algorithms to create two different inversion products, a sample-by-sample (SBS) Geoscience Australia Layered Earth Inversion (GA-LEI) product and a line-by-line (LBL) GA-LEI product. Both the SBS GA-LEI and the LBL GA-LEI were examined to determine their usefulness in interpreting the sub-surface geology of the region. Data from the SBS GA-LEI were gridded at a 500 m grid cell size (one fifth of the line spacing) to create the conductance images, conductivity depth slices and elevation slices available in the public release dataset. At the scale of the

The Frome airborne electromagnetic survey, South Australia: implications for energy, minerals and regional geology

investigation presented here, the gridded Frome AEM survey data offered little new information within the area of the Marree uranium project, because of the large cell size and the relatively small area studied. Therefore individual SBS GA-LEI and LBL GA-LEI conductivity sections, at full resolution with along-line samples every ~12.5 m to 400 m depth, were found to be more suitable for interpretation purposes. The gridded data are, however, more useful in a regional investigation.

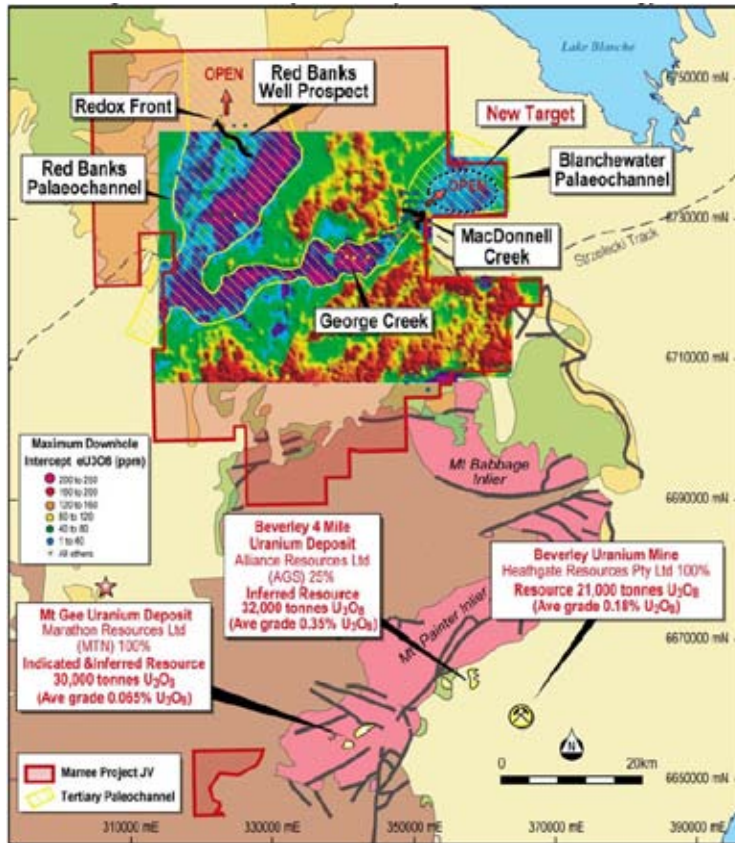


Figure 5.4.4: Location of Cauldron's AEM survey, showing a depth slice generated from their RepTEM™ survey using EM Flow™ software overlain on the regional geology (Cauldron Energy Ltd, 2011a).

The SBS GA-LEI conductivity sections for the Frome AEM survey are published with a logarithmic colour stretch and a linear colour stretch. The two colour stretches highlight electrically conductive or resistive features in geological settings with different conductivity ranges. The logarithmic colour stretch was found to be more useful in areas where overall range of conductivities is low, because it enhances the response of weakly conductive materials. The linear colour stretch was found to be useful where the overall range of conductivities is high, as in the Marree uranium project area, because it suppresses the responses of moderately conductive materials and separates them from highly conductive materials (e.g. the Eyre Formation versus the Marree Subgroup).

Both the SBS GA-LEI and LBL GA-LEI conductivity section data were used to create stacked section maps in ArcGIS™ (SBS GA-LEI shown in Figure 5.4.6) to correlate surface geological features with the 1:1 million Surface Geology of Australia Map (Raymond and Retter, 2010) and also more detailed 1:250 000 scale mapping by DMITRE. The SBS GA-LEI and LBL GA-LEI conductivity section data were also used to create GOCAD™ triangulated surfaces to construct a 3D model of the Blanchewater area, together with other data gathered from Cauldron's company announcements and drill hole data from SARIG. These maps and 3D models are shown in the following section.

The Frome airborne electromagnetic survey, South Australia: implications for energy, minerals and regional geology

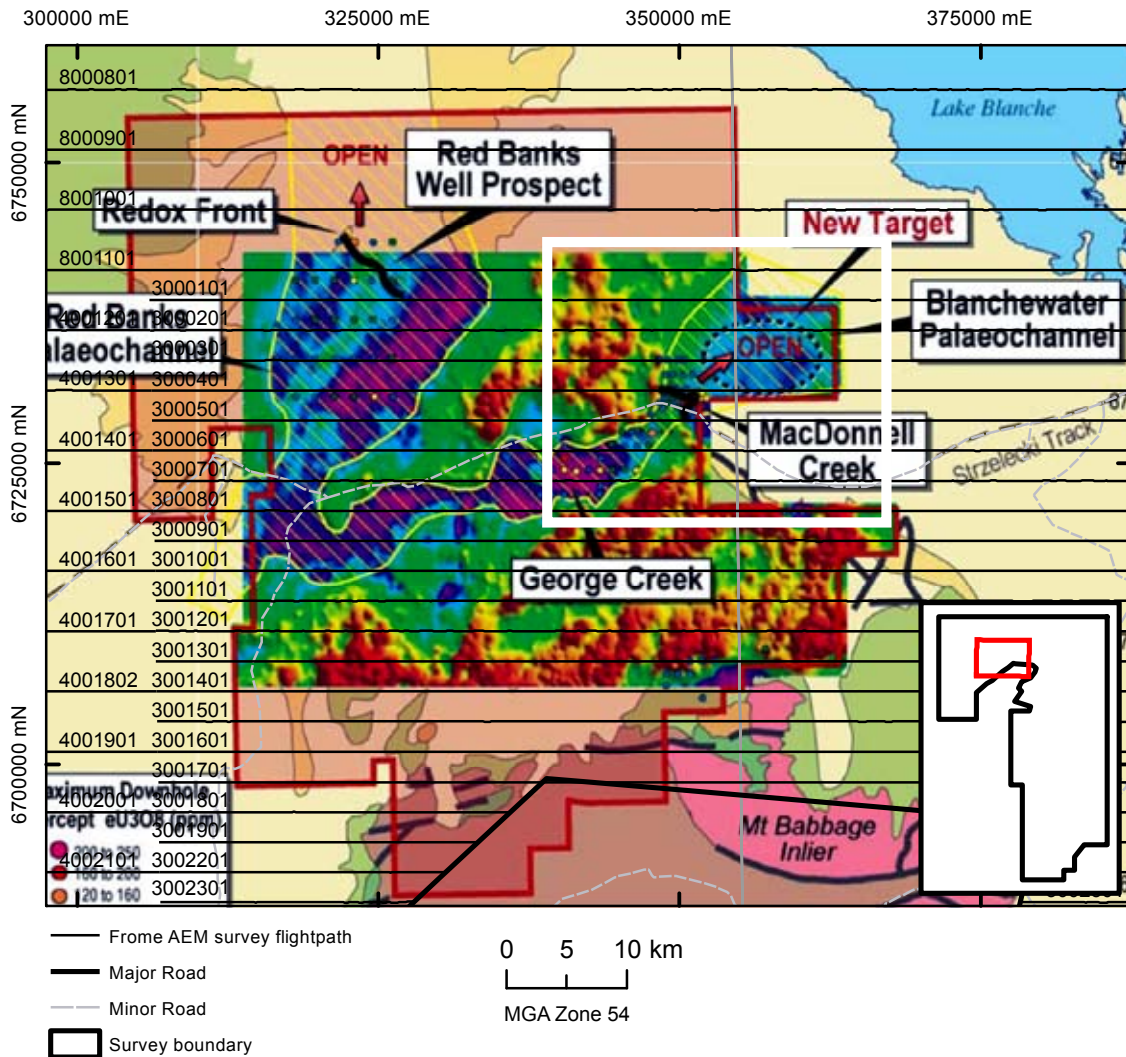


Figure 5.4.5: Location of Frome AEM survey flight lines, with line numbers labelled, overlain on a Cauldron RepTEMTM survey image, Blanchewater Palaeovalley. Modified from Cauldron (2011a). The white box shows the approximate location of Figure 5.4.2.

5.4.5 Interpretations from the Frome AEM Survey

Figure 5.4.6 illustrates linear colour stretched SBS GA-LEI conductivity sections overlain on the 1:1 million Surface Geology of Australia Map (Raymond and Retter, 2010) in the vicinity of the Blanchewater Palaeovalley. It is immediately apparent that the strong conductor visible in each conductivity section is well correlated with outcropping Mesozoic units (Marree Subgroup). In the southwest, Eyre Formation sediments overlying the Marree Subgroup in the Blanchewater Palaeovalley are apparent as a resistor overlying a strong conductor. In the northeast, Namba Formation sediments are apparent as a resistive unit with a thin, weak, conductor overlying Eyre Formation and Marree Subgroup. Experience in other parts of the Callabonna Sub-basin indicates that the weak conductor in the Namba Formation is most likely a sandy, saline water-filled interbed (perhaps a thin anastomosing sandy channel system) within the clay-dominated Namba Formation. This weak conductor also lenses in and out within successive conductivity sections, indicating lateral facies change within the Namba Formation. A number of fault lines, marked on the Cauldron geology map (Figure 5.4.2, 5.4.6), are apparent as steep offsets in the basal conductor in conductivity sections as annotated in Figure 5.4.6.

The Frome airborne electromagnetic survey, South Australia: implications for energy, minerals and regional geology

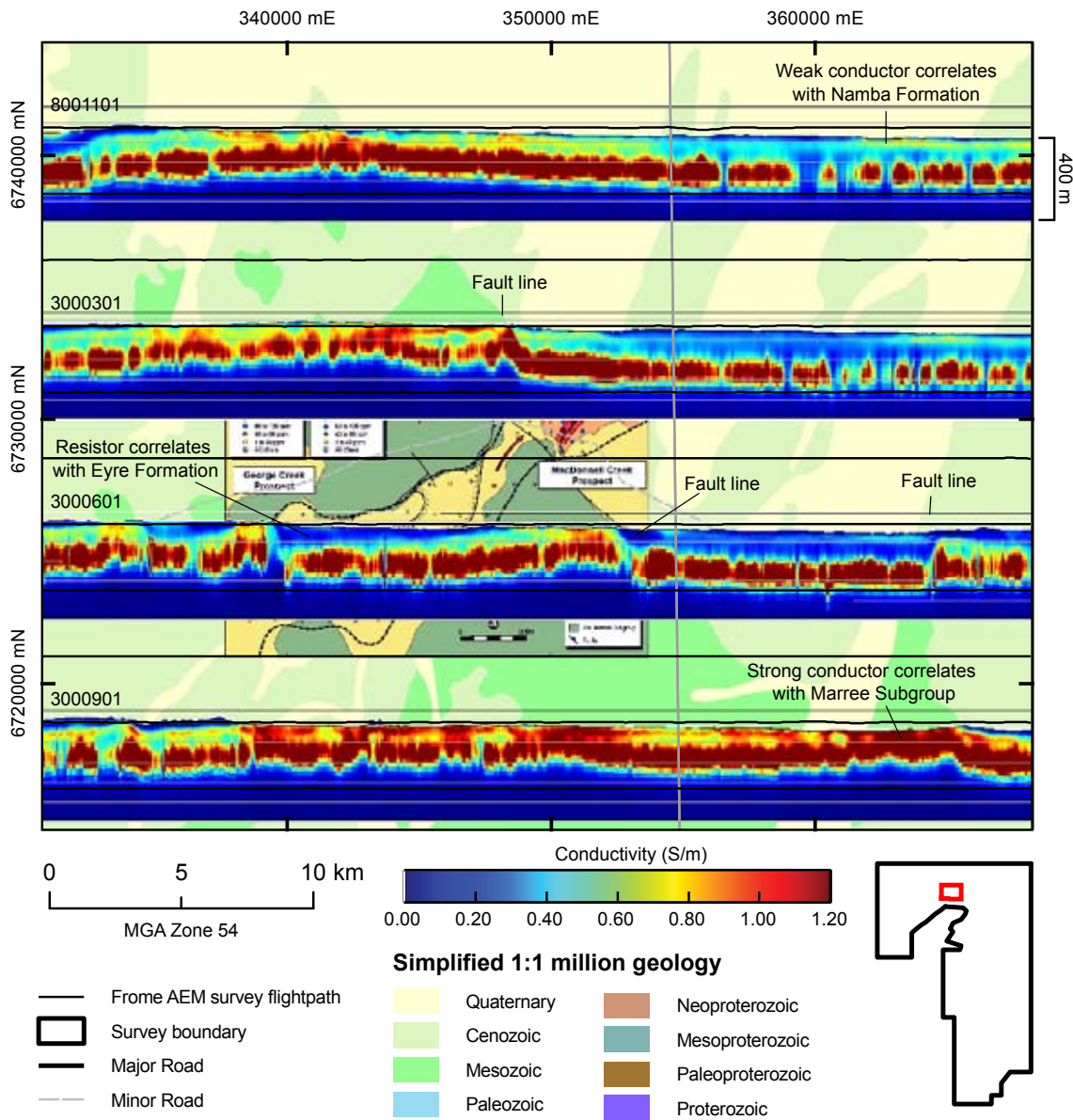


Figure 5.4.6: A stacked section map with linear colour-stretched SBS GA-LEI conductivity sections overlain on the 1:1 million scale Surface Geology of Australia Map (Raymond and Retter, 2010) and the Blanchewater Palaeovalley map shown in Figure 5.4.2, taken from Cauldron Energy Ltd (2011b).

The correlations noted on the surface geology map can be further explored, and taken into 3D, with the addition of drill hole geological data. Figure 5.4.7 illustrates the same SBS GA-LEI data from flight line 3000801, located in the vicinity of Cauldron’s Marree uranium project area. The upper section has a logarithmic colour stretch and the lower section has a linear colour stretch. The diagram serves to illustrate the difference in interpretability between the two different colour stretches, for the reasons listed in Section 5.4.4, but also the importance of conducting a dedicated drilling campaign and capturing calibrated drill hole conductivity data when conducting AEM surveys. Figure 5.4.7 highlights that the Marree Subgroup is a relatively strong conductor within the Frome AEM survey area, and while the Eyre Formation, Namba Formation and overlying Quaternary sediments may be relatively conductive, they can be effectively separated from the more conductive Marree Subgroup by image processing. Most of the drill holes shown in Figure 5.4.7 lie some distance from the flight line, however hole MPE 7 (far left of Figure 5.4.7) lies only 62 m

south of the flight line and is illustrative of the ability of calibrated AEM data to map weathering zones on conductive rocks. In this instance, the Marree Subgroup appears to have an at least 30 m thick weathering zone between the Eyre Formation-Marree Subgroup unconformity and the underlying strong conductor. The Marree Subgroup is known to be a thick sequence of pyritic, carbonaceous marine clays and silts with abundant plant fragments (Kreig and Rogers, 1995) and is generally very conductive. The stratigraphic log for drill hole MPE 7 states that the interval of Marree Subgroup sampled within the hole contains “Clay, plastic, yellow-pale grey-grey/green, common oxidised yellowish zones” (Pechiney, 1973). The presence of yellow clay reflects the weathering and oxidation of pyrite in the Marree Subgroup, the presence of a thick weathered zone and the consequent loss of bulk conductivity.

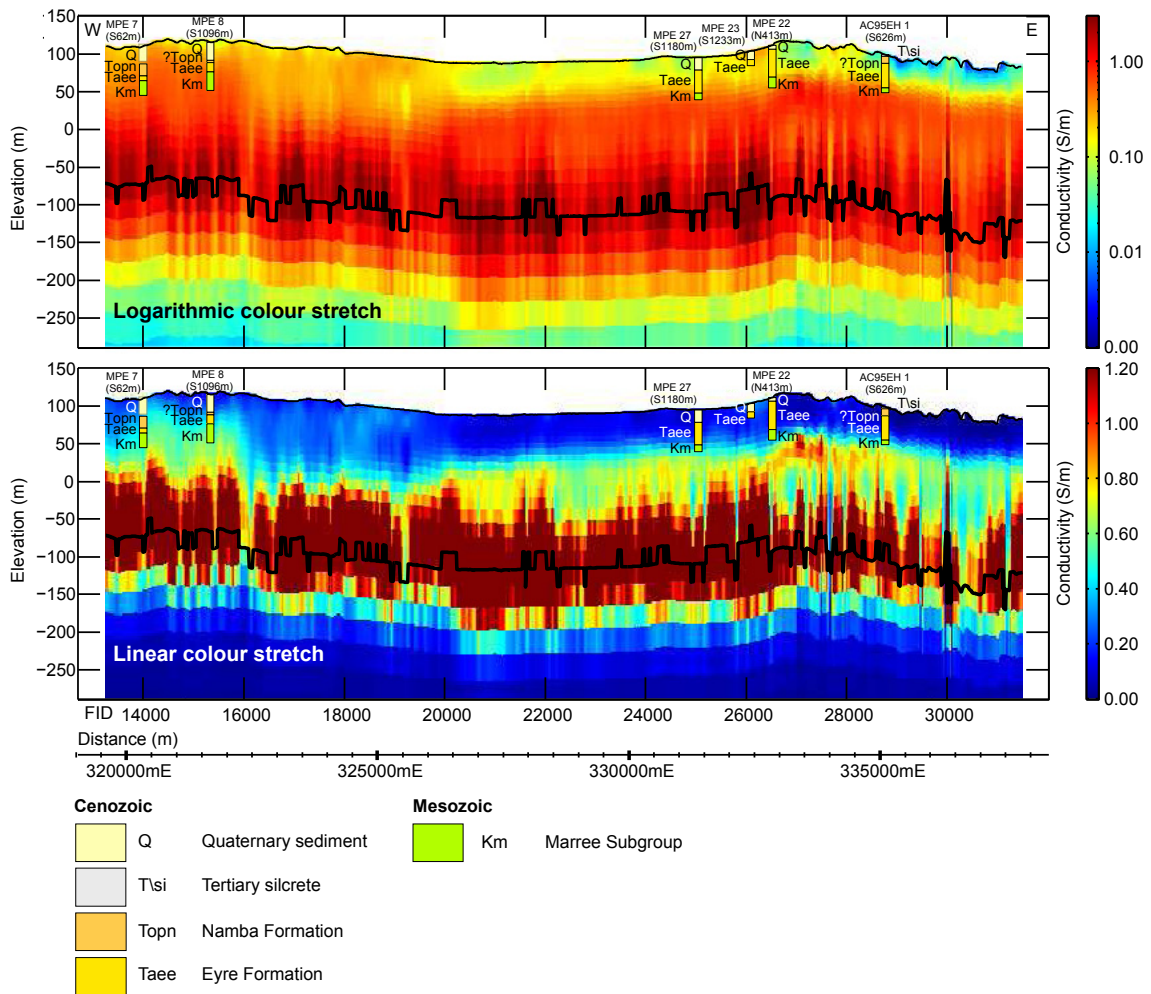


Figure 5.4.7: Drill hole geology overlain on logarithmic (upper) and linear (lower) colour stretched SBS GA-LEI conductivity sections. The sections illustrate the difference in interpretability between the two colour stretches, and internal facies variations visible within the Cenozoic and Mesozoic sequences in the Frome AEM survey area. Drill holes are labelled with the drill hole name and an alphanumeric indicating the distance of each drill hole from the flight line, e.g. MPE 27 S1180m indicating that hole MPE 27 is 1180 m south of the flight line (out of the paper, towards the reader). Drill hole locations and stratigraphic logs are from SARIG.

Internal lithostratigraphic variation within the Marree Subgroup is also apparent in the eastern portion of the conductivity section. This may represent a facies variation within the Bulldog Shale, or another unit within the Marree Subgroup such as the Coorikiana Sandstone or Mackunda

The Frome airborne electromagnetic survey, South Australia: implications for energy, minerals and regional geology

Sandstone (see Figure 3.11 for a stratigraphic column of the Mesozoic sequence). These are mapped in the local area, and are presumably filled with relatively fresh to brackish water. Unfortunately, drilling in this area is shallow and the geology of this conductivity variation can not be resolved.

The three-dimensional (3D) morphology of the Blanchewater Palaeovalley is readily apparent in Frome AEM survey conductivity sections of the area when displayed as stacked sections. Figure 5.4.6 illustrates only every third flight line, and similar correlations are visible within the intervening conductivity sections in different flight lines. The 3D morphology is better captured in a 3D rendering program, and Frome AEM survey data have been added to a GOCAD™ project of the Blanchewater Creek and wider northern Flinders Ranges flank, together with drill hole data, to map the unconformity between the Cenozoic and Mesozoic sequences, as well as interpret faults that control the location of uranium mineralisation.

Figure 5.4.8 illustrates part of a GOCAD™ model of the northern Flinders Ranges, including Cauldron's Marree uranium project and the Beverley area. The Northern Flinders Range Geology map of Sheard *et al.* (1996) is draped onto the SRTM DEM, together with uranium occurrences and interpreted Eyre Formation palaeovalley outlines (see Figure 6.1). Important uranium-bearing felsic rocks are indicated (the Yerrilla Granite and the Mount Neill Granite) as part of the Mount Babbage and Mount Painter inliers. This figure illustrates the surface geology of the northern Flinders Ranges flank, which is dominated by Mesozoic sediments of the Marree Subgroup (green colours) and Cenozoic sediments of the Namba and Eyre formations (yellow-orange colours).

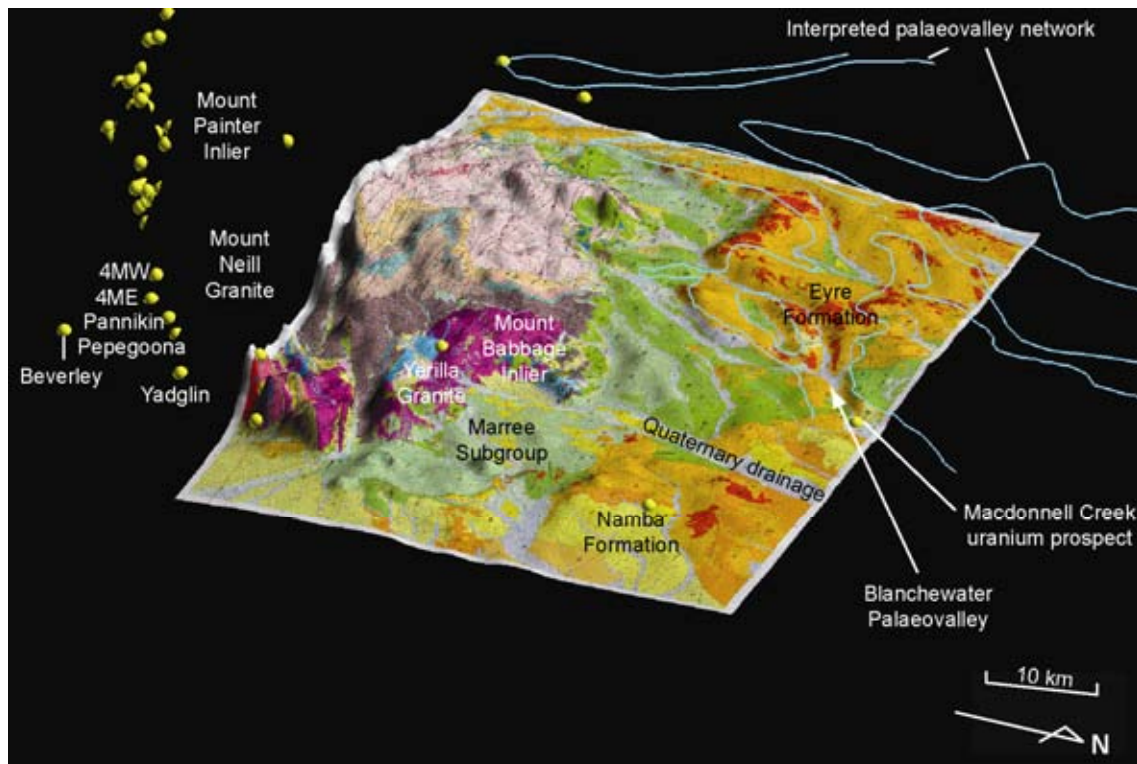


Figure 5.4.8: GOCAD™ model of the northern Flinders Ranges including the MacDonnell Creek prospect and the Beverley area. The model includes the Northern Flinders Ranges Geology map of Sheard *et al.* (1996), draped onto the SRTM DEM, uranium occurrences and interpreted Eyre Formation palaeovalley outlines.

Palaeovalley boundaries for the Eyre Formation have been interpreted using Frome AEM Survey gridded data (depth slices), conductivity sections and the Cauldron Marree uranium project map, shown in Figure 5.4.4, within an ArcGIS™ project. The palaeovalley boundaries were then imported into the GOCAD™ model. These boundaries represent areas where thick (> ~ 20 m) Eyre Formation is incised into the Marree Subgroup and where there is a noticeable resistivity anomaly associated with the Eyre Formation. The Eyre Formation is regarded as a resistor in this region.

The Marree Subgroup is exposed around the flanks of the northern Flinders Ranges by neotectonic uplift and erosion. Modern drainage cross-cuts the interpreted palaeovalley boundaries in many places, indicating that palaeovalleys are being eroded and removed by modern surface processes. This will be discussed further, below.

Figure 5.4.9 depicts the same scene as Figure 5.4.8, except the base map has been replaced with the map of Cauldron's Marree uranium project shown in Figure 5.4.4, again draped onto the SRTM DEM. The Cauldron RepTEM™ data included in the map was flown at closer line spacing (1000 m) than the Frome AEM Survey and consequently the gridded images contains much more detail than the Frome AEM Survey, but over a smaller area, allowing detailed interpretation of palaeovalleys within Cauldron's RepTEM™ survey.

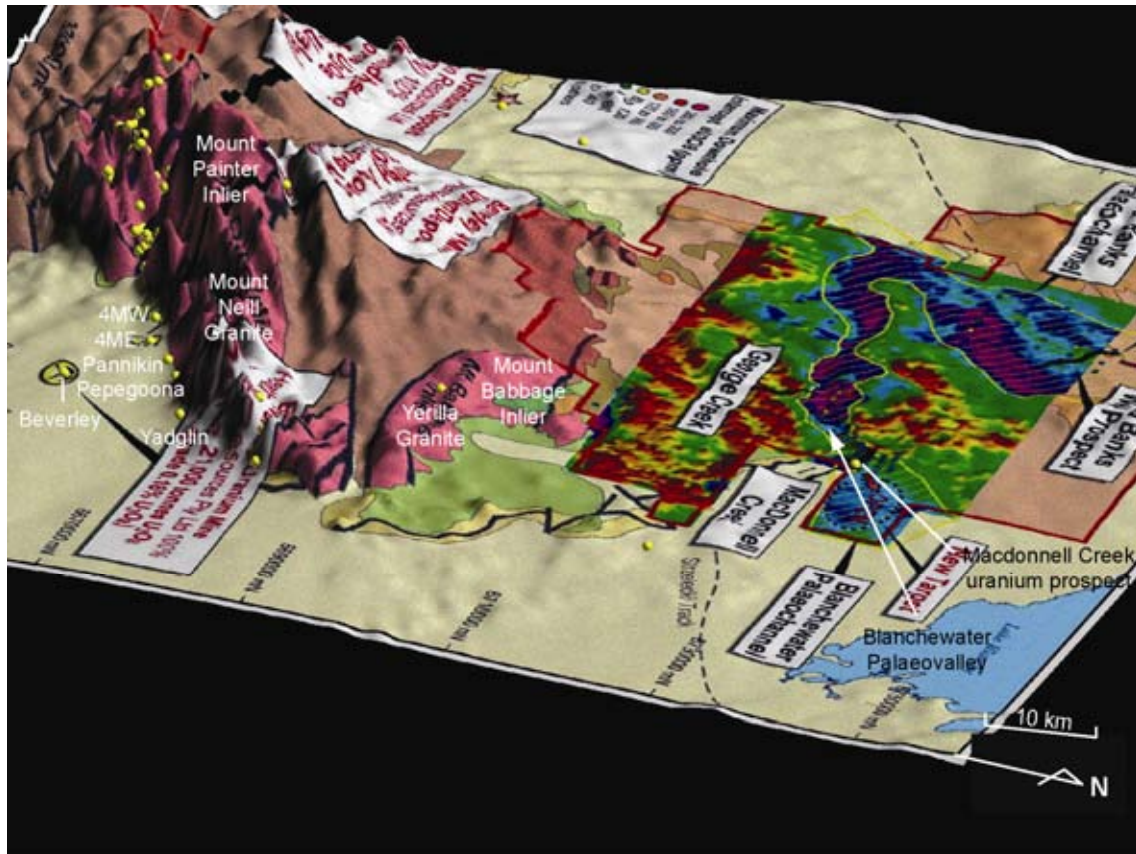


Figure 5.4.9: GOCAD™ model of the northern Flinders Ranges including the MacDonnell Creek prospect and the Beverley area. The model includes the Marree Joint Venture map of Cauldron Energy Ltd (2011a) draped onto the SRTM DEM, uranium occurrences and Cauldron's interpreted palaeovalley outlines.

Figure 5.4.10 illustrates the GOCAD™ model of the northern Flinders Ranges developed using the Frome AEM Survey, with all geological maps removed. The model includes a surface defining the

top of the Mesozoic, representing the Marree Subgroup-Eyre Formation unconformity, interpreted from individual conductivity sections. Fault planes within the model are modified from those mapped by Sheard *et al.* (1996) and also include new faults mapped using the Frome AEM Survey data. Generally speaking there was good agreement between Sheard *et al.*'s mapped faults and those visible within individual conductivity sections. There were also areas where faulting was clearly visible within conductivity sections that was not recognised and mapped because of cover. Faults within the model area are most commonly low- to high-angle thrust faults, but are shown as vertical within the model because of the high vertical exaggeration used (25x). There were instances where the mapped geology could not be correlated with the AEM signatures within conductivity sections, so some geological boundaries have been slightly altered to accommodate the new AEM data. The Marree Subgroup-Eyre Formation unconformity was extrapolated along individual flight lines using picks from stratigraphic drill holes scattered throughout the region. The polygons for uranium-bearing felsic rocks in the Mount Painter and Mount Babbage inliers have been draped over the SRTM DEM to indicate where these rocks are exposed at the surface. The implications for uranium prospectivity of these rocks are discussed in Section 3.6 and are summarised in Table 6.1. Construction lines for the Top Mesozoic surface, visible in the centre of the image, have been left to demonstrate how the model was constructed.

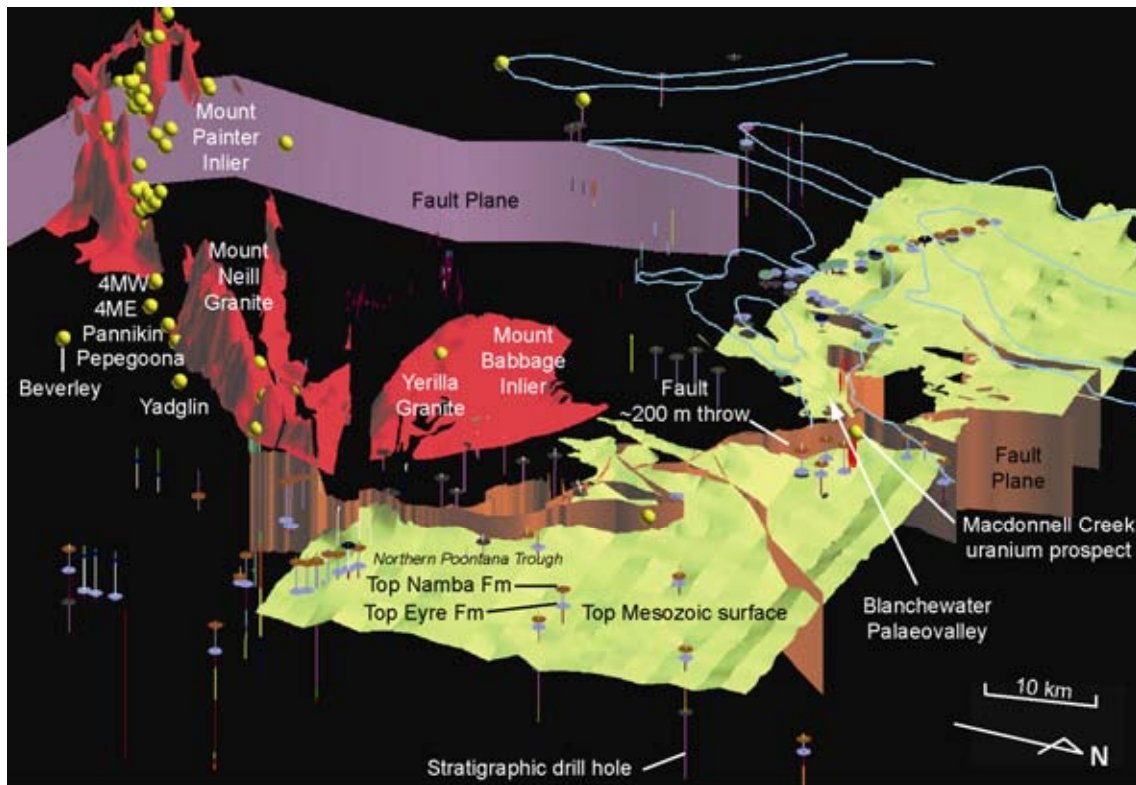


Figure 5.4.10: GOCADTM model of the northern Flinders Ranges area incorporating Cauldron's MacDonnell Creek prospect (Marree Joint Venture area) and northern Poontana Trough. The model incorporates stratigraphic drill holes from SARIG, faults modified from Sheard *et al.* (1996) using AEM data and surface exposures of uranium-bearing granites draped onto the SRTM DEM.

The site of Cauldron Energy's Marree uranium project, and other uranium occurrences along the northern Flinders Ranges flank, occurs in close proximity to a major fault system, with a throw of ~200 m indicated in Figure 5.4.10, which separates the up-thrown block of the northern Flinders Ranges from the down-thrown block of the lowlands between Lake Blanche and Lake Callabonna. On the up-thrown side the palaeodrainage has clearly incised the Marree Subgroup and has been filled with Eyre

Formation. The Marree Subgroup here includes the strong conductor of the Bulldog Shale and other slightly relatively weaker conductors like the Oodnadatta Formation (see [Figure 5.2.7](#) and Costelloe and Roach, 2012), making the task of mapping the unconformity with AEM relatively easy. On the up-thrown side, it can be surmised that the Namba Formation has largely been removed by erosion, whereas it occurs as a cap over Eyre Formation on the down-thrown side to the north. The Eyre Formation on either side of the major fault system is generally resistive, indicating that it is saturated with relatively fresh groundwater. The Namba Formation, where it exists, is seen to be more conductive, and it can be surmised that it is saturated with more saline groundwater as it lies closer to the playas of Lake Blanche and Lake Callabonna. The sharp conductivity contrasts between the Marree Subgroup, Eyre Formation and Namba Formation are readily mappable using AEM.

The model highlights the location of Cauldron's MacDonnell Creek uranium prospect and other similar environments along the northern Flinders Ranges flank. The MacDonnell Creek discovery occurs on the down-thrown side of the major fault system and is protected from oxidation and dissolution by a cap of Namba Formation sediments (acting as an aquitard) and by the sheer depth of burial, unlike uncovered Eyre Formation sediments on the south side of the major fault system. Uranium-bearing fluids would have travelled through the Blanchewater Palaeovalley to the site, precipitating uranium minerals along the Palaeovalley, where remnant uranium mineralisation can still be found (as shown in [Figures 5.4.2](#) and [5.4.3](#)). Importantly, uranium is now being oxidised and dissolved from the upper reaches of the Blanchewater Palaeovalley by oxidised groundwater, indicated by the variable redox state of the Palaeovalley shown in [Figure 5.4.3](#). However, uranium mineralisation in the MacDonnell Creek prospect seems to be unaffected by these modern processes.

It could be surmised that uranium is presently being carried by oxidised groundwater through the Blanchewater Palaeovalley, across the major fault system (where it travels ~150 m downwards) and enters the fault-offset Eyre Formation where it is fixed by reduction in the MacDonnell Creek prospect location. Without accurate groundwater chemistry data, and without knowledge of the timing of movement on the major fault system, the MacDonnell Creek site is probably best regarded as a site of uranium preservation, rather than one of active precipitation.

There are several potential sources for the uranium carried within the Blanchewater Creek Palaeovalley. The GOCADTM model shows the close proximity of the MacDonnell Creek site to the Yerilla Granite (up to ~270 ppm U) in the Mount Babbage Inlier. This would be the most obvious source of uranium, however, another source could be granitoids and metamorphic rocks of the Mount Painter Inlier via a less direct route following a major palaeodrainage system that could have existed at the time of sedimentation in the Eyre Formation. This is indicated as a fault plane connecting the Mount Painter Inlier with the southern Blanchewater Palaeovalley in [Figure 5.4.10](#). The Blanchewater Palaeovalley is not currently directly connected to the Mount Babbage Inlier by Eyre Formation sediments, however uplift and erosion of the northern Flinders Ranges has most likely removed these sediments.

5.4.6 Conclusions

Data from the Frome AEM survey can be used, in conjunction with drill hole stratigraphy and other more detailed AEM data, to more accurately map the architecture of palaeovalley systems. The mapped features include:

- The unconformities between the Proterozoic basement and the onlapping Eromanga Basin and Lake Eyre Basin and the boundary between the Eyre Formation and the Namba Formation
- The overall shape of the palaeovalley system running north and northeast from the Mount Babbage Inlier;
- Sediments (Eyre Formation) infilling incisions into Mesozoic rocks of the Marree Sub-group;
- Thickness of Eyre Formation; and,
- Major structures that could have controlled the shape of the palaeovalley system as well as areas in which Eyre Formation sediments and/or overlying Namba Formation sediments have been preserved.

These features can be used to assess the fertility of sandstone-hosted uranium systems in this area. The mapped architecture of the palaeovalley systems shows that:

- Eyre Formation sediments in the channels were hydrogeologically connected to felsic rocks enriched in leachable uranium (Yerilla Granite in the Mount Babbage Inlier, and possibly Mount Neill Granite in the Mount Painter Inlier);
- Palaeo fluid-flow direction was broadly north and northeast from the source area, which means that the redox fronts which control mineralisation are located to north and northeast of the source; and,
- The area is highly prospective for sandstone-uranium deposits (see [Chapter 6](#), [Figure 6.1](#) and [Table 6.1](#) for more details). One possible limiting factor is the movement along faults which could have selectively eroded parts of palaeovalley systems in-filled with prospective sediments of the Eyre Formation.

A number of juxtapositions of deeply-buried Eyre Formation against uplifted Mesozoic sediments occur along the entire northern Flinders Ranges flank, similar to that at MacDonnell Creek, as shown in [Figure 5.4.10](#). A number of shorter palaeovalleys (too short to be accurately mapped using the Frome AEM Survey data) exist between the MacDonnell Creek prospect and the northern Poontana Trough. We regard these juxtapositions as being prospective for sandstone-hosted uranium mineralisation throughout the region, provided that there was once a hydraulic connection to a felsic rock enriched in leachable uranium.

5.4.7 References

- Cauldron Energy Ltd, 2009. ASX Announcement 24 November 2009: Drilling by Cauldron and Korean partners confirms presence of large uranium target in South Australia. West Perth. Online: http://www.cauldronenergy.com.au/_content/documents/370.pdf.
- Cauldron Energy Ltd, 2011a. ASX Announcement 14 July 2011: New uranium target uncovered at Marree Project, South Australia. Leederville WA. Online: http://www.cauldronenergy.com.au/_content/documents/536.pdf.
- Cauldron Energy Ltd, 2011b. ASX Announcement: Quarterly Report for period ended 30 September 2011. Leederville WA, 19 pp. Online: http://www.cauldronenergy.com.au/_content/documents/548.pdf.
- Cauldron Energy Ltd, 2011c. Cauldron Energy Ltd Annual Report for the year ended 30 June 2011. Leederville WA. Online: http://www.cauldronenergy.com.au/_content/documents/543.pdf.
- Cauldron Energy Ltd, 2012. Marree Project, SA. Online: <http://www.cauldronenergy.com.au/marree.asp>.
- Costelloe, M. T. and Roach, I. C., 2012. The Frome AEM Survey, uncovering 10% of South Australia. Preview **158**.
- Kreig, G. W. and Rogers, P. A., 1995. Stratigraphy - marine succession. In: Drexel, J. F. and Preiss, W. V. (editors), *The Geology of South Australia Volume 2 - The Phanerozoic*. Geological Survey of South Australia, Adelaide. 112-123 p.
- Pechiney, 1973. Pechiney (Australia) Exploration Pty Ltd Murnpeowie. Progress and final reports to licence expiry/surrender for the period 15/1/1970 to 9/2/1973. Primary Industries and Resources SA, Adelaide. **Envelope 01327**.
- Raymond, O. L. and Retter, A. J., 2010. Surface geology of Australia 1:1 000 000 scale. Geoscience Australia, Canberra. 2010. Online: <http://www.ga.gov.au/mapconnect/>.
- Sheard, M. J., Reid, P. W. and White, M. R., 1996. Northern Flinders Ranges Geology. Geological Atlas 1:75 000 series, Geological Survey of South Australia, Adelaide.

5.5 MAPPING BASIN ARCHITECTURE AND SALINITY: A TEMPEST™ AEM INTERPRETATION OF THE POONTANA TROUGH, NORTHWESTERN LAKE FROME REGION

*B. H. Michaelsen, A. B. Marsland-Smith, P. D. Magarey, A. J. Fabris, I. C. Roach, T. Dhu,
L. F. Katona and J. L. Keeling*

5.5.1 Introduction

The Poontana Trough is a major depocentre within the Callabonna Sub-basin, Lake Eyre Basin. The trough is developed between the subsurface Benagerie Ridge (which lies to the east) and the Flinders Ranges (which lie to the west), within the northwestern region of the modern-day Lake Frome watershed, South Australia (Figure 5.5.1, 5.5.2).

The western margin of the Poontana Trough is probably South Australia's most prospective area for sandstone-hosted, redox-related uranium. The region is actively explored, mainly by Heathgate Resources Pty Ltd (Heathgate) with various joint venture partners. The principal method of exploration is by rotary-mud drilling. Potential mineralised targets are within a depth range of ca. 110 to 240 m in strata of Cretaceous (Frome Embayment), Paleogene and Neogene (Callabonna Sub-basin) age.

Several uranium deposits have been discovered in the Paralana-Beverley area (Figure 5.5.1, 5.5.2, 5.5.3): Beverley (discovered 1969), Four Mile East (discovered 2005), Four Mile West (discovered 2005), Pepegoona (discovered 2009) and Pannikin (discovered 2010). The Beverley ore body is possibly tabular, however, the most common style of mineralisation in the region is roll-front, ranging from classic, crescent-shaped rolls (e.g. Pannikin), to stacked mini-rolls (e.g. Pepegoona) of complicated geometries (Marsland-Smith *et al.*, 2011).

With the exception of Beverley, the other deposits (i.e. Four Mile West and Four Mile East, Pannikin, Pepegoona and Pepegoona West) are on strike with the Paralana Fault Zone (Figure 5.5.3), and are therefore collectively and conveniently referred to here as the "Paralana uranium field". At the Beverley deposit, mineralisation is developed in the uppermost sedimentary sequence (the "Beverley sequence") of the Namba Formation (mid-Miocene), within a sub-unit informally termed the "Beverley sands", and predominantly within the Beverley Palaeochannel (Heathgate Resources, 1998). In contrast, deposits of the Paralana uranium field are hosted mostly within fluvial sands of the stratigraphically older Eyre Formation; in the case of Four Mile West, mineralisation is within a sandy glacial diamictite, equivalent in age to the Early Cretaceous Bulldog Shale (Cross *et al.*, 2010; Figure 5.5.4).

In this contribution we have reviewed an area of approximately 5780 km² over the northern and central Poontana Trough, using data released from the Frome AEM Survey flown across the Lake Frome drainage basin in 2010. This case study presents an opportunity to document some geological aspects of some of South Australia's largest sandstone-hosted uranium deposits. The recoverable uranium mineralisation is within unlithified sand and only minor quantities of uranium are bound within silica-cemented sands above, for example, the main Pepegoona ore horizons. These groundwater silcretes form at major unconformities which act as important fluid conduits; in the case of Pepegoona, at the Eyre Formation/Namba Formation unconformity (see Figure 5.5.5). The cemented lithologies are quartz arenites or conglomeratic arenites (if they contain coarse detritus).

Silicified unconformities, such as at the Pepegoona deposit, are impervious layers (aquitards). Not only do they modify fluid flow, they also function as cap rocks to unconventional, shallow petroleum systems. At Pepegoona, petroleum pools beneath the silicified layer within the same horizon as the uranium ore.

New terminology used in this manuscript is summarised in Table 5.5.1, and geographic localities referred to are shown in Figures 5.5.1-5.5.3, 5.5.6 and 5.5.7.

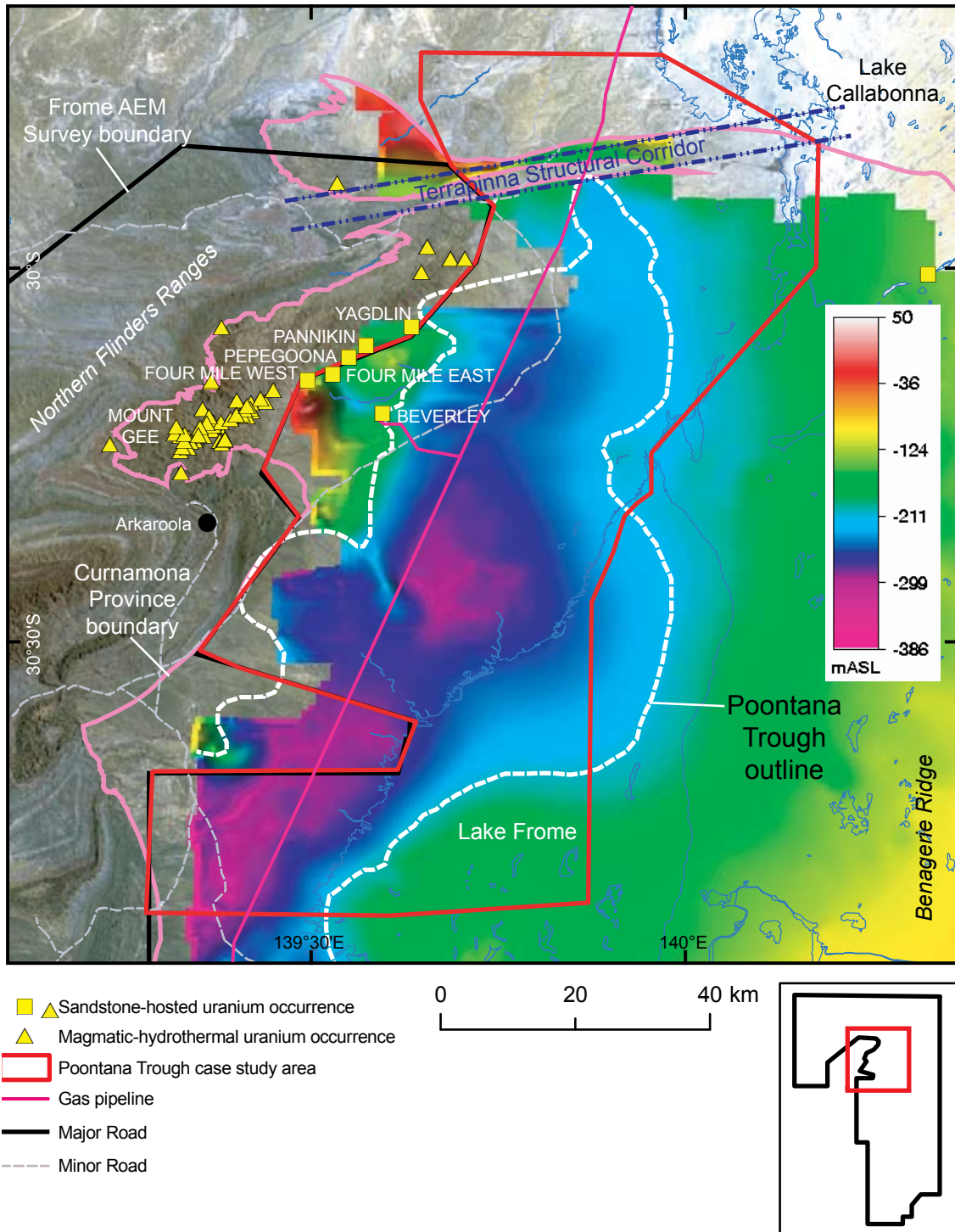


Figure 5.5.1: Map of the Poontana Trough study area showing the modelled extent and depth of the Poontana Trough in the Callabonna Sub-basin (from Fabris et al., 2010) and uranium occurrences in the Beverley and northern Flinders Ranges area. Background: Landsat MSS mosaic of Australia.

The Frome airborne electromagnetic survey, South Australia: implications for energy, minerals and regional geology

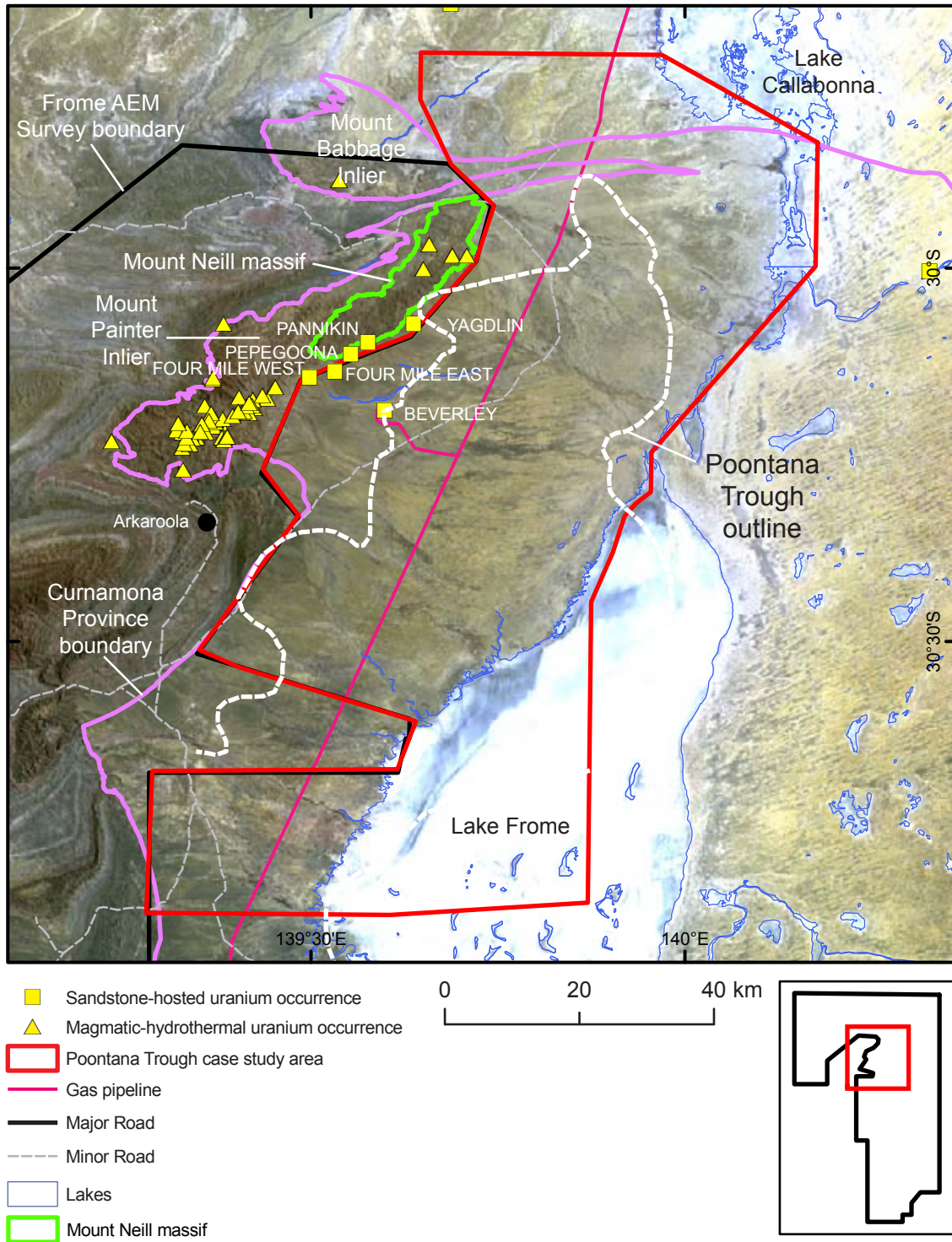


Figure 5.5.2: Landsat MSS mosaic of the Poontana Trough study area showing the northern Flinders Ranges, comprising the Mt Painter Inlier (including the Mount Neill massif), the Mt Babbage Inlier, the folded strata of the Adelaide Geosyncline and the Lake Frome playa.

The Frome airborne electromagnetic survey, South Australia: implications for energy, minerals and regional geology

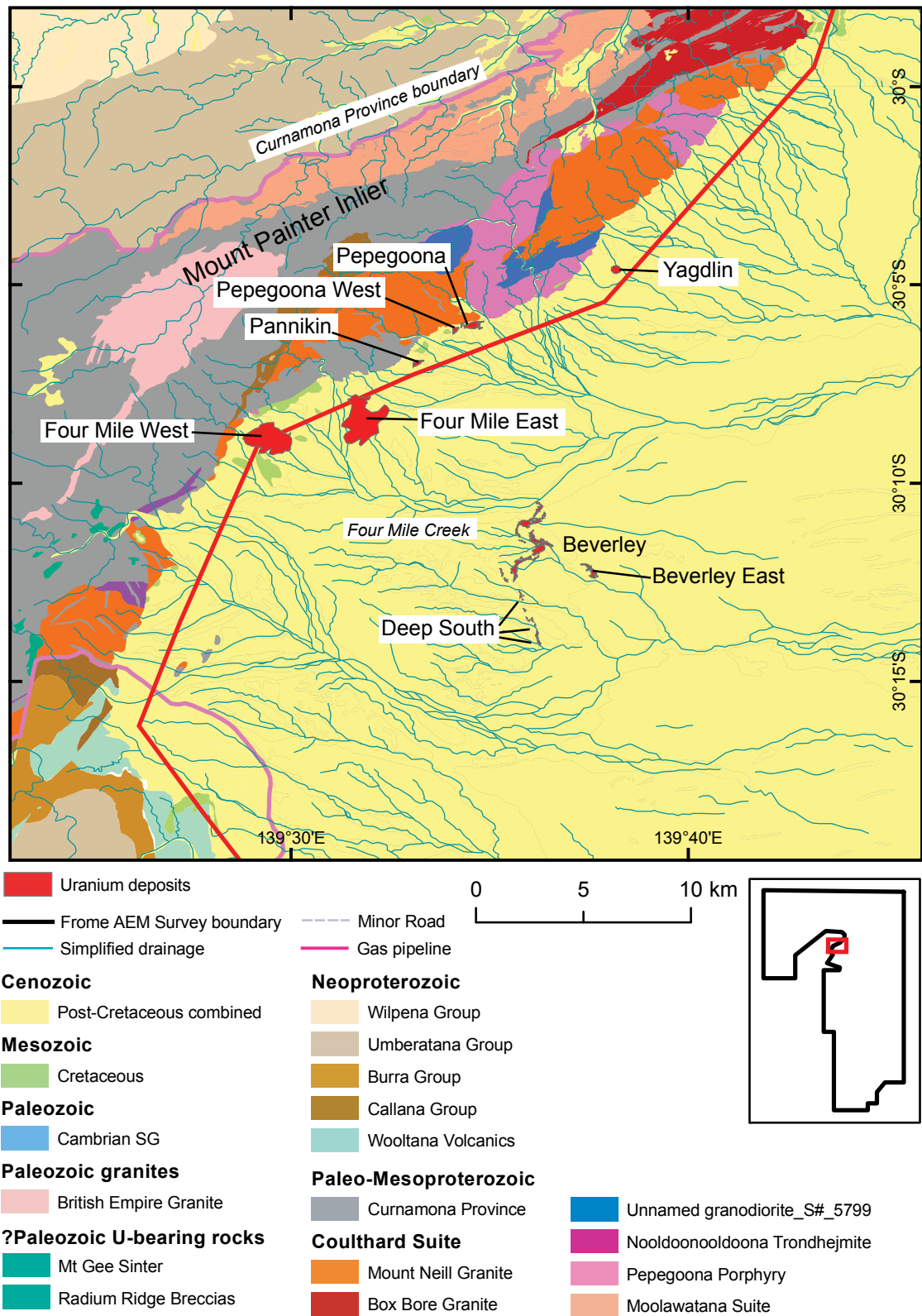


Figure 5.5.3: Surface geology of the Paralana Embayment area within the central Poontana Trough, showing outlines of known uranium deposits with respect to the northern Flinders Ranges and simplified surface drainage.

The Frome airborne electromagnetic survey, South Australia: implications for energy, minerals and regional geology

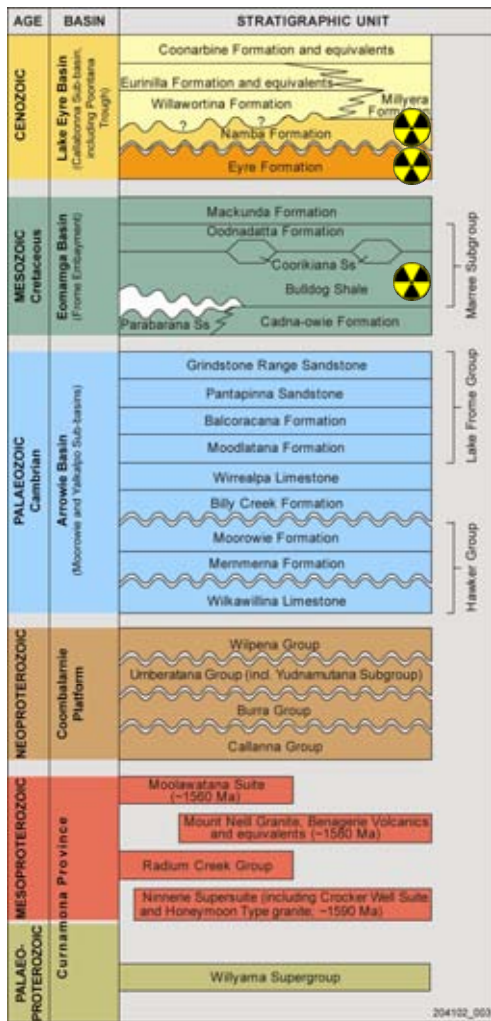


Figure 5.5.4: Stratigraphy of the northern Flinders Ranges and Poontana Trough area, highlighting the known strata containing uranium deposits. Modified after Fabris et al. (2010).

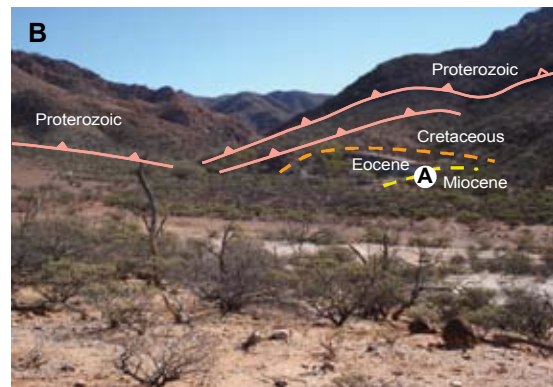


Figure 5.5.5: **A:** Outcrop of Eyre Formation/Namba Formation unconformity at the Dead Tree Section (Hore and Hill, 2009) (MGA 54 354011 mE 6664802 mN), ~430 m northwest of the Four Mile West uranium deposit. **B:** Panoramic photograph indicating the position of the Dead Tree Section, where a headwater tributary of Four Mile Creek exits the rugged outcrop of the northern Flinders Ranges. Annotations illustrate the approximate geological contacts between Proterozoic intrusions, Cretaceous conglomerate and diamictite, Eocene Eyre Formation, and Miocene Namba Formation. The sense of thrusting of Proterozoic rocks over the sedimentary cover is also indicated. The location of photograph A is indicated.

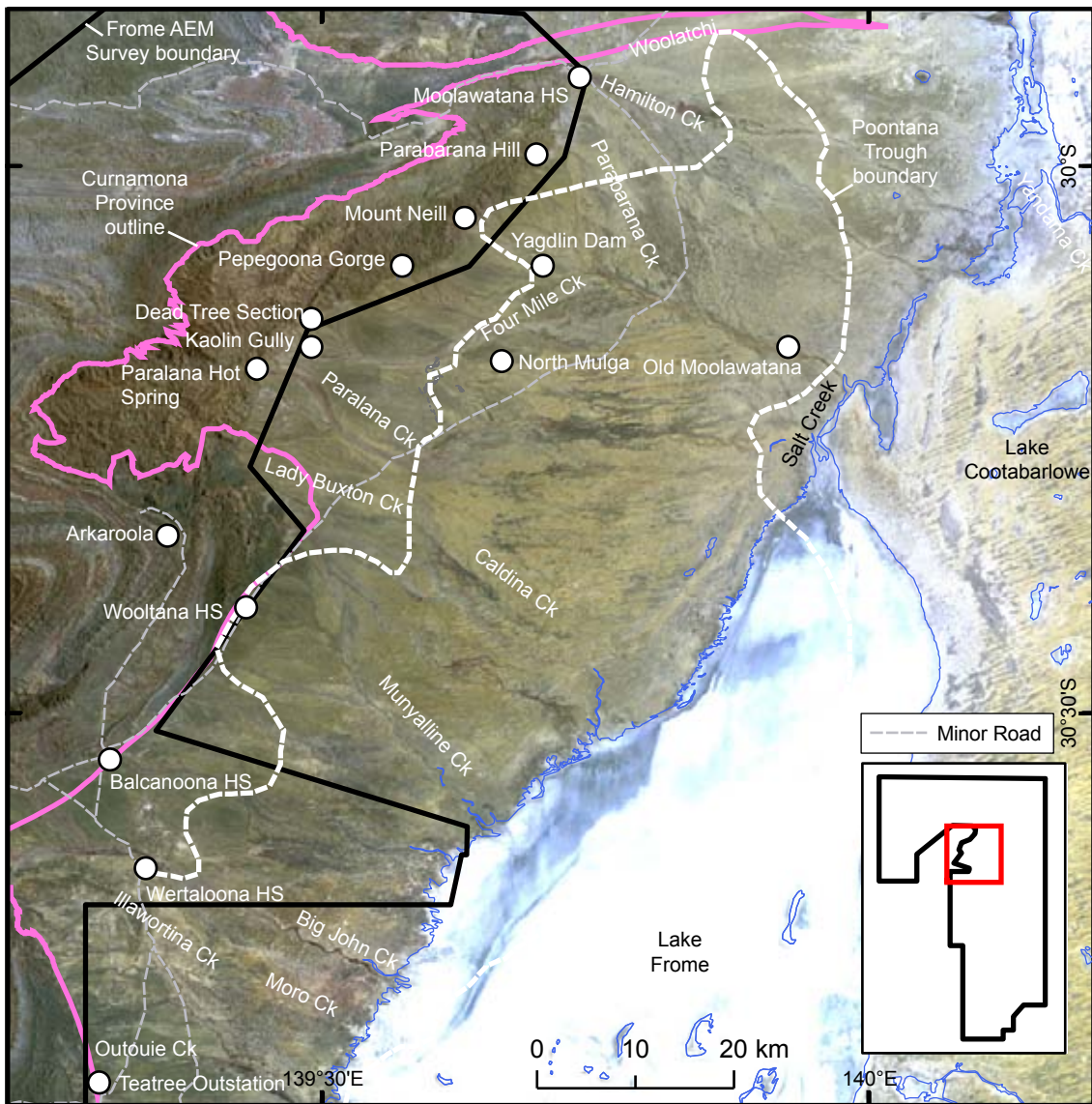


Figure 5.5.6: Localities described in the text.

5.5.2 Basin-wide aquifer salinity model

Some features within the Frome AEM Survey data set are best explained by a basin-wide aquifer salinity model. To that end, sub-surface salinity data, based on open-file water-bore data for the northern Lake Frome region, is shown in Figure 5.5.8. We have stratigraphically-attributed most of these data using drill hole depth and lithology, and added these to drill hole records contained in SAGEodata, the Government of South Australia's corporate geoscientific data repository, accessible via SARIG (<http://www.sarig.dmitre.gov.au>). The groundwater salinity data provide a regional picture of fresh water recharge into Cenozoic sediments that abut the northern Flinders Ranges range front, i.e. along the western margin of the Poontana Trough. In particular recharge occurs in the vicinity of:

- Moolawatana Homestead and Parabarana Hill where, via Hamilton Creek, water drains directly from Early Mesoproterozoic Moolawatana Suite granitoids (Figure 5.5.3) of the northern Mount Painter and Mount Babbage Inliers, as well as Neoproterozoic metasediments of the Umberatana Group, particularly glacial deposits and limestone;

The Frome airborne electromagnetic survey, South Australia: implications for energy, minerals and regional geology

- Balcanoona and Wooltana homesteads, where fresh water extends ~20 km basin-ward towards Lake Frome. The headwaters of the creeks in this area also flow over and through various Neoproterozoic strata including the Wooltana Volcanics, glacial deposits, reduced shales with interbedded dolomites and limestone;
- Wertaloona Homestead (Figure 5.5.6), where the southeast extension of Italowie Ridge is covered by Cenozoic sediments. Recharge occurs via Italowie Creek and Big John Creek, and also via Illawortina and Moro creeks, that flow southeast and drain the Stirrup Iron Range, an area of bedrock comprising Neoproterozoic metasediments (Umberatana and Wilpena groups) and Cambrian carbonates of the Arrowie Basin; and,
- Teatree Outstation immediately east of Wearing Gorge, where recharge occurs via the funnelling of water through Outouie Creek that drains the Wearing Hills comprising folded Late Neoproterozoic metasediments of the Adelaide Geosyncline.

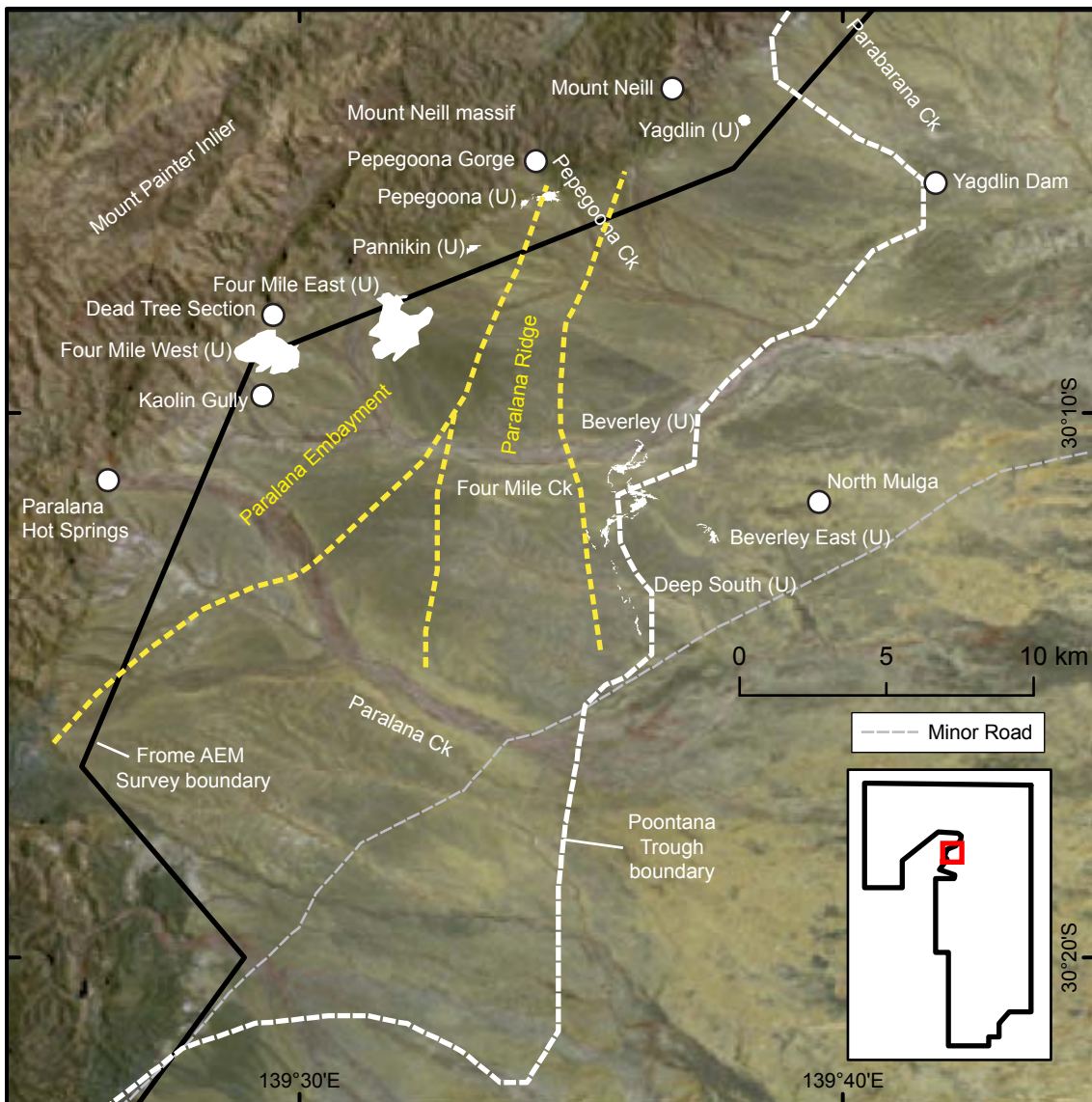


Figure 5.5.7: Close-up of the Paralana Embayment showing localities described in the text and uranium deposit outlines. The dashed yellow lines show the positions of important sub-surface features.

The Frome airborne electromagnetic survey, South Australia: implications for energy, minerals and regional geology

In contrast to the fresh water recharge areas described above, bores in the vicinity of Yagdlin Dam (Figure 5.5.6-5.5.8) contain saline water. The most saline of these is Yagdlin Bore No. 2 (drill hole no. 87778; Figure 5.5.8) that produces water of ~20 300 ppm TDS (total dissolved solids) from the Willawortina Formation at a depth of 54 m. This high salinity is in contrast to the overall regional picture of < 5000 ppm TDS.

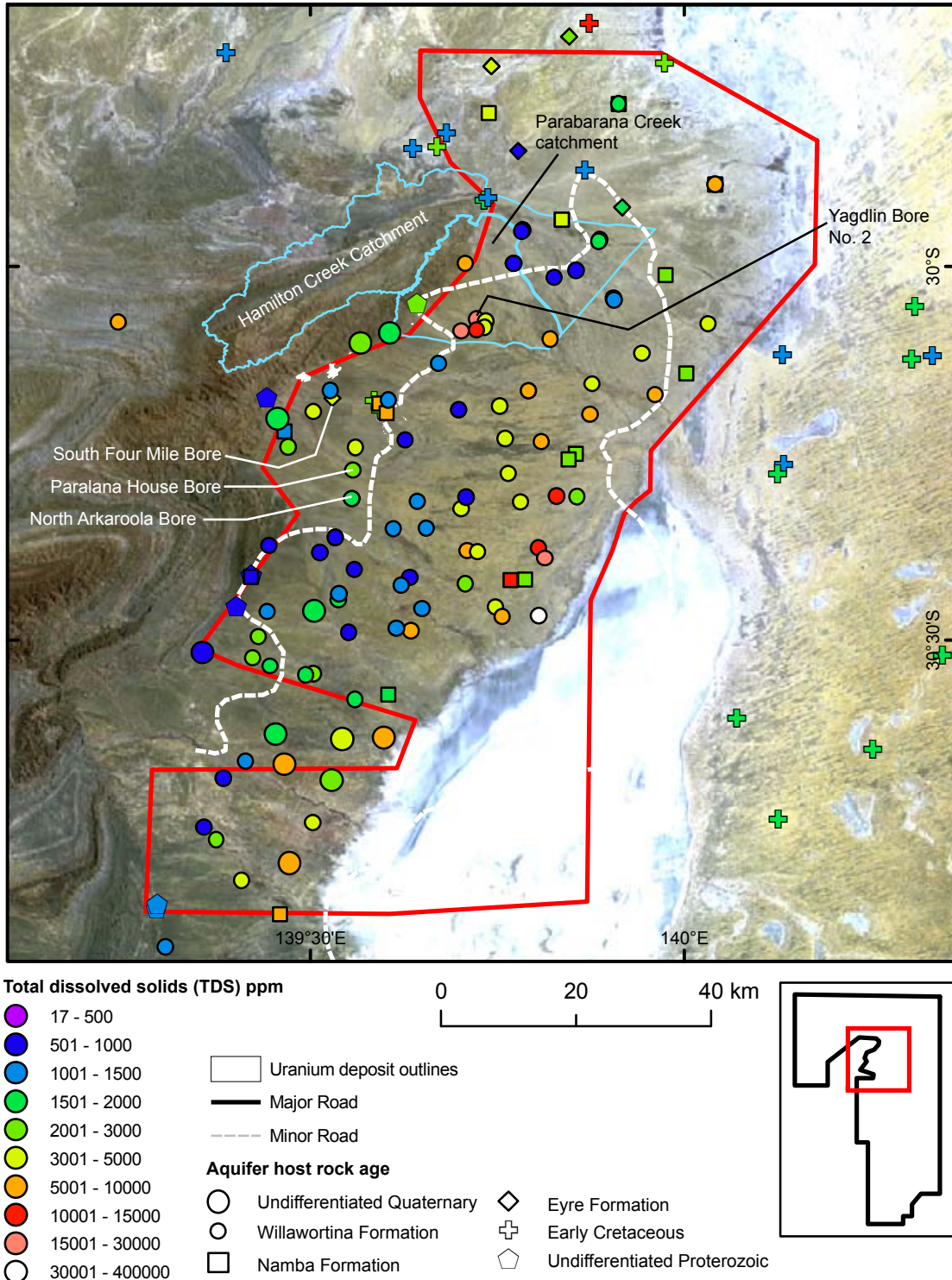


Figure 5.5.8: Lake Frome watershed and northern Flinders Ranges: regional salinity of bore-hole waters expressed as total dissolved solids (TDS). Units in parts per million (ppm).

The significance of this saline body of water with respect to sandstone-hosted uranium systems is discussed below; however, empirical evidence suggests that groundwater that abuts the ruggedly-outcropping granitoids of the Mt Neill massif (Figure 5.5.2) is saline. This could be from:

- A higher proportion of recharge from adjacent, more saline aquifers (via flow from fractured-rock aquifers within strongly altered intrusives); and/or,
- A consequence of diffuse recharge of brackish/saline water through shallow Quaternary sediments (via surficial recharge from the relatively small Parabarana Creek catchment; Figure 5.5.2).

Table 5.5.1: New terminology.

NEW TERMINOLOGY	DESCRIPTION
Beverley-type deposit (or prospect)	A uranium deposit or prospect hosted in unlithified palaeochannel sand within the clay and silt-dominant Namba Formation.
Beverley salinity plume	Saline plume of groundwater between Beverley uranium deposit (east) and Paralana Ridge (west). It extends from near Pepegoona uranium deposit (north) to 6.5 km south of Beverley. See Figures 5.5.11C, 5.5.13 and 5.5.15-5.5.17.
Paralana-type deposit	A uranium deposit hosted in predominantly sandy sediments, i.e. amalgamated fluvial sands and pebbly gravels of the Eyre Formation at Four Mile East, Pannikin and Pepegoona; or sandy diamictite (Bulldog Shale equivalent) at Four Mile West. Paralana-type deposits are capped with a diagenetic (relatively impervious) lithology, usually quartz arenite (“groundwater silcrete”).
Paralana Embayment	The area corresponding to a low Bouger gravity feature between the outcropping northern Flinders Ranges (west) and the Paralana Ridge (east). See Figures 5.5.7, 5.5.15 and 5.5.16.
Paralana Gravity Trough	Conspicuous area with a low Bouger gravity signal, situated between Four Mile East (SW), the Paralana Ridge (east) and the northern Flinders Ranges (NW). Pepegoona uranium deposit. See Figure 5.5.14.
Paralana Ridge	Conspicuous north-northwest-striking Bouger gravity high corresponding to shallow stratigraphy. The Paralana Ridge separates the Paralana Embayment from the rest of the Callabonna Sub-basin, including the Beverley area. The northern extension of the Paralana Ridge corresponds only approximately to the area between the northern extension of the Wooltana Fault and Vidnee Yarta Fault. See Figures 5.5.7 and 5.5.14. Previously referred to as the Poontana Inlier.
Yagdlin salinity plume	Saline plume of groundwater centred on Yagdlin Dam, and extending from the outcropping Mt Neill massif (northern Flinders Ranges) to the Salt Creek-Lake Frome drainage axis. See Figure 5.5.11B.
Paralana uranium field	Collective name for the uranium deposits that occur along strike with, and in the vicinity of the Paralana Fault zone: Four Mile West, Four Mile East, Pannikin, Pepegoona West and Pepegoona uranium deposits, and also Yagdlin uranium prospect. See Figures 5.5.1, 5.5.2 and 5.5.7.
Vidnee Yarta Fault	Newly-defined regional fault, striking NNW, positioned approximately mid-way between Wooltana Fault (west) and Poontana Fault (east). See Figures 5.5.15 and 5.5.16.

5.5.3 Results and discussion

5.5.3.1 Anthropogenic anomalies in the AEM data

The identification of anthropogenic anomalies is an important exercise when interpreting any AEM data. In the area under consideration, anthropogenic AEM responses are associated with the Moomba to Adelaide gas pipeline, which runs through the entire length of the Poontana Trough (Figure 5.5.1). From time to time, 50 Hz electricity is passed along the pipe as a measure to prevent corrosion. These electrical events create anthropogenic AEM anomalies recorded in two regions: a northern area, ~12 km east of Moolawatana Homestead; and a southern area, ~18 km southeast of Wooltana Homestead. These anthropogenic anomalies are most easily seen in the LBL GA-LEI conductivity sections (Figure 5.5.9). In all cases, signal disturbance is restricted to within 2 km (usually less) of the pipeline, but does little to detract from the usability of the data once identified.

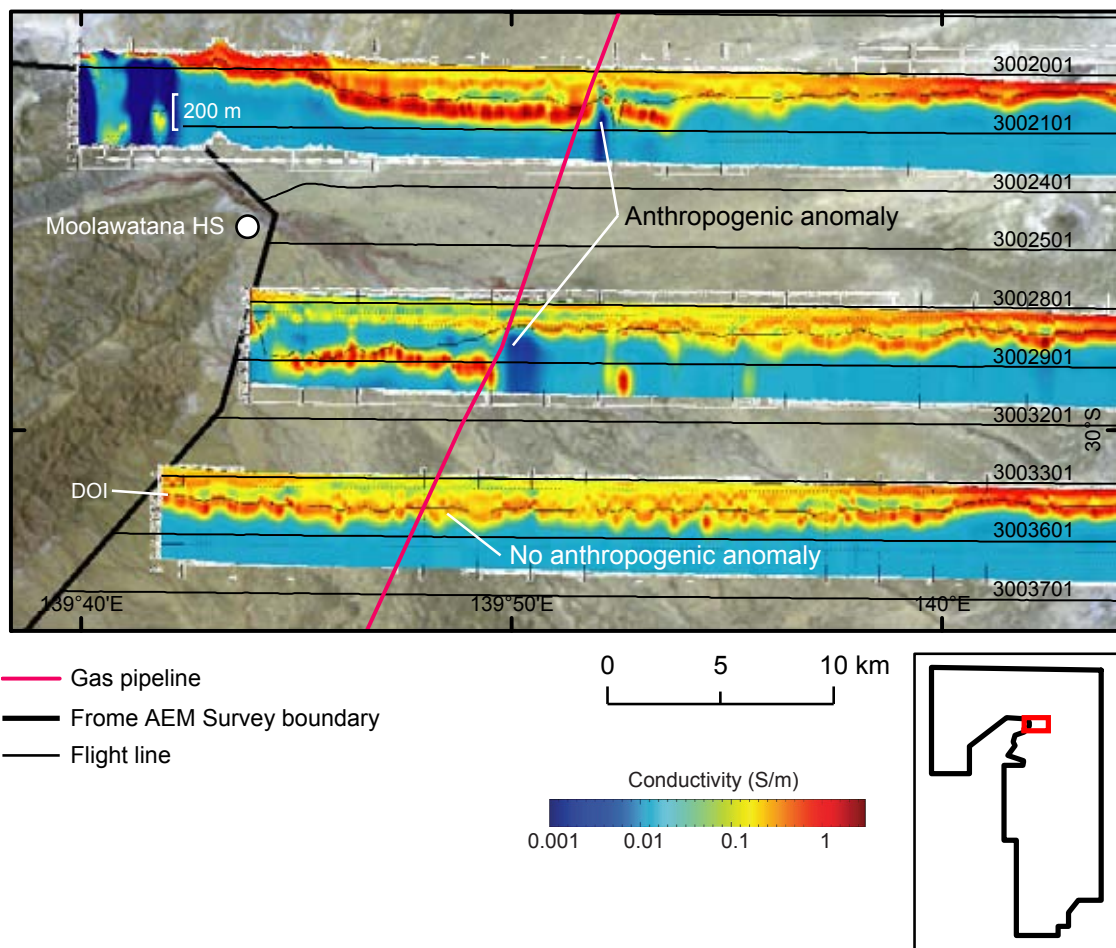


Figure 5.5.9: Examples of anthropogenic AEM anomalies associated with the Moomba to Adelaide gas pipeline near Moolawatana Homestead, northern Poontana Trough. DOI: Depth of investigation.

5.5.3.2 Regional AEM response

5.5.3.2.1 0-200 m conductance image

The most prominent feature of the Frome AEM survey is an area of high conductivity corresponding to Lake Frome, which is a hypersaline playa (both surface and shallow subsurface waters; Draper and Jensen, 1976). The peripheral ~5 to 8 km around the western margin of the lake is also affected by high salinity; this area is characterised by very high near-surface AEM conductivity (Figures 5.5.10 and 5.5.11). Almost the entire northeast Lake Frome watershed is a broad zone of relatively high conductivity.

The Poontana Trough receives significant fresh water recharge as surface water from the northern Flinders Ranges which percolates into sediment fill of the Poontana Trough.

Conductivity data illustrated in [Figures 5.5.10](#) and [5.5.11](#) indicate that Hamilton Creek near Moolawatana Homestead is a local site of substantial fresh water recharge. This is confirmed from bore-water salinity data ([Figure 5.5.8](#)). Other areas of recharge are the Paralana Embayment ([Figure 5.5.7](#)) where several large creeks exit the Flinders Ranges, and the range front south of Paralana Creek ([Figure 5.5.6, 5.5.7](#)).

5.5.3.2.2 Conductivity depth slices

[Figure 5.5.11](#) depicts a series of four depth-slices ranging from shallow (0-5 m: [Figure 5.5.11A](#)) to deep (100-150 m: [Figure 5.5.11D](#)). Fresh water sourced from Hamilton Creek is apparent in the deepest of these (100-150 m) and in the more shallow depth-slices ([Figure 5.5.11A, B, C](#)). Viewed in totality, the depth-slices may indicate fresh water recharge centred on the catchment of East Painter Creek, which feeds into Paralana Creek. However, a probable scenario is that this low-conductivity feature is largely due to shallow basement of Mount Painter Inlier rocks.

Slices of intermediate depth (i.e. 60-80 m and 80-100 m) record that the size of the low conductivity feature at East Painter Creek diminishes with increasing shallowness; it is eventually replaced with a feature bearing a heterogeneous but relatively high conductivity in the 0-5 m depth slice ([Figure 5.5.11A](#)) which shows that the creeklet valleys within the Paralana Creek watershed are subtle low-conductivity features. [Figure 5.5.11C](#) also shows an interconnection between the high conductivity domain immediately west of Beverley and a high-conductivity feature at South Four Mile Bore (drill hole no. 87835; see also [Figure 5.5.8](#)). This conspicuous feature is interpreted as an area containing a high salinity aquifer within both the Willawortina Formation and the underlying Namba Formation.

By way of contrast to the aforementioned high conductivity feature, at near-surface depths (i.e. 0-5 m depth-slice: [Figure 5.5.11A](#)) a large low conductivity feature is developed at Arkaroola Creek, 20 km south-southwest of Beverley.

A simplistic interpretation could be that the infiltration of runoff into the shallow aquifers of the Paralana Embayment is brackish to saline. This idea is supported by water analyses from bores in the Paralana Embayment ([Figure 5.5.8](#)). We suspect that the salinity of the groundwater in the Paralana Embayment may be partly derived from surficial runoff over sodium-rich intrusions immediately to the west; these include outcropping Mount Neill Granite and the albite-rich Nooldoonooldoona Trondhjemite ([Figure 5.5.3](#)). However, fractured-rock aquifers within these altered intrusives would possibly deliver most of the saline water into the Cenozoic sediments buried within the Poontana Trough due to hydrological head.

Overall, the depth-slice conductivity data confirms that deep fresh water recharge occurs along the range front near Wooltana Homestead and Munyallina Creek, and also at Illawortina Creek in the southern area of the Poontana Trough ([Figure 5.5.6, 5.5.11](#)). Groundwater salinity data confirm the presence of fresh water within the Willawortina Formation in this vicinity ([Figure 5.5.8](#)). The broad scale conductivity model derived from AEM ([Figure 5.5.12](#)) is in excellent agreement with the known groundwater salinity.

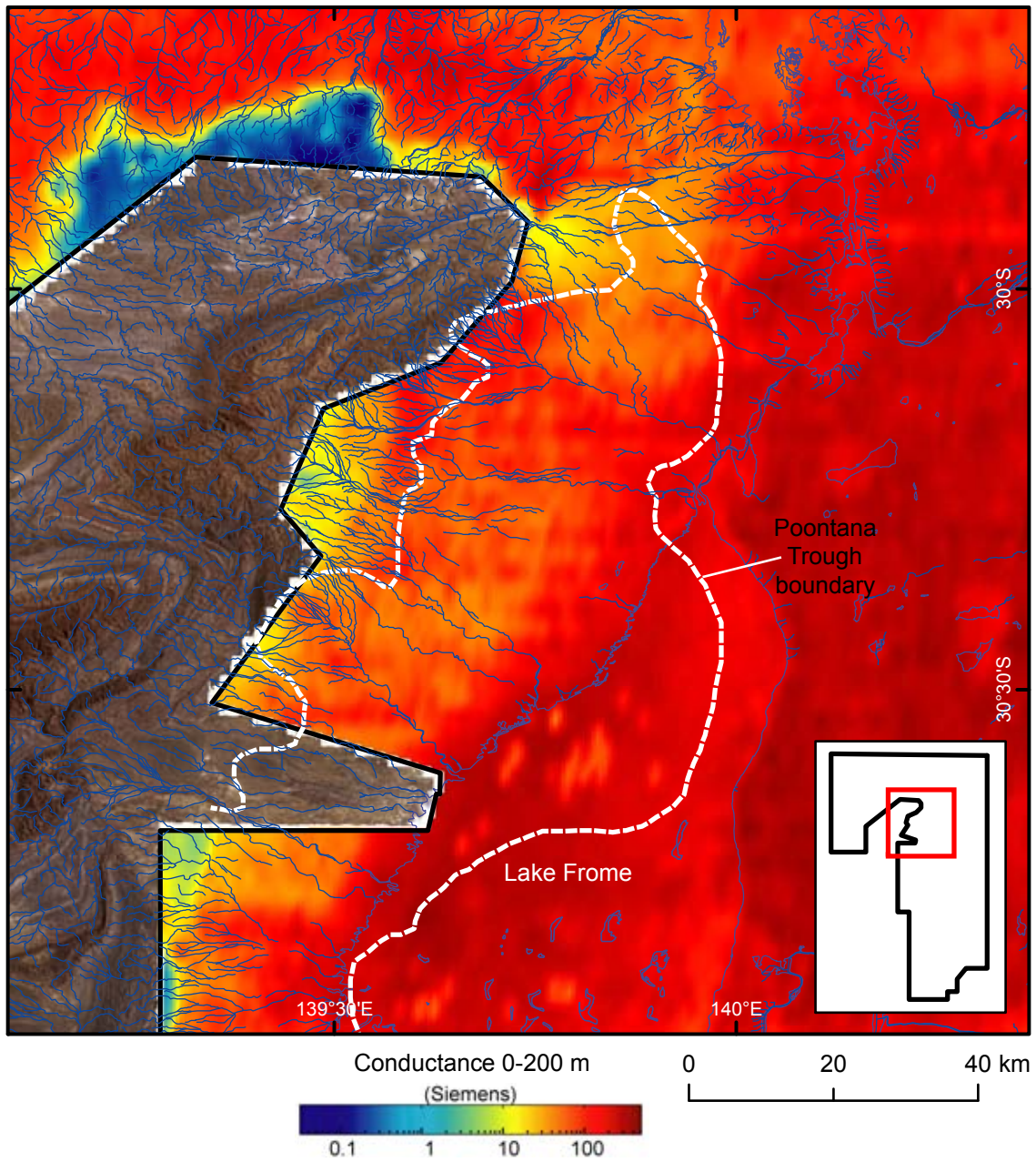


Figure 5.5.10: 0-200 m conductance image of the Poontana Trough area, showing simplified drainage.

Recognition of areas with fresh water versus more saline recharge is important: uranium at depth may be sourced from the chemical break-down of uranium-rich minerals in granitic boulders (within either Willawortina Formation or Namba Formation alluvial sediments). Uranium transported in solution as complexed uranyl ion (UO_2^{2+}), will percolate from shallow to deeper aquifers. Reduction and precipitation of uranium will then take place at depth within the Poontana Trough, generally below 100 m, provided suitable reductants are present in the sediment.

Airborne electromagnetic data in Figures 5.5.10 and 5.5.11 indicate that fresh water infiltration also occurs at Arkaroola Creek and at Teatree Outstation in the extreme southwest corner of the study area.

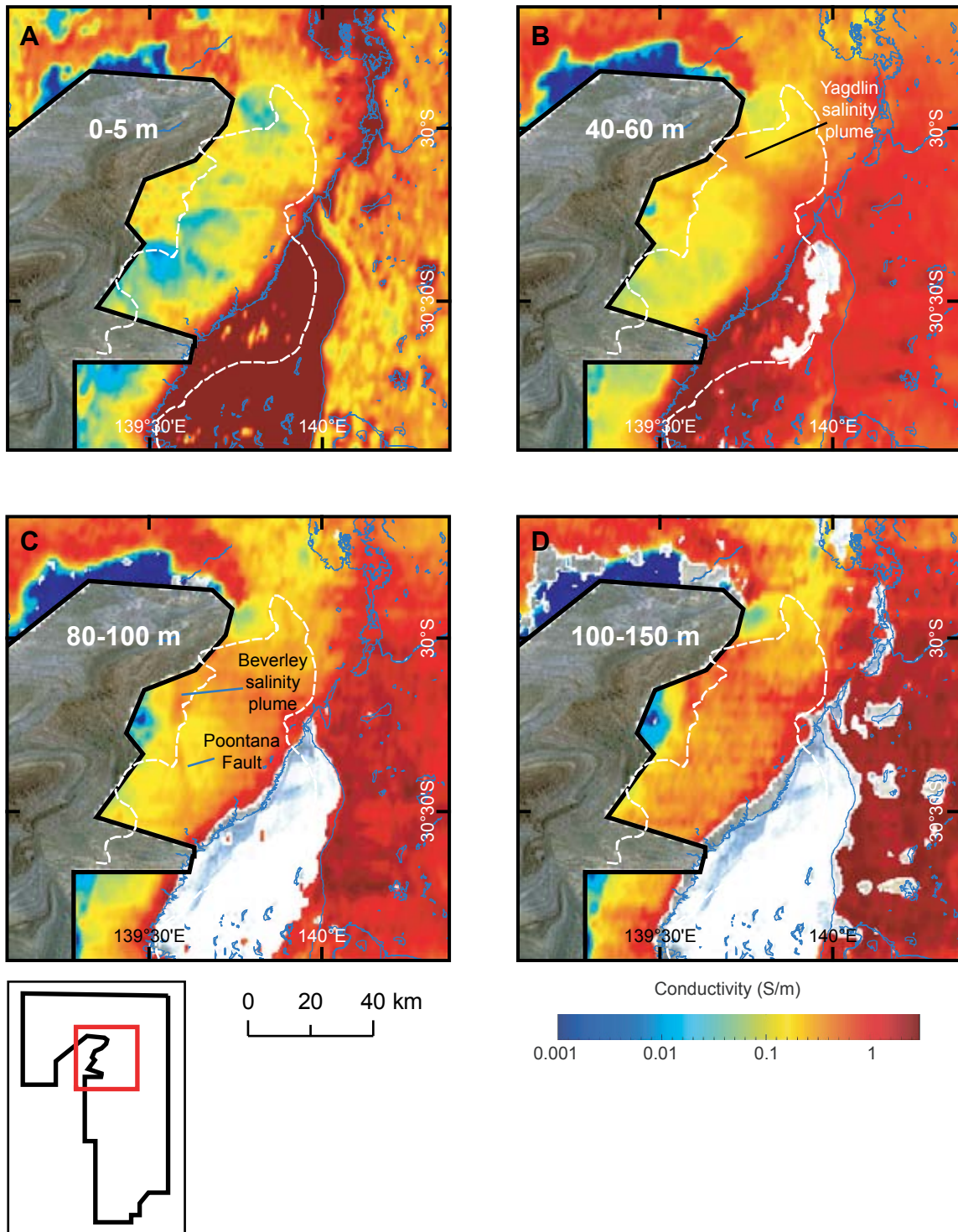


Figure 5.5.11: Conductivity depth slices from the Frome AEM Survey showing the Poontana Trough outline and selected groundwater salinity features. A: 0-5 m; B: 40-50 m; C: 80-100 m; D: 100-150 m.

5.5.3.2.3 Yagdlin salinity plume

A high conductivity feature is present between Parabarana Creek (labelled on Figure 5.5.6) to the north and the area immediately west of Beverley. The feature is apparent in all the depth-slices and is most obvious in the 40-60 m and 80-100 m conductivity depth slices (Figures 5.5.11B, C). The

feature extends along the range front from immediately northeast of Parabarana Hill to beyond the Yagdlin uranium prospect. Viewed in the 100-150 m conductivity depth-slice (Figure 5.5.11D), the western margin of the high conductivity feature strikes almost due north–south, between a point near the Pepegoona uranium deposit to a point to the west and south of Beverley. At relatively shallow depths (e.g. 40-60 m: Figure 5.5.11B), the salinity plume extends westward into the Paralana Embayment and just to the south of the Four Mile uranium deposits. This is in accord with public-domain geochemical analyses of groundwater within the Paralana Embayment, and those from Beverley, that indicate variable salinities ranging from moderately fresh to saline within the Namba and Willawortina formations (Figure 5.5.8).

We have interpreted the conspicuous high conductivity feature (centred on Yagdlin Dam; Figure 5.5.11B) as a salinity plume, referred to here as the “Yagdlin salinity plume” (Table 5.5.1). This plume is most probably formed by groundwater through-flow in adjacent fractured-rock aquifers within the deformed, altered and weathered intrusive units of the ~1580 Ma Coulthard Suite (Wade, 2011; including the Mount Neill Granite, Nooldoonooldoona Trondhjemite and Box Bore Granite), an unnamed granodiorite (SAGeodata stratigraphy number 5799) and the Pepegoona Porphyry, a coarse-grained, rhyodacitic, feldspar porphyry. With the probable exception of the Box Bore Granite, we speculate that alteration (i.e. albitisation) and chemical weathering of the Coulthard Suite will contribute substantially higher amounts of dissolved salts with abundant Na^+ and Cl^- , and also Ca^{2+} , Mg^{2+} and K^+ . By contrast, Moolawatana Suite intrusives, north of Parabarana Hill, are typically coarse-grained rapakivi-type granitoids with minor adamellite, all with significantly fewer sodic minerals than the Coulthard Suite. The lower relief and more stable potassium feldspar compositions are likely to weather more slowly and produce less saline groundwaters. Moreover, the catchment area of Hamilton Creek is large compared to the catchment of Parabarana Creek. Therefore, volumetrically less fresh water runoff is contributed from the steep and rugged Parabarana Creek catchment to reduce the build-up of saline waters within the Yagdlin salinity plume.

Based on the argument above, it is logical that surface runoff from the Flinders Ranges catchment of Hamilton Creek would have a fresh water character and, as discussed previously, this is evident in the conductivity depth slices that show a large low conductivity volume of sediment at the mouth of Hamilton Creek. This is confirmed in groundwater analyses from bores in the area where Hamilton Creek discharges across the northeast Lake Frome watershed. When compared to the other creeks that drain the northern Flinders Ranges, the catchment of Hamilton Creek is significantly larger. It also drains large areas of Neoproterozoic metasediments (Figure 5.5.8) that are not altered in the style of the Mt Neill intrusions.

In the absence of basin-wide piezometric data, the AEM mapping of salinity plumes within Cenozoic sediments of the Poontana Trough may provide a de facto means of mapping aquifer flow, and therefore also hydrocarbon migration fairways. It is not known whether the petroleum accumulated at Pepegoona has affinity with either fresh water or more saline aquifer waters, nor has the petroleum been geochemically analysed to determine its source affinity. However, if hydrocarbons are important for the reduction of uranyl complexes to uranium ore within the Paralana and Beverley uranium deposits, then the AEM conductivity data may provide a means of modelling more likely hydrocarbon migration scenarios.

5.5.3.2.3 *Southern Poontana Trough*

The southern Poontana Trough is located between Teatree Outstation, Wooltana Homestead and Lake Frome (Figure 5.5.6).

Flight line 3006001 has similar latitude to the Wooltana 1 stratigraphic drill hole (Figure 5.5.12), which was terminated at 244.5 m in basal Namba Formation. The Wooltana 1 drill hole is one of several type-sections for the Namba Formation (Callen and Tedford, 1976); at this locality, most of the Namba Formation sediments represent facies distal to the Ranges, i.e. mud and micritic, dolomitic palygorskite. The AEM data indicate that elevated salinity associated with Lake Frome is

mapped by very high surficial conductivity around its shoreline. Within the Wooltana 1 drill hole, the top of the Namba Formation, at 72 m, is in good agreement with the top of a more conductive volume as indicated upon flight line 3006001 (Figure 5.5.12).

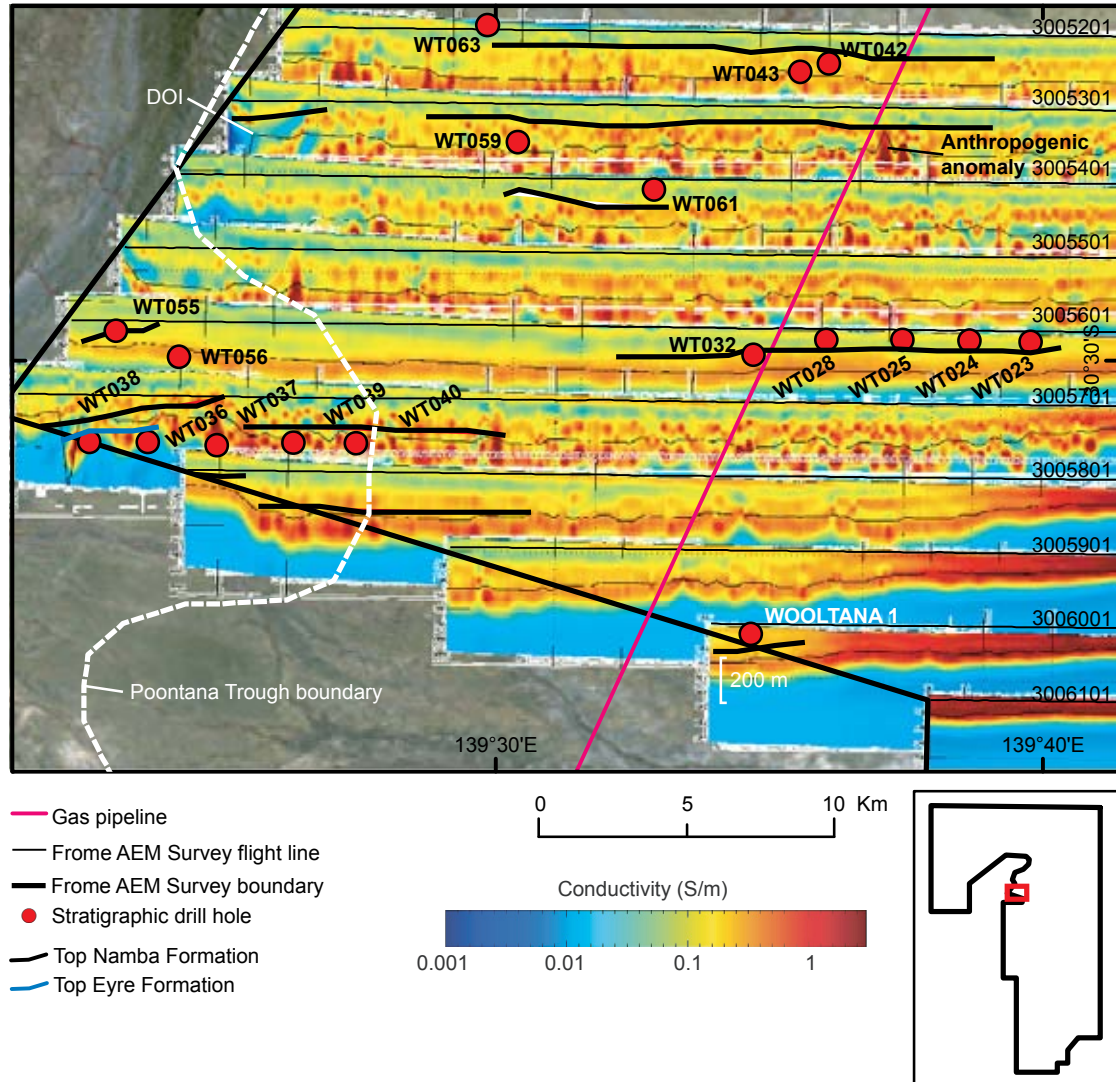


Figure 5.5.12: LBL GA-LEI conductivity sections, drill holes and unconformity interpretations in the southern part of the Poontana Trough case study area near the Wooltana 1 stratigraphic drill hole.

To the north of the Wooltana 1 drill hole, we have used wireline logs from Heathgate’s exploration drill holes to constrain and geologically validate the Frome AEM Survey data (flight lines 3005201 to 3005701). From wireline down-hole geophysics, the top of the Namba Formation (i.e. the Namba Formation/Willawortina Formation unconformity) can be identified in all the drill holes. Moreover, in three of these, the Eyre Formation/Namba Formation unconformity is also evident. In drill holes WT038 and WT036 (western end of flight line 3005701) the volume of sediment equated to the Namba Formation shows variable conductivity. Relatively resistive features in WT038 and WT036 are probably sandy facies of the Namba Formation filled with relatively fresh water. Fresh water is also indicated in the overlying Willawortina Formation sediments. A distinctive resistive (clayey) sedimentary volume is apparent within 80 m of the surface. To the east of WT037 the Namba Formation surface slopes eastward. Relatively resistive sediment in WT039 and WT040 is also likely to be sandy lithologies within the Namba Formation, saturated with fresh water. There is

displacement of strata and conductors in the LBL GA-LEI conductivity sections between WT037 and WT039, which is interpreted as due to faulting sub-parallel to the Flinders Ranges range front.

On flight line 3005701 the Namba Formation thins towards the west and the Namba Formation surface also dips in that direction. A similar picture emerges at the western end of flight line 3005601 (see drill holes WT055 and WT056; 2.5 km north of 3005701); in this area the Namba Formation is thickest where the overlying Pliocene-Quaternary sediments are thinnest in the vicinity of WT037. The relatively resistive Willawortina Formation suggests that fresh water is present in the vicinity of drill holes WT039 and WT040.

In most cases the Namba Formation surface derived from down-hole geophysics correlates with an increase in conductivity as demonstrated in the LBL GA-LEI conductivity sections. For example, on flight line 3005601 (Figure 5.5.12) the Namba Formation surface in drill holes WT023, WT024, WT025, WT028 and WT032 correlate very well with the top of the high conductivity layer represented as orange hues on Figure 5.5.12. Nonetheless, in flight line 3005401, an anomalously resistive feature is evident within the uppermost Namba Formation. Based on drill hole data of WT059 about 1.2 km to the north (of flight line 3005401) this feature may represent a palaeochannel carrying fresh water.

Several drill holes have been projected onto flight lines 3005201 and 3005301, the northernmost lines shown in Figure 5.5.12. The top of the Namba Formation correlates well with the top of a moderately conductive layer. This conductivity contrast represents a change from the dominantly gravely Willawortina Formation to predominantly clay of the underlying Namba Formation. Notwithstanding, low conductivity intra-Namba Formation sediments are indicated on flight line 3005301 near the vicinity of drill holes WT043 and WT042 and closer to the Flinders Ranges on flight line 3005201, west of WT063. The Namba Formation closer to the range front is more likely to contain coarser-grained sediments. The less conductive zones within the Namba Formation may represent more sandy facies containing fresher water and therefore these conductivity sections have significant potential to provide exploration targets for sandstone-hosted uranium.

Overall, the conductivity data show a trough-like basin. However, the highly-conductive area around Lake Frome makes it impossible to resolve the eastern margin due to limited depth of penetration in the Frome AEM Survey data.

5.5.3.2.4 Central Poontana Trough

The central region of the Poontana Trough includes the Paralana Embayment, the area of the Paralana uranium field, and Beverley ore body (Figure 5.5.13A, B). Similar to the area of the southern Poontana Trough, a salinity (conductivity) halo is present around the western margin of Lake Frome. To the west of this conductivity feature, the broad depression of the Poontana Trough is clearly resolved in the Frome AEM Survey data set (Figure 5.5.13).

As discussed previously, the Beverley ore body is at the eastern margin of a conspicuous conductivity high which is elongated north-south. It is referred to here as the “Beverley salinity plume”. This feature is resolved in the LBL GA-LEI conductivity sections through the Beverley area and also in the gridded data (Figure 5.5.13B). The Poontana Fault is also apparent in the same images and forms a southern extension to the Beverley salinity plume.

The Frome airborne electromagnetic survey, South Australia: implications for energy, minerals and regional geology

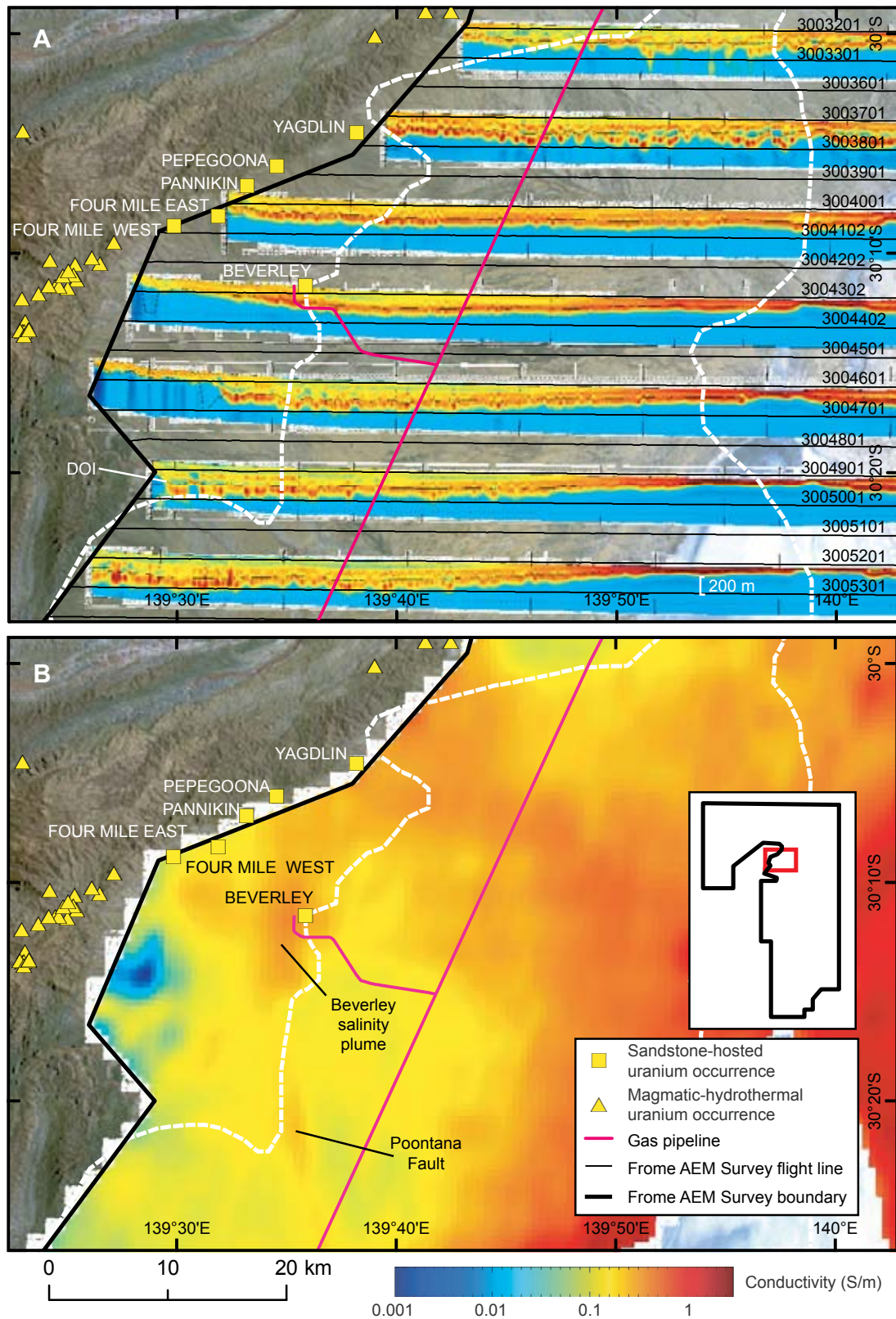


Figure 5.5.13: *A: The central Poontana Trough expressed as basin conductivity structures in LBL GA-LEI conductivity sections. B: The Beverley salinity plume and the Poontana Fault trace visible as conductivity anomalies in the 60-80 m depth slice.*

5.5.3.2.5 Stratigraphy and structure of the Paralana-Beverley area

The Frome AEM Survey data indicate that the Poontana Fault is the most significant subsurface structure in the greater Paralana-Beverley area. It connects the Beverley deposit with the deepest parts of the Poontana Trough; potentially it is a regional conduit for reduced fluids to migrate from depth into overlying strata including the Beverley palaeochannel within the upper Namba Formation. However, the Poontana Fault is not the only regional discontinuity resolved by the data set. Other notable linear features include several fault zones in the immediate Paralana-Beverley area.

The total magnetic intensity (TMI) and gravity images of the Paralana-Beverley area are shown in Figures 5.5.14A and B respectively. These geophysical images help to delineate the Paralana and Wooltana faults and the Vidnee Yarta and Poontana fault zones (Figure 5.5.14B; a slightly different model is given in Figure 3.42). With the exception of the Poontana Fault Zone, which has a width of about 2 km immediately south of Beverley, the regional faults trend mostly north-northeast to south-southwest. The gravity image defines a north-south trending gravity high, the Paralana Ridge, which most likely represents upthrust basement (a buried ridge of the Mount Painter Inlier). It separates the Paralana Embayment (see Figure 3.42 Paralana Trough) on the west from the rest of the Callabonna Sub-basin on the east. Overall, the structural fabric of the area is one of north-south- to northeast-southwest-striking faults, possibly thrusts, active during compressional neotectonics.

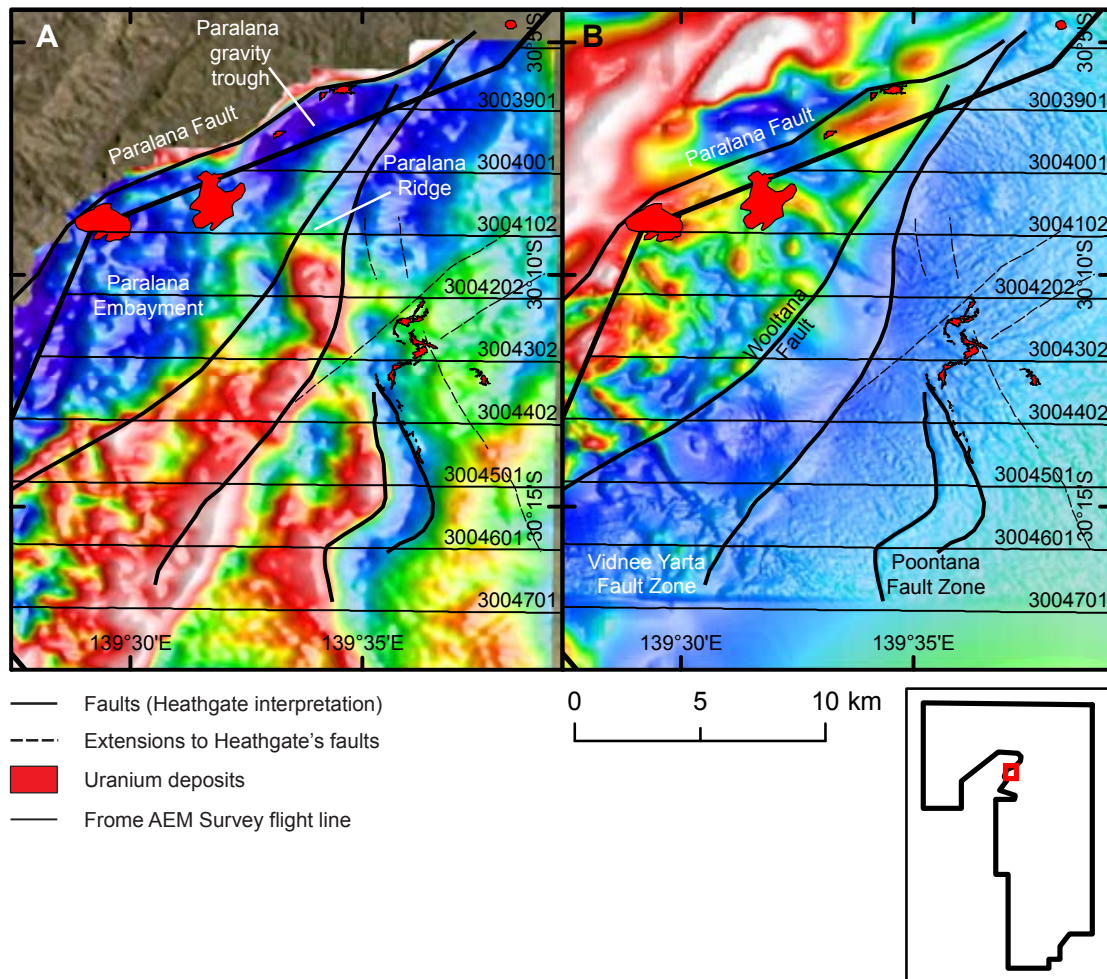


Figure 5.5.14: Paralana-Beverley region, central Poontana Trough. A: Gravity image showing locations of the Paralana Ridge and Paralana Embayment. B: Total magnetic intensity image showing major fault zones. Gravity and magnetic images from Heathgate.

The structure and stratigraphy within the immediate vicinity of Beverley is also evident in the LBL GA-LEI conductivity sections shown in Figure 5.5.15. The inversions delineate the known faults, including the Paralana and Wootana faults and the Vidnee Yarta and Poontana fault zones. Moreover, other significant faults may be indicated by disruptions to conductivity anomalies in the inverted data. These strike predominantly northeast-southwest and form a conjugate fault set, identified by dashed lines in Figure 5.5.15. The palaeochannel, host to the Beverley ore body, is developed at the intersection of this conjugate fault-set, which may have been growth faults that provided accommodation space for development of thick (Beverley) channel sands during the mid-Eocene.

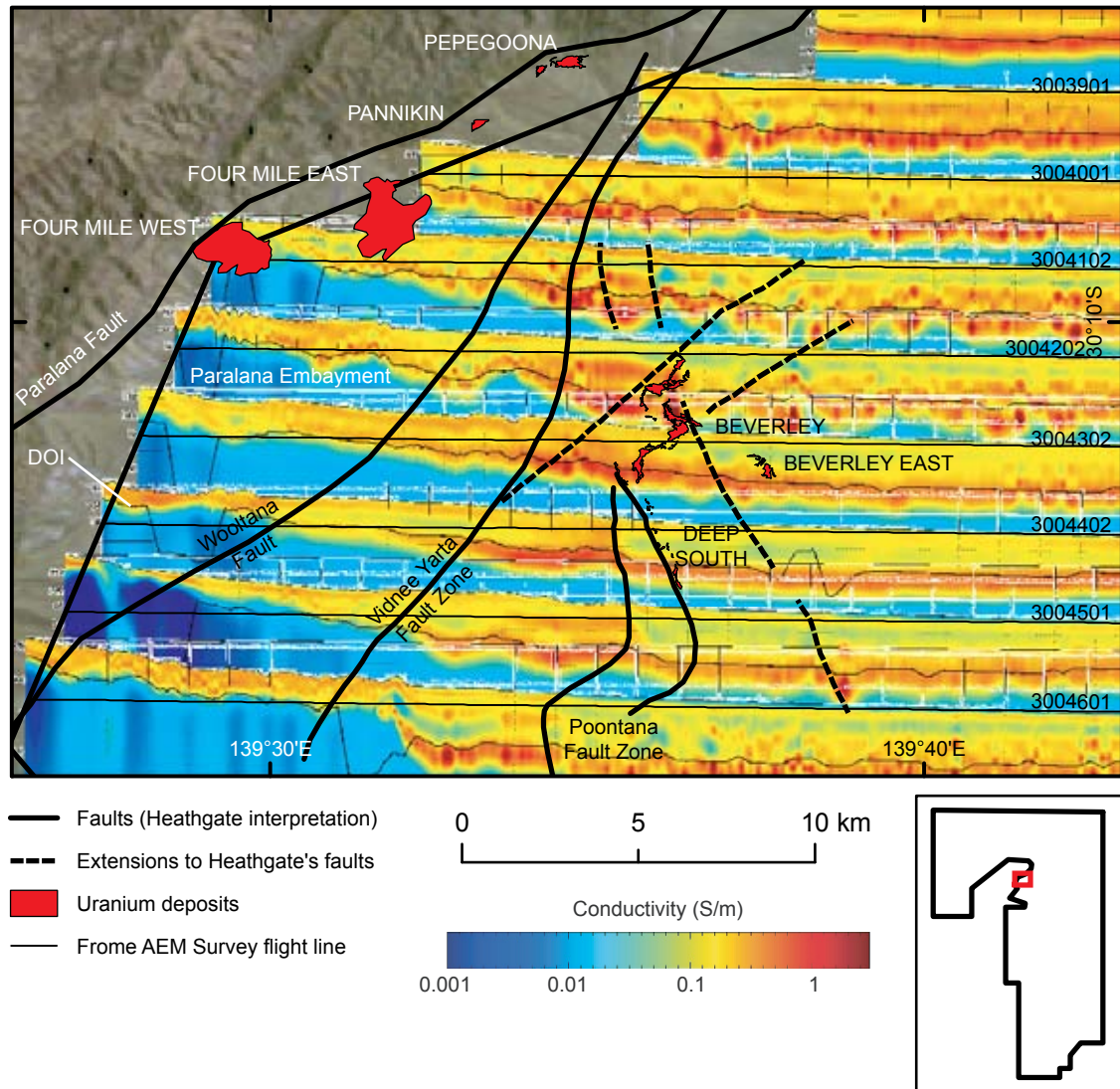


Figure 5.5.15: LBL GA-LEI conductivity sections highlighting interpreted structural features in the Beverley area.

In the area between the Beverley and Four Mile East deposits, the Paralana Ridge (a local gravity high: Figure 5.5.14A), is bounded on the west by the Wootana Fault and on the east by the Vidnee Yarta Fault zone, is also mappable by AEM (Figure 5.5.15). In the western portion of Figure 5.5.15, drilling shows that resistive crystalline basement occurs at shallow depth (≤ 100 m but often considerably less) and is depicted as various shades of blue (resistive) on the conductivity sections. The mostly resistive basement slopes eastward towards the depocentre of the Poontana Trough.

The Frome airborne electromagnetic survey, South Australia: implications for energy, minerals and regional geology

In Figure 5.5.16, drill hole WT074 is projected onto flight line 3004601. WT074 intersected the Namba Formation/Willawortina Formation unconformity at 50 m and Eyre Formation at 158 m. In this hole the Eyre Formation is only 13 m thick and, therefore, at the scale depicted, the top of the Bulldog Shale (strong conductor at base of sections in Figure 5.5.16) acts as a proxy for the top of the Eyre Formation (green line). Here both the Eyre and Namba formations are saturated with relatively fresh water. This is one of the few localities where the AEM signal penetrates both the Namba and Eyre formations. Analysis of down-hole geophysical logs shows that the Namba Formation in the vicinity of WT074 is arenaceous. This is consistent with closer proximity to the range front. Our interpretation is that the Beverley salinity plume extends from the southern extremity of the main Beverley deposit to the immediate vicinity of WT074. Within this 6.5 km tract, the Namba Formation contains more saline groundwater (see Figure 5.5.8).

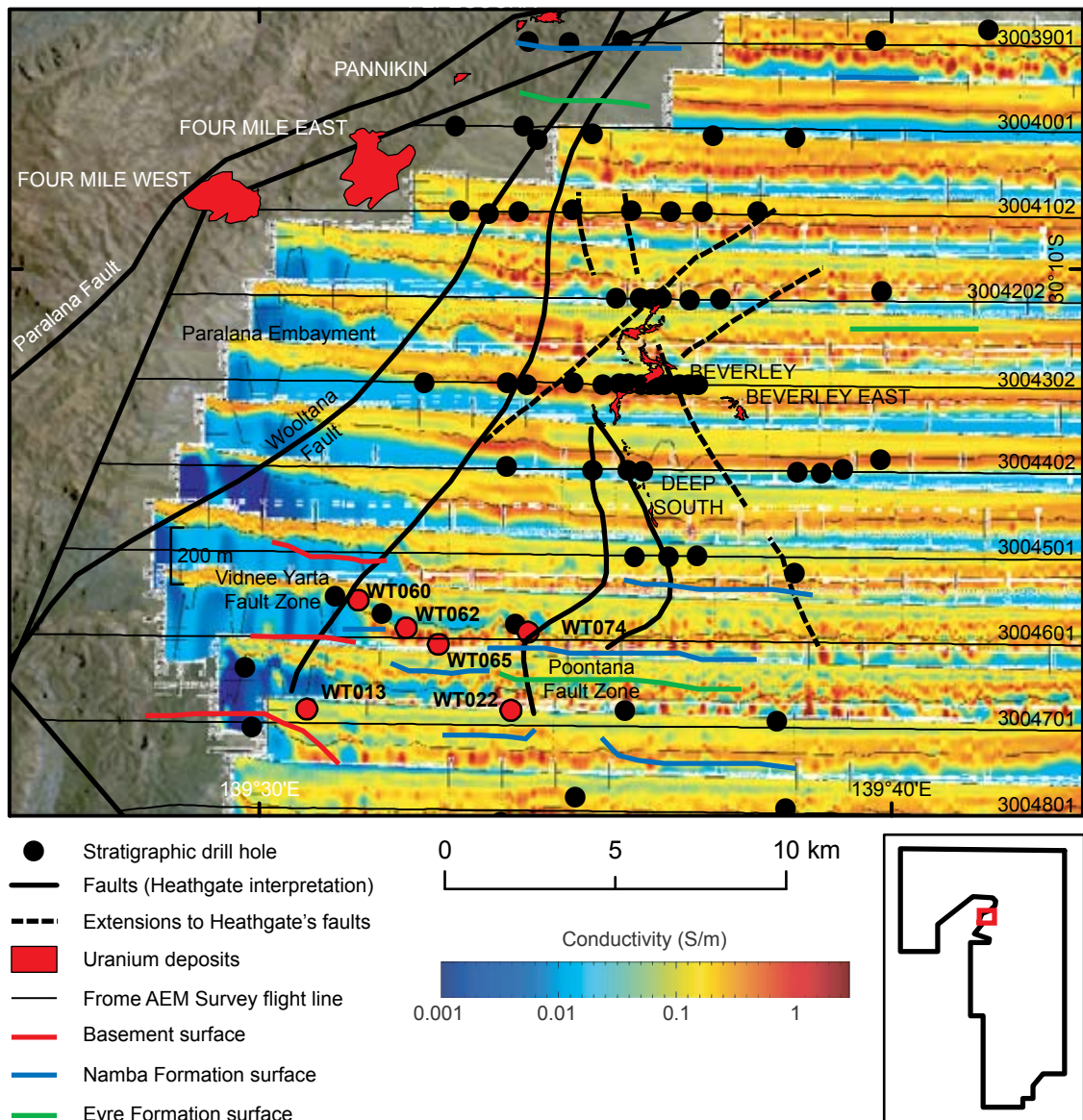


Figure 5.5.16: Interpreted unconformities within the greater Paralana-Beverley area. Interpretations are based on drill hole and wireline geophysical interpretations. Note the highly conductive volume of sediment immediately west of Beverley deposit, part of the Beverley salinity plume.

In the conductivity section just south of the Beverley salinity plume (flight line 3004601; [Figure 5.5.16](#)), the relatively resistive nature of the Namba Formation is shown in the vicinity of drill holes WT062 and WT065, and also immediately east of WT074. This situation is similar to the conductivity section from flight line 3004701 (2.5 km south), where the sedimentary units intersected in WT022 and the shallow buried crystalline basement in WT013 appear to be saturated by comparatively fresh water. Therefore in this area the Namba Formation must also be coarse and sandy. This interpretation is further supported by the low salinities in two local water-bores: Paralana House Bore (drill hole no. 87831; 2028 ppm TDS at ~ 110 m: Namba Formation) and North Arkaroola Bore (drill hole no. 87772; 1542 ppm TDS at ~ 64 m: Namba Formation) ([Figure 5.5.8](#)).

Coarse-grained facies of the Namba Formation not only occur in the subsurface. Indeed, there is also considerable evidence in outcrop for gravelly and sandy facies of the Namba Formation. Closer to the northern Flinders Ranges range front in the Four Mile West area (northern Paralana Embayment) the Namba Formation is exposed as a gravelly and sandy facies, capable of transmitting water in the sub-surface. One such locality is the Dead Tree Section ([Figures 5.5.5-5.5.7](#)) where the Eyre Formation/Namba Formation unconformity is exposed (MGA54 354011 mE 6664802 mN). Here a coarse-grained, alluvial fan of Namba Formation has incised the fluvial-aeolian sediments of the upper Eyre Formation ([Figure 5.5.5A](#)). Palaeo-fluids have used this unconformity as a hydrological conduit and ferruginous roll-fronts (typically 5 to 10 cm thick) are preserved in the uppermost metre of the Eyre Formation along the unconformity. Hore and Hill (2009) demonstrated that the Dead Tree Section roll-fronts are enriched in uranium and thorium. Around 2.3 km south of the Dead Tree Section, at “Kaolin Gully” (MGA54 354407 mE 6662504 mN; [Figure 5.5.6, 5.5.7](#)), gully erosion has exposed a section through gravelly Namba Formation. Here Namba Formation is weathered to a permeable residuum of sub-angular coarse sand, granules and quartz pebbles, in a matrix of kaolin. This locality forms part of the southern headwaters of Four Mile Creek and the expected high permeability of this stratum would facilitate local recharge of the Namba Formation and Willawortina Formation aquifers. Infiltration of recharge water through the gravelly, kaolin-rich alluvial facies of the Namba Formation, outcropping close to the Flinders Ranges range front, provides a likely means for soluble ions to enter the Cenozoic aquifers of the Paralana Embayment.

The interpreted top of Namba Formation from holes WT062 and WT065 are projected onto the AEM section of flight line 3004601 ([Figure 5.5.16](#)). At this locality Namba Formation sediments are over-thrust from the west and faulted to form a graben filled with Willawortina Formation.

5.5.3.2.6 Beverley deposit and northern Paralana Embayment

Flight lines 3004501 and 3004402 cross an area where many exploration drill holes are available to aid the interpretation of the conductivity sections ([Figure 5.5.17](#)). The top of Namba Formation unconformity surface interpreted from these holes indicates a down-throw to the east of 65-75 m on the Poontana Fault between drill holes PR305 and PR700 (flight line 3004402). On the same flight line the apparent dip of the top of Namba Formation surface (between drill holes PR305 and W592) is westward towards the northern Flinders Ranges and the unconformity is overprinted by the Beverley salinity plume. This is in contrast to the apparent easterly slope of the Namba Formation surface interpreted on flight line 3004302, some 2.5 km to the north, which crosses the main southern Beverley ore body. The slope is towards the depocentre of the Poontana Trough. The conductivity of the Namba Formation along flight line 3004302, between the Beverley ore body and the Paralana Ridge is considerably higher (a consequence of the Beverley salinity plume); this contrasts with less conductive Namba Formation immediately to the east and west of this zone. Conductivity sections for flight lines 3004202 and 3004302 also indicate that the lower Willawortina Formation is more conductive between the Beverley deposit and the Paralana Ridge. By contrast, east of the southern Beverley ore body (i.e. eastward of drill hole WD1298 projected onto flight line 3004302), and across the Beverley East ore body, the mid-Willawortina Formation has overall low conductivity.

Flight line 3004102 was flown 2.5 km north of Beverley and crosses the Paralana Ridge and Four Mile West deposit within the northern Paralana Embayment. The corresponding section (Figure 5.5.17) possibly indicates the repetition of a prominent conductor interpreted as the top of the Namba Formation. Note the vertical repetition of the inclined Namba Formation unconformity indicated on flight line 3004102 at drill holes PR980 and BV128. The interpreted data indicate that the Vidnee Yarta Fault Zone is a reverse-thrust zone variously dipping eastward. It is sub-parallel to the main thrusting along the Paralana Fault that defines the eastern margin of the range front, consistent with compressional neotectonism reported for this region of the northern Flinders Ranges (e.g. Sandiford, 2003). Some 2.5 km north of Beverley, conspicuous resistive volumes of (lower) Willawortina Formation between BV147 and BV131, and also between BV131 and PR1525 on flight line 3004102, are bodies of fresh water superimposed upon sandy and gravelly alluvial fan sequence.

The AEM survey did not cover the immediate vicinity of Pepegoona deposit. Consequently we are not able to scrutinise the AEM response to silicification and the presence of groundwater silcretes associated with the Paralana uranium field.

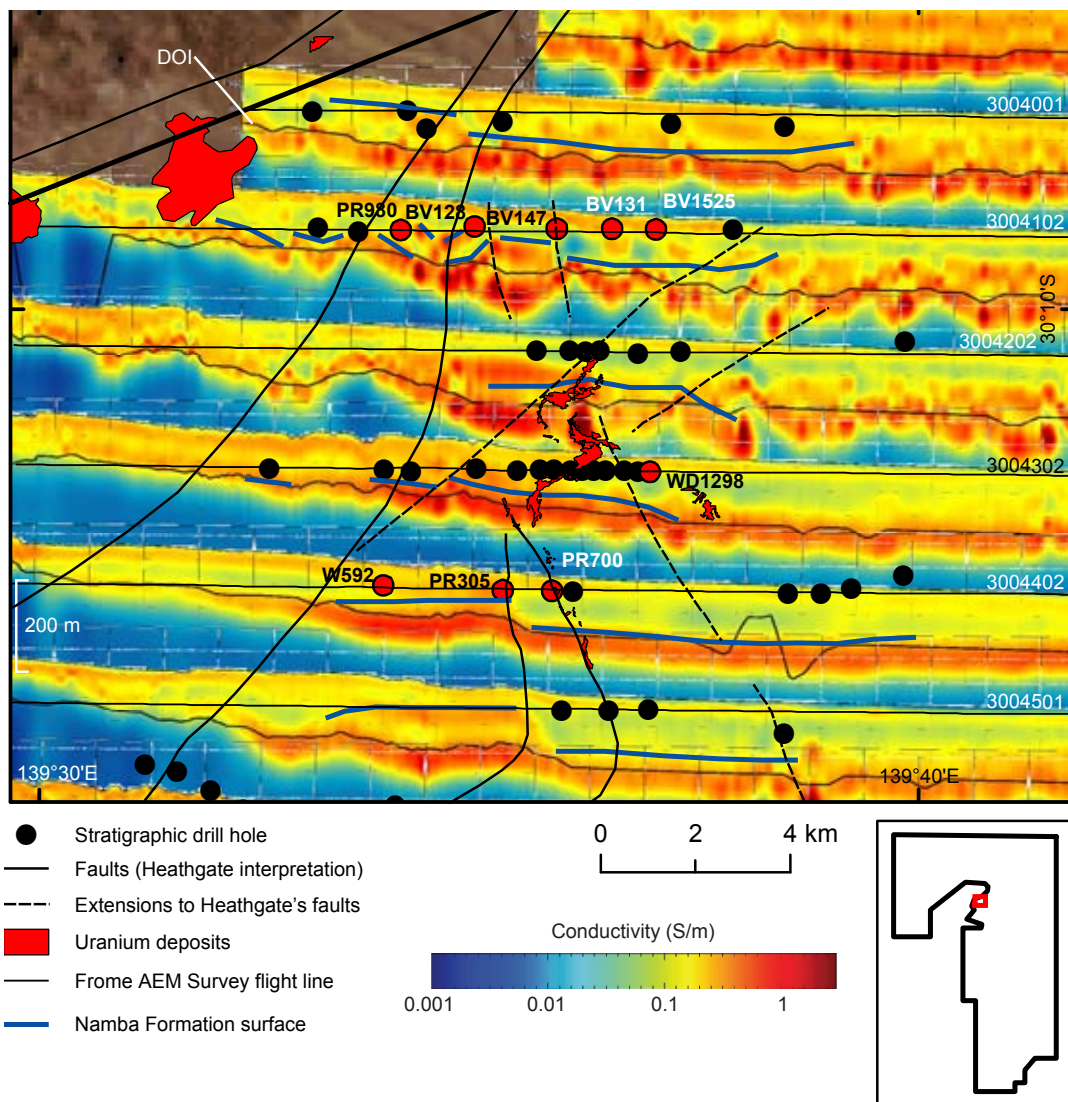


Figure 5.5.17: Namba Formation unconformity interpretation over LBL GA-LEI conductivity sections, Beverley area.

5.5.3.2.7 *Hydrochemistry of the Beverley water-monitoring bores*

Water monitoring bores are situated on the periphery of Beverley uranium deposit as a regulatory measure to detect any excursions of acidic mining solution beyond the well-fields. Pre-mining groundwater analyses from these holes in the immediate vicinity of Beverley uranium ore confirm that water within the Namba Formation east of the Beverley ore zone is relatively fresh ($1800 < \text{TDS} < 4900$ ppm, $n = 57$) compared with groundwater immediately west ($5100 < \text{TDS} < 13500$ ppm, $n = 58$) of the deposit (Figure 5.5.18A). Salinity data for the overlying Willawortina Formation (Figure 5.5.18B) show a similar trend. This is an important observation because it may help to partly explain why the Beverley ore body is located precisely where it is. Our working hypothesis is as follows: uranium is mobilised in (fresh water) solution as a uranyl (UO_2^{2+}) complex, for example with carbonate ions. With an influx of saline groundwater, uranyl and carbonate become disassociated due to the preference for the formation of (for example) Na_2CO_3 in solution. Thus U^{6+} within uranyl is made available for reduction, especially by mobile reductants within the aquifer. Irrespective of the specific chemical transformations that give rise to uranium ore, mixing of groundwaters of different salinities clearly occurs in the vicinity of the Beverley ore zone. The salinity gradient is evident in the Frome AEM Survey data across the deposit. This observation provides explorers for sandstone-hosted uranium with an additional technique to reduce exploration risk.

5.5.3.2.8 *Northern Poontana Trough*

Down-hole geophysics from eighteen drill holes was interpreted from the area of the northern Poontana Trough. Interpreted unconformity surfaces are superimposed on the LBL GA-LEI conductivity sections shown in Figure 5.5.19. In the southwest of the area, the Namba Formation/Willawortina Formation unconformity is the uppermost conductor of significance. In drill hole PR1567 the depth to the top of Namba surface is 124 m; this depth is consistent across a cluster of holes drilled at the western end of flight lines 3003601 and 3003801 near the Yagdlin prospect. Here the lithofacies of the Namba Formation are similar to those at Beverley. The Namba Formation comprises multiple cycles of clayey silt with minor intervals of fine sand, the latter presumably deposited within channels; some of the upper sand contains uranium mineralisation. In this area, the conductivity profiles on AEM sections indicate relatively flat-lying, highly-conductive clays and silts with no indication of low-conductivity sandy units saturated with fresh water.

The western ends of flight lines 3003201, 3002901 and 3002801 show a volume of low conductivity sediment within 5 km of the Flinders Ranges. In drill hole YR040, this corresponds to sandy Eyre Formation. In more northern sections (flight lines 5001901 and 5001801), drill hole and AEM data indicate that relatively resistive features in the upper parts of the sections correspond to a fresh water aquifer within the Namba Formation (with fresh water runoff from the relatively large Hamilton Creek catchment as the likely source of recharge).

The stratigraphy near the Yagdlin prospect is different to that in the northwest corner of the study area, where highly conductive Bulldog Shale is known to outcrop or occur beneath thin cover. The Bulldog Shale is expressed in the conductivity sections as near-surface highly conductive layers with an apparent easterly dip. The true dip orientation of the Cretaceous and Cenozoic strata is more towards the northeast and the depocentre of the Cooper and Eromanga basins near the South Australia/Queensland border.

The AEM response is strongly perturbed in the area of the Terrapinna Structural Corridor (Figure 5.5.1), that separates the Mt Painter and Mt Babbage Inliers, and extends basin-ward along a west-southwest—east-southeast strike. In Figure 5.5.19 this faulted zone is evident in the western end of the section corresponding to flight line 5001901, the eastern end of flight line 3001601, and flight line 3002001, ~3 km east of drill hole YR042. Low-conductivity material between 50 and 100 m of the surface indicates a significant volume of low-salinity groundwater within Pliocene-Quaternary cover between Moolawatana Station and Lake Callabonna.

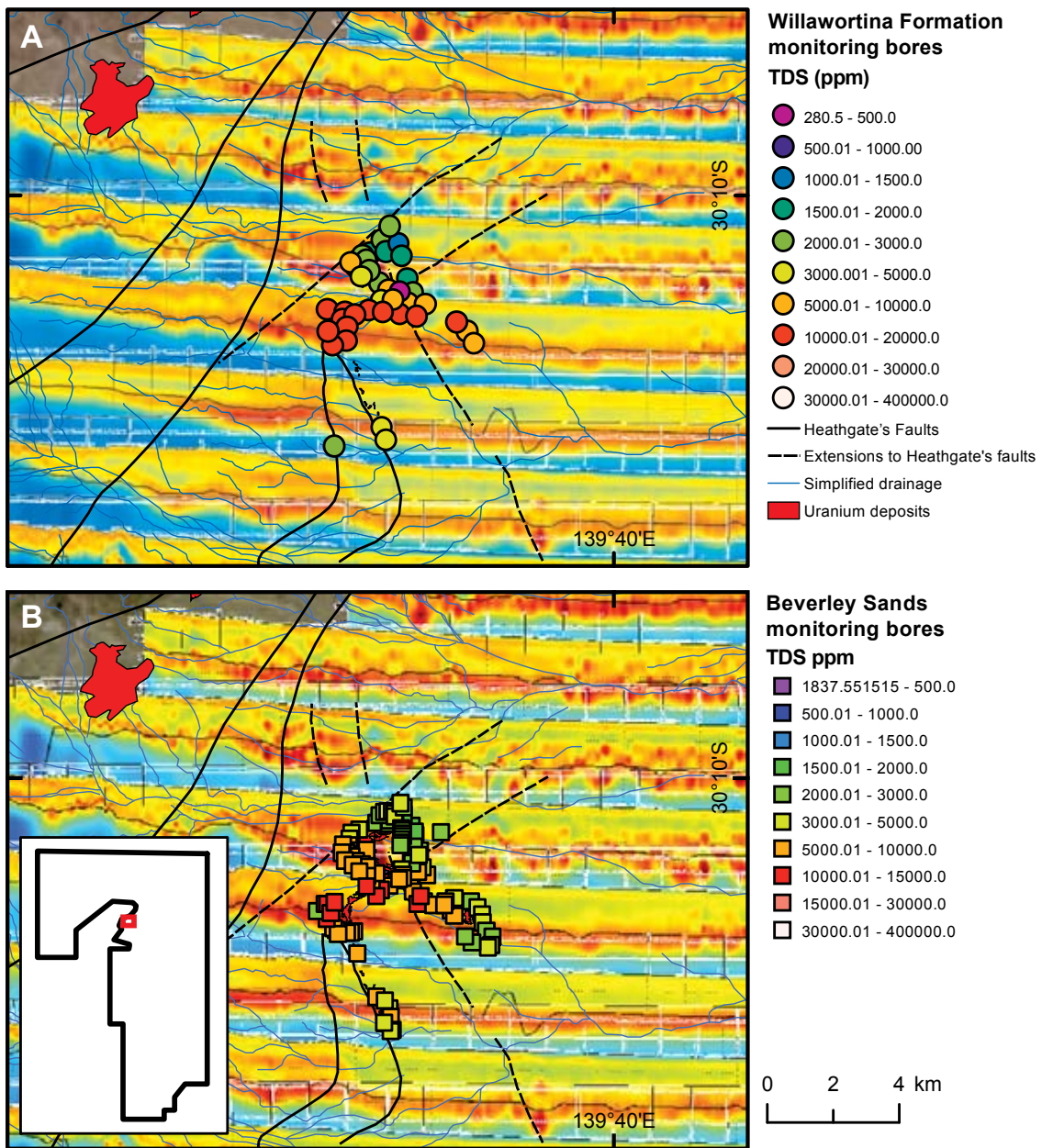


Figure 5.5.18: Salinity (TDS ppm) of compliance water-monitoring bores on the periphery of Beverley uranium deposit. **A:** Willawortina Formation. **B:** Upper Namba Formation (“Beverley Sands”).

5.5.4 Conclusions

Inverted data from the 2010 Frome AEM Survey provides useful insights into the stratigraphic and structural architecture of the Poontana Trough, including aspects of the uranium mineralising system(s). These are summarised below:

1. The broad structure of the Poontana Trough is well delineated by AEM. The data can be used to improve previous models of the Poontana Trough that were based on publicly-available drill hole and seismic data (e.g. Fabris *et al.*, 2010);
2. Clayey sediments within the upper Namba Formation are easily recognised as a conductor beneath the surface in the Poontana Trough; therefore the Namba Formation/Willawortina Formation unconformity is readily mapped. This conductive volume is perturbed in many areas, notably close to the Flinders Ranges range front where faulting is known to displace

the Cenozoic units. The Frome AEM Survey data can assist to resolve the magnitude and extent of displacement;

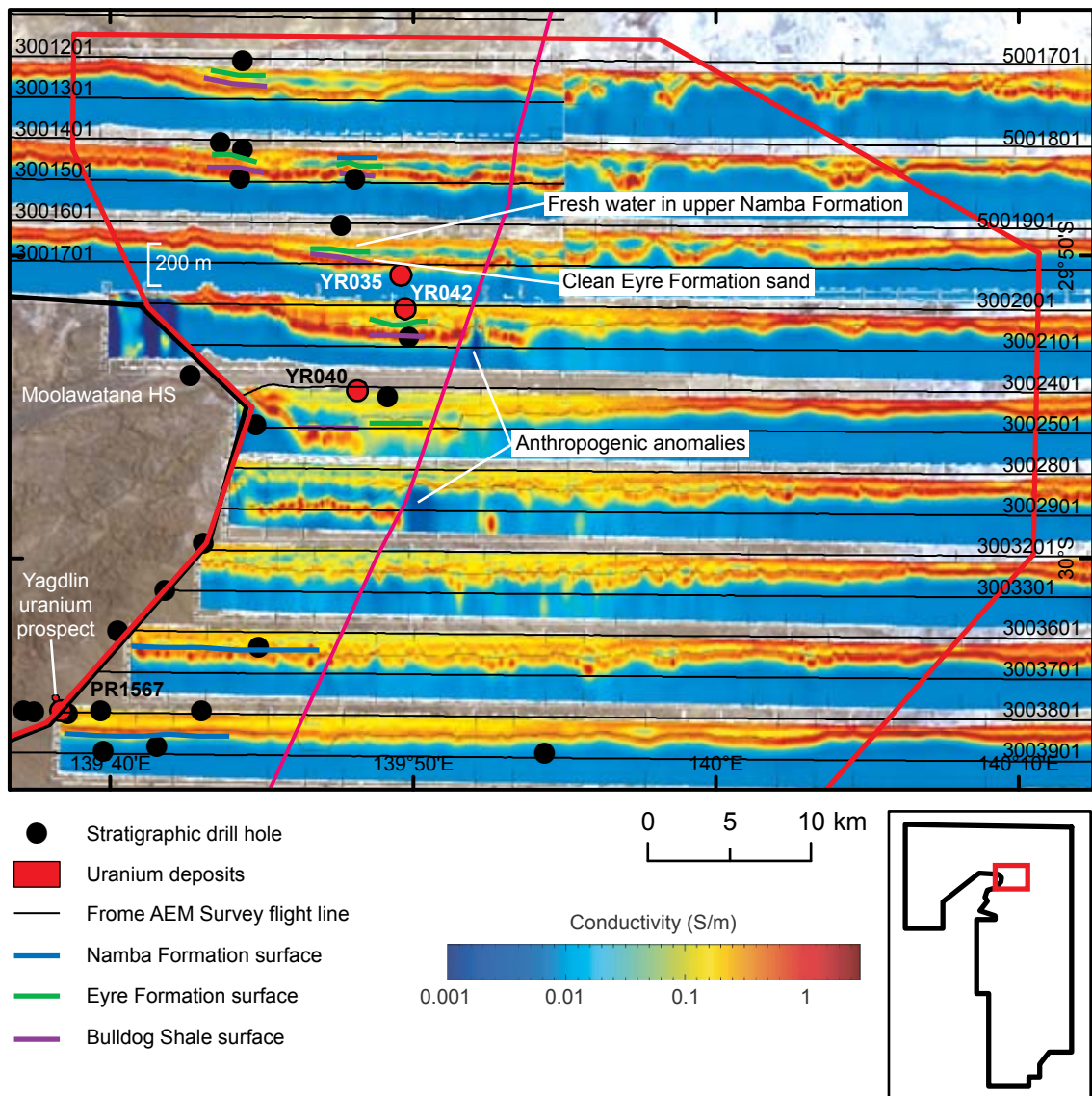


Figure 5.5.19: Northern Poontana Trough in the vicinity of Moolawatana Homestead showing stratigraphic, groundwater and anthropogenic features in LBL GA-LEI sections.

3. In the Beverley-Paralana area, electrical conductivity changes are associated with several known faults including the Paralana and Wooltana faults and the Vidnee Yarta and Poontana fault zones. These regional features are also mappable using high-resolution magnetic and gravity data. The faults mostly have a northeast-southwest orientation. An exception is the Poontana Fault Zone, that has an overall north-northwest—south-southeast trend. Moreover, additional faults, which also strike predominantly northeast-southwest, are apparent in the AEM survey data. These may be significant with respect to uranium deposition. The Beverley palaeochannel is developed at the intersection of an interpreted conjugate fault-set, associated with the intersection of the Vidnee Yarta and Poontana fault zones. Dextral movement and reactivation of the faulted blocks is indicated, and dilation arising from interaction between faults may have facilitated the migration of reducing fluids from the deeper Poontana Trough into the shallower Cenozoic units;

4. In the area between the Beverley and Four Mile East deposits, the Paralana Ridge (a local gravity high), bounded on the west by the Wooltana Fault and on the east by the Vidnee Yarta Fault Zone, is also apparent in the AEM data. Stacked repetition of an inclined conductive volume adjacent to the Vidnee Yarta Fault Zone, north of Beverley, is consistent with thrust faulting. The interpretation is also consistent with geophysical log data from drill holes in the area. A throw of up to 75 m on the Poontana Fault Zone is estimated from the conductivity sections, between 2.5 and 5 km south of the Beverley deposit;
5. A volume of sediment containing high salinity water is inferred between Beverley uranium deposit and the Vidnee Yarta Fault Zone. This high conductivity feature, the “Beverley salinity plume” is mappable between the vicinity of Pepegoona uranium deposit near the Flinders Ranges range front, to an area ~6.5 km south of the main Beverley deposit. Conductivity sections demonstrate that the salinity anomaly straddles the Namba Formation/Willawortina Formation unconformity. The source of the saline plume appears to be related to the small bedrock catchment of the Mt Neill massif. Albitised rocks, which predominate in the catchment, are potential sources of highly weatherable plagioclase to produce saline groundwater in fractured-rock aquifers that are in connection with groundwater in adjacent Cenozoic sediments of the Poontana Trough;
6. Fresh water recharge is evident in AEM data along the northern Flinders Ranges range front especially where: Hamilton Creek discharges from the Flinders Ranges just south of Moolawatana Homestead; within the Paralana Embayment; and, near Teatree Outstation and Moro Creek near the southeast corner of the study area; and,
7. The Beverley uranium deposit is located where fresh groundwater mixes with saline groundwater of the “Beverley salinity plume”. The distribution of fresh and saline groundwater is mappable using data inverted data from the Frome AEM Survey, which offers a new approach to target sites of uranium deposition and thereby reduce exploration risk.

5.5.5 References

- Callen, R. A. and Tedford, R. H., 1976. New Late Cainozoic rock units and depositional environments, Lake Frome area, South Australia. *Transactions of the Royal Society of South Australia* **100(3)**, 125-167.
- Cross, A., Jaireth, S., Hore, S. B., Michaelsen, B. and Schofield, A., 2010. SHRIMP U-Pb detrital zircon results, Lake Frome region, South Australia. *Geoscience Australia, Canberra. Record* **2010/46**, 28 pp.
- Draper, J. J. and Jensen, A. R., 1976. The geochemistry of Lake Frome, a playa lake in South Australia. *BMR Journal of Australian Geology and Geophysics* **1**, 83-104.
- Fabris, A. J., Gouthas, G. and Fairclough, M. C., 2010. The new 3D sedimentary basin model of the Curnamona Province: geological overview and exploration implications. *MESA Journal* **58(September 2010)**, 16-24.
- Heathgate Resources, 1998. Beverley Uranium Mine: Environmental Impact Statement. Main report. Heathgate Resources Ltd, Adelaide.
- Hore, S. B. and Hill, S. M., 2009. Palaeoredox fronts: setting and associated alteration exposed within a key section for understanding uranium mineralisation at the Four Mile West deposit. *MESA Journal* **December 2009**, 34-39.
- Marsland-Smith, A. B., Huddleston, A., Packer, B. and Smith, A., 2011. Uranium exploration and recently discovered uranium deposits in the Frome Embayment, South Australia. In: Forbes, C. J. (editor): 6th Sprigg Symposium, Adelaide. *Geological Society of Australia Abstracts* **100**, 43-46 pp.
- Sandiford, M., 2003. Chapter 8-Neotectonics of southeastern Australia: linking the Quaternary faulting record with seismicity and in situ stress. In: Hillis, R. R. and Muller, R. D. (editors), *Evolution and dynamics of the Australian plate*. Geological Society of Australia, Sydney. **Special Publication No. 22**, 101-113 p.
- Wade, C. E., 2011. Definition of the Mesoproterozoic Ninnerie Supersuite, Curnamona Province, South Australia. *MESA Journal* **62**, 25-42.

5.6 MAPPING STRUCTURES: INTERPRETATION OF THE FROME AEM SURVEY FOR THE LEIGH CREEK- MARREE REGION, SOUTH AUSTRALIA

T. Wilson and I. C. Roach

5.6.1 Introduction

In the Frome Embayment, recent airborne electromagnetic survey data are typically used to explore for minerals in shallow, relatively undeformed sedimentary environments, predominantly for sandstone-hosted uranium. During the mid to late 1990s, BHP Minerals Pty Ltd used airborne EM surveys to explore for copper oxide and sulphide mineralisation associated with diapirs throughout the Adelaide Geosyncline (Rennison and Rutley, 1996).

The Frome AEM survey area is dominated by extensive sedimentary basins, however, it also includes areas of the Neoproterozoic Adelaide Geosyncline, specifically the Nackara Arc and the northwest Flinders and Willouran ranges (Figure 3.6). As the Frome AEM Survey covers these structurally complex areas it provides an opportunity to assess whether reliable structural information can be derived from AEM data.

This case study includes an area of interest of approximately 9000 km² in the northwest Flinders Ranges and Willouran Ranges from south of Leigh Creek to the township of Marree in the north (Figure 5.6.1).

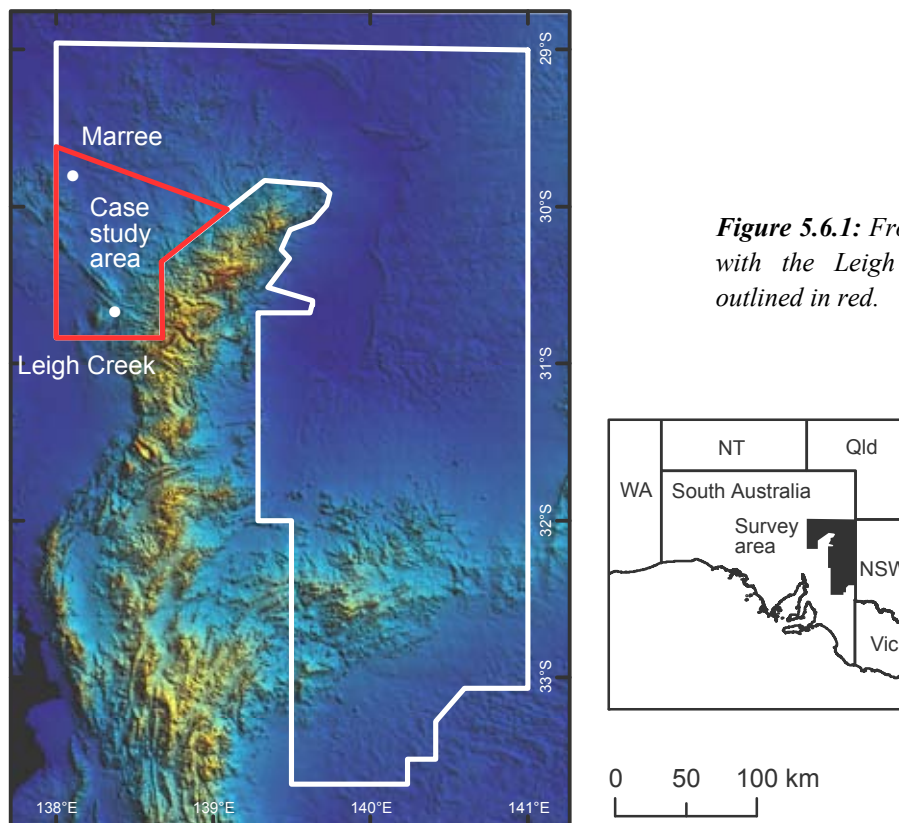


Figure 5.6.1: Frome AEM survey area with the Leigh Creek-Marree area outlined in red.

For this particular area, the focus of interpretive work was on outcropping Neoproterozoic sequences and the overlying Triassic-Jurassic Telford Basin. Sedimentary sequences of the Cambrian Arrowie Basin, Cretaceous Eromanga Basin and Cenozoic Pirie-Torrens and Lake Eyre basins and the Beltana Sub-basin were not included in the interpretation.

5.6.2 Outline of regional geology

The area covers the northwest corner of the MARREE and southwest corner of the COPLEY 1:250 000 map sheets which include sequences of the Neoproterozoic Callana Group, Burra Group, Umberatana Group and Wilpena Group, as well as the younger Triassic-Jurassic Telford Basin (see [Figure 3.10](#)). The complete stratigraphic succession of the Adelaide Geosyncline is shown in [Figures 3.6](#) and [3.7](#), however, in the area not all units are present. Those units outcropping in the area are briefly outlined below. Further detail is available in Drexel *et al.* (1993), Drexel and Preiss (1995) and Preiss (1987).

5.6.2.1 Callanna Group

The oldest rocks in the area are the Callana Group, representing the oldest sequences of the Adelaide Geosyncline, and have been subdivided into the Arkaroola and Curdimurka subgroups. In the Mount Painter region to the east and the Peake and Denison inliers to the north of the area, coarse clastics of the basal Arkaroola Subgroup unconformably overlie pre-Adelaidean basement. Within the area, the Black Knob Marble and the Wooltana Volcanics are the only units represented from the Arkaroola Subgroup. The Black Knob Marble occurs as disrupted blocks within the Willouran Ranges (Preiss, 1993).

Approximately 50 km to the west of the area, within the Willouran Ranges, is the Clara Saint Dora copper mine, where over 6000 t of ore were extracted in the early 1900s (Preiss, 1993). A very minor occurrence of the Wooltana Volcanics occurs in the area near the Boolooroo Diapir. Within the area, an incomplete stratigraphic sequence of the Curdimurka Subgroup is observed and consists of the basal Dome Sandstone, Recovery Formation, Cooranna Formation and the Boorloo Siltstone.

In general, the Callanna Group has undergone more deformation than other Neoproterozoic units in the Flinders Ranges. In particular, the Curdimurka Subgroup varies from intact bedded sediments to remobilised, carbonate-cemented breccia forming diapiric structures that intrude younger sedimentary sequences. These diapiric structures are common throughout the Flinders and Willouran ranges (Preiss, 1993).

5.6.2.2 Burra Group

Within the area the Burra Group is represented by the Top Mount Sandstone Beds, Willawalpa Formation and the Copley and Witchelina quartzites of the basal Emeroo Subgroup.

The Emeroo Subgroup is conformably overlain by the Skillogalee Dolomite of the Mundiallo Subgroup. Repetitive lithologies of intraclastic dolomite and magnesite, cryptalgal laminated dolomite (including stromatolite biostromes), siltstone and sandstone characterise the Skillogalee Dolomite. In the eastern Willouran Ranges the Skillogalee Dolomite is notably sandier, reflecting a cratonic clastic source (Hearon *et al.*, 2010; Preiss, 1993).

Magnesite mud-pellet conglomerates are typical of the Skillogalee Dolomite, particularly in the Willouran Ranges, where the thickest beds have been mined for magnesite near Myrtle Springs and Witchelina Station ([Figure 5.6.5](#)) (Preiss, 1993). In the central Flinders Ranges, at Burra, the Skillogalee Dolomite is host to copper mineralisation where 2 Mt was mined between 1845 and 1981 (Preiss, 1993). In the northern Flinders and Willouran ranges, the Skillogalee Dolomite is conformably overlain by the shallow marine Myrtle Springs Formation of the Bungarider Subgroup (Preiss, 1993).

Widespread diapirism and extensional faulting are associated with the depositional break between the Burra Group and overlying Umberatana Group (Preiss, 1993).

5.6.2.3 Umberatana Group

The Umberatana Group encompasses all of the glacial deposits of the Adelaide Geosyncline and consists of four subgroups ranging from Sturtian to Early Marinoan age (Preiss, 1993).

In the area the basal Yudnamutana Subgroup is comprised of the Bolla Bollana and Merinjina tillites and the Lyndhurst and Wilyerpa formations. Unconformably overlying is the Nepouie Subgroup which includes the Serle Conglomerate, the Tapley Hill Formation with the basal Tindelpina Shale Member and the Balcanoona Formation.

The Tapley Hill Formation is an interglacial sequence dominated by very thinly laminated carbonaceous, partly calcareous, siltstone. The basal Tindelpina Shale Member is pyritic and carbonaceous, with thin laminated grey dolomite interbeds and lenses and is the host unit for several small copper mines in the northern Flinders Ranges. Copper deposits occur elsewhere in the upper units of the Tapley Hill Formation, at Kapunda in the southern Flinders Ranges and at Mount Gunson on the Stuart Shelf. Gold bearing quartz-carbonate-sulphide veins also occur in the Tapley Hill Formation. Subsequent erosion of these veins resulted in the alluvial gold deposits of the Teetulpa Goldfield (Preiss, 1993; Robertson, 1991).

Unconformably overlying the Nepouie Subgroup is the Upalinna Subgroup consisting of the Angepena and Yankaninna formations, the Amberoona Formation, the Enorama Shale and the Trezona Formation. The overlying Yerelina Subgroup is represented by the Fortress Hill Formation, the Mount Curtis Tillite, the Balparana Sandstone and the Elatina Formation.

5.6.2.4 Wilpena Group

The youngest subdivision of the Adelaidean succession, the Wilpena Group, represents two major marine transgressive-regressive cycles. The first is interpreted as due to melting of extensive Marinoan icesheets (Preiss, 1993) and includes the Nuccaleena Formation at the base overlain by the Brachina Formation including the Moolooloo Siltstone Member, the ABC Range Quartzite and equivalent Ulupa Siltstone.

The second transgressive-regressive cycle is represented by the Pound Subgroup, which in the area consists of the Bunyeroo Formation, the Wonoka Formation, including the Wearing Dolomite Member and the Rawnsley Quartzite. Several small copper prospects associated with the Wearing Dolomite Member occur around Beltana in the northern Flinders Ranges (Preiss, 1993).

5.6.2.5 Delamarian Orogeny

Broad, open, dome and basin structures throughout the central Flinders area formed during folding and deformation associated with the Cambro-Ordovician Delamarian Orogeny. Diapiric activity throughout the area is particularly associated with a late, tensional phase of the Delamarian Orogeny (Preiss, 1987).

5.6.2.6 Telford Basin and associated basins

Several isolated structural depressions, or intramontane basins, contain Late Triassic fluvial and freshwater lacustrine deposits including the Leigh Creek Coal Measures. Due to tectonism these sediments are now preserved in synclines surrounded by the Neoproterozoic sequences in the Leigh Creek area (Kwitko, 1995).

5.6.3 Methods

As outlined in [Chapter 4](#), the Geoscience Australia Layered Earth Inversion (GA-LEI) uses a 1D layered earth conductivity structure that assumes the earth is a series of horizontal layers stacked in a layer-cake fashion. Each layer extends infinitely in the horizontal direction and each layer has a constant conductivity. In a relatively undeformed sedimentary basin environment the GA-LEI performs particularly well. In a structurally complex environment, however, many of the datasets produced by the GA-LEI process were less useful for interpretation, e.g. the Line-By-Line GA-LEI (LBL GA-LEI). The most informative and useful GA-LEI datasets for interpreting structural information in this area were the Sample-By-Sample GA-LEI (SBS GA-LEI) 400 m inversion conductivity sections and conductivity depth slices. An explanation of the two inversions is included in [Chapter 4](#).

The SBS GA-LEI conductivity sections and conductivity depth slices were imported into an ArcGIS™ project along with the South Australian 1:100 000 scale geology layer, tectonic sketches for the COPLEY and MARREE 1:250 000 scale map sheets and all available digital field observation sites for the state. The conductivity sections and the 1:100 000 scale geology were also imported into a GOCAD™ project to assist with 3D visualisation and interpretation.

Using the ArcGIS™ and GOCAD™ projects the AEM data were scrutinised for variations in conductivity which might be correlated to the known geology. Conductivity variations of interest were then compared to the 1:100 000 scale geology, tectonic sketches and field observation data to determine a possible cause for the variation. In areas where dip directions were interpreted from the conductivity sections a comparison was made with measured field observations. Interpretations using the conductivity depth slices, such as regional scale faulting, were validated using the 1:100 000 scale geology and 1:250 000 tectonic sketches.

The emphasis of the interpretation was on outcropping Neoproterozoic sequences and the Triassic-Jurassic Telford Basin.

5.6.4 Results

5.6.4.1 Regional Scale Faults

Within the conductivity depth slices, several abrupt changes from resistive to conductive structure can be observed in the southwest corner of the area (Figure 5.6.2). These variations in conductivity are persistent to depths of approximately 80 m, at which point the areas of high conductivity fall below the Depth Of Investigation (DOI) and consequently are not represented in the data.

These abrupt changes in the conductivity structure coincide with the Norwest, Mount Deception and Ediacara faults, which juxtapose resistive Neoproterozoic sequences against the more conductive sedimentary sequences of the Pirie-Torrens Basin and the Beltana Sub-basin (Figure 5.6.2).

5.6.4.2 Bedding

By the nature of AEM data collection in 3-dimensional geological environments, combined with the SBS GA-LEI process, which forces the data to fit a layered earth model, a considerable number of artefacts may be introduced into the conductivity sections. Despite this, it is still possible to extract meaningful dip or apparent dip directions.

In many places conductivity variations in the conductivity sections coincide with bedding in the Neoproterozoic sequences. In some areas where the conductivity sections are at a high angle to the strike direction, dipping conductive structures can be observed consistent with the known dip direction.

Line 4003301 coincides with an area where the flight direction and strike of the Neoproterozoic sequences are sub-parallel. In this area sub-horizontal conductivity structures correlated with bedding are observed in the AEM data (Figure 5.6.3A), although these are not consistently present throughout the data. Similar conductivity structures occur elsewhere in the area, however, the flight lines are at a high angle to the strike direction, indicating that conductivity anomalies may merely be artefacts in the data (Figure 5.6.3B) or that they are strongly influenced by sub-vertical fractures or conductive objects out of the plane of the flight line.

The Frome airborne electromagnetic survey, South Australia: implications for energy, minerals and regional geology

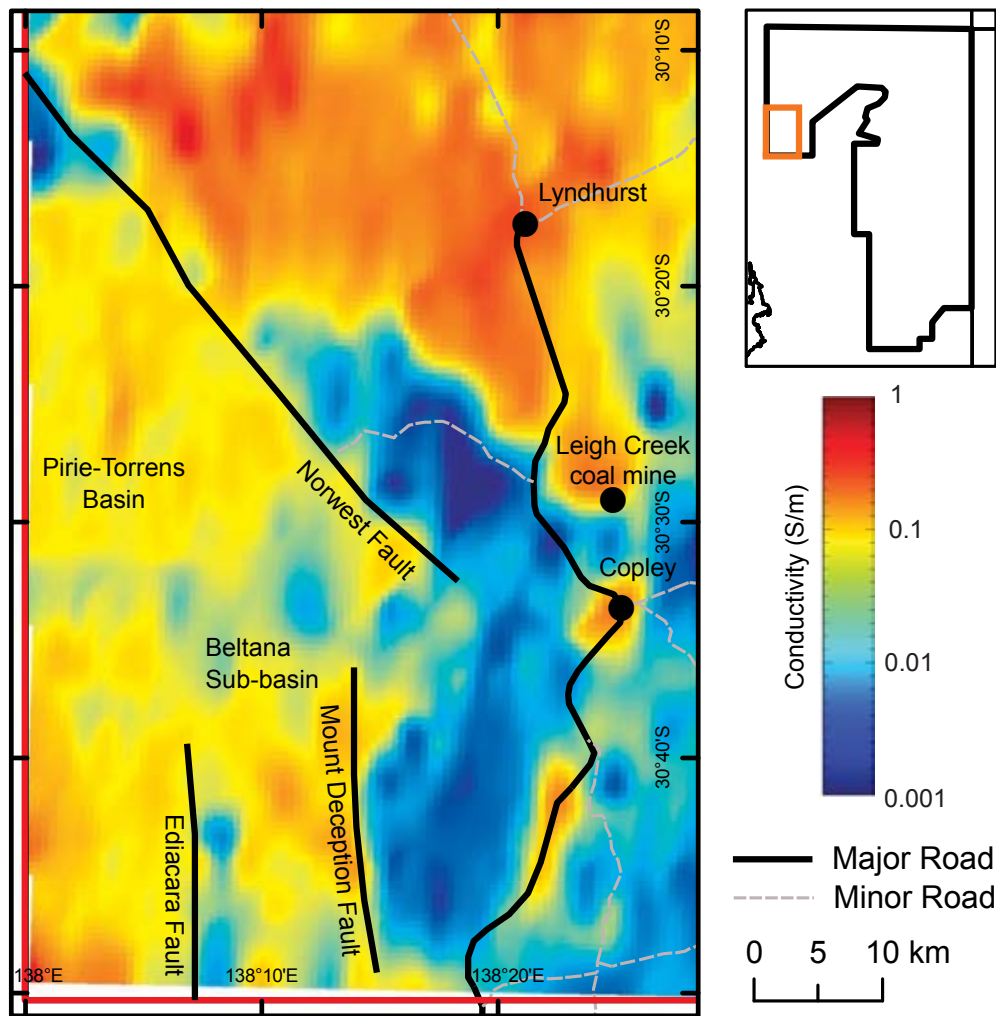


Figure 5.6.2: SBS GA-LEI conductivity depth slice (5-10 m) showing abrupt changes from resistive Neoproterozoic sequences to conductive sedimentary sequences associated with regional scale faults.

The Frome airborne electromagnetic survey, South Australia: implications for energy, minerals and regional geology

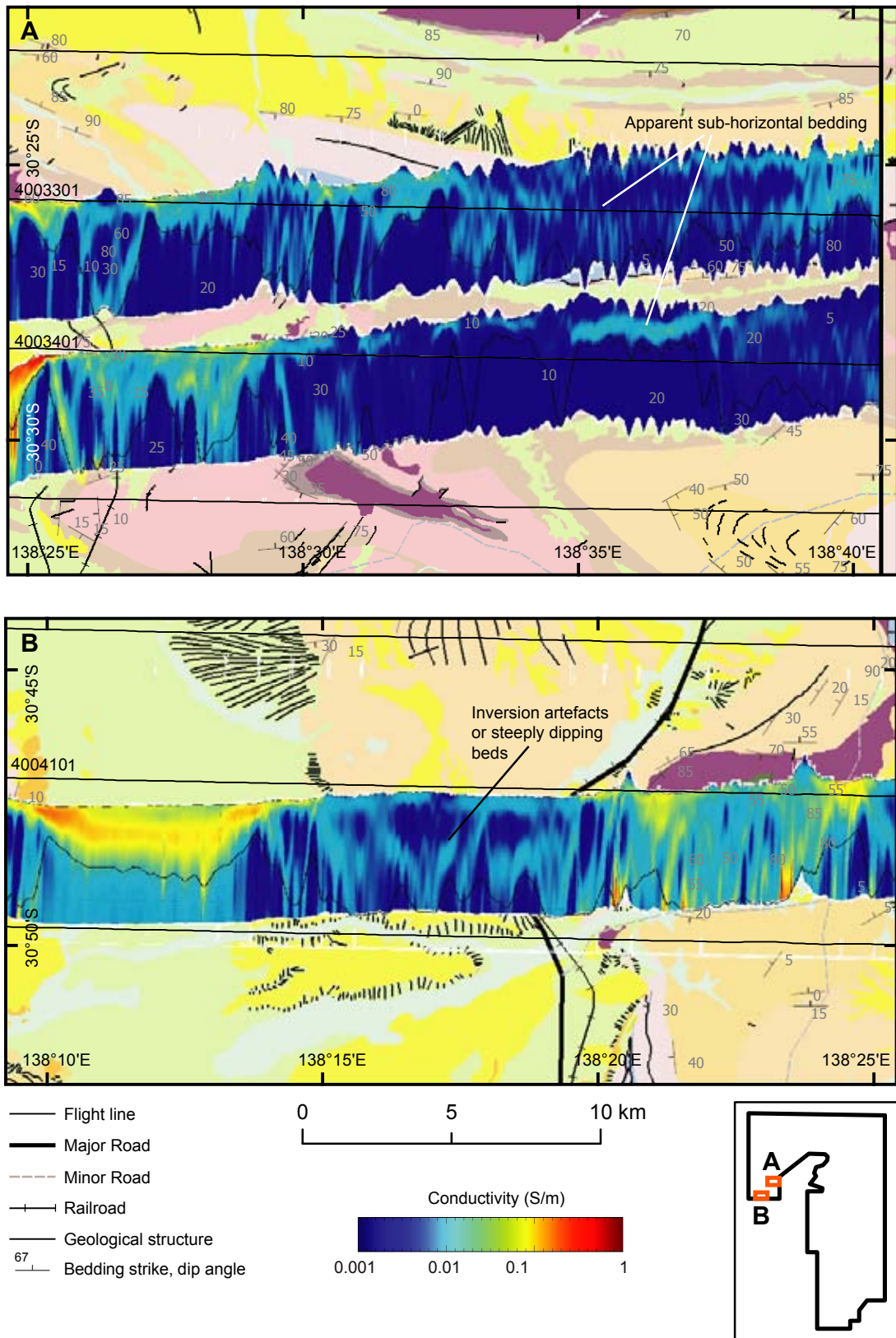


Figure 5.6.3: *A*: Conductivity anomalies associated with bedding; *B*: Conductivity anomalies that are not associated with bedding and appear to be inversion artefacts or steeply-dipping fractures.

5.6.4.3 Diapiric Structures

Numerous diapirs have been mapped within the region, including the Witchelina, Lyndhurst, Burr, Boolooroo, Coffin, Copley, Moolooloo and Beltana diapirs.

The Witchelina Diapir, in the northwest of the area, is intersected by line 4002301. A clear truncation of the conductivity structure associated with bedding either side of the diapir and disrupted structure coinciding with the diapir are apparent in the AEM data (Figure 5.6.4). In this figure, the Witchelina Diapir contains the Curdimurka Subgroup (labelled Nk in Figure 5.6.4B) which disrupts the Witchelina Quartzite (Now) and the Skillogalee Dolomite (Nms). Figure 5.6.4C is an annotated version of the conductivity section shown in Figure 5.6.4A.

The Lyndhurst Diapir, intersected by lines 4002601, 4002701 and 4002801, coincides with a high conductivity structure. Similarly, the Burr Diapir (lines 4002902, 4003001, 4003101), the Coffin Diapir (line 4003401), the Copley Diapir (line 4003601), the Moolooloo Diapir (line 4003801) and the Beltana Diapir (line 4004101) all coincide with high conductivity structures. The disrupted conductivity structure observed in the Witchelina Diapir is absent in the other diapirs.

The Boolooroo Diapir is situated between lines 4003301 and 4003401 and, therefore, is not represented in the AEM data.

5.6.4.4 Magnesite deposits in the Skillogalee Dolomite

Sedimentary magnesite beds are present within the Skillogalee Dolomite and are thicker or more concentrated at several localities including Mount Playfair, Myrtle Springs, Mount Hutton, Mount Hutton South and Camel Flat. Where flight lines coincide with these localities a pronounced conductivity high is observed in the AEM data, for example Myrtle Springs, Mount Hutton South and Camel Flat (Figure 5.6.5).

5.6.4.5 Tapley Hill Formation

In the southeast region of the area lines 4003701 and 4003801 show an approximately 10 km by 12 km area of high conductivity. This high conductivity structure coincides with an anticlinal core developed in the Tapley Hill Formation (Figure 5.6.6). A similar conductivity feature occurs in known basal Tapley Hill Formation in the Olary Spur region of the Frome AEM survey.

The Frome airborne electromagnetic survey, South Australia: implications for energy, minerals and regional geology

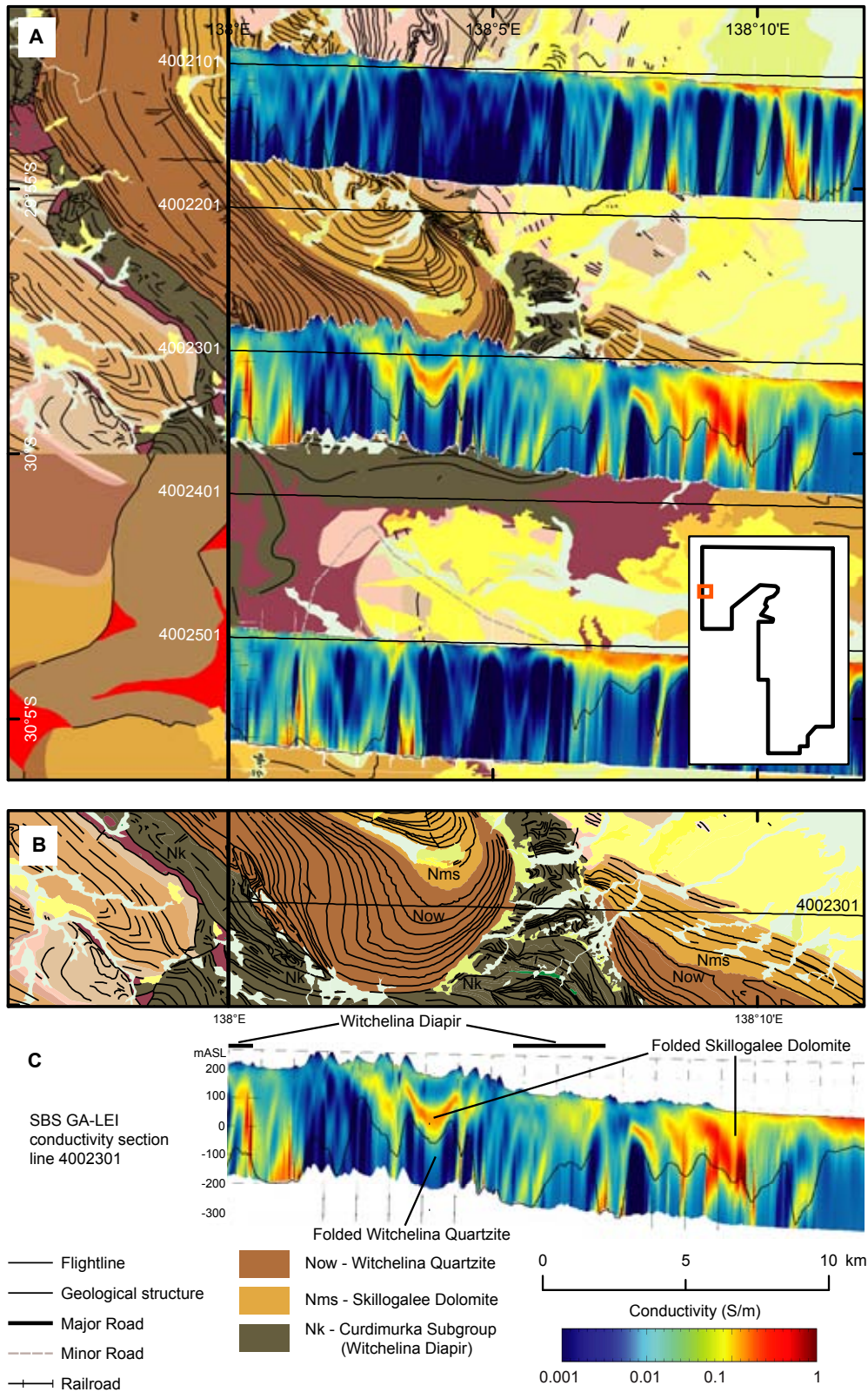


Figure 5.6.4: Conductivity structures associated with the Witchelina Diapir. **A:** Overview of the Witchelina Diapir with 1:100 000 geology and SBS GA-LEI conductivity sections; **B:** Detailed geology of line 4002301 with generalised geological structures; **C:** Annotated conductivity section of line 4002301.

The Frome airborne electromagnetic survey, South Australia: implications for energy, minerals and regional geology

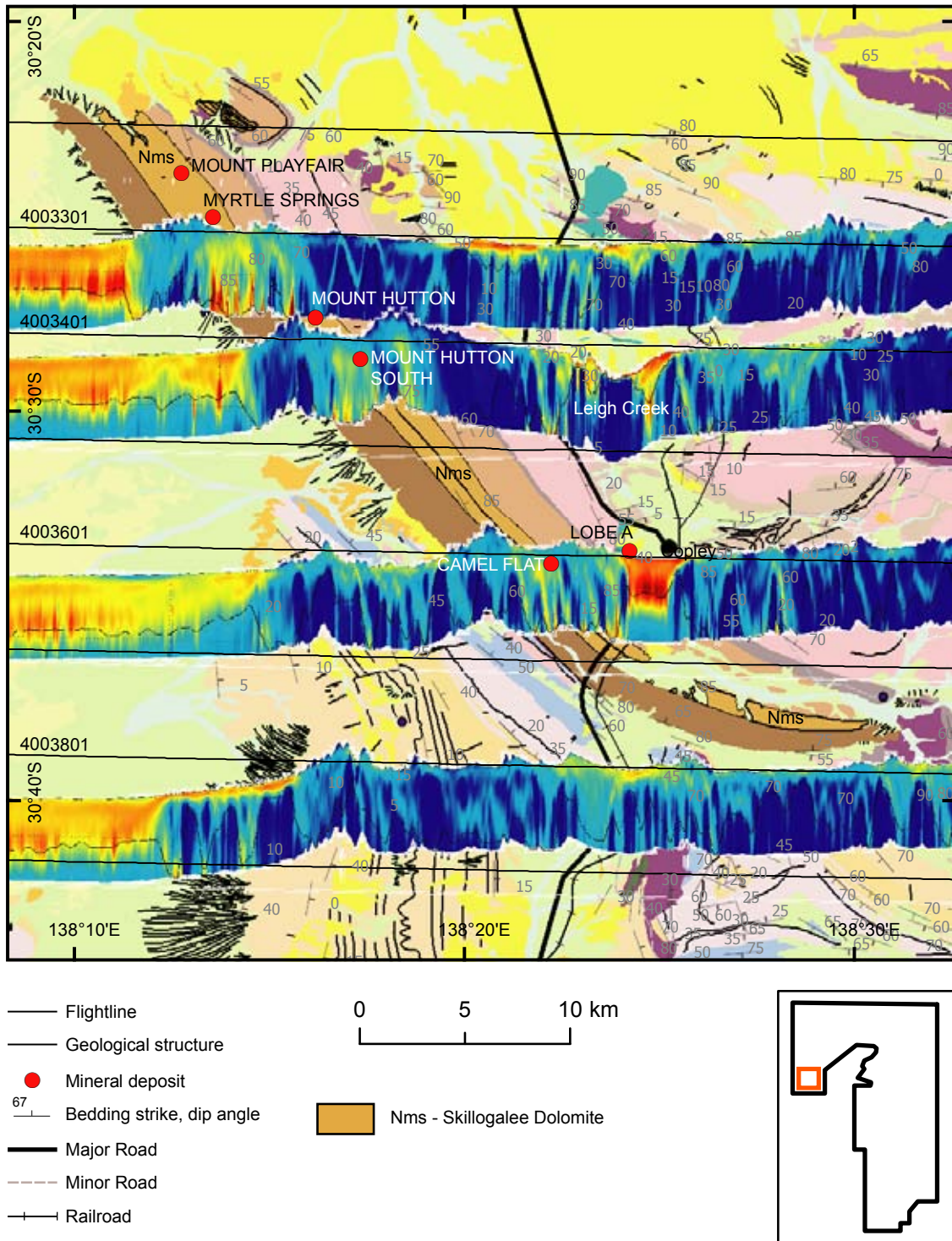


Figure 5.6.5: Conductivity structures associated with known magnesite deposits in the Skillogeale Dolomite (Nms) shown in SBS GA-LEI conductivity sections.

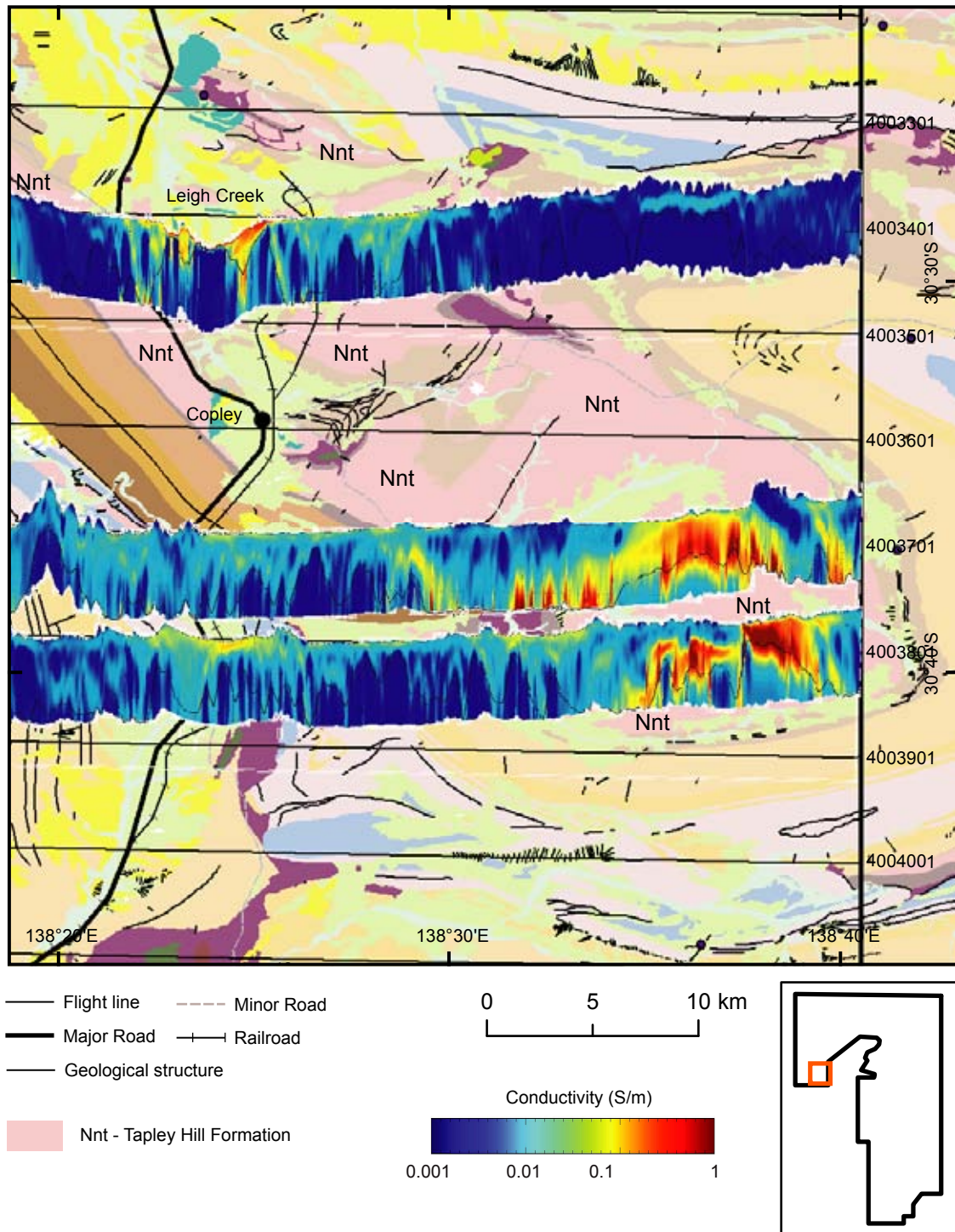


Figure 5.6.6: A high conductivity structure associated with an anticlinal core in the Tapley Hill Formation (Nnt) shown in SBS GA-LEI conductivity sections. Note the conductivity anomaly associated with the Leigh Creek coal mine, most likely due to a combination of porous and permeable, sulfidic coal deposits and dust suppression using saline water.

5.6.4.6 Leigh Creek Coal Measures

Several high conductivity features can be observed in the conductivity depth slices in the central southern part of the area. These distinct areas of anomalous conductivity correspond to the four

known lobes of the Leigh Creek Coal Measures hosted by the Triassic-Jurassic age Telford Basin and associated basins (Figure 5.6.7). These anomalies are persistent in the depth slice data to depths of approximately 250 metres, where they are then lost due to the encroachment of the DOI.

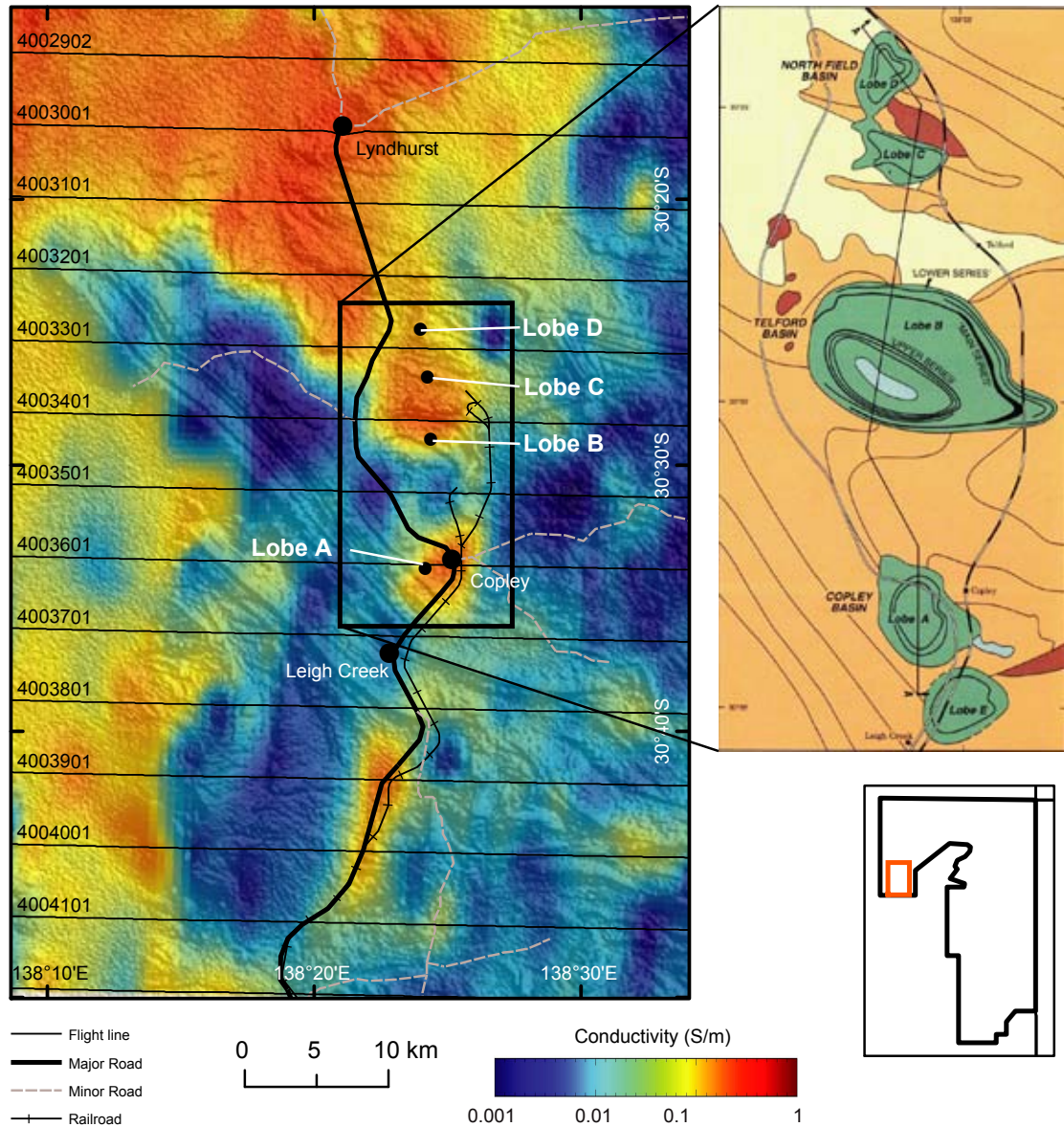


Figure 5.6.7: Conductivity anomalies associated with the Leigh Creek Coal Measures in the SBS GA-LEI 5-10 m conductivity depth slice. SRTM DEM as background. Inset geology map is from Kwitko (1995).

5.6.5 Discussion

Airborne electromagnetics is typically used for mineral exploration in relatively undeformed sedimentary environments, however, this investigation has demonstrated that AEM data can be useful in other areas such as the Neoproterozoic Adelaide Geosyncline, in particular the northern Flinders and Willouran ranges, which is a deformed, structurally complex region.

The strong conductivity contrast, as observed in the conductivity depth sections, between the resistive Neoproterozoic sequences of the Adelaide Geosyncline and the conductive sedimentary sequences of the Pirie-Torrens Basin and Beltana Sub-basin enables the identification of regional scale faults bounding the Neoproterozoic.

In some cases AEM is capable of imaging lithological variations at a formation level, down to bedding scale. Comparison between AEM-derived bedding dip direction and known structural data is critical as the GA-LEI process introduces a significant number of artefacts to the datasets.

Diapiric structures throughout the area typically show a high conductivity response, possibly due to sulphide mineralisation transported in brines associated with diapir emplacement. This response indicates the potential for AEM to be used in the mapping of diapirs under cover. The disrupted conductivity “texture” observed in the Witchelina Diapir suggests that AEM can provide information on the internal diapir structure. With closer line spacing three dimensional mapping of internal structures may be possible.

Distinct conductivity highs associated with magnesite deposits in the Skillogee Dolomite and the Leigh Creek Coal Measures indicates that the AEM technique may be useful as an exploration tool in deformed basement environments as coal, in particular, typically has a high conductivity response.

The conductivity anomaly associated with an anticlinal core within the Tapley Hill Formation is interpreted as being due to pyrite and carbon in the basal section of the formation. The basal Tindelpina Shale Member is known to contain up to 5% pyrite (Preiss, 1987). Groundwater salinity in this region is relatively low (TDS 1500 mg/L), further supporting the interpretation of pyrite causing the observed conductivity anomaly.

5.6.6 Conclusion

Airborne electromagnetics in structurally complex regions is capable of delineating regional scale structures such as faults, and may provide information on bedding trends where there is conductivity contrast in the lithologies, however, this is not consistent throughout the area and care needs to be taken not to over-interpret the data.

Of particular interest is the potential, as highlighted by this investigation, for the AEM technique to be useful for three dimensional modelling of diapirs, for detecting facies variations as in the Tapley Hill Formation and for target generation for the exploration industry.

5.6.7 References

- Drexel, J. F. and Preiss, W. V. (editors), 1995. The Geology of South Australia: Volume 2, The Phanerozoic. **Bulletin 54(2)**, 357 pp.
- Drexel, J. F., Preiss, W. V. and Parker, A. J. (editors), 1993. The Geology of South Australia: Volume 1, The Precambrian. **Bulletin 54(1)**, 249 pp.
- Hearon, T. E., Lawton, T. F. and Hannah, P. T., 2010. Subdivision of the upper Burra Group in the eastern Willouran Ranges, South Australia. *MESA Journal* **59**, 36-46.
- Kwitko, G., 1995. Triassic intramontaine basins. In: Drexel, J. F. and Preiss, W. V. (editors), South Australia Geological Survey, The Geology of South Australia Volume 2 The Phanerozoic. **Bulletin 54**, 98-101 p.
- Preiss, W. V., 1987. The Adelaide Geosyncline. Late Proterozoic Stratigraphy, Sedimentation, Palaeontology and Tectonics. Geological Survey of South Australia, Department of Mines and Energy, Adelaide. **Bulletin 53**, 441 pp.
- Preiss, W. V., 1993. Chapter 6: Neoproterozoic. In: Drexel, J. F., Preiss, W. V. and Parker, A. J. (editors), The Geology of South Australia Volume 1: The Precambrian. Geological Survey of South Australia, Adelaide. **Bulletin 54**, 171-202 p.
- Rennison, M. W. and Rutley, A. J., 1996. Exploration Licence 2100 ‘Broken Range’ Flinders Project, SA – First Annual Report for the period ending 3 August 1996. Geological Survey of South Australia. **Open File Envelope 9983**.
- Robertson, R. S., 1991. Major South Australian Gold Deposits – Summaries. Department of Mines and Energy, South Australia, Adelaide. **Report Book 91/66**, 23 pp.

5.7 MAPPING STRUCTURE-RELATED MINERAL DEPOSITS: GOLD DEPOSITS IN THE NACKARA ARC AND COPPER-MOLYBDENUM PROSPECTS ASSOCIATED WITH THE ANABAMA GRANITE

S. Jaireth

5.7.1 Introduction

The Nackara Arc is an arcuate belt of folded and metamorphosed Neoproterozoic sediments of the Adelaide Geosyncline (Figures 3.6 and 5.7.1). Several small gold deposits and prospects are located in the Arc, hosted predominantly by the rocks of the Burra and Umberatana groups (Table 5.7.1), with more than 85% of known resources hosted by the Umberatana Group (Morris and Horn, 1990).

Structurally, the rocks have been folded into broad upright folds. Burra Group rocks are generally located in the cores of anticlines and the younger Wilpena Group rocks in the cores of synclines. Several salt diapirs were emplaced in the anticlinal cores of the Burra Group (Morris and Horn, 1990).

The sediments were metamorphosed regionally to greenschist facies. They also underwent almandine-amphibolite facies contact metamorphism caused by the intrusion of the Cambro-Ordovician (Delamerian) Anabama Granite.

Mineralised veins show regional and local-scale structural control. Regionally they are located near northwest-trending lineaments.

Mineralogically and geochemically, gold deposits in the Nackara Arc are similar. The mineralisation is hosted within stratabound quartz veins containing pyrite, arsenopyrite, chalcopyrite, locally galena, and carbonate. Quartz veins are accompanied by alteration zones comprising silicification, sericitisation and locally kaolinisation. Fluid inclusion studies show that gold-bearing quartz veins resulted in mineral systems similar to orogenic lode gold systems. The relation of mineralisation with granitoids is unclear. In some gold fields (such as the Wadnaminga gold field) mineralisation could have some input from felsic rocks (such as the Anabama Granite).

The age of mineralisation is unknown. It is possible that it is associated with Delamerian deformation and metamorphism (514-485 Ma).

A number of copper-molybdenum occurrences with variable amounts of gold, silver and zinc have been reported, either within or in close proximity to the Anabama Granite, dated at 468 ± 62 Ma (Stevenson and Webb, 1976; Table 5.7.1). The granite intrudes rocks of the Umberatana Group and forms a magnetically zoned, elliptical body with its long axis trending northeast. It comprises biotite granodiorite interlayered with microgranodiorites and is crosscut by several quartz porphyry and dacite porphyry dykes. Locally the granite is completely altered to a greisen-like assemblage containing quartz and muscovite. The abundant iron-staining observed in the alteration is thought to be due to oxidation of pyrite. In less altered areas granite minerals are replaced by secondary muscovite, chlorite and epidote. Pyrite and traces of chalcopyrite occur as irregular disseminations. Locally molybdenite forms scattered flakes.

The Anabama Granite shows two prominent sets of joints, one striking between north-northeasterly and north-northwesterly and the other east-west (Morris, 1981). Many of the joints appear to have channelled fluids and controlled quartz veins, alteration and breccia zones, and dykes. Some steeply dipping shears are parallel to the joints.

This case study discusses some of the mineral deposits in the Nackara Arc, but focuses on the Anabama Granite area.

The Frome airborne electromagnetic survey, South Australia: implications for energy, minerals and regional geology

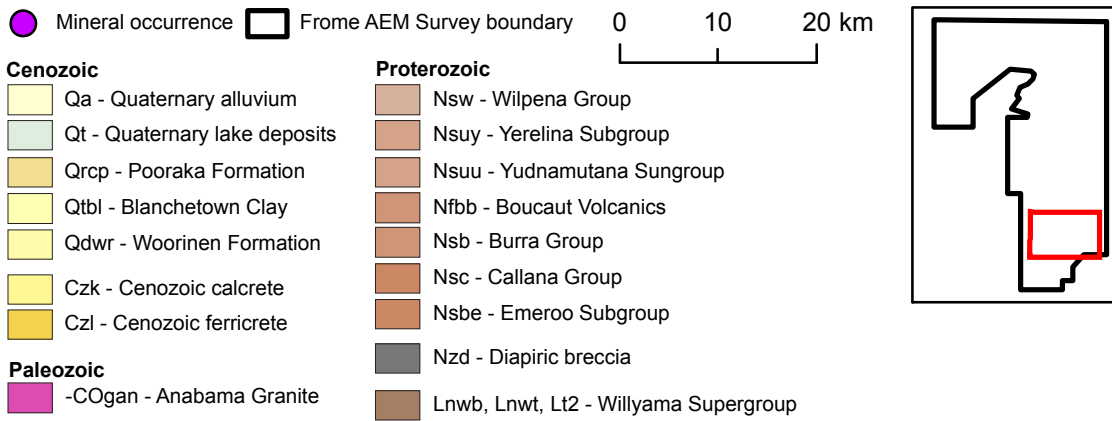
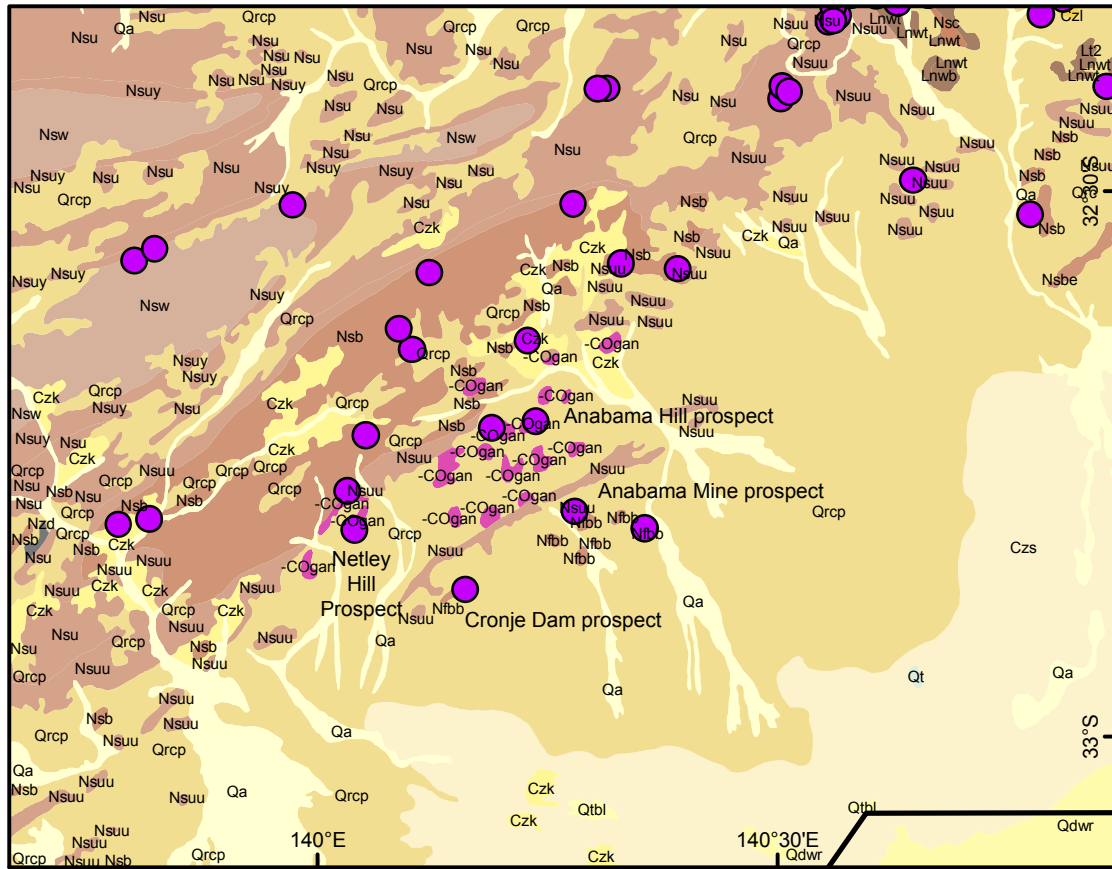


Figure 5.7.1: Location map of gold and copper-molybdenum deposits associated with the Anabama Granite in the Nackara Arc region.

Table 5.7.1: Significant orogenic lode gold and porphyry copper-molybdenum prospects.

DEPOSIT/FIELD	COMMODITY	HOST ROCK	GROUP	AEM RESPONSE (HOST ROCK)	LITHOLOGY	STYLE
Teetulpa	Au	Tapley Hill Formation	Umberatana	Conductive	Calcareous, pyritic siltstone,	Vein
Mannahill	Au	Enorama Shale	Umberatana	Resistive	Calcareous siltstone, shale, sandstone	Vein
Wadnaminga	Au	Mintaro Shale, Saddleworth Formation	Burra	Mintaro Shale conductive; Saddleworth Formation resistive	Micaceous slate	Vein
Anabama Mine Prospect	Cu, Ag, Au, Mo, Zn	Boucaut Volcanics/Blind Siltstone	Umberatana	Resistive	Rhyolite, basalt	Vein
Cronje Dam Prospect	Cu, Ag, Au, Mo, Zn	Boucaut Volcanics	Umberatana	Resistive	Rhyolite, basalt	Vein
Anabama Hill Prospect	Cu, Mo, Ag	Anabama Granite	Anabama Granite	Resistive	Biotite Granite	Vein
Anabama Hill Kaolin Prospect	Clay	Anabama Granite	Anabama Granite	Resistive	Biotite Granite	Alteration zone
Netley Hill Prospect	Cu, Mo	Anabama Granite	Anabama Granite	Resistive	Biotite Granite	Vein, dissemination

Mineralisation at the Anabama Hill prospect is in the form of quartz veins within greisen envelopes. The veins and thin zones of greisenisation are structurally controlled by northeast trending faults, contain up to 20% pyrite, minor magnetite and traces of chalcopyrite and stibnite. Chalcopyrite is more common in veinlets with secondary biotite. Some joints show kaolinite alteration. Locally veins contain molybdenite and fluorite. The veins and alteration zones are similar to those associated with copper±gold porphyry systems. The area was targeted for Climax-style copper-molybdenum deposits (Morris and Horn, 1990).

The Cronje Dam Copper prospect is also spatially and genetically associated with the Anabama Granite (Morris, 1981). The mineralisation is hosted by quartz-muscovite schist (possibly metamorphosed Yudnamutana Group). The host rocks also include partially recrystallised rhyolite that contains alteration pyrite and tourmaline.

At the Netley Hill prospect exploration drilling identified low-grade disseminated and vein-type copper-molybdenum mineralisation containing chalcopyrite, molybdenite, and pyrite (SARIG).

The mineralisation is interpreted to be genetically associated with the Anabama Granite and hence may be of Delamerian age.

5.7.2 AEM signatures of orogenic lode gold and porphyry copper-molybdenum deposits

This section is devoted to characterising the AEM signatures of selected mineral deposits in the Nackara Arc by describing the host rock, the location of gold prospects and by a general description of the deposit's AEM signature including relative conductivity or relative resistivity, gleaned from SBS GA-LEI conductivity sections that intersect the selected deposits.

5.7.2.1 Wadnaminga Goldfield

Host rock:

- Saddleworth Formation (dark grey siltstone, dolomite and rare sandstone); and,
- Mintaro Shale (siltstone, dolomite, quartzite and schist).

Gold prospects:

- Located along the northwest limb of an anticline (northeast-southwest axis).

Major minerals in veins:

- Quartz, pyrite, arsenopyrite, chalcopyrite, galena and calcite. Gold was formed along with sulfides, the presence of which can generate zones of conductivity along ore-localising structures.

AEM signature:

- Saddleworth Formation: predominantly resistive;
- Mintaro Shale: more conductive than Saddleworth Formation; and,
- Most shallow conductive zones are probably related to Cenozoic sediments in the creeks, however, a zone containing gold prospects contains steeply dipping noise of higher conductivity which can be identified in some conductivity sections.

5.7.2.2 Teetulpa Goldfield

Host rock:

- Tapley Hill Formation (calcareous, often pyritic siltstone with dolomite and fine sandstone).

Gold prospects:

- Located along the northwestern limb of an anticline trending northeast. Gold mineralisation is hosted by quartz veins.

Major minerals in veins:

- Quartz, muscovite, siderite and pyrite.

AEM signature:

- Tapley Hill Formation is generally conductive. Dolomitic units within are relatively more resistive than pyritic siltstones. As the host rocks are conductive, possible conductivity contrasts generated due to interaction between rocks and ore-forming fluid are too weak to be able to be identified on AEM conductivity sections.

5.7.2.3 Mannahill Goldfield

Host rock:

- Enorama Shale (calcareous siltstone and shale with fine sandstone beds).

Gold prospects:

- Located on the northern limb of a fold trending east-northeast.

Major minerals in veins:

- Quartz, muscovite, calcite, pyrite, pyrrhotite and chalcopyrite.

AEM signature:

- The Enorama Shale is resistive. In principle, ore-controlled structures with sulfides should generate conductivity contrasts detectable on SBS GA-LEI conductivity sections. The area is cross cut by a northwest-trending regional structure (the Teetulpa Fracture) which is filled with Quaternary alluvial sediments. Conductivity generated by these clay-rich sediments and pockets of saline water appears to mask the conductivity contrast generated by ore fluids along ore-forming structures.

5.7.2.4 Anabama Cu-Mo (Ag, Au, Zn) field

Host rock:

- Mineral prospects are either hosted by the Anabama Granite or by rocks intruded by it (Boucaut Volcanics or Blind Siltstone). The Anabama Granite intrudes the core of a northeast-trending anticlinal structure. Most of the intrusion is under cover, delineated by a prominent, zoned magnetic low of elliptical shape on the first vertical derivative total magnetic image (1VD TMI; [Figure 5.7.2](#)). It also produces a distinct Bouguer gravity low of the same elliptical shape. In the southeastern part of the Granite, it appears to be overprinted by a concentrically-zoned circular body suggesting that the Anabama Granite may be composed of more than one intrusion. The 1VD TMI image also shows several northeast-trending faults and/or major joints. They are parallel to number of major faults (e.g. the Anabama-Redan Shear Zone) in the area. The western segment of the Shear Zone follows the eastern margin of the Anabama Granite.

Mineral deposits/prospects:

- All known mineral prospects are either located within the Granite or under cover in the host rocks in proximity to the Granite ([Figure 5.7.3](#), [Table 5.7.1](#)). The prospects appear to be structurally controlled, located along northeast-trending structures visible on the 1VD TMI image ([Figure 5.7.2](#)). The Anabama Mine prospect, hosted by the Boucaut Volcanics and/or the Blind Siltstone, and the Cronje Dam prospect are located in close proximity to the Anabama-Redan Shear Zone ([Figure 5.7.2](#))

Major minerals in ore zones:

- Vein and disseminated mineralisation comprises pyrite, minor magnetite and traces of chalcopyrite, stibnite and molybdenite. The mineralisation is associated with biotite, greisen and clay alteration.

AEM signature:

- The Anabama Granite appears resistive on SBS GA-LEI conductivity sections. In contrast, the country rocks, especially the Tapley Hill Formation (along the western margin of the Granite) are distinctly more conductive (Figure 5.7.3). Steeply dipping conductive zones observed within the Granite follow the structures visible on the 1VD TMI image. All known mineral prospects are located along these structures. The ore-bearing fluids which altered the Granite (mica and clay alteration) also deposited sulfide minerals which could have created conductivity contrasts detected on SBS GA-LEI conductivity sections. The AEM data thus add to the information provided by 1VD TMI data by showing structures which could channel ore-forming fluids. This example shows that a more dense (closer line spacing) AEM survey would be able to map alteration and mineralised zones in more detail.

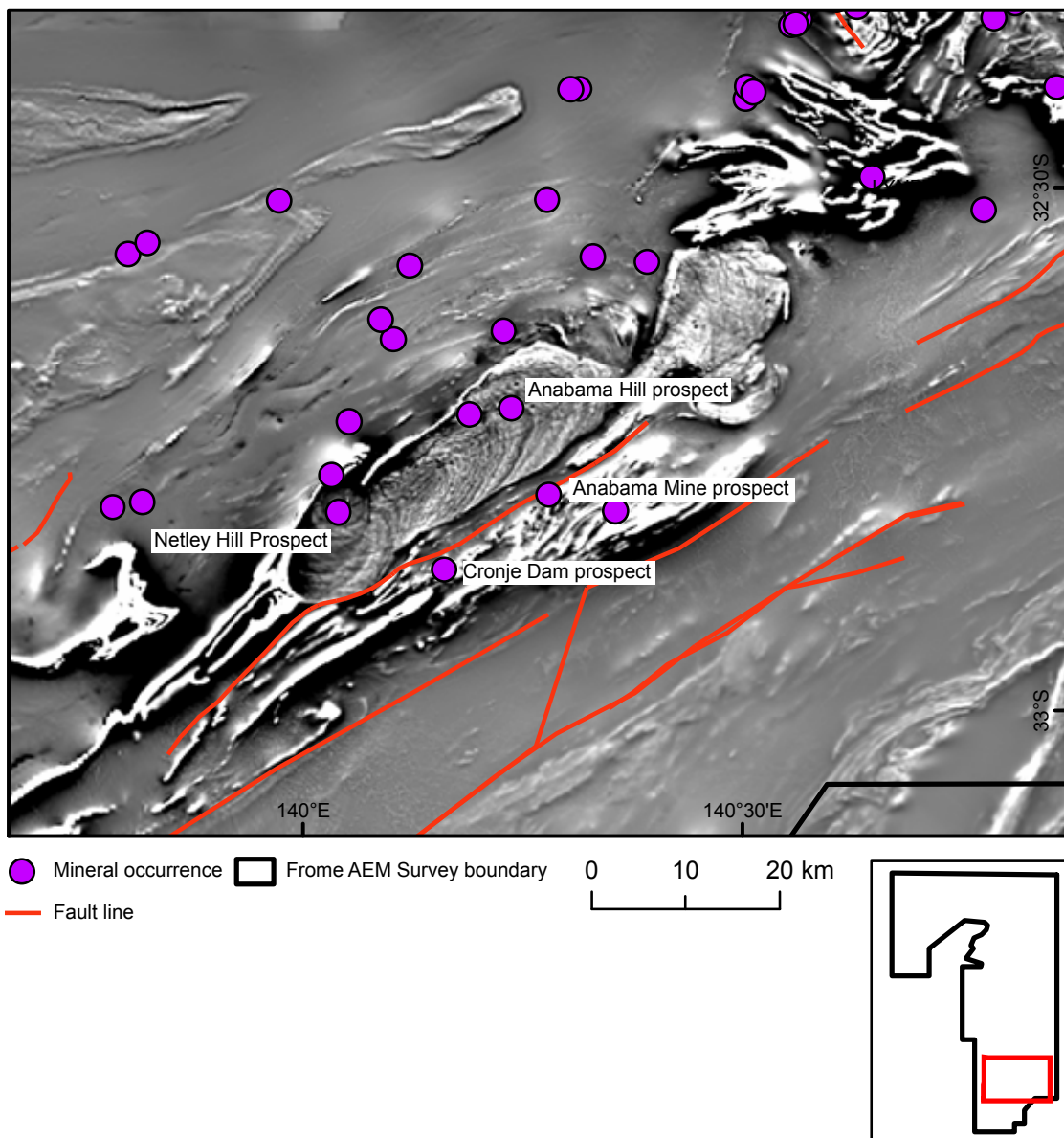


Figure 5.7.2: 1VD TMI image showing the undercover extension of the Anabama Granite. Gold and copper-molybdenum prospects are shown as dots. Note that prospects are located along northeast-trending structures.

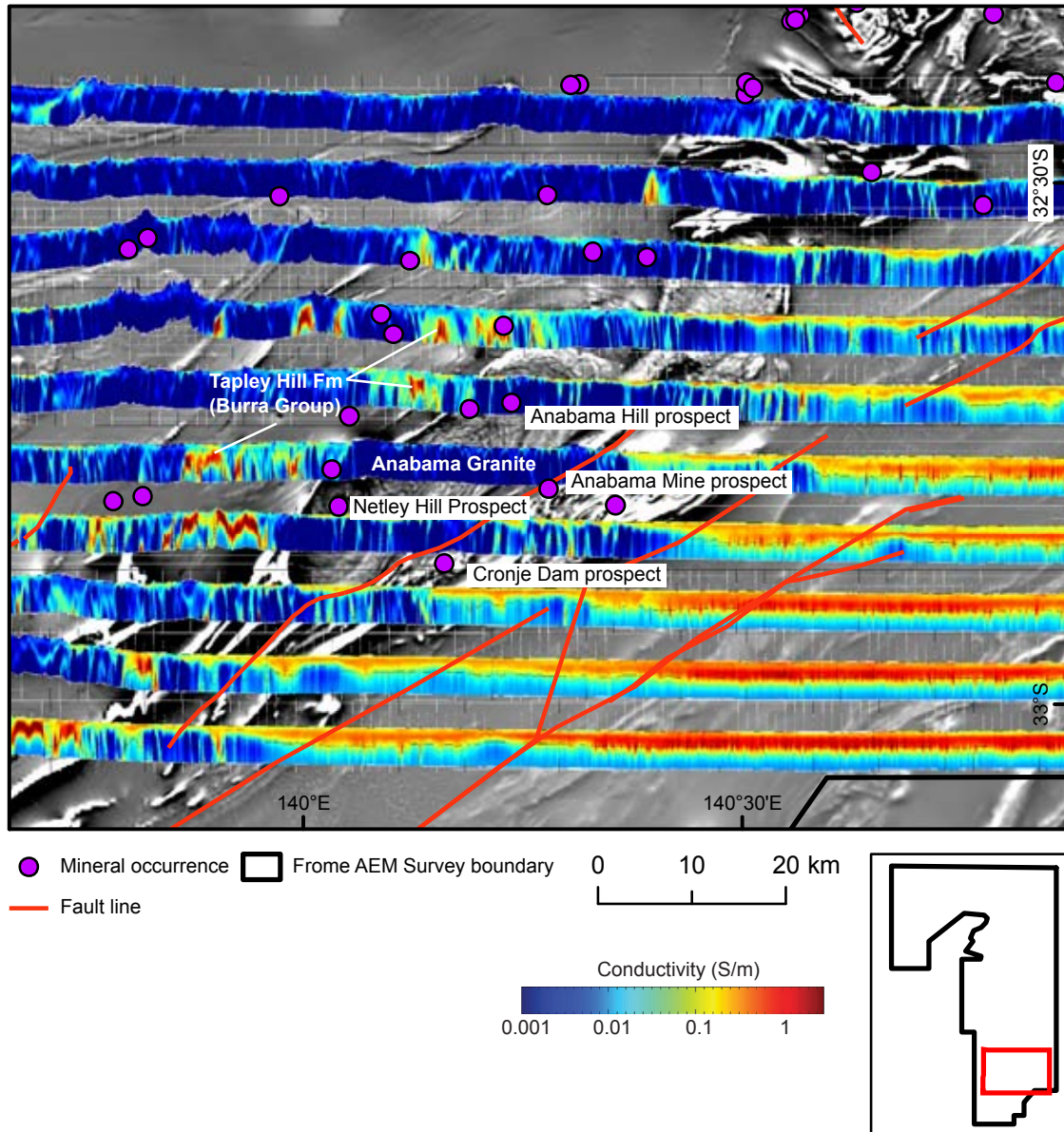


Figure 5.7.3: 1VD TMI image overlain by SBS GA-LEI conductivity sections. The Anabama Granite is strongly resistive compared to the country rocks, which in the west contain the Tapley Hill Formation. Note the steeply-dipping, high conductivity zones following northeast-trending structures seen on the 1VD TMI image (Figure 5.7.2). The high conductivity zones may be caused by deposition of conductive minerals (sulfides and clay) due to reaction of the ore-forming fluid with the Granite.

5.7.3. Conclusions

Regional AEM data from the Frome AEM Survey have provided new data on the three dimensional nature of fracture systems that may have controlled gold and copper-molybdenum mineralisation in the Nackara Arc region, particularly around the Anabama Granite. Data provide information on the continuation of potentially mineralised fracture systems under cover, as well as the three dimensional geology of potential redox conditions including the Tapley Hill Formation, by mapping the destruction or addition of electrically conductive minerals within rock bodies. The Frome AEM data set can help improve exploration for these mineral systems in the Nackara Arc by helping to locate

potentially mineralised fracture systems and providing widespread depth of cover information by allowing drill hole information to be extrapolated laterally.

5.7.4 References

- Morris, B. J., 1981. Porphyry style copper/molybdenum mineralization at Anabama Hill. Mineral Resources Review, South Australia **150**, 5-24.
- Morris, B. J. and Horn, C. M., 1990. Review of gold mineralisation in the Nackara Arc. Mines and Energy Review, South Australia, 51-58 pp.
- Stevenson, B. G. and Webb, A. W., 1976. The geochronology of the granitic rocks of southeastern South Australia: AMDEL Progress Report 14. South Australia Department of Mines and Energy, Adelaide. **Open File Envelope 2136**.

5.8 MAPPING GEOLOGICAL SURFACES: BENAGERIE RIDGE RESISTIVE BASEMENT AND BASIN STRATIGRAPHY

I. C. Roach

5.8.1 Introduction

The Benagerie Ridge is a buried, north-striking basement feature in the central Frome Embayment, composed of Paleo-Mesoproterozoic rocks of the Curnamona Province under Cenozoic, Mesozoic and Paleozoic cover of the Callabonna Sub-basin (Lake Eyre Basin), the Eromanga Basin and the Arrowie Basin (Moorowie and Yalkalpo sub-basins) respectively (Figure 5.8.1).

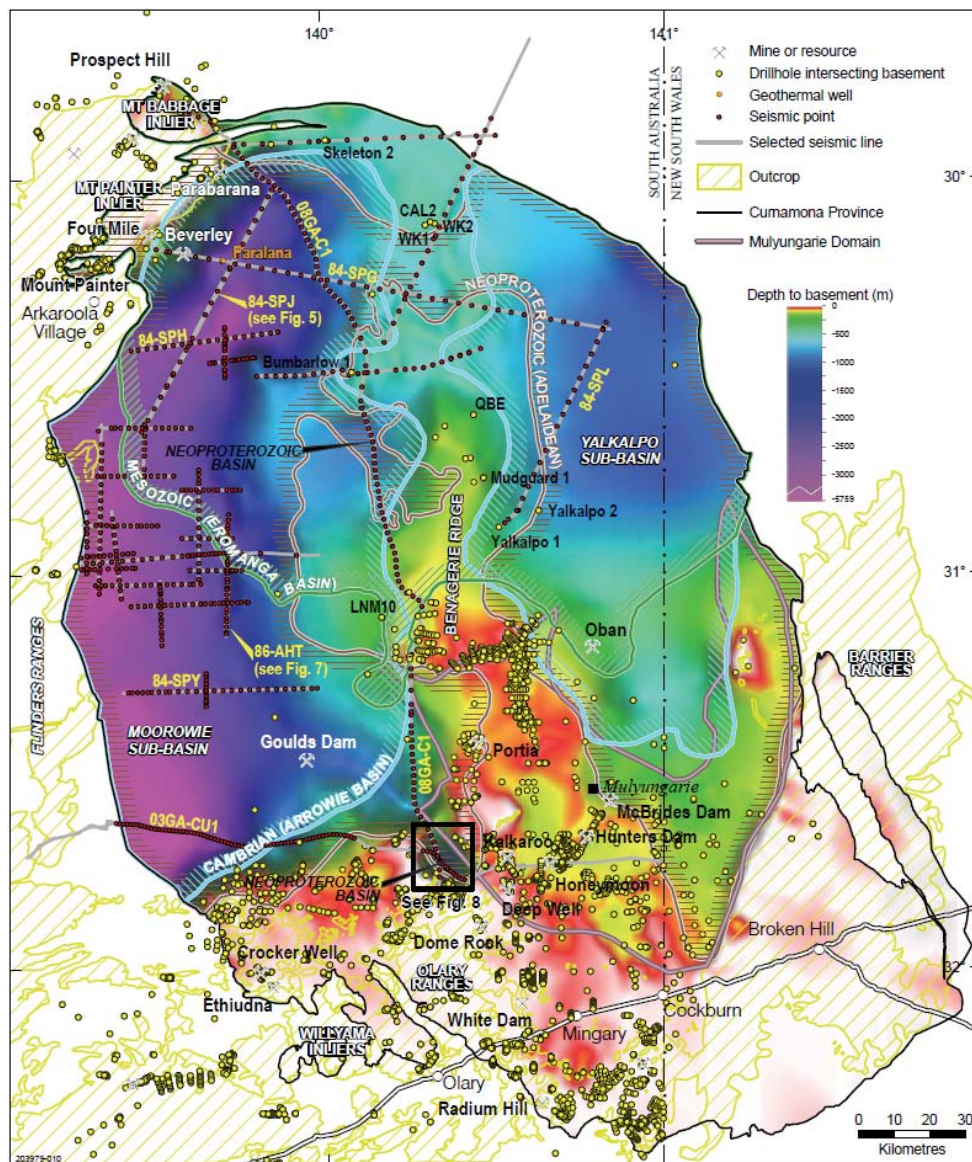


Figure 5.8.1: Benagerie Ridge depth to basement model from Fabris et al. (2010).

The Benagerie Ridge consists of Lower and Upper Willyama Supergroup (Paleo-Mesoproterozoic) of the Olary and Mulyungarie domains in the south, Mesoproterozoic granites and Benagerie Volcanics of the Mudguard Domain in the centre and undifferentiated granites and metamorphic rocks of the Moolawatana Domain in the north, where it outcrops in the northern Flinders Ranges as

the Mount Painter and Mount Babbage inliers (Figure 5.8.2) (Conor, 2004; Conor and Preiss, 2008; Kositcin, 2010). The Benagerie Ridge does not include overlying Neoproterozoic sediments of the overlying and rift-juxtaposed Adelaide Geosyncline (Fabris *et al.*, 2010).

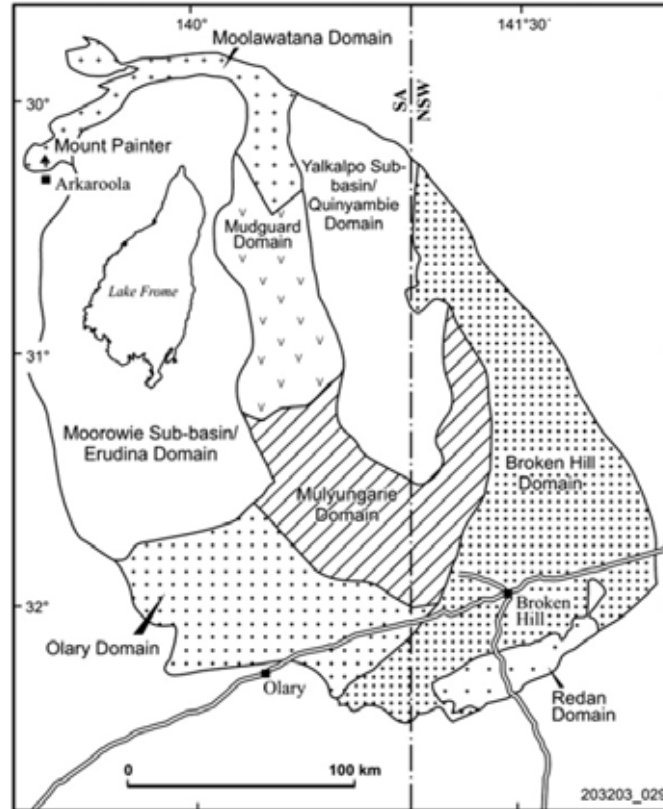


Figure 5.8.2: Geological domains of the Curnamona Province. From Conor and Preiss (2008).

The Benagerie Ridge has potential for iron oxide copper gold (IOCG) deposits, Broken Hill-style lead-zinc-silver deposits and magmatic-hydrothermal uranium deposits. Numerous deposits and prospects occur over the outcropping portions of the Curnamona Province in the south of the Benagerie Ridge, as well as within the shallowly-buried portions including: White Dam (gold); Portia and North Portia (gold-copper); Shylock (gold-copper); Kalkaroo (copper-gold); Dome Rock (copper); Mutooroo (copper); Hunters Dam (lead-zinc-silver); Crocker Well (uranium); Mt Victoria (uranium); and, Radium Hill (uranium). Overlying the Benagerie Ridge, the Cenozoic sediments of the Callabonna Sub-basin host sandstone-hosted uranium deposits including Goulds Dam, Honeymoon and Oban. The Benagerie Ridge is fault-bound on its eastern and western sides and has controlled the form of depocentres associated with the Arrowie and Eromanga basins and the Callabonna Sub-basin (see Chapter 3). The Benagerie Ridge has also shaped the morphology of palaeovalley systems associated with sandstone-hosted uranium systems in the southern Callabonna Sub-basin.

A new Benagerie Ridge surface model developed by Fabris *et al.* (2010) describes the 3D extent of the top of the Benagerie Ridge, based on exploration and stratigraphic drilling and seismic sections. The Fabris *et al.* model includes surfaces describing the modelled top of the Benagerie Ridge (including the Paleo-Mesoproterozoic Curnamona Province and the Neoproterozoic Adelaide Geosyncline combined), the top of the Cambrian (Arrowie Basin), the top of the Mesozoic (Eromanga Basin) and the top of the Cenozoic (Callabonna Sub-basin).

In this case study a new resistive basement surface is shown, derived from the Frome AEM survey data and stratigraphic drill holes. The resistive basement surface includes the Proterozoic rocks of the Curnamona Province and Adelaide Geosyncline and Cambrian sediments of the Arrowie Basin as a single surface, and is comparable to the Benagerie Ridge surface of Fabris *et al.* (2010). The two surfaces are compared to demonstrate the efficacy of regional AEM for the development of 3D palaeosurface models in the Frome Embayment.

5.8.2 Creating the model

The Benagerie Ridge resistive basement surface is derived from Frome AEM Survey conductivity sections and conductivity elevation slices, and drill hole geological data from the SARIG database. The model was constructed using GOCAD™ software at Geoscience Australia (GA).

Conductivity depth interval (CDI) sections generated using EM Flow™ software, sample-by-sample (SBS) GA-LEI conductivity sections and elevation grids were entered into GOCAD™ as triangulated surfaces to preserve the integrity of the original data, rather than as raster images, which are down-sampled by GOCAD™. Line-by-line (LBL) GA-LEI conductivity sections were also used where available, giving a different treatment to data. Drill hole geological data (locations shown in [Figure 5.8.1](#)) were entered in bulk from ASCII collar and down hole geology tables created for the GA Lake Frome Uranium Systems Project (Skirrow, 2009). Markers were created at the bases of horizon picks within the drill hole data including the base of Cenozoic, base of Mesozoic and top of Proterozoic, in keeping with the Benagerie Ridge surface of Fabris *et al.* (2010). The geological interpretation process involved using the 3D drill hole information to recognise conductivity features (conductivity contrasts and/or conductivity textures) that correlated to known geological features (unconformities or rock volumes) at points along flight lines. Examples of use of stratigraphic drill holes to correlate electrical conductivity features with geology in the Benagerie Ridge area can be seen in [Figures 5.2.10](#), [5.2.11](#), [5.3.8](#) and [5.3.12](#). These features were then extrapolated along flight lines and between flight lines using the conductivity elevation slices and other geological information including magnetic and gravity images and solid geology mapping. Geological boundaries were digitised along flight lines within GOCAD™ and were converted to surfaces using along-line picks and markers in the drill hole geological data as constraints. The resistive basement surface was additionally constrained using the 1:1 million scale outcrop geology polygons for Proterozoic rocks in the area. The outcrop polygons were transferred from ArcGIS™ and were draped onto the digital elevation model created for the GOCAD™ project to give a representation of the 3D geometry of the basement-cover boundary.

5.8.3 Results and discussion

The following figures illustrate the process of creating the Benagerie Ridge resistive basement surface and geological features that are visible within the data. [Figure 5.8.3](#) illustrates the surface geology of the Southern Lake Frome area, looking southwest towards the under-cover extent of the Benagerie Ridge. The surface uses the 1:1 million Surface Geology of Australia Map (Raymond and Retter, 2010) draped over a resampled digital elevation model, derived from the SRTM DEM, of the Frome AEM Survey area. Prominent features in the image include the Olary Spur in the south (background; which contains felsic, uranium-bearing rocks of the Ninnerie Supersuite; Fricke and Hore, 2010; Wade, 2011) and the northern Flinders Ranges in the west (right) of the image. The surface of the southern Lake Frome area is covered with variably conductive Quaternary alluvial and colluvial sediment.

[Figure 5.8.4](#) illustrates EM Flow™ CDI sections across the southern Lake Frome area, highlighting the location of the resistive basement that was picked to create the surface. Note the high conductivity of saline sediments associated with the Lake Frome playa. Other smaller playas and salinas occur in the southern Lake Frome area, indicated by high conductivities in the near-surface and a lack of signal penetration in these high conductivity areas.

In [Figure 5.8.5](#), the boundary between the conductive Cenozoic cover (here including the Quaternary and the Cenozoic Namba and Eyre formations) and the underlying resistive basement has been traced with aid of stratigraphic drill hole control, and converted into the resistive basement surface. The boundary can be interpreted with relative certainty, to within ~20 m vertically of the boundary logged in stratigraphic drill holes, above the depth of investigation (DOI; see [Section 4.7.7](#)). Below the DOI it is not possible to pick geological boundaries because of the uncertainty in the inverted data. Some difficulty was also encountered in the southeast of the resistive basement surface area where the weak to moderately conductive Cenozoic sediments overlie basement of highly-conductive Willyama Supergroup rocks of the Strathearn Group (see [Figure 3.4](#) and [Section 5.3.6.1.3](#)). In this area, judicious use of logarithmic and linear colour stretches ensured that sufficient electrical contrast could be recognised, allowing the successful discrimination of cover from basement.

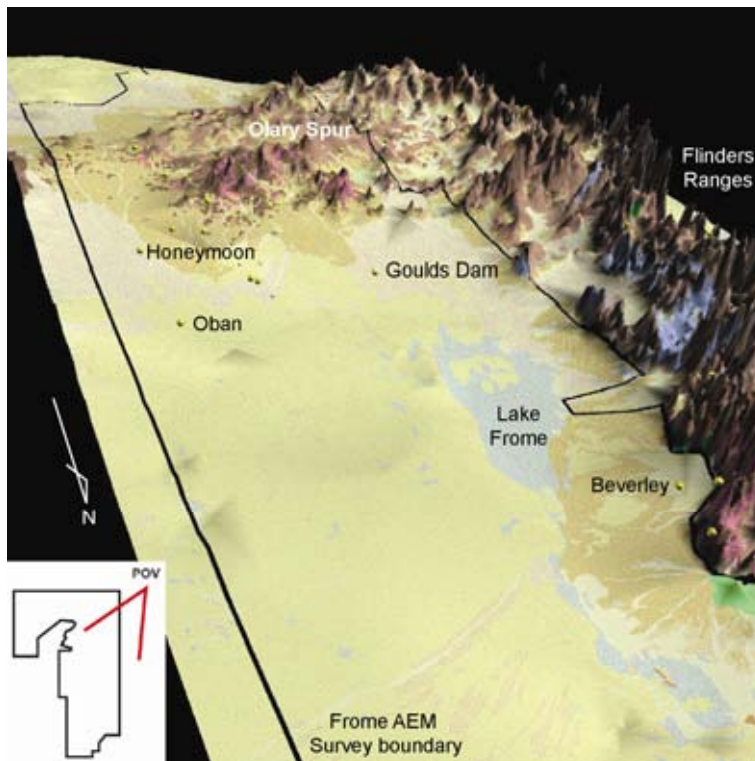


Figure 5.8.3: 1:1 million scale Surface Geology of Australia Map (Raymond and Retter, 2010) draped over the resampled SRTM DEM highlighting the relative relief of the Frome AEM Survey area compared to the Flinders Ranges at right. The locations of major uranium deposits in the Lake Frome area are also shown.

[Figure 5.8.6](#) compares the resistive basement surface to the Benagerie Ridge surface of *Fabris et al.* (2010). The resistive basement surface traces the unconformity between conductive cover and resistive basement to a depth of 150-200 m, which is the level where the DOI indicates that the inversions are dominated by the reference model rather than geological data. The depth of the DOI is heavily influenced by surface electrical conductivity conditions: where the surface is highly conductive, the DOI is very shallow (< 50 m); and, where surface conductivity is low, the DOI is very deep (up to 400 m; see [Section 4.5.7](#) and [Figure 4.8](#)). Thus the continuity of the resistive basement surface depends on the depth of the DOI in individual flight lines.

The resistive basement surface is well correlated with the Benagerie Ridge surface of *Fabris et al.* (2010) in the central Benagerie Ridge area to the west of the Oban uranium deposit, and can be seen merging in and out of the modelled surface. This area consists principally of Benagerie Volcanics in the northern Mulyungarie Domain and southern Mudguard Domain lying at ~100-150 m below surface. Here thick resistive saprolite covers resistive felsic volcanics, forming a good electrical contrast with the overlying relatively weak to moderately conductive Cenozoic sediments of the Eyre and Namba Formations and a small fringe of Mesozoic sediments of the Bulldog Shale in the north of the resistive basement surface. The resistive basement surface has helped infill the sparse drilling and seismic data in this area, providing more certainty in depth of cover information.

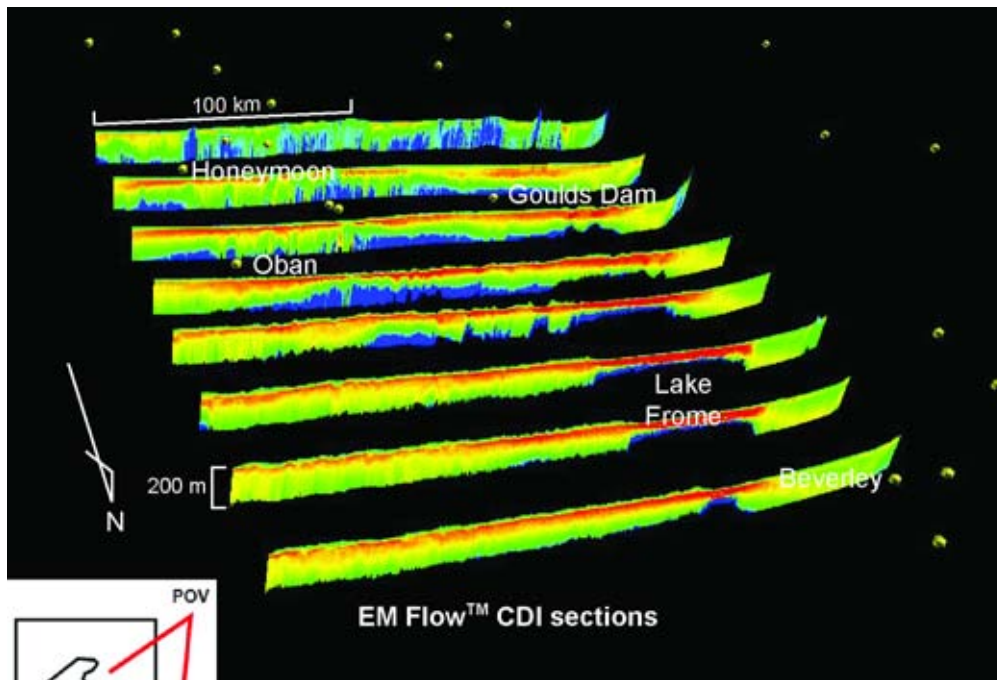


Figure 5.8.4: EM Flow™ CDI sections for AEM flight lines across the southern Lake Frome area. The resistive basement model traces the dark blue basement resistor in these CDI sections. Colours in the CDI sections do not conform exactly to the GA logarithmic colour stretch, however hot colours equate to high conductivity (~ 1000 mS/m) and cold colours equate to low conductivity (~ 1 mS/m).

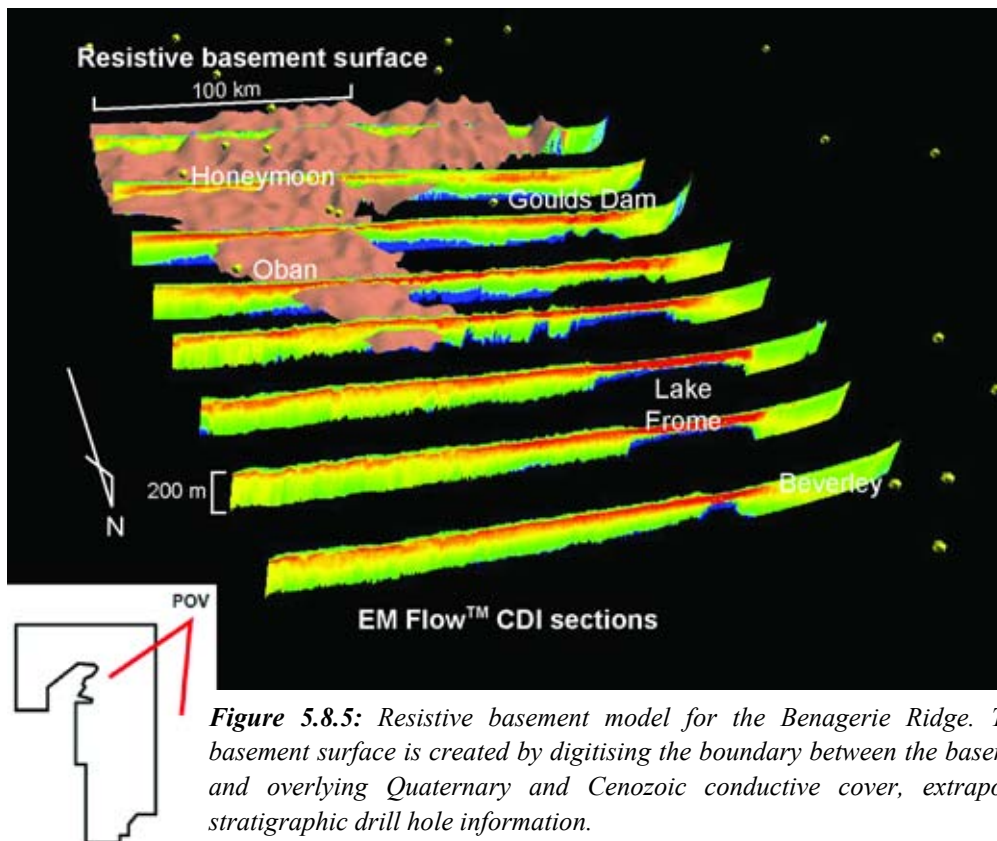


Figure 5.8.5: Resistive basement model for the Benagerie Ridge. The resistive basement surface is created by digitising the boundary between the basement resistor and overlying Quaternary and Cenozoic conductive cover, extrapolating from stratigraphic drill hole information.

Further to the south, in the Goulds Dam area, the resistive basement surface and the Benagerie Ridge surface of Fabris *et al.* (2010) diverge because the inverted AEM data can not adequately discriminate between resistive Willyama Supergroup rocks, resistive Neoproterozoic rocks and resistive Cambrian Arrowie Basin rocks. These rocks tend to have their own electrical conductivity “texture”, in that the Cambrian rocks behave like a massive, textureless resistor whereas the Willyama Supergroup rocks have a varied electrical conductivity texture related to complex folding, faulting and mixture of resistive and weakly conductive slivers of rock. Neoproterozoic rocks in this area are slightly folded (similar to those in the Leigh Creek-Marree area; see Section 5.6) and faulted and tend to have an electrical conductivity pattern reflecting this (see Sections 5.6 and 5.7). The boundaries between the rock masses are, however, problematic to pick.

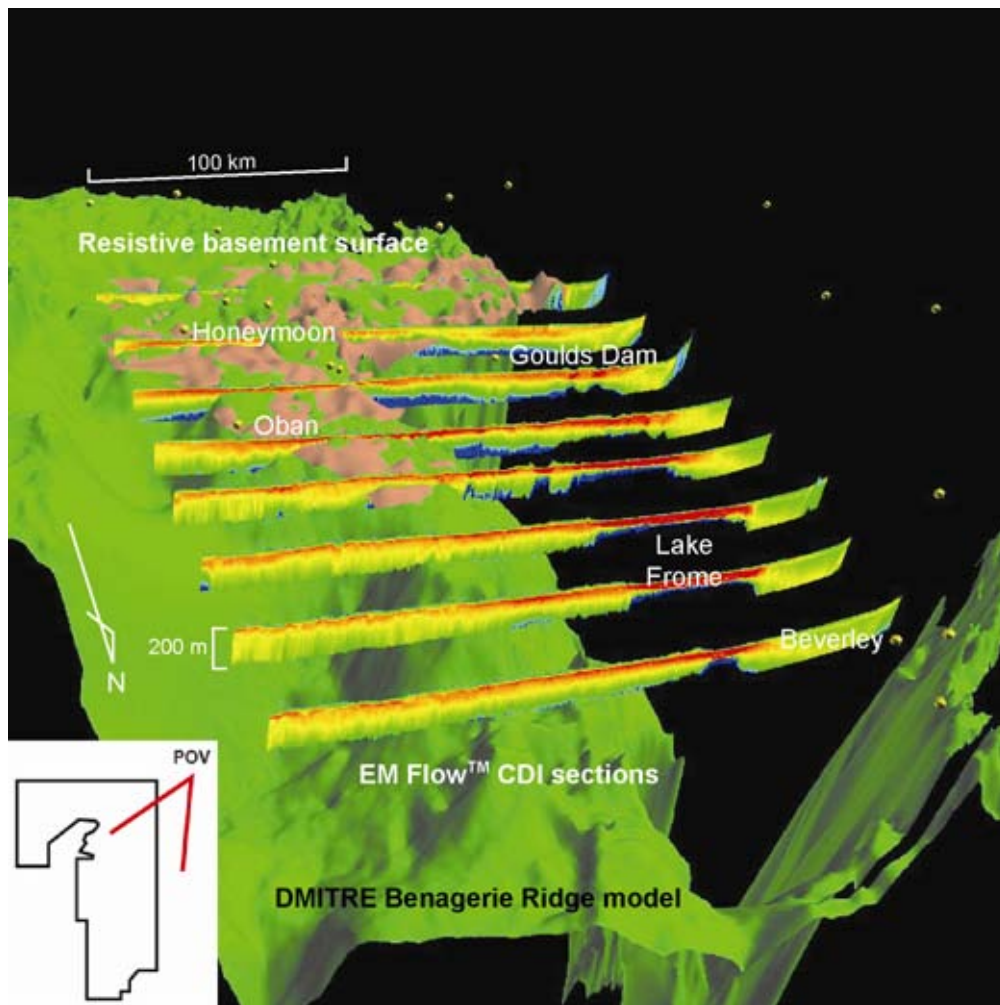


Figure 5.8.6: Comparison of the Benagerie Ridge resistive basement model and the Benagerie Ridge model of Fabris *et al.* (2010). The resistive basement model is in good agreement with the Benagerie Ridge model in the central Benagerie Ridge, but diverges in the Goulds Dam area.

A variety of geological features are mappable in the Frome AEM Survey data over the Benagerie Ridge area. Figure 5.8.7 is a close-up view of the resistive basement surface shown in the previous figures. The vertically exaggerated (25x), foreshortened views of individual SBS GA-LEI conductivity sections in this image allow a number of sedimentary features to be recognised and mapped, including:

- Resistive Quaternary cover consisting of sand dunes and sand sheets. These occur as a thin (< 30 m thick) mantle over the Cenozoic sediments of the Callabonna Sub-basin;

- Moderately conductive sediments in sandy interbeds in the Namba Formation. These sediments can be mapped (see Figures 5.2.7, 5.2.10, 5.2.11 and 5.3.8) by their conductivity contrast with surrounding clayey sediments, especially where they are saturated with brine as they are in the southern Callabonna Sub-basin at Oban (Oban Energy Pty Ltd, 2009). Lateral sedimentary facies variation within the Namba Formation is mapped as a lateral change in conductivity due to a change in the sand:clay ratio and a consequent change in bulk conductivity of the unit. This lateral change is also partially due to changes in the salinity of groundwater within the local area (Oban Energy Pty Ltd, 2009);
- Weak to relatively highly conductive Eyre Formation. At the Oban uranium deposit the Eyre Formation contains a brine pool in its lower part (Oban Energy Pty Ltd, 2009) which makes it electrically indistinguishable from the upper Bulldog Shale of the Eromanga Basin. Careful mapping can, however, resolve the upper Eyre Formation below the Namba Formation sandy conductor and above the thick, highly conductive Bulldog Shale;
- Highly conductive (~1000 mS/m) Bulldog shale. The top of the Bulldog Shale and the base of the Eyre Formation (the Mesozoic-Cenozoic unconformity) may not be readily distinguishable, but the extent of the Bulldog Shale as the lower-most strong conductor in the Frome Embayment is apparent in conductivity sections and grids.

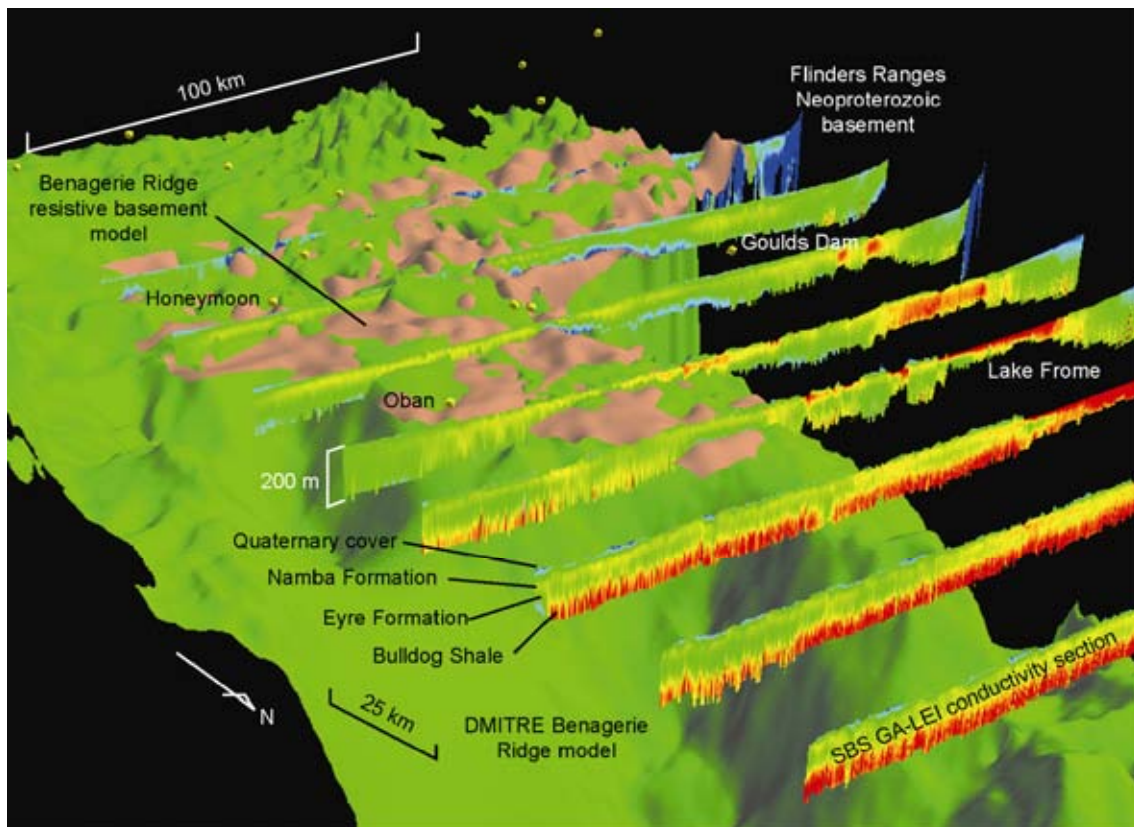


Figure 5.8.7: Close-up view of the Benagerie Ridge resistive basement surface and the Benagerie Ridge surface of Fabris et al. (2010). This figure highlights the ability of the Frome AME Survey data, here showing the SBS GA-LEI, to map different sedimentary units within the Callabonna Sub-basin and Eromanga Basin. Colours in the conductivity sections do not conform exactly to the GA logarithmic colour stretch, however hot colours equate to high conductivity (~1000 mS/m) and cold colours equate to low conductivity (~1 mS/m).

5.8.4 Conclusions

The Benagerie Ridge resistive basement surface demonstrates how regional AEM data can be used to extrapolate from sparsely-distributed drill hole stratigraphic data to create interpreted geological surfaces over wide areas. These surfaces assist in the search for minerals by providing thickness of cover and depth to basement information, which can be adapted for a variety of commodities. In the southern Callabonna Sub-basin, the term “cover” has different connotations, depending on the commodity sought. For uranium exploration, “cover” refers to the Quaternary sand cover, playas, salinas and the Namba Formation, whereas for copper-gold and lead-zinc-silver exploration, “cover” refers to the entire Cenozoic and Mesozoic sedimentary succession. The resistive basement surface demonstrates how the unconformity between the Callabonna Sub-basin, Eromanga Basin and the Paleozoic and Proterozoic basement can be mapped in three dimensions. Further subdivision of the regional AEM data is possible; the Namba Formation sands and the upper Eyre Formation can be recognised within the Frome AEM Survey data set, provided adequate stratigraphic drill hole control is available. The release of the regional data from the Frome AEM Survey now means that it is possible to map Namba Formation sands over a wide area to aid in exploration of Beverley-style sandstone-hosted uranium deposits, and to map upper Eyre Formation to explore for Honeymoon-Goulds Dam-Oban style sandstone-hosted uranium deposits within the southern Callabonna Sub-basin.

5.8.5 References

- Conor, C. H. H., 2004. Geology of the Olary Domain, Curnamona Province, South Australia. South Australia. Department of Primary Industries and Resources, Adelaide, **Report Book 2004/8**, 86 pp.
- Conor, C. H. H. and Preiss, W. V., 2008. Understanding the 1720-1640 Ma Palaeoproterozoic Willyama Supergroup, Curnamona Province, Southeastern Australia: Implications for tectonics, basin evolution and ore genesis. *Precambrian Research* **166(1-4)**, 297-317.
- Fabris, A. J., Gouthas, G. and Fairclough, M. C., 2010. The new 3D sedimentary basin model of the Curnamona Province: geological overview and exploration implications. *MESA Journal* **58(September 2010)**, 16-24.
- Fricke, C. E. and Hore, S., 2010. Definition of the Mesoproterozoic Ninnerie Supersuite, Curnamona Province, South Australia. Department of Primary Industries and Resources South Australia, Adelaide. **Report Book 2010/20**, 55 pp.
- Kositcin, N. (editor) 2010. Geodynamic synthesis of the Gawler Craton and Curnamona Province. Geoscience Australia, Canberra **Record 2010/27**.
- Oban Energy Pty Ltd, 2009. Mining and rehabilitation plan on Retention Lease 123 for uranium field leach trial at Oban, South Australia. Oban Energy Pty Ltd, Glenside, SA. Online: http://www.pir.sa.gov.au/_data/assets/pdf_file/0005/97079/Oban_MARP_Voll.pdf.
- Raymond, O. L. and Retter, A. J., 2010. Surface geology of Australia 1:1 000 000 scale. Geoscience Australia, Canberra. 2010. Online: <http://www.ga.gov.au/mapconnect/>.
- Skirrow, R. G. (editor) 2009. Uranium ore-forming systems of the Lake Frome Region, South Australia: Regional spatial controls and exploration criteria. Geoscience Australia, Canberra. **Record 2009/40**, 151 pp.
- Wade, C. E., 2011. Definition of the Mesoproterozoic Ninnerie Supersuite, Curnamona Province, South Australia. *MESA Journal* **62**, 25-42.

6 Summary and conclusions

I. C. Roach and S. Jaireth

6.1 MEETING THE AIMS OF THE SURVEY

I. C. Roach

The Frome AEM Survey was designed to deliver reliable, low noise, calibrated, fit-for-purpose, pre-competitive AEM data to aid research into the energy potential within the Lake Frome, Leigh Creek, Marree and northeastern Murray-Darling Basin region. The aims of the Survey were to reduce exploration risk and promote mineral exploration, principally for uranium energy resources, but also for other commodities, by mapping:

- Palaeovalley systems;
- Basin architecture;
- Sedimentary facies;
- Geological structures that may control mineralisation;
- Geological surfaces; and,
- Groundwater resources.

The following summary details the outcomes of the Survey in achieving these aims, and discusses the implications of the survey outcomes for uranium, lode gold and porphyry copper systems and other commodities.

6.1.1 Mapping palaeovalley systems

New data from the Frome AEM Survey give a regional overview of the distribution and electrical conductivity characteristics of palaeovalley systems across the entire Survey area. Palaeovalley systems were previously mapped from sparsely-distributed drill holes, small tenement-scale AEM surveys and small induced-polarization (IP) surveys. The Frome AEM Survey has provided a regional overview of palaeovalley systems, together with along-line detail, to allow the seamless integration of earlier mapping with the regional AEM data. Palaeovalley systems targeted by industry are generally of a size that is readily resolved within the gridded Frome AEM Survey data, especially those in the southern Callabonna Sub-basin and northern Flinders Ranges flank areas. New outcomes from the interpretation of palaeovalley features include:

- Comprehensively re-interpreting the palaeovalley boundaries in the southern Callabonna Sub-basin, including the Curnamona, Billeroo, Lake Namba and Yarramba palaeovalleys (see [Section 5.3](#));
- Mapping the Olary Palaeovalley in the Murray-Darling Basin (see [Section 5.2](#));
- Extending the boundaries of the Blanchewater Palaeovalley on the northern Flinders Ranges flank (see [Figure 6.1](#)); and,
- Interpretation of several entirely new palaeovalley systems in the southern Callabonna Sub-basin area (see [Section 5.3](#)).

6.1.2 Mapping basin architecture

The Frome AEM Survey has provided new data and interpretations of the basin architecture of the Lake Eyre Basin—Callabonna Sub-basin, the Eromanga Basin flanking the northern Flinders Ranges and the Murray-Darling Basin flanking the Nackara Arc. The Survey data complement shallow seismic data in the area by providing detailed information to the depth of investigation (DOI), ~150-200 m depth, in the sedimentary basins.

The Frome AEM Survey data have provided new information regarding:

- The morphology and stratigraphy of the Poontana Trough, running parallel to the eastern Flinders Ranges range front and extending into the Strzelecki Desert region in the north of the Survey area (see [Section 5.5](#));
- The southern extent of the Eromanga Basin in the Frome Embayment underneath the Callabonna Sub-basin (see [Section 5.8](#));
- The morphology and thickness of the Callabonna Sub-basin (see [Section 5.3](#) and [5.8](#));
- The morphology and thickness of the Lake Eyre Basin in the north of the Survey area (see [Section 5.4](#));
- Regional stratigraphy of the Murray-Darling Basin including the extent of Murray Group marine sediments (see [section 5.2](#)); and,
- Mapping conductivity anomalies associated with Triassic coal-bearing basins in the Leigh Creek-Copley area (see [Section 5.6](#)).

6.1.3 Mapping sedimentary facies

The Frome AEM Survey data provide detailed along-line information on the bulk conductivity of the Earth that can be interpreted for sedimentary facies implications with the aid of detailed stratigraphic logging and groundwater salinity data. Interpretations have provided new information regarding:

- The discrimination and mapping of Namba Formation sands in the Callabonna Sub-basin (see [Sections 5.2, 5.3](#) and [5.8](#));
- The discrimination and mapping of the Eyre Formation in the Callabonna Sub-basin (see [Sections 5.2, 5.3](#) and [5.8](#));
- The mapping of Willawortina Formation sediments in the Poontana Trough of the Callabonna Sub-basin along the eastern Flinders Ranges range front (see [Sections 5.3](#) and [5.5](#));
- Discriminating and mapping Mesozoic sedimentary units including the Bulldog Shale, the Oodnadatta Formation and the Mackunda Formation in the MacDonnell Creek area along the northern Flinders Ranges flank, and the Bulldog Shale in the Frome Embayment underneath the Callabonna Sub-basin (see [Sections 5.2](#) and [5.4](#)); and,
- Discriminating and mapping Cenozoic sedimentary units in the Murray-Darling Basin including marine sediments of the Murray Group (Winnambool Formation and Ettrick Formation as well as generic Murray Group sediments) and the Renmark Group, as well as the Pliocene Loxton-Parilla Sand and the Blanchetown Clay (see [Section 5.2](#)).

6.1.4 Mapping geological structures

Faults and fracture zones are visible within the Frome AEM Survey data as electrical conductivity contrasts between themselves and surrounding rocks. These systems may be filled with electrically conductive minerals and saline groundwater, or hydrothermal waters may have destroyed pre-existing conductivity within host rocks. Fault and fracture systems observed within the Frome AEM data set, and their implications, include:

- Major thrust faults associated with the Anabama-Redan Fault Zone bounding the Nackara Arc and Murray-Darling Basin, and parallel fractures, associated with gold and copper mineralisation in the Anabama area (see [Sections 5.2](#) and [5.7](#));
- Major thrust faults on the eastern side of the Flinders Ranges, thrusting resistive Neoproterozoic rocks over conductive Cenozoic sediments;
- Major thrust, strike-slip and scissor faults in the northern Flinders Ranges flank area, visible as juxtapositions of highly conductive Marree Subgroup sediments against weakly to moderately conductive Cenozoic sediments (see [Section 5.4](#)); and,
- Thrust and strike-slip faults in the Leigh Creek-Marree area, visible as resistive Neoproterozoic rocks of the Willouran Ranges thrust over conductive sediments of the Torrens Basin and vertical conductivity structures associated with strike-slip faults, normal faults and diapirs (see [Section 5.6](#)).

6.1.5 Mapping geological surfaces

The Frome AEM Survey data demonstrate the efficacy of using regional AEM data to map geological surfaces on a regional scale. Using detailed drill hole stratigraphy, high-resolution seismic data and detailed geological mapping, the data have been used to help reduce exploration risk by providing better cover thickness and depth to target information for a variety of commodities. The data have been used to:

- Map a resistive basement surface between the Nackara Arc and Murray-Darling Basin, highlighting sedimentary fill in the Olary Palaeovalley and demonstrating fault offsets of Murray Group sediments by neotectonic activity along the Anabama-Redan Fault Zone for gold and copper-molybdenum exploration (see [Sections 5.2](#) and [5.7](#));
- Map a resistive basement surface associated with the Benagerie Ridge, allowing extrapolation between sparsely-distributed drill holes and better targeting of drill holes for gold-copper and lead-zinc-silver exploration (see [Section 5.8](#));
- Map the top surface of the Mesozoic Marree Subgroup around the entire northern Fringe of the Flinders Ranges, allowing better targeting of uranium exploration efforts in the region (see [Section 5.4](#)); and,
- Map the lower Namba Formation across the Callabonna Sub-basin and Lake Eyre basin to the north of the Flinders Ranges to better define uranium exploration targets for sandstone-hosted uranium deposits hosted by the Namba Formation (e.g. Beverley) and the Eyre Formation (e.g. the Four Mile deposits, Honeymoon, Oban and Goulds Dam) (see [Section 5.4](#)).

6.1.6 Mapping groundwater resources

The Frome AEM Survey data have allowed the first regional overview of salinity conditions in groundwater over the entire Survey area, and will allow the groundwater chemistry results from scattered water bores to be amalgamated into a regional data set. The Frome AEM Survey data have mapped:

- Saline groundwater plumes associated with major playas in the Survey area including Lake Frome, Lake Callabonna and Lake Blanche, as well as numerous small salt lakes in the dune fields of the Strzelecki Desert to the northeast of Lake Frome. The Geoscience Australia Layered Earth Inversion (GA-LEI) product provides conductivity images with sufficient detail to be able to map strata in the Callabonna Sub-basin up to the fringes of the large playas and salt lakes (see [Section 5.5](#));
- Saline plumes associated with uranium mineralisation around the Beverley area (see [Section 5.5](#));
- Saline groundwater associated with the Namba Formation sands in the southern Callabonna Sub-basin and the Lake Eyre Basin to the north of the Flinders Ranges (see [section 5.4](#));
- Saline groundwater used for mine site dust suppression in the Leigh Creek coal mine area; and;
- Saline surface and groundwater in the Murray-Darling Basin, especially groundwater associated with the Marine Murray Group sediments (see [Section 5.2](#));
- Relatively fresh groundwater associated with surface recharge in the Strzelecki Desert region (see [Section 5.2](#));
- Fresh surface water in the Murray-Darling Basin;
- Fresh near-surface groundwater in the Olary Spur merging with saline groundwater lower in alluvial systems leading into the Lake Frome area; and,
- Fresh to brackish groundwater in the Poontana Trough on the eastern side of the Flinders Ranges (see [Sections 5.4](#) and [5.5](#)).

6.1.7 Data collection and inversion products

The Frome AEM Survey was an innovative survey in many respects, from the way the data were collected to the range of products released to the public (see [Chapter 4](#)). New innovations for the collection and release of regional AEM survey data include:

- A low flying height (~100 m nominal height), enhancing the signal-to-noise ratio of the entire survey. This survey was the first TEMPEST™ survey to fly at this height in Australia, which resulted in very low noise data over the entire survey area;
- Releasing a line-by-line (LBL GA-LEI) product, which enhances horizontal structure within the AEM data, together with a sample-by-sample (SBS GA-LEI) product;
- Releasing new interpretation products including GOCAD™ triangulated surfaces, which can be directly imported into 3D modelling software without loss of resolution;
- Releasing two different colour stretches for each inversion product. A logarithmic and a linear colour stretch of the conductivity section images was released for the first time, allowing users to effectively discriminate between weak to moderate conductors and strong conductors within the georeferenced conductivity section images;
- Improvements to the method used to calculate the Depth of Investigation (DOI); and,
- Release of a 400 m and a 200 m GA-LEI suite of interpretation products.

6.2 IMPLICATIONS FOR URANIUM SYSTEMS

S. Jaireth

Important features of sandstone-hosted uranium mineral systems in the Lake Frome region were described in [Section 3.6](#). Critical elements which determine the fertility of such systems, and which can be used to assess the prospectivity of an area, are:

- Sources of leachable uranium (felsic rocks containing uranium-bearing minerals such as uraninite, monazite and xenotime);
- Highly permeable sandstones (aquifers) confined by relatively less permeable shales (aquitards);
- Organic and/or inorganic reductants (*in situ* or mobile) in the aquifers or in the shales under- or over-lying the sandstone aquifer; and,
- Basin architecture favourable to creating hydrogeological conditions under which fluids (shallow groundwater) can bring uranium from source rocks with leachable uranium in to the aquifer.

Sandstone-hosted uranium deposits are formed at reduction-oxidation (redox) fronts in a sandstone aquifer, either as roll-fronts, or as tabular bodies often formed in proximity to faults. The mineralogy of redox fronts is dominated by hematite in the oxidised part and by sulfides at the ‘nose’ part of the roll front, with organic material dominating the reduced side of the redox front. As most sandstone hosts are active aquifers, the presence of moderate to high-salinity groundwater (as is the case in the Lake Frome region) masks the conductivity contrast generated by sulfides and clay minerals. As a result regional-scale AEM datasets (>2.5 km line spacing) are unable to map the location and shape of the redox front in the sandstone aquifer in this instance.

Interpretation of AEM data discussed in the preceding chapters has shown that it can map many critical features of a uranium mineral system, especially the architecture of the Callabonna Sub-basin in mineralised and prospective areas of the Lake Frome region:

1. Paralana Trough. This northeast-southwest trending trough is located to the west of the Poontana Inlier ([Figure 3.42](#)). The Trough hosts major uranium deposits (Four Mile East, Four Mile West, Pepegooona) and prospects. The presence of felsic source rocks with leachable uranium and several vein and breccia hosted primary deposits (e.g. Mount Gee and Mount Painter) in the Mount Painter Inlier to the west most probably explains the high uranium endowment of the Paralana Trough;
2. Mount Babbage Inlier palaeovalley system ([Figure 6.1](#)). The system, which includes the Blanchewater Palaeochannel, has been defined by mapping the surface of the Eyre Formation incising Mesozoic and/or Proterozoic basement. The system runs northward from the highlands

- of the Mount Babbage Inlier. Its present-day architecture is defined by movements along faults mappable by AEM. The general northward direction of the palaeovalley and alluvial fan system suggests that redox fronts in the Eyre Formation aquifers will be located in the northward direction, and not to the east of the Mount Babbage Inlier. Neotectonic movements (most probably post-mineralisation) along this fault system have produced horst and graben structures and scissor faults, causing erosion of the Eyre Formation in some areas and preservation in others, thereby defining prospective areas (e.g. the MacDonnell Creek area);
3. Poontana Trough. This trough is a region of sedimentary fill running parallel to the eastern Flinders Ranges range front, and extends northwards into the Strzelecki Desert beyond the northeastern tip of the Flinders Ranges. The Poontana Trough is gently down-warped and is filled with sediment of the Adelaide Geosyncline, the Arrowie Basin, the Eromanga Basin and the Callabonna Sub-basin, indicating that it has been active for a very long time interval in response to periodic uplift of the Flinders Ranges. The most recent sediment fill of the Willawortina Formation thickens towards the range front, indicating recent sedimentation after the most recent pulse of uplift in the Flinders Ranges (< 5 Ma). The Poontana Trough contains Cenozoic sediments of the Eyre and Namba formations, that are targets for uranium exploration throughout the region;
 4. Palaeovalley and palaeochannel systems in the southern Lake Frome region ([Figure 6.1](#)). The Palaeovalleys and palaeochannels mapped by Fabris *et al.* (2010), Fricke (2008) and (Hou *et al.*, 2007) have been updated using AEM data. Some palaeovalleys have been extended and the architecture of others has been more accurately defined. A better definition of palaeochannels is essential to assess their potential to generate fertile uranium systems. The architecture of the palaeochannels controls:
 - a. Sediment transport and groundwater flow direction;
 - b. Whether the groundwaters were hydrologically connected to source rocks of leachable uranium;
 - c. The meandering bends and sites of confluences with tributary-channels which constitute favourable sites of uranium deposition; and,
 - d. The position and thickness of basement scours or thalwegs filled with more permeable sands; and,
 5. Mapping of permeable sands in the Eyre and Namba formations. Uranium mineralisation is hosted in more permeable sandstone, rich in organic material, or in sandstone close to the contact with less permeable, organic-rich shales (for instance, near the contact between the Beverley Sands and the Alpha Mudstone). Airborne electromagnetic data and drill hole logs assist in mapping the spatial extent of permeable sands in both the Eyre and Namba formations.

The Lake Frome region remains the focus of exploration for sandstone-hosted uranium deposits. One of the major requirements in the generation of fertile sandstone-hosted systems, capable of forming significant deposits, is the presence of felsic rocks with leachable uranium. In the Lake Frome region such rocks are present in the Mount Painter and Mount Babbage inliers and in the Curnamona Province in the Olary Spur. Airborne electromagnetic data summarised in previous chapters has shown important features of favourable basin architecture that hydrogeologically links source rocks of uranium with permeable sandstones in the Eyre and Namba formations. The prospectivity of selected areas in the Lake Frome region is summarised in [Table 6.1](#). Palaeovalley and alluvial fan systems to the north of the Mount Babbage Inlier (the Mount Babbage palaeovalley system; [Figure 6.1](#)) are considered to have high potential for sandstone-hosted deposits of significant size.

6.3 IMPLICATIONS FOR OROGENIC LODE GOLD AND PORPHYRY COPPER GOLD SYSTEMS

Chemically reactive rocks (those containing large amounts of carbon, pyrite or carbonate) are potential targets for exploration because of their ability to react with ore fluids and precipitate metals. Both the Tapley Hill Formation and the Saddleworth Formation, in the Nackara Arc, are considered to be prospective for copper-uranium and gold mineralisation because they contain black

shale facies with abundant carbon and pyrite, and may act as chemical reductants for ore fluids. Rocks of the Broadhurst Formation in the Paterson Province of Western Australia are of a similar age and mineralogy and host the Nifty copper mine, plus a number of copper, copper-uranium and copper-gold prospects, and are also electrically conductive (Huston *et al.*, 2010; Roach *et al.*, 2010).

Several orogenic lode gold deposits of Delamerian age are located in the Nackara Arc. Most gold deposits are hosted in the Tapley Hill Formation, which is characterised by high relative conductivity and is thought to mask the conductivity contrast possibly generated by gold-bearing fluids reacting with the host rocks. Gold deposits hosted in slightly less conductive rocks (such as the relatively moderately conductive Saddleworth Formation) show steeply-dipping conductivity textures which may be related to sulfides formed from reaction with gold-bearing fluids. It is possible that AEM surveys of closer line-spacing would be able to map fluid-channelling structures.

Interestingly, the regional AEM data can map structures when the host rock is relatively more resistive (such as the Anabama Porphyry). All known copper, gold and molybdenum prospects in and around the porphyry are structurally controlled, and these structures show steeply-dipping, distinct conductivity contrasts generated by clay- and sulfide-bearing alteration (see [Figure 5.7.3](#))

6.4 REFERENCES

- Fabris, A. J., Gouthas, G. and Fairclough, M. C., 2010. The new 3D sedimentary basin model of the Curnamona Province: geological overview and exploration implications. *MESA Journal* **58**(September 2010), 16-24.
- Fricke, C., 2008. Definitions of Mesoproterozoic igneous rocks of the Curnamona Province: The Ninnerie Supersuite. Primary Industries and Resources South Australia, Adelaide. **Report Book 2008/4**, 86 pp.
- Hou, B., Zang, W., Fabris, A., Keeling, J., Stoian, L. and Fairclough, M., 2007. Palaeodrainage and coastal barriers of South Australia 1:2 000 000. CRC LEME, Geological Survey Branch, Primary Industries and Resources South Australia, Adelaide. Online: http://www.pir.sa.gov.au/_data/assets/pdf_file/0005/41486/palaeochannels_sa_map.pdf.
- Huston, D. L., Czarnota, K., Jaireth, S., Williams, N. C., Maidment, D., Cassidy, K. F., Duerden, P. and Miggins, D., 2010. Mineral systems of the Paterson Region. In: Roach, I. C. (editor), Geological and energy implications of the Paterson Province airborne electromagnetic (AEM) survey, Western Australia. Geoscience Australia, Canberra. **Record 2010/12**, 155-218 p.
- Roach, I. C., Costelloe, M. T. and Hutchinson, D. K., 2010. Interpretations of AEM data. In: Roach, I. C. (editor), Geological and energy implications of the Paterson Province airborne electromagnetic (AEM) survey. Geoscience Australia, Canberra. **Record 2010/12**, 107-154 p.

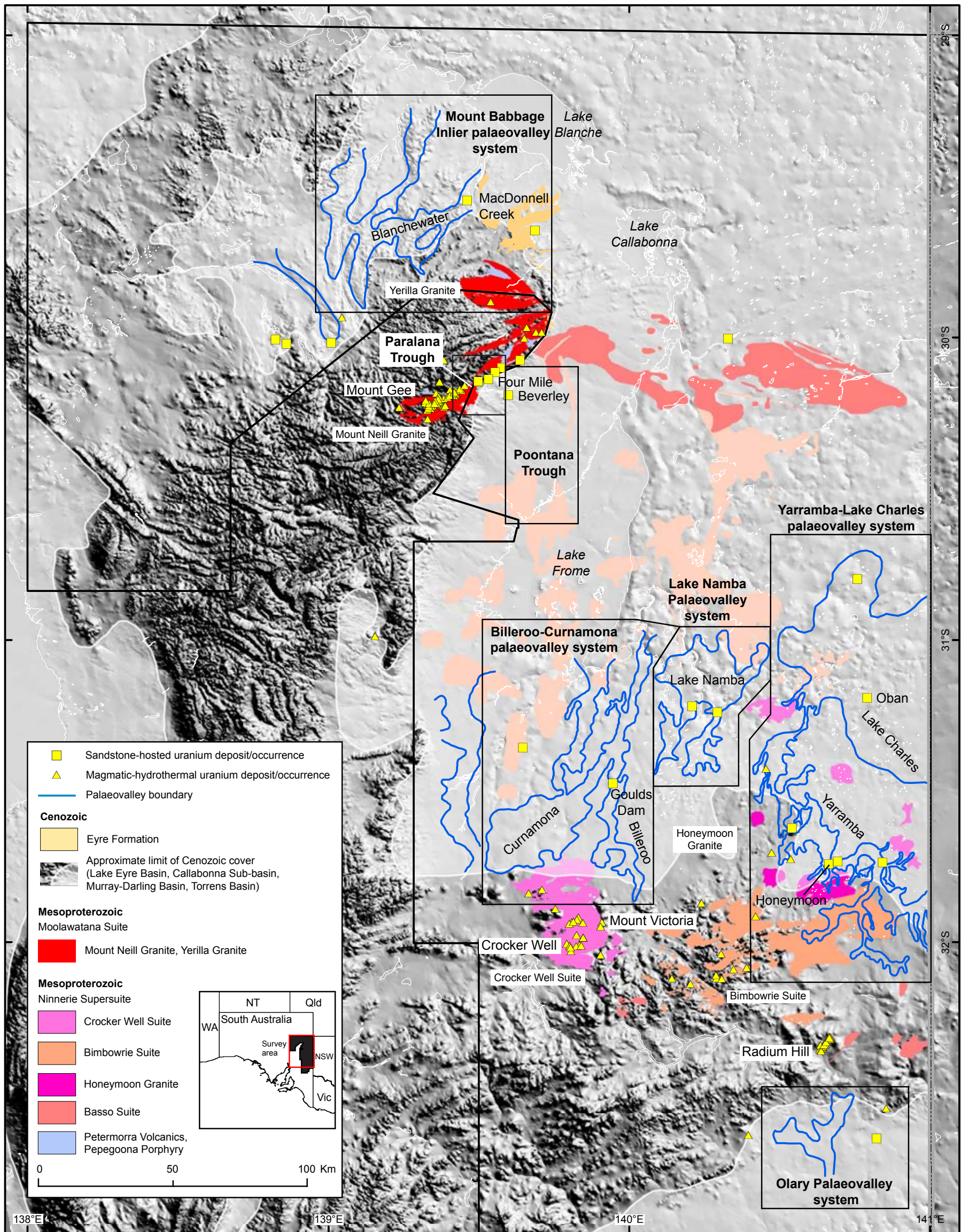


Figure 6.1: Map of the Frome AEM Survey area detailing the prospectivity analysis areas discussed in Table 6.1. The map depicts the SRTM DEM (greyscale background) with the interpreted boundaries of the Cenozoic Lake Eyre Basin—Callabonna Sub-basin and Murray-Darling Basin cover (from SARIG), outcropping Eyre Formation (from SARIG), uranium-bearing felsic rocks (from SARIG) and palaeovalley systems interpreted or reinterpreted using the Frome AEM Survey data set.

Blank page

Table 6.1: Critical features of sandstone-hosted uranium systems in the Lake Frome region and the mineral potential of selected areas.

CRITICAL FEATURE	MOUNT BABBAGE PALAEOVALLEY SYSTEM	PARALANA TROUGH	POONTANA TROUGH	BILLEROO-CURNAMONA PALAEOVALLEY SYSTEM	YARRAMBA-LAKE CHARLES PALAEOVALLEY SYSTEM	LAKE NAMBA PALAEOVALLEY SYSTEM	OLARY PALAEOVALLEY SYSTEM
Source of leachable uranium.	Yerilla Granite (up to 270 ppm U); felsic rocks contain uraninite, monazite, xenotime, allanite); Yerilla uranium prospect.	Mount Neill Granite (up to 380 ppm U); Hot Springs Gneiss (up to 470 ppm U); rock contain uraninite, allanite, monazite, xenotime; Mount Gee and Mount Painter deposits.	Unclear. If palaeo fluid-flow direction was southward from Mount Babbage Inlier, Yerilla Granite could have provided U.	Mindamereeka Trondhjemite (Crocker Well Suite, with up to 110 ppm U); felsic rock contains allanite, monazite and thorian brannerite (not easily leachable). Mount Victoria, Crocker Well deposits (brannerite, davidite, minor monazite, xenotime, uranophane).	Honeymoon Granite (up to 40 ppm U) and felsic intrusives and metamorphic rocks in the Broken Hill Block (up to 20 ppm U); Honeymoon Granite contains uranium oxides, monazite, allanite.	Unclear. Benagerie Volcanics (up to 20 ppm U). No information about leachable uranium minerals in the source rocks.	Possibly Bimbowrie Suite (up to 35 ppm U) and uranium deposits such as Radium Hill.
Permeable sandstone.	Eyre Formation; sands in Namba Formation.	Eyre Formation; Namba Formation; Bulldog Shale/Cadna-owie Formation.	Beverley Sands in the Namba Formation; Eyre Formation; Cadna-owie Formation.	Eyre Formation.	Eyre Formation.	Eyre Formation.	Murray Group (marine) in the lower reaches, Renmark Group (terrestrial) in the upper part.
Organic material or mobile reductant.	Organic in Eyre Formation.	Organic material in Eyre Formation and Bulldog Shale and mudstone facies in the Namba Formation; possible mobile reductant.	Organic material in mudstones in the Namba Formation, Eyre Formation and Bulldog Shale. Possible mobile reductant.	Eyre Formation is rich in organic material.	Eyre Formation is rich in organic material.	Eyre Formation is rich in organic material.	Lignitic and carbonaceous shale in the Murray Group.
Architecture.	Palaeovalley/palaeochannel and/or alluvial fan system. Eyre Formation incised into Marree Subgroup.	Trough. Eyre Formation overlying Bulldog Shale.	Eyre and Cadna-owie formations as alluvial fans. Beverley Sands form a palaeochannel incised into Alpha-mudstone. Palaeochannel marked with meandering bends and sites of confluences with tributaries.	Eyre Formation palaeochannels incised into Bulldog Shale and/or Willyama Supergroup. The system runs generally northward from the Olary Spur with felsic rocks containing leachable uranium. Palaeochannel with basement scours, meandering bends and sites of confluences with tributaries.	Eyre Formation palaeochannels incised into Bulldog Shale and/or Willyama Supergroup. The system runs generally northward from the Olary Spur with felsic rocks containing leachable uranium. Palaeochannel with basement scours, meandering bends and sites of confluences with tributaries.	Eyre Formation palaeochannels incised into Benagerie Volcanics and/or Willyama Supergroup. The system runs generally northward from the Olary Spur. Palaeochannel with basement scours, meandering bends and sites of confluences with tributaries present. It is not clear if the channel system was hydrogeologically connected to uranium-enriched felsic rocks in the Olary Spur.	Palaeochannel incised into Neoproterozoic rocks (Adelaide Geosyncline). Terrestrial sediments (Renmark Group?) covered by marine transgression. Shape of palaeovalley/palaeochannels yet to be defined.
Palaeo fluid-flow direction of shallow groundwater.	Generally northward from Mount Babbage Inlier.	Generally southwest to northeast connecting felsic rocks with leachable uranium.	Unclear; Possibly northwest to southeast.	Most probably northward from the Olary Block.	Most probably northward from the Olary Spur the and northwest from the Barrier Ranges.	Most probably northward from the Barrier Ranges.	Most probably southward from the Barrier Ranges and Olary Spur.
Known prospects or deposits.	MacDonnell Creek area.	Four Mile East, Four Mile West, Pepegoona.	Beverley; Yagdlin.	Goulds Dam.	Honeymoon, Kalkaroo, Yarramba, Junction Dam, Oban.	Lake Namba, Lake Tinko.	Unnamed U prospects associated with lignitic shales in the Murray Group (Kinloch Dam and Gairloch Dam prospects).
Comments on potential.	High potential for relatively large deposits.	Moderate potential for new deposits as two large deposits have been found.	Moderate potential for mineralisation in the Namba Formation; high potential in Eyre and Cadna-owie formations.	High potential for relatively smaller deposits. Interpretation of AEM data has extended the palaeovalley system to the north and defined its shape more accurately. Low potential in Namba Formation.	High potential for relatively smaller deposits. Interpretation of AEM data has extended the palaeovalley system to the north and defined its shape more accurately. Low potential in the Namba Formation. Eyre Formation in the palaeochannel system in NSW has not been explored.	Moderate potential for relatively smaller deposits. Low potential in the Namba Formation.	Low potential for uranium deposits of significant size. Murray Group sediments less prospective than the sands of the Renmark Group.

Blank page

7 Acknowledgements

The Geoscience Australia and the Geological Survey of South Australia acknowledge the invaluable assistance of the following people and organisations in the production of this volume.

Geophysical contractor:

Fugro Airborne Surveys Pty Ltd.

Reviewers:

Ross C. Brodie (GA), Mike Craig (GA), Tania Dhu (GSSA), Stephen Hore (GSSA), David Huston (GA), John Keeling (GSSA), Aden McKay (GA), Wolfgang Preiss (GSSA), Murray Richardson (GA), Ned Stolz (GA), Anthony Schofield (GA), Alan Whitaker (GA).

Geoscience Australia:

Andy Barnicoat, Ross S. Brodie, Jonathan Clarke, Dave Gibson, David Hutchinson, Richard Lane, Steven Lewis, Daniel Rawson, Murray Richardson, Camilla Sorensen, Nick Williams and Lisa Worrall.

Geological Survey of South Australia:

Tim Baker, Martin Fairclough, George Gouthas, Malcolm Sheard and Ted Tyne.

Interpretation workshop contributors:

Graham Heinson (University of Adelaide) and Tim Munday (CSIRO).

Industry contacts:

- Adelaide Resources Ltd (Chris Drown) provided access to drill holes, geophysical and geophysical data;
- Alinta Energy Ltd (Leigh Creek Coal Mine; Max Duval and Laurie Mills) provided access to drill holes, geophysical and geophysical logs and discussion;
- Areva Australia Pty Ltd (Philippe Portella) provided geophysical data;
- Callabonna Uranium Ltd (Mike Raetz, George Ross and Andrew Wilde) led the industry infill consortium, provided geological and geophysical data, access to drill holes, accommodation and discussion and contributed to the interpretation workshop;
- Cameco Australia Pty Ltd (Tyler Matheson) for discussion;
- Curnamona Energy Ltd (Mark Randell) provided access to drill holes, geophysical and geophysical data, accommodation and discussion;
- Eromanga Uranium Ltd (Steve Abbott) for discussion;
- Gold Fields Australasia (Chris Wawryk) provided drill hole data;
- Havilah Resources NL (Chris Giles and Bob Johnson) for discussion;
- Heathgate Resources (Lynelle Bienke, Michaela Jennings, Geoff McConachy and Adam Huddleston) provided access to drill holes, geophysical and geophysical data, accommodation and discussion;
- Maximus Resources (Kevin Wills) for discussion;
- SinoSteel-PepinNini Curnamona Management Pty Ltd (Brett Rava and Andrew Querzoli) for discussion;
- Scimitar Resources Ltd (now Cauldron Energy Ltd; Andrew Rust) provided geophysical data;
- Toro Energy Ltd (David Rawlings) for discussion; and,
- Uranium One Australia Pty Ltd (Leon Faulkner and Katherine Kingma) provided access to drill holes, geophysical and geophysical data, discussion and accommodation.

Steven Hill (University of Adelaide) for discussions on landscape evolution.

The Frome airborne electromagnetic survey, South Australia: implications for energy, minerals and regional geology

Appendix 1: Additional climate data

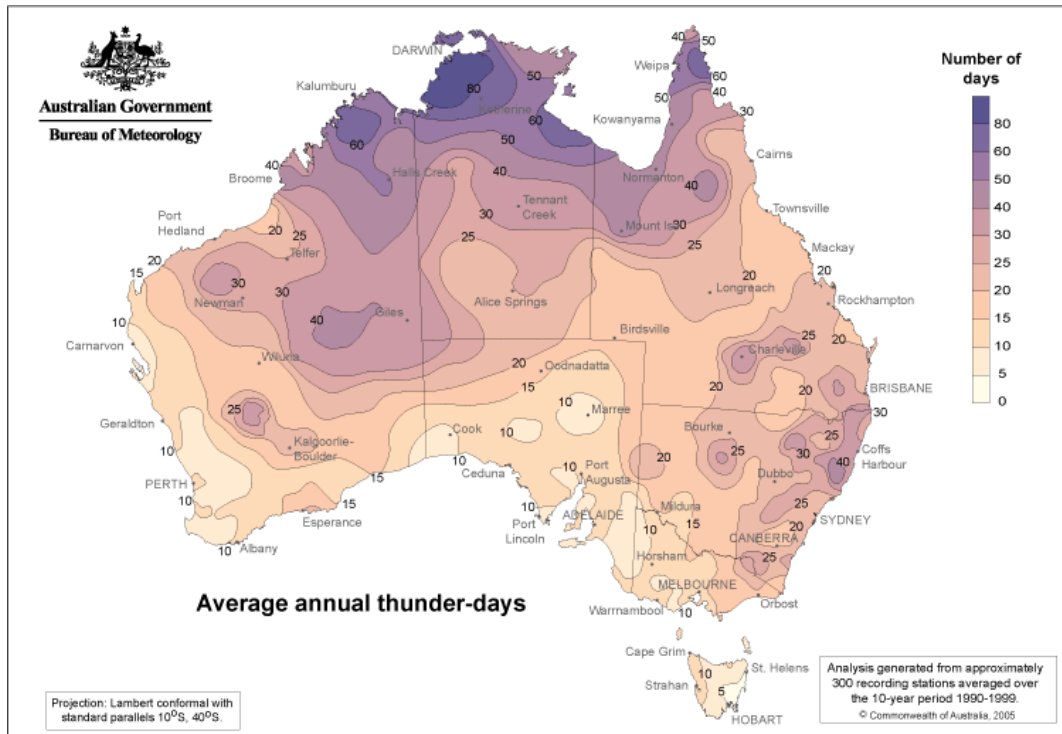


Figure A1.1: Average number of thunder days for Australia (BOM, 2011).

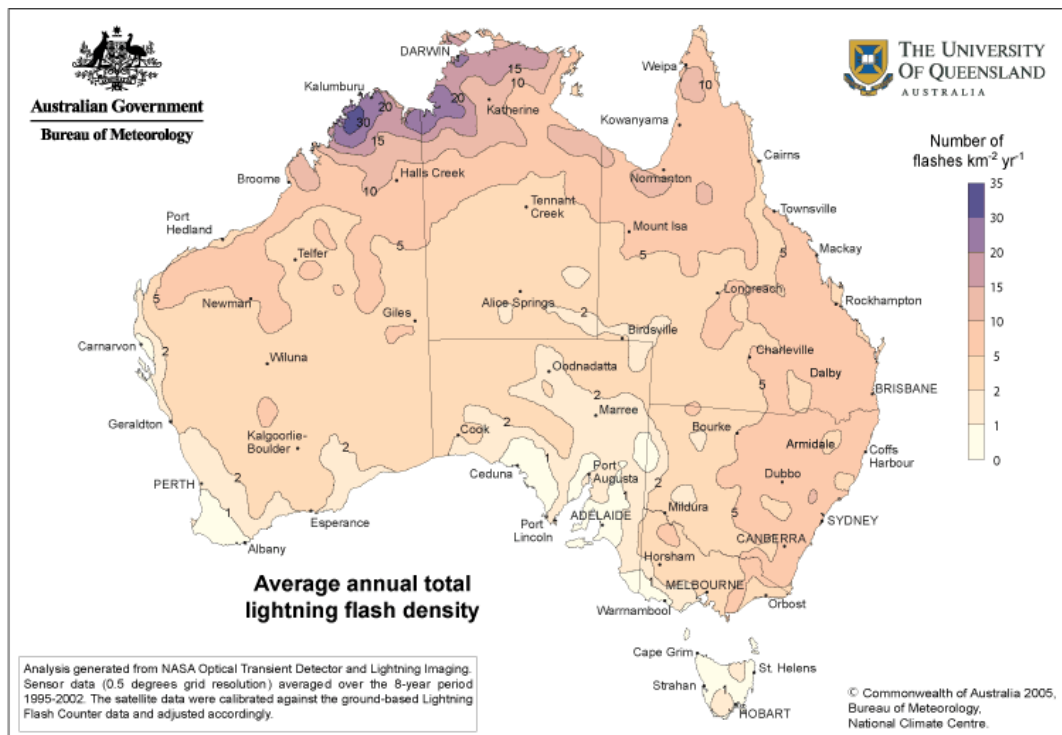


Figure A1.2: Average annual total lightning flashes for Australia (BOM, 2011).

The Frome airborne electromagnetic survey, South Australia: implications for energy, minerals and regional geology

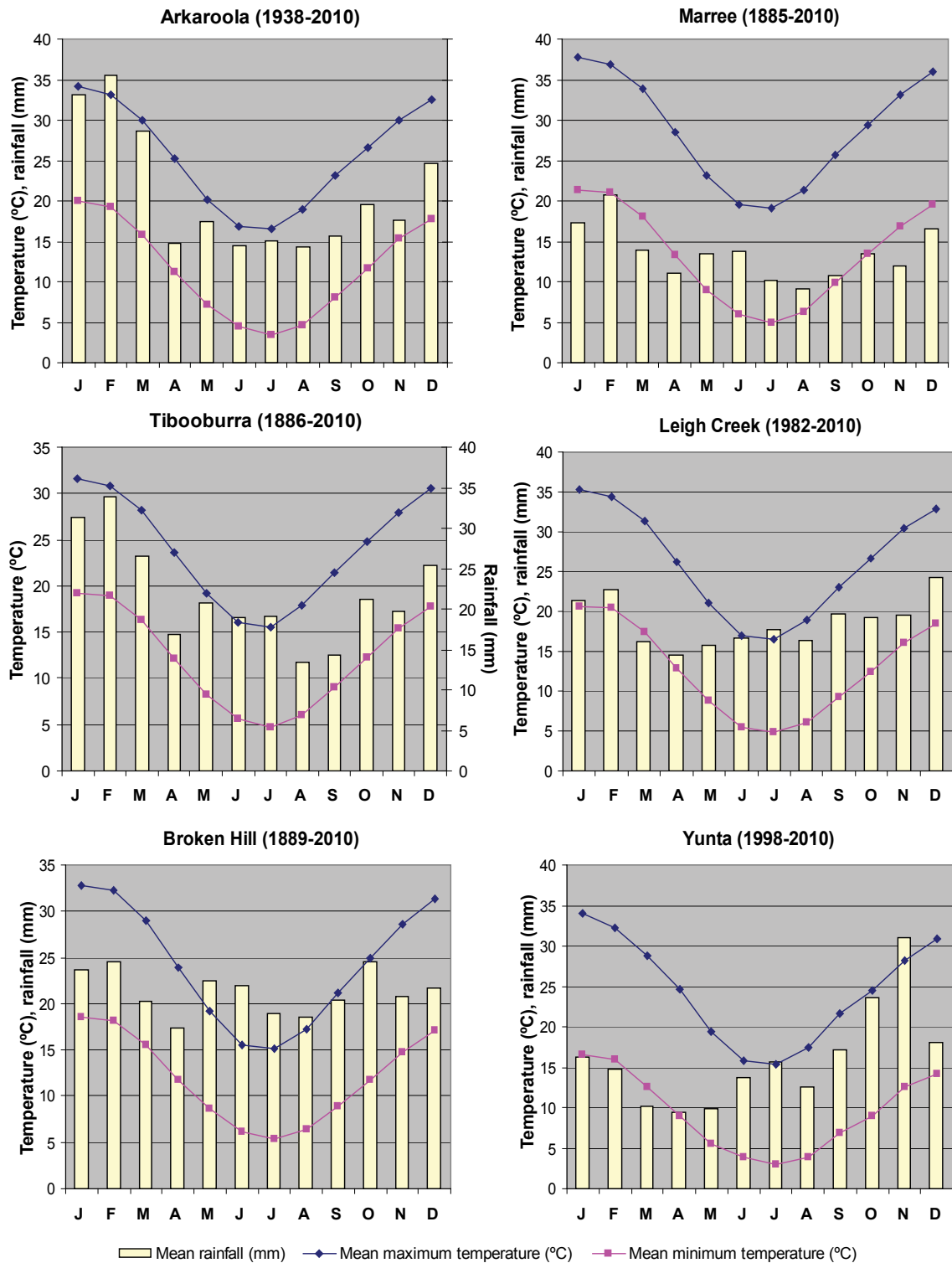


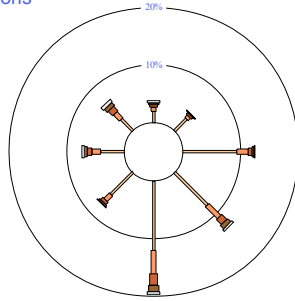
Figure A1.3: Rainfall and temperature averages for settlements within or near the survey area (BOM, 2011). Bracketed figures are the years during which data were collected.

The Frome airborne electromagnetic survey, South Australia: implications for energy, minerals and regional geology

ARKAROOLA

Rose of Wind direction versus Wind speed in km/h (01 Dec 1977 to 28 Feb 2010)

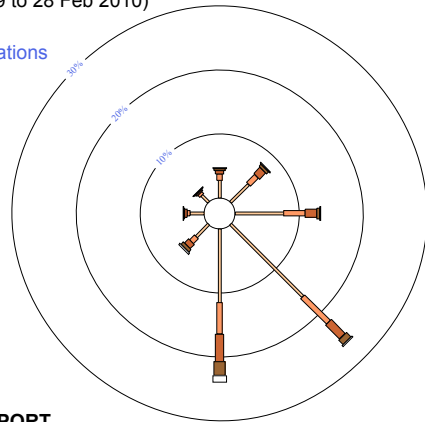
9 am
11176 Total Observations
Calm 25%



MARREE COMPARISON

Rose of Wind direction versus Wind speed in km/h (01 Apr 1939 to 28 Feb 2010)

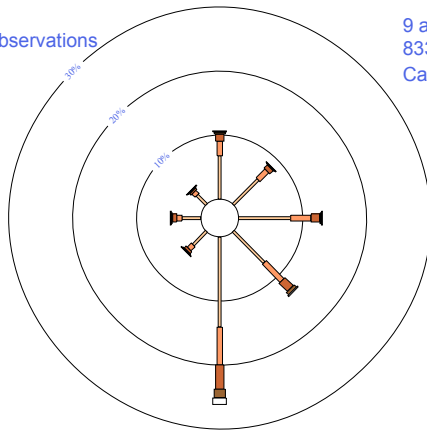
9 am
24806 Total Observations
Calm 12%



TIBOOBURRA POST OFFICE

Rose of Wind direction versus Wind speed in km/h (01 Jan 1910 to 28 Feb 2010)

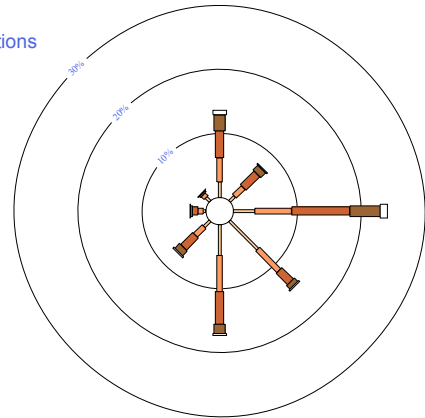
9 am
33308 Total Observations
Calm 15%



LEIGH CREEK AIRPORT

Rose of Wind direction versus Wind speed in km/h (01 May 1982 to 28 Feb 2010)

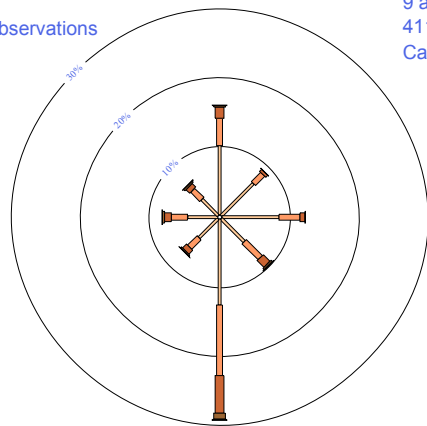
9 am
8331 Total Observations
Calm 11%



BROKEN HILL (PATTON STREET)

Rose of Wind direction versus Wind speed in km/h (01 May 1959 to 28 Feb 2010)

9 am
15606 Total Observations
Calm 1%



YUNTA AIRSTRIP

Rose of Wind direction versus Wind speed in km/h (09 Jul 1998 to 26 Feb 2010)

9 am
4114 Total Observations
Calm 6%

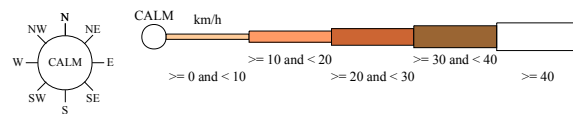
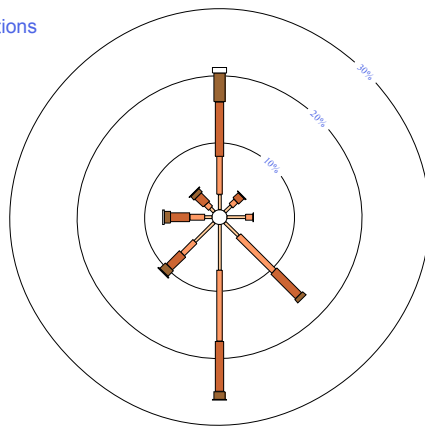


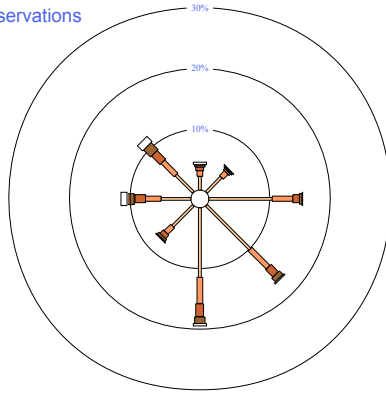
Figure A1.4: Wind roses for 9 am wind directions and wind speeds (BOM, 2011).

The Frome airborne electromagnetic survey, South Australia: implications for energy, minerals and regional geology

ARKAROO LA

Rose of Wind direction versus Wind speed in km/h (01 Dec 1977 to 28 Feb 2010)

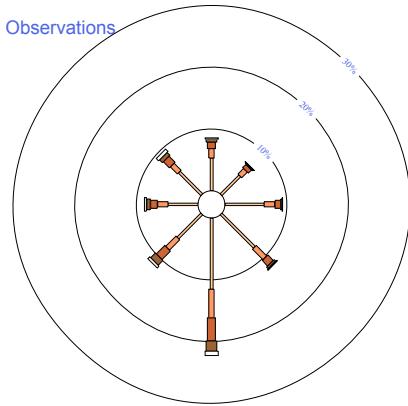
3 pm
11113 Total Observations
Calm 7%



MARREE COMPARISON

Rose of Wind direction versus Wind speed in km/h (01 Apr 1939 to 28 Feb 2010)

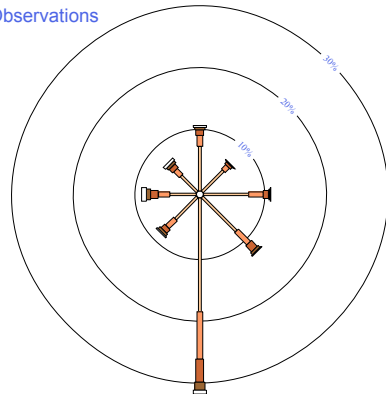
3 pm
24672 Total Observations
Calm 11%



TIBOOBURRA POST OFFICE

Rose of Wind direction versus Wind speed in km/h (01 Jan 1910 to 28 Feb 2010)

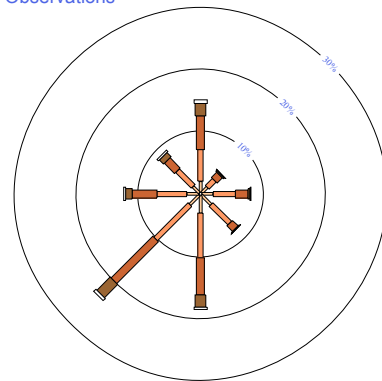
3 pm
19790 Total Observations
Calm 3%



LEIGH CREEK AIRPORT

Rose of Wind direction versus Wind speed in km/h (01 May 1982 to 28 Feb 2010)

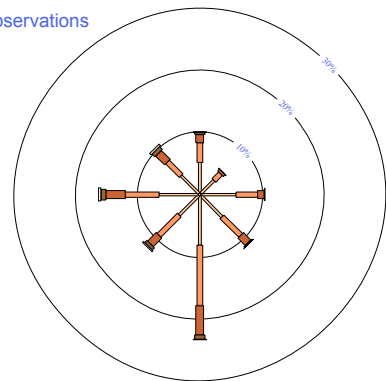
3 pm
8230 Total Observations
Calm 1%



BROKEN HILL (PATTON STREET)

Rose of Wind direction versus Wind speed in km/h (01 May 1959 to 28 Feb 2010)

3 pm
15575 Total Observations
Calm 1%



YUNTA AIRSTRIP

Rose of Wind direction versus Wind speed in km/h (09 Jul 1998 to 26 Feb 2010)

3 pm
4129 Total Observations
Calm *

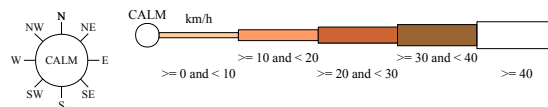
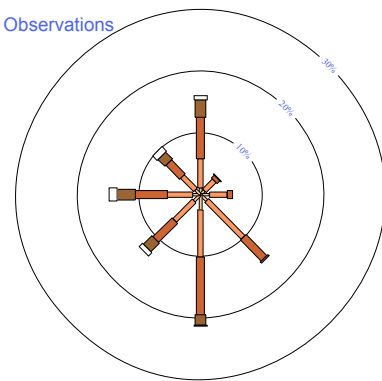


Figure A1.5: Wind roses for 3 pm wind directions and wind speeds (BOM, 2011).

Appendix 2: Summary of inversion products for the 400 m GA-LEI inversion

NAME	FORMAT	DESCRIPTION	COMMENTS
grids			
Conductance_ers	.ers	Total conductance grids for 0-100 m and 0-200 m depth	4 files
Conductance_jpg	.jpg and associated .jgw	Conductance grids in georeferenced JPEG format	4 files
Depth_of_Investigation_ers	.ers	Depth of investigation grid	2 files
Depth_of_Investigation_jpg	.jpg and associated .jgw	Depth of investigation grid in georeferenced JPEG format	2 files
Depth_Slices_ers	.ers	Conductivity grids in slices of depth below surface	30 files
Depth_Slices_jpg	.jpg and associated .jgw	Depth slices in georeferenced JPEG format	30 files
Elevation_slices_ers	.ers	Conductivity grids in slices of elevation above sea level (10 m slices)	120 files
Elevation_Slices_jpg	.jpg and associated .jgw	Elevation slices in georeferenced JPEG format	120 files
sbs_inversion		Sample-by-sample inversion products	
linedata			
Frome.sbs.inversion.part1.dat	ASCII .dat	ASCII data file containing SBS inversion (part 1 of 2)	1 file containing 124 lines of data
Frome.sbs.inversion.part1.des	ASCII .des	ASEG-GDF2 header descriptor file (Free form)	1 file
Frome.sbs.inversion.part1.dfn	ASCII .dfn	ASEG-GDF2 header definition file	1 file
Frome.sbs.inversion.part2.dat	ASCII .dat	ASCII data file containing SBS inversion (part 2 of 2)	1 file containing 143 lines of data
Frome.sbs.inversion.part2.des	ASCII .des	ASEG-GDF2 header descriptor file (Free form)	1 file
Frome.sbs.inversion.part2.dfn	ASCII .dfn	ASEG-GDF2 header definition file	1 file

The Frome airborne electromagnetic survey, South Australia: implications for energy, minerals and regional geology

georef_images

Linenumbr.jpg	.jpg and	Georeferenced JPEG images of	582 files
Linenumbr.jgw	associated .jgw	conductivity line sections	
Colorbar_image.jpg	.jpg	Conductivity colour scale	1 file

gocad_tsurf	.ts	GOCAD™ triangulated surfaces of conductivity line sections	291 files
--------------------	-----	--	-----------

sections

Linenumbr.pdf	.pdf	Multiplots showing conductivity, AEM system geometry and data misfit	291 files
---------------	------	--	-----------

lbl_inversion		Line-by-line inversion products	
----------------------	--	---------------------------------	--

linedata

Frome.lbl.inversion.dat	ASCII .dat	ASCII data file containing LBL inversion	1 file containing 162 lines of data
Frome.lbl.inversion.des	ASCII .des	ASEG-GDF2 header descriptor file (Free form)	1 file
Frome.lbl.inversion.dfn	ASCII .dfn	ASEG-GDF2 header definition file	1 file

georef_images

Linenumbr.jpg	.jpg and	Georeferenced JPEG images of	372 files
Linenumbr.jgw	associated .jgw	conductivity line sections	
Colorbar_image.jpg	.jpg	Conductivity colour scale	1 file

gocad_tsurf	.ts	GOCAD™ triangulated surfaces of conductivity line sections	186 files
--------------------	-----	--	-----------

sections

Linenumbr.pdf	.pdf	Multiplots showing conductivity, AEM system geometry and data misfit	186 files
---------------	------	--	-----------

Report

Frome_AEM_inversion_report.pdf	.pdf	Explanatory notes	1 file
--------------------------------	------	-------------------	--------

The Frome airborne electromagnetic survey, South Australia: implications for energy, minerals and regional geology

Shapefiles

Frome_TEMPEST_flightpath.shp	.shp and associated files	Frome Flight path shape file	4 files
Frome_boundary.shp	.shp	Frome boundary shape file	4 files
Frome_C1_infill_boundary.shp	.shp	Frome C1 Infill boundary shape file (commercial-in-confidence data)	4 files

Appendix 3: GA-LEI Inversion of TEMPEST Data

R. C. Brodie

A3.1 INTRODUCTION

The GA-LEI inversion program is capable of inverting data from most airborne time-domain AEM systems. It has the capability of inverting for layer conductivities, layer thicknesses, and system geometry parameters, or some subset of these. There are options to use a multi-layer smooth-model formulation (Constable *et al.*, 1987) or a few-layer blocky-model formulation (Sattel, 1998). For the sake of simplicity, only the aspects of the algorithm that are relevant to the inversion of TEMPEST™ data using a multi-layer smooth-model are described here.

TEMPEST™ data consist of a collection (tens of thousands to millions) of point located multi-channel samples acquired at 0.2 s (approximately 12 m) intervals along survey flight lines. The algorithm independently inverts each sample. The data inputs to the inversion of each sample are the observed total (primary plus secondary) field X-component and Z-component data. Auxiliary information input into the algorithm are the measured and assumed elements of the system geometry, the thicknesses of the layers, and prior information on the unmeasured elements of the system geometry and ground conductivity. The unknowns solved for in the inversion (outputs) are the electrical conductivity of the layers and the unmeasured elements of the system geometry.

Since each sample is inverted independently, the user may elect to invert all samples or some subset of them. The inversion of each sample results in an estimate of a one dimensional (1D) conductivity structure associated with that sample. Each estimated 1D conductivity structure, although theoretically laterally constant and extending infinitely in all directions, is only supported by the data within the system footprint which is approximately a square of side length 470 m centred about the sample point (Reid and Vrbancich, 2004). So by progressively inverting all the samples and stitching together the resultant 1D conductivity structures a depiction of the overall laterally variable 3D conductivity structure is built up.

A3.2 FORMULATION

Figure A3.1 shows the overall framework under which the inversion of a single airborne sample is carried out. The elements of the figure are progressively described in the following sections.

A3.2.1 Coordinate System

Since each sample is inverted separately the coordinate system is different for the inversion of each sample. A right handed xyz Cartesian coordinate system is used. The origin of the coordinate system is on the Earth's surface directly below the centre of the transmitter loop. The x-axis is in the direction of flight of the aircraft at that sample location, the y-axis is in the direction of the left wing and the z-axis is directed vertically upwards.

A3.2.2 System Geometry

The centre of the transmitter loop is located at $(0, 0, TX_h)$. Roll of the transmitter loop (TX_r) is defined as anti-clockwise rotation, about an axis through $(0, 0, TX_h)$ and parallel to the x-axis, so that a positive roll will bring the left wing up. Pitch of the transmitter loop (TX_p) is defined as anti-clockwise rotation, about an axis through $(0, 0, TX_h)$ and parallel to the y-axis, so that positive pitch will bring the aircraft's nose down. Yaw of the transmitter loop (TX_y) is defined as anti-clockwise rotation, about an axis through $(0, 0, TX_h)$ and parallel to the z-axis, so that a positive yaw would turn the aircraft left. However since the x-axis is defined to be in the direction of flight at each

sample, the transmitter loop yaw is always zero by definition. The order of operations for calculating the vector orientations is to apply the pitch, roll then yaw rotations respectively.

The position of the receiver coils relative to the transmitter loop is defined by the transmitter to receiver horizontal in-line separation (D_x), the transmitter to receiver horizontal transverse separation (D_y), and the transmitter to receiver vertical separation (D_z). The receiver coils are thus located at $(D_x, D_y, RX_h=TX_h+D_z)$. The receiver coils are always behind and below the aircraft ($D_x < 0, D_z < 0$). The receiver coils' roll (RX_r), pitch (RX_p) and yaw (RX_y) have the same rotational convention as for the transmitter loop except that they are rotations about the point (D_x, D_y, D_z) . The receiver coils are always assumed to be located on the y-axis ($D_y = 0$) and to have zero yaw ($RX_y = 0$). Although this is not in reality the case, the position and orientation is not measured and there is not enough information available to solve for these since Y-component data is not available.

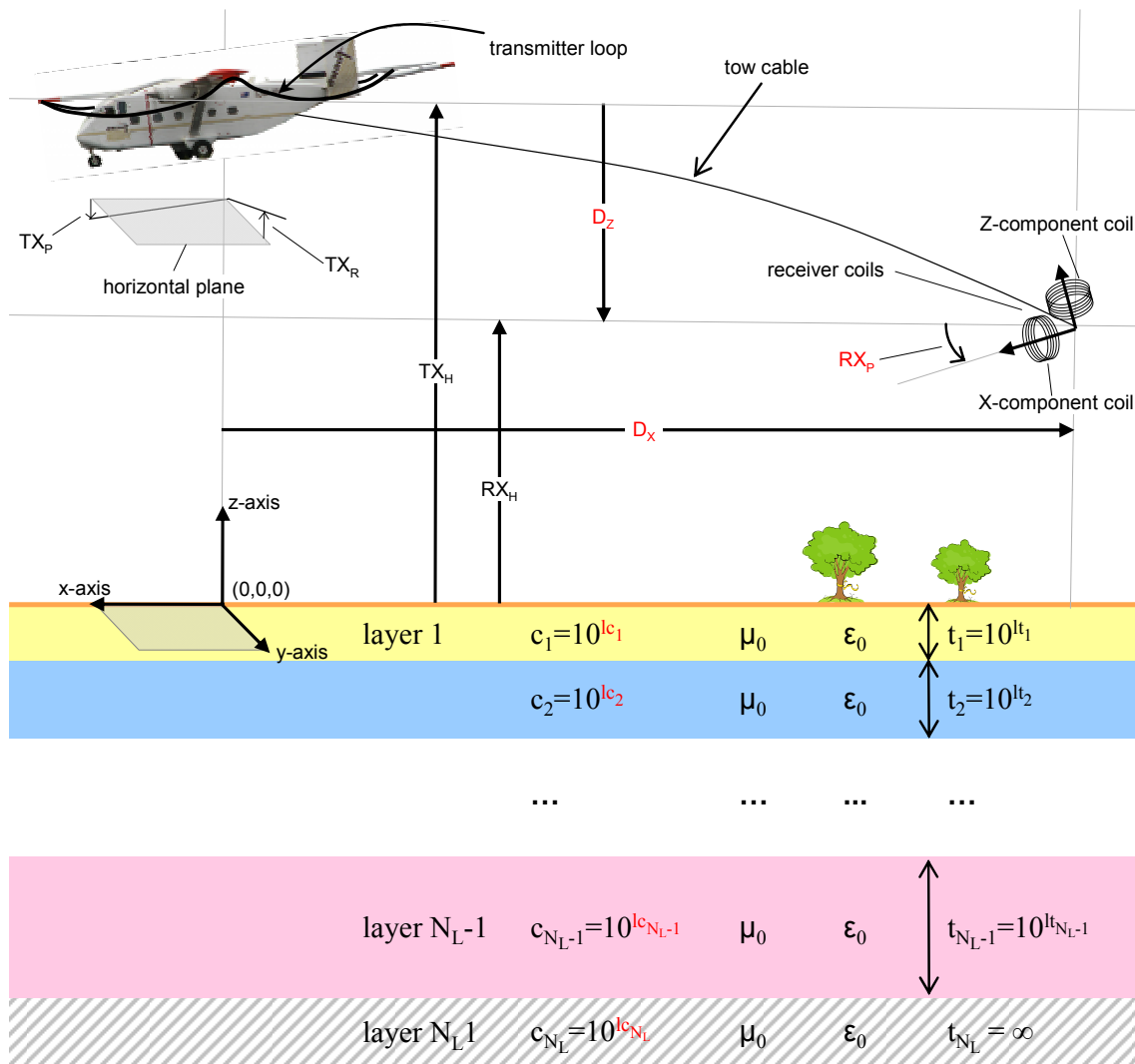


Figure A3.1: Schematic representation of the framework for GA-LEI inversion of TEMPESTTM AEM data. Red elements are the unknowns to be solved for.

Note that transmitter loop pitch data supplied by Fugro Airborne Surveys in processed TEMPEST data uses the convention where a positive transmitter pitch is nose up, and accordingly the supplied pitch is reversed in sign before being used in the inversion algorithm.

A3.2.3 Layered Earth

The layered earth model is independent at each inverted sample location. The layered earth consists of N_L horizontal layers stacked on top of each other in layer cake fashion. The k^{th} layer has constant thickness t_k and the bottom layer is a halfspace that has infinite thickness ($t_{NL} = \infty$), extending to infinite depth. The electrical conductivity of the k^{th} layer is c_k and it is constant throughout the layer. The magnetic permeability of all layers is assumed to be equal to the magnetic permeability of free space μ_0 . The dielectric permittivity of all layers is assumed to be equal to the permittivity of free space ϵ_0 .

A3.2.4 Data

Part of the TEMPEST data processing sequence involves partitioning the total (secondary plus primary) field response that is actually observed into estimates of the unknown primary and secondary field components. Then an estimate of the transmitter to receiver horizontal in-line and vertical separations D_x and D_z are made from the partitioned primary field component. The procedure uses the measured transmitter pitch (TX_p) and roll (TX_r) and assumes the receiver coils are flying straight, level and directly behind the aircraft ($D_y=0$, $RX_r=0$, $RX_p=0$, and $RX_y=0$). It is the estimated secondary field data, the measured elements of the system geometry (TX_h , TX_p , TX_r , and TX_y) and the associated estimates of the unmeasured elements of the system geometry (D_x and D_z) that are delivered to clients. Implicit in the delivered dataset are the assumed elements of the system geometry ($D_y=0$, $RX_r=0$, $RX_p=0$, and $RX_y=0$). However the estimated primary field data are not delivered to clients.

Since the GA-LEI algorithm makes its own estimate of system geometry as part of the inversion procedure it works with total field data. The input data are the total (primary plus secondary) field X-component and Z-component data. Therefore the total field data are first reconstructed. This is a simple matter of recomputing the primary field from magnetic dipole formulae (Wait, 1982) using the delivered (measured, estimated and assumed) elements of the system geometry then adding them to the delivered secondary field data. Note that the height, pitch, roll and geometry corrected data that are usually delivered as part of TEMPESTTM datasets are not used because the GA-LEI algorithm makes its own estimate of system geometry as part of the inversion procedure.

The reconstructed X-component and Z-component total field data for the k^{th} window are $X_k = X^P + X_k^S$ and $Z_k = Z^P + Z_k^S$ respectively. Here the super scripts ^P and ^S represent primary and secondary field components. Since the TEMPESTTM system has $N_w = 15$ windows, the observed data vector of length $N_D = 2 \times N_w = 30$ used in the inversion is,

$$\mathbf{d}^{obs} = [X_1 \ X_2 \ \dots \ X_{N_w} \ Z_1 \ Z_2 \ \dots \ Z_{N_w}]^T \quad (1)$$

where ^T represents the matrix and vector transpose operator.

Errors on the data are calculated outside of the program and input along with the data. Errors are assumed to be uncorrelated and Gaussian distributed. They are estimated as standard deviations of the Gaussian error distribution for each window and receiver component. Typically errors are calculated from the parameters of an additive plus multiplicative noise model (Green and Lane, 2003). Parameters of the noise model are determined from analysis of high altitude and repeat line data. If X_k^{err} and Z_k^{err} , represent the estimated standard deviation of the error in the k^{th} window of the X- component and Z-component data respectively then the data error vector of length $N_D=30$ is,

$$\mathbf{d}^{err} = [X_1^{err} \ X_2^{err} \ \dots \ X_{N_w}^{err} \ Z_1^{err} \ Z_2^{err} \ \dots \ Z_{N_w}^{err}]^T. \quad (2)$$

A3.2.5 Model Parameterisation

The unknown model parameter vector (\mathbf{m}) to be solved for in the inversion comprises earth model parameters and system geometry model parameters.

For the inversion of the TEMPESTTM dataset described here we choose to use a multi-layer smooth-model formulation (Constable *et al.*, 1987) rather than a few-layer blocky-model formulation (Sattel, 1998). Therefore we solve for the N_L conductivities of the layers but not the thicknesses. The layer thicknesses are inputs into the algorithm and are kept fixed throughout. To maintain positivity of the layer conductivities we actually invert for the base ten logarithms of the conductivities of each layer.

We solve for $N_G=3$ system geometry parameters: the transmitter to receiver horizontal in-line separation (D_x), the transmitter to receiver vertical separation (D_z), and the pitch of the receiver coil assembly (RX_p).

The unknown model parameter vector of length $N_p=N_G + N_L$ to be solved for is the concatenated vector of log base ten layer conductivities $\mathbf{lc} = [\log c_1 \log c_2 \cdots \log c_{N_L}]^T$ and the geometry parameters $\mathbf{g} = [D_x \ D_z \ RX_p]^T$, such that,

$$\mathbf{m} = [\mathbf{lc} \ | \ \mathbf{g}] = [\log c_1 \ \log c_2 \ \cdots \log c_{N_L} \ D_x \ D_z \ RX_p]^T \quad (3)$$

A3.2.6 Forward Model Derivatives

The forward model is the non-linear multi-valued function,

$$\mathbf{f}(\mathbf{m}) = [f_1(\mathbf{m}, \mathbf{p}) \ f_2(\mathbf{m}, \mathbf{p}) \ \cdots \ f_{ND}(\mathbf{m}, \mathbf{p})], \quad (4)$$

which for a given a set of model parameters (\mathbf{m}) calculates the theoretical total field data equivalent to that which would be produced for an ideal system, after the measurement and transformation by the data processing steps (Lane *et al.*, 2000). Here each $f_k(\mathbf{m}, \mathbf{p})$ is a function, not only of the layer conductivities and system geometry parameters in the inversion model vector \mathbf{m} , but also of several other fixed parameters \mathbf{p} (layer thicknesses; transmitter height, pitch and roll; receiver roll and yaw, transmitter to receiver horizontal transverse separation; system waveform and window positions *etc.*).

The implementation of (4) is based upon the formulation of Wait (1982) in which he develops the frequency-domain expressions for the magnetic fields due to vertical and horizontal magnetic dipole sources above a horizontally layered medium. The formulation does not account for the contribution due to displacement currents. We also assume that effects of dielectric permittivity and magnetic susceptibility are negligible compared to electrical conduction, and set each layer's dielectric permittivity and magnetic permeability to that of free space ($\epsilon_k=\epsilon_0$; $\mu_k=\mu_0$).

The full transient (0.04 s) equivalent square current waveform, to which TEMPESTTM data are processed, was linearly sampled at 75,000 Hz (3000 samples) and transformed to the frequency domain via fast Fourier transform (FFT). Using Wait's expressions the secondary B-field was calculated for ~20 discrete frequencies between 25 Hz and 37,500 Hz (6 logarithmically equi-spaced frequencies per decade). The inphase and quadrature parts of each component were then individually splined to obtain linearly spaced values at the same frequencies as the nodes of the FFT transformed current waveform. Complex multiplication of splined B-field with the FFT transformed current waveform, followed by inverse FFT, yielded the B field transient response.

The transient was then windowed (boxcar) into the 15 windows by averaging those samples that fell within each window. The primary field, which is constant over all 15 windows, was then computed from Wait's expressions and added to yield the total field window response in the *x-axis* and *z-axis*

directions. Finally these were rotated to be aligned with the X-component receiver coil's axis and Z-component receiver coil's axis according to the receiver pitch model parameter (RX_p) to yield $\mathbf{f}(\mathbf{m})$.

The inversion also requires the partial derivatives of $\mathbf{f}(\mathbf{m})$ with respect to the model parameters (see Equation 19). These were all calculated analytically. For computation of Wait's coefficient R_0 , we took advantage of the propagation matrix method (Farquharson *et al.*, 2004) because it is efficient for computation of the partial derivatives with respect to the multiple layer conductivities.

A3.2.7 Reference Model

The algorithm uses the concept of a reference model (Farquharson and Oldenburg, 1993) to incorporate prior information from downhole conductivity logs or lithologic/stratigraphic logging in order to improve inversion stability and to reduce the trade-off between parameters that are not well resolved independently. Since prior information is not available everywhere within the survey area, and the inversions are carried out in independent sample by sample fashion, it is not plausible to place hard reference model constraints on the model parameters. Instead the reference model provides a soft or probabilistic constraint only. If, from prior information, it is concluded that the likely distribution of the model parameter m_k is a Gaussian distribution with mean m_k^{ref} and standard deviation m_k^{unc} , then we would define the reference model vector as,

$$\mathbf{m}^{ref} = [lc_1^{ref} \quad lc_2^{ref} \quad \dots \quad lc_{N_L}^{ref} \quad D_x^{ref} \quad D_z^{ref} \quad RX_p^{ref}]^T \quad (5)$$

and the reference model uncertainty vector as,

$$\mathbf{m}^{unc} = [lc_1^{unc} \quad lc_2^{unc} \quad \dots \quad lc_{N_L}^{unc} \quad D_x^{unc} \quad D_z^{unc} \quad RX_p^{unc}]^T \quad (6)$$

The reference model mean values and uncertainties are inputs to the inversion algorithm and they may be different from sample to sample. The uncertainty values assigned to the reference model control the amount of constraint that the reference model places on the inversion results. A large uncertainty value for a particular parameter implies that the assigned reference model mean value is not well known and thus is allowed to vary a long way from the mean. On the other hand a low uncertainty implies the parameter is well known.

A3.3 OBJECTIVE FUNCTION

The inversion scheme minimises a composite objective function of the form,

$$\Phi = \Phi_d + \lambda (\alpha_c \Phi_c + \alpha_g \Phi_g + \alpha_v \Phi_v) \quad (7)$$

where Φ_d is a data misfit term, Φ_c is a layer conductivity reference model misfit term, Φ_g is a system geometry reference model misfit term, and Φ_v is a vertical roughness of conductivity term. The relative weighting of the data misfit Φ_d and the collective model regularisation term,

$$\Phi_m = \alpha_c \Phi_c + \alpha_g \Phi_g + \alpha_v \Phi_v \quad (8)$$

is controlled by the value of regularisation factor λ . The three model regularisation factors α_c , α_g and α_v control the relative weighting within the model regularisation term Φ_m . The algorithm requires that the α values be set by the user on an application by application basis and they remain fixed throughout the inversion. However the λ is automatically determined within the algorithm by the method described in Section 0.

A3.3.1 Data Misfit

The data misfit Φ_d is a measure of the misfit, between the data (\mathbf{d}^{obs}) and the forward model of the model parameters ($\mathbf{f}(\mathbf{m})$), normalised by the expected error and the number of data. It is defined as,

$$\begin{aligned}\Phi_d &= \frac{1}{N_D} \sum_{k=1}^{N_D} \left(\frac{d_k^{obs} - \mathbf{f}(\mathbf{m})}{d_k^{err}} \right)^2 \\ &= [\mathbf{d}^{obs} - \mathbf{f}(\mathbf{m})]^T \mathbf{W}_d [\mathbf{d}^{obs} - \mathbf{f}(\mathbf{m})]\end{aligned}\quad (9)$$

The diagonal $N_D \times N_D$ matrix \mathbf{W}_d is,

$$\mathbf{W}_d = \frac{1}{N_D} \begin{bmatrix} \frac{1}{(d_1^{err})^2} & & & \\ & \frac{1}{(d_2^{err})^2} & & \\ & & \dots & \\ & & & \frac{1}{(d_{N_D}^{err})^2} \end{bmatrix}\quad (10)$$

A3.3.2 Conductivity Reference Model Misfit

The conductivity reference model misfit term Φ_c is a measure of the misfit, between the logarithmic conductivity model parameters ($\mathbf{l}\mathbf{c}$) and the corresponding layer reference model values ($\mathbf{l}\mathbf{c}^{ref}$) normalised by the layer thicknesses and reference model uncertainty. It is defined as,

$$\begin{aligned}\Phi_c &= \sum_{k=1}^{N_L} \frac{t_k}{T/N_L} \left(\frac{lc_k^{ref} - lc_k}{lc_k^{unc}} \right)^2 \\ &= [\mathbf{m}^{ref} - \mathbf{m}]^T \mathbf{W}_c [\mathbf{m}^{ref} - \mathbf{m}]\end{aligned}\quad (11)$$

where $T = \sum_{k=1}^{N_L} t_k$, and the diagonal $N_p \times N_p$ matrix \mathbf{W}_c is,

$$\Delta \mathbf{m}_n = \mathbf{m}_{n+1} - \mathbf{m}_n. \quad (18)$$

The forward model at the new set of model parameters \mathbf{m}_{n+1} is approximated by a Taylor series expansion about \mathbf{m}_n , which, after excluding high order terms reduces to,

$$\mathbf{f}(\mathbf{m}_{n+1}) \approx \mathbf{f}(\mathbf{m}_n) + \mathbf{J}_n(\mathbf{m}_{n+1} - \mathbf{m}_n) \quad (19)$$

where $\mathbf{J}_n = \partial \mathbf{f}(\mathbf{m}) / \partial \mathbf{m}$ is the Jacobian matrix whose $i^{\text{th}}, j^{\text{th}}$ element is the partial derivative of the i^{th} datum with respect to the j^{th} model parameter evaluated at \mathbf{m}_n in model space. Making use of Equation 19 and substituting $\mathbf{m} = \mathbf{m}_{n+1}$, allows Equation 17 to be rewritten as,

$$\begin{aligned} \Phi(\mathbf{m}_{n+1}) = & \left[\mathbf{d}^{obs} - \mathbf{f}(\mathbf{m}_n) - \mathbf{J}_n(\mathbf{m}_{n+1} - \mathbf{m}_n) \right]^T \mathbf{W}_d \left[\mathbf{d}^{obs} - \mathbf{f}(\mathbf{m}_n) - \mathbf{J}_n(\mathbf{m}_{n+1} - \mathbf{m}_n) \right] \\ & + \lambda \alpha_c \left[\mathbf{m}^{ref} - \mathbf{m}_{n+1} \right]^T \mathbf{W}_c \left[\mathbf{m}^{ref} - \mathbf{m}_{n+1} \right] \\ & + \lambda \alpha_g \left[\mathbf{m}^{ref} - \mathbf{m}_{n+1} \right]^T \mathbf{W}_g \left[\mathbf{m}^{ref} - \mathbf{m}_{n+1} \right] \\ & + \lambda \alpha_v \mathbf{m}_{n+1}^T \mathbf{L}_v^T \mathbf{L}_v \mathbf{m}_{n+1} \end{aligned} \quad (20)$$

Since the value of Φ will be minimised when $\partial \Phi / \partial \mathbf{m}_{n+1} = 0$, we differentiate Equation 20 with respect to \mathbf{m}_{n+1} and set the result to zero and get,

$$\begin{aligned} 0 = & -2\mathbf{J}_n^T \mathbf{W}_d \left[\mathbf{d}^{obs} - \mathbf{f}(\mathbf{m}_n) - \mathbf{J}_n(\mathbf{m}_{n+1} - \mathbf{m}_n) \right] \\ & + \lambda \left[-2\alpha_c \mathbf{W}_c \left[\mathbf{m}^{ref} - \mathbf{m}_{n+1} \right] - 2\alpha_g \mathbf{W}_g \left[\mathbf{m}^{ref} - \mathbf{m}_{n+1} \right] + 2\alpha_v \mathbf{L}_v^T \mathbf{L}_v \mathbf{m}_{n+1} \right] \end{aligned} \quad (21)$$

Collecting terms in the unknown vector \mathbf{m}_{n+1} on the left hand side yields,

$$\begin{aligned} \left[\mathbf{J}_n^T \mathbf{W}_d \mathbf{J}_n + \lambda (\alpha_c \mathbf{W}_c + \alpha_g \mathbf{W}_g + \alpha_v \mathbf{L}_v^T \mathbf{L}_v) \right] \mathbf{m}_{n+1} = & \dots \\ \mathbf{J}_n^T \mathbf{W}_d \left[\mathbf{d}^{obs} - \mathbf{f}(\mathbf{m}_n) + \mathbf{J}_n \mathbf{m}_n \right] + \lambda \left[\alpha_c \mathbf{W}_c + \alpha_g \mathbf{W}_g \right] \mathbf{m}^{ref} \end{aligned} \quad (22)$$

Since Equation 22 is in the familiar form of a system of linear equations ($\mathbf{A} \mathbf{m}_{n+1} = \mathbf{b}$) we are able to solve for \mathbf{m}_{n+1} using a variety of linear algebra methods. We use Cholesky decomposition.

A3.4.2 Choice of the value of λ

An initial value of λ is chosen such that the data and model objective functions will have approximately equal weight. This is automatically realised by computing the ratio of the data and model objective functions, from the reference model perturbed by 1%, and computing the ratio of the data and model misfits,

$$\lambda_{start} = \frac{\Phi_d(\mathbf{f}(1.01 \times \mathbf{m}_0))}{\Phi_m(1.01 \times \mathbf{m}_0)}. \quad (23)$$

Then at each iteration the inversion employs a 1D line search where, in solving for \mathbf{m}_{n+1} in Equation 22 different values of λ are trialled, until a value of λ_n is found such that,

$$\Phi_d(\mathbf{f}(\mathbf{m}_{n+1})) \approx \Phi_d^{arg et} = 0.7 \times \Phi_d(\mathbf{f}(\mathbf{m}_n)), \quad (24)$$

thus reducing Φ_d to 0.7 of its previous value.

A3.4.3 Convergence Criterion

The iterations continue until the inversion terminates when one of the following conditions is encountered;

- Φ_d reaches a user defined minimum value $\Phi_d^{\min} = 1$;
- Φ_d has been reduced by less than 1% in two consecutive iterations;
- Φ_d can no longer be reduced; or,
- The number of iterations reaches a maximum of 100 iterations.

A3.5 REFERENCES

- Constable, S.C., Parker, R.L. and Constable, C.G., 1987. Occam's inversion: a practical inversion method for generating smooth models from electromagnetic sounding data. *Geophysics*, 52, 289-300.
- Farquharson, C.G., and Oldenburg, D.W., 1993. Inversion of time domain electromagnetic data for a horizontally layered earth. *Geophysical Journal International*, 114, 433–442.
- Farquharson, C. G., D. W. Oldenburg, and P. S. Routh, 2004, Simultaneous 1D inversion of loop-loop electromagnetic data for magnetic susceptibility and electrical conductivity. *Geophysics*, 68, 1857–1869.
- Green, A., and Lane, R., 2003. Estimating Noise Levels in AEM Data. Extended Abstract, ASEG 16th Geophysical Conference and Exhibition, February 2003, Adelaide.
- Lane, R., Green, A., Golding, C., Owers, M., Pik, P., Plunkett, C., Sattel, D. and Thorn, B., 2000. An example of 3D conductivity mapping using the TEMPEST airborne electromagnetic system. *Exploration Geophysics*, 31: 162-172.
- Reid, J.E., and Vrbancich, J., 2004. A comparison of the inductive-limit footprints of airborne electromagnetic configurations. *Geophysics*, 69, 1229–1239.
- Sattel, D., 1998, Conductivity information in three dimensions. *Exploration Geophysics*, 29, 157–162.
- Wait, J.R., 1982, Geo–electromagnetism. Academic Press Inc.

Appendix 4: GA-LEI inversion output ASCII header information

The conductivity ASCII data are provided in ASEG-GDF2 format, with accompanying .dfn and .des header files. The .des header files for both the sample-by-sample and line-by-line inversions are provided below.

A4.1 SAMPLE-BY-SAMPLE INVERSION CONDUCTIVITY HEADER

COMM Coordinate System Notes:

COMM -----

COMM The Transmitter Pitch (tx_pitch) in this dataset is the negative value of
COMM the transmitter pitch measured by the contractor (in the TEMPEST Phase-1
COMM data release). The contractor used a convention where aircraft nose-up is a
COMM positive pitch whereas the inversion algorithm uses a convention where
COMM aircraft nose-down is a positive pitch angle. The tx_pitch in this data
COMM uses the inversion coordinate system.

COMM

COMM The Tx-Rx transverse separation estimate is also of opposite sign to the
COMM corresponding GPS transverse separation as measured by the contractor. The
COMM contractor's coordinate system for the Tx-Rx separation is positive forward,
COMM upward and to the right of the plane direction, whereas the inversion's
COMM coordinate system is positive forward, upward and to the left of the plane
COMM direction.

COMM

COMM	Field Channel	Description	Units	Undefined	Format
COMM	----	-----	-----	-----	-----
COMM	1	uniqueid	Sample ID	-99999	I7
COMM	2	survey	GA survey ID		-9999 I5
COMM	3	date	Date (yyyymmdd)		-99999 I9
COMM	4	flight	Flight Number		-9999 I5
COMM	5	line	Line Number		-99999 I11
COMM	6	fid	Fiducial Number		-99999 F11.2
COMM	7	easting	Easting, PROJECTION:GDA94/MGA54 (m)	-99999	F9.1
COMM	8	northing	Northing, PROJECTION:GDA94/MGA54 (m)	-99999	F10.1
COMM	9	elevation	Ground Elevation, DATUM:AHD (m)	-99999	F8.2
COMM	10	altimeter	LIDAR Altimeter (m)	-99999	F8.2
COMM	11	tx_height	Transmitter Height (measured) (m)	-99999	F9.2
COMM	12	tx_roll	Transmitter Roll (measured) (deg)	-99999	F9.2
COMM	13	tx_pitch	Transmitter Pitch (measured) (deg)	-99999	F9.2
COMM	14	tx_yaw	Transmitter Yaw (assumed) (deg)	-99999	F9.2
COMM	15	txrx_dx	Tx-Rx horizontal separation (estimate) (m)	-99999	F9.2
COMM	16	txrx_dy	Tx-Rx transverse separation (estimate) (m)	-99999	F9.2
COMM	17	txrx_dz	Tx-Rx vertical separation (estimate) (m)	-99999	F9.2
COMM	18	rx_roll	Rx Roll (assumed) (deg)	-99999	F9.2
COMM	19	rx_pitch	Rx Pitch (estimate) (deg)	-99999	F9.2
COMM	20	rx_yaw	Rx Yaw (assumed) (deg)	-99999	F9.2
COMM	21	nlayers	Number of inversion layers	-999	I4
COMM	22	conductivity_01	Conductivity Layer 01 0.00m to 4.00m (S/m)	-99999	F14.8
COMM	23	conductivity_02	Conductivity Layer 02 4.00m to 8.40m (S/m)	-99999	F14.8

The Frome airborne electromagnetic survey, South Australia: implications for energy, minerals and regional geology

COMM	24	conductivity_03	Conductivity Layer 03 8.40m to 13.24m (S/m)	-99999	F14.8
COMM	25	conductivity_04	Conductivity Layer 04 13.24m to 18.56m (S/m)	-99999	F14.8
COMM	26	conductivity_05	Conductivity Layer 05 18.56m to 24.42m (S/m)	-99999	F14.8
COMM	27	conductivity_06	Conductivity Layer 06 24.42m to 30.86m (S/m)	-99999	F14.8
COMM	28	conductivity_07	Conductivity Layer 07 30.86m to 37.95m (S/m)	-99999	F14.8
COMM	29	conductivity_08	Conductivity Layer 08 37.95m to 45.74m (S/m)	-99999	F14.8
COMM	30	conductivity_09	Conductivity Layer 09 45.74m to 54.32m (S/m)	-99999	F14.8
COMM	31	conductivity_10	Conductivity Layer 10 54.32m to 63.75m (S/m)	-99999	F14.8
COMM	32	conductivity_11	Conductivity Layer 11 63.75m to 74.12m (S/m)	-99999	F14.8
COMM	33	conductivity_12	Conductivity Layer 12 74.12m to 85.54m (S/m)	-99999	F14.8
COMM	34	conductivity_13	Conductivity Layer 13 85.54m to 98.09m (S/m)	-99999	F14.8
COMM	35	conductivity_14	Conductivity Layer 14 98.09m to 111.90m (S/m)	-99999	F14.8
COMM	36	conductivity_15	Conductivity Layer 15 111.90m to 127.09m (S/m)	-99999	F14.8
COMM	37	conductivity_16	Conductivity Layer 16 127.09m to 143.80m (S/m)	-99999	F14.8
COMM	38	conductivity_17	Conductivity Layer 17 143.80m to 162.18m (S/m)	-99999	F14.8
COMM	39	conductivity_18	Conductivity Layer 18 162.18m to 182.40m (S/m)	-99999	F14.8
COMM	40	conductivity_19	Conductivity Layer 19 182.40m to 204.64m (S/m)	-99999	F14.8
COMM	41	conductivity_20	Conductivity Layer 20 204.64m to 229.10m (S/m)	-99999	F14.8
COMM	42	conductivity_21	Conductivity Layer 21 229.10m to 256.01m (S/m)	-99999	F14.8
COMM	43	conductivity_22	Conductivity Layer 22 256.01m to 285.61m (S/m)	-99999	F14.8
COMM	44	conductivity_23	Conductivity Layer 23 285.61m to 318.17m (S/m)	-99999	F14.8
COMM	45	conductivity_24	Conductivity Layer 24 318.17m to 353.99m (S/m)	-99999	F14.8
COMM	46	conductivity_25	Conductivity Layer 25 353.99m to 393.39m (S/m)	-99999	F14.8
COMM	47	conductivity_26	Conductivity Layer 26 393.39m to 436.73m (S/m)	-99999	F14.8
COMM	48	conductivity_27	Conductivity Layer 27 436.73m to 484.40m (S/m)	-99999	F14.8
COMM	49	conductivity_28	Conductivity Layer 28 484.40m to 536.84m (S/m)	-99999	F14.8
COMM	50	conductivity_29	Conductivity Layer 29 536.84m to 594.52m (S/m)	-99999	F14.8
COMM	51	conductivity_30	Conductivity Layer 30 594.52m to infinity (S/m)	-99999	F14.8
COMM	52	sensitivity_01	Layer Sensitivity 01	-99999	F19.4
COMM	53	sensitivity_02	Layer Sensitivity 02	-99999	F14.8
COMM	54	sensitivity_03	Layer Sensitivity 03	-99999	F14.8
COMM	55	sensitivity_04	Layer Sensitivity 04	-99999	F14.8
COMM	56	sensitivity_05	Layer Sensitivity 05	-99999	F14.8
COMM	57	sensitivity_06	Layer Sensitivity 06	-99999	F14.8
COMM	58	sensitivity_07	Layer Sensitivity 07	-99999	F14.8
COMM	59	sensitivity_08	Layer Sensitivity 08	-99999	F14.8
COMM	60	sensitivity_09	Layer Sensitivity 09	-99999	F14.8
COMM	61	sensitivity_10	Layer Sensitivity 10	-99999	F14.8
COMM	62	sensitivity_11	Layer Sensitivity 11	-99999	F14.8
COMM	63	sensitivity_12	Layer Sensitivity 12	-99999	F14.8
COMM	64	sensitivity_13	Layer Sensitivity 13	-99999	F14.8
COMM	65	sensitivity_14	Layer Sensitivity 14	-99999	F14.8
COMM	66	sensitivity_15	Layer Sensitivity 15	-99999	F14.8
COMM	67	sensitivity_16	Layer Sensitivity 16	-99999	F14.8
COMM	68	sensitivity_17	Layer Sensitivity 17	-99999	F14.8
COMM	69	sensitivity_18	Layer Sensitivity 18	-99999	F14.8
COMM	70	sensitivity_19	Layer Sensitivity 19	-99999	F14.8
COMM	71	sensitivity_20	Layer Sensitivity 20	-99999	F14.8
COMM	72	sensitivity_21	Layer Sensitivity 21	-99999	F14.8
COMM	73	sensitivity_22	Layer Sensitivity 22	-99999	F14.8
COMM	74	sensitivity_23	Layer Sensitivity 23	-99999	F14.8
COMM	75	sensitivity_24	Layer Sensitivity 24	-99999	F14.8

The Frome airborne electromagnetic survey, South Australia: implications for energy, minerals and regional geology

COMM	76 sensitivity_25	Layer Sensitivity 25	-99999	F14.8
COMM	77 sensitivity_26	Layer Sensitivity 26	-99999	F14.8
COMM	78 sensitivity_27	Layer Sensitivity 27	-99999	F14.8
COMM	79 sensitivity_28	Layer Sensitivity 28	-99999	F14.8
COMM	80 sensitivity_29	Layer Sensitivity 29	-99999	F14.8
COMM	81 sensitivity_30	Layer Sensitivity 30	-99999	F14.8
COMM	82 x_primary_pred	X Primary Field Predicted	(fT) -99999	F15.3
COMM	83 x_window_pred_01	X Window 01 Predicted	(fT) -99999	F14.8
COMM	84 x_window_pred_02	X Window 02 Predicted	(fT) -99999	F14.8
COMM	85 x_window_pred_03	X Window 03 Predicted	(fT) -99999	F14.8
COMM	86 x_window_pred_04	X Window 04 Predicted	(fT) -99999	F14.8
COMM	87 x_window_pred_05	X Window 05 Predicted	(fT) -99999	F14.8
COMM	88 x_window_pred_06	X Window 06 Predicted	(fT) -99999	F14.8
COMM	89 x_window_pred_07	X Window 07 Predicted	(fT) -99999	F14.8
COMM	90 x_window_pred_08	X Window 08 Predicted	(fT) -99999	F14.8
COMM	91 x_window_pred_09	X Window 09 Predicted	(fT) -99999	F14.8
COMM	92 x_window_pred_10	X Window 10 Predicted	(fT) -99999	F14.8
COMM	93 x_window_pred_11	X Window 11 Predicted	(fT) -99999	F14.8
COMM	94 x_window_pred_12	X Window 12 Predicted	(fT) -99999	F14.8
COMM	95 x_window_pred_13	X Window 13 Predicted	(fT) -99999	F14.8
COMM	96 x_window_pred_14	X Window 14 Predicted	(fT) -99999	F14.8
COMM	97 x_window_pred_15	X Window 15 Predicted	(fT) -99999	F14.8
COMM	98 z_primary_pred	Z Primary Field Predicted	(fT) -99999	F14.8
COMM	99 z_window_pred_01	Z Window 01 Predicted	(fT) -99999	F14.8
COMM	100 z_window_pred_02	Z Window 02 Predicted	(fT) -99999	F14.8
COMM	101 z_window_pred_03	Z Window 03 Predicted	(fT) -99999	F14.8
COMM	102 z_window_pred_04	Z Window 04 Predicted	(fT) -99999	F14.8
COMM	103 z_window_pred_05	Z Window 05 Predicted	(fT) -99999	F14.8
COMM	104 z_window_pred_06	Z Window 06 Predicted	(fT) -99999	F14.8
COMM	105 z_window_pred_07	Z Window 07 Predicted	(fT) -99999	F14.8
COMM	106 z_window_pred_08	Z Window 08 Predicted	(fT) -99999	F14.8
COMM	107 z_window_pred_09	Z Window 09 Predicted	(fT) -99999	F14.8
COMM	108 z_window_pred_10	Z Window 10 Predicted	(fT) -99999	F14.8
COMM	109 z_window_pred_11	Z Window 11 Predicted	(fT) -99999	F14.8
COMM	110 z_window_pred_12	Z Window 12 Predicted	(fT) -99999	F14.8
COMM	111 z_window_pred_13	Z Window 13 Predicted	(fT) -99999	F14.8
COMM	112 z_window_pred_14	Z Window 14 Predicted	(fT) -99999	F14.8
COMM	113 z_window_pred_15	Z Window 15 Predicted	(fT) -99999	F14.8
COMM	114 PhiD	PhiD: Data Misfit (Target = 1.0)	-99999	F14.8
COMM	115 PhiM	PhiM: Model regularisation term	-99999	F14.8
COMM	116 PhiC	PhiC: Conductivity model misfit	-99999	F14.8
COMM	117 PhiT	PhiT: Not used in this inversion	-99999	I14
COMM	118 PhiG	PhiG: System geometry model misfit	-99999	F14.8
COMM	119 PhiS	PhiS: Vertical smoothness term	-99999	F14.8
COMM	120 Lambda	Lambda: Regularisation factor	-99999	F14.5
COMM	121 AlphaC	AlphaC: Conductivity model weight	-99999	I14
COMM	122 AlphaT	AlphaT: Not used in this inversion	-99999	I14
COMM	123 AlphaG	AlphaG: System geometry model weight	-99999	I14
COMM	124 AlphaS	AlphaS: Smoothness weight	-99999	F14.5
COMM	125 Iterations	Inversion Iterations	-999	I4

A4.2 LINE-BY-LINE INVERSION CONDUCTIVITY HEADER

COMM Coordinate System Notes:

COMM -----

COMM The Transmitter Pitch (tx_pitch) in this dataset is the negative value of the transmitter pitch measured by the contractor (in the TEMPEST Phase-1 data release). The contractor used a convention where aircraft nose-up is a positive pitch whereas the inversion algorithm uses a convention where aircraft nose-down is a positive pitch angle. The tx_pitch in this data uses the inversion coordinate system.

COMM

COMM The Tx-Rx transverse separation estimate is also of opposite sign to the corresponding GPS transverse separation as measured by the contractor. The contractor's coordinate system for the Tx-Rx separation is positive forward, upward and to the right of the plane direction, whereas the inversion's coordinate system is positive forward, upward and to the left of the plane direction.

COMM

COMM Field	Channel	Description	Units	Undefined	Format
COMM -----	-----	-----	-----	-----	-----
COMM	1 survey	GA survey ID	-999	I4	
COMM	2 date	Date	(yyyymmdd)	-99999	I9
COMM	3 flight	Flight Number	-9999	I5	
COMM	4 line	Line Number	-99999	I8	
COMM	5 fid	Fiducial Number	-99999	F11.2	
COMM	6 linedistance	Line Distance	-99999	F9.1	
COMM	7 easting	Easting, PROJECTION:GDA94/MGA54	(m)	-99999	F9.1
COMM	8 northing	Northing, PROJECTION:GDA94/MGA54	(m)	-99999	F10.1
COMM	9 elevation	Ground Elevation, DATUM:AHD	(m)	-99999	F8.2
COMM	10 altimeter	LIDAR Altimeter	(m)	-99999	F8.2
COMM	11 tx_height	Transmitter Height (measured)	(m)	-99999	F8.2
COMM	12 tx_roll	Transmitter Roll (measured)	(deg)	-99999	F7.2
COMM	13 tx_pitch	Transmitter Pitch (measured)	(deg)	-99999	F7.2
COMM	14 tx_yaw	Transmitter Yaw (assumed)	(deg)	-99999	F7.2
COMM	15 trrx_dx	Tx-Rx horizontal separation (estimate)	(m)	-99999	F8.2
COMM	16 trrx_dy	Tx-Rx transverse separation (estimate)	(m)	-99999	F8.2
COMM	17 trrx_dz	Tx-Rx vertical separation (estimate)	(m)	-99999	F8.2
COMM	18 rx_roll	Rx Roll (assumed)	(deg)	-99999	F7.2
COMM	19 rx_pitch	Rx Pitch (estimate)	(deg)	-99999	F7.2
COMM	20 rx_yaw	Rx Yaw (assumed)	(deg)	-99999	F7.2
COMM	21 nlayers	Number of inversion layers	-999	I4	
COMM	22 conductivity_01	Conductivity Layer 01 0.00m to 4.00m	(S/m)	-99999	F9.5
COMM	23 conductivity_02	Conductivity Layer 02 4.00m to 8.40m	(S/m)	-99999	F9.5
COMM	24 conductivity_03	Conductivity Layer 03 8.40m to 13.24m	(S/m)	-99999	F9.5
COMM	25 conductivity_04	Conductivity Layer 04 13.24m to 18.56m	(S/m)	-99999	F9.5
COMM	26 conductivity_05	Conductivity Layer 05 18.56m to 24.42m	(S/m)	-99999	F9.5
COMM	27 conductivity_06	Conductivity Layer 06 24.42m to 30.86m	(S/m)	-99999	F9.5
COMM	28 conductivity_07	Conductivity Layer 07 30.86m to 37.95m	(S/m)	-99999	F9.5
COMM	29 conductivity_08	Conductivity Layer 08 37.95m to 45.74m	(S/m)	-99999	F9.5
COMM	30 conductivity_09	Conductivity Layer 09 45.74m to 54.32m	(S/m)	-99999	F9.5
COMM	31 conductivity_10	Conductivity Layer 10 54.32m to 63.75m	(S/m)	-99999	F9.5

The Frome airborne electromagnetic survey, South Australia: implications for energy, minerals and regional geology

COMM	32 conductivity_11	Conductivity Layer 11 63.75m to 74.12m	(S/m)	-99999	F9.5
COMM	33 conductivity_12	Conductivity Layer 12 74.12m to 85.54m	(S/m)	-99999	F9.5
COMM	34 conductivity_13	Conductivity Layer 13 85.54m to 98.09m	(S/m)	-99999	F9.5
COMM	35 conductivity_14	Conductivity Layer 14 98.09m to 111.90m	(S/m)	-99999	F9.5
COMM	36 conductivity_15	Conductivity Layer 15 111.90m to 127.09m	(S/m)	-99999	F9.5
COMM	37 conductivity_16	Conductivity Layer 16 127.09m to 143.80m	(S/m)	-99999	F9.5
COMM	38 conductivity_17	Conductivity Layer 17 143.80m to 162.18m	(S/m)	-99999	F9.5
COMM	39 conductivity_18	Conductivity Layer 18 162.18m to 182.40m	(S/m)	-99999	F9.5
COMM	40 conductivity_19	Conductivity Layer 19 182.40m to 204.64m	(S/m)	-99999	F9.5
COMM	41 conductivity_20	Conductivity Layer 20 204.64m to 229.10m	(S/m)	-99999	F9.5
COMM	42 conductivity_21	Conductivity Layer 21 229.10m to 256.01m	(S/m)	-99999	F9.5
COMM	43 conductivity_22	Conductivity Layer 22 256.01m to 285.61m	(S/m)	-99999	F9.5
COMM	44 conductivity_23	Conductivity Layer 23 285.61m to 318.17m	(S/m)	-99999	F9.5
COMM	45 conductivity_24	Conductivity Layer 24 318.17m to 353.99m	(S/m)	-99999	F9.5
COMM	46 conductivity_25	Conductivity Layer 25 353.99m to 393.39m	(S/m)	-99999	F9.5
COMM	47 conductivity_26	Conductivity Layer 26 393.39m to 436.73m	(S/m)	-99999	F9.5
COMM	48 conductivity_27	Conductivity Layer 27 436.73m to 484.40m	(S/m)	-99999	F9.5
COMM	49 conductivity_28	Conductivity Layer 28 484.40m to 536.84m	(S/m)	-99999	F9.5
COMM	50 conductivity_29	Conductivity Layer 29 536.84m to 594.52m	(S/m)	-99999	F9.5
COMM	51 conductivity_30	Conductivity Layer 30 594.52m to infinity	(S/m)	-99999	F9.5
COMM	52 thickness_01	Thickness 01	(m)	-99999	F9.5
COMM	53 thickness_02	Thickness 02	(m)	-99999	F9.5
COMM	54 thickness_03	Thickness 03	(m)	-99999	F9.5
COMM	55 thickness_04	Thickness 04	(m)	-99999	F9.5
COMM	56 thickness_05	Thickness 05	(m)	-99999	F9.5
COMM	57 thickness_06	Thickness 06	(m)	-99999	F9.5
COMM	58 thickness_07	Thickness 07	(m)	-99999	F9.5
COMM	59 thickness_08	Thickness 08	(m)	-99999	F9.5
COMM	60 thickness_09	Thickness 09	(m)	-99999	F9.5
COMM	61 thickness_10	Thickness 10	(m)	-99999	F9.5
COMM	62 thickness_11	Thickness 11	(m)	-99999	F9.5
COMM	63 thickness_12	Thickness 12	(m)	-99999	F9.5
COMM	64 thickness_13	Thickness 13	(m)	-99999	F9.5
COMM	65 thickness_14	Thickness 14	(m)	-99999	F9.5
COMM	66 thickness_15	Thickness 15	(m)	-99999	F9.5
COMM	67 thickness_16	Thickness 16	(m)	-99999	F9.5
COMM	68 thickness_17	Thickness 17	(m)	-99999	F9.5
COMM	69 thickness_18	Thickness 18	(m)	-99999	F9.5
COMM	70 thickness_19	Thickness 19	(m)	-99999	F9.5
COMM	71 thickness_20	Thickness 20	(m)	-99999	F9.5
COMM	72 thickness_21	Thickness 21	(m)	-99999	F9.5
COMM	73 thickness_22	Thickness 22	(m)	-99999	F9.5
COMM	74 thickness_23	Thickness 23	(m)	-99999	F9.5
COMM	75 thickness_24	Thickness 24	(m)	-99999	F9.5
COMM	76 thickness_25	Thickness 25	(m)	-99999	F9.5
COMM	77 thickness_26	Thickness 26	(m)	-99999	F9.5
COMM	78 thickness_27	Thickness 27	(m)	-99999	F9.5
COMM	79 thickness_28	Thickness 28	(m)	-99999	F9.5
COMM	80 thickness_29	Thickness 29	(m)	-99999	F9.5
COMM	81 x_primary_observed	X Primary Field Observed	(fT)	-99999	F13.6
COMM	82 x_window_observed_01	X Window 01 Observed	(fT)	-99999	F13.6
COMM	83 x_window_observed_02	X Window 02 Observed	(fT)	-99999	F13.6

The Frome airborne electromagnetic survey, South Australia: implications for energy, minerals and regional geology

COMM 84	x_window_observed_03	X Window 03 Observed	(fT) -99999	F13.6
COMM 85	x_window_observed_04	X Window 04 Observed	(fT) -99999	F13.6
COMM 86	x_window_observed_05	X Window 05 Observed	(fT) -99999	F13.6
COMM 87	x_window_observed_06	X Window 06 Observed	(fT) -99999	F13.6
COMM 88	x_window_observed_07	X Window 07 Observed	(fT) -99999	F13.6
COMM 89	x_window_observed_08	X Window 08 Observed	(fT) -99999	F13.6
COMM 90	x_window_observed_09	X Window 09 Observed	(fT) -99999	F13.6
COMM 91	x_window_observed_10	X Window 10 Observed	(fT) -99999	F13.6
COMM 92	x_window_observed_11	X Window 11 Observed	(fT) -99999	F13.6
COMM 93	x_window_observed_12	X Window 12 Observed	(fT) -99999	F13.6
COMM 94	x_window_observed_13	X Window 13 Observed	(fT) -99999	F13.6
COMM 95	x_window_observed_14	X Window 14 Observed	(fT) -99999	F13.6
COMM 96	x_window_observed_15	X Window 15 Observed	(fT) -99999	F13.6
COMM 97	z_primary_observed	Z Primary Field Observed	(fT) -99999	F13.6
COMM 98	z_window_observed_01	Z Window 01 Observed	(fT) -99999	F13.6
COMM 99	z_window_observed_02	Z Window 02 Observed	(fT) -99999	F13.6
COMM 100	z_window_observed_03	Z Window 03 Observed	(fT) -99999	F13.6
COMM 101	z_window_observed_04	Z Window 04 Observed	(fT) -99999	F13.6
COMM 102	z_window_observed_05	Z Window 05 Observed	(fT) -99999	F13.6
COMM 103	z_window_observed_06	Z Window 06 Observed	(fT) -99999	F13.6
COMM 104	z_window_observed_07	Z Window 07 Observed	(fT) -99999	F13.6
COMM 105	z_window_observed_08	Z Window 08 Observed	(fT) -99999	F13.6
COMM 106	z_window_observed_09	Z Window 09 Observed	(fT) -99999	F13.6
COMM 107	z_window_observed_10	Z Window 10 Observed	(fT) -99999	F13.6
COMM 108	z_window_observed_11	Z Window 11 Observed	(fT) -99999	F13.6
COMM 109	z_window_observed_12	Z Window 12 Observed	(fT) -99999	F13.6
COMM 110	z_window_observed_13	Z Window 13 Observed	(fT) -99999	F13.6
COMM 111	z_window_observed_14	Z Window 14 Observed	(fT) -99999	F13.6
COMM 112	z_window_observed_15	Z Window 15 Observed	(fT) -99999	F13.6
COMM 113	x_primary_predicted	X Primary Field Predicted	(fT) -99999	F13.6
COMM 114	x_window_predicted_01	X Window 01 Predicted	(fT) -99999	F13.6
COMM 115	x_window_predicted_02	X Window 02 Predicted	(fT) -99999	F13.6
COMM 116	x_window_predicted_03	X Window 03 Predicted	(fT) -99999	F13.6
COMM 117	x_window_predicted_04	X Window 04 Predicted	(fT) -99999	F13.6
COMM 118	x_window_predicted_05	X Window 05 Predicted	(fT) -99999	F13.6
COMM 119	x_window_predicted_06	X Window 06 Predicted	(fT) -99999	F13.6
COMM 120	x_window_predicted_07	X Window 07 Predicted	(fT) -99999	F13.6
COMM 121	x_window_predicted_08	X Window 08 Predicted	(fT) -99999	F13.6
COMM 122	x_window_predicted_09	X Window 09 Predicted	(fT) -99999	F13.6
COMM 123	x_window_predicted_10	X Window 10 Predicted	(fT) -99999	F13.6
COMM 124	x_window_predicted_11	X Window 11 Predicted	(fT) -99999	F13.6
COMM 125	x_window_predicted_12	X Window 12 Predicted	(fT) -99999	F13.6
COMM 126	x_window_predicted_13	X Window 13 Predicted	(fT) -99999	F13.6
COMM 127	x_window_predicted_14	X Window 14 Predicted	(fT) -99999	F13.6
COMM 128	x_window_predicted_15	X Window 15 Predicted	(fT) -99999	F13.6
COMM 129	z_primary_predicted	Z Primary Field Predicted	(fT) -99999	F13.6
COMM 130	z_window_predicted_01	Z Window 01 Predicted	(fT) -99999	F13.6
COMM 131	z_window_predicted_02	Z Window 02 Predicted	(fT) -99999	F13.6
COMM 132	z_window_predicted_03	Z Window 03 Predicted	(fT) -99999	F13.6
COMM 133	z_window_predicted_04	Z Window 04 Predicted	(fT) -99999	F13.6
COMM 134	z_window_predicted_05	Z Window 05 Predicted	(fT) -99999	F13.6
COMM 135	z_window_predicted_06	Z Window 06 Predicted	(fT) -99999	F13.6

The Frome airborne electromagnetic survey, South Australia: implications for energy, minerals and regional geology

COMM	136	z_window_predicted_07	Z Window 07 Predicted	(fT)	-99999	F13.6
COMM	137	z_window_predicted_08	Z Window 08 Predicted	(fT)	-99999	F13.6
COMM	138	z_window_predicted_09	Z Window 09 Predicted	(fT)	-99999	F13.6
COMM	139	z_window_predicted_10	Z Window 10 Predicted	(fT)	-99999	F13.6
COMM	140	z_window_predicted_11	Z Window 11 Predicted	(fT)	-99999	F13.6
COMM	141	z_window_predicted_12	Z Window 12 Predicted	(fT)	-99999	F13.6
COMM	142	z_window_predicted_13	Z Window 13 Predicted	(fT)	-99999	F13.6
COMM	143	z_window_predicted_14	Z Window 14 Predicted	(fT)	-99999	F13.6
COMM	144	z_window_predicted_15	Z Window 15 Predicted	(fT)	-99999	F13.6
COMM	145	SamplePhiD	Sample Data Misfit (target = 1.0)		-99999	F12.5
COMM	146	LinePhiD	Line Data Misfit (target = 1.0)		-99999	F12.6
COMM	147	Iterations	Inversion Iterations		-999	I4

Appendix 5: Technical specifications of map projections

Projection Name: Map Grid of Australia, Zone 54
Units: Metres
Datum: Geocentric Datum of Australia 1994 (GDA94)
Epoch: 1994.0
Ellipsoid: GRS80
Semi-major axis (a): 6,378,137.0 metres
Inverse flattening (1/f): 298.257
Central meridian 142°00'00''
False Easting: 500 000 metres
False Northing: 10 000 000 metres

The Frome airborne electromagnetic survey, South Australia: implications for energy, minerals and regional geology